Des microquasars aux systèmes binaires enfouis: enquête dans l'Univers des astres extrêmes...

Sylvain Chaty

▶ **To cite this version:**

Sylvain Chaty. Des microquasars aux systèmes binaires enfouis: enquête dans l'Univers des astres extrêmes.... Cosmologie et astrophysique extra-galactique [astro-ph.CO]. Université Paris-Diderot - Paris VII, 2007. tel-00274649

HAL Id: tel-00274649

https://theses.hal.science/tel-00274649

Submitted on 20 Apr 2008

HAL is a multi-disciplinary open access archive for the deposit and dissemination of scientific research documents, whether they are published or not. The documents may come from teaching and research institutions in France or abroad, or from public or private research centers.

L'archive ouverte pluridisciplinaire **HAL**, est destinée au dépôt et à la diffusion de documents scientifiques de niveau recherche, publiés ou non, émanant des établissements d'enseignement et de recherche français ou étrangers, des laboratoires publics ou privés.

HABILITATION À DIRIGER DES RECHERCHES
de l'Université Paris 7 - Denis Diderot

présentée par

Dr. Sylvain CHATY

Spécialité : Astrophysique

Des microquasars aux systèmes binaires enfouis : enquête dans l'Univers des astres extrêmes...

Soutenue le 26 Novembre 2 007 à 14h00,
à l'Amphithéâtre Claude Bloch du CEA de Saclay,
devant le jury composé de :

Monsieur Didier Barret	Rapporteur
Monsieur Anthony J. Dean	Rapporteur
Monsieur Gilles Henri	Président du jury
Monsieur Jacques Le Bourlot	Rapporteur
Monsieur I. Félix Mirabel	Examinateur

AIM - Astrophysique Interactions Multi-échelles
Unité Mixte de Recherche CEA/CNRS/Université Paris 7 Denis Diderot n°7158
CEA/Saclay, DSM/DAPNIA/Service d'Astrophysique, Bât. 709
L'Orme des Merisiers, FR-91 191 Gif-sur-Yvette cedex, France
Tél :+33 1 69 08 43 85 / Fax :+33 1 69 08 65 77 / *chaty@cea.fr*
http ://www.aim.univ-paris7.fr/CHATY/

HABILITATION À DIRIGER DES RECHERCHES
de l'Université Paris 7 - Denis Diderot

présentée par

Dr. Sylvain CHATY

Spécialité : Astrophysique

Des microquasars aux systèmes binaires enfouis : enquête dans l'Univers des astres extrêmes...

Soutenue le 26 Novembre 2 007 à 14h00,
à l'Amphithéâtre Claude Bloch du CEA de Saclay,
devant le jury composé de :

Monsieur Didier Barret	Rapporteur
Monsieur Anthony J. Dean	Rapporteur
Monsieur Gilles Henri	Président du jury
Monsieur Jacques Le Bourlot	Rapporteur
Monsieur I. Félix Mirabel	Examinateur

AIM - Astrophysique Interactions Multi-échelles
Unité Mixte de Recherche CEA/CNRS/Université Paris 7 Denis Diderot n°7158
CEA/Saclay, DSM/DAPNIA/Service d'Astrophysique, Bât. 709
L'Orme des Merisiers, FR-91 191 Gif-sur-Yvette cedex, France
Tél :+33 1 69 08 43 85 / Fax :+33 1 69 08 65 77 / *chaty@cea.fr*
http ://www.aim.univ-paris7.fr/CHATY/

Traversant ce vide, devine :
Il me manque, terriblement.

Petit, les étoiles me consolaient,
Aujourd'hui, ma petite lumière me guide...

À Nuria

Et qu'on ne s'imagine pas que j'allège la tâche du physicien ou du naturaliste : rien de plus difficile que de bien observer ; rien de plus difficile que de bien faire une expérience ; rien de plus difficile que de ne tirer de l'expérience ou de l'observation que des conséquences rigoureuses ; rien de plus difficile que de se garantir de la séduction systématique, du préjugé et de la précipitation.

Il ne peut y avoir qu'une théorie sur une machine qui est une, et la découverte de cette théorie est d'autant plus éloignée que la machine est plus compliquée.

Quelle machine que l'univers !

Denis Diderot, 1782
Essais sur les règnes de Claude et de Néron, Les questions naturelles

Première partie

Curriculum Vitae

Curriculum Vitae

CHATY Sylvain ; *Né le :* 16/10/1971 à Maisons-Alfort (94) ; *Nationalité :* française

AIM Astrophysique Interactions Multi-echelles (Unité Mixte de Recherche n^{o}7158 CEA-CNRS-Université Paris 7 - Denis Diderot), Service d'Astrophysique, CEA-Saclay DSM/DAPNIA/SAp, Bât. 709, L'Orme des Merisiers, FR-91 191 Gif-sur-Yvette Cedex, France
Tél : +33 1 69 08 43 85 ; Fax : +33 1 69 08 65 77, e-mail : chaty@cea.fr
http ://www.aim.univ-paris7.fr/CHATY/

Carrière :

- • depuis 09/2002 : Maître de conférences de l'Université Paris 7 - Denis Diderot et Service d'Astrophysique, CEA Saclay, France.
- • 09/1999-08/2002 : Chercheur du département de Physique et d'Astronomie de l'Open University, Royaume-Uni, financement de la fondation Leverhulme.
- • 09/1998-08/1999 : Attaché Temporaire d'Enseignement et de Recherche, Université Paul Sabatier – Toulouse III et C.E.S.R. - Centre d'Etude Spatiale des Rayonnements, Toulouse, France.
- • 09/1994-09/1995 et 08/1996-08/1998 : Doctorant au Service d'Astrophysique du CEA Saclay, contrat CFR (10/1995-07/1996 : Scientifique du contingent, Direction Générale de l'Armement)

Diplômes :

- • Habilitation à Diriger des Recherches de l'Université Paris Diderot, soutenue le 26/11/2007 : *Des microquasars aux systèmes binaires enfouis : enquête dans l'Univers des astres extrêmes*, Jury : Dr. D. Barret, Pr. A.J. Dean, Pr. J. Le Bourlot (rapporteurs), Pr. G. Henri (président), et Dr. I.F. Mirabel (examinateur).
- • Doctorat d'Astrophysique et de Techniques Spatiales de l'Université Paris 11, Service d'Astrophysique CEA/Saclay, dirigé par Dr. I.F. Mirabel, soutenu le 29/09/1998 : *Étude multi-longueur d'onde du microquasar GRS 1915+105 et de sources binaires de haute énergie de la Galaxie*, Mention Très Honorable avec les Félicitations du Jury, Jury : Dr. C. Motch et Pr. J.M. Paredes (rapporteurs), Pr. B. Rocca-Volmerange (présidente), Dr. L.F. Rodríguez et Dr. M. Boër (examinateurs).
- • DEA d'Astrophysique et de Techniques Spatiales (1994, Université Paris 7 - Denis Diderot et Observatoire de Meudon, Mention Bien)
- • Licence & Maîtrise de Physique Fondamentale (1992&1993, Université Paris 6, Mention Bien)

Activités administratives et Comités :

- • depuis 2007 : Membre élu du conseil d'UFR de Physique de l'Université Paris Diderot
- • depuis 2007 : Membre élu de la Commission de Spécialistes de l'Enseignement Supérieur 34 (Astronomie-Astrophysique) de l'Université Paris Diderot

- • depuis 2005 : Membre élu du conseil de laboratoire AIM (Astrophysique Interactions Multi-échelles, UMR n^{o}7158)
- • depuis 2005 : Responsable de “Astrophysique enseignement” (L3 SPE), “Instrumentation de l’IR aux hautes énergies” et “Traitement d’Images en astronomie X/γ (M2 Recherche Astrophysique)”, Université Paris Diderot
- • depuis 2007 : Scientifique affilié à la collaboration du Satellite GLAST (groupe multi-longueur d’onde)
- • 2004 : Membre de la commission d’attribution de temps du satellite Chandra (systèmes binaires X ; Boston, USA)
- • depuis 2007 : Représentant de l’Université Paris Diderot pour l’Année Mondiale de l’Astronomie 2009
- • depuis 2005 : Membre du comité national des Olympiades Nationales de Physique
- • depuis 2004 : Membre du comité scientifique d’organisation du Festival d’Astronomie de Fleurance
- • depuis 2006 : Membre du comité scientifique du Pôle de Rayonnement Culturel “A ciel ouvert”

Distinctions :

- • 01/2007 : Sélection des travaux de recherche, et invitation à la conférence de presse du 1er symposium du satellite GLAST, Stanford Univ., USA :
  http ://www.nasa.gov/centers/goddard/news/topstory/2007/gas_cocoon.html
- • depuis 1997 : Orateur invité dans 13 congrès internationaux
- • depuis 1995 : > 50 propositions de temps acceptées sur les observatoires/satellites internationaux radio $\rightarrow \gamma$: VLA, ESO/VLT, INTEGRAL, etc.
- • depuis 2002 : Financement CNES : MINE (Multiwavelength *INTEGRAL* NEtwork) 200 k€ pour 5 ans, renouvelable : post-doc, équipement, missions
- • 1999-2002 : Financement GdR Hautes Energies : 20 k€ pour 4 ans : missions

Activités de recherche

Étude multi-échelle des phénomènes relativistes de l'Univers

I. Thèmes de recherche

La recherche que je conduis est par nature transverse : non seulement j'étudie des objets de différents types, des astres galactiques (contenant des étoiles à neutron et des trous noirs) aux astres extragalactiques (noyaux actifs de galaxie et sursauts de rayons γ), mais de plus je les étudie par des observations multi-longueur d'onde –sur l'ensemble du spectre électromagnétique–. Mes résultats les plus importants, concernant la découverte du lien entre les phénomènes d'accrétion et d'éjection dans les microquasars, et la découverte d'une nouvelle population d'objets de haute énergie enfouis derrière un cocon de poussière, montrent que ma recherche porte sur les questions actuelles en Astrophysique. Ceci est aussi montré par le nombre de citations de mes articles (plus de 1000), les conférences où j'ai été invité à donner des communications et revues de sujets, et le temps d'observation que j'ai obtenu sur de nombreux télescopes au sol et dans l'espace. Finalement, j'ai dirigé les travaux de recherche de plusieurs post-doctorants, doctorants et étudiants du L1 au M2 recherche.

• Accrétion et éjection de matière dans les *microquasars*

Mes activités de recherche portent sur une étude multi-longueur d'onde de sources transitoires de haute énergie de notre Galaxie. Ce sont des systèmes binaires constitués d'un astre compact (étoile à neutron ou trou noir de masse stellaire) attirant la matière d'une étoile compagnon. Parfois, des sursauts d'activité se produisent lorsque la matière s'accumulant sous la forme d'un disque d'accrétion devient instable, se traduisant par une intense augmentation d'émission sur l'ensemble du spectre électromagnétique. Parmi ces objets, ceux présentant des jets relativistes, – les *microquasars*–, sont des laboratoires idéaux d'étude des phénomènes relativistes de physique de haute énergie, car ils posent des questions essentielles à la compréhension de la nature et du fonctionnement de ces formidables puits gravitationnels : quels sont les processus physiques permettant l'éjection à partir de l'accrétion, quelle est la nature des jets, quelle est l'énergie des électrons du jet, quelle est la fraction de masse qui est éjectée ? De plus, ces microquasars éjectant de la matière de façon sporadique ou même parfois continue, ces éjections de matière se propagent et interagissent, à différentes échelles, avec le milieu les environnant.

• Différentes populations, et évolution de systèmes binaires de haute énergie

Notre Galaxie regorge de systèmes binaires de haute énergie différents de par leur nature, et leurs propriétés : l'astre compact peut être soit une étoile à neutron soit un trou noir, et l'étoile compagnon peut être une étoile de faible masse ou de grande masse. Ajoutons à cela des caractéristiques différentes liées à la taille de l'orbite et au rapport des masses des deux objets, et nous obtenons des systèmes aux propriétés complètement différentes. L'observation étant à l'astrophysique ce que l'expérimentation est à la physique, seule une étude exhaustive de ces systèmes aux caractéristiques différentes mais liée par une même physique permet de comprendre leur

formation, leur fonctionnement et leur évolution. Chaque système binaire contient deux objets dont l'évolution est accélérée par son compagnon : à la fois l'objet compact et l'étoile compagnon évoluent différemment du fait de la présence de l'autre objet. L'étude de cette évolution à long terme, en particulier de l'étoile compagnon, permet de mieux comprendre les modèles de population d'étoiles dans les systèmes binaires.

• Comparaison avec les noyaux actifs de galaxie et les sursauts de rayons γ

Les microquasars présentent une morphologie et des phénomènes dynamiques analogues aux quasars, mais sur une échelle de longueur des millions de fois inférieure. L'échelle de temps des phénomènes se produisant autour d'un trou noir étant proportionnelle à sa masse, les phénomènes d'accrétion-éjection se déroulent beaucoup plus vite au sein des microquasars que des quasars. La comparaison entre quasars et microquasars permet donc de mieux comprendre le processus des éjections relativistes. En outre, s'il existe des blazars, des quasars dont le jet pointe vers nous, existe-t-il aussi des microblazars, leur analogue pour les microquasars ? Enfin, on retrouve au sein des sursauts γ des phénomènes d'éjection similaires à ceux présents dans les (micro-)quasars. Le but ultime de cette recherche est ainsi de comprendre les phénomènes relativistes se produisant dans ces laboratoires de physique fondamentale.

II. Résumé des résultats marquants et publications les plus significatives

• Découverte du lien entre accrétion et éjection au sein du microquasar GRS 1915+105

Grâce à un ensemble de campagnes d'observations simultanées multi-longueur d'onde, dans le cadre d'une collaboration internationale, j'ai découvert le précurseur synchrotron infrarouge aux sursauts radio, lié à l'expansion adiabatique du nuage de plasma relativiste éjecté. J'ai ensuite mis en évidence le lien entre les phénomènes d'accrétion et d'éjection de matière se produisant autour du candidat trou noir et microquasar GRS 1915+105 (Chaty, Thèse 1998 ; Mirabel, Dhawan, Chaty et al. 1998, A&A, 330, L9, cf Figure 1). Ce résultat est essentiel pour la compréhension des objets que sont les microquasars, mais aussi pour l'ensemble des sources à jets présentes dans l'Univers tout entier, dont les quasars et les noyaux actifs de galaxie.

• Découverte de deux nouvelles populations de systèmes binaires de haute énergie

Le satellite de haute énergie *INTEGRAL* a découvert dans la direction du centre et du plan de notre Galaxie plusieurs sources de nature inconnue. Grâce à mes observations en optique, infrarouge proche et moyen, j'ai montré que IGR J16318-4848, le premier astre détecté par *INTEGRAL*, était un système très rare dans la Galaxie : un système binaire de grande masse contenant une étoile supergéante B[e], l'ensemble du système étant enfoui derrière un cocon de poussière (Chaty, S. & Filliatre, P., 2005, ApSS, 297, 235 ; Filliatre & Chaty, 2004, ApJ, 616, 469). Fort de cette découverte, j'ai ensuite étudié d'autres sources *INTEGRAL*, et montré que leurs propriétés étaient principalement dues à la présence de l'étoile supergéante. Dans la lignée de ce résultat, j'ai découvert que certains systèmes binaires de grande masse vus par *INTEGRAL*, contenant eux aussi une étoile évoluée, étaient variables sur de petites échelles de temps, alors que jusqu'à maintenant, seuls les systèmes binaires de faible masse étaient variables sur de telles échelles de

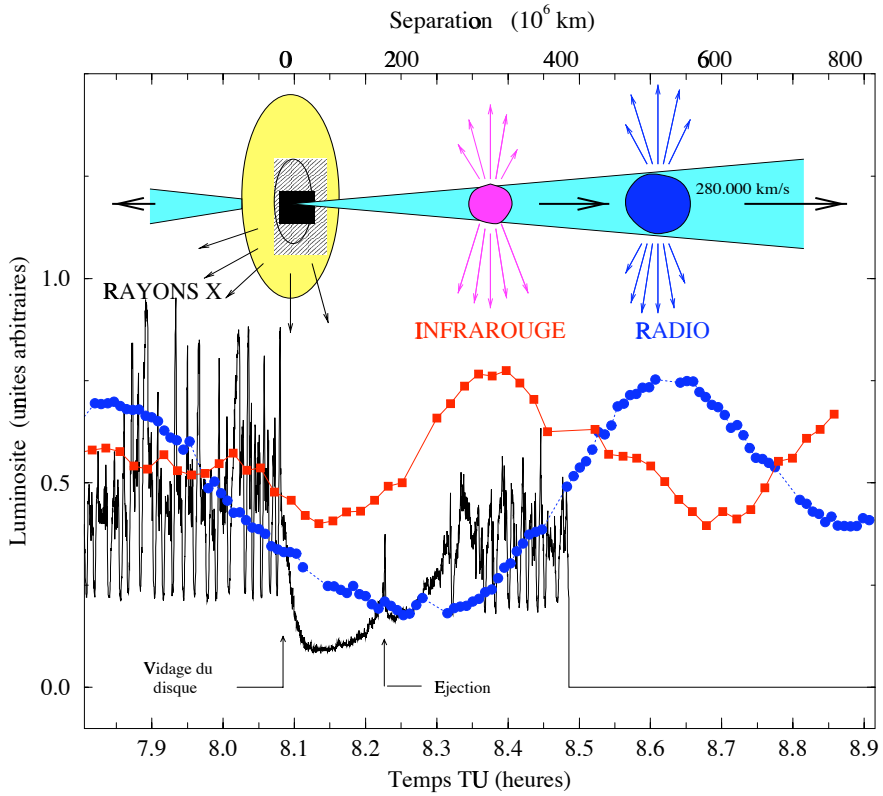

FIG. 1 – Observations du lien entre accrétion et éjection au sein du microquasar GRS 1915+105. Disparition rapide de la partie interne du disque d'accrétion, remplissage (rayons X), et éjection de nuages de plasma relativistes (émission synchrotron, en infrarouge puis en radio) (Chaty, Thèse 1998 ; Mirabel, Dhawan, Chaty et al. 1998, A&A, 330, L9 ; voir aussi Chaty 2006 in "Frontier Objects in Astrophysics and Particle Physics", Italy (2006).

temps. Il s'agit entre autres des sources IGR J11215-5952, IGR J16465-4507 et IGR J17544-2619 (Pellizza, Chaty, Negueruela, 2006, A&A, 455, 653). Cette découverte de deux nouvelles populations d'astres émettant dans les hautes énergies révolutionne notre vision sur la formation, l'évolution et le destin des systèmes binaires de haute énergie, en remettant en cause les schémas classiques d'évolution. Les questions qu'elle pose devraient permettre de mieux comprendre l'évolution de l'ensemble des systèmes binaires (Chaty et al. 2008, A&A in press), cf conférence de presse : http ://www.nasa.gov/centers/goddard/news/topstory/2007/gas_cocoon.html

• Les jets émettent depuis la radio jusqu'aux hautes énergies, lien accrétion/éjection

Grâce à mon réseau d'observations multi-longueurs d'onde, j'ai observé le candidat trou noir XTE J1118+480 depuis la radio jusqu'aux rayons γ, en le suivant tout au long de son sursaut d'activité, jusqu'à son retour à l'état calme. La richesse de ces observations m'a permis de modéliser précisément l'émission provenant du disque d'accrétion, des jets, et de l'étoile compagnon. L'évolution de ces émissions tout au long du sursaut suggère que le jet émet depuis la radio jusqu'aux hautes énergies, et que l'énergie transportée par l'accrétion est corrélée à l'énergie injectée dans les jets. Ce résultat est très important car il montre d'une part que l'énergie associée aux jets est plus importante que ce qui était communément admis dans la communauté travaillant sur les microquasars, et d'autre part que l'éjection est un phénomène commun dans les systèmes binaires de haute énergie, qui est présent chaque fois que se produit une accrétion de matière (Chaty et al., 2003, MNRAS, 346, 689).

• Mise en évidence d'interactions éjections– milieu environnant

En observant en optique/infrarouge certains sursauts du microquasar GRS 1915+105 et d'une source qui pourrait être le premier microblazar –V4641 Sgr–, et en les comparant aux observations radio, j'ai montré que la matière éjectée par chaque source est entrée en collision avec leur environnement (Chaty et al., 2003, MNRAS, 343, 169 ; Chaty et al., 2001, A&A, 366, 1035).

• Éjection : propagation d'une onde de choc

En appliquant les modèles d'éjection des quasars aux observations d'éjection effectuées sur le microquasar GRS 1915+105, j'ai montré que les éjections représentent la propagation d'une onde de choc moyennement relativiste, et non de nuages de plasma, contrairement à ce qui était communément admis dans la communauté scientifique travaillant sur les microquasars (Türler, Courvoisier, Chaty et al. 2004, A&A, 415, L35).

• Découverte de la contrepartie infrarouge de sources de haute énergie

J'ai découvert la contrepartie optique et/ou infrarouge des objets XTE J1118+480, XTE J1720-318, XTE J1859+226, XTE J1908+094, GRO J1655-40, GRS 1734-292, GX 354-0, IGR J16318-4848, IGR J17544-2619, V4641 Sgr, et je les ai étudiées, afin de contraindre leur nature, leur distance, etc.

III. Moyens mis en oeuvre : Observations multi-longueurs d'onde

Chaque élément du système binaire émet dans des domaines de longueurs d'onde variés : le disque d'accrétion émet des X/γ à l'infrarouge, l'étoile compagnon de l'ultraviolet à l'infrarouge et les jets de l'infrarouge (ou des X ?) à la radio. L'approche multi-longueur d'onde s'avère donc indispensable. De plus, ces microquasars n'étant pas toujours en activité, il faut les observer au bon moment, et de façon très rapide, et donc disposer par avance de temps d'observation dans différents observatoires. J'ai donc dirigé deux programmes internationaux d'observation multi-longueur d'onde sur les plus grands observatoires terrestres, qui nous permettent d'obtenir un **droit prioritaire d'observation** (cible d'opportunité interrompant les programmes en cours) au cas où une nouvelle source apparaisse, ou si une source déjà connue redevient active.

• Organisation de **programmes internationaux** d'observation en "cible d'opportunité"

– • 1999-2003 : Lors de mon post-doc au Royaume-Uni : collaboration d'une dizaine de chercheurs britanniques et américains, sur l'étude des microquasars. Observation de XTE J1859+226, XTE J1118+480.
– • Depuis le lancement d'*INTEGRAL* (2002) : Réseau MINE (Multi-wavelength *INTEGRAL* network) : collaboration d'une cinquantaine de chercheurs dans plus de 20 instituts dans le monde. Organisation de campagnes d'observations multi-longueurs d'onde de sources *INTEGRAL* et microquasars (GRS 1915+105, Cyg X-1) avec des instruments sol et espace.

• Plus de 50 propositions de temps acceptées sur les grands observatoires/satellites radio $\rightarrow \gamma$

– • **ESO VLT**, (ISAAC, NAOS-CONICA, VISIR) ; **NTT** (SOFI, EMMI, SUSI2) et **2.2m**, (IRAC2b), Chili : plus de 30 propositions de temps acceptées (20 en tant que PI), 30 heures par semestre de ToO (temps prioritaire) depuis 1997, plus de 35 nuits d'observation en mode visiteur sur une quinzaine de missions (optique/infrarouge)
– • **UKIRT** (IRCAM, UFTI), Mauna Kea, Hawaii, USA : 5 propositions de temps acceptées (3 en tant que PI) 12 heures de ToO depuis 1999, 5 nuits d'observation en mode visiteur (infrarouge)
– • **HST, WHT, NOT, INT, JKT**, Canary Islands, **Gemini-N/S**, Hawaii, Chile : observations ToO (UV/optique/infrarouge).
– • **IRAM**, Granada, Espagne : + de 5 semaines d'observations (radiotélescope mm de 30m)
– • **VLA**, Socorro, USA, **VLBA** (interférométrie radio)
– • **Chandra, FUSE, HESS, HETE-2, INTEGRAL, RXTE, Swift, XMM :** plus de 20 propositions acceptées (EUV, X, γ)

IV. Obtentions de financement

– • depuis 2002 : MINE (co-I) : Multiwavelength *INTEGRAL* NEtwork. Organisation de campagnes d'observation avec instruments internationaux sol/espace, simultanées au sa-

tellite *INTEGRAL*. Financement du CNES (Centre National d'Études Spatiales, 200 k€ pour 5 ans, financement d'un post-doc (actuellement J.A. Zurita Heras 2006-2008), équipement et missions.

– •1999 – 2002 : Financement GdR Hautes Energies : 20 k€ pour 4 ans : missions

V. Séminaires et communications orales

– **Conférence de presse :** 1er symposium scientifique *GLAST*, Stanford, USA, Fév. 2007 http ://www.nasa.gov/centers/goddard/news/topstory/2007/gas_cocoon.html

– • 22 congrès internationaux, dont 7 invités :
  – Observational Evidence for Black Holes in the Universe, Calcutta, India, Feb. 10-15, 2008, **invité**
  – A Population Explosion : The Nature and Evolution of X-ray Binaries in Diverse Environments, St. Petersburg Beach, Florida USA, 28 Octobre - 2 Novembre 2007, **invité**
  – Frascati Workshop (Vulcano, Italie) 28 mai-02 juin 2007, **invité**
  – Vulcano Workshop (Italy) 22nd - 27th May, 2006, **invité**
  – 1st *GLAST* scientific symposium (Stanford, USA), 02/2007 **invité**, conférence de presse
  – VIth Microquasar Workshop : Como, Italie, 09/2006
  – Vth Microquasar Workshop : Beijing, 06/2004
  – IVth Microquasar Workshop : Cargese, France, 05/2002
  – IIIrd Microquasar Workshop, Granada, Espagne, 11-13/09/2000
  – IInd microquasar workshop, Institut d'Astrophysique de Paris, Déc. 1998
  – Ist microquasar workshop, Goddard Space Flight Center, Baltimore Avril 1997
  – VIth *INTEGRAL* Workshop : The transparent Universe, Moscou, Russie, 07/2006
  – Vth *INTEGRAL* Workshop : The *INTEGRAL* Universe, Münich, D, 16-20/02/2004
  – IVth *INTEGRAL* Workshop, Alicante, Espagne, 4-8/09/2000,
  – IInd *INTEGRAL* workshop, Saint Malo, France, 16-20/09/1996
  – Cozumel Triggering relativistic jets Mexico, 03-04/2005
  – XXXVIth Rencontres de Moriond Astrophysics "Very High Energy Phenomena in the Universe", La Thuile, 03/2005, **invité**
  – XXXIInd Rencontres de Moriond Astrophysics "Very High Energy Phenomena in the Universe", Les Arcs, France, 01/1997
  – XXIInd Rencontres de Moriond Astrophysics, "The Gamma-Ray Universe", Les Arcs, France, 9-16/03/2002.
  – Unidentified High Energy Sources, Hong Kong, 06/2004
  – IAU Col. 194 "Compact Binaries in the Galaxy and Beyond", La Paz, Mexico, 17-22/11/2003,
  – RAS meeting on Microquasars, Londres (UK), 11/05/2001, **invité**
  – CV & LMXB Workshop, Manchester, Royaume-Uni, 17-18/08/2000

– • 13 congrès nationaux en France et au Royaume-Uni dont 6 invités :

- Atelier APC/LISA, 01/2005, **invité**
- Atelier MAX, une lentille gamma, IAP, 23/03/2004, **invité**
- Final Leverhulme/X-ray binary meeting, Southampton (UK), 09/2002, **invité**
- BAA Variable Star Section Meeting, Northampton (UK), 14/10/2000, **invité**
- 2nd Leverhulme/X-ray binary meeting, Leicester (UK), 01/2000, **invité**
- Réunion GdR Radiosources Extragalactiques et AGNs, IAP, 12/1997, **invité**
- Stades ultimes de l'évolution stellaire, École d'Aussois, 16-21/09/2001
- Congrès 2001 de la Société Française de Physique, Strasbourg, 9-13 juillet 2001
- SF2A, Semaine de l'Astrophysique Française, Lyon, 28 Mai - 1er Juin 2001
- UK X-ray astronomy, Leicester (UK), 28/06/2000
- Réunion du Groupe de Recherche Accrétion-Disques-Jets, Strasbourg, 11/1998,
- Réunion Binaires X, Strasbourg, 06/1995
- Journées SF2A, Paris, 05/1995

- • 15 séminaires internationaux :
  Allemagne (ESO-Garching), Argentine (IAFE, La Plata), Chili (ESO, Université de Santiago) (5), États-Unis (JAC-Hawaii), Mexique (Morelia) (2), Royaume-Uni (Keele, Open University, Oxford, Southampton) (4)

- • 15 séminaires nationaux (en France) :
  Grenoble (LAOG) (2), Paris (IAP, IAS, LPNHE, Obs. de Meudon, SAp) (7), Montpellier (GAM), Strasbourg (Observatoire) (2), Toulouse (CESR) (3)

VI. Activités d'encadrement & de formation

Post-docs :

- • 2006-2010 : Responsable du post-doc Juan Antonio Zurita Heras (SAp, 4 ans) : Étude des sources de haute énergie *INTEGRAL*
- • 2003-2004 : Co-responsable du post-doc Philippe Filliatre (SAp, 7 mois) : (La contrepartie optique et proche-infrarouge de la source *INTEGRAL* obscurcie IGR J16318-4848 : une étoile sgB[e] dans un système binaire de grande masse, Filliatre & Chaty, 2004, ApJ, 616, 469)
- • 2003-2005 : Co-responsable (50%) du post-doc William Clarkson avec Carole A. Haswell (Obtention d'un an de financement de l'Open University) : Organisation/analyse de campagnes d'observation multi-longueurs d'onde.

Thèses :

- • 2006-2008 : Directeur de thèse de Farid Rahoui, co-financement ESO-CEA, co-encadrement avec Félix Mirabel, Sujet : Étude multi-longueur d'onde de sources binaires de haute énergie *INTEGRAL* de la Galaxie
- • 2000-2004 : Co-directeur de thèse de Craig R. Powell (Open University). Co-encadrement à 50% avec Carole A. Haswell. Observations et interprétation de sources binaires X (Chaty, Powell et al.).

Stages M2, M1, divers :

– • 2007 : Directeur de stage de M2 d'Anand Raichoor (SAp, 4 mois) : étude du candidat trou noir de notre Galaxie XTE J1550-564.
– • 2004 : Directeur de stage de M2 de Nicolas Bessolaz (SAp, 4 mois) : étude du candidat trou noir de notre Galaxie XTE J1720-318 (Chaty & Bessolaz, 2006, A&A, 455, 639).
– • 2006 : Directeur de 2 stages de M1 (2 mois) au SAp de Guillaume Bacques et Vincent Le Gallo : étude du candidat trou noir de notre Galaxie H1743-322 (Chaty & Dubus in prep.).
– • 2005 : Directeur de stage ingénieur (Sébastien Delautier, 1 mois) et stage L1 (Claudia Conde Cespedes, 2 semaines) : Bibliographie sur microquasars et sources *INTEGRAL* (http ://www.aim.univ-paris7.fr/CHATY/)

VII. Arbitrages :

– • depuis 1999 : Rapporteur de 11 articles pour *Astronomy & Astrophysics*, *Astrophysical Journal*, *Monthly Notices of the Royal Astronomical Society* et *Publications of the Astronomical Society of Japan*.
– • 2007 : Rapporteur de projet ANR
– • depuis 1999 : Rapporteur d'une dizaine de propositions de temps de télescopes UKIRT
– • 2002 : Rapporteur européen de la thèse de Marc Ribó (Université de Barcelone)
– • 2003 : Rapporteur de candidature de contrat post-doctoral PPARC (Royaume-Uni)

VIII. Personnalités scientifiques pouvant être contactées :

– **Dr. Didier Barret** ; Centre d'Etude Spatiale des Rayonnements 9, avenue du Colonel Roche Boite postale 44346 31028 Toulouse Cedex 4 ; Tel : +33 (0) 5 61 55 83 71 ; Fax : +33 (0) 5 61 55 67 01 ; e-mail : didier.barret@cesr.fr
– **Prof. Philip A. Charles** ; Director, South African Astronomical Observatory, P.O. Box 9, Observatory, 7935, South Africa tel : (27)-21-460-9303/9321 fax : (27)-21-447-3639 e-mail : pac@saao.ac.za
– **Prof. Anthony J. Dean** ; School of Physics and Astronomy ; University of Southampton ; Highfield, Southampton, Hampshire SO17 1BJ ; U.K. Tel : +44 (0) 23 8059 2111 ; Fax : +44 (0)23 8059 3910 ; e-mail : ajd@astro.soton.ac.uk
– **Prof. Gilles Henri** ; Laboratoire d'Astrophysique Observatoire de Grenoble BP 53 F-38041 Grenoble Cedex 9 Tel : +33 (0) 476 51 42 11 ; Fax : +33 (0) 476 44 88 21 e-mail : Gilles.Henri@obs.ujf-grenoble.fr
– **Dr. I. F. Mirabel** ; European Southern Observatory. Casilla 19001. Santiago 19. Chile Tel : +56-2-463 3260 e-mail : fmirabel@eso.org

Enseignement et Activités pédagogiques

I. Enseignement universitaire

Université Paris 7 :

Créations et responsabilités de modules d'enseignement (depuis 2004) :

• Cours M2R Astrophysique IdF "Instrumentation de l'infrarouge aux hautes énergies" (15h)

• Méthodologie M2R Astrophysique IdF "Traitement d'images en astronomie X/γ" (25h)

• Cours L3 SPE–Sciences Physiques pour l'Enseignement "Astrophysique enseignement" (36h)

• Cours L2 LLSH–Lettres Langues Sciences Humaines "Astrophysique pour Littéraires, Evolution dans l'Univers" (36h)

• Formation continue (IUFM/rectorats Créteil/Paris) "Phénomènes physiques élémentaires en Astrophysique" (18h)

Autres enseignements effectués (depuis 2002) :

• TDs/TPs Physique, L1 Sciences de la Matière (80h)

• TDs Physique PCEM (Préparation Concours d'Entrée en Médecine) Lariboisière (192h)

Open University (Royaume-Uni) :

• 1999-2002 : Formation doctorale, processus de rayonnement et moyens instrumentaux en astrophysique multi-longueur d'onde (20h/an)

Université Toulouse 3 Paul Sabatier :

• 1998-1999 : A.T.E.R. (Attaché Temporaire d'Enseignement et de Recherche) (100h) : TPs électricité/électronique en DEUG A, TDs/TPs électromagnétisme licence/maîtrise de physique

Université Paris 6 :

• 1996-1998 : Tutorat Pédagogique de physique en DEUG (64h/an)

Service d'Astrophysique CEA Saclay :

• 2006 : Création des séminaires multi-échelles

II. Diffusion des connaissances en Physique

Olympiades Nationales de Physique :

• Membre du jury national de 1998 à 2005, Président du jury en 2003 et 2005, Membre du comité national depuis 2005

• Réalisation du film du concours 2005 "Olympiades Nationales de Physique" (de Sylvain Chaty et Jean-Paul Flourat, Production Studio-Vidéo de Paris 7)

• Rédaction du livre "Olympiades de Physique" décrivant des projets expérimentaux, édité en 1997 par le CNDP, en collaboration avec la SFP et l'UDP, préfacé par P. Léna.

• Création du prix "Olympiades de Physique" de Paris 7 (2005)

• Rapporteur pour le concours d'Objectif Science (depuis 2003)

• Edition du livre "Multimédias et Réseaux", 8^{emes} entretiens de la Villette, CNDP 1998

III. Diffusion des connaissances en Astrophysique

Animation scientifique :

• depuis 2007 : Représentant de l'Université Paris 7 pour l'organisation de l'Année Mondiale de l'Astronomie 2009

Film :

• 2005 : Le ciel, la cordillère et l'astrophysicien, réalisation Jean-Louis Berdot, film de Jean-Louis Berdot, Sylvain Chaty et Jean-Paul Flourat, coproduction CEA et Paris 7, 2005

Radio :

• 2006 : entretiens sur Radio Hôp', Escapades Célestes : "les Trous Noirs"

Podcast :

• 2007 : podcast sur Ciel et Espace : "Trous Noirs, étoiles à neutron et observations multi-longueurs d'onde"

Conférences :

• 2006-2007 : Conférences invitées au Palais de la Découverte, Club d'Astronomie Uranoscope, Université Inter-Âges du Val-de-Marne et Géospace Hérault : "Les secrets des astres X poussiéreux : une nouvelle population d'astres"

• 2005-2007 : Conférences lors de "Science en Fête" à Paris 7 : "Comment percer les secrets de l'Univers ?" et "Promenade dans le bestiaire des sources extrêmes"

• 2004-2007 : Conférences invitées et ateliers aux Festivals d'Astronomie de Fleurance (Gers) sur les microquasars, les mécanismes d'émission et l'observation multi-longueurs d'onde en astrophysique.

• 2002 : Conférence invitée à la Société d'Astronomie de Londres

• 1996-1998 : Conférences au Palais de la Découverte lors des Nuits des étoiles

• 1997 : Conférence au CEA lors de Science en Fête

• 1992 : Chargé d'exposés dans le département de Physique du Palais de la Découverte : optique, hydrostatique, physique nucléaire et électrostatique.

Rencontres :

• 2006 : Cosmogonies, rencontre "Art et Science" entre des étudiants, l'astrophysicien Sylvain Chaty et l'artiste Julien Discrit (Galerie de Noisy-le-Sec et Musée des Arts et Métiers).

• 2007-2008 : Projet "Art et Science" avec des collégiens du 93, Fondation 93

• 2006-2007 : Projet "Eurêka" (gravitation) avec des collégiens du 93, Fondation 93, rencontres à la Cité des Sciences et au Musée Arts et Métiers ; Conférence : "La gravitation dans l'Univers, des naines blanches aux trous noirs".

Planétarium :

• 1991-1998 : **Séances de planétarium** (plus de 400) au Palais de la Découverte et à la Cité des Sciences et de l'Industrie de la Villette

Formation :

• 1989-1993 : **Encadrement de stages** d'astronomie, soirées d'observation, à l'Observatoire Astronomique d'Aniane (Hérault). Stage de formation d'animateurs en Astronomie.

Astronomie amateur :

• 1994-1999 : Conférences et organisations d'observations : éclipses de Lune, de Soleil (dont 11/08/99)

• 1997-1998 : Création du club d'Astronomie du CEA-Saclay

• 1994 : Expédition en Islande, Observations d'Aurores polaires boréales, Lauréat d'une Bourse de l'Aventure de la Mairie de Paris

• 1991 : Expédition d'observation de l'éclipse totale de Soleil en Finlande (22/07/1991), "À la recherche des plus beaux cieux d'Europe", Lauréat d'une bourse Zellidja

Exposition :

• 1998-1999 : Membre du comité scientifique de l'exposition itinérante AN 2000 – Planète vivante, Cité de l'Espace, Toulouse et Cité des Sciences, Paris.

Articles de Vulgarisation (10) :

• Rédaction de 10 articles de vulgarisation dans Pour la Science, La Recherche, etc...

Liste des publications nationales et internationales

Publications de recherche (125) :

• **54 publications de rang A dans des revues internationales à comité de lecture :** 14 en 1^{er} auteur, 10 en 2^{e} auteur, 16 en 3^{e} auteur (moyenne de 4.5 co-auteurs)
• **45 publications de rang B, dans les mémoires de colloques internationaux :** dont 7 publications de revues invitées, 1 ayant fait l'objet d'un communiqué de presse en 2007 : http ://www.nasa.gov/centers/goddard/news/topstory/2007/gas_cocoon.html
• **22 circulaires IAU, GCN et Astronomer Telegram,**
• **1 HDR, 1 thèse, 1 rapport de DEA et 1 rapport technique,**
• $\sim$ 1000 citations de mes articles, h-index = 17

Publications de vulgarisation (11) :

• 1 livre et 10 articles de vulgarisation,
• + 1 édition de livre, et 3 articles de journalistes scientifiques écrits sur ma recherche

– **Chaty, S.**, 2007, Habilitation à Diriger des Recherches de l'Université Paris Diderot, *Des microquasars aux systèmes binaires enfouis : enquête dans l'Univers des astres extrêmes*
– **Chaty, S.**, 1998, Thèse de doctorat de l'Université Paris Sud (XI), *Étude multi-longueur d'onde du microquasar GRS 1915+105 et de sources binaires de haute énergie de la Galaxie*

Publications de rang A dans des revues internationales à comité de lecture (54) :

2008

– **Chaty S.**, Rahoui F., Foellmi C., Tomsick J., Rodriguez J., Walter R., 2008, A&A, in press, *Galactic hard X-ray sources discovered by INTEGRAL brought to light by multi-wavelength observations. I. The nature of the companion star*
– Rahoui F., **Chaty S.**, Lagage P.-O., Pantin E., 2008, A&A in press, *Galactic hard X-ray sources discovered by INTEGRAL brought to light by multi-wavelength observations. II. The environment of the companion star*
– Rodriguez J., Tomsick J., **Chaty S.**, 2008, A&A subm., *Swift follow-up observations of INTEGRAL sources of unknown nature*
– Testa, V., Rea, N., Mignani, R.P., Israel, G.L., Perna, R., **Chaty, S.**, Stella, L., Covino, S., Turolla, R., Zane, S., Lo Curto, G., Campana, S., Marconi, G., Mereghetti, S., 2008, A&A in press, *Adaptive Optics Near-infrared Observations of Magnetars : XTE J1810-197 , 1RXS J1708-4009 , 1E 1841-045 and SGR1900+14*
– Zurita Heras J.A., **Chaty S.**, 2008, A&A, subm., *INTEGRAL, XMM-Newton and ESO/NTT identification of AX J1749.1-2733 : an obscured and likely-distant Be/X-ray binary ?*

2007

- Cadolle Bel M., Ribo M., Rodriguez J., **Chaty S.**, Corbel S., Goldwurm A., 2007, ApJ, 659, 549, *Simultaneous multiwavelength observations of the Low/Hard state of the X-ray transient source SWIFT J1753.5-0127*
- **Chaty, S.**, Dubus, G., Kern, B., 2007, Revista Mexicana de Astronomia y Astrofisica, 27, 207, *Infrared and Optical Polarisation of Microquasars*
- Healey, S.E., Romani, R.W., Cotter, G., Michelson, P.F., Schlafly, E.F., Readhead, A.C.S., Giommi, P., **Chaty, S.**, Grenier, I.A., Weintraub, L.C., 2007, ApJ, in press (astrop-ph/0709.1735), *CGRaBS : An All-Sky Survey of Gamma-Ray Blazar Candidates*
- Paizis, A., Nowak, M.A., **Chaty, S.**, Rodriguez, J., Courvoisier, T. J.-L., Del Santo, M., Ebisawa, K., Farinelli, R., Ubertini, P., Wilms, J., 2007, ApJL, 657, L109, *Hunting the nature of IGR J17497-2821 with X-ray and NIR observations*
- Pellizza, L. J., **Chaty, S.**, Negueruela, I., 2007, Revista Mexicana de Astronomia y Astrofisica, 27, 225 *ESO Optical/ir Observations of Igr J17544-2619*

2006 .

- **Chaty, S.**, Bessolaz N., 2006, A&A, 455, 639, *Optical/near-infrared observations of the black hole candidate XTE J1720-318 : from high-soft to low-hard state*
- **Chaty, S.**, Mignani, R.P. ; Israel, G.L., 2006, MNRAS, 365, 1387, *A closer look at the X-ray transient XTE J1908+094 : identification of two new near-infrared candidate counterparts*
- Combi J.A., Ribó M., Martí J., **Chaty S.**, 2006, A&A, 458, 761, *Multiwavelength properties of the high energy bright Seyfert 1 Galaxy IGR J18027-1455*
- Dubus G., **Chaty, S.**, 2006, A&A, 458, 591, *Infrared polarimetry of the microquasars H1743-322, XTE J1550-564 and GRO J1655-40*
- Filliatre, P., **Chaty, S.**, 2006, Advances in Space Research, 38, 1365, *Optical and near-infrared observations of new INTEGRAL galactic sources*
- Malzac J, Petrucci P.O., Jourdain E., Cadolle M., Sizun P., Pooley G., Cabanac C., **Chaty S.**, Belloni T., Rodriguez J., Roques J.P., Durouchoux P., Goldwurm A., Laurent P., 2006, A&A, 448, 1125, *Bimodal spectral variability of Cygnus X-1 in an intermediate state*
- Pellizza L., **Chaty, S.**, Negueruela I., 2006, A&A, 455, 653, *IGR J17544-2619 : a new supergiant fast X-ray transient revealed by optical/infrared observations*
- Sutaria F.K., Kolb U., Barnard R., Charles P.A., **Chaty S.** et al., 2006, A&A subm. *XMM-Newton Observations of J2123-058 in quiescence*
- Tomsick J.A., **Chaty S.**, Rodriguez J., Foschini L., Walter R., Kaaret P., 2006, ApJ, 647, 1309, *Identifications of Four INTEGRAL Sources in the Galactic Plane via Chandra Localizations*

2005

- **Chaty, S.**, Filliatre, P., 2005, Astrophysics and Space Science, 297, 235, *Revealing the nature of the obscured High Mass X-ray binary IGR J16318-4848*
- **Chaty, S.**, Filliatre, P., 2005, Chinese Journal of Astronony and Astrophysics, Proceedings Beijing, 5, 104, *INTEGRAL reveals a new class of obscured high mass X-ray binaries : focus on IGR J16318-4848*
- Foschini L., Chiaberge M., Grandi P., Grenier I.A., Guainazzi M., Hermsen W., Palumbo G.G.C., Rodriguez J., **Chaty S.** et al., 2005, A&A, 433, 515 *Investigating the EGRET-radio galaxies link with INTEGRAL : the case of 3EG J1621+8203 and NGC 6251*

2004

- Di Cocco, G., Foschini, L., Grandi, P., Malaguti, G., Castro-Tirado, A.J., **Chaty, S.** et al., 2004,

A&A, 425, 89, *INTEGRAL observation of 3EG J1736-2908*

– Filliatre, P., **Chaty, S.**, 2004, ApJ, 616, 469, *The Optical/Near-Infrared Counterpart of the INTEGRAL Obscured Source IGR J16318-4848 : An sgB[e] in a High-Mass X-Ray Binary ?*
– Türler, M., Courvoisier, T.J.-L., **Chaty, S.**, Fuchs, Y., 2004, A&A, 415, L35, *Quasar jet emission model applied to the microquasar GRS 1915+105*

2003

– **Chaty, S.** ; Charles, P.A. ; Martí, J. et al., 2003, MNRAS, 343, 169, *Optical and near-infrared observations of the microquasar V4641 Sgr during the 1999 September outburst*
– **Chaty, S.**, Haswell, C.A., Malzac, J. et al., 2003, MNRAS, 346, 689, *Multiwavelength observations revealing the evolution of the outburst of the black hole XTE J1118+480*
– Fuchs, Y. ; Rodriguez, J. ; Mirabel, I.F. ; **Chaty, S.** et al., 2003, A&A, 409, L35, *Simultaneous multiwavelength observations of GRS 1915+105*
– Greenhough, J. ; Chapman, S.C. ; **Chaty, S.** et al., 2003, MNRAS, 340, 851, *Identification of a 12-17 d time-scale in X-ray observations of GRS 1915+105*
– Hynes, R.I., Haswell, C.A., ..., **Chaty, S.** et al., 2003, MNRAS, 345, 292, *The remarkable rapid X-ray, ultraviolet, optical and infrared variability in the black hole XTE J1118+480*

2002

– **Chaty, S.**, Mignani, R.P. ; Israel, G.L., 2002, MNRAS, 337, L23, Discovery of the near-infrared counterpart of the X-ray transient XTE J1908+094
– **Chaty, S.**, Mirabel, I.F., Goldoni, P. et al., 2002, MNRAS, 331, 1065, *Near-Infrared Observations of Galactic Black Hole Candidates*
– Greenhough, J., Chapman, S.C., **Chaty, S.** et al., 2002, A&A, 385, 693, *Characterising anomalous transport in accretion disks from X-ray observations*
– Hynes, R.I., Haswell, C.A., **Chaty, S.** et al., 2002, MNRAS, 331, 169, *The Evolving Accretion Disc in the Black Hole X-ray Transient XTE J1859+226*
– Mignani, R.P., **Chaty, S.**, Mirabel, I.F., Mereghetti, S., 2002, A&A, 389, L11 *The Infrared Counterpart of the X-ray burster KS 1731-260*
– Ogley, R.N., **Chaty, S.**, Crocker, M. et al. 2002, MNRAS, 330, 772, *Radio emission from Galactic supersoft X-ray sources*
– Ueda, Y., Yamaoka, K., Sánchez-Fernández, C., Dhawan V., **Chaty, S.** et al., 2002, ApJ, 571, 918, *Study of the Largest Multiwavelength Campaign of the Microquasar GRS 1915+105*

2001

– **Chaty, S.**, Mirabel, I. F., Martí, J., Rodríguez, L. F., 2001, Astrophysics and Space Science Supplement, 276, 153, *On the Nature of the Microquasar V4641 Sagittarii*
– **Chaty, S.**, Rodríguez, L.F., Mirabel, I.F., 2001, AIP Conf. Proc. 599 : X-ray Astronomy : Stellar Endpoints, AGN, and the Diffuse X-ray Background, 599, 574, *Search for interactions between ejections of GRS 1915+105 and its environment*
– **Chaty, S.**, Rodríguez, L.F., Mirabel, I.F. et al., 2001, A&A, 366, 1035, *A search for possible interactions between ejections from GRS 1915+105 and the surrounding interstellar medium*
– Hynes, R. I., Haswell, C. A., **Chaty, S.** et al., 2001, Astrophysics and Space Science Supplement, 276, 61, *Recent Hubble Space Telescope results on X-ray Novae*
– McClintock, J.E., Haswell, C.A., ..., **Chaty, S.** et al., 2001, ApJ, 555, 477, *Complete and Simultaneous Spectral Observations of the Black-Hole Candidate XTE J1118+480*
– Mereghetti, S., Mignani, R.P., Covino, S., **Chaty, S.** et al., 2001, MNRAS, 321, 143, *A Search for*

the Optical/Infrared Counterpart of the Anomalous X-ray Pulsar 1E 1841-045

– Ueda, Y., Yamaoka, K., Grove, J.E., ..., **Chaty, S.** et al., 2001, Astrophysics and Space Science Supplement, 276, 25, *The 2000 April multiwavelength campaign of GRS 1915+105*

2000

– Hynes, R. I., Mauche, C. W., ..., **Chaty, S.**, 2000, ApJ, 539, L37, *The X-Ray Transient XTE J1118+480 : Multiwavelength Observations of a Low-State Minioutburst*
– Martí, J., Mirabel, I.F., **Chaty, S.**, Rodríguez, L.F., 2000, A&A, 363, 184, *VLT search for the infrared counterpart of 1E 1740.7-2942*
– Martí, J., Mirabel, I.F., **Chaty, S.**, Rodríguez, L.F., 2000, A&A, 356, 943, *VLT Observations of GRS 1915+105*

1999

– Fuchs, Y., Mirabel, I.F., **Chaty, S.** et al., 1999, A&A, 350, 891, *ISO observations of the environment of the soft gamma-ray repeater SGR 1806-20*
– Vreeswijk, P.M., Galama, T.J., Owens, A.N., ..., **Chaty, S.** et al., 1999, ApJ, 523, 171, *The X-ray, Optical and Infrared Counterpart to GRB 980703*

1998

– Martí, J., Mereghetti, S., **Chaty, S.** et al., 1998, A&A, 338, L95, *Search for the optical and infrared counterpart of GRS 1758-258*
– Martí, J., Mirabel, I.F., **Chaty, S.**, Rodríguez, L.F., 1998, A&A, 330, 72, *The hard X-ray source GRS 1734-292 : a Seyfert 1 galaxy behind the Galactic center*
– Martí, J., Mirabel, I.F., **Chaty, S.**, Rodríguez, L.F., 1998, New Astronomy Review, 42, 621, *Radio counterparts to GRANAT sources*
– Martí, J., Mirabel, I.F., Rodríguez, L.F., **Chaty, S.**, 1998, A&A, 332, L45, *The radio counterparts of GX 354-0 and Terzan 1*
– Mirabel, I.F., Dhawan, V., **Chaty, S.** et al., 1998, A&A, 330, L9, *Accretion instabilities and jet formation in GRS 1915+105*

1996

– **Chaty, S.**, Mirabel, I.F., Duc, P.-A. et al., 1996, A&A, 310, 825, *Infrared and millimeter observations of the galactic superluminal source GRS 1915+105*
– Mirabel, I.F., Rodríguez, L.F., **Chaty, S.** et al., 1996, ApJ, 472, L111, *Infrared Observations of an Energetic Outburst in GRS 1915+105*

Publications de rang B dans les mémoires des congrès internationaux (45) :

– Boër, M., Atteia J.-L., Bringer M., **Chaty S.**, Klotz, A., Morand, F., Pedersen H., Pollas, C., Toublanc, D., 2000, Proceedings of the Fifth Huntsville Gamma-Ray Burst Symposium, 1999 October 18-22, 255, *Preliminary Results from the TAROT Experiment*
– Cadolle Bel M., Ribo M., Rodriguez J., **Chaty S.**, Corbel S., Goldwurm A., Proceedings of Microquasars and Beyond, 18-22 September 2006, Italie (2006) (astro-ph/0611217) *Broad-band spectral changes of the microquasars Cygnus X-1 and SWIFT J1753.5-0127*
– Chadwick, P.M., **Chaty, S.**, Daniel, M.K., Haswell, C.A., Kolb, U. et al., 2001, Proceedings of High Energy Gamma-Ray Astronomy, International Symposium held 26-30 June, 2000, in Heidelberg, Germany. American Institute of Physics (AIP) Proceedings, volume 558. Edited by Felix A.

Aharonian and Heinz J. Völk, 757 *VHE Gamma Rays from Binary Systems*

- **Chaty, S.**, 2008, St Petersburg conference, in press, *Multi-wavelength observations of the most obscured high-energy sources of our Galaxy, discovered by INTEGRAL*
- **Chaty, S.**, 2007, 1st GLAST scientific symposium, in press, *How to reveal the mysteries of the most obscured high-energy sources of our Galaxy, discovered by INTEGRAL ?*
- **Chaty S.**, Proceedings of the VIth Microquasar Workshop : "Microquasars and beyond" (Como, Italy), eds : T. Belloni et al. September 2006, *Multi-wavelength observations of the microquasar XTE J1720-318 : a transition from high-soft to low-hard state* (astro-ph/0611558)
- **Chaty S.**, Proceedings of Frontier Objects in Astrophysics and Particle Physics, Vulcano (Italie) 22nd - 27th May, 2006, *The role of microquasars in astroparticle physics* (astro-ph/0607668)
- **Chaty S.**, Proceedings of Rencontres de Moriond, Very High Energy Phenomena in the Universe, La Thuile, Italy (March 12-19, 2005) *Microquasars and Jets* (astro-ph/0506008)
- **Chaty, S.**, 2004, 35th COSPAR Scientific Assembly, 2239, *Optical and near-infrared observations of new INTEGRAL galactic sources*
- **Chaty, S.**, 1999, Proceedings Atelier Accrétion - Disques - Jets, 3-5 Novembre 1998, Strasbourg, éd. Hameury, J.-M., *Étude multi-longueur d'onde du microquasar GRS 1915+105*
- **Chaty, S.**, 1998, Proceedings Atelier Radiosources Extragalactiques et Noyaux Actifs de Galaxies : Implications en Cosmologie (session II), 16-17 décembre 1997, Institut d'Astrophysique de Paris et Observatoire de Paris, éd. Rocca-Volmerange B., Sol, H., 115, *Observations Multi-longueur d'onde de GRS 1915+105 : un microquasar dans la Galaxie*
- **Chaty, S.**, 1995, JAF, 49, 47, *Observations multi-longueur d'onde de la source superluminique GRS 1915+105, permettant de déterminer son absorption visuelle, sa distance et sa nature*
- **Chaty, S.**, Filliatre, P., 2004, Proceedings IAU Colloquium 194 : Compact Binaries in the Galaxy and Beyond, La Paz, Mexico, Revista Mexicana de Astronomia y Astrofisica Conference Series, 20, 65, *Revealing the nature of the highly obscured galactic source IGR J16318-4848*
- **Chaty, S.**, Filliatre, P., 2004, Proceedings 5th INTEGRAL Workshop, Münich, Allemagne, "The Transparent Universe", 365, *Revealing the nature of the highly obscured galactic source IGR J16318-4848*
- **Chaty, S.**, Haswell, C. A., Hynes, R. I. et al., 2001, Proceedings of IVth INTEGRAL Workshop, Alicante, Spain, "Exploring the Gamma-Ray Universe", September 4-8, 2000, ESA SP-459, 491, (astro-ph/0102103), *Multi-wavelength observations revealing the outbursts of two new soft X-ray transients : XTE J1859+226 and XTE J1118+480*
- **Chaty, S.**, Haswell, C.A., Hynes, R.I., Shrader, C.R., Cui, W., Abstracts from SF2A-2001 : Semaine de l'Astrophysique Francaise, meeting held in Lyon, France, May 28-June 1st, 2001, Eds. : F. Combes, D. Barret, F. Thévenin, to be published by EdP-Sciences, Conference Series, 349 *Multi-wavelength observations revealing the outbursts of the two soft X-ray transients XTE J1859+226 and XTE J1118+480*
- **Chaty, S.** ; Haswell, C. A. ; Malzac, J. et al., New Views on MICROQUASARS, the Fourth Microquasars Workshop, Institut d'Etudes Scientifiques de Cargèse, Corsica, France, May 27 - June 1, 2002. Edited by Ph. Durouchoux, Y. Fuchs, and J. Rodriguez. Published by the Center for Space Physics : Kolkata (India), 23, *Multiwavelength Observations Revealing the Evolution of the Outburst of the Black Hole XTE J1118+480*
- **Chaty, S.**, Mirabel, I.F., 1997, Proceedings of the 4th Compton Symposium on Gamma-ray Astronomy and Astrophysics, 1997 April 27-30, Williamsburg, Virginia, AIP Conference Proceedings 410, 917, *Infrared Observations and Energetic Outburst of GRS 1915+105*

- **Chaty, S.**, Mirabel, I.F., 1997, Proceedings of the XXXIInd Rencontres de Moriond, Les Arcs, France, 1997 January 18-25, "Very High Energy Phenomena in the Universe", ed. Trân Thanh Vân, J., Éditions Frontières, Paris, 3 (astro-ph/9703127), *Infrared jet of the galactic superluminal source GRS 1915+105*
- **Chaty, S.**, Mirabel, I.F., Duc, P.-A., Wink, J.E., Rodríguez, L.F., 1996, Proceedings "Röntgenstrahlung from the Universe", International Conference on X-ray Astronomy and Astrophysics, September 25-29, 1995, Würzburg, Germany, eds. Zimmermann, H.U., Trümper, J., Yorke, H., MPE Report 263, 129, *Infrared and millimeter observations of the galactic superluminal source GRS 1915+105*
- **Chaty, S.**, Mirabel, I.F., Martí, J. et al., 2001, Proc. of IVth INTEGRAL Workshop, Alicante, Spain, "Exploring the Gamma-Ray Universe", 4-8/09/2000, ESA SP-459, 479 (astro-ph/0102105), *On the nature of the microquasar V 4641 Sagittarii*
- **Chaty, S.**, Mirabel, I.F., Rodríguez, L.F., 1999, Proceedings of the American Astronomical Society, HEAD meeting 31, 1601, *Multi-wavelength study of the microquasar GRS 1915+105 and of high-energy binary sources in the Galaxy*
- **Chaty, S.**, Mirabel, I.F., Rodríguez, L.F. et al., 1997, Proceedings 2nd INTEGRAL Workshop, St. Malo, France, "The Transparent Universe", March 1997, ESA SP-382, 241 (astro-ph/9612192), *Infrared observations and energetic outburst of GRS 1915+105*
- **Chaty, S.**, Rahoui, F., 2007, Proceedings of the VIth INTEGRAL Workshop, "The Obscured Universe", Space Research Institute, Moscow, Russia, July 2-8, 2006, ESA's Publications Division : Special Publication SP-622, (astro-ph/0609474), *Optical to Mid-Infrared observations revealing the most obscured high-energy sources of the Galaxy*
- Di Cocco, G., Castro-Tirado, A.J., **Chaty, S.** et al., 2004, Proceedings 5th INTEGRAL Workshop, Münich, Allemagne, "The Transparent Universe", 683 (astro-ph/0403676), *Study of Unidentified EGRET sources with INTEGRAL : first results and future prospects*
- Dubus, G., **Chaty, S.**, and Kern, B., SF2A-2005 : Semaine de l'Astrophysique Francaise, 2005, editor Casoli, F., Contini, T., Hameury, J.M. and Pagani, L, 451, *Infrared and optical polarisation of microquasars*
- Fuchs, Y., Mirabel, I.F., **Chaty, S.** et al., 1998, 19th Texas Symposium on Relativistic Astrophysics and Cosmology, Paris, France, Dec. 14-18, 1998. eds. : Paul, J., Montmerle, T., Aubourg, E., 236, *ISOCAM preliminary results on the environment of the Soft Gamma-ray Repeater SGR 1806-20*
- Fuchs, Y., Rodriguez, J., **Chaty, S.** et al.,2003, SF2A-2003 : Semaine de l'Astrophysique Francaise, 409, *The MINE collaboration : multi-wavelength observations of microquasars with INTEGRAL, prospects with HESS and ANTARES*
- Fuchs, Y. ; Rodriguez, J. ; **Chaty, S.** et al. SF2A-2003 : Semaine de l'Astrophysique Française, meeting held in Bordeaux, France, June 16-20, 2003. Eds. : F. Combes, D. Barret and T. Contini. EdP-Sciences, Conference Series, p. 409, *The MINE collaboration : multi-wavelength observations of microquasars with INTEGRAL, prospects with HESS and ANTARES*
- Fuchs, Y., Rodriguez, J., Mirabel, I. F., Shaw, S. E., Kretschmar, P., Ribó, M., **Chaty, S.** et al., 2004, Revista Mexicana de Astronomia y Astrofisica Conference Series, 2004, 20, 28, *Simultaneous multi-wavelength observations of microquasars (the MINE collaboration)*
- Fuchs, Y., Rodriguez, J., Shaw, S.E., Kretschmar, P., Ribo, M., **Chaty, S.** et al., 2004, Proceedings 5th INTEGRAL Workshop, Münich, Allemagne, "The Transparent Universe", 321 (astro-ph/0404030), *Multi-wavelength INTEGRAL NEtwork (MINE) observations of the microquasar GRS 1915+105*

- Greenhough, J. ; Chapman, S. C. ; **Chaty, S.** et al., In : Statistical challenges in astronomy. Third Statistical Challenges in Modern Astronomy (SCMA III) Conference, University Park, PA, USA, July 18 - 21 2001. Eric D. Feigelson, G. Jogesh Babu (eds.). New York : Springer, ISBN 0-387-95546-1, 2003, 423 *Characterising anomalous transport in accretion disks from X-ray observations*
- Hynes, R.I., Haswell, C.A., **Chaty, S.**, Cui, W., Shrader, C.R., 2000, Proceedings of the American Astronomical Society, HEAD meeting 32, 3107, *Multiwavelength Rapid Variability in XTE J1118+480*
- Hynes, R. I. ; Haswell, C. A. ; **Chaty, S.** et al., New Views on MICROQUASARS, the Fourth Microquasars Workshop, Institut d'Etudes Scientifiques de Cargèse, Corsica, France, May 27 - June 1, 2002. Edited by Ph. Durouchoux, Y. Fuchs, and J. Rodriguez. Published by the Center for Space Physics : Kolkata (India), 27 *X-ray/UV correlations in XTE J1118+480 : disc, jet, or something else ?*
- Malzac J., Petrucci, P.O., Jourdain, E., Sizun, P., Cadolle M., Pooley, G., Cabanac, C., **Chaty, S.**, Belloni, T., Rodriguez, J., Roques J.P., Durouchoux P., Goldwurm A., Laurent P., 2004, Proceedings 5th INTEGRAL Workshop, Münich, Allemagne, "The Transparent Universe", in press, *INTEGRAL observation of Cyg X-1 in June 2003*
- Malzac J., Petrucci, P.O., Jourdain, E., Sizun, P., Cadolle M., Pooley, G., Cabanac, C., **Chaty, S.**, Belloni, T., Rodriguez, J., Roques J.P., Durouchoux P., Goldwurm A., Laurent P., Proceedings of the "The X-ray Universe 2005", 26-30 September 2005, El Escorial, Madrid, Spain. Ed. by A. Wilson. ESA SP-604, Volume 1, Noordwijk : ESA Publications Division, ISBN 92-9092-915-4, 2006, p. 223 *Spectral Variability of Cygnus X-1 during an Intermediate State*
- Martí, J., Mirabel, I.F., **Chaty, S.** et al., Rodríguez, L.F., 2001, Proceedings of "The nature of Unidentified Galactic high-energy gamma-ray sources" (Tonantzintla, INAOE, Mexico, 9-11 oct 2000), Astrophysics and Space Science Library (ASSL), Kluwer Academic Publishers, eds. Carramiñana, Reimer & Thompson, 255, *VLT Observations of Galactic Microquasars*
- Martí, J., Mirabel, I.F., **Chaty, S.**, Rodríguez, L.F., March 1997, Proceedings 2nd INTEGRAL Workshop, St Malo, France, "The Transparent Universe", ESA SP-382, 323, *VLA observations of SIGMA hard X-ray sources in the galactic bulge*
- Mirabel, I.F., Fuchs, Y., **Chaty, S.**, 2000, Proceedings of the Fifth Huntsville Gamma-Ray Burst Symposium, 1999 October 18-22, 814 (astro-ph/9912446), *Soft Gamma-ray Repeaters in Clusters of Massive Stars*
- Negueruela I., Smith D.M., Reig P., **Chaty S.**, Torrejon J.M., Proceedings of the "The X-ray Universe 2005", 26-30 September 2005, El Escorial, Madrid, Spain. Ed. by A. Wilson. ESA SP-604, Volume 1, Noordwijk : ESA Publications Division, ISBN 92-9092-915-4, 2006, p. 165, *Supergiant Fast X-ray Transients : A new class of high mass X-ray binaries unveiled by INTEGRAL*
- Ogley, R. N. ; **Chaty, S.** ; Crocker, M. ; Eyres, S. P. S. ; Kenworthy, M. A., Richards, A. M. S. ; Rodriguez, L. F. ; Stirling, A. M., 2001, Proceedings of the American Astronomical Society Meeting 199, #133.13, *A Search for Radio Emission from Galactic Supersoft X-ray Sources*
- Pellizza L.J., **Chaty S.**, 2006, Revista Mexicana de Astronomia y Astrofisica Conference Series, Proceedings of XI Latin American Regional IAU Meeting, 204, *ESO Optical/NIR Observations of IGR J162834838*
- Türler, M. ; Courvoisier, T. J.-L. ; **Chaty, S.**, High Energy Blazar Astronomy, Astronomical Society of the Pacific Conference Series, Vol. 299, held 17-21 June 2002 at Tuorla Observatory, Piikkio, Finland. Edited by Leo O. Takalo and Esko Valtaoja, 2003., 299, 239, *Comparing the Properties of Synchrotron Outbursts in Quasars and Microquasars*

- Türler, M., Courvoisier, T., **Chaty, S.**, Fuchs, Y., Lindfors, E.J., 2004, 35th COSPAR Scientific Assembly, 2797, *Modelling the Variable Synchrotron Emission of Galactic and Extragalactic Jets*
- Ueda, Y. ; Yamaoka, K. ; Sánchez-Fernández, C. ; Dhawan, V. ; **Chaty, S.** et al., New Views on MICROQUASARS, the Fourth Microquasars Workshop, Institut d'Etudes Scientifiques de Cargèse, Corsica, France, May 27 - June 1, 2002. Edited by Ph. Durouchoux, Y. Fuchs, and J. Rodriguez. Published by the Center for Space Physics : Kolkata (India), 295, *Study of the largest multiwavelength campaign of the microquasar GRS 1915+105*

Circulaires IAU, GCN et Astronomer Telegram (ATEL) (22) :

- **Chaty, S.**, 1999, ATel, 48, 1, *Multiwavelength observations of XTE J1859+226*
- **Chaty, S.** ; Haswell, C. A. ; Smith, G. P. ; Smail, I. ; Hynes, R. I., 2000, IAUC, 7394, 3, *XTE J1118+480*
- **Chaty, S.**, Haswell, C. A., Norton, A. J., Hynes, R. I. et al., 1999, IAUC, 7284, 1, *XTE J1859+226*
- **Chaty, S.** ; Matsuoka, Y. ; Nagata, T., Ueda, Y., 2006, ATEL, 897, 1, *Infrared observations of IGR J17497-2821 : 3 candidate counterparts*
- **Chaty, S.** ; Hatano, H ; Matsuoka, Y. ; Nagata, T., 2006, ATEL, 906, 1, *Infrared observations of IGR J17497-2821 : new position, new candidate counterparts*
- **Chaty, S.** ; Hatano, H ; Matsuoka, Y. ; Nagata, T., 2006, ATEL, 936, 1, *Follow-up near-infrared observations of IGR J17497-2821*
- **Chaty, S.** ; Mignani, R. P. ; Vanzi, L., 2002, IAUC, 7897, 2, *XTE J1908+094*
- Haswell, C. A. ; **Chaty, S.** ; Cui, W. ; Casares, J. V. ; Hynes, R. I., 2000, ATel, 55, 1, *Multiwavelength observations of XTE J1859+226*
- Haswell, C. A., **Chaty, S.**, Norton, A. J., Chen, W., Hynes, R. I., 1999, ATel, 51, 1, *Multiwavelength observations of XTE J1859+226 on 1999, November 6th*
- Haswell, C. A., **Chaty, S.**, Norton, A. J., Chen, W., Hynes, R. I., 1999, ATel, 49, 1, *Multiwavelength observations of XTE J1859+226*
- Heise, J., **Chaty, S.**, 1999, IAUC, 7099, 1, *GRB 990123*.
- Hynes, R. I., Haswell, C. A., Norton, A. J., **Chaty, S.** et al., 1999, ATel, 50, 1, *Optical and near-IR observations of XTE J1859+226*
- Hynes, R. I., Haswell, C. A., Norton, A. J., **Chaty, S.** et al., 1999, IAUC, 7294, 2, *XTE J1859+226*
- Martí, J., Mirabel, I.F., **Chaty, S.** et al., 1997, IAU Circ. 6601, *SAX J1750.8-2900*
- Maury, A., Boër, M., **Chaty, S.**, 1999, IAU Circ. 7099, 2 *GRB 990123*
- Maury, A., Boër, M., **Chaty, S.**, 1999, GCN Circ. 220, *GRB 990123 Optical Observations*
- Negueruela, I. and Smith, D. M. and **Chaty, S.**, 2005, The Astronomer's Telegram, 429, 1, *Optical counterpart to IGR J16465-4507*
- Negueruela, I. and Smith, D. M. and **Chaty, S.**, 2005, The Astronomer's Telegram, 470, 1, *HD 306414 and IGR J11215-5952*
- Norton, A. J., Haswell, C. A., **Chaty, S.** et al., 1999, IAUC, 7279, 2, *XTE J1859+226*
- Tomsick, J.A., **Chaty S.**, Rodriguez J., Walter R., Kaaret P., 2006, ATEL 959, 1, *IGR J06074+2205 is a Be X-ray Binary*
- Tomsick, J. A., **Chaty, S.**, Rodriguez, J., Walter, R., 2007, ATEL 1018, 1, *Chandra Position and Possible IR Identification for IGR J09026-4812*
- Zurita Heras, J. A., **Chaty, S.**, Rodriguez, J., 2007, ATEL 1035, 1, *Discovery of a likely-period of 185 days in AX J1749.1-2733*

Autres publications de recherche (4) :

- **Chaty, S.**, 2007, Habilitation à Diriger des Recherches de l'Université Paris Diderot, *Des microquasars aux systèmes binaires enfouis : enquête dans l'Univers des astres extrêmes*
- **Chaty, S.**, 1998, Ph.D. Thesis, Doctorate of the University Paris Sud (XI), *Étude multi-longueur d'onde du microquasar GRS 1915+105 et de sources binaires de haute énergie de la Galaxie (Multiwavelength study of the microquasar GRS 1915+105 and of high energy binary sources of the Galaxy)*
- **Chaty, S.**, 1994, Rapport de stage de D.E.A. de doctorat de l'Université Paris Sud (XI), *Microquasars et objets compacts observés en infrarouge*
- **Chaty, S.**, 1999, Technical Report CESR, *Procédure de traitement rapide des alertes TAROT*

Livre (1) :

- **Chaty, S.**, 1997, edited by CNDP (Centre National de Documentation Pédagogique), collection Documents, Actes et Rapports pour l'Education, in collaboration with the SFP (Société Française de Physique) and UDP (Union des Physiciens), under the direction of D. Le Quéau, preface de P. Léna, *Olympiades de Physique*

Articles de vulgarisation dans des revues nationales (3) :

- **Chaty, S.**, Martí, J., Mirabel, I.F., 1998, Pour la Science, 243, 34, *Disparition dans un trou noir*
- **Chaty, S.**, 1998, La Recherche, 313, 18, *Découverte d'un chaînon manquant chez les pulsars*
- Martí, J., **Chaty, S.**, Mirabel, I.F., 1999, Investigacion y ciencia, 272, 37, *Agujero negro : Fases de su vida*

Articles de vulgarisation dans des revues locales (7) :

- **Chaty, S.**, 1998, Le journal du centre CEA/Saclay, 5, 12, *Actualités du ciel*
- **Chaty, S.**, 1998, Le journal du centre CEA/Saclay, 4, 12, *Actualités du ciel*
- **Chaty, S.**, 1998, Le journal du centre CEA/Saclay, 3, 12, *Actualités du ciel*
- **Chaty, S.**, Martí, J., Mirabel, I.F., 1998, Le journal du centre CEA/Saclay, 3, 12, *Un trou noir se dévoile*
- Mirabel, I.F., **Chaty, S.**, Martin, J., 1998, Scintillations, *La première preuve directe de l'existence d'un trou noir*
- **Chaty, S.**, 1997, Le journal du centre CEA/Saclay, 2, 12, *Actualités du ciel*
- **Chaty, S.**, 1997, Le journal du centre CEA/Saclay, 1, 12, *Actualités du ciel*

Édition de livre (1) :

- Multimédias et réseaux : Actes des 9èmes Entretiens de la Villette, 1998, édité par le CNDP (Centre National de Documentation Pédagogique) en collaboration avec la Cité des Sciences et de l'Industrie, collection Documents, Actes et Rapports pour l'Education

Articles publiés à partir de ma recherche (3) :

- Un nouveau couple d'étoiles dans notre Galaxie, J. Bourdet, 21/11/2005, Le Figaro, 14
- Les excentricités d'un trou noir, P. Henarejos, 2000, Ciel et Espace, 362, 25
- L'univers des plasmas, du big bang aux technologies du III^{e} millénaire, Bradu, P., 1999, ed. Flammarion, 79

Deuxième partie

Travaux de Recherche

Table des matières

I Curriculum Vitae **i**

II Travaux de Recherche **1**

1 Préliminaires **11**
1.1 Découverte d'astres X dans notre Galaxie 13
1.2 Caractéristiques, formation et évolution des systèmes binaires 13
1.2.1 Les systèmes binaires X de faible masse 14
1.2.2 Les systèmes binaires X de grande masse 20
1.3 Originalité de mes travaux de recherche 23

2 Microquasars **27**
2.1 Prélude à l'ère des microquasars : SS 433 29
2.2 L'entrée dans l'ère des microquasars 29
2.2.1 Interlude : définition et étude des microquasars 29
2.2.2 Analogie avec les quasars 30
2.3 L'âge d'or des microquasars : accrétion et éjection 31
2.4 L'âge d'or des microquasars : processus d'émission 32
2.4.1 Des microquasars dans tous leurs états 32
2.4.2 Jet ou pas jet ? *That is the question !* 34
2.5 La face cachée des microquasars : interaction avec leur environnement 36
2.6 Mais où sont les microblazars ? 38
2.7 Les microquasars et leur rôle dans la physique des astroparticules 39
2.7.1 Les microquasars en tant qu'émetteurs de photons THE 39
2.7.2 Les microquasars en tant qu'émetteurs de neutrinos 40
2.7.3 Les microquasars en tant qu'émetteurs de rayons cosmiques 41
2.8 Conclusions 41
2.9 Quelques articles publiés parmi les plus significatifs 43
2.9.1 Une recherche d'éventuelles interactions entre les éjections de GRS 1915+105 et le milieu interstellaire environnant 45
2.9.2 Observations en infrarouge proche de candidats trous noirs Galactiques . 59
2.9.3 Observations en optique et infrarouge proche du microquasar V4641 Sgr au cours du sursaut de septembre 1999 69

2.9.4 Observations multi-longueurs d'onde révélant l'évolution du sursaut du trou noir XTE J1118+480 77
2.9.5 Observations en optique et infrarouge proche du candidat trou noir XTE J1720-318 : de l'état haut-mou à l'état bas-dur 95

3 Astres binaires de grande masse 103
3.1 Introduction 107
3.2 Localisation des sources *INTEGRAL* dans le plan Galactique 110
3.3 Observations multi-longueurs d'onde de sources *INTEGRAL* 111
3.3.1 IGR J16318-4848 : représentant extrême des astres de haute énergie obscurcis 112
3.3.2 IGR J17544-2619 : archétype des supergéantes transitoires rapides de rayons X 116
3.3.3 Étude d'un échantillon de sources *INTEGRAL* en optique et infrarouge proche 121
3.3.4 Étude d'un échantillon de sources *INTEGRAL* en infrarouge moyen . . . 122
3.4 Discussion et conclusions 125
3.5 Quelques articles publiés parmi les plus significatifs 133
3.5.1 La contrepartie optique/infrarouge proche de la source *INTEGRAL* obscurcie IGR J16318-4848 : une sgB[e] dans une binaire de rayons X de grande masse ? 135
3.5.2 Identifications de quatre sources *INTEGRAL* dans le plan Galactique à partir de localisations *Chandra* 153
3.5.3 IGR J17544-2619 : Une nouvelle transitoire rapide de rayons X à supergéante révélée par des observations en optique/infrarouge 169
3.5.4 Sources Galactiques de rayons X durs découvertes par *INTEGRAL* révélées par des observations multi-longueurs d'onde : I. Nature de l'étoile compagnon 177
3.5.5 Sources Galactiques de rayons X durs découvertes par *INTEGRAL* révélées par des observations multi-longueurs d'onde : II. Environnement de l'étoile compagnon 205

4 Conclusions et perspectives scientifiques 223
4.1 Étude de population de sources Galactiques 225
4.1.1 Poursuite de l'étude des microquasars 225
4.1.2 Détermination de la nature des sources *INTEGRAL* 225
4.1.3 Contraintes sur les modèles de synthèse de population 226
4.1.4 L'apport de GLAST 227
4.2 Formation et évolution des systèmes binaires serrés 228
4.2.1 Formation des systèmes binaires : lien avec leur environnement 229
4.2.2 Evolution des systèmes binaires : importance du donneur 230
4.3 À la recherche des progéniteurs de trous noirs et d'étoiles à neutron 235
4.3.1 Formation, évolution et fin de vie des étoiles massives 236

4.3.2 Étude des phénomènes physiques à chaque étape de l'évolution 238
4.4 Le mot de la fin 239
4.4.1 Le rêve d'un observateur 239

Table des figures

1 Observations du lien accrétion–éjection au sein du microquasar GRS 1915+105. . vii

1.1 Distribution des systèmes binaires 15
1.2 Systèmes binaires de grande masse et de faible masse 16
1.3 Diagramme Hertzsprung-Russell. 17
1.4 Evolution des LMXBs. 19
1.5 Diagramme de Corbet 21
1.6 Catalogue *INTEGRAL* 22
1.7 Evolution des HMXBs. 24

2.1 Schéma illustrant les analogies entre quasars et microquasars. 31
2.2 Observation du lien entre l'accrétion et l'éjection. 32
2.3 Observation du lien entre l'accrétion et l'éjection (détail en X) 33
2.4 Distribution spectrale d'énergie du microquasar XTE J1720-318 35
2.5 Distribution spectrale d'énergie du microquasar XTE J1118+480 36
2.6 Schéma illustrant le débat concernant les émetteurs à haute énergie 40

3.1 Répartition sur la voûte céleste des astres IBIS/ISGRI (17–100 keV). 108
3.2 Image du bulbe de la Galaxie 109
3.3 Diagramme HI de notre Galaxie 109
3.4 Images *Chandra* 0.3–10 keV de 6 sources *INTEGRAL*. 111
3.5 Distribution spectrale d'énergie de IGR J16207–5129. 112
3.6 Spectres en infrarouge proche de IGR J16318-4848 115
3.7 Distribution spectrale d'énergie optique–infrarouge moyen de IGR J16318-4848 . 117
3.8 Spectre optique de IGR J17544-2619 119
3.9 Distribution spectrale d'énergie optique–infrarouge moyen de IGR J17544-2619 . 120
3.10 Distribution spectrale d'énergie de IGR J16195-4945 et IGR J16358-4726 129
3.11 Diagramme de Corbet 130
3.12 Diagramme de la période orbitale en fonction de la séparation 131
3.13 Schémas illustrant les 2 types de sources *INTEGRAL* 132

4.1 Distribution spatiale des sources *INTEGRAL* 231
4.2 Distribution Galactique des systèmes binaires de grande masse 232

Liste des tableaux

3.1 Résumé des caractéristiques des sources *INTEGRAL* étudiées. 123
3.2 Résumé des résultats en infrarouge moyen sur les astres *INTEGRAL* étudiés. . . . 125

Chapitre 1

Préliminaires

Ou comment naissent, vivent et meurent deux étoiles en orbite serrée l'une autour de l'autre...

Sommaire

1.1 Découverte d'astres X dans notre Galaxie 13
1.2 Caractéristiques, formation et évolution des systèmes binaires 13
1.2.1 Les systèmes binaires X de faible masse 14
1.2.2 Les systèmes binaires X de grande masse 20
1.3 Originalité de mes travaux de recherche 23

Mots clés : Variable cataclysmique, naine blanche, étoile à neutron, trou noir, système binaire X de faible masse, système binaire X de grande masse

Abstract :

In this introduction chapter I describe the general characteristics, the formation and evolution of different types of high energy binary systems, and also the general context inside which resides my research. I finish by the important current questions, and by describing the originality of my research activities.

Résumé :

Dans ce chapitre d'introduction je décris les caractéristiques générales, la formation et l'évolution des différentes familles de systèmes binaires de haute énergie, ainsi que le contexte général dans lequel s'inscrit ma recherche. Je finis par les grandes questions actuelles, et par la description de l'originalité de mes travaux de recherche.

1.1 Découverte d'astres X dans notre Galaxie

Notre Galaxie contient environ 100 sources X brillantes aux flux supérieurs à 10^{-10} erg s^{-1}cm^{-2}, dans la bande d'énergie 1-10 keV (observables uniquement au-dessus de l'atmosphère terrestre). La distribution de ces sources montre une concentration claire vers le centre Galactique et aussi vers le plan Galactique, indiquant que la majorité de ces sources appartient bien à notre Galaxie (cf Figure 1.1). De plus, une douzaine de sources brillantes sont observées dans des amas globulaires Galactiques et dans les nuages de Magellan. Peu après la découverte de la première source X, Sco X-1, par Giacconi et al. (1962), Zeldovich & Guseynov (1966), Novikov & Zel'Dovich (1966) et Shklovsky (1967) ont suggéré que les sources X brillantes de notre Galaxie étaient des étoiles à neutron ou des trous noirs dans des systèmes binaires, ces systèmes émettant dans le domaine des hautes énergies (principalement en rayons X) à cause de l'objet compact accrétant de la matière de l'étoile compagnon. Le processus d'accrétion de matière sur un trou noir supermassif avait déjà été suggéré quelques années plus tôt comme une source d'énergie pour les quasars et les noyaux actifs de galaxie par Salpeter (1964), Zel'Dovich (1964) et Zel'Dovich & Novikov (1964).

La première évidence d'un système binaire accrétant provint de Webster & Murdin (1972) et Bolton (1972). Ils découvrirent que Cyg X-1 était un système binaire avec une période orbitale de 5.6 jours. Ils mesurèrent l'amplitude de la courbe de vitesse radiale (72 km/s) de la contrepartie optique supergéante O9.7, et conclurent indépendamment que l'émission X était le résultat de l'accrétion sur un objet compact, probablement un trou noir, vu que la masse déduite de l'objet compact était $> 3\,M_{\odot}$ en supposant une masse réaliste ($> 15\,M_{\odot}$) pour la supergéante O9.7. Plusieurs centaines d'astres émettant dans les hautes énergies sont aujourd'hui connus. Nous nous focalisons ici sur les systèmes binaires de haute énergie, et laissons donc de côté les sursauts de rayons γ et noyaux actifs de galaxies.

1.2 Caractéristiques, formation et évolution des systèmes binaires

Un système binaire de rayons X contient un objet compact –soit une étoile à neutron soit un trou noir de masse stellaire–, accrétant de la matière d'une étoile compagnon. La matière accrétée transporte du moment angulaire et sur son chemin vers l'objet compact peut former un disque d'accrétion, en fonction de la géométrie du système et des masses respectives des deux composantes. Ce disque d'accrétion est alors responsable de l'émission X. Les variables cataclysmiques (CV), des systèmes binaires contenant des naines blanches, n'appartiennent pas aux systèmes binaires de rayons X, car la densité de colonne entourant une naine blanche lors de l'accrétion de matière est trop importante (de l'ordre de 16 g/cm^{-2}) pour permettre aux rayons X de s'échapper. Seuls les étoiles à neutron et trous noirs accrétants présentent des densités de colonne d'accrétion suffisamment basse (0.5 et 0.3 g/cm^{-2} respectivement) pour permettre l'émission de rayons X sans qu'ils soient stoppés. Il existe actuellement 280 systèmes binaires de rayons X connus (cf Liu et al. 2001 ; Liu et al. 2000 ; Liu et al. 2006). Plus de 90% des sources

de rayons X brillantes de notre Galaxie appartiennent à deux classes distinctes, selon la masse de l'étoile compagnon : les systèmes binaires X de grande masse (HMXBs) et les systèmes binaires X de faible masse (LMXBs). Ces deux groupes, illustrés dans la figure 1.2, diffèrent par un certain nombre de caractéristiques physiques. Leurs distributions respectives dans la Galaxie sont montrées dans la figure 1.1.

1.2.1 Les systèmes binaires X de faible masse

Caractéristiques générales

L'étoile compagnon des systèmes binaires X de faible masse est une étoile de faible masse (en général moins d'une masse solaire, étoile appartenant aux populations I et II, voir le diagramme Hertzsprung-Russell dans la figure 1.3), qui transfère de la matière par remplissage de son lobe de Roche. Parmi les étoiles compagnon de faible masse, se trouvent des naines blanches, des étoiles de séquence principale de type plus tardif que B : des étoiles de type A, et des sous-géantes de type F-G. La dernière catégorie d'étoiles compagnons est probablement le rémanent d'étoiles qui originellement étaient de masse intermédiaire (M $\sim 1.5 \rightarrow 4\ M_{\odot}$) et qui ont perdu de la masse par transfert de masse à l'intérieur du système binaire, ainsi que cela a été suggéré récemment pour Cygnus X-2 (cf. Podsiadlowski & Rappaport 2000, Tauris et al. 2000). Les contreparties optiques des binaires X de faible masse sont intrinsèquement des objets faibles, la plupart présentant des spectres avec peu de raies d'émission caractéristiques, superposées à un continuum plutôt plat. Ce continuum optique est dominé par l'émission d'un disque d'accrétion situé autour de l'objet compact, qui est de façon prédominante le résultat du reprocessing d'une fraction des rayons X en photons optiques dans le disque. La contribution de l'étoile secondaire est généralement négligeable. Il arrive cependant que la présence de la secondaire soit détectée dans le spectre (ou les couleurs) de la binaire X de faible masse. Ceci est le cas en particulier des systèmes contenant des donneurs qui sont ou étaient des étoiles de masse intermédiaire, comme Her X-1 et Cyg X-2. Pour une description plus complète des binaires X de faible masse, le lecteur est encouragé à se reporter au livre de Lewin et al. (1995).

La classification en tant que système binaire X de faible masse est principalement basée sur les spectres obtenus lors de l'identification optique, et/ou de la fonction de masse à partir de mesures temporelles des arrivées de pulsations X, ou encore de la mesure de vitesse radiale à partir des raies du spectre optique. Si aucune de ces mesures n'est disponible, une classification peut-être effectuée en se basant sur la similitude des propriétés X avec d'autres systèmes identifiés. Un système non identifié est classifié comme système binaire X de faible masse contenant une étoile à neutron si une ou plusieurs des propriétés suivantes sont observées : des sursauts X de type I (qui jusqu'ici ont uniquement été vus chez les étoiles à neutrons dans les systèmes binaires X de faible masse), un spectre 1-10 keV mou avec une température caractéristique de 5-10 keV et/ou une période orbitale inférieure à 12 heures.

En 1983 le nombre de binaires X de faible masse était de 33 (van Paradijs 1983, Bradt & McClintock 1983). En 1995 ce nombre a atteint 119 (van Paradijs, 1995). En 2000 il est de 150 (Liu et al., 2001). Ce nombre a donc été multiplié par 4.5 en 17 ans.

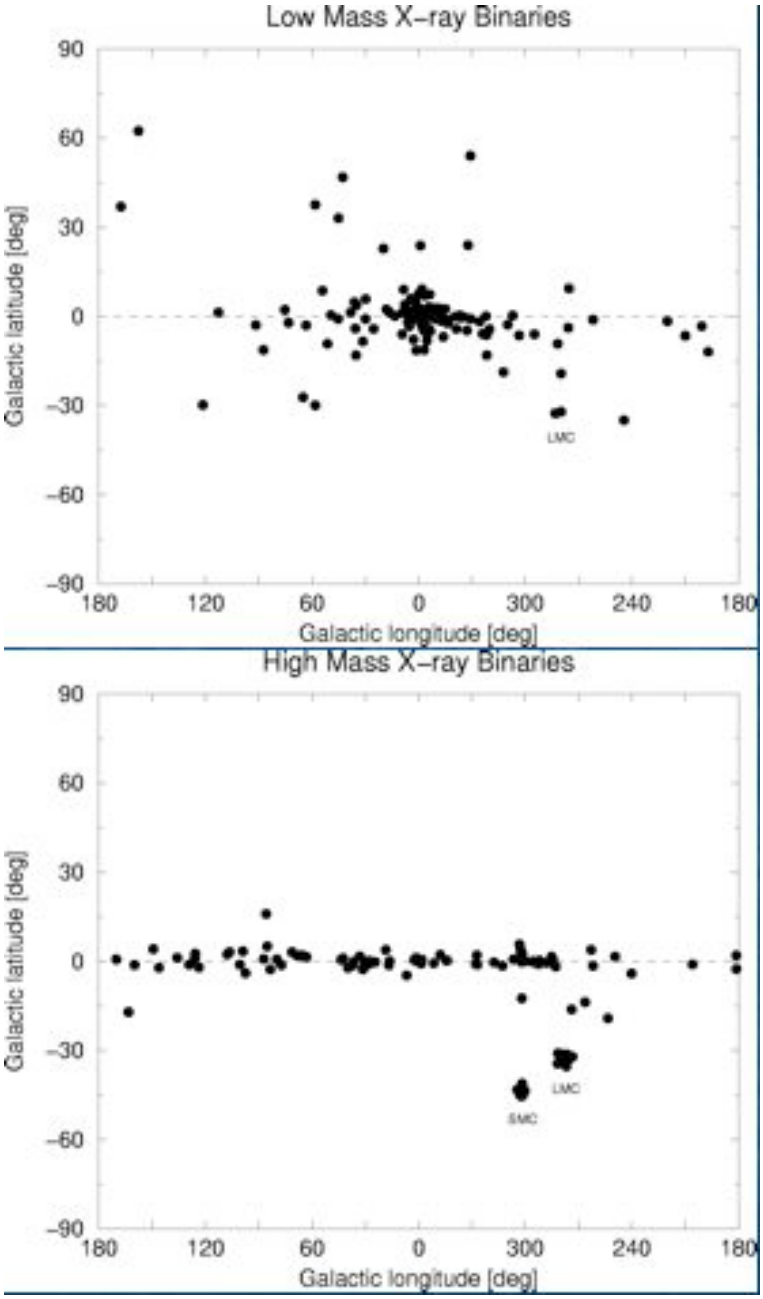

FIG. 1.1 – Diagramme représentant les distributions de systèmes binaires X de faible masse (en haut, Liu et al. 2001) et de grande masse (en bas, Liu et al. 2006).

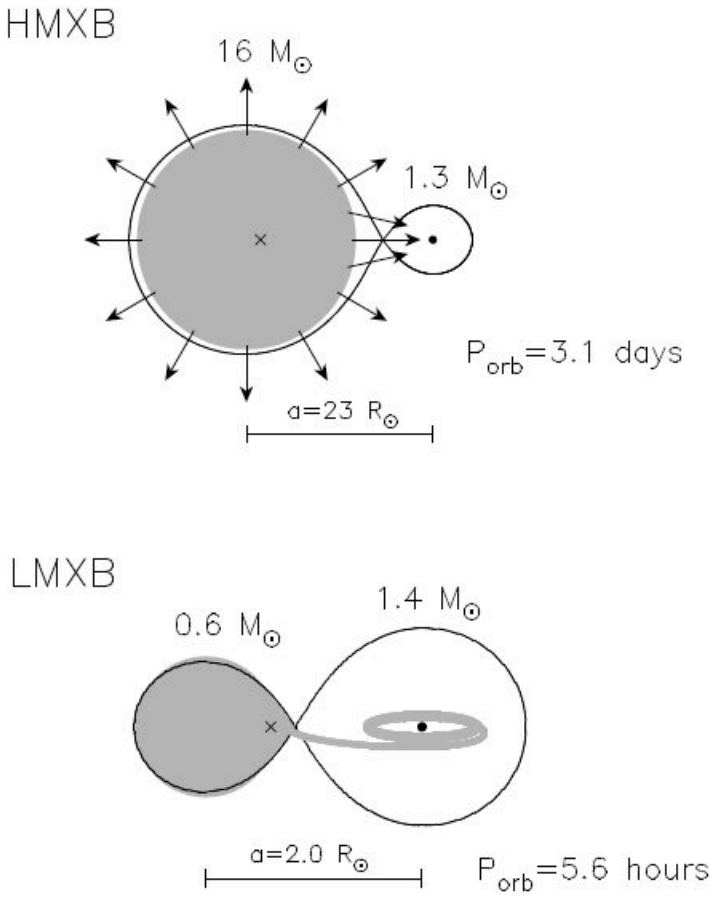

FIG. 1.2 – Systèmes binaires de grande masse et de faible masse : schémas typiques de HMXB (en haut) et LMXB (en bas). L'étoile à neutron dans une HMXB accrète un fort vent stellaire de grande vitesse et/ou l'atmosphère de l'étoile commençant à dépasser le lobe de Roche. L'étoile à neutron dans une LMXB est entourée d'un disque d'accrétion qui est alimenté par dépassement du lobe de Roche. Il existe aussi des évidences observationnelles que certaines HMXBs et LMXBs contiennent des trous noirs. Figure tirée de Tauris & van den Heuvel (2006).

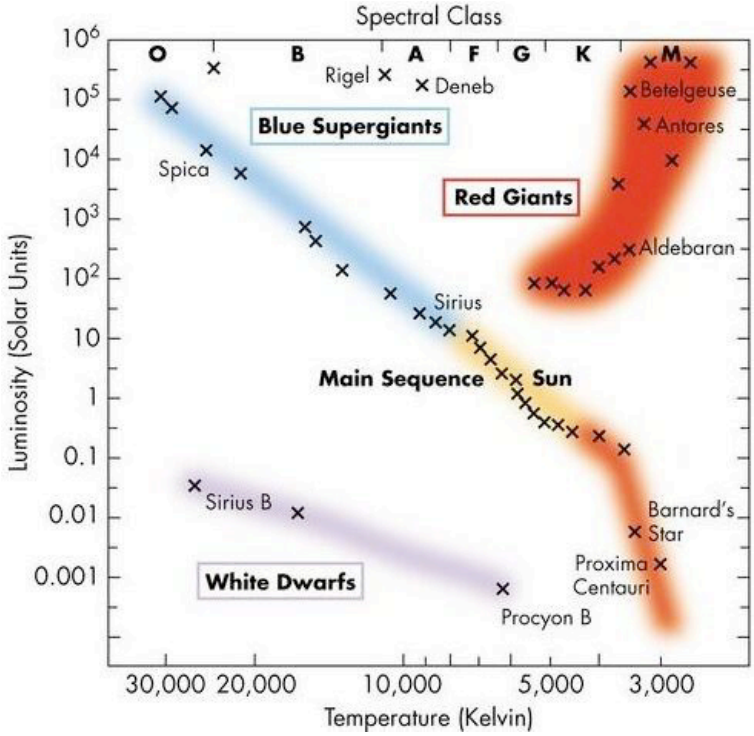

FIG. 1.3 – Diagramme Hertzsprung-Russell. Ce diagramme montre l'évolution des étoiles en fonction de leur type spectral (ou de leur température de surface) et de leur luminosité.

Formation et évolution

La formation et l'évolution des LMXBs est illustrée dans la figure 1.4, jusqu'à la formation de systèmes de pulsars millisecondes. Tout commence par un couple d'étoiles relativement massives de la séquence principale, orbitant l'une autour de l'autre en quelques milliers de jours. Au bout d'une dizaine de millions d'années, lorsque l'étoile la plus massive (à gauche sur le schéma) évolue jusqu'à devenir une supergéante, elle dépasse son lobe de Roche, et transfère de la matière à son compagnon (à droite). L'étoile massive évolue encore et englobe son compagnon, le système passant alors par la phase d'enveloppe commune. A cause de la perte de moment angulaire, le compagnon orbite en spiralant vers l'étoile massive, ce qui a pour effet de réduire la période orbitale de quelques milliers de jours à moins d'une journée. Cette étoile massive perd alors son enveloppe, et devient un coeur d'hélium, avant d'exploser en supernova. L'étoile compagnon gravite alors autour d'une étoile à neutron, sur une orbite de quelques jours. Le compagnon évolue à son tour, dépasse son lobe de Roche, et transfère de la matière à l'étoile à neutron : un système binaire de rayons X de faible masse est né ! Puis le compagnon implose en naine blanche, et orbite autour d'un pulsar milli-seconde.

Nous connaissons aujourd'hui plus de 40 pulsars binaires millisecondes dans le disque Galactique. Ils peuvent être grossièrement divisés en 3 classes (Tauris, 1996) : la classe A contient les systèmes à grande orbite ($P_{orb} > 20$ jours) avec comme compagnon une naine blanche de faible masse ($M_{NB} < 0.45\, M_{\odot}$) composée d'hélium, alors que les systèmes à petite orbite ($P_{orb} < 15$ jours) sont constitués de systèmes avec soit des compagnons naines blanches de faible masse composées d'hélium (classe B), soit des systèmes avec des naines blanches relativement lourdes, composées de CO/O-Ne-Mg (classe C). La dernière classe a évolué à travers une phase caractérisée par une perte significative de moment angulaire (soit une évolution par enveloppe commune soit un transfert de masse extrême sur une échelle de temps subthermique), et descend des systèmes binaires de rayons X de masse intermédiaire avec des donneurs de masse comprise entre $2 < M_2/\, M_{\odot} < 8$. Les pulsars millisecondes isolés proviennent de systèmes serrés de la classe B où le compagnon a été détruit ou évaporé -soit par irradiation de rayons X lorsque l'étoile à neutron accrétait, soit sous la forme d'un vent/rayonnement de particules relativistes provenant du pulsar (cf van den Heuvel & van Paradijs 1988 ; Ruderman et al. 1989 ; Podsiadlowski 1991 ; Ergma & Fedorova 1991). Une évidence observationnelle de ce scénario est trouvée dans des pulsars millisecondes à éclipse avec des compagnons ultra-légers –par exemple PSR 1957+20 ($P_{orb} = 0.38$ jour ; $M_2 \sim 0.02\, M_{\odot}$) et le pulsar planétaire PSR 1257+12 (Wolszczan, 1994). Pour les systèmes binaires de rayons X de faible masse, Pylyser & Savonije (1988) et Pylyser & Savonije (1989) ont montré qu'une bifurcation de période orbitale sépare la formation de systèmes convergents (qui évoluent avec une période orbitale décroissante jusqu'à ce que l'étoile compagnon devienne dégénérée et qu'une binaire ultracompacte se forme), des systèmes divergents (qui évoluent avec une période orbitale croissante jusqu'à ce que l'étoile compagnon perde son enveloppe et qu'une binaire largement détachée se forme). Cette bifurcation de période, aux conséquences importantes, est de 2-3 jours, et dépend principalement de la force du couple de freinage magnétique.

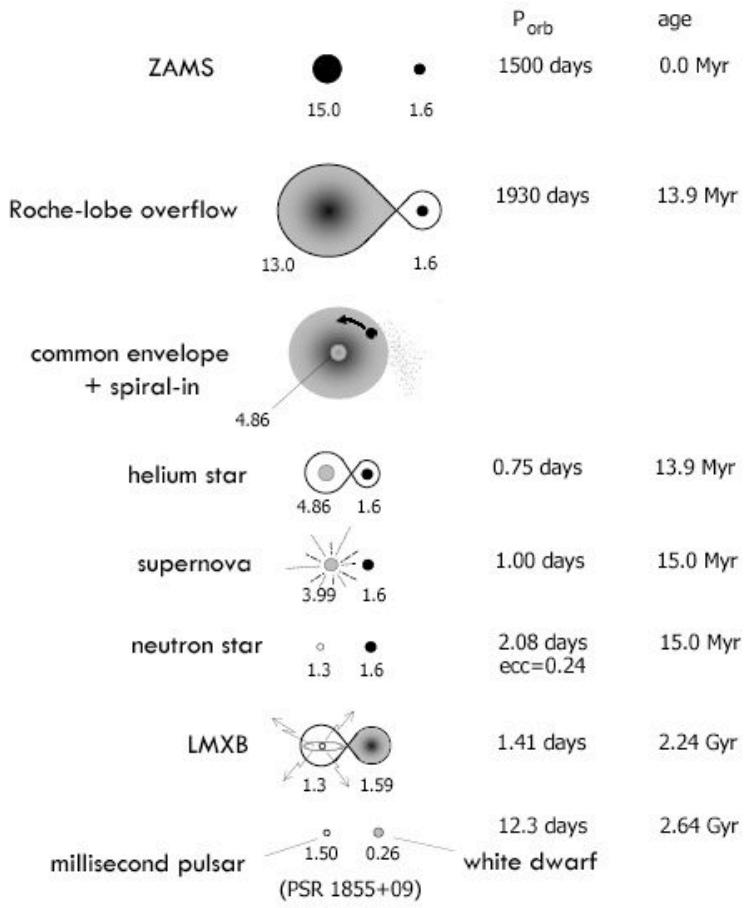

FIG. 1.4 – Evolution des LMXBs. Schéma tiré de Tauris & van den Heuvel (2006) décrivant l'évolution d'un système binaire conduisant à une LMXB et finalement à la formation d'un pulsar binaire milliseconde. Les paramètres gouvernant le moment angulaire orbital spécifique de la matière éjectée, l'enveloppe commune et la phase de mouvement spiral interne, l'explosion de supernova asymétrique et l'évolution stellaire de l'étoile constituée d'un coeur d'hélium nu ont tous un grand impact sur l'évolution exacte. Les paramètres sont donnés pour un scénario conduisant à la formation du pulsar binaire milliseconde PSR 1855+09 tel qu'il est observé actuellement. Les masses stellaires sont données en unités solaires.

1.2.2 Les systèmes binaires X de grande masse

Caractéristiques générales

Les systèmes binaires X de grande masse se séparent en deux groupes distincts. Le premier groupe, qui contient la majorité des systèmes binaires X de grande masse (~ 60 %), est constitué de systèmes binaires de rayons X avec étoiles Be, connus ou suspectés ("BeXRBs"). Dans les systèmes avec Be, le donneur est une étoile Be, et l'objet compact est une étoile à neutron, typiquement sur une grande orbite, modérément excentrique, et passe peu de temps à proximité du disque circumstellaire dense entourant le compagnon Be, appelé disque de décrétion (car il provient de l'étoile elle-même, cf Coe 2000 et Negueruela 2004). Les sursauts de rayons X se produisent lorsque l'objet compact passe à travers le disque de décrétion de l'étoile Be, accrétant le vent de faible vitesse et de grande densité présent autour des étoiles Be, et sont caractérisés par des spectres de rayons X durs. Pour cette raison ces objets sont appelés transitoires de rayons X avec Be.

Le deuxième groupe de systèmes binaires X de grande masse, qui représente environ un tiers de la population totale ($\sim$ 32 %), est composé de binaires de rayons X avec supergéantes de type spectral O ou B (cf diagramme Hertzsprung-Russell dans la figure 1.3), où l'objet compact orbite profondément à l'intérieur du vent hautement supersonique présent autour d'une étoile supergéante de type précoce, de type spectral O ou B, et qui joue le rôle de l'étoile donneur (Kaper et al., 2004). Il faut ici encore distinguer deux cas distincts : en effet, la luminosité de rayons X est produite soit par accrétion du vent stellaire intense provenant du compagnon optique, soit par remplissage du lobe de Roche. Dans le premier cas, c'est-à-dire dans un système d'accrétion par vent stellaire, la luminosité de rayons X est persistante et atteint 10^{35-36} erg/s, alors que dans le deuxième cas, c'est-à-dire dans un système à remplissage du lobe de Roche, la matière s'écoule par le point de Lagrange interne, pour former un disque d'accrétion. Une luminosité de rayons X bien supérieure est alors produite : $\sim 10^{38}$ erg s^{-1}.

Les différentes classes de systèmes binaires de grande masse sont indiquées dans un diagramme nommé diagramme de Corbet, montré dans la figure 1.5, et qui est adapté des diagrammes de Corbet (1986). Il montre les trois types de binaires de rayons X de grande masse. Les systèmes à supergéantes d'accrétion par disque avec remplissage du lobe de Roche, localisés dans la partie inférieure du diagramme, ont des périodes orbitales et de spin courtes, et sont des sources persistantes brillantes avec des couples d'accrétion relativement réguliers. Les systèmes avec supergéantes d'accrétion par vent (dans la partie supérieure du diagramme) ont des périodes de spin et orbitales plus longues, et sont des sources persistantes moins lumineuses avec des couples d'accrétion hautement variables. Finalement, les binaires transitoires Be, dans la partie droite du diagramme, présentent une corrélation marquée entre les périodes de spin et orbitale, et tendent à avoir les périodes orbitales les plus longues (cf Reig 2007 sur l'interaction entre l'étoile Be et l'étoile à neutron).

En 1983 le nombre de binaires X de grande masse était de 30 (van Paradijs 1983 ; Bradt & McClintock 1983). En 1995 ce nombre a atteint 69 (van Paradijs, 1995). En 2001 il est de 130 (Liu et al., 2000). En 2005 il y a 114 HMXBs dans la Galaxie et 128 dans les nuages de Magellan (Liu et al., 2006). Le nombre de systèmes binaires X de grande masse, multiplié par 8 en 22 ans,

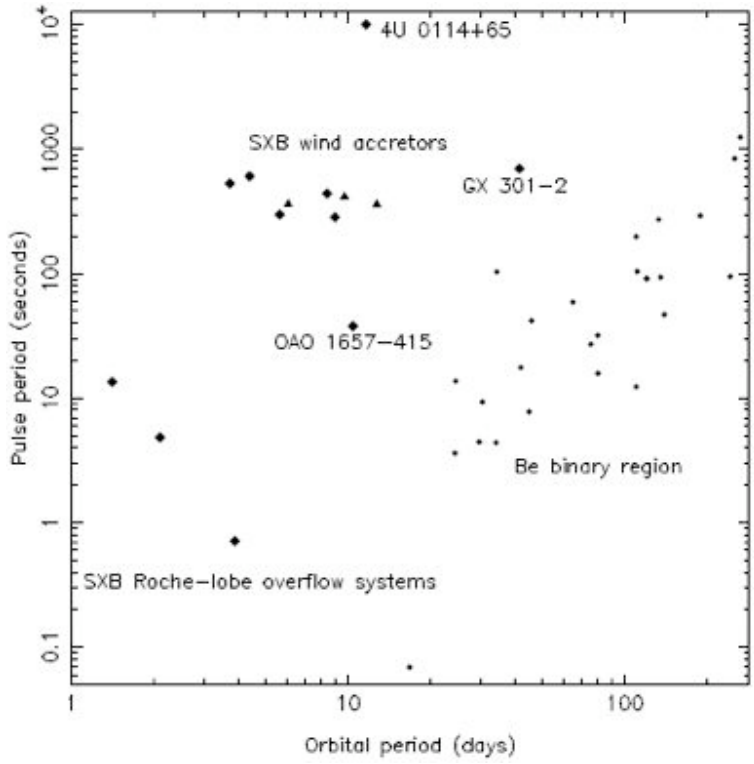

FIG. 1.5 – Diagramme de Corbet. Période de spin des étoiles à neutron accrétantes en fonction de la période du système binaire. Les différents symboles indiquent les différents types de systèmes binaires. Diagramme adapté de Corbet (1986).

a donc augmenté presque deux fois plus vite que celui des systèmes binaires X de faible masse. La situation au bout de cinq ans d'observation avec le satellite *INTEGRAL* est la suivante : ce satellite a observé 79 LMXBs et 65 HMXBs (Bird et al. 2006 ; cf Figure 1.6).

Parmi les 114 HMXBs, il y a 39(13) binaires X avec Be confirmées(suspectées) (quatre de ces systèmes semblent être douteux : il s'agit probablement de naines blanches avec un compagnon Be), 18(11) binaires X avec supergéantes, et 6 autres sources avec des propriétés particulières (il s'agit de CI Cam, IGR J16318-4848, Cyg X-3, LS 5039, V4641 Sgr et SS 433). Le reste concerne des candidats HMXBs. Finalement, il est intéressant de noter que la plupart des sources de rayons X ultra-lumineuses présentes dans les galaxies spirales et à flambée d'étoiles semblent être des binaires X de grande masse avec trou noir (Liu & Mirabel, 2005).

Formation et évolution

L'évolution des HMXBS est illustrée dans la figure 1.7, jusqu'à la formation de systèmes binaires constitués de deux étoiles à neutron ou trous noirs. La formation des HMXBs nécessite deux étoiles massives ($> 12\ M_{\odot}$) orbitant l'une autour de l'autre en une centaine de jours. Alternativement l'étoile secondaire (à droite sur le schéma) appartenant au début de sa vie à la séquence principale (ZAMS : Zero Age Main Sequence) peut être moins massive initialement,

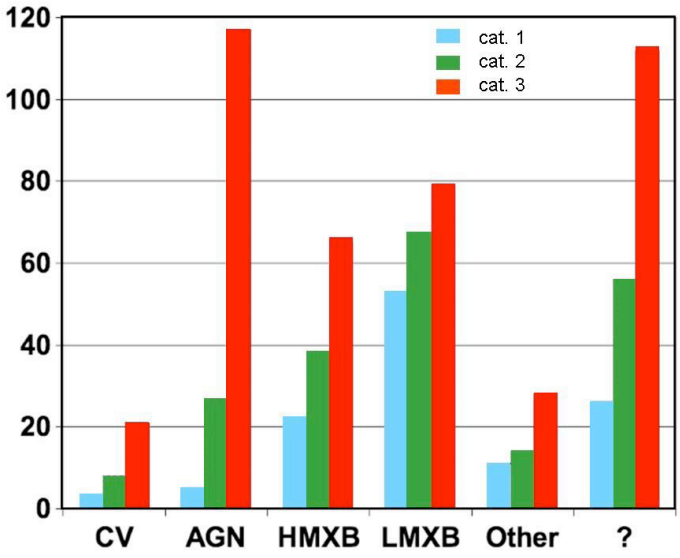

FIG. 1.6 – Catalogue *INTEGRAL*. Ce catalogue compte plus de 400 sources. Cet histogramme, résultat des trois catalogues *INTEGRAL* publiés jusqu'à présent, indique la classification des objets. L'excès proportionnellement supérieur des sources extragalactiques (AGN) dans le 3ème catalogue (en rouge) reflète une exposition plus importante sur des régions du ciel à haute latitude galactique. Une fraction importante des sources est jusqu'à présent de nature inconnue et est l'objet de nombreuses études (Bird et al., 2006).

tant qu'elle accrète assez de matériel de l'étoile primaire (à gauche sur le schéma), lorsque celle-ci ayant évolué dépasse son lobe de Roche, afin de finir plus tard au-dessus du seuil de masse et donner lieu à une explosion de supernova (comme l'étoile primaire). La première phase de transfert de masse, de l'étoile primaire à la secondaire, est habituellement supposée être dynamiquement stable (semi-conservative) si le rapport de masse au démarrage du dépassement du lobe de Roche n'est pas trop extrême. Au cours de ce premier transfert de masse, l'étoile primaire perd une grande partie de sa masse, jusqu'à devenir une étoile au coeur d'hélium nu, puis finit en étoile à neutron, après une explosion de supernova. L'étoile secondaire, qui est devenue très massive au cours du premier transfert de masse, fournit alors du matériau qui est accrété par l'étoile à neutron nouvellement formée : un système binaire de grande masse est né ! Il a alors une période orbitale de plusieurs milliers de jours. Plus tard au cours de leur évolution, toutes les HMXBs finissent dans une phase d'enveloppe commune, lorsque l'étoile à neutron (ou le trou noir de faible masse) est englobée par l'enveloppe étendue de son compagnon, sur une orbite qui décroît rapidement à cause de la perte importante de moment angulaire orbital. L'instabilité de la présence du compagnon dans l'enveloppe commune fait perdre son enveloppe à l'étoile secondaire, qui devient une étoile à coeur d'hélium nu. Un troisième transfert de masse se produit alors, où le coeur d'hélium transfère du matériau à l'étoile à neutron, par dépassement du lobe de Roche. Puis le coeur d'hélium évoluant explose alors en supernova, devient elle-même pulsar, et on obtient finalement un système binaire de jeunes pulsars. Ces systèmes doubles et serrés d'étoiles à neutron entreront en coalescence à cause du rayonnement d'ondes gravitationnelles, des collisions qui devraient être détectées par les détecteurs d'ondes gravitationnelles avancés tels que LIGO II/VIRGO.

Cependant il existe beaucoup d'incertitudes dans ce modèle, car les vents stellaires d'étoiles massives, comme les noyaux d'hélium nus (étoiles Wolf-Rayet), sont quelques-uns des aspects les plus incertains des modèles d'évolution des HMXBs. Les conditions physiques qui déterminent la formation d'une étoile à neutron par rapport à un trou noir sont aussi quelque peu inconnues. Il se pourrait que la masse du coeur ne soit pas le seul facteur important déterminant la nature de l'astre compact créé. Le champ magnétique et la rotation du coeur effondré pourraient aussi jouer un rôle important (Ergma & van den Heuvel, 1998). De plus, les observations semblent montrer qu'il y a un recouvrement dans l'échelle de masse conduisant finalement à une étoile à neutron ou à un trou noir.

1.3 Originalité de mes travaux de recherche

Notre Galaxie regorge donc de systèmes binaires de haute énergie différents de par leur nature, et leurs propriétés : l'astre compact peut être soit une étoile à neutron soit un trou noir, et l'étoile compagnon peut être une étoile de faible masse ou de grande masse. Ajoutons à cela des caractéristiques différentes liées à la taille de l'orbite et au rapport des masses des deux objets, et nous obtenons des systèmes aux propriétés complètement différentes. L'observation étant à l'astrophysique ce que l'expérimentation est à la physique, seule une étude exhaustive de ces systèmes aux caractéristiques différentes mais liés par une même physique permet de comprendre leur formation, leur fonctionnement et leur évolution.

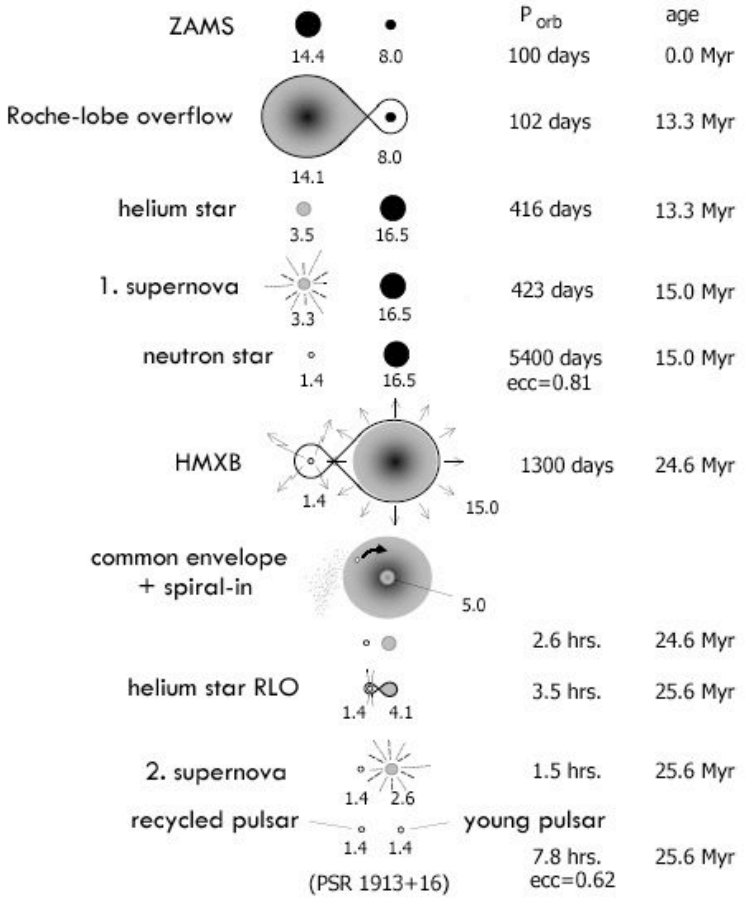

FIG. 1.7 – Evolution des HMXBs. Schéma tiré de Tauris & van den Heuvel (2006) décrivant la formation d'une HMXB avec étoile Be et finalement un système double d'étoiles à neutron. Un tel système binaire sera le siège de deux explosions de supernova. C'est toujours le pulsar recyclé qui est observé dans un système pulsar double comme le résultat de sa très longue échelle de temps de ralentissement comparé au jeune pulsar (un facteur $\sim 10^2$). Des systèmes binaires serrés d'étoiles à neutron entreront en coalescence après une phase de mouvement spiral interne due au rayonnement d'ondes gravitationnelles, des collisions qui devraient être détectées par les détecteurs d'ondes gravitationnelles avancés tels que LIGO II/VIRGO.

Les systèmes binaires constituent des objets intéressants à étudier, non seulement parce qu'il s'y produit des phénomènes relativistes extrêmes, mais aussi de par le fait que l'échange de matière et de moment angulaire entre les deux composantes modifie, certainement accélère, leur évolution : à la fois l'objet compact et l'étoile compagnon évoluent différemment du fait de la présence de l'autre objet. L'étude de cette évolution à long terme, en particulier de l'étoile compagnon, permet de mieux comprendre les modèles de population d'étoiles dans les systèmes binaires.

Mes travaux de recherche portent à la fois sur les systèmes binaires de faible et de grande masse, contenant étoiles à neutron et trous noirs, et dans une moindre mesure sur les astres extragalactiques (noyaux actifs de galaxie et sursauts de rayons γ). Le chapitre 2 de ce manuscrit décrit mes travaux sur les *microquasars*, ces sources présentant des jets relativistes, qui sont principalement des systèmes binaires de rayons X de faible masse. Ces astres sont des laboratoires idéaux d'étude des phénomènes relativistes de physique de haute énergie, car ils posent des questions essentielles à la compréhension de la nature et du fonctionnement de ces formidables puits gravitationnels : quels sont les processus physiques permettant l'éjection à partir de l'accrétion, quelle est la nature des jets, quelle est l'énergie des électrons du jet, quelle est la fraction de masse qui est éjectée, quels sont les effets des interactions entre la matière éjectée et le milieu environnant ? L'originalité de mes travaux sur les microquasars porte principalement sur une approche multi-longueur d'onde, fondée sur des observations dans différents domaines, des rayons X à la radio en passant par l'infrarouge. Par cette approche, j'ai tout d'abord mis en évidence le lien entre les phénomènes d'accrétion et d'éjection de matière dans l'archétype des microquasars, GRS 1915+105, puis j'ai montré qu'une composante non-thermique était présente dans l'ensemble de la distribution spectrale d'énergie d'un autre microquasar, XTE J1118+480. Ces observations ont permis d'apporter des contraintes et des tests sévères aux modèles et théories décrivant les phénomènes d'accrétion–éjection.

La suite de ce manuscrit, dans le chapitre 3, concerne les systèmes binaires de grande masse récemment découverts par le satellite de rayons X et γ *INTEGRAL*. Là encore, l'originalité de mon travail provient d'une approche multi-longueur d'onde. Grâce à un travail d'identification et d'étude sur l'ensemble du spectre électromagnétique, j'ai pu identifier la première source détectée par ce satellite, IGR J16318-4848, comme un système binaire de grande masse contenant une étoile compagnon supergéante d'un type rarement vu dans notre Galaxie, et enfoui derrière ce qui semble être un cocon de poussière et/ou de gaz froid. Cette source est ensuite devenue le prototype d'une nouvelle population d'astres émettant dans les hautes énergies, dont la découverte révolutionne notre vision sur la formation, l'évolution et le destin des systèmes binaires de haute énergie, en remettant en cause les schémas classiques d'évolution, et en imposant des contraintes nouvelles sur les modèles de synthèse de population. L'étude de ces sources INTEGRAL, ainsi que les questions que pose cette nouvelle population, devraient permettre de mieux comprendre l'évolution de l'ensemble des systèmes binaires.

L'approche multi-longueur d'onde n'est pas qu'une technique, car elle requiert de se confronter à des phénomènes différents, émettant à des énergies différentes, et permettant de sonder diverses parties de l'astre étudié. Ainsi, mon approche s'est avérée toujours être "multi-échelle" au sens où j'ai à chaque fois étudié les astres de haute énergie sous différentes coutures, et en les comparant à d'autres astres de haute énergie. J'ai étudié les microquasars sous différentes

coutures, depuis le disque d'accrétion au niveau de sa dernière orbite stable autour de l'objet compact, jusqu'à l'interaction entre matière éjectée et milieu environnant. J'ai comparé les microquasars à d'autres astres de haute énergie, en commençant par les quasars, par une analogie morphologique assez évidente, dont il fallait montrer si elle était justifiée par une analogie physique, puis en continuant par les microblazars et blazars, avant de comparer les phénomènes d'accrétion–éjection à ceux présents dans les phénomènes de sursauts γ. Enfin, la découverte d'une nouvelle population de sources X révélée par *INTEGRAL* impose d'étudier les propriétés de l'étoile supergéante, ainsi que le type d'accrétion sphérique à partir du vent stellaire. Ce sont en effet principalement le type de l'étoile et de l'accrétion qui donnent à cette population ses caractéristiques inhabituelles.

Je finis ce manuscrit par des conclusions, ainsi que des perspectives, dans le chapitre 4, portant principalement sur l'étude de la formation, de l'évolution et de la fin de vie des systèmes binaires de grande masse, en insistant sur l'importance de l'environnement et de l'interaction entre les deux composantes, sur leur évolution, et leur destin final... Je montre ainsi que l'avenir de l'Astrophysique des hautes énergies s'avère radieux, avec bientôt l'avénement du satellite GLAST, qui augmentera drastiquement le nombre d'astres célestes de haute énergie.

Pour conclure, et avant d'entrer dans le vif du sujet, l'originalité de mes travaux de recherche réside donc dans l'approche à la fois multi-longueur d'onde et multi-échelle, qui elle-seule peut permettre de dévoiler les secrets des astres célestes émettant dans les hautes énergies...

Chapitre 2

Microquasars

Ou comment la présence de jets permet à certains astres de ressembler à leurs grands frères, et de s'immiscer dans la physique des hautes énergies et des particules

Sommaire

2.1 Prélude à l'ère des microquasars : SS 433 29
2.2 L'entrée dans l'ère des microquasars 29
2.2.1 Interlude : définition et étude des microquasars 29
2.2.2 Analogie avec les quasars 30
2.3 L'âge d'or des microquasars : accrétion et éjection 31
2.4 L'âge d'or des microquasars : processus d'émission 32
2.4.1 Des microquasars dans tous leurs états 32
2.4.2 Jet ou pas jet ? *That is the question !* 34
2.5 La face cachée des microquasars : interaction avec leur environnement . . 36
2.6 Mais où sont les microblazars ? 38
2.7 Les microquasars et leur rôle dans la physique des astroparticules 39
2.7.1 Les microquasars en tant qu'émetteurs de photons THE 39
2.7.2 Les microquasars en tant qu'émetteurs de neutrinos 40
2.7.3 Les microquasars en tant qu'émetteurs de rayons cosmiques 41
2.8 Conclusions 41
2.9 Quelques articles publiés parmi les plus significatifs 43
2.9.1 Une recherche d'éventuelles interactions entre les éjections de GRS 1915+105 et le milieu interstellaire environnant 45
2.9.2 Observations en infrarouge proche de candidats trous noirs Galactiques 59
2.9.3 Observations en optique et infrarouge proche du microquasar V4641 Sgr au cours du sursaut de septembre 1999 69
2.9.4 Observations multi-longueurs d'onde révélant l'évolution du sursaut du trou noir XTE J1118+480 77
2.9.5 Observations en optique et infrarouge proche du candidat trou noir XTE J1720-318 : de l'état haut-mou à l'état bas-dur 95

Mots clés : microquasar, SS 433 ; GRS 1915+105 ; 1E 1740.7-2942 ; V4641 Sgr ; XTE J1118+480 ; XTE J1720-318 ; optique, infrarouge proche, radio

Abstract :

I present an overview of past, present and future research on microquasars and jets, showing that microquasars, i.e. galactic jet sources, are among the best laboratories for high energy phenomena and astroparticle physics. After reminding the analogy with quasars, I focus on one of the best microquasar representatives, probably the archetype, namely GRS 1915+105, and present accretion and ejection phenomena, showing that only a multi-wavelength approach allows a better understanding of phenomena occurring in these sources. Thereafter, I review jets at different scales : compact jets, large-scale jets, and the interactions between ejection and the surrounding medium. I finish this review by showing that microquasars are good candidates to be emitters of astroparticles : very high energy photons, cosmic rays and neutrinos.

Résumé :

Je présente un exposé synthétique de la recherche passée, présente et future sur les microquasars et les jets, et je vais montrer que les microquasars, c'est-à-dire les sources galactiques présentant des jets, sont parmi les meilleurs laboratoires d'étude des phénomènes de haute énergie et de physique des particules. Je vais tout d'abord rappeler l'analogie avec les quasars, puis je me concentrerai sur l'un des meilleurs représentants des microquasars, probablement l'archétype : l'astre GRS 1915+105. Je présenterai les phénomènes d'accrétion et d'éjection s'y produisant, en montrant que seule une approche multi-longueur d'onde permet une meilleure compréhension des phénomènes ayant lieu au sein de ces sources. Puis, je présente les jets à différentes échelles : les jets compacts, les jets à large échelle, ainsi que les interactions entre les éjections et le milieu environnant. Je finis cet exposé en montrant que les microquasars sont de bons candidats pour être des astres émetteurs d'astroparticules : photons de très haute énergie, rayons cosmiques et neutrinos.

2.1 Prélude à l'ère des microquasars : SS 433

En 1979 est découvert le prototype des microquasars : SS 433, une source de haute énergie présentant des jets précessant, et se déplaçant à une vitesse de $0.26c$ dans le référentiel de la source, avec des raies d'émission observées en optique, preuve que le contenu du jet était baryonique (Margon, 1984). SS 433 est entouré d'un rémanent de supernova : W50, et il existe des signatures claires d'interaction entre les jets de SS 433 et la nébuleuse W50 (cf Dubner et al. 1998). La question qui est alors rapidement apparue était : comment un objet galactique peut-il éjecter de la matière à de telles vitesses relativistes (Γ=1.04) ? Cet objet présentait des propriétés tellement inhabituelles, qu'il était probablement impossible de prévoir que, deux décades plus tard, les sources montrant des jets deviendraient tellement communes. SS 433 avait donc tout d'un microquasar, à part le nom...

2.2 L'entrée dans l'ère des microquasars

En 1990 était lancé le télescope *SIGMA*, en orbite à bord de l'observatoire *Granat*. Ce télescope avait été conçu pour observer les candidats trous noirs galactiques, car la bande d'énergie dans laquelle il observait correspondait à l'énergie libérée par l'accrétion autour des objets compacts. En 1992 était identifié le premier -ainsi nommé- "microquasar", 1E 1740.7-2942 (Mirabel et al., 1992). Cet astre présentait des jets radio bipolaires s'étalant sur plusieurs années-lumières. C'était la première observation de ce type dans notre Galaxie, cependant des jets avaient déjà été observés autour de galaxies distantes. Ainsi cette observation permis de montrer clairement l'existence d'une analogie morphologique entre les quasars et les microquasars.

2.2.1 Interlude : définition et étude des microquasars

Bien qu'il n'existe pas de définition claire d'un microquasar, on peut le caractériser comme un système binaire galactique –constitué d'un objet compact (trou noir de masse stellaire ou étoile à neutron) entouré d'un disque d'accrétion et d'une étoile compagnon)– émettant dans les hautes énergies et présentant des jets relativistes. Le schéma d'un microquasar, comparé aux quasars, est donné dans la figure 2.1. En prenant cette définition au sens large, une vingtaine de microquasars a été observée dans notre Galaxie, et il s'agit de l'un des principaux sujets d'étude des missions spatiales actuelles.

Les microquasars, comme la majorité des systèmes binaires de haute énergie, étant situés la plupart du temps dans le plan de la Galaxie, ou même dans les régions du centre Galactique, leur rayonnement doit traverser une grande quantité de poussière et de gaz froid. Les rayons X, l'infrarouge et la radio ne sont presque pas affectés par cette absorption. Par contre, quasiment l'ensemble du rayonnement, depuis l'extrême ultra-violet jusqu'à l'optique, est absorbé. Les rayons X provenant des parties internes du disque d'accrétion, l'infrarouge étant émis principalement par l'étoile compagnon, et la radio émanant des jets, ces trois rayonnements sont très complémentaires, et nous permettent d'avoir une vision complète des microquasars. Comme on le verra dans la suite, ces trois domaines vont donc jouer un rôle clé dans la compréhension

des phénomènes se produisant au sein de ces formidables puits gravitationnels. Ainsi, puisque chaque composante du système émet à des longueurs d'onde différentes, il est nécessaire d'effectuer des observations multi-longueurs d'onde, afin de comprendre les phénomènes se produisant au sein de ces objets.

Lors de la découverte d'un microquasar, qui a généralement lieu dans les hautes énergies, puis de sa localisation en radio, les paramètres les plus importants à acquérir sont la distance et la nature de l'objet compact et de l'étoile compagnon. En effet, la nature de l'étoile compagnon permet de déterminer la nature du système binaire, à savoir s'il s'agit d'un système binaire de faible masse ou de grande masse. Ceci a en effet beaucoup d'implications sur le type d'accrétion (voir le chapitre 1). Un exemple d'une telle étude, concernant la détermination de la nature de l'étoile compagnon et donc du système, est donnée dans Chaty et al. (2002)[1]. Puis viennent les paramètres tels que la période orbitale, la masse des deux objets, etc. C'est en effet lorqu'on connaît l'ensemble de ces caractéristiques que l'on peut tenter de mieux comprendre les phénomènes qui se produisent au sein de ces microquasars, et que les microquasars deviennent des laboratoires d'étude des phénomènes de haute énergie à part entière. Cependant, rares sont les microquasars pour lesquels nous disposions de toutes ces données. Le champ d'étude des microquasars passe donc par la collecte de ces données. J'ai au cours de ma recherche sur les microquasars participé à cette quête, à partir de l'identification de ces objets, principalement en optique et infrarouge.

2.2.2 Analogie avec les quasars

En 1992, le télescope WATCH/GRANAT découvre le candidat trou noir GRS 1915+105 (Castro-Tirado et al., 1994), qui allait devenir par la suite l'archétype des microquasars. Deux ans plus tard, en observant cet astre avec le VLA (à l'échelle de la seconde d'arc), Mirabel & Rodríguez (1994) détectent des mouvements en apparence superluminique, alors que la vitesse dans le référentiel de l'objet était de $v \sim 0.92c$. Il devient alors rapidement clair que les avantages des microquasars, comparés aux quasars, sont : i. leur proximité, ii. il est possible d'observer à la fois le jet qui s'approche et celui qui s'éloigne de nous, et iii. l'échelle de temps des phénomènes d'accrétion et d'éjection est beaucoup plus courte. Après cette observation de mouvements superluminiques, l'analogie morphologique avec les quasars se trouva renforcée, et la question clé devint alors : cette analogie morphologique est-elle due à la physique ? Si la réponse s'avérait positive, alors les microquasars seraient réellement des "micro-"quasars. De plus, si l'analogie avec les quasars était physique, elle impliquait alors l'existence de microblazars (des microquasars dont l'un des jets pointe dans la direction de l'observateur).

Nous verrons dans la suite que cette analogie entre quasars et microquasars est rapidement devenue très fructueuse, vu que le champ d'étude des quasars bénéficiait de celui des microquasars, et inversement. Par exemple, parce que l'échelle de temps des phénomènes d'accrétion et d'éjection est proportionnelle à la masse du trou noir, il est plus facile (car plus court) d'observer des cycles d'accrétion et d'éjection au sein de microquasars que de quasars[2]. Inversement,

[1] cf l'article présenté dans la sous-section 2.9.2

[2] L'échelle de temps caractéristique des phénomènes se produisant très près de la dernière orbite stable autour

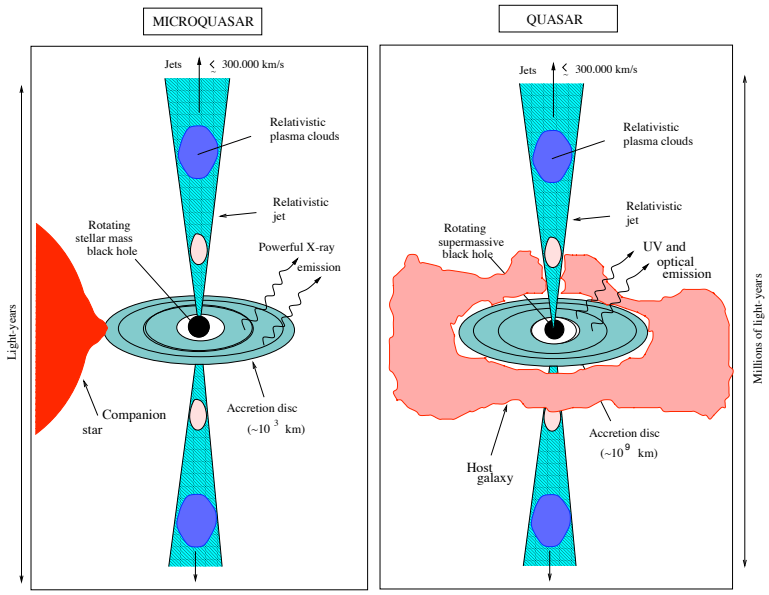

FIG. 2.1 – Schéma illustrant les analogies entre quasars et microquasars. Il est à noter la différence des échelles de masse et de longueur entre les deux types d'objets (Chaty, 1998).

la compréhension des phénomènes d'éjection au sein des microquasars a largement bénéficié de l'existence de modèles de jets qui avaient été développés pour les galaxies actives.

2.3 L'âge d'or des microquasars : accrétion et éjection

GRS 1915+105 va encore une fois jouer un rôle important dans la compréhension des microquasars. En 1997, après avoir entrepris plusieurs campagnes d'observations multi-longueurs d'onde de cet astre, le lien entre les phénomènes d'accrétion et d'éjection a pu être découvert (Chaty 1998 ; Mirabel et al. 1998). En examinant la figure 2.2, on peut voir la disparition de la partie interne du disque d'accrétion, visible sous la forme d'une décroissance du flux de rayons X, suivie par l'éjection d'un nuage de plasma relativiste, correspondant à une oscillation dans l'infrarouge proche puis dans la radio, le nuage devenant progressivement optiquement mince. L'analyse des flux de rayons X et des rapports de dureté, montrés dans la figure 2.3, suggère que c'est principalement la partie émettant à plus haute énergie qui est éjectée au moment du pic visible dans les rayons X. Ceci permet d'appuyer l'interprétation qu'une partie de la couronne (entourant l'objet compact dans la partie centrale du disque d'accrétion) est éjectée au cours de ce cycle (Chaty, 1998). Chacun de ces cycles d'accrétion/éjection dure une dizaine de minutes, et se répètent, se produisant environ toutes les 30–45 minutes. Il est intéressant de relever le fait que non seulement ces observations n'avaient pas été conduites sur les quasars, même après quelques

d'un trou noir de masse M est donnée par $\tau \sim \frac{r_g}{c} \sim M$, où r_g est le rayon de Schwarzschild. Ainsi, cette échelle de temps est proportionnelle à la masse du trou noir. Alors qu'un trou noir de masse stellaire présente des cycles d'accrétion et d'éjection durant quelques minutes, un trou noir supermassif présentera des cycles correspondants sur plusieurs milliers d'années.

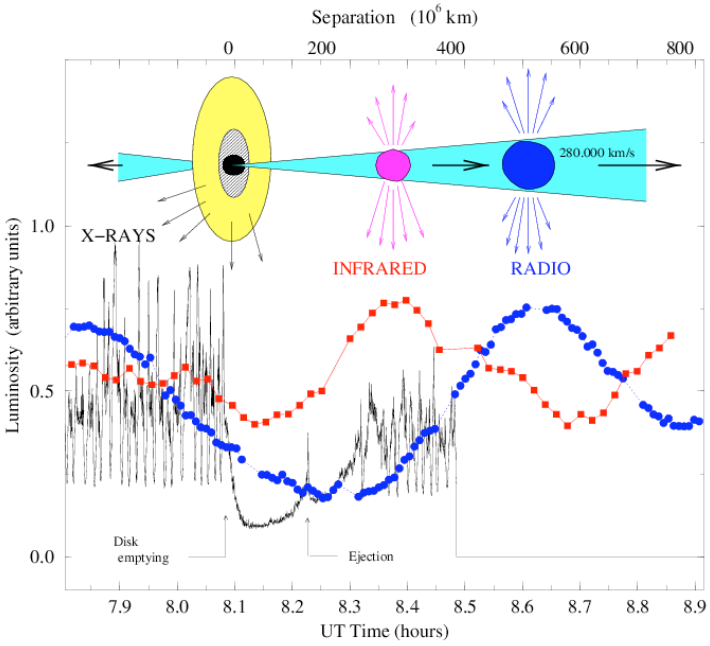

FIG. 2.2 – Observation du lien entre l'accrétion et l'éjection. Courbes de lumière en rayons X, infrarouge et radio de GRS 1915+105 au cours de la campagne d'observations multi-longueurs d'onde du 9 septembre 1997. La disparition de la partie interne du disque d'accrétion (décroissance du flux de rayons X) est suivie de l'éjection d'un nuage de plasma relativiste (oscillation en infrarouge proche et en radio) (Chaty 1998 ; Mirabel et al. 1998).

quarante années d'étude, mais qu'en plus, pour la première fois, les microquasars étaient en train de dépasser les quasars, en apportant de nouvelles découvertes, qui permettront de mieux comprendre le fonctionnement de ces trous noirs accrétants, qu'ils soient stellaires ou supermassifs. Cinq années plus tard, des phénomènes similaires allaient être observés sur le quasar 3C120, en compilant trois années d'observations (Marscher et al., 2002). Ces observations des deux types d'objets confirment alors que l'analogie morphologique entre quasars et microquasars était bien due à la physique sous-jacente[3].

2.4 L'âge d'or des microquasars : processus d'émission

2.4.1 Des microquasars dans tous leurs états

Il n'est pas question de discuter ici des différents modèles d'accrétion et d'éjection, et je renvoie plutôt le lecteur curieux à l'article de Fender (2001) pour une description de ces modèles,

[3]Une autre évidence contraignante de cette analogie est donnée par le trou noir supermassif situé au centre de notre Galaxie : avec une masse de $3.6 \times 10^6\ M_\odot$ il présente des oscillations quasi-périodiques (QPO) en infrarouge proche de quelques dizaines de minutes (Genzel et al. 2003), alors que les trous noirs de masse stellaire présentent des QPOs dans les rayons X de quelques milli-secondes, en accord avec les rapport de masse.

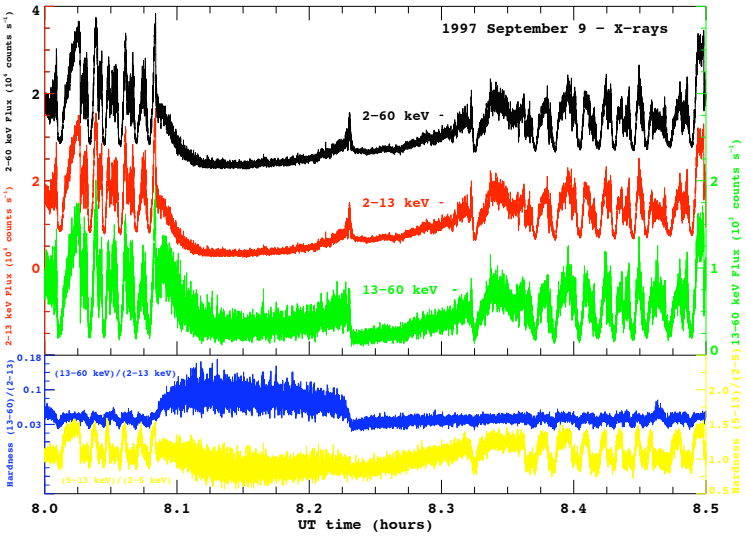

FIG. 2.3 – Observation du lien entre l'accrétion et l'éjection. Mêmes observations que la figure précédente, mais seules les observations en rayons X sont montrées, et agrandies sur l'intervalle TU [8.0-8.5] heures. De haut en bas : Flux de rayons X 2-60 keV, 2-13 keV et 13-60 keV ; rapport de dureté $\frac{13-60keV}{2-13keV}$ et $\frac{5-13keV}{2-5keV}$. Ces observations suggèrent que c'est une partie de la couronne qui est éjectée au moment du pic de rayons X (Chaty, 1998).

et comment ils sont reliés aux différents états d'éjection. Je rappelle ici simplement les grandes lignes de ces processus d'émission. L'état haut/mou (termes historiques se référant aux rayons X) se caractérise par un flux X élevé et mou, et une absence d'émission radio. Le modèle standard interprétant cet état invoque naturellement une émission thermique provenant d'un disque d'accrétion formé d'une émission de corps noir multicolore, et se caractérise par une absence d'émission non-thermique (donc de jet) dans le domaine radio. Inversement, l'état bas-dur se caractérise principalement par un flux faible et dur dans les rayons X, sous la forme d'une émission non-thermique en loi de puissance, ainsi que d'une détection d'émission non-thermique en radio. Certains microquasars émettent à haute énergie, leur émission étant dominée par une loi de puissance (indice spectral 2.5-3), sans aucune coupure (Grove et al., 1998). Le modèle standard invoque pour cet état une émission X provenant vraisemblablement d'une couronne de plasma, et une émission non-thermique en radio provenant d'un jet, ou plus généralement d'une éjection de particules relativistes émettant du rayonnement synchrotron. C'est en effet dans l'état bas-dur que sont résolus les jets en radio. Un exemple typique de ces différents états haut-mou et bas-dur, ainsi que leurs caractéristiques principales, est donné dans la figure 2.4, tiré de Chaty & Bessolaz (2006)[4].

Cependant la question de l'origine de l'émission à haute énergie, en particulier dans l'état bas/dur n'est pas close, car certains modèles, concurrents au modèle standard, invoquent une émission synchrotron des jets de la radio aux rayons X. Ainsi l'incertitude majeure dans ce domaine concerne le processus physique sous-jacent : est-ce de la comptonisation, du rayonnement

[4]cf l'article présenté dans la sous-section 2.9.5

synchrotron, ou un mélange des deux ?

2.4.2 Jet ou pas jet ? *That is the question !*

Une réponse pourrait être fournie par des observations de polarisation. Les instruments de haute énergie ne le permettent pas encore, et les observations polarimétriques en infrarouge proche ne font que débuter. Dubus & Chaty (2006) ont publié des observations polarimétriques en infrarouge proche du microquasar XTE J1550-564, qui ont été exécutées en 2003 au New Technology Telescope (NTT), à l'observatoire La Silla de l'European Southern Observatory (ESO). Ces observations ont été acquises pendant la phase de décroissance (à ~ 2.5 coups/s) d'un sursaut de petite amplitude (maximum à 4.5 coups/s) détecté par *Rossi-XTE*/ASM (Sturner & Shrader, 2005) et qui a duré environ un mois. En infrarouge proche, l'astre était 3.2 magnitudes plus brillant qu'en quiescence. La polarisation de XTE J1550-564 est supérieure à celle des autres étoiles du champ de vue au niveau 2.5σ, ce qui suggère une polarisation intrinsèque en infrarouge proche p=0.9–2.0%, peut-être due à l'émission synchrotron du jet, associée au sursaut (Dubus & Chaty, 2006). Si ce résultat est confirmé par de futures observations, il montre qu'une partie de l'émission infrarouge est due au rayonnement synchrotron du jet.

Afin de comprendre les modèles d'accrétion et d'éjection, il est donc nécessaire d'entreprendre une approche multi-longueurs d'onde et d'obtenir la distribution spectrale d'énergie de plusieurs sources. Il existe un petit nombre de microquasars pour lesquels ceci a été fait de façon intensive, le microquasar et candidat trou noir XTE J1118+480 étant l'un des meilleurs exemples, favorisé par la très faible absorption le long de sa ligne de visée (Chaty et al., 2003b)[5]. Dans la figure 2.5 est montrée la distribution spectrale d'énergie de cet astre, incluant six époques différentes d'observations multi-longueurs d'onde simultanées depuis la radio jusqu'aux rayons X, acquises avec huit instruments différents. Sur cette figure j'ai de plus reporté : l'émission thermique du disque d'accrétion de corps noir multicolore, l'émission de l'étoile compagnon, et l'émission non-thermique qui apparaît nécessaire afin de rendre compte de l'émission dans les domaines radio, infrarouge radio et rayons X. J'ai montré dans Chaty et al. (2003b), en utilisant une simulation Monte-Carlo non-linéaire, que la présence d'une sphère de plasma chaud au centre, par des processus de comptonisation, peut rendre compte de l'émission de l'astre depuis l'optique jusqu'aux rayons X. Cependant d'autres modèles montrent que cette émission peut aussi être décrite par un jet émettant depuis la radio jusqu'aux rayons X, un modèle adapté de celui qui décrit l'émission des jets des galaxies actives (Markoff et al., 2001). Cette question de la contribution du jet dans l'ensemble du spectre électromagnétique est donc encore matière à débat, et il sera certainement nécessaire d'avoir plus de sensibilité et de résolution temporelle, et de lier ces observations fines à des prédictions des modèles théoriques, pour arriver à y répondre.

Il est intéressant de comparer les distributions spectrales d'énergie des microquasars XTE J1118+480 et GRS 1915+105. Au cours d'importantes campagnes multi-longueurs d'onde, de la radio aux rayons X durs, Ueda et al. (2002) et Fuchs et al. (2003) ont montré la présence d'un spectre radio plat, pendant l'état "plateau" (ou bas/dur) de GRS 1915+105. Ils confirment aussi que le jet contribue à l'émission dans l'infrarouge proche. Une comparaison des rapports

[5] cf l'article présenté dans la sous-section 2.9.4

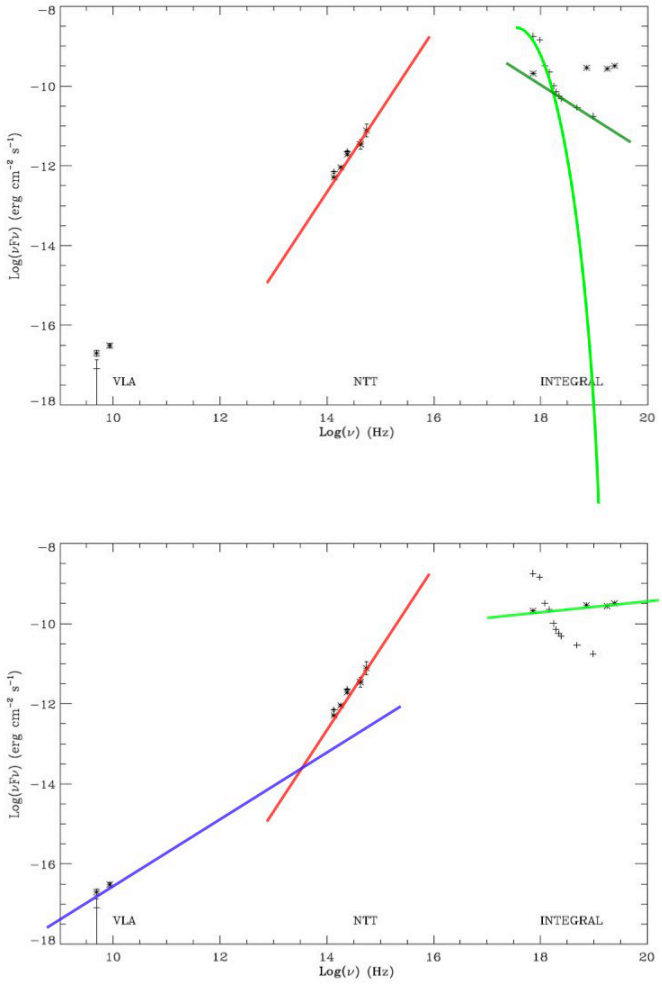

FIG. 2.4 – Distribution spectrale d'énergie du microquasar XTE J1720-318 dans deux états différents, à deux époques différentes (Chaty & Bessolaz, 2006) : état haut-mou le 28 février 2003 ('+') et bas-dur le 24 avril 2003 ('$*$') respectivement. Les observations ont été acquises simultanément en radio au VLA, en optique et infrarouge proche avec le NTT/EMMI et SOFI, et dans les hautes énergies avec *INTEGRAL/IBIS*. L'état haut-mou se caractérise par un flux X élevé et mou, et une absence d'émission radio, et l'état bas-dur par un flux X faible et dur, et une détection d'émission radio. Les flux en optique et infrarouge proche restent remarquablement stables pendant les 2 observations.
Dans la figure du haut sont superposées aux observations les caractéristiques de l'état haut-mou : en vert l'émission d'un disque d'accrétion de corps noir multicolore, en bleu la loi de puissance molle et en rouge l'émission optique et infrarouge proche.
Dans la figure du bas sont superposées aux observations les caractéristiques de l'état bas-dur : en vert la loi de puissance dure des X, en rouge l'émission optique et infrarouge proche, et en bleu l'émission non-thermique (loi de puissance) en radio.

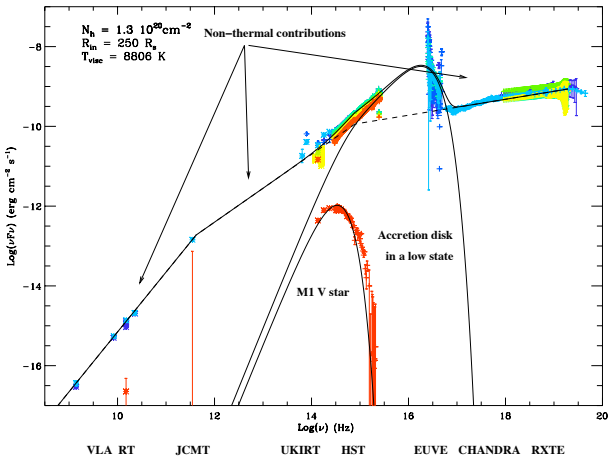

FIG. 2.5 – Distribution spectrale d'énergie du microquasar XTE J1118+480, qui peut être décrite par la somme des émissions du disque d'accrétion à corps noir multicolore, une contribution non-thermique du jet, et l'émission thermique de l'étoile compagnon M1 V (Chaty et al., 2003b).

d'énergie d'accrétion et d'éjection des deux sources XTE J1118+480 & GRS 1915+105 montre qu'elles tombent toutes les deux dans le régime des quasars silencieux en radio (Chaty et al., 2003b).

Des observations multi-longueurs d'onde simultanées des deux types d'objets, microquasars et quasars, apporteront vraisemblablement des contraintes sévères sur les modèles d'accrétion et d'éjection (par exemple Blandford-Payne, Blandford-Znajek, l'instabilité magnéto-rotationnelle...), et sur la nature des jets (sont-ils baryoniques ou leptoniques ?). Par exemple, la compilation d'observations en radio et en rayons X suggère qu'un couplage existe entre ces deux domaines, $F_{\rm rad} \propto F_{\rm X}^{+0.7}$, pour les sources à jet galactiques (Gallo et al., 2003) et extragalactiques (Falcke et al., 2004), mais il nous manque toujours une bonne compréhension de ce couplage. Ceci montre qu'il n'y a pas de forte amplification Doppler, et que les jets présentent une faible vitesse ($\beta < 0.8c, \Gamma < 2$). Existe-t-il un couplage à plus haute énergie ? Des réponses viendront peut-être de la détection de raies d'émission d'annihilation (décalées par effet Doppler ?), et aussi d'observations de QPOs dans les microquasars. Cependant il faut aussi souligner que beaucoup de sources (par exemple la source SWIFT J1753.5-0127, Cadolle Bel et al. 2007) ne suivent pas ce couplage, pour des raisons encore inconnues, mais certainement dues à des subdivisions subtiles dans les états de ces sources.

2.5 La face cachée des microquasars : interaction avec leur environnement

Les jets des microquasars peuvent être observés à différentes échelles, correspondant à diverses tailles et énergies déployées. Des observations d'éjections sporadiques à grande échelle

furent d'abord effectuées, comme décrit dans le paragraphe 2.2. Un jet compact stable a été observé dans quelques microquasars, comme par exemple dans GRS 1915+105 (à l'échelle de la milli-seconde d'arc, où 10 mas = 1 u.a. ; Dhawan et al. 2000 ; Fuchs et al. 2003 ; Ribó et al. 2004). Etant donné que ces sources à jet éjectent une grande quantité de matière dans l'espace interstellaire, qui est loin d'être vide, il apparut rapidement fructueux de chercher des interactions entre ces jets et l'environnement des microquasars. Le premier exemple est 1E 1740.7-2942, qui présente un jet stable, probablement dû au freinage de son jet continu dans le milieu interstellaire. La signature d'une telle interaction pourrait être l'observation, directement au sein des jets, d'une raie d'annihilation étroite à 511 keV, due aux positrons e^+ entrant en collision avec le milieu interstellaire[6]. Des jets à grande échelle sont maintenant régulièrement observés dans les rayons X. Corbel et al. (2002) ont observé de tels jets émanant du microquasar XTE J1550-564, à $45''$ de la source centrale. Pour émettre à de telles énergies, les particules doivent être accélérées jusqu'à des énergies proches du TeV, ce qui renforce encore l'analogie avec les quasars. Cependant, la question de l'énergie maximale des électrons est encore ouverte.

Lorsqu'on étudie les interactions entre les jets et le milieu interstellaire, on ne peut évidemment pas oublier GRS 1915+105 : source X toujours active, transitoire, et le siège d'éjections très énergétiques. De telles interactions dans les environs de GRS 1915+105 avaient déjà été suggérées il y a une dizaine d'années par Mirabel et al. (1996). En août 1995, au cours d'un sursaut X de GRS 1915+105, de grande puissance et de longue durée, la source radio a été résolue en deux jets, et l'émission en proche infrarouge augmenta de façon significative entre 2 et 5 jours après le sursaut radio. Mirabel et al. (1996) interprétèrent ce phénomène comme la signature de la présence d'un cocon étendu de poussière, chauffée par l'éjection de plasma concomitante au sursaut. Cette poussière dans l'environnement de ce microquasar fut confirmée plus tard par des observations dans les hautes énergies (*Chandra* ; Lee et al. 2002) et en infrarouge (*ISO* ; Fuchs et al. 2001). Cependant le mystère reste entier sur le moment de la création de ce cocon : a-t-il été créé par de précédentes éjections, ou par accumulation de poussière du milieu interstellaire ? Allons maintenant à plus large échelle : que savons-nous de l'environnement à grande échelle de GRS 1915+105 ? Une carte centimétrique de basse résolution présente 2 sources alignées avec la source centrale (Chaty et al., 2001)[7]. En observant ces sources à plus grande résolution, j'ai découvert une étrange émanation non-thermique dans le lobe sud-est, qui pourrait être une signature synchrotron d'interactions entre les jets émis par GRS 1915+105, et le milieu interstellaire (Chaty et al., 2001). Cependant, la conclusion d'une étude intensive sur ces deux sources est la suivante : il est possible qu'il y ait eu interaction, si on se base sur l'énergie déployée et sur l'observation de cette signature non-thermique, mais il n'existe pas plus de signature observationnelle permettant de confirmer de façon certaine que cette étrange émanation est réellement le signe d'interactions entre les jets de GRS 1915+105 et le milieu interstellaire.

Finalement, toutes ces observations de jets nous amènent à une autre question importante dans le champ des sources à jets : est-ce que les jets sont une propagation de nuages de plasma ou d'ondes de choc ? La première interprétation est courante au sein de la communauté travaillant

[6]Des raies d'annihilation ont été rapportées sur cet astre (et pour cette raison aussi appelé "le grand annihilateur de la Galaxie") mais provenant probablement de l'astre central, et donc reliée au processus d'accrétion (Bouchet et al., 1991).

[7]cf l'article présenté dans la sous-section 2.9.1

sur les microquasars, et la seconde est favorisée par la communauté extragalactique. En appliquant un modèle décrivant les éjections du quasar 3C273 au microquasar GRS 1915+105, j'ai pu montrer dans Türler et al. (2004) que les éjections dans GRS 1915+105 pouvaient être décrites comme la propagation d'une onde de choc se formant à 1 UA, avec un courant dissipatif de vitesse $v = 0.6c$.

2.6 Mais où sont les microblazars ?

Même si les microquasars ne sont pas partout, ils sont de plus en plus présents ! Nous avons vu dans le paragraphe 2.2 que les microblazars devraient exister si l'analogie morphologique avec les quasars était justifiée par une analogie physique. Cependant le problème avec les microblazars est qu'ils sont difficiles à observer puisque les sursauts, bien que puissants, sont courts[8]. La précession des jets pourrait produire des microblazars intermittents (voir par exemple Massi et al. 2004). Il existe quelques indications suggérant que des microblazars ont été observés. La source V4641 Sgr a présenté un sursaut qui a duré une journée, devenant pour un court laps de temps la source de rayons X la plus brillante du ciel, augmentant de 1.6 à 12.2 Crab, et de 14 à 8.8 magnitudes en optique, présentant une vitesse de vent de 5000 km/s (Chaty et al., 2003a)[9]. Cette source a rapidement été perçue comme pouvant être un microblazar, puisqu'à la distance de 6 kpc, les jets auraient eu une vitesse apparente sur le fond du ciel de $v \sim 10c$. Cependant cette vitesse apparente est fondée sur un mouvement incertain du lobe radio, dû à l'absence de couverture observationnelle complète en radio. Il n'y a donc pas d'évidence observationnelle permettant de prouver de façon irréfutable que cette source est un microblazar.

Nous avons donc quelques difficultés à trouver des microblazars dans notre Galaxie, mais nous en avons peut-être trouvé en dehors de la Voie Lactée. En effet, des sources de rayons X ultra-lumineuses (ULXs ; cf Liu & Mirabel 2005) sont observées la plupart du temps près des noyaux actifs de galaxie spirales à fort taux de formation stellaire. Sont-elles des jets collimatés émanant de microquasars dans des systèmes binaires de grande masse (et dans ce cas les microblazars ne manqueraient plus à la famille), ou des trous noirs de masse intermédiaire ($\sim 1000 M_{sol}$; Körding et al. 2002) ? Cette question nous ramène d'ailleurs immédiatement à notre Galaxie : s'il existe des ULXs dans les autres galaxies, pourquoi n'en voit-on pas dans notre Galaxie ? Et cette question ouvre aussi un autre mystère : pourquoi voit-on des trous noirs de masse stellaire (par exemple au sein des microquasars) et des trous noirs supermassifs (au sein des quasars) mais pas de trous noirs de masse intermédiaire ? Est-ce que ces objets ne peuvent pas se former, ou n'ont-ils pas eu le temps de se former ?

[8] Pour un microblazar dont la vitesse du jet dans le référentiel de la source est $v = 0.98c$, la durée du sursaut est diminuée d'un facteur 10, le flux étant multiplié par 1000, et l'énergie du photon augmentée, par rapport à un microquasar présentant la même vitesse.

[9] cf l'article présenté dans la sous-section 2.9.3

2.7 Les microquasars et leur rôle dans la physique des astroparticules

Dans cette revue j'ai montré que les microquasars étaient le siège de phénomènes d'accrétion, d'éjection et d'interaction des jets avec le milieu interstellaire. Les microquasars sont donc des laboratoires de haute énergie qui contiennent tous les ingrédients nécessaires à l'émission d'astroparticules : photons de très haute énergie (appelés dans la suite photons THE), rayons cosmiques et neutrinos.

2.7.1 Les microquasars en tant qu'émetteurs de photons THE

Plusieurs modèles existent, qui prédisent l'émission de photons THE par les microquasars. Un modèle récent est le modèle leptonique à large bande pour les microquasars émettant des rayons γ, par Bosch-Ramon et al. (2006), dans lequel le jet est dominé dynamiquement par des protons froids, et radiativement par des leptons relativistes, le champ magnétique étant à l'équipartition. Dans ce modèle l'émission de la radio aux THE est due aux processus synchrotron, Bremsstrahlung relativistes et Compton inverse. Ce modèle fournit des prédictions sur la forme de la distribution spectrale d'énergie et prédit que les microquasars sont des émetteurs de photons THE.

Il existe des observations d'une émission au GeV par EGRET (Paredes et al., 2000) jusqu'aux photons de rayons γ THE au TeV par HESS (Aharonian et al., 2005), émanant du candidat microquasar LS 5039. Un second exemple a été la détection par MAGIC d'une émission variable de photons γ THE provenant du candidat microquasar LS I +61 303 (Albert et al., 2006).

Mais ces observations d'une émission à haute énergie ne constituent pas la preuve que le jet, ou son interaction avec le disque d'accrétion, émette à haute énergie. En effet, l'émission γ peut aussi être créée par l'interaction entre le rayonnement de l'objet compact (s'il s'agit d'une étoile à neutron magnétisée) et le vent de l'étoile compagnon de type spectral précoce, ainsi que l'a proposé Dubus (2006)[10]. Or, ce débat a été partiellement clos lors du 6^{me} congrès sur les microquasars, qui s'est tenu en septembre 2006, où des observations interférométriques en radio acquises au VLBA montrent de façon claire que l'émission radio de LSI +61 303 est périodique, corrélée à la période orbitale de l'objet, et suit l'orbite de l'objet compact autour de son étoile compagnon[11]. Ces observations montreraient donc que l'émission γ est due à la nature binaire de l'objet, plutôt qu'au jet. Dans le cas de LSI +61 303, aucun jet n'est donc requis, et sa nature de microquasar est fortement remise en cause. Il subsiste encore le cas de LS 5039... Un schéma des deux objets du débat est représenté en figure 2.6.

[10]Ce type d'objet a été habilement appelé "pulsars déguisés" ("pulsars in disguise") par cet auteur.

[11]"LSI +61 303 revisited : it sits, it spits, and it spins." (Dhawan, Mioduzewski, Rupen, communications du VIeme congrès de microquasars, Como, Italie, Sept. 2006.)

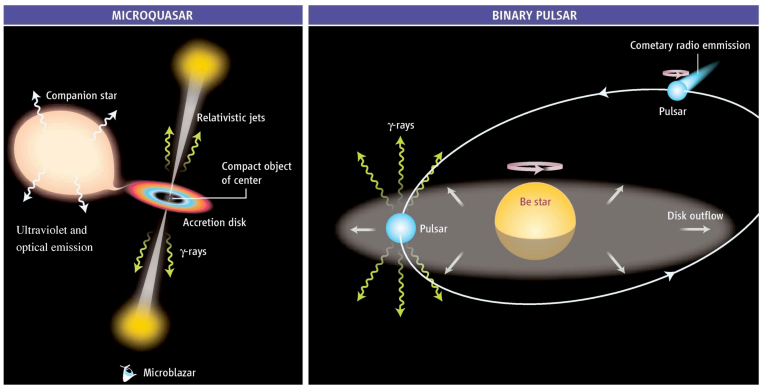

FIG. 2.6 – Schéma illustrant le débat concernant les émetteurs à haute énergie : les microquasars et les sources binaires constituées d'une étoile à neutron magnétisée orbitant autour d'une étoile massive de type précoce (Mirabel, 2006).

2.7.2 Les microquasars en tant qu'émetteurs de neutrinos

Le modèle de Romero & Orellana (2005) prédit une émission de neutrinos et de photons de rayons γ provenant de microquasars non alignés, c'est-à-dire dont le jet n'est pas aligné avec la perpendiculaire au plan orbital (ce qui pourrait être en fait assez courant : par exemple, le jet est incliné de $35°$ par rapport au plan orbital de V4641 Sgr ; il existe une précession du jet dans les microquasars SS 433 et Cygnus X-3), et pour lesquels l'étoile compagnon est une étoile de type précoce. Si ces deux conditions sont remplies, alors le jet entre en collision avec le vent stellaire, et un choc stable se crée entre l'objet compact et la surface stellaire. Finalement, si le contenu du jet est hadronique, les protons d'énergie du TeV pourraient diffuser dans un vent interne et dense, produisant une émission de rayons γ. Ce modèle prédit une augmentation et une variabilité périodique de l'émission de rayons γ du TeV (qui pourrait être détectée par HESS, MAGIC, Veritas), et aussi un signal d'émission de neutrino à 3 σ (ICECUBE, AMANDA, ANTARES), pour un temps d'observation de 15 ans, d'une source située à 2 kpc... mais seulement s'il existe un alignement serré du jet le long de la ligne de visée, afin d'obtenir un cycle effectif ("duty cycle") de 20%.

Ainsi, même si les microquasars sont des émetteurs de neutrinos au TeV, leur détection sera probablement uniquement possible avec les télescopes neutrinos d'une surface atteignant au moins 1 km^2. Pour voir quel pourrait être le signal, on peut prendre le modèle de Distefano et al. (2002), où il y a production de photopion dans le jet, avec la condition que le jet est protonique, et qu'une fraction de quelques pourcents de l'énergie du jet est dissipée sur une échelle de taille suffisamment petite. Dans ce cas, on peut s'attendre à un signal de quelques 252 neutrinos provenant de SS 433, avec un temps d'intégration d'une année. Nous pourrions probablement même identifier de nouveaux microquasars par leur émission de neutrinos et de rayons γ, s'ils présentent des facteurs de Lorentz de volume élevés, et si les jets sont dirigés le long de notre ligne de visée.

2.7.3 Les microquasars en tant qu'émetteurs de rayons cosmiques

Si les jets contiennent des protons froids et des ions lourds (comme c'est le cas dans SS 433), les rayons cosmiques provenant de microquasars pourraient représenter une composante étroite à 3-10 GeV du spectre de rayons cosmiques (Heinz & Sunyaev, 2002). Par exemple, un seul microquasar comme GRS 1915+105, actif pendant 10^7 ans, présentant une luminosité de 10^{38}ergs/s, et situé à une distance de 1 kpc, produirait un signal détectable dans le spectre de rayons cosmiques du bruit de fond galactique. Enfin, leur prédiction est que s'il n'y a pas de telle détection, cela signifie que les jets seraient leptoniques...

2.8 Conclusions

Nous avons vu que les microquasars sont d'excellents laboratoires d'étude de la physique des hautes énergies, et qu'ils sont la clé de beaucoup de questions encore présentes, reliées aux mécanismes d'accrétion et d'éjection, à l'interaction entre les jets et le milieu interstellaire, et leur propagation. Afin de répondre à ces questions, il sera nécessaire d'étudier simultanément les émissions multi-longueurs d'onde provenant de plusieurs microquasars à différentes époques. Ceci permettra de mieux mesurer quelle est dans leur distribution spectrale d'énergie la contribution de l'émission non-thermique (synchrotron) provenant des jets. L'une des questions clés, peut-être la plus importante, concerne la nature –baryonique ou leptonique– des jets. En effet, nous avons vu que les microquasars ne joueront pas le même rôle dans la physique des astroparticules dans chacun de ces cas, puisqu'il y a beaucoup plus de possibilités pour eux d'être des émetteurs de photons de très haute énergie, de rayons cosmiques et de neutrinos si les jets sont de nature baryonique.

Nous sommes actuellement à une étape charnière où l'ensemble du spectre électromagnétique est maintenant exploré et accessible, depuis la radio jusqu'aux photons de très haute énergie, en ajoutant les rayons cosmiques, et nous serons bientôt capables d'observer les neutrinos[12]. Le regroupement de toutes ces informations, et le lien de ces observations avec la théorie et les modèles, devraient nous aider à mieux comprendre les microquasars, ces astres excitants mais recélant encore beaucoup de mystères.

[12]Les instruments actuels ou à venir dans un futur proche, les plus à même de répondre à ces questions sont : en radio le VLA/VLBA et SKA, en sub-mm ALMA et HERSCHEL ; en optique/infrarouge : VLT ; en hautes énergies : XMM, Chandra, RXTE, Swift, Suzaku, INTEGRAL, HESS(-2) ; MAGIC, AGILE, GLAST ; pour les rayons cosmiques : AUGER ; pour les neutrinos : AMANDA, ANTARES.

2.9 Quelques articles publiés parmi les plus significatifs

2.9.1 Une recherche d'éventuelles interactions entre les éjections de GRS 1915+105 et le milieu interstellaire environnant

"A search for possible interactions between ejections from GRS 1915+105 and the surrounding interstellar medium" par S. Chaty, L.F. Rodríguez, I.F. Mirabel, T.R. Geballe, Y. Fuchs, A. Claret, C.J. Cesarsky and D. Cesarsky, 2001, A&A, 366, 1035

Dans cet article est inspecté l'environnement du microquasar GRS 1915+105, afin de repérer d'éventuelles signatures d'interactions entre les éjections de cette source, et le milieu interstellaire environnant. Après la description d'observations multi-longueurs d'onde, la conclusion de cet article est que, bien qu'il y ait quelques signes d'interaction possible, et en particulier une émanation non-thermique partant d'un lobe éloigné de GRS 1915+105, et dirigé dans sa direction, il n'y a pas de preuve irréfutable permettant de conclure sur une possible interaction. Dans cet article est aussi présenté un budget énergétique de ces éjections, qui montre bien qu'il est tout à fait possible qu'il y ait interaction entre les éjections et la matière environnante, même à grande distance (voir le paragraphe 2.5 pour plus de détails).

A&A 366, 1035–1046 (2001)
DOI: 10.1051/0004-6361:20000266
© ESO 2001

Astronomy & Astrophysics

A search for possible interactions between ejections from GRS 1915+105 and the surrounding interstellar medium

S. Chaty[1,2], L. F. Rodríguez[3], I. F. Mirabel[2,4], T. R. Geballe[5], Y. Fuchs[2], A. Claret[2], C. J. Cesarsky[6], and D. Cesarsky[7,8]

[1] Department of Physics and Astronomy, The Open University, Walton Hall, Milton Keynes, MK7 6AA, UK
[2] Service d'Astrophysique, DSM/DAPNIA/SAp, CEA/Saclay, L'Orme des Merisiers, Bât. 709, 91191 Gif-sur-Yvette Cedex, France
[3] Instituto de Astronomía, UNAM, Campus Morelia, Morelia, Michoacán 58190, Mexico
[4] Instituto de Astronomía y Física del Espacio C.C. 67, Suc. 28. 1428, Buenos Aires, Argentina
[5] Gemini Observatory, 670 N. A'ohoku Place, Hilo, HI 96720, USA
[6] ESO, Karl-Schwarzschild Strasse 2, 85748 Garching-bei-München, Germany
[7] Université Paris XI, Institut d'Astrophysique Spatiale, Bât. 121, 91450 Orsay Cedex, France
[8] Max Plank Institut für Extraterrestrische Physik, Postfach 1603, 85740 Garching, Germany

Received 25 July 2000 / Accepted 13 November 2000

Abstract. We have observed an extended region surrounding the first discovered galactic superluminal source GRS 1915+105, seeking evidence of interaction between the relativistic ejecta of that object and the interstellar medium. We find two radio sources axisymmetrically aligned along the sub-arcsecond relativistic ejecta of GRS 1915+105 and roughly 17′ distant from it, which coincide with the luminous IRAS sources 19124+1106 and 19132+1035. We have observed these sources at centimeter (VLA), millimeter (IRAM 30 m), and infrared (ISO, UKIRT, ESO/MPI 2.2 m) wavelengths in both line and continuum emission. At centimeter wavelengths a non-thermal jet-like feature aligned along the outflow axis is located adjacent to the inner edge of the southern source. Strong density enhancements are found in the millimeter tracers CO and $H^{13}CO^+$ at the positions of both sources and some of the morphology is reminiscent of shock-like interactions; however, linewidths are narrow. At infrared wavelengths strong hydrogen recombination lines and weak lines of molecular hydrogen are observed at the southern source. We discuss these results as possible evidence of the sought-after interaction, both in terms of the regions undergoing ongoing shock-heating and in terms of them being locations of shock-induced star formation. The evidence for each of these is inconclusive. Millimeter line mapping of a portion of W 50 where the relativistic jets of the X-ray binary SS 433 interact with the interstellar medium shows roughly similar morphology as GRS 1915+105, suggesting that the phenomena observed at the IRAS sources may not be unusual for such a long distance interaction.

Key words. stars: individual: GRS 1915+105, SS 433 – ISM: individual objects: IRAS 19124+1106, IRAS 19132+1035 – ISM: jets and outflows – X-rays: stars

1. Introduction

The hard X-ray transient GRS 1915+105 was discovered in 1992 by the all-sky monitor WATCH on GRANAT (Castro-Tirado et al. 1994). It has been intensively studied since then in many wavebands, including the radio, where ejected plasma clouds with apparently superluminal velocities, a common extragalactic phenomenon, were found for the first time in our Galaxy (Mirabel & Rodríguez 1994). Material ejected from GRS 1915+105 would be expected to interact with the surrounding interstellar medium, providing an opportunity to study in detail for the first time such a relativistic interaction (for a review see Mirabel & Rodríguez 1999).

In a program to look for these interactions we have detected two compact sources of bright radio emission, each coincident with a bright IRAS source near GRS 1915+105. These sources are located axisymetrically with respect to GRS 1915+105 and at same position angle as its normal sub-arsec ejections, suggesting that they could be the zones of interaction between the ejecta and the interstellar medium as described in Sect. 2. We have observed these two IRAS sources at near-infrared (ESO/MPI 2.2 m, UKIRT), mid-infrared (ISO), millimeter (IRAM 30 m) and centimeter (VLA) wavelengths. The observations are detailed in Sect. 3. We discuss in

Send offprint requests to: S. Chaty,
e-mail: S.Chaty@open.ac.uk

Sect. 4 the possibility of a physical association between the ejections of GRS 1915+105 and the two IRAS sources, comparing some of the results obtained in the putative interaction zones with new measurements of the interaction between one of the jets of SS 443 and the interstellar medium. Some of the observations and results described here have been briefly described in Chaty (1998), Chaty et al. (2000) and Rodríguez & Mirabel (1998) (hereafter RM98).

2. The context: Two axisymmetric sources around GRS 1915+105

In order to search for interactions involving the energetic and relativistic ejections of GRS 1915+105, the region surrounding GRS 1915+105 was observed at radio wavelengths as described by RM98. This search was performed at $\lambda = 20$ cm, using the Very Large Array (VLA) of NRAO[1], in its C-configuration, giving a resolution of 15″. The resulting map is shown in Fig. 1. The region in the map referred to as G45.45+0.06 was mislabelled G45.46+0.06 in the original papers (e.g., RM98). Characteristics of this radio source are given in Downes et al. (1980) and in Feldt et al. (1998). No evidence of jets or elongated clouds appears in the figure. However, two small radio continuum sources positioned nearly axisymmetrically with respect to GRS 1915+105 were found at angular separations of 17′ each from GRS 1915+105 (RM98). These small sources are coincident with the bright IRAS sources, 19124+1106 and 19132+1035. Their coordinates are given in Table 1. The position angle of the line connecting the northwest source and GRS 1915+105 is 157.°9, and their separation is 16.′6, the equivalent values for the southeastern source and GRS 1915+105 are 156.°6 and 16.′9. The position angles are very similar to the position angle of the sub-arcsec radio-ejections from GRS 1915+105 (∼150°) (Mirabel & Rodríguez 1994; Fender et al. 1999). The angle between these ejections and the line of sight towards GRS 1915+105 is 70°, with the southeastern ejection approaching and the northwestern one receding (Mirabel & Rodríguez 1994).

The distance to GRS 1915+105 is crucial for determining many of the physical parameters of the object (e.g., mass loss rate, velocity of ejecta, energetics). It was estimated to be 12.5±1.5 kpc by Mirabel & Rodríguez (1994) and by Chaty et al. (1996). Recent VLBA observations are consistent with this value (Dhawan et al. 2000). However, the uncertainty may be larger than 1.5 kpc, as the above lower limit was based on a distance to G45.45+0.06 of 8.8 kpc, whereas Feldt et al. (1998) have placed the HII region at only 6.6 kpc. Moreover, Fender et al. (1999), who derived an upper limit of 11.2 ± 0.8 kpc, consider that the source is constrained to lie between 7 and 12 kpc.

[1] The National Radio Astronomy Observatory is operated by Associated Universities, Inc., under cooperative agreement with the USA National Science Foundation.

Table 1. Positions of GRS 1915+105, IRAS 19124+1106 and IRAS 19132+1035. These coordinates are the positions of peak signal at 20 cm as observed by the VLA

Source	J2000.0 coord.	gal. coord.
GRS 1915+105	$\alpha = 19^h15^m11.^s545$	$l^{II} = 45.^\circ40$
	$\delta = 10^\circ56'44.''80$	$b^{II} = -0.^\circ29$
IRAS 19124+1106	$\alpha = 19^h14^m45.^s77$	$l^{II} = 45.^\circ54$
	$\delta = 11^\circ12'06.''4$	$b^{II} = -0.^\circ007$
IRAS 19132+1035	$\alpha = 19^h15^m39.^s13$	$l^{II} = 45.^\circ19$
	$\delta = 10^\circ41'17.''1$	$b^{II} = -0.^\circ44$

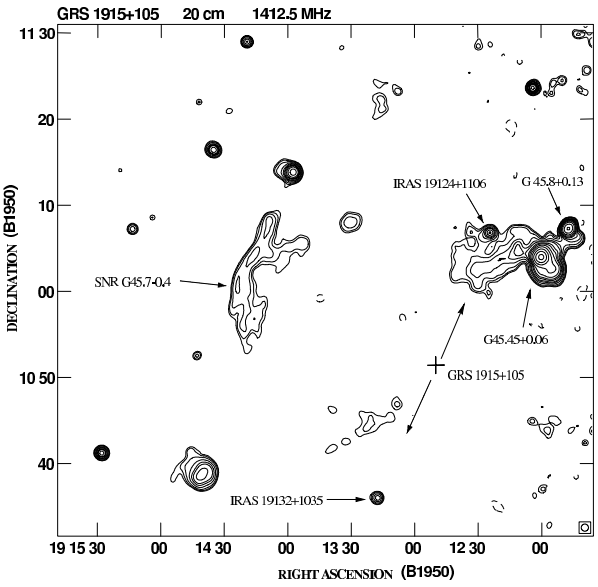

Fig. 1. Map of the surroundings of GRS 1915+105, taken with the VLA-C at $\lambda = 20$ cm. Contour levels are −3, 3, 4, 6, 10, 15, 20, 30, 40, 60, 100, 200, 400 and 800 ×3 mJy beam^{-1}. The half power contour of the beam is shown in the bottom right corner. The arrows around GRS 1915+105 indicate the position angle of the sub-arc relativistic ejecta

If the radio sources are at the same distances from the Sun as GRS 1915+105, and if we assume that the distance of this source is 12.5 ± 1.5 kpc, their angular separations correspond to the distance of 60 pc from GRS 1915+105.

3. Observations and results

3.1. Centimeter

High-resolution maps of the two radio sources have been obtained with the VLA. Details of these observations can be found in RM98. These maps, at three different wavelengths, 2, 6 and 20 cm, are shown in Fig. 2. The morphology of the northern source resembles that of a cometary

Table 2. Flux densities of IRAS 19124+1106 and IRAS 19132+1035. All the flux densities with λ from 12 μm to 20 cm come from RM98. We refer to Table 3 for the fluxes at mid-infrared wavelengths

Source	1.25 μm	2.2 μm	12 μm	25 μm	60 μm	100 μm	2 cm	6 cm	20 cm
	mag	mag	Jy	Jy	Jy	Jy	mJy	mJy	mJy
IRAS 19124+1106	17.9 ± 0.1	12.1 ± 0.1	3.9	19.6	260.6	581.5	114 ± 6	130 ± 4	114 ± 4
IRAS 19132+1035	17.45 ± 0.1	10.7 ± 0.1	6.9	34.0	277.4	488.8	52 ± 6	63 ± 4	60 ± 4
IRAS 19132+1035 "jet"							≤ 1	2	5

HII region, but it also shows a bow shock-like structure to the South-East, e.g. towards GRS 1915+105. At the southern lobe a non-thermal jet extends to the northwest along the line between the source and GRS 1915+105. The flux densities of this jet are $\lesssim$1, 2 and 5 mJy at 2, 6 and 20 cm, respectively, indicating a spectral index of $\alpha = -0.8$ ($f_\nu \propto \nu^\alpha$), therefore noticeably different than that of the rest of the southern radio lobe, which exhibits thermal emission, as it can be seen in the Table 2. We also reported in Fig. 3[2] a spectral index map of IRAS 19132+1035 made from the 20 and 6-cm maps. The southern lobe also shows a sharp edge to the south, which could be either a bow shock, or the ionization front of an H II region.

Additional radio observations of these sources in the H92α recombination line and adjacent continuum at 3.6 cm are detailed in RM98. The line strengths, profiles, and radial velocities are typical of H II regions at kinematic distances of 7.4 ± 1.4 kpc for the north lobe and 6.0 ± 1.4 kpc for the south lobe (distance errors are estimated from the mean value for deviations of circular rotation of 12 km s^{-1} given by Brand & Blitz 1993). We note that the distance uncertainties are large because of the low velocity resolution ($\pm$12 km s^{-1}) of the H92 observations (RM98). These estimates are most consistent with the distance to G45.45+0.06 given by Feldt et al. (1998). The radio luminosities of the sources derived using these distances are similar to those of H II regions powered by O9.5 ZAMS and B0 ZAMS stars (RM98). If instead they are at the nominal distance of GRS 1915+105 hotter individual stars or two stars of the above spectral types would be required to power each source. However, the interpretation of these objects as normal H II regions does not explain the presence of the non-thermal jet-like structure in IRAS 19132+1035. Furthermore, given the large uncertainty in the distance of GRS 1915+105, we cannot a priori rule out the possibility that GRS 1915+105 is roughly at the kinematic distance of the H II regions.

A search for OH maser emission was performed with the VLA in the vicinity of GRS 1915+105, at 1720 MHz. Such emission can be a signpost for interaction between a SNR and molecular gas (as in the case of IC 443, e.g. Denoyer 1979). No detection was obtained. However, this does not imply necessarily that there is no interaction (Rodríguez, Goss, Mirabel, private communication).

[2] On the color page at the end of this article.

3.2. Infrared

3.2.1. Near-infrared

Broad-band imaging[3]

We imaged the IRAS sources in the J (1.25 μm) and K (2.2 μm) bands. The observations were made on 1997, April 5, with IRAC2b installed on the Max Planck Institute's 2.2 m telescope at the European Southern Observatory (ESO). The IRAC2b camera, which contains a Rockwell 256 × 256 pixel Hg:Cd:Te NICMOS 3 array detector was mounted at the f/35 infrared adapter of the telescope. It was used with lens C, providing an image scale of 0.49 arcsec/pixel and a field of 136×136 arcsec^2. The typical seeing for these observations was 1.2 arcsec. Each final image is the median of 5 frames, each exposed for 2 min. After taking each image of the object, an image of adjacent sky was taken, to allow subtraction of sky emission. The images were processed by removing bias and dark current, and applying a flat field correction. These steps were performed using IRAF procedures, in particular the DAOPHOT package for the photometry in crowded fields.

The images reveal a compact near-infrared counterpart at the position of IRAS 19124+1106, with $J = 17.9 \pm 0.1$ mag and $K = 12.1 \pm 0.1$ mag, and a brighter and more extended counterpart of IRAS 19132+1035, with $J = 17.45 \pm 0.1$ mag and $K = 10.7 \pm 0.1$ mag. Figure 4 shows the central portions of the images containing IRAS 19132+1035.

Spectroscopy

A low resolution K-band spectrum of IRAS 19132+1035 was obtained with the facility instrument CGS4 on the UK Infrared 3.8 m Telescope (UKIRT) on UT 1997 July 13, as part of the UKIRT Service Program. The 75 l/mm grating was used in CGS4 together with a slit of width 1.2″ to provide a spectral coverage of 0.67 μm at a resolution of 0.0026 μm (370 km s^{-1} at 2.15 μm) on the 256 × 256 array of InSb detectors. The slit was oriented at a position angle of 148° and the telescope was moved to center the peak signal from the infrared counterpart in one row of the array. Observations were obtained in the standard

[3] Based on observations collected at the European Southern Observatory, Chile.

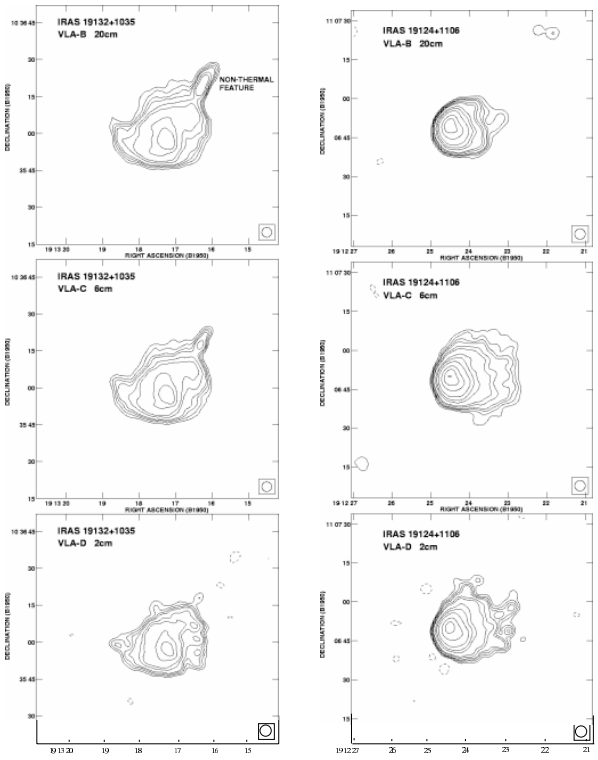

Fig. 2. Maps of the two continuum radio sources IRAS 19132+1035 (left) and IRAS 19124+1106 (right), acquired with the VLA respectively in the D-configuration for the $\lambda = 2$ cm map (bottom), in the C-configuration for the $\lambda = 6$ cm map (middle) and in the B-configuration for the $\lambda = 20$ cm map (top). Contour levels are $-4, 4, 6, 8, 10, 15, 20, 40, 60, 100, 200, 300$ and $400\times$ the rms noise of 0.05 mJy beam^{-1}. The half power contour of the beam, with diameter of $4''$, is shown in each bottom right corner

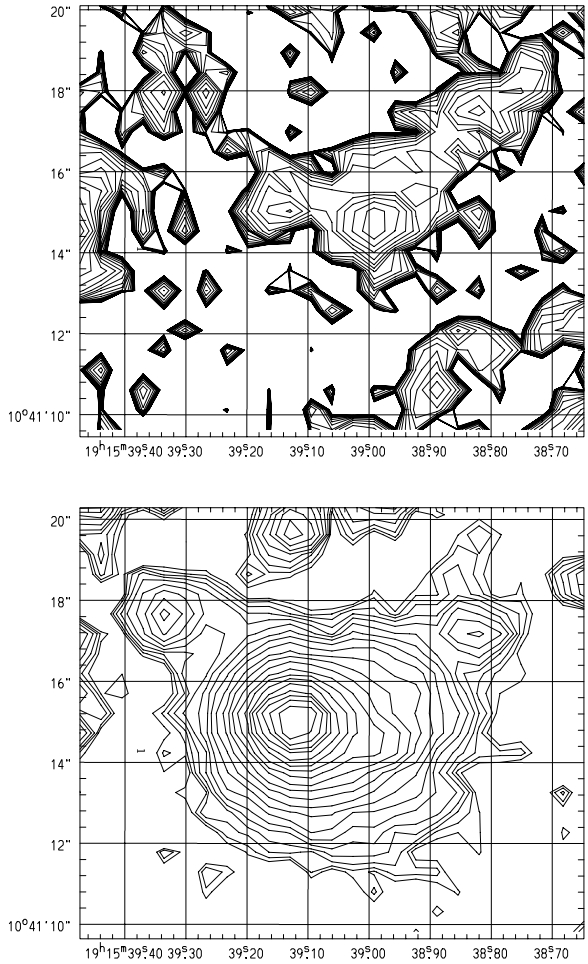

Fig. 4. J (top) and K (bottom) band images of the source IRAS 19132+1035, taken with IRAC2b on the 2.2 m of the ESO. The coordinates are for the J2000 equinox. The ADU flux contour levels are in a logarithmic scale, each separated by a factor $\sqrt{2}$, the first one is equal respectively to 0.864 for the J band and to 25.501 for the K band

stare/nod-along-slit mode. The total integration time was 8 minutes. A near simultaneous spectrum of the F3V star HR 6987 ($T = 6700$ K, $K = 4.50$ assumed) was obtained at the same airmass; in order to remove telluric absorption lines (the Brackett γ (7–4) absorption line, with a central depth of 0.88 of the continuum at this spectral resolution, was artificially removed from the spectrum of the comparison star prior to ratioing). Wavelength calibration was obtained from observations of an argon arc lamp and is accurate to 0.0005 μm.

The spectrum of IRAS 19132+1035 is shown in Fig. 5. It is the sum of the spectra of three adjacent rows, covering an area of 1.2×3.6 arcsec. Most of the flux is contained in the central row. The spectrum exhibits a very red continuum and a number of emission lines. Most prominent are three recombination lines of atomic hydrogen: a very strong Paschen α (4–3) line at 1.876 μm, and weaker Brackett γ (7–4) and Brackett δ (8–4) lines, at 2.166 μm and 1.945 μm, respectively. The Pa α and Br δ lines are uncorrected for the absorption due to the same line in the comparison star and both it and the Br δ line occur near strong telluric absorption lines of water vapor; thus their strengths and profiles are subject to systematic errors.

The peak of the Br γ emission line occurs at $+45 \pm 70$ kms^{-1} in the Local Standard of Rest (LSR). The Full Width at Half Maximum (FWHM) of the profile is only marginally broader than the instrumental resolution, but the profile appears to exhibit a weak high-velocity wing, displaced towards the red. No such wing is present in the profile of either of the other two atomic hydrogen lines. We note that lines displaced towards the blue are much more common in the H II regions, because the front part of an expanding H II region is more easily detected.

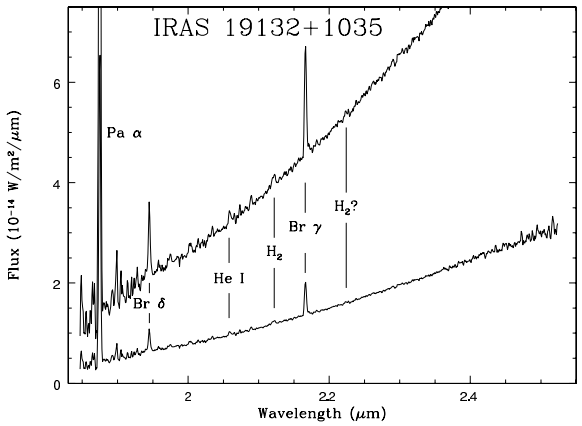

Fig. 5. K-band spectrum of IRAS 19132+1035 obtained with CGS 4 on UKIRT. The upper trace is multiplied by a factor of 3.33 to allow an easier reading of the weakest lines. Identifications and positions of detected and marginal lines are indicated

Two fainter emission lines also are visible: the singlet He I 2P–2S transition at 2.059 μm and the H_2 1–0S(1) line at 2.122 μm. The flux in the H_2 line is $\sim$1 10^{-17} W m^{-2}. There is also evidence for the presence of the H_2 2 – 1 S(1) line at 2.224 μm, at roughly one-fourth the strength of the 1–0 line, which suggests that most of the excitation of H_2 is due to absorbed UV radiation rather than collisions. The 1–0 line appears partly resolved with a deconvolved FWHM of $\sim$500 km s^{-1}, but new measurements are required to confirm this. The signal-to-noise ratio of the 2–1 line is too low to determine if its profile is resolved.

3.2.2. Mid-infrared

Both infrared sources were imaged in six wavebands from 7 to 15 μm with the infrared camera ISOCAM[4] (Cesarsky et al. 1996), on the Infrared Space Observatory (ISO) satellite mission as part of the Guaranteed and Open Time Programme. The observations were performed on 1996 April 28 and on 1997 October 20. The log of the observations and the derived fluxes in all bands are found in Table 3. The images were taken through the Large Width (LW) filters at angular resolutions given in this Table. Data reduction used the CIA package and included subtraction of the dark current, suppression of the cosmic ray impacts by a multiresolution median method, correction of the detector transient behaviour, flat field correction and when necessary a distortion correction (see Starck et al. 1999 and references therein).

The observation at 7 μm of the south lobe, shown at the bottom of Fig. 6[5], is particularly striking, because it shows thermal emission, presumably from heated dust, exactly coincident with the radio counterpart. One component of this emission is localized, between the maximum and the jet feature seen at radio wavelengths, on a line connecting GRS 1915+105 and IRAS 19132+1035. The other component is more extended, and closely resembles the remainder of the radio image with its bow-shock morphology at the south-east edge. The 15 μm image of the north lobe is shown at the top of Fig. 6. The morphology is similar to the radio images, resembling a common cometary H II region, but with two bow shock-like structures facing each other.

3.3. Millimeter

We used the 30 m radio telescope of the Instituto de Radio Astronomía Milimetrica (IRAM[6]) to observe molecular lines which are good density tracers and are diagnostics of shock excitation and chemistry.

The observations, totalling 70 hours, took place during 1997 April 17–24, November 29–December 3, and during 1997 December 31–1998 January 5. The observed molecules and transitions, together with their respective frequencies were: ^{12}CO ($J = 2-1$) at $\nu = 230.5$ GHz, ^{13}CO ($J = 2-1$) at $\nu = 220.4$ GHz, H^{13}CO$^+$($J = 1-0$) at $\nu = 89.2$ GHz, SiO ($J = 2-1$, $v = 0$) at $\nu = 86.8$ GHz, SiO ($J = 3-2$, $v = 0$) at $\nu = 130.3$ GHz, SiO ($J = 5-4$, $v = 0$) at $\nu = 217.1$ GHz and CS ($J = 2-1$) at $\nu = 98.0$ GHz. Details are given in Table 4.

We used position switching during the observations, with the off-source position located ($-500''$, $-1200''$) from the position of GRS 1915+105. Tests demonstrated that the off position contained no significant line emission. The treatment and analysis of the millimetric data were standard, consisting for each spectrum of a subtraction of a polynomial baseline of first or second order, in order to remove instrumental fringes.

3.3.1. IRAS 19132+1035

For each of the ^{12}CO, ^{13}CO, H^{13}CO$^+$ and SiO 2–1 transitions, we obtained 23 spectra at positions separated by $6''$, along the line joining GRS 1915+105 to the South lobe and crossing the maximum of the centimetric continuum shown at the bottom left panel of Fig. 2; this maximum was defined as the (0, 0) position. Integration times were 15 min per point, except at the (0, 0) position where it was 45 min, (–13, 20) where it was 135 min, and (–10, 15) where it was 90 min. The two latter locations correspond to the jet-like feature. In addition we obtained spectra at eight locations adjacent to the jet. The observations of CS, SiO 3–2 and SiO 5–4 each

[4] ISOCAM was constructed under the scientific direction and the technical expertise of the Service d'Astrophysique of the CEA/Saclay. The ISOCAM Consortium is led by the PI C. Cesarsky.

[5] On the color page at the end of this article.

[6] IRAM is an European institute for millimeter astronomy, founded by the French Centre National de la Recherche Scientifique (CNRS) and the German Max-Planck-Gesellschaft (MPG), in collaboration with the Spanish Instituto Geografico Nacional (IGN).

Table 3. Log, characteristics and fluxes of the sources from ISO observations. PFOV = Pixel Field Of View

Source	Date	Filter	PFOV	Flux
IRAS 19132+1035	28/04/96	LW2 (5–8.5 μm)	3″	13.2 ± 2.6 Jy
IRAS 19132+1035	28/04/96	LW7 (8.7–10.7 μm)	6″	5.9 ± 1.2 Jy
IRAS 19132+1035	28/04/96	LW3 (12–18 μm)	6″	10.7 ± 2.2 Jy
IRAS 19132+1035	20/10/97	LW10 (8–15 μm)	1.5″	6.3 ± 1.2 Jy
IRAS 19124+1106	20/10/97	LW9 (14–16 μm)	3″	3.3 ± 0.66 Jy

Table 4. Frequencies of the transitions and receivers used at IRAM. The filter bank b3*, divided into sections b31, b32, b33 and b34, provides a low resolution of 1 MHz, and contains 4×256 channels, for a total bandwidth of 1 GHz; the filterbank b20 provides a high resolution of 100 kHz, and contains 2×128 channels, for a total bandwidth of 25.3 MHz; the autocorrelator b4*, divided into sections b41, b42, b43 and b44 offers resolutions ranging from 10 kHz to 1.25 MHz, a variable number of channels, and a variable total bandwidth from 20 MHz to 1 GHz

Abbr	**Transition**	**Frequency**	**Receiver**	**Banks**	**Beam**
^{12}CO	^{12}CO ($J = 2-1$)	$\nu = 230.537\,990$ GHz	230g2	b44 b34	10.9″
^{13}CO	^{13}CO ($J = 2-1$)	$\nu = 220.398\,686$ GHz	230g1	b43 b33 b20	11.4″
H^{13}CO$^+$	H^{13}CO$^+$($J = 1-0$)	$\nu = 89.188\,523$ GHz	3mm1	b42 b32	28.2″
CS	CS ($J = 2-1$)	$\nu = 97.980\,968$ GHz	3mm1	b41 b31	25.7″
SiO 2-1	SiO ($J = 2-1$, $v = 0$)	$\nu = 86.846\,891$ GHz	3mm2	b41 b31	29″
SiO 3-2	SiO ($J = 3-2$, $v = 0$)	$\nu = 130.268\,702$ GHz	2mm	b42 b32	19.4″
SiO 5-4	SiO ($J = 5-4$, $v = 0$)	$\nu = 217.104\,935$ GHz	230g1	b43 b33 b20	11.6″

consisted of 15 spectra at 6″ separation along the same line, with integration times of 15 min per position with the exception of (0, 0) and (10, –15) where the times were 30 and 7 min, respectively.

Results for ^{12}CO, ^{13}CO, $H^{13}CO^+$ and CS

Figure 7[7] contains position-velocity plots with an expanded velocity scale for the observed lines of ^{12}CO, ^{13}CO, H^{13}CO$^+$ and CS.

For all transitions the line peak occurs at an LSR velocity of 67 km s^{-1}, close to the velocity of 75.7 km s^{-1} of the H92α recombination line observations as seen by RM98 with much lower velocity resolution. The intensity distributions of the millimeter lines are not symmetric, each showing a sharper edge to the south (positive RA offset), as seen in the VLA images, and a slightly shifted peak velocity. The CS transition, which is a high density tracer, exhibits a peak shifted to the northwest (more negative RA offsets), towards the jet-like feature.

SiO

The SiO 2–1 transition was detected only close to the position (–10, 14); the spectrum at that location is shown in Fig. 8. The line is weak, but its velocity, 67.6 ± 0.5 km s^{-1} and width, 4.4 ± 1.2 km s^{-1} are similar to those seen for much stronger lines and give us confidence that it is real. The 3–2 transition was not detected at any individual position, but the average of the spectra between (0, 0) and (–17, 25) yields a 3σ detection

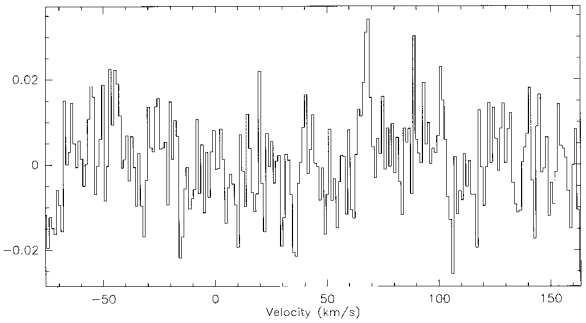

Fig. 8. Spectrum of the SiO 2–1 line at IRAS 19132+1035, obtained at the offset (α, δ) = (−10″, +14″). In this and the following spectra, the y-axis is the antenna temperature in K and the x-axis is the radial velocity with respect to the LSR

of a narrow (1.0 ± 0.3 km s^{-1}) line at 67.3 km s^{-1} ± 0.2, exhibiting an antenna temperature of $T_A^* = 0.044$ K and an intensity of 0.05 ± 0.01 K km s^{-1} (Fig. 9). The SiO 5–4 transition was not detected at any individual location or when all of the spectra were averaged.

Discussion

Figure 7 demonstrates clearly that brightness maxima for transitions with higher critical densities are displaced increasingly towards the northwest where the non-thermal jet-like structure is located. What little SiO emission is detected also originates largely in this region. The very densest region could be the main interaction zone between the putative jet and the ambient medium. However, the narrow lines that are observed are difficult to explain in

[7] On the color page at the end of this article.

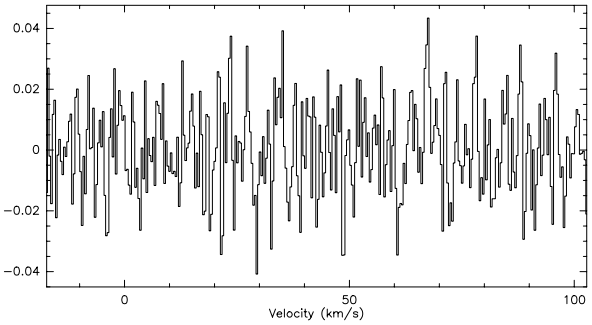

Fig. 9. Spectrum of the SiO 3–2 line at IRAS 19132+1035, averaged over all positions from (0, 0) to (–17, 25)

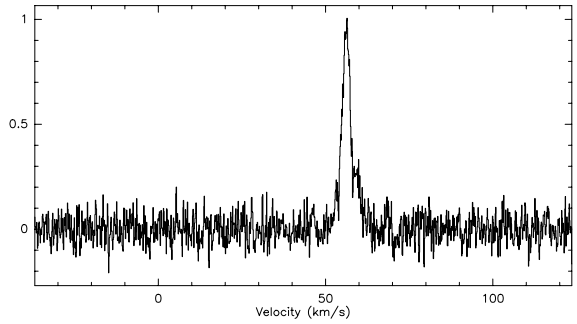

Fig. 11. IRAS 19124+1106, CS, b41, spectrum taken at the position (0, 0)

the above scenario, as an energetic shock might be expected to lead to line emission over a much wider range of velocities than is observed. If a shock is present, it apparently must be of very low velocity.

3.3.2. IRAS 19124+1106

For the ^{12}CO, ^{13}CO, H^{13}CO$^+$ and SiO 2–1 transitions, we acquired 24 spectra at positions separated by 6″, along the line joining GRS 1915+105 to the northern lobe. As in the case of the southern lobe, the reference position (0, 0) is defined as the position of maximum radio continuum signal in the northern lobe, as observed by the VLA. The integration time at each position was 5 min, except at the reference position, where it was 10 min. Each of the above transitions was detected over a wide range of positions. Spectra of the CS 2–1, SiO 3–2 and SiO 5–4 transitions were obtained only at the (0, 0) position, each with an integration time of 15 min. None of the three SiO transitions were detected at any position at an upper limit of 0.05 K, or when all positions were averaged.

Results for ^{12}CO, ^{13}CO and H^{13}CO$^+$

Position velocity diagrams for ^{12}CO, ^{13}CO and H^{13}CO$^+$ are presented using an expanded velocity scale in Fig. 10[8]. Two strong velocity components are readily apparent in all three transitions. For ^{12}CO at the (0, 0) position, the strongest component is centered at $53.95 \pm 0.03\ \mathrm{km\,s^{-1}}$, with a width of $4.05 \pm 0.09\ \mathrm{km\,s^{-1}}$, an intensity of 12.9 K, and an integrated brightness of $55.5 \pm 0.09\ \mathrm{K\,km\,s^{-1}}$. For ^{13}CO, this component is peaked at $55.10 \pm 0.04\ \mathrm{km\,s^{-1}}$, and has a width of $3.88 \pm 0.10\ \mathrm{km\,s^{-1}}$, an intensity of 7.32 K, and an integrated brightness of $30.3 \pm 0.60\ \mathrm{K\,km\,s^{-1}}$. A second velocity component occurs at $59.5 \pm 0.1\ \mathrm{km\,s^{-1}}$ with a width of $3.9 \pm 0.2\ \mathrm{km\,s^{-1}}$, an intensity of 3.11 K and an integrated brightness of $12.8 \pm 0.6\ \mathrm{K\,km\,s^{-1}}$ at the ^{12}CO (0, 0) position. The velocities of these two components are close to that of the H92α recombination line peak at $57.3\ \mathrm{km\,s^{-1}}$ (RM98). A third velocity component, at $\sim 6\ \mathrm{km\,s^{-1}}$ is visible in the northwestern part of this cloud for CO and in the southeastern part for H^{13}CO$^+$. Given the very different velocity the line emission probably originates in a foreground or background cloud.

Results for CS

The single spectrum obtained at (0, 0), shown in Fig. 11, contains a strong component centered at $56.17 \pm 0.03\ \mathrm{km\,s^{-1}}$, of width $3.039 \pm 0.07\ \mathrm{km\,s^{-1}}$, intensity 0.937 K and integrated brightness $3.03 \pm 0.06\ \mathrm{K\,km\,s^{-1}}$. Adjacent to it is a weaker component at $59.91 \pm 0.11\ \mathrm{km\,s^{-1}}$, with width $1.589 \pm 0.22\ \mathrm{km\,s^{-1}}$, intensity 0.298 K and integrated brightness $0.504 \pm 0.07\ \mathrm{K\,km\,s^{-1}}$. These velocities are similar to those detected in other molecules and in H92α (RM98).

Discussion

As already noted by RM98 from the centimeter observations, the morphology of the northern source is that of a cometary H II region. The millimeter wave spectroscopy, which reveals two velocity components, is consistent with this morphology.

4. Discussion

The new data do not definitively prove or disprove an association between GRS 1915+105 and either of the IRAS sources. The strongest lines of evidence supporting an association are (1) the axisymmetric locations of the two sources at nearly the same position angle as the recent sub-arcsecond ejections observed at radio wavelengths, (2) the spatial coincidence of the non-thermal radio jet with the inner edge of the southern source, IRAS 19132+1035, as well as the orientation of this jet along the axis, (3) the location of the highest densities in IRAS 19124+1106 and IRAS 19132+1035 on the sides closest to GRS 1915+105 and, in the case of IRAS 19132+1035, close to the non-thermal jet, and (4) the bow shock – like structure in the portion of IRAS 19132+1035 most distant from GRS 1915+105. Some of these lines of evidence are associated only with the southern source. Evidence against

[8] On the color page at the end of this article.

an association includes (1) the lack of detected high velocity gas at the IRAS sources, (2) the luminosities of the IRAS sources, which are consistent with each of them being powered by one or more hot stars, and (3) the cometary morphology of the northern source, IRAS 19124+1106, which is common in star forming regions.

Although the physical alignment of the IRAS sources could be a background coincidence, the probability of this is low in view of the small number of IRAS sources, the existence of a jet at IRAS 19132+1035, and the locations of these sources within the Galaxy. It remains possible that the jet at IRAS 19132+1035 is an extragalactic background source. This should be tested by radio observations at higher resolution. Because an association between GRS 1915+105 and these objects may be real we explore in the following the potential characteristics of interactions of ejecta from GRS 1915+105 with the interstellar gas and compare these examples with observations of another somewhat similar source.

4.1. Production of a large scale cavity

The angular separation between each IRAS sources and GRS 1915+105 is 17′. The measured proper motions of the most recent ejections from GRS 1915+105 are respectively for the approaching and receding ejecta in the interval $\mu_{\rm app} = [17.6, 23.6] \pm 0.5$ mas/d and $\mu_{\rm rec} = [9.0, 10.0] \pm 0.5$ mas/d (Mirabel & Rodríguez 1994; Fender et al. 1999). This implies typical travel times to reach the lobes of 140 years for the approaching ejecta and of 300 years for the receding ejecta. It is therefore interesting to note that the impact due to the South lobe with the southern IRAS source would appear to occur much earlier than that of the North lobe with the northern IRAS source. Evidence for precession of the jets during the last five years is marginal (Rodríguez & Mirabel 1999), with the maximum angle no more than 10 degrees. Thus a close alignment of currently observed jets close to GRS 1915+105 with those from long past outbursts that may be responsible for the IRAS sources may not be a coincidence.

It is perhaps surprising that the separations from GRS 1915+105 of the two possible interaction zones are identical to better than two percent. These are determined not only by properties of the outflow from GRS 1915+105, but also by the density and uniformity of the interstellar medium. In order for ejected matter to travel up to 60 pc, a large scale cavity must have been created around GRS 1915+105. Over time this cavity could tend to extend an equal distance in each direction. The probable existence of a cavity around GRS 1915+105 already has been pointed out by Mirabel & Rodríguez (1996). The plasma clouds ejected during the last few years exhibit ballistic motions (i.e., with no evidence of deceleration), indicating that the density in the interstellar medium through which they have passed is less than 0.05 protons cm^{-3} (Mirabel & Rodríguez 1996). These clouds have been observed until their emission faded out or became unobservable with the available VLA configuration, typically at distances of one arcsecond from the central source.

Although direct evidence for a cavity is limited to a region very close to GRS 1915+105, it is likely that the cavity extends well beyond one arcsecond from it. Apart from the two IRAS sources, no phenomena that might be associated with deceleration of recent ejecta have been observed from 1″ angular separation from GRS 1915+105 to 17′. In order to produce a cavity with a linear dimension of many tens of parsecs, even a relativistic source must be active for a much longer period of time than GRS 1915+105 has been observed. From EXOSAT measurements (Reynolds et al. 1999) GRS 1915+105 was active in 1985 but much fainter than it has been since 1992. For the second discovered superluminal galactic source, GRO J1655−40, Kolb et al. (1997) suggested that the activity of the source is caused by the companion crossing the Hertzsprung gap, a transient phase lasting ∼1 Myr. The companion of GRS 1915+105 (Martí et al. 2000) is believed to be more massive than the companion of GRO J1655−40 (Shahbaz et al. 1999), and thus the duration of the active phase would be much shorter, although still sufficiently long, especially since GRS 1915+105 has been much more active than GRO J1655−40.

4.2. Interaction between ejecta and ambient material

Considerable heating of the gas must occur at the ends of the cavities, where the ejecta, whether or not partially decelerated en route, impact ambient material. One would expect that much of heating would occur via shock excitation. For the case of GRS 1915+105 the speed and density of the incident material and the relative amounts of atomic and molecular gas (both in the incident and impacted material) are not known, and thus the spectrum of the shock-heated gas is uncertain. The southern IRAS source shows strong infrared lines of atomic hydrogen and weak infrared line emission from molecular hydrogen, very unlike the emission observed in molecular clouds impacted by protostellar winds having speeds of up to 100 km s^{-1}, in which lines of molecular hydrogen dominate and hydrogen recombination lines are nearly non-existent (e.g. Geballe & Garden 1987).

We note that if the non-thermal feature near the southern lobe is an element of the interaction involving the ejecta of GRS 1915+105, the collimation of the jet is $f_{\rm coll} = \frac{\rm length_{jet}}{\rm width_{jet}} = \frac{15'}{7''} \gtrsim 100$, ten times larger than the most highly collimated Herbig-Haro objects (see e.g. Bachiller 1996). This implies a jet opening angle of $\lesssim 0.5°$ which is consistent with the limit of $< 8°$ derived by Fender et al. (1999) based on observations of the core, but is more highly constraining. This jet opening angle seems to be in agreement with the jet full opening angle as function of distance from the core for M 87 (Junor et al. 1999), if we take into account the scaling factor between galactic and extragalactic black holes. Therefore,

as for extragalactic jets, it would require in the galactic case ongoing confinement of the jet at large distances from the source, ruling out free expansion of a relativistic gas.

Induced star formation?

The similarity of the luminosities of the IRAS sources to those of compact H II regions containing one or more massive stars, as well as the spectrum of IRAS 19132+1035, which shows strong hydrogen recombination line emission, suggest the possibility that ejecta from GRS 1915+105 have induced massive star formation at the locations of the IRAS sources, via compression of the interstellar gas. In this scenario the non-thermal radio jet observed at IRAS 19132+1035 might be interpreted as a Herbig-Haro-like feature, the result of a protostellar wind breaking out of the natal cloud. However, given the length of time for star formation to proceed to this phase, such an explanation would require activity from GRS 1915+105 at a much earlier time than mentioned above. Moreover, there appears to be no reason for star formation at IRAS 19132+1035 to produce a close coincidence between the position angle of the radio jet at IRAS 19132+1035 and that of the line connecting GRS 1915+105 and IRAS 19132+1035, as is observed. Finally, the radio emission from Herbig-Haro jets usually is thermal (free-free; Rodríguez 1999). In view of these arguments, we do not regard induced star formation to be a likely explanation for the luminosities of IRAS 19124+1106 and IRAS 19132+1035. Dubner et al. (1998) note that in the case of the relativistic jets from SS 433 there is no evidence of induced star formation in the impacted gas.

4.3. Comparison with SS 433

In view of the inconclusive evidence linking the IRAS sources with activity originating at GRS 1915+105, it is perhaps useful to examine other possible examples of such an interaction. Like GRS 1915+105, the famous X-ray binary SS 433 ejects beams of material at relativistic speeds. This object is located inside the radio shell/supernova remnant W50, which exhibits two lateral extensions with dimensions of tens of parsecs (Dubner et al. 1998). The morphology can be attributed to continuous ejection of magnetic field and high-energy particles from the central source. Sub-arcsecond jets are present at SS 433, with 5 orders of magnitude difference between their extents and those of the far lobes. The power injected into these jets is $\sim 10^{39}$ erg s^{-1} according to Dubner et al. (1998), who also estimate that the kinetic energy transferred to the surroundings of SS 433 during the last $\sim 2\ 10^4$ years amounts to $2\ 10^{51}$ erg.

Major ejection events in GRS 1915+105 are more sporadic than in SS 433, and therefore the average kinetic energy injected into the surroundings over long periods of time may be smaller (Mirabel & Rodríguez 1999). The kinetic energy of the 1994 March 19 event in GRS 1915+105 was $\sim 10^{43}$ erg (Rodríguez & Mirabel 1999). GRS 1915+105 would need to exhibit one ejection event per hour similar to this one in order to match SS 443. A more likely rate is one event per month (Rodríguez & Mirabel 1999), in which case $\sim 2\ 10^7$ years would be required to equal the energy output of SS 443 in $2\ 10^4$ years. However, we note also that the jets emanating from GRS 1915+105 always are compact close to the source (Dhawan et al. 2000), which indicates that a continuous injection of energy from GRS 1915+105 is occuring. In addition to the large events described above, there are also smaller ones, observed at X-ray, radio and infrared wavelengths, where the mechanical luminosities are in the range $10^{37}-10^{39}$ erg s^{-1}, and where the synchrotron emission is seen up to the infrared wavelengths (e.g. Mirabel et al. 1998; Fender & Pooley 2000). A comparison of the energetics of GRS 1915+105 with SS 433 and a Herbig-Haro object is reported in Table 5.

Despite the differences between GRS 1915+105 and SS 433, each may have created a cavity of similar linear extent. In view of the uncertainty as to what effects might be observable at the putative ends of the cavity produced by GRS 1915+105, we have observed the western tip of W50 where the ejecta of SS 443 and the shell remnant interact, in some of the same millimeter lines of ^{12}CO, ^{13}CO, H^{13}CO$^+$ and SiO as were observed for the IRAS sources. The observed region in W50 is at the constant declination 05°00′00″ and right ascensions between $19^h05^m27^s$ and $19^h06^m24^s$ (B1950) (see Dubner et al. 1998, Figs. 1a and 1b). The off position was 15 arcmin east and north of the reference point located at $19^h06^m00^s$; 05°00′00″. Measurements at W50 were separated by 24″, with integration times of 5 min each, except at (0, 0) where the integration time was 10 min.

The results are shown in Fig. 12[9] over the relevant velocity range. Emission from ^{12}CO, ^{13}CO and H^{13}CO$^+$ are found roughly 200–300″ west of the reference position, at the westernmost edge of the radio shell (Dubner et al. 1998, Figs. 1a and 1b).

The emission from the high density tracer H^{13}CO$^+$ is the most compact and probably indicates the location of the strongest interaction. The line profiles of all three species are asymmetric but narrow. SiO 2–1 emission was not detected. These results are very similar to those for IRAS 19132+1035. These similarities between SS 433/W50 and GRS 1915+105/IRAS 19132+1035 and IRAS 19124+1106 suggest that high density, low velocity molecular clumps may not be unusual products of the interaction of the ejecta of a distant energetic source and the surrounding medium.

[9] On the color page at the end of this article.

Table 5. Characteristics of jets from different sources. HH = Herbig-Haro. The range is the ratio of distance between the far lobes and the subarcsec jets, the collimation factor is the ratio between the length of the jet and its width, and the kinetic power of the ejections is a time average

	HH	SS 433	GRS 1915
Velocity	1–500 $\mathrm{km\,s^{-1}}$	0.26 c	0.92 c
Separation	1 au–10 pc	50 pc	60 pc
Range	10^6	10^5	$10^4 - 10^5$
Collimation	2–10	≥ 12	~ 100?
Kinetic Pow.	10^{32} $\mathrm{erg\,s^{-1}}$	10^{39} $\mathrm{erg\,s^{-1}}$	10^{36-39} $\mathrm{erg\,s^{-1}}$

5. Conclusions

We have performed extensive multi-wavelength observations from IR to radio of two radio/IRAS sources axisymetrically located with respect to GRS 1915+105 and aligned with the position angle of the subarcsec jets. The northern source has the morphology of a common cometary H II region. The observations of the southern cloud reveal a collimated non-thermal structure which may be the far end of a jet of material from GRS 1915+105. Both sources contain dense clumps of molecular material. Overall the evidence for these regions being interaction zones seems inconclusive. An abbreviated study of what may be a very similar interaction between the ejecta of SS 433 and the surrounding interstellar medium reveals strikingly similar (and also apparently inconclusive) phenomena, perhaps indicating that such phenomena might be produced by sources which via their violent behavior have created large cavities over long periods of time.

Acknowledgements. We thank F. Comeron for allowing us to use part of his time at the ESO/MPI 2.2 m telescope of the ESO/La Silla. S.C. thanks the astronomers on duty at IRAM, particularly R. Moreno and D. Reynaud, for much assistance and many fruitful discussions during the observations. He thanks also G. Pineau des Forêts and B. Le Floch for helpful discussions. S. C. would like to acknowledge the invitation to work in the dynamic Instituto de Astronomia de Morelia, group of the Universidad Nacional Autonoma de Mexico (UNAM), and the fruitful discussions leading to some of the ideas in this paper. He thanks also the Groupe de Recherche Accrétion-Disque-Jets (GdR ADJ) of the French Centre National de la Recherche Scientifique (CNRS) altogether with the UNAM for the financial support of this journey. We thank R. P. Fender for pointing out to us the previous mislabelling of the region G 45.45+0.06. We also thank the anonymous referee for prompt and useful comments, which allowed us to improve the manuscript. S. C. acknowledges support from grant F/00-180/A from the Leverhulme Trust. I. F. M. acknowledges support from CONICET/Argentina. The UK Infrared Telescope is operated by the Joint Astronomy Centre on behalf of the UK Particle Physics and Astronomy Research Council. The ISOCAM data presented in this paper were analysed using "CIA", a joint development by the ESA Astrophysics Division and the ISOCAM Consortium.

References

Bachiller, R. 1996, ARA&A, 34, 111
Brand, J., & Blitz, L. 1993, A&A, 275, 67
Castro-Tirado, A. J., Brandt, S., Lund, N., et al. 1994, ApJS, 92, 469
Cesarsky, C. J., Abergel, A., Agnese, P., et al. 1996, A&A, 315, L32
Chaty, S. 1998, Ph.D. Thesis, University Paris XI
Chaty, S., Mirabel, I. F., Duc, P.-A., Wink, J. E., & Rodríguez, L. F. 1996, A&A, 310, 825
Chaty, S., Rodríguez, L. F., & Mirabel, I. F. 2000, in A. Letters and Communications (eds.), Proceedings of X-ray Astronomy '999 – Stellar Endpoints, AGN and the Diffuse Background, ed. G. Malaguti, G. Palumbo & N. White (Gordon & Breach Singapore), in press
Denoyer, L. K. 1979, ApJ, 232, L165
Dhawan, V., Mirabel, I., & Rodríguez, L. 2000, ApJ, 543
Downes, D., Wilson, T., Bieging, J., & Wink, J. 1980, A&AS, 40, 379
Dubner, G., Holdaway, M., Goss, M., & Mirabel, I. F. 1998, A&AS, 116, 1842
Feldt, M., Stecklum, B., Henning, T., et al. 1998, A&A, 339, 759
Fender, R. P., Garrington, S. T., McKay, D. J., et al. 1999, MNRAS, 304, 865
Fender, R. P., & Pooley, G. G. 2000, MNRAS, 318, L1
Geballe, T. R., & Garden, R. 1987, ApJ, 317, L107
Junor, W., Biretta, J. A., & Livio, M. 1999, Nature, 401, 891
Kolb, U., King, A., Ritter, H., & Frank, J. 1997, ApJ, 485, L33
Martí, J., Mirabel, I. F., Chaty, S., & Rodríguez, L. F. 2000, A&A, 356, 943
Mirabel, I. F., & Rodríguez, L. F. 1999, ARA&A, 37, 409
Mirabel, I. F., Dhawan, V., Chaty, S., et al. 1998, A&A, 330, L9
Mirabel, I. F., & Rodríguez, L. F. 1994, Nature, 371, 46
Mirabel, I. F. and Rodríguez, L. F. 1996, in Solar and Astrophysical Magnetohydrodynamic Flows ed. K. Tsinganos (Kluwer Academic Publishers), 683
Reynolds, A. P., Parmar, A. N., Hakala, P. J., et al. 1999, A&AS, 134, 287
Rodríguez, L. F. 1999, in Star Formation 1999, Proceedings of Star Formation 1999, ed. N. R. O. T. Nakamoto, held in Nagoya, Japan, June 21–25, 1999, 257
Rodríguez, L. F., & Mirabel, I. F. 1998, A&A, 340, L47 (RM98)
Rodríguez, L. F., & Mirabel, I. F. 1999, A&J, 511, 398
Shahbaz, T., van der Hooft, F., Casares, J., Charles, P., & van Paradijs, J. 1999, MNRAS, 306, 89
Starck, J. L., Abergel, A., Aussel, H., et al. 1999, A&AS, 134, 135

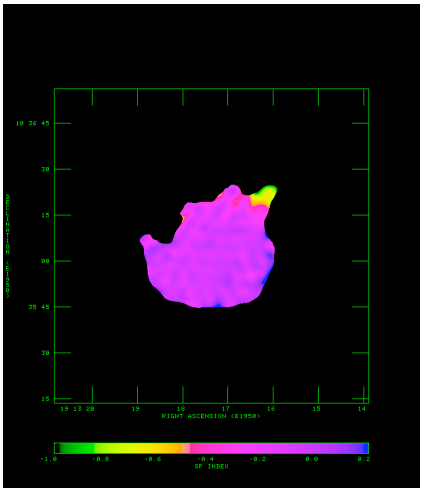

Fig. 3. Spectral index map of IRAS 19132+1035 made from the 20 and 6-cm maps. The color coding for the spectral index is given at the bottom of the figure. Note the negative, non-thermal spectral index of the jet feature to the northwest

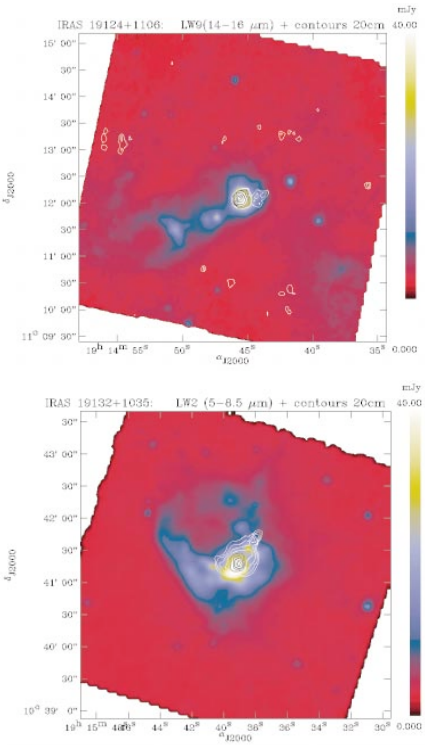

Fig. 6. Top: ISO map of the source IRAS 19124+1106, at $\lambda = 15$ μm, taken with the LW9 filter. Superimposed are the 20cm radio contours at 0.4, 0.6, 1, 2, 5, 10 and 15 mJy. Bottom: ISO map of the source IRAS 19132+1035, at $\lambda = 7$ μm, taken with the LW2 filter. Superimposed are the 20 cm radio contours at the levels 0.2, 0.4, 0.7, 1.2, 1.8, 2.5, 3, 4 and 5 mJy

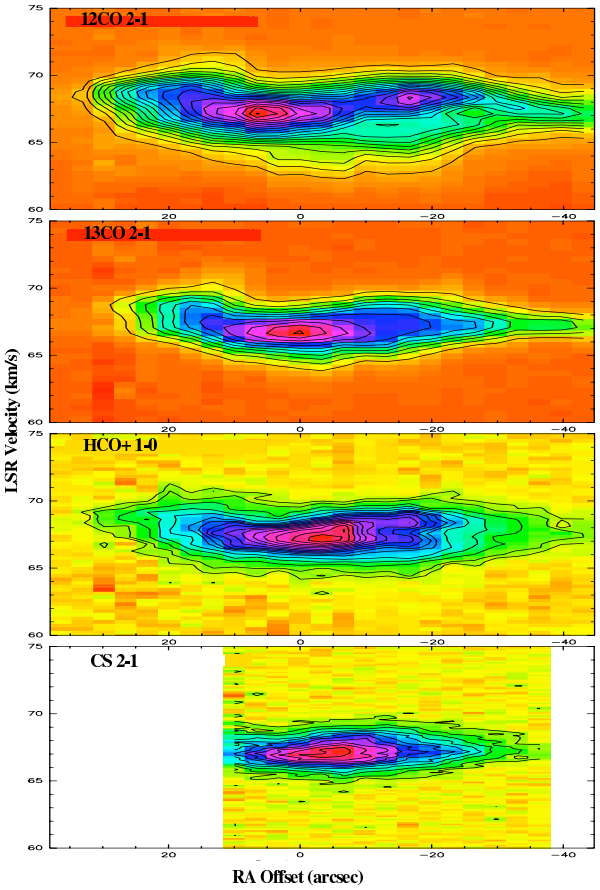

Fig. 7. Observations of IRAS 19132+1035. Offsets are relative to the position of maximum radio emission observed at the VLA. The black contours are antennae iso-temperature: ^{12}CO: $T_{\rm A}^{*} = -1$, and from 1 to 20 K separated by an interval of 1 K; ^{13}CO: $T_{\rm A}^{*} = -1$, and from 1 to 11 K separated by an interval of 1 K; H^{13}CO^{+}: $T_{\rm A}^{*} = -1$, and from 0.2 to 2.1 K separated by an interval of 0.1 K; CS: $T_{\rm A}^{*} = -1$, and from 0.2 to 2.2 K separated by an interval of 0.2 K

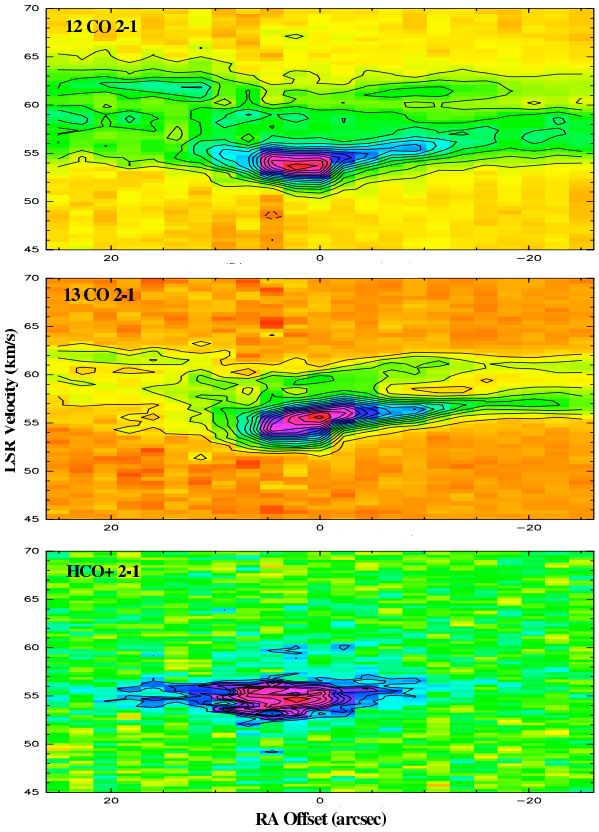

Fig. 10. Observations of IRAS 19124+1106. Offsets are relative to the position of maximum radio emission observed at the VLA. The black contours are antennae iso-temperatures: ^{12}CO: $T_{\rm A}^{*}$ = –1, and from 1 to 14 K separated by an interval of 1 K; ^{13}CO: –1 and from 0.5 to 8 K separated by an interval of 0.5 K; H^{13}CO^{+}: –1 0.3 0.4 and from 0.5 to 0.8 K separated by an interval of 0.05 K

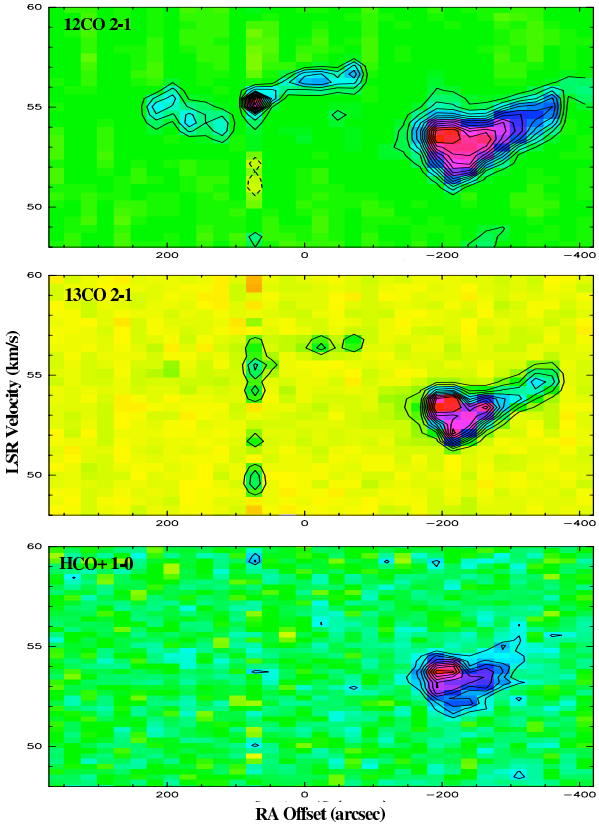

Fig. 12. Observations of W50, the supernova remnant shell surrounding SS 433. Offsets are relative to the position of the central source. The black contours are antennae iso-temperatures: ^{12}CO: $T_{\rm A}^{*}$ = –1 and from 1 to 12 K separated by 1 K; ^{13}CO: –1 and from 0.5 to 5 K separated by 1 K; H^{13}CO^{+}: –1 and from 0.2 to 1 K separated by 0.1 K

2.9.2 Observations en infrarouge proche de candidats trous noirs Galactiques

"Near-infrared observations of Galactic black hole candidates" par S. Chaty, I.F. Mirabel, P. Goldoni, S. Mereghetti, P.-A. Duc, J. Martí, and R.P. Mignani, 2002, MNRAS, 331, 1065

Dans cet article est publié un ensemble d'observations dans l'infrarouge proche de candidats trous noirs de notre Galaxie. Le but ultime de cette recherche est de découvrir la nature du système binaire, à savoir s'il s'agit d'un système binaire de faible ou de grande masse. Pour accéder à cette connaissance, il faut donc étudier la nature de l'étoile compagnon (voir le paragraphe 2.2.1 pour plus de détails).

Mon. Not. R. Astron. Soc. **331,** 1065–1071 (2002)

Near-infrared observations of Galactic black hole candidates★

S. Chaty,[1,2]† I. F. Mirabel,[2,3] P. Goldoni,[2] S. Mereghetti,[4] P.-A. Duc,[2] J. Martí[5] and R. P. Mignani[6]

[1]*Department of Physics and Astronomy, The Open University, Walton Hall, Milton Keynes MK7 6AA*
[2]*Service d'Astrophysique, DSM/DAPNIA/SAp, CEA/Saclay, L'Orme des Merisiers, Bât. 709, F-91 191 Gif-sur-Yvette, Cedex, France*
[3]*Instituto de Astronomía y Física del Espacio C. C. 67, Suc. 28. 1428, Buenos Aires, Argentina*
[4]*Istituto di Fisica Cosmica 'G. Occhialini', via Bassini 15, I-20133 Milano, Italy*
[5]*Departamento de Física, Escuela Politécnica Superior, Universidad de Jaén, Calle Virgen de la Cabeza, 2, E-23071 Jaén, Spain*
[6]*ESO, Karl-Schwarzschild Strasse 2, D-85748 Garching-bei-München, Germany*

Accepted 2001 December 7. Received 2001 December 4; in original form 2001 February 26

ABSTRACT

We report on several European Southern Observatory (ESO) near-infrared (NIR) observational campaigns aimed at understanding the nature of Galactic black hole candidates. Our results, including NIR photometry of the sources GRO J1655−40, GRS 1739−278, GRS 1716−249, GRS 1121−68 and GX 339−4, show that all the sources but GRO J1655−40 are consistent with low-mass stars as the companion star of the binary system.

By locating the counterparts on a colour–magnitude diagram (CMD), we better constrain the spectral type of the companion star of three of the systems considered here, and confirm a fourth one. The spectral types are respectively: M0–5 V for GRS 1716−249, F8–G2 III for GX 339−4 and later than F5 V for GRS 1739−278. We confirm the already known spectral type of the companion in GRS 1121−68 (K0–5 V). The location of GRO J1655−40 on the CMD is consistent with the sub-giant luminosity class and with this source crossing the Hertzsprung gap. However, a non-stellar emission seems to contribute to the NIR flux of this source.

Key words: stars: individual: GRO J1655−40 – stars: individual: GRS 1739−278 – stars: individual: GRS 1716−249 – stars: individual: GRS 1121−68 – stars: individual: GX 339−4 – infrared: stars.

1 INTRODUCTION

Optical follow-up observations of transient X-ray sources are fundamental to fully understand the nature of these systems and characterize the accretion. Most important, the measurement of their mass function through optical observations performed in quiescence is the best way to confirm the presence of a black hole (see, e.g., Charles 1999). Most of the bright transient X-ray sources discovered in recent years are located in the Galactic bulge region. Owing to the strong absorption present along this direction of the Galaxy, NIR observations are one of the best ways of constraining the properties of these systems. Furthermore, the disc emission is much weaker in the NIR band allowing a much better probe of the nature of the companion star. One approach is to perform spectroscopic observations (see, e.g., Bandyopadhyay et al. 1999), but for faint sources or for the sources lacking prominent emission lines, photometric observations are more efficient for deriving the NIR spectral energy distribution of the source (see, e.g., Chaty et al. 1996).

We observed the infrared counterparts of several Galactic bulge hard X-ray sources, in order to better constrain the spectral type of the mass donor star. Here we report on our results on five Galactic black hole candidates: GRO J1655−40, GRS 1739−278, GRS 1716−249, GRS 1121−68 and GX 339−4. Since all the sources we observed show variations, we concentrate on the magnitudes obtained around the emission minimum of our observations. Assuming that all the emission at this time came from the photosphere of the companion star, we can compare our data with infrared magnitudes of different stellar spectral types. Any anomalous colour distribution can then be related to the source spectral state, known from high-energy observations. Obviously, this method has limitations, since the infrared flux may be contaminated. There are a number of possible sources of contamination: emission from the accretion disc; X-ray heating of the secondary; the presence of ejected material, as was the case during flares of the superluminal source GRS 1915+105 (Mirabel et al. 1998); the presence of surrounding dust or of an extended

★ Based on observations collected at the European Southern Observatory, La Silla, Chile (proposals: 51.6-0018, 53.6-0015, 59.D-0719 & 61.D-0542.
†E-mail: S.Chaty@open.ac.uk

© 2002 RAS

© Royal Astronomical Society • Provided by the NASA Astrophysics Data System

atmosphere. None the less, since the emission provides at least an upper limit to the source flux, this constrains the nature of the companion star, and in addition can also give some information regarding sources of contamination.

In Section 2 we describe our method, and then go through each source in turn, summarizing the current knowledge and describing our observations and results. Discussion of the results and conclusions are in Section 3. Some of the results presented here were partly reported in Chaty (1998).

2 OBSERVATIONS AND RESULTS

The general parameters of these sources, including the distance and the absorption that will be used in this paper, are given in Table 1.

Table 1. Parameters of the sources: coordinates, fluxes in different energy domains, orbital period when known, distance, hydrogen column density N_H and absorption A_V. The variations, if any, are given by [*min* − *max*]. The error is given in the following line. The reader should refer to Table 2 to see the NIR variations of these sources. Concerning the distance and column density, we reported the interval in which they are constrained, including the error, by [*min*/*max*], and the value chosen in this paper is given in the following line. The references are: bai92: Bailyn (1992), bai95: Bailyn et al. (1995), bor96: Borozdin et al. (1996), cal92: Callanan et al. (1992), del91: Della Valle et al. (1991), del94: Della Valle et al. (1994), dox79: Doxsey et al. (1979), fen97: Fender et al. (1997), gre94: Greiner et al. (1994), gre96a: Greiner (1996), gre96b: Greiner et al. (1996), gri79: Grindlay (1979), hje95: Hjellming & Rupen (1995), hje96: Hjellming et al. (1996), kes91: Kesteven & Turtle (1991), mar97: Martí et al. (1997), mas96: Masetti et al. (1996), mcc92: McClintock et al. (1992), nag94: Nagase et al. (1994), oro97: Orosz & Bailyn (1997), pre91: Predehl et al. (1991), rub98: Rubin et al. (1998), sha97: Shahbaz et al. (1997), sha01: Shahbaz et al. (2001), tan93: Tanaka (1993)), zdz98: Zdziarski et al. (1998).

Source	Gal. coord.	$L_{2-10\,keV}$ erg s^{-1}	L_{opt} (m_V mag)	$L_{6\,cm}$ (mJy)	Period	Distance (kpc)	N_H (10^{22} cm^{-2})	A_V (mag)
GRO J1655−40	$l = 344.°98$	2×10^{37}	[17.4−16.8]	[0−2500]	2.62157 d	3.0	[0.3/0.8]	2.46
Nova Scorpii 94	$b = +2.°46$				±13 s		0.44	
	bai95	gre96a	oro97	hje95	oro97	gre96a	nag94	
GRS 1739−278	$l = 0.°66$	5×10^{37}	23.2	[1.1−4.7]	–	8.5	[1.1/4.8]	11.18
	$b = +1.°17$		±0.3				2.0	
	mar97	gre96b	mar97	hje96		mar97	gre96b/bor96	
GRS 1716−249	$l = 0.°20$	2×10^{38}	16.65	[0.5−4.4]	∼14.7 h	[2/2.8]	0.4	2.24
Nova Ophiuchi 93	$b = +6.°99$			±0.1		2.4		
	del94	del94	del94	del94	mas96	del94	tan93	
GRS 1121−68	$l = 295.°30$	10^{37}	[20.35−13.3]	[3−137]	10.5 h	[1.4/4]	0.22	1.23
Nova Muscae 91	$b = -7.°07$		±0.05			2.8		
	del91	del91	mcc92/del91	kes91	bai92	del91/sha97	gre94	
GX 339−4	$l = 338.°94$	2×10^{36}	[21−15]	[0−6.5]	14.8 h	[5.6/7]	0.6	3.72
4U 1658−48	$b = -4.°33$					5.6		
	dox79	rub98	dox79/gri79	fen97	cal92	sha01	pre91	zdz98

Table 2. Infrared observations of the sources. The exposure times were respectively 10, 10, 15 and 9 min in 1993, 1994, 1997 and 1998. The two magnitudes quoted for GRO J1655−40 in 1999 are the interval of the ellipsoidal variations. gre01: Greene et al. (2001); mar97: Martí et al. (1997); sha97: Shahbaz et al. (1997). 2.2: 2.2-m La Silla Telescope (ESO, Chile), with the instrument IRAC2b. AAT: 3.9-m Anglo-Australian Telescope (AAT), with the infrared array IRIS. CITO: Cerro Tololo Inter-American Observatory, with ANDICAM on the 1.0-m Yale telescope

Source	Date	JD	Tel	ref	J (1.25 μm)	H (1.65 μm)	K (2.2 μm)
GRO J1655−40	19/07/97	245 0648	2.2		13.43 ± 0.03	12.87 ± 0.02	12.07 ± 0.01
	07/10/99	245 1421	CTIO	gre01	13.7−14	–	13.1−13.4
GRS 1739−278	01/04/96	245 0174	2.2	mar97	16.3 ± 0.1	15.5 ± 0.2	14.9 ± 0.1
	20/07/97	245 0649	2.2		18.7 ± 0.6	–	15.4 ± 0.25
	07/07/98	245 1001	2.2		≥19.2	–	≥18.4
GRS 1716−249	08/07/94	244 9539	2.2		16.2 ± 0.3	–	15.5 ± 0.3
	19/07/97	245 0648	2.2		19.4 ± 1.2	19.2 ± 1	18.3 ± 1
	06/07/98	245 1000	2.2		≥19.38	≥18.72	≥17.77
GRS 1121−68	07/07/94	244 9540	2.2		17.5 ± 0.25	–	16.7 ± 0.25
	18/02/95	244 9766	AAT	sha97	–	17.12 ± 0.12	–
	19/07/97	245 0648	2.2		–	–	17.23 ± 0.25
	06/07/98	245 1000	2.2		≥17.5	17.2 ± 0.5	≥16.5
GX 339−4	03/06/93	244 9141	2.2		–	–	15.2 ± 0.3
	04/06/93	244 9142	2.2		16.2 ± 0.3	–	–
	06/07/94	244 9539	2.2		15.3 ± 0.1	14.9 ± 0.1	14.5 ± 0.1
	08/07/94	244 9541	2.2		15.4 ± 0.1	–	14.4 ± 0.1
	19/07/97	245 0648	2.2		14.21 ± 0.03	13.13 ± 0.01	12.41 ± 0.01

© Royal Astronomical Society • Provided by the NASA Astrophysics Data System

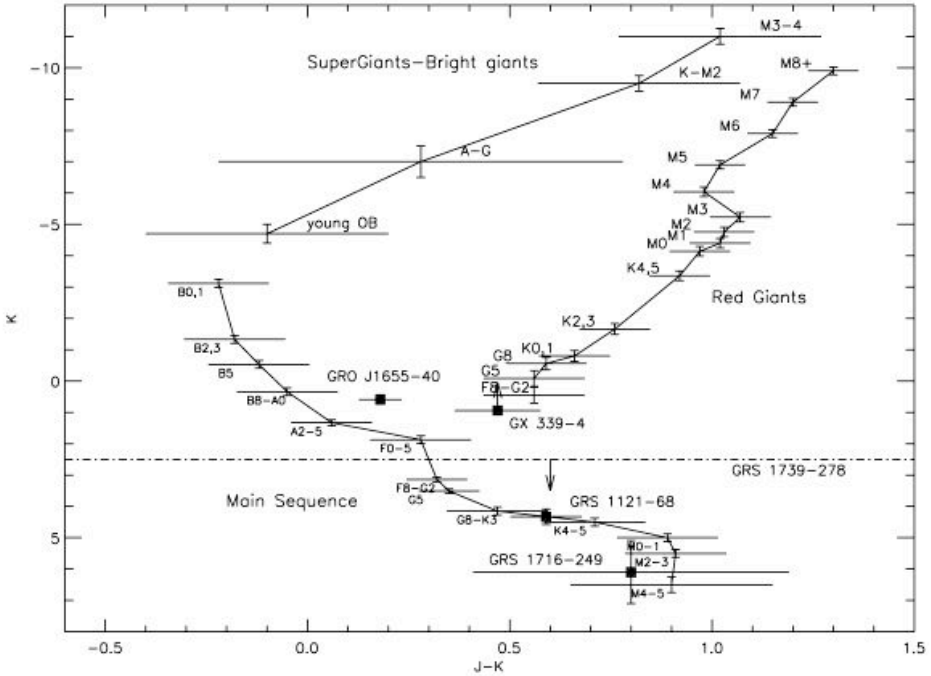

Figure 1. Near-infrared colour–magnitude diagram of Galactic stars (Ruelas-Mayorga 1991), with the superimposed counterparts of GRO J1655−40, GX 339−4, GRS 1716−249 and GRS 1121−68. The error bars on GRO J1655−40 are due to the ellipsoidal variations, and the position of GX 339−4 corresponds to the lower limit of the distance. The dash–dot line is the upper limit for GRS 1739−278 (see Section 2.2.2). This diagram shows that except for GRO J1655−40, which is consistent with an intermediate mass system, all sources are consistent with low-mass systems.

In Table 2 we give a log of the observations that were mostly obtained at the ESO/MPI (Max Planck Institute) 2.2-m telescope in La Silla (Chile) using the IRAC2b camera. The IRAC2b camera, mounted at the F/35 infrared adapter of the telescope, is a Rockwell 256 × 256 pixel Hg:Cd:Te NICMOS 3 infrared array detector. It was used with the lens C, providing an image scale of 0.49 arcsec pixel^{-1} and a field of 136 × 136 arcsec^2. The typical seeing for these observations was 1.2 arcsec.

Each final image is the result of the median-filtering of at least nine frames of 1 min exposure each (depending on the observations). An image of the sky was taken after each image of the object (offset by 30 arcsec), to allow subtraction of the infrared sky emission. The images were further treated by removal of the dark current and correction with a dome flat-field, and we carried out absolute photometry by calibration obtained with the observation of different standard stars. This work was performed with the IRAF procedures, using the DAOPHOT package for photometry in crowded fields.

To estimate the nature of the companion stars, we compare their NIR absolute magnitudes with those of template stars, using the relations between the magnitudes and the spectral type reported by Ruelas-Mayorga (1991) and Johnson (1966). Absolute magnitudes have been computed from the distances reported in Table 1, and correction of the reddening has been estimated from the absorption measured either from X-ray or optical observations, based on the relation $A_v(\mathrm{mag}) = 5.59 \times 10^{-22} N_{\mathrm{H}}$ (cm^{-2}) (Predehl & Schmitt 1995). The absorption in the infrared bands J, H and K is given by $A_J/A_V = 0.282$, $A_H/A_V = 0.175$ and $A_K/A_V = 0.112$ (Rieke & Lebofsky 1985). We report the absolute infrared magnitudes of our targets on a CMD in Fig. 1. We report in Fig. 2 the X-ray light curves of the sources as observed by the All Sky Monitor (ASM) of the *Rossi X-ray Timing Explorer* (*RXTE*) in the interval of our observations.

2.1 GRO J1655−40

2.1.1 Introduction

GRO J1655−40 (Nova Scorpii 1994) was discovered with BATSE as a hard X-ray nova (Zhang et al. 1994) and was the second superluminal source to be discovered in the Galaxy (Hjellming & Rupen 1995). The column density was estimated to be in the range $3–8 \times 10^{21}$ cm^{-2} (Hynes et al. 1998; Inoue et al. 1994; Greiner 1996; Inoue, Nagase & Ueda 1995). Following Hynes et al. (1998), we adopt the intermediate *ASCA* measurement of $N_{\mathrm{H}} = 4.4 \times 10^{21}$ cm^{-2} (Nagase et al. 1994). Assuming a mean extinction along the line of sight, the distance of the source has been estimated as 3 kpc (Greiner 1996). GRO J1655−40 has a bright variable optical counterpart (Bailyn et al. 1995): $B \sim [19–18.4]$, $V \sim [17.4–16.8]$, $R \sim [16.4–15.8]$ and $I \sim [15.4–14.8]$ (Orosz & Bailyn 1997, Greene et al. 2001). Comparing the spectrum of the source in quiescence with many standard stellar spectra of type M and K, the companion star was estimated to have a spectral type F3–F6. Following arguments on the size of the star compared to its Roche lobe, it was argued that the star was a sub-giant (Orosz & Bailyn 1997).

The masses of the two components of the system have been precisely determined thanks to optical observations: the compact object mass is in the range 4.1–7.9 $M_\odot$ (see Phillips et al. 1999; Shahbaz et al. 1999; Soria et al. 1998), making GRO J1655−40 a

© Royal Astronomical Society • Provided by the NASA Astrophysics Data System

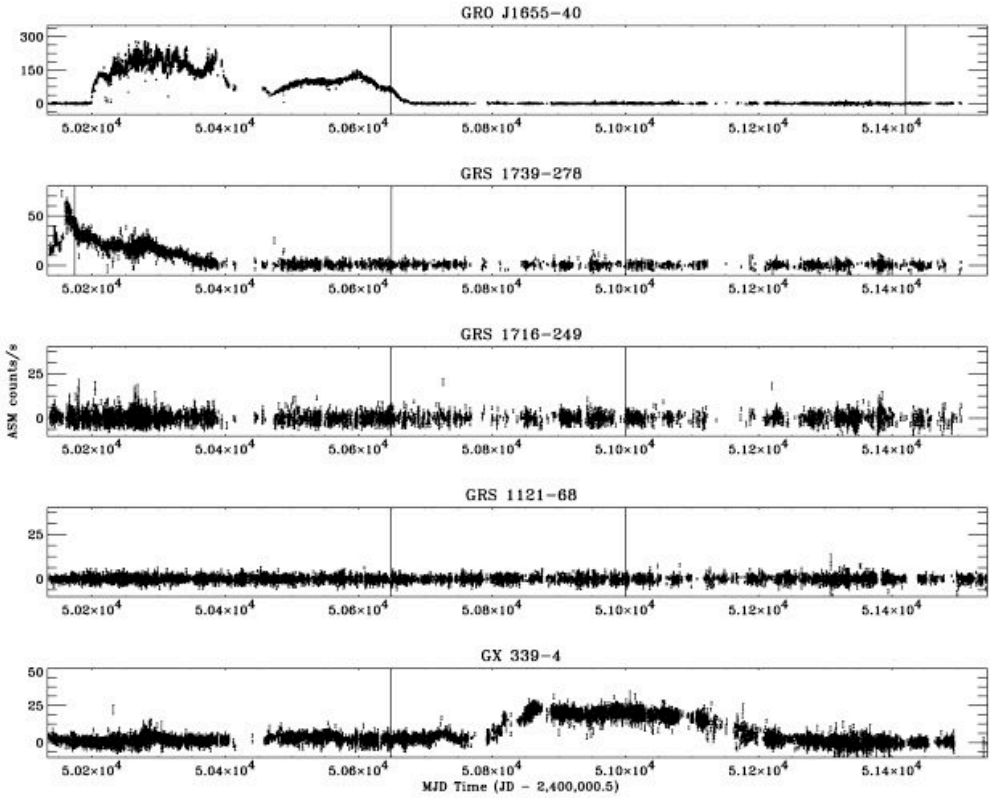

Figure 2. *RXTE/ASM* light curves of GRO J1655−40, GRS 1739−278, GRS 1716−249, GRS 1121−68 and GX 339−4 from 1996 February 20 to 1999 December 31. These quick-look results show the observations in the high-energy band 2−12 keV. The time of observations are indicated by the vertical lines. For comparison, the Crab nebula flux is about 75 ASM count s^{-1}. Concerning the uncertainties, the light curve of the Crab nebula gives a measure of the rms error of 5 per cent. However, the error bars are an underestimate of the error, if sources present different spectral shape than the Crab, are located in crowded regions, and/or for different reasons. Therefore, we point out that, although we show here all the sources for completeness, there is no flux detected by the *ASM* from the sources GRS 1716−249 and GRS 1121−68 during the period of observation shown here.

very good black hole candidate while the secondary star mass was estimated at 1.7−3.3 $M_\odot$, both with 95 per cent confidence (Shahbaz et al. 1999). The spectroscopic period is 2.62157 ± 0.00015 d (Orosz & Bailyn 1997), with a radial velocity semi-amplitude of $K = 215.5 \pm 2.4\,km\,s^{-1}$ and a mass function $f(M) = 2.73 \pm 0.09\,M_\odot$ (Shahbaz et al. 1999). The position of the secondary on the Hertzsprung−Russell diagram has been claimed to be consistent with a star of ∼2.3 $M_\odot$, which evolved from the main sequence, and is now mid-way between the main sequence and the beginning of the giant branch (Kolb et al. 1997).

2.1.2 *The observations*

As it has a bright optical counterpart, GRO J1655−40 has not been studied in great detail in NIR. In Table 2 we present the only NIR photometry which has been reported for this source, the counterpart being seen in the three filters. Our 1997 observations were performed at the end of an X-ray outburst (see Fig. 2), consequently the NIR emission is likely contaminated by an external source. We take therefore the magnitudes corresponding to the observations in an almost quiescent state by Greene et al. (2001). The absolute magnitudes are $M_J = 0.77 \pm 0.15$ and $M_K = 0.59 \pm 0.15$, the error quoted being due to the ellipsoidal variation.

We can see in Fig. 1 that the colours and magnitudes of the source in quiescence locate it on the CMD between the main sequence and giant star branches. This is therefore consistent with the sub-giant luminosity class derived by Orosz & Bailyn (1997) and also with the fact that the source is crossing the Hertzsprung gap. However, the position in the CMD shows a discrepancy with the F3−6 spectral type mentioned earlier. Therefore, there is an emission which is not of stellar origin in the NIR emission of GRO J1655−40. Furthermore, this emission does not seem to be due to irradiation since the ellipsoidal light curve of the 1999 observations is well fitted by a model without any disc (Greene et al. 2001). This discrepancy was also pointed out by Beer & Podsiadlowski (2002) in their recent analysis of its quiescent light curve. Monitoring of the NIR emission during different states of activity of this source will be necessary to reveal the origin of this emission.

2.2 GRS 1739−278

2.2.1 *Introduction*

GRS 1739−278 is a hard X-ray transient source, discovered by SIGMA on 1996 March 18 (Paul et al. 1996). The hardness of its spectrum immediately suggested that it was an X-ray nova

© Royal Astronomical Society • Provided by the NASA Astrophysics Data System

containing an accreting black hole. GRS 1739−278 seems to be located near the Galactic Centre, therefore at the distance of ~8.5 kpc (Martí et al. 1997). Vargas et al. (1997) inferred a peak luminosity of $8.6 \pm 2.0 \times 10^{36}$ erg s^{-1} in the 40–300 keV energy band. A variable radio source in the hard X-ray error box was proposed as the counterpart of GRS 1739−278 (Hjellming et al. 1996). A candidate optical/infrared counterpart was soon discovered at the position of the radio counterpart with a constant luminosity in a range of 0.2 mag on a time-scale of several weeks during 1996 (Mirabel et al. 1996). The observed optical magnitudes of GRS 1739−278 are $V = 23.2 \pm 0.3$, $R = 20.5 \pm 0.1$ and $I = 18.3 \pm 0.3$ (Martí et al. 1997). The magnitudes and colours of the companion star of GRS 1739−278 seemed to suggest either a low-mass X-ray binary with a giant companion, or a high-mass X-ray binary. The major problem in distinguishing between them was the great uncertainty in the value of the hydrogen column density (Martí et al. 1997). The GRS 1739−278 column density estimates range from $1.2 \pm 0.1 \times 10^{22}$ cm^{-2} (Greiner et al. 1996) to $4.1 \pm 0.7 \times 10^{22}$ cm^{-2} (Borozdin et al. 1996).

2.2.2 *The observations*

The counterpart is confirmed by our observations, showing a continuous decline in the luminosity of this source (see Table 2). The source dropped by ≥3 mag in both J and K between 1996 and 1998. For our analysis we will consider the magnitudes of 1998 as upper limits. Taking the assumed distance of $D \sim 8.5$ kpc, and the intermediate value of the column density $N_{\rm H} = 2.0 \times 10^{22}$ cm^{-2} (Martí et al. 1997), we can derive the absolute magnitudes respectively in the J and K bands: $M_J \geq 1.40$ and $M_K \geq 2.5$. $J - K$ is not constrained; this source lies below the line $M_K = 2.5$ on the CMD (Fig. 1). If GRS 1739 − 278's companion star is on the main sequence then it must be F5 V or later. By examining the optical and near-infrared colours of the system, Martí et al. (1997) derived two possibilities for the nature of the secondary star: either a luminous early/middle B type main-sequence star, or a middle G/early K giant star. Clearly, the implicit assumption by Martí et al. (1997) that the source had reached the quiescent level was premature at that time, and the magnitudes reported here allow us to better constrain the spectral type of this system.

2.3 GRS 1716−249

2.3.1 *Introduction*

GRS 1716−249 (Nova Ophiuchi 1993) is an X-ray transient source, detected on 1993 September 25 by SIGMA on *GRANAT* and by BATSE on the γ-ray observatory *Compton* (GRO J1719−24) (Ballet et al. 1993). Its light curve during the flare was very similar to the one of GRS 1121−68, and the (0.1–100 keV) X-ray luminosity at maximum was $L_X \sim 2.1 \times 10^{38}$ erg s^{-1}, which is close to the Eddington limit for a compact object of 1.6 $M_\odot$. This X-ray luminosity is similar to those of A 0620−00 and of GRS 1121−68, both of which are, like GRS 1716−249, transient radio sources. *ASCA* observations gave an estimation of the column density of $N_{\rm H} = 4 \times 10^{21}$ cm^{-2} (Tanaka 1993). The optical counterpart was soon discovered (Della Valle et al. 1994). From $V = 16.65$ Della Valle et al. (1994) derived that the companion star was a low-mass main-sequence star of spectral type ~K or later. This classification was consistent with the photometric and spectroscopic properties of this object.

The distance of this source remains subject to uncertainties. Estimated from the equivalent width of the NaD absorption lines the derived distance is $D \sim 2$ kpc, while taking the mean absolute magnitude at the maximum of the low-mass X-ray binaries, the distance has been estimated to be ~2.8 kpc, giving an absolute magnitude $M_V \geq 6$ (Della Valle et al. 1994). Masetti et al. (1996) discovered a superhump period at 14.7 h, therefore indicative of the orbital period at a few per cent accuracy. They estimated the mass respectively of the primary and the companion star to be ≥4.9 $M_\odot$ and 1.6 $M_\odot$. As noted by the authors, the secondary would then be substantially brighter than claimed by Della Valle et al. (1994), suggesting either the distance has been underestimated, or the secondary is a slightly evolved late-type star.

2.3.2 *The observations*

GRS 1716−249 was not detected in our 1998 observations (see Table 2), which were less sensitive that the 1997 ones in which the source was still visible at faint fluxes. Other observations with more powerful telescopes are needed in order to see if GRS 1716−249 has now reached its minimum, or if its luminosity is still decreasing. We will take for this analysis the magnitudes of 1997, assuming that they correspond to a minimum. Adopting a distance of $D \sim 2.4$ kpc and a column density $N_{\rm H} = 4 \times 10^{21}$ cm^{-2}, we can deduce the absolute magnitudes respectively in the J, H and K bands: $M_J = 6.9 \pm 1.2$, $M_H = 6.9 \pm 1$ and $M_K = 6.1 \pm 1$. This allows us to say that the counterpart is a main-sequence star of spectral type M0−5 V. This is not consistent with the possible masses of the companion star derived by Masetti et al. (1996). It seems likely therefore that the secondary is a slightly evolved late-type star. Therefore, our NIR absolute magnitudes are consistent with the absolute magnitude $M_V \geq 6$ of the optical counterpart identified by Della Valle et al. (1994), and furthermore allow us to constrain better the nature of the companion star.

2.4 GRS 1121−68

2.4.1 *Introduction*

This X-ray nova (Nova Muscae 1991) was discovered by *Ginga* on 1991 January 8 and by *GRANAT* on 1991 January 9 (Lund et al. 1991). The column density has been derived from *ROSAT* and *Ginga* observations: $N_{\rm H} = 2.2 \times 10^{21}$ cm^{-2} (Greiner et al. 1994). The optical counterpart was identified by Della Valle et al. (1991) with a star which rose from $R \sim 20$ to $V \sim 13.3$. The distance of this object has been subject to many uncertainties. The estimation from $E(B - V)$ gives $D = 2.3 \pm 2.1$ kpc, but using the linear relation between the equivalent width of the Na D line and the distance, a distance of $D = 1.4$ kpc could be derived (Della Valle et al. 1991). A distance of 2.8 kpc was estimated from observations in the H band, with an upper limit of 4 kpc (Shahbaz et al. 1997). Optical observations in quiescence, when its magnitude after dereddening was $B_0 = 19.8$, showed that GRS 1121−68 is a low-mass X-ray binary composed of a black hole of mass greater than ~3 $M_\odot$ and of a 0.7 $M_\odot$ low-mass companion of spectral type in the interval K0−4 V (Remillard et al. 1992). Further optical spectroscopic observations in quiescence suggested the donor star to be a low main-sequence star of spectral type of K3−5 V (Orosz et al. 1996) and allowed the detection of a 10.5-h orbital period (Bailyn 1992).

© Royal Astronomical Society • Provided by the NASA Astrophysics Data System

2.4.2 The observations

To estimate the nature of the binary system, we selected from Table 2 the magnitudes of the source near minimum luminosity, i.e. in 1994. Following Shahbaz et al. (1997), we choose 2.8 kpc as the most likely distance. The absolute magnitudes estimated in the J and K bands are respectively: $M_J = 4.92 \pm 0.25$ and $M_K = 4.33 \pm 0.25$. We can see on Fig. 1 that the location of this point on the CMD is consistent with the companion star being a main sequence star of spectral type K0–5 V, so fully consistent with the previous spectroscopic observations. This shows that in the case where the NIR only comes from the companion star, i.e. when there is no contamination, this method can be efficiently used to constrain the spectral type of the companion star.

2.5 GX 339−4

2.5.1 Introduction

GX 339−4 was discovered in 1973 by the 1–60 keV X-ray MIT detector on the satellite *OSO-7* (Markert et al. 1973). Because of its X-ray spectral behaviour similar to that of Cygnus X-1 and of its rapid temporal variations (from 0.010 to 10 s), GX 339−4 was classified as a black hole candidate (Tanaka & Shibazaki 1996). The counterpart of GX 339−4 was identified as a blue star of typical $V = 16.6$ mag but variable between $15 < V < 21$ mag (Doxsey et al. 1979; Grindlay 1979). A 14.8-h modulation of the optical luminosity was interpreted as the orbital period of the binary system (Callanan et al. 1992). However, because of the substantial optical emission from the accretion disc, the orbital parameters of GX 339−4 have not yet been established in order to clearly demonstrate that it is a black hole binary: the estimated mass of the compact object is $\leq 2.5\,M_\odot$ (Cowley et al. 1987).

Recent optical observations of GX 339−4 in an extended 'off' state allowed to estimate a lower limit to the distance of 5.6 kpc and an evolved spectral type later than F8 (Shahbaz et al. 2001). Zdziarski et al. (1998) derived the extinction $E(B-V) = 1.2 \pm 0.1$ mag which is equivalent to $A_v = 3.72 \pm 0.1$ mag (see e.g. Cardelli et al. 1989).

2.5.2 The observations

The results (Table 2) show that the luminosity changed appreciably during this period: by 2 mag in J; 1.8 in H; and ~2.6 in K. The X-ray activity is shown in Fig. 2. We take the magnitudes corresponding to the minimum luminosity of this source in 1993, the two observations being taken with a one day interval. At this date the source was not detected with BATSE: the source was certainly in a low state (off state or low/hard state; S. Corbel, private communication). Using the distance $D = 5.6$ kpc and an absorption of 3.72 mag in the V band, we obtain the absolute magnitudes respectively in the J and K bands: $M_J = 1.41 \pm 0.3$ and $M_K = 1.04 \pm 0.3$.

From the location of GX 339−4 on the CMD, it appears that the companion star is a red giant of spectral type F8–G2 III. This evolved type is consistent with the analysis of Shahbaz et al. (2001) and with the orbital period of 14.8 h of the binary system.

3 DISCUSSION AND GENERAL CONCLUSIONS

NIR photometry is useful for constraining the stellar spectral type of the secondary star when the source is heavily obscured at optical wavelengths. We have determined constraints on the stellar spectral type of the counterparts of the galactic black hole candidates GRO J1655−40, GRS 1739−278, GRS 1716−249, GRS 1121−68 and GX 339−4. Our results are summarized in Table 3 and displayed in Fig. 1. All the sources but GRO J1655−40 are consistent with low-mass stars as the companion star of the binary system. The position of each source in this CMD allows us to roughly estimate the evolutionary state of the secondary while its $J-K$ colour allows us to see if the infrared emission only comes from the photosphere of the companion or is contaminated by an external source.

The most important results are our constraints on the companion stars in GRS 1716−249, GRS 1121−68 and GX 339−4, along with the weaker constraint on the companion of GRS 1739−278. For the sources GRS 1716−249 and GRS 1121−68, the location in the CMD diagram is fully consistent with their magnitudes, indicating that the infrared emission mainly emanates from the companion star, without the need for any other source of emission.

Table 3. Results corresponding to the minimum of luminosity chosen during all our observations. We report here the absorption, and the corresponding derived absolute magnitudes. We note that the spectral type of GRO J1655−40 does not come from our analysis, but from preceding optical observations. Only the sub-giant luminosity class is consistent with the NIR observations.

Source	A_J	A_H	A_K	M_J (mag)	M_H	M_K	Spectral type
GRO J1655−40	1.10	0.59	0.44	0.77 ±0.15	– –	0.59 ±0.15	F3–6 IV
GRS 1739−278	3.15	1.96	1.25	≥1.40	–	≥2.5	≥F5 V
GRS 1716−249	0.63	0.39	0.25	6.9 ±1.2	6.9 ±1	6.1 ±1	M0–5 V
GRS 1121−68	0.35	0.22	0.14	4.92 ±0.25	–	4.33 ±0.25	K0–5 V
GX 339−4	1.05	0.65	0.42	1.41 ±0.3	–	1.04 ±0.3	F8–G2 III

© Royal Astronomical Society • Provided by the NASA Astrophysics Data System

The derived spectral types are respectively M0−5 V for GRS 1716−249, K0−5 V for GRS 1121−68 and F8−G2 III for GX 339−4. If the companion of GRS 1739−278 is on the main sequence then it must be a low-mass star of spectral type F5 V or later. Concerning GRO J1655−40, its location, between the main sequence and giant star branches, is consistent with the sub-giant luminosity class and with this source crossing the Hertzsprung gap. However, there is a discrepancy with the optically determined F3−6 spectral type, showing that a non-stellar emission seems to contribute to the NIR flux of this source.

ACKNOWLEDGMENTS

SC is grateful to U. Kolb for stimulating discussions, to J. A. Orosz for comments on GRO J1655−40, to C. A. Haswell for improving the language of the manuscript and for useful suggestions, and finally to S. J. Bell Burnell for a careful rereading of the manuscript. SC also acknowledges the anonymous referee for useful comments which allowed to improve the paper. We acknowledge the quick-look results provided by the ASM/*RXTE* team, used to produce Fig. 2. SC acknowledges support from grant F/00-180/A from the Leverhulme Trust. IFM acknowledges support from CONICET/Argentina. JM acknowledges partial support by DGICYT (PB97-0903) and by Junta de Andalucía (Spain).

REFERENCES

Bailyn C. D., 1992, ApJ, 391, 298
Bailyn C. D. et al., 1995, Nat, 374, 701
Ballet J., Denis M., Gilfanov M., Sunyaev R., Harmon B., Zhang S., Paciesas W., Fishman G., 1993, IAU Circ., 5874
Bandyopadhyay R. M., Shahbaz T., Charles P. A., Naylor T., 1999, MNRAS, 306, 417
Beer M. E., Podsiadlowski P., 2001, MNRAS, submitted (astro-ph/0109136)
Borozdin K., Alexandrovich N., Sunyaev R., 1996, IAU Circ., 6350
Callanan P. J., Charles P. A., Honey W. B., Thorstensen J. R., 1992, MNRAS, 259, 395
Cardelli J. A., Clayton G. C., Mathis J. S., 1989, ApJ, 345, 245
Charles P., 1999, in ASSL Vol. 234, Observational Evidence for the Black Holes in the Universe. p. 279
Chaty S., 1998, PhD thesis, Univ. Paris XI
Chaty S., Mirabel I. F., Duc P.-A., Wink J. E., Rodríguez L. F., 1996, A&A, 310, 825
Cowley A., Crampton D., Hutchings J., 1987, AJ, 93, 195
Della Valle M., Jarvis B., West R., 1991, Nat, 353, 50
Della Valle M., Mirabel I. F., Rodríguez L. F., 1994, A&A, 290, 803
Doxsey R., Grindlay J., Griffiths R., Bradt H., Johnston M., Leach R., Schwarz D., 1979, ApJ, 228, L67
Fender R., Spencer R., Newell S., Tzioumis A., 1997, MNRAS, 286, L29
Greene J., Bailyn C. D., Orosz J. A., 2001, ApJ, 554, 1290
Greiner J., 1996, A&AS, 120, 239
Greiner J., Hasinger G., Molendi S., Ebisawa K., 1994, A&A, 285, 509
Greiner J., Dennerl K., Predehl P., 1996, A&A, 314, L21
Grindlay J. E., 1979, ApJ, 232, L33
Hjellming R., Rupen M., 1995, Nat, 375, 464
Hjellming R., Rupen M., Martí J., Mirabel I., Rodríguez L., 1996, IAU Circ., 6383
Hynes R. I. et al., 1998, MNRAS, 300, 64
Inoue H., Nagase F., Ishida M., Sonobe T., Ueda Y., 1994, IAU Circ., 6063, 3
Inoue H., Nagase F., Ueda Y., 1995, IAU Circ., 6210, 2
Johnson H. L., 1966, ARA&A, 4, 193
Kesteven M., Turtle A., 1991, IAU Circ., 5181
Kolb U., King A., Ritter H., Frank J., 1997, ApJ, 485, L33
Lund N., Brandt S., Makino F., McNaught R. H., Jones A., Nelson N., West R. M., 1991, IAU Circ., 5161
Markert T. H., Canizares C. R., Clark G. W., Lewin W. H. G., Schnopper H. W., Sprott G. F., 1973, ApJ, 184, L67
Martí J., Mirabel I. F., Duc P.-A., Rodríguez L. F., 1997, A&A, 323, 158
Masetti N., Bianchini A., Bonibaker J., della Valle M., Vio R., 1996, A&A, 314, 123
McClintock J., Bailyn C., Remillard R., 1992, IAU Circ., 5499
Mirabel I. F., Marti J., Duc P. A., Rodríguez L. F., Duerbeck H., Benetti S., 1996, IAU Circ., 6427, 1
Mirabel I. F., Dhawan V., Chaty S., Rodríguez L. F., Martí J., Robinson C. R., Swank J., Geballe T. R., 1998, A&A, 330, L9
Nagase F., Inoue H., Kotani T., Ueda Y., 1994, IAU Circ., 6094, 2
Orosz J. A., Bailyn C. D., 1997, ApJ, 477, 876
Orosz J. A., Bailyn C. D., McClintock J. E., Remillard R. A., 1996, ApJ, 468, 380
Paul J., Bouchet L., Churazov E., Sunyaev R., 1996, IAU Circ., 6348
Phillips S. N., Shahbaz T., Podsiadlowski P., 1999, MNRAS, 304, 839
Predehl P., Braeuninger H., Burkert W., Schmitt J., 1991, A&A, 246, L40
Predehl P., Schmitt J., 1995, A&A, 293, 889
Remillard R. A., McClintock J. E., Bailyn C. D., 1992, ApJ, 399, L145
Rieke G., Lebofsky M., 1985, ApJ, 288, 618
Rubin B., Harmon B., Paciesas W., Robinson C., Zhang S., Fishman G., 1998, ApJ, 492, L67
Ruelas-Mayorga R. A., 1991, Rev. Mex. Astron. Astrofis., 22, 27
Shahbaz T., Fender R., Charles P. A., 2001, A&A, 376, L17
Shahbaz T., Naylor T., Charles P., 1997, MNRAS, 285, 607
Shahbaz T., van der Hooft F., Casares J., Charles P., van Paradijs J., 1999, MNRAS, 306, 89
Soria R., Wickramasinghe D. T., Hunstead R. W., Wu K., 1998, ApJ, 495, L95
Tanaka Y., 1993, IAU Circ., 5877
Tanaka Y., Shibazaki N., 1996, ARA&A, 34, 607
Vargas M. et al., 1997, ApJ, 476, L23
Zdziarski A. A., Poutanen J., Mikolajewska J., Gierlinski M., Ebisawa K., Johnson W. N., 1998, MNRAS, 301, 435
Zhang S. N., Wilson C. A., Harmon B. A., Fishman G. J., Wilson R. B., Paciesas W. S., Scott M., Rubin B. C., 1994, IAU Circ., 6046, 1

This paper has been typeset from a TEX/LATEX file prepared by the author.

© Royal Astronomical Society • Provided by the NASA Astrophysics Data System

2.9.3 Observations en optique et infrarouge proche du microquasar V4641 Sgr au cours du sursaut de septembre 1999

"Optical and near-infrared observations of the microquasar V4641 Sgr during the 1999 September outburst" par S. Chaty, P.A. Charles, J. Martí, I.F. Mirabel, L.F. Rodríguez and T. Shahbaz, 2003, MNRAS, 343, 169

Cet article rassemble des observations en optique et infrarouge proche du microquasar V4641 Sgr, qui a présenté un sursaut d'activité très rapide, devenant pendant une journée la source de rayons X la plus brillante du ciel. Ses variations sont tout aussi spectaculaires dans les domaines optique et infrarouge. Cette source a été proposée comme un possible microblazar par certains auteurs, cependant ceci est encore sujet à débat (voir le paragraphe 2.6 pour plus de détails).

Mon. Not. R. Astron. Soc. **343,** 169–174 (2003)

Optical and near-infrared observations of the microquasar V4641 Sgr during the 1999 September outburst

S. Chaty,[1,2⋆] P. A. Charles,[3] J. Martí,[4] I. F. Mirabel,[2,5] L. F. Rodríguez[6] and T. Shahbaz[7]

[1]*Department of Physics and Astronomy, The Open University, Walton Hall, Milton Keynes MK7 6AA*
[2]*Université Paris 7 and Service d'Astrophysique, CEA-Saclay, F-91191 Gif-sur-Yvette, Cedex, France*
[3]*Department of Physics and Astronomy, University of Southampton, Southampton SO17 1BJ*
[4]*Departamento de Física, Escuela Politécnica Superior, Universidad de Jaén, C/Virgen de la Cabeza, 2, E-23071 Jaén, Spain*
[5]*Instituto de Astronomía y Física del Espacio, Conicet, CC 67, Suc. 28 (1428), Buenos Aires, Argentina*
[6]*Instituto de Astronomía, Campus UNAM, Morelia, Michoacán, 58190, Mexico*
[7]*Instituto de Astrofísica de Canarias, C/Vía Láctea, s/n, 38205, La Laguna, Tenerife, Spain*

Accepted 2003 March 20. Received 2003 March 10; in original form 2002 July 19

ABSTRACT

We present photometric and spectroscopic optical and near-infrared (NIR) observations taken during the outburst of the microquasar V4641 Sgr = SAX J1819.3 − 2525 in 1999 September. We observed an increase in the $J - K_s$ colour between 5 and 8 d after the outburst, which we interpret as likely evidence for the presence of dust around the source. We also observed an extraordinarily strong, broad and variable Hα line, with a velocity width of 4560 km s^{-1}, suggesting the presence of a high-velocity outflow component. We constrain the distance of the system between 3 and 8 kpc, locating it further away than previously derived from radio observations, but consistent with results from Orosz et al. We then discuss the nature of this system, showing that the companion star is either a B3–A2 main-sequence star or a B3–A2 subgiant crossing the Hertzsprung gap. The system is therefore an intermediate- or high-mass X-ray binary system (IMXB or HMXB). The distance derived by these optical/NIR observations implies that the jets observed by Hjellming et al. would then exhibit apparent velocities of $\sim$10c. We finally discuss the possibility of an interaction between the jets and surroundings of the source, and also of this source being a 'microblazar'.

Key words: stars: individual: V4641 Sgr – stars: individual: SAX J1819.3 − 2525 – stars: individual: XTE J1819 − 254 – ISM: jets and outflows – infrared: stars – X-rays: binaries.

1 INTRODUCTION

The variable V4641 Sgr attracted considerable attention after the detection of a giant optical outburst on 1999 September 15.7 UT, from $V \sim 14.0$ to 8.8 (Stubbings 1999). Located in the direction of the Galactic bulge (Galactic coordinates $l, b = 6.^{\circ}77, -4.^{\circ}79$), V4641 Sgr was initially confused with GM Sgr, and most of the references to this X-ray source are reported under that name. After this confusion was clarified by Williams (1999) and Samus et al. (1999), the source was then designated V4641 Sgr (Kazarovets, Samus & Durlevich 2000). The X-ray source XTE J1819 − 254 flared, from 1.6 to 12.2 Crab on 1999 September 14, as observed by *RXTE* in the 2–12 keV band, through a brief but dramatic eruption (at its peak it was the brightest X-ray source in the sky), its position being coincident with the optical transient (Smith, Levine & Morgan 1999). Less than 10 h later, the source was fainter than 50 mCrab. It was also identified with the previously detected faint X-ray transient, SAX J1819.3 − 2525, discovered by *BeppoSAX* on 1999 February 20 (flux 0.012–0.3 Crab, in't Zand et al. 1999), and independently detected by *RXTE* (designated XTE J1819 − 254) 2 d earlier (Markwardt, Swank & Marshall 1999), with a flux between 3 and 80 mCrab in the 2–10 keV energy band.

Three other flares followed, each lasting less than 2 h in the X-ray band, some of the fastest events ever seen. The observations by *RXTE* (Wijnands & van der Klis 2000) allowed the observation of some strong flaring activity: fluctuations by factors of 4 and 500 on time-scales of seconds and minutes, respectively. The spectrum was harder when the count rate was decreasing. During quiescent intervals, the X-ray spectrum was much softer. No quasi-periodic object (QPO) was detected, but some red noise at < 30 Hz was present. The observations by *BeppoSAX* (in't Zand et al. 2000) revealed a strong Fe-K emission line at 6.85 ± 0.02 keV, interpreted as fluorescence from a highly photoionized plasma. A

⋆E-mail: chaty@cea.fr

© 2003 RAS

© Royal Astronomical Society • Provided by the NASA Astrophysics Data System

later analysis of the same data by Miller et al. (2002) derived an inclination of $i = 43^\circ \pm 15^\circ$. No sign of eclipse or periodic signal due to a binary orbit was detected during 19 h, which was consistent with the 2.5-d period found later. The best fit for the column density was $N_{\rm H} = 0.05 \pm 0.02 \times 10^{22}$ cm^{-2} (in't Zand et al. 2000).

The VLA radio telescope detected a strong radio source (0.4 Jy) at 4.9 GHz on September 16.02 UT, at the position of the variable star ($\alpha = 18^{\rm h}19^{\rm m}21\overset{\rm s}{.}636$, $\delta = -25^\circ\,24'\,25\overset{''}{.}6$ J2000; Hjellming, Rupen & Mioduszewski 1999a). The flux rapidly decreased on a time-scale of hours, with an e-fold decay time of 0.6 d. The source was resolved, with the presence of an elongation extending 0.25 arcsec between 0.6 and 1.2 d after the huge X-ray flare. On September 17.93, 22.00 and 24.1 UT, the elongation was at the same position (Hjellming, Rupen & Mioduszewski 1999b), implying a proper motion of 0.5 arcsec d^{-1}, but this is strongly dependent upon the time of the ejection. This allowed the source to be classified as a new microquasar (for a review on jet sources see Mirabel & Rodríguez 1999). An H I absorption measurement towards the source implied a distance $d >$ 0.4 kpc (Hjellming et al. 2000), and these authors proposed a likely distance of 0.5 kpc.

Goranskij (1978, 1990) reported a single short outburst of V4641 Sgr in 1978, recorded on Moscow photographic plates, reaching B = 12.4. He also suggested the possible presence of a periodicity of 0.7365 d from analysis of the quiescent data. Another optical outburst occurred in 1999 August (Watanabe 1999), followed by a period of apparently increasing activity. Kato et al. (1999) reported unusual optical activity 6 d prior to the 1999 September giant optical and X-ray outburst, through a ∼1 mag increase combined with a modulation of 2.5 d, which they claimed to correspond to the orbital period. More recently, during 2002 May, V4641 Sgr was active again, exhibiting in the optical chaotic 0.5-mag variations on a time-scale of a few seconds. In the radio domain, the source was also flaring on time-scales of minutes to hours (Rupen, VSNET communication). Details of this outburst are reported at http://vsnet.kusastro.kyoto-u.ac.jp/vsnet/Xray/v4641sgr02.html.

Orosz et al. (2001) derived from European Southern Observatory (ESO) spectroscopic optical observations of the source in quiescence a mass function of 2.74 ± 0.12 M$_\odot$, which, combined with their information on the inclination ($60^\circ \leqslant i \leqslant 70^\circ$, Orosz et al. 2001), makes V4641 Sgr a black hole system with a mass of the compact object in the range $8.73 \leqslant M_1 \leqslant 11.70$ M$_\odot$. They also found a spectroscopic period of 2.816 78 ± 0.000 56 d, and assuming an extinction $E(B - V) = 0.32 \pm 0.10$, quoted a distance between 7.40 and 12.31 kpc (note that this is larger than previously derived by Orosz et al. 2000).

Through our on-going ESO Target of Opportunity (ToO) programme aimed at observing new X-ray flaring sources, we quickly obtained near-infrared (NIR) and optical imaging and spectroscopic observations of this new microquasar during the 1999 outburst and we followed it during its decline from 1999 September to 2000 June. We report the observations, including the first near-infrared observations of this source yet published, in Section 2, and the results and a discussion are given in Section 3.

2 OBSERVATIONS

All the observations took place at European Southern Observatory, La Silla, Chile, except the NIR spectroscopy of 1999 September 17, performed at United Kingdom Infrared Telescope (UKIRT), Hawaii, and the optical imaging of 2000 June 24, performed at the 1.23-m telescope of the Centro Astronómico Hispano Alemán at Calar Alto, with the CCD optical camera and exposure times between 30 and 60 s (more details on these observations are reported in Martí et al. 2001). The log of the optical and NIR imaging and spectroscopic observations is reported, respectively, in Tables 1 and 2.

The optical observations were performed with the 3.58-m New Technology Telescope (NTT) equipped with the spectrograph and imaging camera EMMI RILD. We imaged the source in V, R and I filters, and took spectra with grism no 1, which gave a resolving power of $R \sim 270$. The exposure times were ∼5 min with each filter for the imaging and 15 min for the spectroscopy. The ESO NIR observations were performed with the NTT, equipped with the infrared spectrograph and imaging camera Son of ISAAC (SOFI). The imaging was taken through J, H and $K_{\rm s}$ filters, in combination with the Large Field, giving a 4.9×4.9 arcmin^2 field of view, with a plate scale of 0.292 arcsec pixel^{-1}. The spectra were taken with the

Table 1. Log of the optical observations.

Date	MJD	Inst	B	V	R	I
1999 September 16	51438.1	EMMI	–	13.60 ± 0.10	13.30 ± 0.10	13.20 ± 0.09
1999 September 17	51439.0	EMMI	–	13.51 ± 0.06	–	13.04 ± 0.08
1999 September 28	51450.0	EMMI	–	13.65 ± 0.06	13.60 ± 0.01	13.25 ± 0.02
1999 September 29	51451.0	EMMI	–	13.87 ± 0.06	–	13.41 ± 0.08
2000 March 21	51625.4	EMMI	–	13.89 ± 0.11	13.71 ± 0.08	13.43 ± 0.04
2000 June 24	51719.5	CA	14.32 ± 0.05	13.98 ± 0.05	13.77 ± 0.05	13.46 ± 0.05

Table 2. Log of the NIR observations. The $K_{\rm s}$ magnitude of September 17 has been estimated from the CGS4 spectrum shown in Fig. 5 (Charles et al. 1999).

Date	MJD	Inst	J	H	$K_{\rm s}$	$J - K_{\rm s}$
1999 September 17	51438.2	CGS4	–	–	12.5 ± 0.3	–
1999 September 19	51441.0	SOFI	13.14 ± 0.11	–	13.10 ± 0.04	0.04 ± 0.15
1999 September 20	51441.98	SOFI	12.99 ± 0.03	–	12.81 ± 0.06	0.18 ± 0.08
1999 September 22	51443.97	SOFI	13.93 ± 0.03	–	13.06 ± 0.06	0.87 ± 0.09
1999 September 24	51445.98	SOFI	14.03 ± 0.03	–	13.72 ± 0.03	0.31 ± 0.06
2000 March 20	51623.42	SOFI	12.94 ± 0.01	12.849 ± 0.01	12.72 ± 0.01	0.22 ± 0.02

© Royal Astronomical Society • Provided by the NASA Astrophysics Data System

Grism Red (GR) and 1-arcsec slit. The exposure times were chosen as 9 min for the NIR imaging (10 alternate images of 60-s exposure time each offset from the centre by nearly 30 arcsec to the east, north, west and south, following the standard procedure) and 15 min for the NIR spectroscopy. The combined magnitudes are the result of these 10 co-added and median filtered 60-s exposures, with random offsets and direction between each exposure. The conditions were photometric for most of the observations, the seeing being typically 0.8 arcsec, and the airmass was always between 1.006 and 1.2.

The images were processed using IRAF reduction software. Each of the images were corrected by a normalized dome-flat field, and the NIR images were sky-subtracted by a sky image created from combining with a median filter a total of 10 consecutive images.

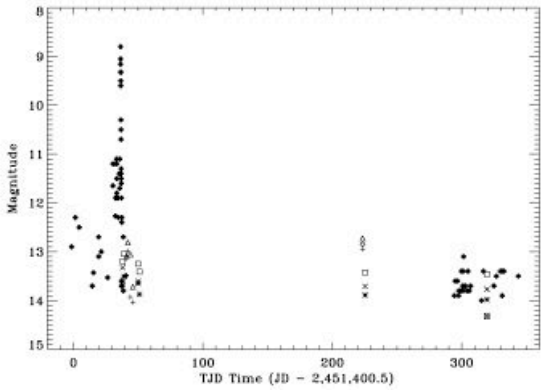

Figure 1. Optical and NIR observations of V4641 Sgr from 1999 August to 2000 July. filled circles, VSNET; boxed crosses, *B*; asterisks, *V*; crosses, *R*; open squares, *I*; pluses, *J*; open diamonds, *H*; open triangles, K_s magnitudes. We first see a brief optical outburst, which occurred in 1999 August, followed by the beginning of a modulation on 1999 September 8 UT (= MJD 51429.5), which leads to the giant outburst of 1999 September 15.7 UT (= MJD 51437). The error bars of our observations are smaller than the size of the symbols used. TJD of 0 corresponds to 1999 August 10.

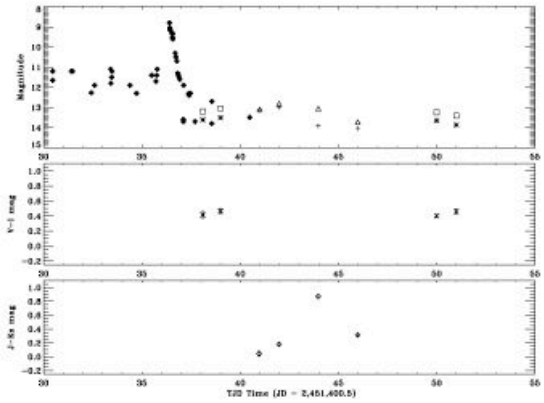

Figure 2. Top: optical light curve of V4641 Sgr during the outburst: middle, $V - I$ colour; bottom, $J - K_s$ colour. filled circles, VSNET; asterisks, *V*; open squares, *I*; pluses, *J*; open triangles, K_s; crosses, $V - I$; open diamonds, $J - K_s$ magnitudes. The error bars of our observations are smaller than the size of the symbols used. TJD of 0 corresponds to 1999 August 10.

The data were then analysed using the IRAF reduction task APPHOT, taking different apertures depending on the photometric conditions of the night.

Absolute photometry was performed using two standard stars from the new system of faint near-infrared standard stars (Persson et al. 1998): no 9164 (HST P565-C) and 9178 (HST S808-C). Each exposure of these standard stars is the average of 7×1.2 s integration time frames, and this is repeated five times by offsetting the images of 1 arcmin to the north-west, north-east, south-east and south-west from the central position, and the final image is the co-add and median filter of those individual frames.

The optical and NIR photometry is plotted in Fig. 1. An enlargement during the outburst interval (September 19–24) and also the $V - I$ and $J - K_s$ colours are shown in Fig. 2. The flux-calibrated optical spectra are shown in Fig. 3, and again in normalized form in Fig. 4. The flux-calibrated NIR spectrum is shown in Fig. 5. The strengths of the spectral features are given in Table 3.

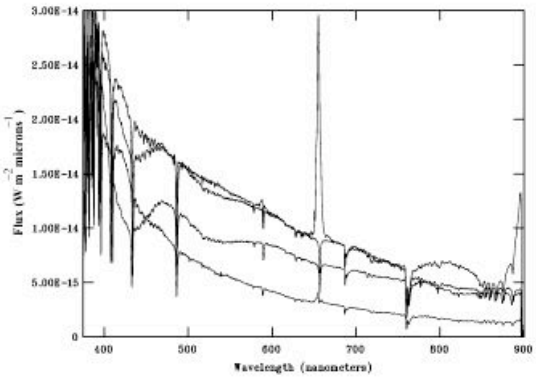

Figure 3. Flux-calibrated optical spectra of V4641 Sgr during the outburst. From top to bottom the spectra were taken, respectively, on 1999 September 17.05, 18.0, 29.0 and 30.0 UT.

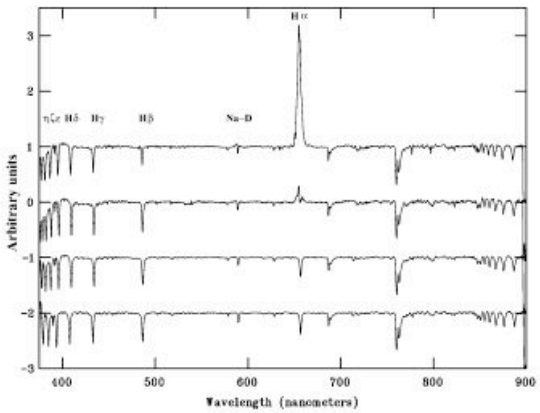

Figure 4. Normalized and offset optical spectra of V4641 Sgr during the outburst. Same order as in Fig. 3. The unlabelled absorption features are telluric ones.

© 2003 RAS, MNRAS **343,** 169–174

© Royal Astronomical Society • Provided by the NASA Astrophysics Data System

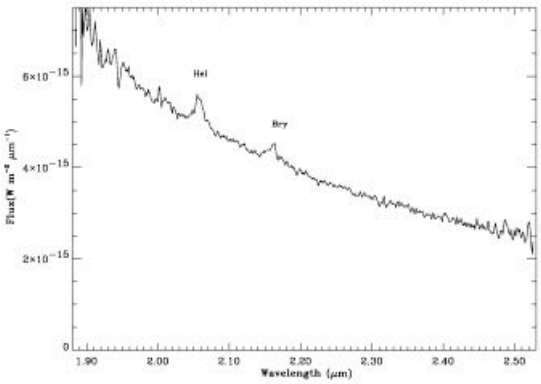

Figure 5. Flux calibrated NIR spectrum of V4641 Sgr during outburst.

3 RESULTS AND DISCUSSION

After the big outburst (from $V = 14$ to 8.8), there was still some flaring activity in V, R and I with variations of ∼0.5 mag but no significant change in the colours. In the NIR there was also some flaring activity with variation of ∼1 mag in J and K_s, and a significant change in $J - K_s$ during the post-outburst interval (between 5 and 8 d after the giant burst, see Fig. 2). This change is due to a much faster decrease in the J band than in K_s, and over more than 3 d, the source emits mainly in K_s. This can be explained either by the emission of a jet, of the appearance of heated dust, or even by the interaction with the interstellar medium, as we will discuss later. We had observed the same phenomenon in GRS 1915+105, which we had interpreted as evidence for an extended cocoon of dust around the source (Mirabel et al. 1996). Later observations by Chandra (Lee et al. 2002) and *ISO* (Fuchs, Mirabel & Ogley 2001) confirmed this presence of dust.

The first striking fact is that on a time-scale of 1 d, the optical lines were changing from emission to absorption. All the H lines from the Balmer series from Hα to Hκ are detected. The Hα emission line is extraordinarily strong and broad: 1 d after the outburst, its equivalent width was ∼100 Å, corresponding to a full width at zero intensity (FWZI) of 4560 km s^{-1} with a blue wing. This broad Hα emission line suggests the presence of a high-velocity outflow component. The single peaked Hα profile suggests a low inclination angle.

There was also a weak He I 5876- Å line. The Na D absorption-line equivalent width of 0.45 Å gives $E(B - V) = 0.25$ (following Munari & Zwitter 1997) implying $N_{\rm H} = 0.14 \times 10^{22}$ cm^{-2} (following Bohlin, Savage & Drake 1978). This value of $E(B - V)$ is consistent with that derived by Wagner (1999). The second interesting fact is that there is a strong variability of the lines, as already pointed out by Garcia, McClintock & Callanan (1999), particularly in Hα, Hβ and also He I. The He II 4680- Å line was claimed to be prominent in emission closer to the outburst time by Ayani, Peiris & Clarke Institute (1999). Since we could not detect it, this line was also very variable. We can also note the blue continuum, visible on the flux-calibrated spectra, suggesting a contribution from an accretion disc or from a corona.

In the NIR, the He I (2.06 μm) and Brγ (2.17 μm) lines were observed as broad emission lines by Charles, Shahbaz & Geballe (1999), in a K-band (1.9–2.5 μm) low-resolution (2.5-nm) UKIRT (+CGS4) spectrum taken on 1999 September 17.22 UT and shown in Fig. 5. He I exhibited an equivalent width of 2.1 nm and Brγ of 1.4 nm, characteristic of large-mass X-ray binaries (LMXBs) and with widths of FWZI = 5900 km s^{-1}. The Brγ profile shows a clearly extended blue wing, again suggesting a high-velocity outflow component. The continuum of our NIR spectrum taken on 1999 September 19 was also blue. However, our NIR spectrum shows only very faint He I (equivalent width 6 Å), He II and Brγ (equivalent width 1 Å) lines, which therefore appear to also be strongly variable.

The broad, strong emission lines and their variability suggest the presence of a high-velocity outflow component (∼6000 km s^{-1})

Table 3. Optical emission and absorption line parameters observed during the outburst of V4641 Sgr. The flux is in W m^{-2} μm^{-1}. The typical uncertainties are ∼0.05 Å for Obs. λ and ∼0.1 Å for equivalent width (EW) and FWHM.

Date 1999 Sept.	Line Id. (Å)	Obs. λ (Å)	Flux	EW (Å)	FWHM (Å)
17.05 UT	Hα 6562	6565.23	9.0e−13	−99.8	45.5
	Hβ 4861	4861.13	−7.4e−14	4.6	13.1
	Hγ 4340	4340.13	−1.3e−13	6.8	14.1
	Hδ 4101	4101.83	−1.6e−13	7.6	14.4
	Hϵ 3970	3970.16	−2.1e−13	8.1	14.2
	Hζ 3889	3889.63	−2.2e−13	8.0	14.3
	Hη 3835	3835.78	−2.0e−13	7.5	13.4
	Hθ 3797	3798.43	−1.5e−13	6.2	11.1
	Hι 3770	3770.67	−1.2e−13	5.6	11.5
	Hκ 3750	3750.51	−8.0e−14	4.2	9.1
	Na D 5780	5785.60	−5.6e−15	0.5	8.9
	Na D 5890	5898.32	−2.2e−14	1.8	10.1
18.0 UT	Hα 6562	6544.13	2.1e−14	−6.9	30.2
	Hβ 4861	4861.08	−7.4e−14	9.5	16.5
	Hγ 4340	4340.82	−1.3e−13	9.2	15.0
	Hδ 4101	4102.20	−1.5e−13	8.7	13.8
	Hϵ 3970	3970.20	−1.9e−13	9.4	14.1
	Hζ 3889	3889.35	−2.0e−13	9.0	14.4
	Hη 3835	3835.29	−1.7e−13	7.7	11.9
	Hθ 3797	3797.50	−1.5e−13	6.8	10.8
	Hι 3770	3770.00	−1.4e−13	6.4	10.6
	Hκ 3750	3749.41	−1.0e−13	5.6	8.6
	Na D 5780	5778.29	−1.8e−15	0.4	9.0
	Na D 5890	5891.15	−8.6e−15	2.0	11.4
29.0 UT	Hα 6562	6561.86	−6.4e−14	7.0	20.1
	Hβ 4861	4861.12	−1.5e−13	9.4	19.2
	Hγ 4340	4339.74	−1.6e−13	9.5	17.8
	Hδ 4101	4101.30	−2.1e−13	9.9	17.6
	Hϵ 3970	3970.08	−2.4e−13	9.4	15.6
	Hζ 3889	3889.70	−2.2e−13	8.7	14.9
	Hη 3835	3835.86	−1.8e−13	8.6	14.3
	Hθ 3797	3799.13	−1.1e−13	6.5	11.4
	Hι 3770	3772.49	−5.9e−14	4.8	10.7
	Hκ 3750	3751.25	−3.9e−14	4.0	9.8
	Na D 5780	5779.41	−6.4e−15	0.5	11.6
	Na D 5890	5891.97	−2.3e−14	2.0	12.8
30.0 UT	Hα 6562	6562.02	−5.0e−14	7.4	19.3
	Hβ 4861	4860.46	−1.0e−13	10.1	19.9
	Hγ 4340	4340.10	−1.1e−13	9.3	16.8
	Hδ 4101	4101.53	−1.1e−13	9.3	16.1
	Hϵ 3970	3969.79	−1.3e−13	9.4	14.9
	Hζ 3889	3889.43	−1.3e−13	8.6	14.6
	Hη 3835	3835.40	−1.2e−13	8.6	14.2
	Hθ 3797	3798.30	−7.9e−14	6.3	11.2
	Hι 3770	3770.75	−5.6e−14	5.2	10.3
	Hκ 3750	3749.82	−4.4e−14	4.8	11.0
	Na D 5780	5777.52	−4.0e−15	0.5	9.1
	Na D 5890	5890.62	−2.1e−14	2.7	14.1

© Royal Astronomical Society • Provided by the NASA Astrophysics Data System

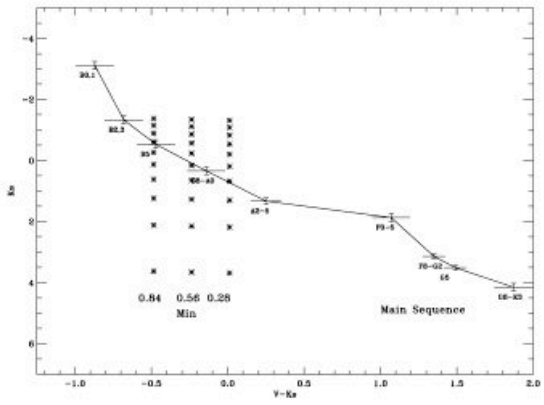

Figure 6. Colour–magnitude $[V - K_s, K_s]$ diagram. asterisks, minimum absolute magnitudes of V4641 Sgr; pluses, typical main-sequence stars (Ruelas-Mayorga 1991). 0.28, 0.56 and 0.84 are the visual absorptions corresponding, respectively, to column densities of 0.05, 0.1 and 0.15 $\times$ 10^{22} cm^{-2}. From bottom to top the asterisks correspond, respectively, to a distance of the source increasing from 1 to 10 kpc. This shows that the distance is constrained to $3 < d < 8$ kpc, and that the spectral type is in this case consistent with an early-type B3–A2 main-sequence star.

blown off from the accretion of matter on to the compact object (see, for example, Schulz & Brandt 2002). It is likely that this outflow component forms an expanding plasma shell or even a cocoon which could have produced the change we observed in the $J - K_s$ colour.

3.1 Nature of the system: the companion star

We plot on a colour–magnitude diagram (CMD, Fig. 6) the optical and NIR absolute magnitudes when the source was faint. In this figure the absolute magnitudes are computed with three different values of absorption and 10 different values of distance from 1 to 10 kpc. The values of the absorption cover the range $N_H = 0.05$ to 0.15×10^{22} cm^{-2}, derived by combining our observations and *BeppoSAX* results (in't Zand et al. 2000). If we constrain the companion to be a main-sequence star, its location on the CMD, taking into account the uncertainty in the absorption, suggests that the distance is constrained to $3 < d < 8$ kpc. Its spectral type is (in this case) consistent with an early-type B3–A2 V main-sequence star.

However, it is interesting to note that the companion star could be crossing the Hertzsprung gap, given the similarities of the system with GRO J1655 − 40 (Chaty et al. (2002); Kolb et al. (1997); Kolb, private communication), although the mass of the companion star in the case of V4641 Sgr is larger than for GRO J1655 − 40. In this view, the location on the CMD would be above the main sequence, the distance of the object could then be larger than $3 < d < 8$ kpc, with this range becoming its minimum distance, and the spectral type would be B3–A2 IV. In both possibilities the mass is constrained between $2 < M < 10$ $M_\odot$, suggesting that it is an IMXB or a HMXB. This is consistent with the A2 V type at 6.1 kpc derived by Orosz et al. (2001).

3.2 Interaction with surroundings

If the elongation seen in the radio was a moving component, the proper motion was between $224 < \mu < 788$ mas d^{-1} depending on the exact time of the ejection. For the sake of discussion, we will take the lower limit, assuming that the approaching (brighter) condensation exhibits $\mu_a = 224$ mas d^{-1}. Since from our results $D \geqslant 3$ kpc, we conclude that the apparent velocity in the plane of the sky would be strongly superluminal, with v_a greater than $4c$. However, no movement of this elongation was detected between September 16.02 and 24.1. This suggests an interaction between matter ejected before the X-ray outburst and its surroundings at 0.25 arcsec $\geqslant 1.5 \times 10^3$ au from the source at the distance of 6 kpc. This is possible if the ejections began to take place at least 10 d before the radio detection, e.g. on September 8, and we can see from Fig. 2 that the source was already showing some activity in the optical range at this date. This interaction with the surroundings is supported by the increase in $J - K_s$ between 5 and 8 d after the outburst.

It then seems that the source activity was not as sporadic as it appears at first glance. Indeed, a previous optical outburst occurred in 1999 August (Watanabe 1999), and *RXTE* detected this source ~270 d before the giant outburst (in't Zand et al. 2000). Furthermore, at least 5 d before the giant outburst, V4641 Sgr was, in the optical band, continuously 2 mag brighter than immediately after, showing a modulation at the orbital period, and with no X-ray emission (typical upper limit of 12 mCrab, in't Zand et al. 2000). All of these facts, combined with the high X-ray variability, show that, even if the Orosz et al. (2001) results suggest that the accretion in the system is of Roche lobe overflow type, there is also the possibility that mass transfer in this source is occurring through irregular wind accretion from the companion star. This would not be too surprising in the case of an IMXB/HMXB system.

At a distance of 6 kpc, the maximum luminosity of the source is ~4×10^{38} erg s^{-1}, which is close to the Eddington limit of a ~10− $M_\odot$ object (1.3×10^{39} erg s^{-1}). If the mass transfer rate is highly super-Eddington such a wind could arise. This wind could be the reason why surrounding matter was present, allowing the interaction between further ejections and surrounding matter to take place. In this case, the companion star is more likely to be a main-sequence star (Kolb, private communication).

In addition, it is interesting to note that Martí et al. (2001) observed V4641 Sgr in order to look for minute to hour variability, discovering 0.05-mag variability on a time-scale of hours. Among the different interpretations considered, they suggested that this variability could originate in an extended corona surrounding the jets, by analogy with SS 433 (Zwitter, Calvani & D'Odorico 1991). Subsequent X-ray analysis also suggest the existence of an extended envelope or outflow surrounding the source (see Revnivtsev et al. 2002a,b). Finally, we mention the possibility that the dust forming this corona could have its origin directly in the jets of X-ray binaries, as in supernova ejecta. If this interaction between the ejections and the surrounding medium is confirmed, this source could therefore be added to the short list of microquasars where such an interaction has been detected (see, e.g., Chaty et al. 2001; Mirabel & Rodríguez 1999).

3.3 A 'microblazar'?

However, V4641 Sgr seems different with respect to other microquasars, since in the latter the outbursts normally fade more slowly, often lasting for weeks. The only similar outburst was that from CI Cam, with an e-fold decay time of ~0.5 d (Belloni et al. 1999), its companion star being a symbiotic B star with an irregular wind. Therefore, V4641 Sgr resembles several sources in behaviour, but differs from them in other aspects: one possibility to explain this is that it might be a 'microblazar', i.e. a microquasar for which the

© Royal Astronomical Society • Provided by the NASA Astrophysics Data System

jet is pointing towards the observer (see, e.g., Mirabel & Rodríguez 1999). Orosz et al. (2001) already mentioned this possibility, based on the new determination of the distance of V4641 Sgr. Indeed, assuming that the radio component was moving (Hjellming et al. 2000) implies that the jets would then exhibit apparent velocities of $\sim 10c$. These large apparent velocities are consistent with the rapid variability in the radio range reported during the 2002 outburst (Rupen, VSNET communication), implying either extremely large Lorentz factors or a jet coming from a microblazar. If V4641 Sgr were a microblazar, we also point out that we would not expect to see any Doppler-shifted emission lines from the ejecta, which is consistent with our spectra (Fig. 4), as these lines would have a much larger blue/redshift than high-inclination systems. For instance, assuming a plausible jet velocity of $0.95c$ with $\leqslant 10^{\circ}$ angle to the line of sight (as expected in a microblazar), the Doppler-shifted wavelengths of Hα would appear in the ultraviolet ($\sim$1000 Å) and NIR ($\sim$4 μm) for the approaching and receding jet, respectively.

4 CONCLUSIONS

We have observed the source V4641 Sgr during its 1999 September outburst at optical and NIR wavelengths, deriving $E(B-V) = 0.25$ and $N_{\rm H} = 0.14 \times 10^{22}$ cm^{-2}. By plotting our optical and NIR colours we have constrained the distance to $3 < D < 8$ kpc, and the companion star would then be a main-sequence star of spectral type B3–A2 V. If the source is crossing the Hertzsprung gap, this determination of the distance would become its minimum distance, and the spectral type of the companion star would be B3–A2 IV. The system is therefore an IMXB or a HMXB. From the NIR colours, and the optical spectra, there is a strong suggestion of interaction of the ejecta of the source with its surroundings. This surrounding matter could have originated from an outflow created by fluctuations around the central object, and in this case the companion star would more certainly be a main-sequence star. Further observations would be useful to confirm the existence of surrounding matter. The bright X-ray outburst of V4641 Sgr in 1999 could have remained unnoticed, because of its very short duration, if the optical detection had not occurred, and if the source was not located so close. This means that there must be many similar (black hole?) objects in our Galaxy, most of them unnoticed when in outburst, because of their short duration and faint flares. This type of source will be a target of prime importance for present and future high-energy missions, such as for example the *INTEGRAL* telescope.

ACKNOWLEDGMENTS

This work was based on observations collected at the European Southern Observatory, La Silla, Chile, under proposal numbers ESO 63.H-0493 and 64.H-0382. SC thanks Rob Hynes for pointing out this new flaring source during 1999 September, Bob Hjellming for all the spontaneous communications he gave on the radio observations of this source and Ulrich Kolb for many stimulating discussions. SC is very grateful to the ESO staff and particularly to the NTT team (Leonardo Vanzi, Olivier Hainaut, Stéphane Brillant and Vanessa Doublier), for their availability and skills in performing service observations for Target of Opportunity programmes (63.H-0493 and 64.H-0382, PI S. Chaty). PAC and TS thank Tom Geballe for his assistance in obtaining the UKIRT CGS4 spectrum. The United Kingdom Infrared Telescope is operated by the Joint Astronomy Centre on behalf of the UK Particle Physics and Astronomy Research Council. We thank VSNET for all their alerts on V4641 Sgr and their optical data used in Figs 1 and 2. SC and PAC gratefully acknowledge support from grant no F/00-180/A from the Leverhulme Trust. JM acknowledges partial support by DGICYT (AYA2001-3092) and by Junta de Andalucía (Spain), he has also been aided in this work by an Henri Chrétien International Research Grant administered by the American Astronomical Society. IFM acknowledges support from grant PIP 0049/98 and Fundacion Antorchas.

REFERENCES

Ayani K., Peiris T.C., Clarke Institute C., 1999, IAU Circ., 7254, 1
Belloni T. et al., 1999, ApJ, 527, 345
Bohlin R.C., Savage B.D., Drake J.F., 1978, ApJ, 224, 132
Charles P.A., Shahbaz T., Geballe T., 1999, IAU Circ., 7267, 2
Chaty S., Rodríguez L.F., Mirabel I.F., Geballe T., Fuchs Y., 2001, A&A, 366, 1041
Chaty S. et al., 2002, MNRAS, 331, 1065
Fuchs Y., Mirabel I.F., Ogley R.N., 2001, Ap&SS Suppl., 276, 99
Garcia M.R., McClintock J.E., Callanan P.J., 1999, IAU Circ., 7271, 4
Goranskij V.P., 1978, Astron. Tsirkulyar, 1024, 3
Goranskij V.P., 1990, Info. Bull. on variable stars, 3464, 1
Hjellming R.M., Rupen M.P., Mioduszewski A.J., 1999a, IAU Circ., 7254, 2
Hjellming R.M., Rupen M.P., Mioduszewski A.J., 1999b, IAU Circ., 7265, 2
Hjellming R.M. et al., 2000, ApJ, 544, 977
in't Zand J., Heise J., Bazzano A., Cocchi M., Di Ciolo L., Muller J.M., 1999, IAU Circ. 7119
in't Zand J.J.M. et al., 2000, A&A, 357, 520
Kato T., Uemura M., Stubbings R., Watanabe T., Monard B., 1999, Inf. Bull. Variable Stars, 4777, 1
Kazarovets E.V., Samus N.N., Durlevich O.V., 2000, Inf. Bull. Variable Stars, 4870, 1
Kolb U., King A., Ritter H., Frank J., 1997, ApJ, 485, L33
Lee J.C., Reynolds C.S., Remillard R., Schulz N.S., Blackman E.G., Fabian A.G., 2002, ApJ, 567, 1102
Markwardt C., Swank J., Marshall F., 1999, IAU Circ. 7120
Martí J., Zamanov R., Paredes J.M., Ribo M., 2001, Inf. Bull. Variable Stars, 5036, 1
Miller J.M. et al., 2002, ApJ, 577, L15
Mirabel I., Rodríguez L., 1999, ARA&A, 37, 409
Mirabel I.F. et al., 1996, ApJ, 472, L111
Munari U., Zwitter T., 1997, A&A, 318, 269
Orosz J.A. et al., 2000, IAU Circ., 7440, 1
Orosz J.A. et al., 2001, ApJ, 555, 489
Persson S.E., Murphy D.C., Krzeminski W., Roth M., Rieke M.J., 1998, AJ, 116, 2475
Revnivtsev M., Gilfanov M., Churazov E., Sunyaev R., 2002a, A&A, 391, 1013
Revnivtsev M., Sunyaev R., Gilfanov M., Churazov E., 2002b, A&A, 385, 904
Ruelas-Mayorga R.A., 1991, Rev. Mex. Astron. Astrofis., 22, 27
Samus N.N., Hazen M., Williams D., Welther B., Williams G.V., Hoffleit D., 1999, IAU Circ., 7277, 1
Schulz N.S., Brandt W.N., 2002, ApJ, 572, 971
Smith D., Levine A., Morgan E., 1999, IAU Circ. 7253
Stubbings R., 1999, IAU Circ. 7253
Wagner R.M., 1999, IAU Circ., 7276, 2
Watanabe T., 1999, VSOLJ Variable Star Bull., 34, 3
Wijnands R., van der Klis M., 2000, ApJ, 528, L93
Williams G.V., 1999, IAU Circ., 7253, 3
Zwitter T., Calvani M., D'Odorico S., 1991, A&A, 251, 92

This paper has been typeset from a TEX/LATEX file prepared by the author.

© Royal Astronomical Society • Provided by the NASA Astrophysics Data System

2.9.4 Observations multi-longueurs d'onde révélant l'évolution du sursaut du trou noir XTE J1118+480

"Multiwavelength observations revealing the evolution of the outburst of the black hole XTE J1118+480" par S. Chaty, C.A. Haswell, J. Malzac, R.I. Hynes, C.R. Shrader and W. Cui, 2003, MNRAS, 346, 689

Cet article rassemble des observations multi-longueurs d'onde du candidat trou noir et microquasar XTE J1118+480, couvrant l'ensemble du spectre électro-magnétique, depuis la radio jusqu'aux hautes énergies. La position inhabituelle de cette source, en dehors du plan de la Galaxie, lui confère une absorption très faible sur la ligne de visée, ce qui a permis de l'observer dans des domaines qui jusqu'ici étaient restés inexplorés, comme par exemple dans les domaines UV et extrême-UV. Cette richesse d'observations a permis de modéliser très précisément cet objet, et en particulier ses différentes composantes : le disque d'accrétion multicolore, l'étoile compagnon et une composante non-thermique présente de la radio aux hautes énergies (voir le paragraphe 2.4.2 pour plus de détails).

Mon. Not. R. Astron. Soc. **346,** 689–703 (2003)

Multiwavelength observations revealing the evolution of the outburst of the black hole XTE J1118+480

S. Chaty,[1,2,3★] C. A. Haswell,[3] J. Malzac,[4,5] R. I. Hynes,[6,7] C. R. Shrader[8] and W. Cui[9]

[1] *Université Paris 7, Fédération APC, 2 place Jussieu, 75005 Paris, France*
[2] *Service d'Astrophysique, DSM/DAPNIA/SAp, CEA-Saclay, Bat. 709, L'Orme des Merisiers F-91 191 Gif-sur-Yvette Cedex, France*
[3] *Department of Physics and Astronomy, The Open University, Walton Hall, Milton Keynes MK7 6AA*
[4] *Institute of Astronomy, Madingley Road, Cambridge CB3 0HA*
[5] *Osservatorio Astronomico di Brera, Via Brera, 28, 20121 Milano, Italy*
[6] *Astronomy department, The University of Texas at Austin, 1 University Station C1400, Austin, TX 78712-0259, USA*
[7] *Department of Physics and Astronomy, University of Southampton, Southampton SO17 1BJ*
[8] *Laboratory for High-Energy Astrophysics, NASA Goddard Space Flight Centre, Greenbelt, MD 20771, USA*
[9] *Department of Physics, Purdue University, 1396 Physics Building, West Lafayette, IN 47907-1396, USA*

Accepted 2003 August 12. Received 2003 July 10; in original form 2002 August 30

ABSTRACT

We report multiwavelength observations of the soft X-ray transient XTE J1118+480, which we observed with UKIRT, *Hubble Space Telescope* (*HST*), *RXTE*, *Extreme Ultraviolet Explorer* (*EUVE*) and many other instruments and facilities. Adding radio (Ryle Telescope, VLA), submillimetre (JCMT) and X-ray (*Chandra* and *SAX*) data from the literature, we assembled the most complete spectral energy distribution (SED) of this source yet published. We followed the evolution of this source for 1 yr, including six observations performed during the outburst, and one observation at the end of the outburst. Because of the unusually high galactic latitude of XTE J1118+480, it suffers from very low extinction, and its SED is nearly complete, including extreme ultraviolet observations. XTE J1118+480 exhibits an unusually low low/hard state (estimated inner radius of $350R_S$) and a strong non-thermal contribution in the radio to optical domain, which is likely to be due to synchrotron emission. We discuss the interstellar column density and show that it is low, between 0.80 and 1.30×10^{20} cm^{-2}. We analyse the evolution of the SED during the outburst, including the contributions from the companion star, the accretion disc, the outflow, and relating irradiation and variability of the source in different bands to the SED. We find no significant spectral variability during the outburst evolution, consistent with the presence of a steady outflow. An analysis of its outflow to accretion energy ratio suggests that the microquasar XTE J1118+480 is analogous to radio-quiet quasars. This, combined with the inverted spectrum from radio to optical, makes XTE J1118+480 very similar to other microquasar sources, e.g. GRS 1915+105 and GX 339−4 in their low/hard state. We model the high-energy emission with a hot disc model, and discuss different accretion models for the broad-band spectrum of XTE J1118+480.

Key words: accretion, accretion discs – stars: individual: XTE J1118+480 – dust, extinction – infrared: stars – ultraviolet: stars – X-rays: binaries.

1 INTRODUCTION

Soft X-ray transients (SXTs), also called X-ray novae, are a class of low-mass X-ray binaries (LMXBs). Among this class of sources, more than 70 per cent are thought to contain black holes (Charles 1998). The compact object accretes matter through an accretion disc from a low-mass star via Roche lobe overflow. The history of these sources is characterized by long periods of quiescence, typically lasting decades, punctuated by very dramatic outbursts. SXTs are usually discovered in X-rays, but outbursts are visible at every wavelength and, in particular, are often accompanied by radio activity. A typical outburst is characterized by soft X-ray emission dominated by thermal emission from the hot inner accretion disc, and optical/ultraviolet (UV) emission produced by reprocessing of X-rays.

★E-mail: chaty@cea.fr

© 2003 RAS

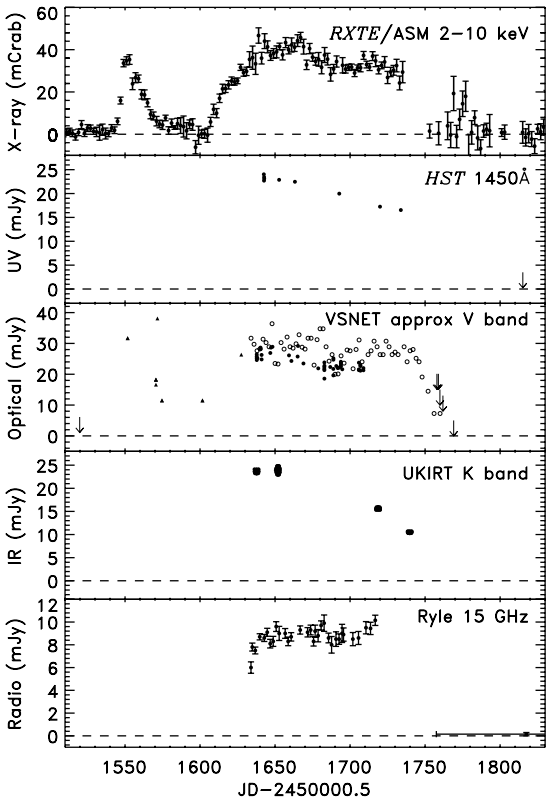

Figure 1. Multiwavelength light curve of XTE J1118+480 in 2000: the six epochs of our observations are indicated by the *HST* points. The top panel shows *RXTE/ASM* 2–10 keV count rates in 2-d averages. Periods with too few dwells for a precise measurement have been excluded for clarity. The second panel is *HST*/STIS far-UV fluxes derived from E140M spectroscopy and an upper limit from the late G140L observation. The middle panel shows VSNET optical measurements (http://www.kusastro.kyoto-u.ac.jp/vsnet/Summary/j1118.html). Open circles are 2-d averages of visual estimates. Solid circles are individual electronic measurements. Triangles are pre-discovery photographic measurements. Arrows are upper limits from all of these sources. The fourth panel shows *K*-band fluxes measured by UKIRT. The lower panel shows 15-GHz radio data from the Ryle Telescope (http://www.mrao.cam.ac.uk/~guy/J1118+480/J1118480.list). The last point is based on the average flux from 2000 August to November.

One such source, XTE J1118+480, was discovered by *RXTE* on 2000 March 29 at the galactic coordinates $(l, b) = (157.62^\circ, +62.32^\circ)$ (Remillard et al. 2000) as a weak (39 mCrab), slowly rising X-ray source, the post-analysis revealing an outburst in 2000 January, with a similar brightness. The outburst history of the source is shown in Fig. 1.

The optical counterpart of XTE J1118+480 in outburst was a 13th magnitude star, coincident with a 18.8-mag object in the USNO catalogue (Uemura et al. 2000). Its optical spectrum was typical of X-ray novae in outburst (Garcia et al. 2000). An infrared counterpart was rapidly identified thereafter (Chaty et al. 2000). Taking the X-ray and optical fluxes given above, it is clear that this system exhibits a very low X-ray to optical flux ratio of 5 (in f_ν, see Remillard et al. 2000; Uemura et al. 2000), compared with a typical value of 500 for SXTs in outburst (see e.g. Tanaka & Shibazaki 1996). A weak 4.1-h (0.170 82-d) photometric modulation was rapidly discovered (Cook et al. 2000), associated with the orbital period of the source, or possibly a superhump period (Uemura et al. 2000). XTE J1118+480 therefore exhibits the shortest orbital period among the black hole candidates. Wagner et al. (2001) took spectra of this source near quiescence and observed a period 0.5 per cent smaller than during the outburst. They suggested that this difference was due to the presence of superhump modulations during the outburst, later confirmed by Zurita et al. (2002). Flickering with an amplitude of ~0.4 mag, and also a quasi-periodic oscillation (QPO) at 10 s, was observed in the optical, in the UV (Haswell et al. 2000) and also in the X-ray range (Revnivtsev, Sunyaev & Borozdin 2000), with an evolving frequency (Wood et al. 2000). A faint radio counterpart was detected at 6.2 mJy, but no jet feature could be spatially resolved (see Fender et al. 2001). Optical observations of the source in quiescence led to the determination of a large value of the mass function, $f(M) = 5.9 \pm 0.4\ \mathrm{M}_\odot$, suggesting that the compact object is a black hole (McClintock et al. 2001a; Wagner et al. 2001).

The location of XTE J1118+480 at an unusually high galactic latitude ($b = +62^\circ$) in the direction to the Lockman Hole implies that there is a very low absorption along the line of sight of the source. Garcia et al. (2000) estimated $E(B-V) \sim 0.024$, leading to a column density of $N_H \sim 1.4 \times 10^{20}$ cm^{-2}. The column density has been estimated as $N_H \sim 0.75$–1×10^{20} cm^{-2} (Hynes et al. 2000), $N_H \sim 0.75$–1.15×10^{20} cm^{-2} (Esin et al. 2001), $N_H \sim 1$–1.3×10^{20} cm^{-2} (McClintock et al. 2001b), $N_H \sim 0.7$–1.5×10^{20} cm^{-2} (Frontera et al. 2001a), all nearly consistent with the mean value in the direction of the Lockman Hole (0.5–1.5×10^{20} cm^{-2}, see Hynes et al. 2000). From analysis of optical spectra, Dubus et al. (2001) derived $N_H \sim 1.77$–4.47×10^{20} cm^{-2}. As we see, the exact column density is still a matter of debate, and will be one of the points discussed in this paper. McClintock et al. (2001a) estimated a distance of 1.8 ± 0.6 kpc, consistent with the value of $\geqslant 1.5$ kpc derived by Uemura et al. (2000).

We triggered our multi-epoch multiwavelength override program with the *Hubble Space Telescope* (*HST*)/*RXTE*/UKIRT to obtain early observations of this system. We also requested Director's Discretionary *Extreme Ultraviolet Explorer* (*EUVE*) observations because of the low value of interstellar absorption, and obtained the first ultraviolet [extreme ultraviolet (EUV)] spectrum of an SXT (Hynes et al. 2000; Mauche et al. 2000). We therefore have unprecedented broad-band coverage, of more than 80 per cent of the electromagnetic spectrum from the radio ($\lambda = 21$cm) to the γ-rays (180 keV) [see the spectral energy distribution (SED) in Fig. 4 in Section 2.8]. The analysis of one of the epochs (corresponding in this paper to epoch 1, see Fig. 3 in Section 2.8) was described in Hynes et al. (2000) and we will briefly report here the main results (see also Esin et al. 2001 and McClintock et al. 2001b for an analysis of epoch 2). The corresponding SED suggested that the system was exhibiting a low-state mini-outburst, with the inner radius of the accretion disc estimated to be rather large, with a maximum value at $\sim 2000 R_\mathrm{s}$ ($R_\mathrm{s} = 2GM/c^2$; the Schwarzschild radius for an object of mass M) demanded by the EUV and X-ray data. One of the most striking features was the strong non-thermal (likely synchrotron) contribution in the optical and near-infrared (NIR) wavelengths, characteristic of outflows seen in jet sources. Indeed, the SED shows a very flat spectrum from the UV to the NIR (~1000–50 000 Å), suggesting that there is another source of NIR flux dominating any thermal disc emission, likely related to the radio emission, and therefore possibly of synchrotron origin.

We followed the evolution of this system from the outburst towards quiescence, to study the mechanisms underlying the outburst. Preliminary results were published in Chaty et al. (2001a,b). In this paper we will concentrate on the analysis and evolution of the SED. A companion paper (Hynes et al. 2003) discusses the multiwavelength variability properties. We describe the

multiwavelength observations in Section 2, present the results in Section 3, and discuss them in Section 4.

2 OBSERVATIONS

Observational details for our VLA, Ryle telescope, JCMT, UKIRT, *HST*, *EUVE*, *SAX*, *Chandra* and *RXTE* data follow.

2.1 Radio observations

All the radio (VLA, Ryle Telescope) and submillimetre (JCMT) observations are taken from references reported in Table 1.

2.2 NIR UKIRT observations

Near-infrared observations were carried out at the UKIRT 3.8-m telescope using UFTI (UKIRT Fast-Track Imager), IRCAM/TUFTI and also CGS4; some of which were already reported in Hynes et al. (2000). The log of the NIR observations is given in Table 2. The UFTI instrument is a cooled 1–2.5-μm camera with a 1024 × 1024 pixels^2 HgCdTe array. The plate scale is 0.091 arcsec pixel^{-1}, giving a field of view of 92 arcsec. The IRCAM/TUFTI instrument is a cooled 1–5-μm camera with a 256 × 256 pixels^2 InSb array. The plate scale is 0.081 arcsec pixel^{-1} with a field of view of 20.8 arcsec.

Images were taken through the wide-band filters J98 ($\lambda = 1.275$; $\Delta\lambda = 0.290$ μm), H98 ($\lambda = 1.670$; $\Delta\lambda = 0.280$ μm) and K98 ($\lambda = 2.205$; $\Delta\lambda = 0.41$ μm) with UFTI, and with all the above plus L′98 ($\lambda = 3.8$; $\Delta\lambda = 0.6$ μm) and M′98 ($\lambda = 4.675$; $\Delta\lambda = 0.250$ μm) with IRCAM/TUFTI.

The exposure times range between 10 and 60 s. The conditions were photometric. After taking each image of the object, an image of the sky was acquired, to allow subtraction of the blank sky. The images were further treated by removal of the dark current, the flat-field and the bright infrared sky. We also took a NIR *K*-band spectrum of this source using the CGS 4 instrument and a 0.6-arcsec slit on June 27.2 UT, which was featureless (see Chaty et al., in preparation).

2.3 Optical and ultraviolet *HST* observations

HST observations were performed with the Space Telescope Imaging Spectrograph (STIS; Leitherer et al. 2001) on the dates indicated in Table 3. These spanned the UV and optical bands at high and

Table 1. Log of radio observations. We tabulate here the epoch, date, Modified Julian Date, instrument and flux in mJy for every band.

Epoch	Date	MJD	Inst	1.4 GHz	8.3 GHz	15 GHz	23 GHz	350 GHz	Ref.
	30–31/03/00	51634	RT	–	–	6.2 ± 0.5	–	–	Pooley & Waldram (2000)
	31/03/00	51635	RT	–	–	7.8 ± 0.35	–	–	Dhawan et al. (2000)
1	02/04/00	51637	RT	–	–	7.5 ± 0.30	–	–	Dhawan et al. (2000)
1	03/04/00	51638	VLA	2.1 ± 0.1	6.0 ± 0.1	–	8.8 ± 0.3	–	Dhawan et al. (2000)
	05/04/00	51640	RT	–	–	8.7 ± 0.3	–	–	Fender et al. (2001)
2–6	16/03–25/06/00	51620–720	VLA	2.6 ± 0.4	6.5 ± 0.7	–	9.3 ± 1.2	–	Fender et al. (2001)
2–6	16/03–25/06/00	51620–720	RT	–	–	9.0 ± 1.0	–	–	Fender et al. (2001)
	08–11/00	51779–872	RT	–	–	0.15 ± 0.17	–	–	Pooley (private communication)
2–6	30–31/05/00	51695	JCMT	–	–	–	–	41 ± 4	Fender et al. (2001)
	09/09/00	51796	JCMT	–	–	–	–	<21	Fender et al. (2001)

Table 2. Log of the infrared observations. The epoch, date, MJD, instrument and magnitudes for every filter are reported. The magnitudes of the first epoch (corresponding to the detection of the infrared counterpart) were reported in Chaty et al. (2000), and those from Sternberg in Taranova & Shenavrin (2000). The observations of epochs 5 and 7 are reported in more details in Chaty et al. (in preparation).

Epoch	Date	MJD	Inst	*I*	*Z*	*J*	*H*	*K*	*L*′	*M*′
1	04/04/00	51638.2	UFTI			12.12 ± 0.02	11.75 ± 0.02	11.06 ± 0.02		
	12–15/04/00	51647.5	Sternberg			12.4 ± 0.2	11.9 ± 0.1	10.9 ± 0.1	9.2 ± 0.1	
2–4	18/04/00	51652.5	TUFTI			11.92 ± 0.07	11.43 ± 0.06	11.05 ± 0.08	9.71 ± 0.14	9.38 ± 0.42
	24/06/00	51719.2	UFTI					11.512 ± 0.004		
5	26/06/00	51721.2	CGS4					spectrum		
6	15/07/00	51740.2	UFTI					11.948 ± 0.006		
7	07/03/01	51975	UFTI	17.41 ± 0.05	17 ± 0.05	16.72 ± 0.05	16.15 ± 0.05	15.77 ± 0.05		

Table 3. Log of the optical and UV observations. The epoch, date, MJD, central wavelength and wavelength range are indicated, with in each case the exposure time in seconds.

Epoch	Date	MJD	E140M	E230M		G430L	G750L
	Central wavelength (Å):		1425	1978	2707	4300	7751
	Wavelength range (Å):		1123–1710	1574–2382	2303–3111	2900–5700	5236–10266
1	08/04/00	51642.7	9150	1300	1200	144	180
2	18/04/00	51652.6	3000	1000	700	1160	150
3	28/04/00	51663.3	1620	820	700	120	150
4	28/05/00	51692.8	1800	1000	750	120	204
5	24/06/00	51720.0	1750	1000	700	158	216
			3000				
6	08/07/00	51733.9	1700	950	750	120	224
7	28/09/00	51815	1250	2050	2050	400	407

Table 4. Log of the *EUVE* observations. The epoch, date, MJD and exposure time in seconds are indicated.

Epoch	Date	MJD	Exp. time
1	8–9/04/00	51642.603–51643.213	19 193.52
	13–14/04/00	51647.821–51648.430	19 553.9
2	16–19/04/00	51651.407–51654.102	80 200.1

Table 5. Log of the *SAX* observations. The epoch, date, MJD, energy bands and exposure time in seconds for the different instruments are indicated. For more details concerning the *SAX* observations see Frontera et al. (2001a).

Epoch	Date	MJD	LECS	MECS	HPGSPC	PDS
	Energy bands (keV):		0.12–4	1.7–10	7–29	15–200
2	14–15/04/00	51648–9	21197	29758	42138	20146

low resolution, respectively, using the E140M, E230M, G430L and G750L modes. For each visit, average calibrated spectra were extracted from standard *HST* pipeline data products. There was useful coverage from 1150 to 10 000 Å, although the region from 1195 to 1260 Å was completely dominated by Lyα absorption and N V emission (Haswell et al. 2002), so was excluded from our spectral energy distributions. On the dates where more than one observation of the same wavelength range was taken, the spectra were averaged to increase the signal-to-noise ratio. The documented absolute calibration accuracy is 5 per cent for the optical (CCD) modes and 8 per cent for the UV (MAMA) modes. The break between them is around 3100 Å, with some overlap. This systematic uncertainty is larger than any statistical uncertainties.

2.4 Extreme ultraviolet *EUVE* observations

EUVE observations of XTE J1118+480 took place during 2000 April 8.10–8.71, 13.32–13.93 and 16.91–19.60 UT. They are described in Hynes et al. (2000). The log of the *EUVE* observations is reported in Table 4. As in Hynes et al. (2000), we considered only the data between 70 and 120 Å, since longer wavelengths are heavily absorbed and dominated by noise. In the following plots showing data from *EUVE*, the vertical error bars are the 1σ errors from the photon statistics.

2.5 X-ray *SAX* observations

Beppo-SAX observed XTE J1118+480 four times, on 2000 April 14, May 4, June 26 and December 12. Here we show the observation taken on 2000 April 14–15, and reported in Table 5. The details of this observation can be found in Frontera et al. (2001a). Since these data were initially corrected with an interstellar absorption of 1.5×10^{20} cm^{-2}, we first uncorrected these data to obtain the observed flux, and then corrected them from the absorption with the desired value of N_H, as described in Section 3.1.

As shown in Fig. 2, although there is a good agreement between *SAX* and *Chandra* data in the interval $\log \nu = 16.6$–17.1 and between *SAX* and *RXTE* data for the interval $\log \nu = 18.5$–18.7, there is an inconsistency between the *SAX* and the *EUVE* observations for the interval $\log \nu = 16.5$–16.7 (probably due to the model used in fitting the *SAX* data combined with the low response of the detector at those wavelengths) and in the interval $\log \nu = 17.0$–18.5 between *SAX* and both *RXTE* and *Chandra* observations. This seems to be a calibration problem.

None the less, the *SAX* spectrum unambiguously shows the presence of a cut-off at an energy of $\log \nu \sim 19.5$, as discussed by

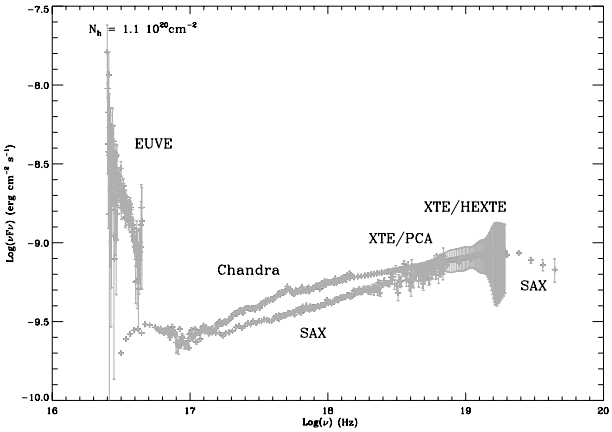

Figure 2. Comparison of epoch 2 SED as observed by the instruments *EUVE*, *Chandra*, *SAX* and *XTE*. The SED is corrected with $N_H = 1.10 \times 10^{20}$ cm^{-2}. This figure can be seen in colour in the on-line version of the journal on *Synergy*.

Table 6. Log of the *Chandra* observations. The epoch, date, MJD and exposure time in seconds are indicated. For more details about the *Chandra* observations see McClintock et al. (2001b).

Epoch	Date	MJD	Exp. time
2	18/04/00	51652.5	27200

Frontera et al. (2001a). Therefore, in the following we will include the *SAX* data only at high energies (in the interval $\log \nu = 18.8$–19.65)

2.6 X-ray *Chandra* observations

There was only one observation by *Chandra*, taken on 2000 April 18, reported in Table 6. Details are given in McClintock et al. (2001b). Since these data were corrected with an interstellar absorption of 1.3×10^{20} cm^{-2}, as for the *SAX* data, we first uncorrected these data to obtain the observed flux, and then corrected them for the absorption with the desired value of N_H, as described in Section 3.1.

2.7 X-ray *RXTE* observations and data analysis

We observed XTE J1118+480 with the *Rossi X-ray Timing Explorer (RXTE)* Proportional Counter Array (PCA) and High-Energy Timing Experiment (HEXTE) at five epochs selected to coincide with the *HST* visits. The log of the *RXTE* observations is reported in Table 7. The method used for the analysis of data is the same as that described in Hynes et al. (2000), therefore in the following we will just give the various parameters derived by analysing the different epochs.

Table 7. Log of the *RXTE* observations. We report here the epoch, date, MJD, exposure time in seconds for the PCA instrument and the observation ID.

Epoch	Date	MJD	Exp. time	Observation ID
1	08/04/00	51642.7	3900	50133-01-01-00
2	18/04/00	51652.6	4700	50133-01-02-00
3	28/04/00	51663.3	10 600	50133-01-03-00
4	28/05/00	51692.8	2400	50133-01-04-00
5	24/06/00	51720.0	5600	50133-01-05-00

Table 8. Log of the different epochs. The date and MJD are indicated. The '–' indicates that we used for the indicated epochs the observations of epoch 2, which is sensible since the SED did not change significantly in these wavelengths during 3 months.

Epoch	Date	MJD	Radio	UKIRT	*HST*	*EUVE*	*SAX*	*Chandra*	XTE	Colour
	log(ν)		9.0–11.6	13.78–14.48	14.47–15.41	16.38–16.61	16.61–19.68	16.76–18.23	17.78–19.68	
1	08/04/00	51642.7	x	x	x	x			x	Dark blue
2	18/04/00	51652.6	x	x	x	x	x	x	x	Light blue
3	28/04/00	51663.3	–	–	x				x	Dark green
4	28/05/00	51692.8	–	–	x				x	Light green
5	24/06/00	51720.0	–	x	x				x	Yellow
6	08/07/00	51733.9	–	x	x					Orange
7	09/00–03/01	51815–52467		x	x					Red

For the PCA, we used the 'standard mode' data (128 spectral channels, 16-s accumulations), selecting subintervals when the number of detectors on remained constant (~90 per cent of the total time). We similarly extracted 256-channel spectral accumulations from the HEXTE science event (SE) data. A subset of PCA and HEXTE detector channels, corresponding typically to approximately 3–100 keV were used in our subsequent model fitting. Background rates for the PCA were estimated using the epoch-4 models, and response matrices were generated using the current calibration files and response-matrix generation software, all from the HEASOFT 5.1 release.

The source intensity was typically in the 30–40 mCrab range for each epoch, with typical PCA count rates of ~80–120 count s^{-1} PCU^{-1} (source; the background is an additional 30 count s^{-1} PCU^{-1}). The spectra thus derived were found to be hard, with photon power-law indices of approximately 1.8 ± 0.1. A thermal Comptonization model (Sunyaev & Titarchuk 1980) with $\tau \simeq 3$ and $T_e \simeq 30$ keV, also provided acceptable fits (in either the power law or thermal Comptonization cases, a typical χ^2 per degree of freedom of the order of unity was obtained). There was no evidence (in terms of statistical improvement to our fits) for a soft-excess component, thus we conclude, as have others, that the source remained in the 'low/hard' spectral state throughout the outburst. In most cases, particularly 50133-01-03-00 for which the PCA exposure was approximately 10 000 s, there was a distinct positive residual corresponding to the 6.4-keV FeK resonance, thus a Gaussian line profile was included to refine the overall fit. The energy coverage was ~3–26 keV with PCA and 11 to 207 keV with HEXTE. In all the figures we show only the data up to 80 keV (except for the first visit where we show them up to 120 keV), since at higher energies the noise dominates.

2.8 Broadband SED

For analysis, we separated the observations into the seven epochs reported in Tables 1–7. Table 8 summarizes the different facilities used at each epoch. For each epoch, observations in all bands are simultaneous or nearly simultaneous. The broad-band SEDs corresponding to all epochs are presented in Figs 3 and 4. In Fig. 3 they are shown with different normalizations for more clarity. We overplot all epochs in Fig. 4, and enlargements in radio, NIR–UV and EUV–X-ray regions are shown, respectively, in Figs 5–7. In all of these figures the data have been corrected with $N_H = 1.1 \times 10^{20}$ cm^{-2} corresponding to $A_v = 0.059$, as will be described in Section 3.1.

3 RESULTS

Before describing the results, in Section 3.1 we present the method used to correct for interstellar absorption.

3.1 Correction of interstellar absorption

The interstellar absorption was corrected in the following way. First, we choose a value for the column density by fitting the UV and EUV fluxes and slopes, as will be discussed in Section 3.5. For example, here we take $N_H = 1 \times 10^{20}$ cm^{-2}.

Using this value of column density, we then correct the *EUVE* data and *SAX* and *Chandra* X-ray data using the absorption cross-sections of Rumph, Bowyer & Vennes (1994) for H I, He I and He II with abundance ratios 1 : 0.1 : 0.01, typical of the diffuse interstellar medium.

Then, we assume that this inferred column density is interstellar, and we adopt an average gas-dust ratio of $\langle N(H_I+H_2)/E(B-V)\rangle = 5.8 \times 10^{21}$ cm^{-2} mag^{-1} (Bohlin, Savage & Drake 1978). This leads to the value of $E(B-V)$, equal to 0.017 in the example taken here. Taking the value of $R_v \equiv A_v/E(B-V) = 3.1$ typical of the diffuse interstellar medium (Cardelli, Clayton & Mathis 1989), we obtain the value of A_v (=0.053 here).

Finally, we correct the infrared (from UKIRT), optical and ultraviolet (*HST*) observations for interstellar absorption with the extinction law of Cardelli et al. (1989), using the derived value of absorption, leading to the inferred SED.

We note that even in the far-ultraviolet (FUV), reddening corrections are $\lesssim$15 per cent [depending on $E(B-V)$] and that the extinction curve and gas-to-dust scaling are not critical. Only in the EUV is the correction large.

3.2 Geometrical parameters of the system

We took a black hole mass of 7.2 ± 1.3 $M_\odot$ (McClintock et al. 2001a), which corresponds to a Schwarzschild radius of $R_s = 21$ km. The mass ratio has been measured as $Q = 1/q = M_1/M_2 = 27 \pm 5$ (an extreme value among SXTs, Orosz 2001), therefore the mass of the donor star $M_2 = 0.27 \pm 0.05$ $M_\odot$. The distance of the system has been determined as 1.71 ± 0.05 kpc (see the discussion in Section 3.3) and the orbital period to $P_{orb} = 0.169\,937(1)$ d ~ 4.08 h (Zurita et al. 2002).

This gives an orbital separation $a = 1.76 \pm 0.1 \times 10^9$ m (Paczyński 1971). To derive the value of the outer radius of the accretion disc, we take the intermediate value between the tidal radius of the disc R_T and the 3:2 resonant radius R_{23}, since the source showed the presence of superhumps (see Section 1). The tidal radius of the disc is taken as 90 per cent of the Roche lobe radius, therefore $R_T/a = 0.58 \pm 0.01$ (Eggleton 1983) and the 3 : 2 resonant radius is $R_{23}/a \sim 0.47$ (Whitehurst & King 1991). Hence the outer radius we take is $r_{out} = 0.52a$. The inclination of the system is chosen to be $70^\circ \pm 10^\circ$, consistent with McClintock et al. (2001a, and also Zurita et al. 2002).

The inner radius of the accretion disc will be a free parameter, but will typically be between 300 and 450 R_s. This corresponds to a low

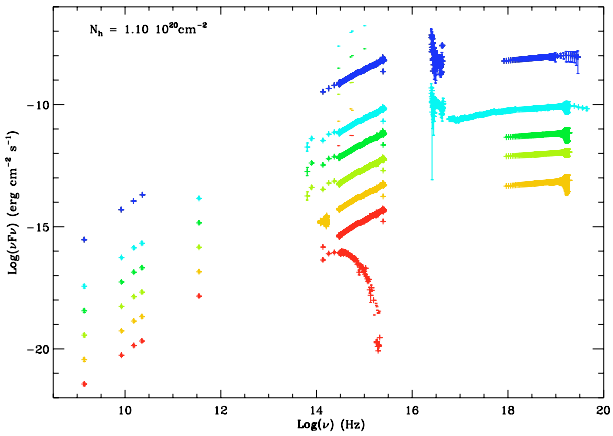

Figure 3. Spectral energy distributions of all the epochs, beginning from the top of the figure. Colour-codings are as given in Table 8. For easier reading, we multiplied epoch 1 by 10, and then divided epoch 2 by 10, epoch 3 by 100, epoch 4 by 10^3, epoch 5 and 7 by 10^4 and epoch 6 by 10^5.

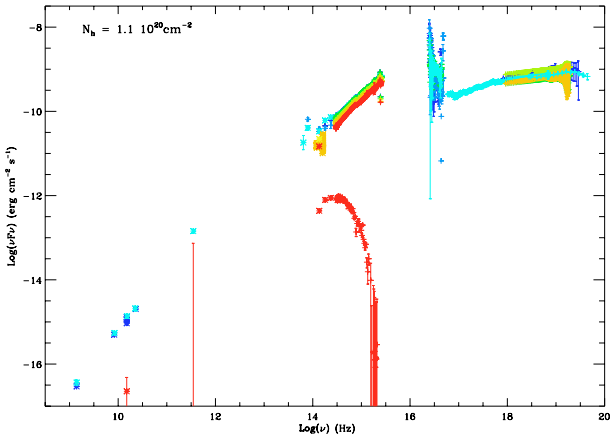

Figure 4. Spectral energy distribution for all the epochs overplotted.

state, in contrast to the high state where the accretion disc extends very close to the compact object, $r_{\rm in} \approx 3R_{\rm s}$, corresponding to the last stable orbit.

3.3 Fit to the nearly quiescent SED

To characterize the nearly quiescent system, we use only the epoch 7 data from UKIRT and *HST*. Since there is probably still some contamination from the accretion disc, we take the combination of two emission models, one representing the companion star and one representing the accretion disc. The spectral type of the companion star has been determined as K5–M1 V (McClintock et al. 2001a; Wagner et al. 2001). In our analysis, we therefore take an M1 V star photosphere ($T_{\rm eff} = 3400$ K, Bessell, Castelli & Plez 1998). The radius of the mass donor star can be estimated with $R_2/a = 0.15 \pm 0.01$ (Eggleton 1983), therefore $R_2 = 0.39$ R$_\odot$. We take a blackbody model for the nearly quiescent accretion disc. We therefore fit the epoch 7 UKIRT and *HST* data with three free parameters: the fractional contribution of the secondary to the total emission, the temperature of the accretion disc, and the distance of the system. We found that the best-fitting parameters were a fractional contribution of 25 ± 2 per cent, a remnant accretion disc at 6000 ± 50 K and a

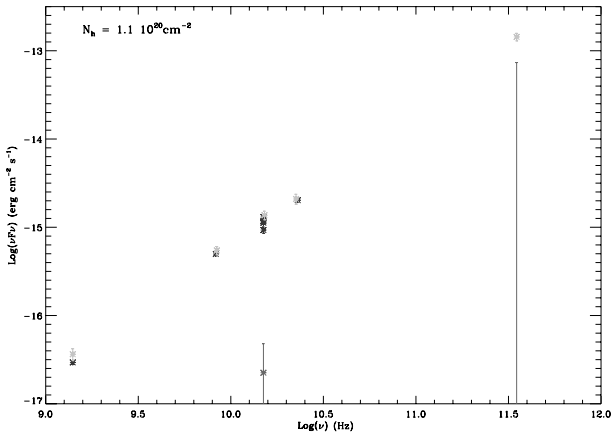

Figure 5. Radio SED for all the epochs. This figure can be seen in colour in the on-line version of the journal on *Synergy*.

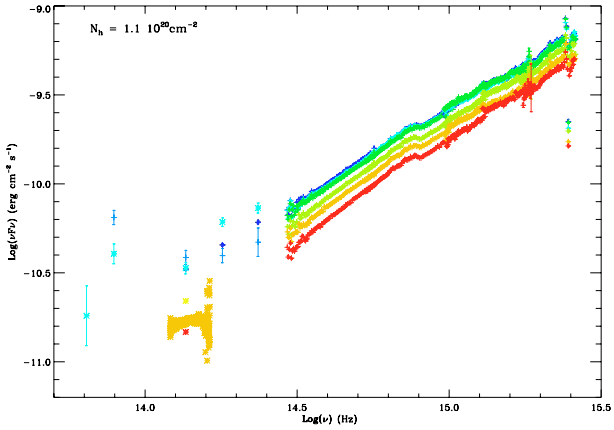

Figure 6. NIR-UV SED for all the epochs.

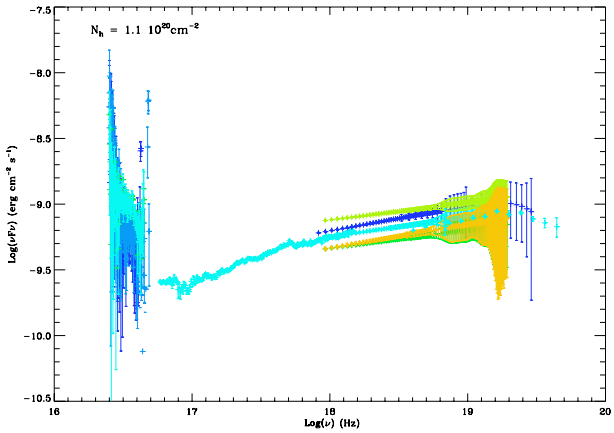

Figure 7. EUV-X SED for all the epochs.

distance of 1.71 ± 0.05 kpc with a reduced $\chi^2 = 1.3$, and a tolerance of 10^{-5} (see Fig. 8). The fractional contribution of the secondary to the total emission which we derived is in agreement with the contribution of ∼28–36 per cent found by Wagner et al. (2001) and $\sim 34 \pm 8$ per cent by McClintock et al. (2001a) from optical spectroscopy. We also tried to replace the blackbody model by a power law, but the fit was worse, showing that the synchrotron contribution

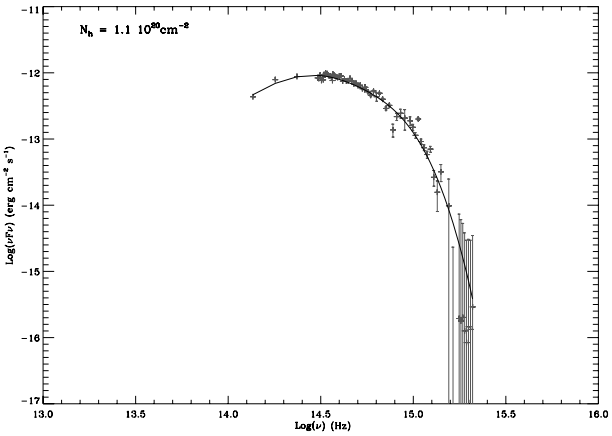

Figure 8. Fit of the epoch 7 (the nearly quiescent system), with a fractional contribution secondary/total emission of ∼25 per cent, a remnant accretion disc at ∼6000 K and a distance of ∼1.7 kpc, taking into account the emission of a M1V star at $T_{\rm eff} = 3400$ K with a radius $R_2 = 0.39\ {\rm R}_{\odot}$. This figure can be seen in colour in the on-line version of the journal on *Synergy*.

had decreased between epochs 1–6 and 7. We finally varied the absorption through the column density interval allowed by the broad-band SED (see Section 3.5) but this did not change the best-fitting parameters substantially. Therefore, our simple model gives a result consistent with the other methods, and in the following we will use the parameters derived from our analysis, to add the contribution from the companion star to the overall fits at other epochs.

It is interesting to point out that, by plotting the infrared colour magnitudes (observed on 2001 March, during the near-quiescence of the source, corresponding to epoch 7) on a Hertzsprung–Russell diagram, we derived that the companion star had a spectral type of M1 V (Chaty et al., in preparation), in agreement with the spectroscopic results. On the other hand, the radius of the companion star that we used for the fit in Fig. 8 is smaller than an isolated main-sequence star by a factor of 2. However, Haswell et al. (2002) showed that the companion star of XTE J1118+480 is an evolved star, consequently it may well have a different radius to an isolated main-sequence star of the same type.

3.4 Epoch 2

As we can see in Fig. 4 (which we will discuss in more detail in Section 3.8), there were no gross changes in the SED between epochs 1 and 6, so in the following we will consider the epoch where we have the most data, i.e. epoch 2. Our analysis differs from previous ones (see Section 1) because, in addition to the disc blackbody, we explicitly include contributions in different bands (for instance power-law spectra in radio, submillimetre–NIR and X-rays), together with the emission in the NIR–optical domain of the nearly quiescent system, using the results from Section 3.3. We are aware that this does not account for irradiation of the mass donor star, however, the fits are just intended to be illustrative. XTE J1118+480 is a unique source in term of its low absorption, allowing us to study its whole SED in great detail, derive some useful constraints and analyse the evolution from the outburst to near quiescence.

3.4.1 Model of the accretion disc

To fit the broad-band emission due to the accretion disc we use the simple parametrized model of Hynes et al. (2002). It is based on a combination of the classic viscously heated blackbody disc spectrum (Shakura & Sunyaev 1973; Frank, King & Raine 1992) and the modified temperature distribution for an irradiated disc (Cunningham 1976; Vrtilek et al. 1990). See these papers for derivations of the relevant temperature distributions, and Dubus et al. (1999) for a critique of the assumptions.

The model spectrum is calculated by summing a series of black bodies over radius. The local effective temperature of a disc annulus is determined by the emergent flux at that radius, such that $T_{\rm eff}^4 \propto F_{\rm bol}$. The emergent flux is the sum of viscous energy release within that annulus, $F_{\rm visc} \propto T_{\rm visc}^4$, and the X-rays reprocessed by the annulus, $F_{\rm irr} \propto T_{\rm irr}^4$. Hence the effective temperature contains contributions from viscous heating ($T \propto R^{-3/4}$) and irradiation ($T \propto R^{-3/7}$). The effective temperature profile of the disc is therefore represented by

$$T_{\rm eff}^4(R) = T_{\rm visc}^4(R) + T_{\rm irr}^4(R).$$

Both profiles are effectively controlled in the model by the temperature at the outer radius of the disc. The viscous temperature, $T_{\rm visc}(R_{\rm out})$, is a free parameter, typically around 7500 K; the irradiation temperature, $T_{\rm irr}(R_{\rm out})$, we usually take to be $T_{\rm irr}(R_{\rm out}) = 0$ K (but see Section 3.6).

The detailed fit is the sum of the secondary star (or nearly quiescent system), the model of the accretion disc in the low state, and three different power laws demanded by the data in the radio, NIR and X-ray bands, with respective spectral indices of 0.5, −0.15 and −0.8, taking the convention

$$f_\nu \propto \nu^\alpha. \qquad (1)$$

As the figures show, these three power laws are natural fits to the SED. They have the respective expressions: $f_{\nu\rm radio} = 7 \times 10^{-31} \times \nu^{1/2}$ between 1×10^9 and 4×10^{11} Hz; $f_{\nu\rm nir} = 2.5 \times 10^{-23} \times \nu^{-0.15}$ between 4×10^{11} and 8×10^{14} Hz; and $f_{\nu\rm x} = 1.2 \times 10^{-13} \times \nu^{-0.8}$ between 8×10^{14} and $10^{19.3}$ Hz.

3.4.2 Examining the SED

We show epoch 2 with the different models and fit in Fig. 9. We clearly see two main characteristics. First, the source is exhibiting

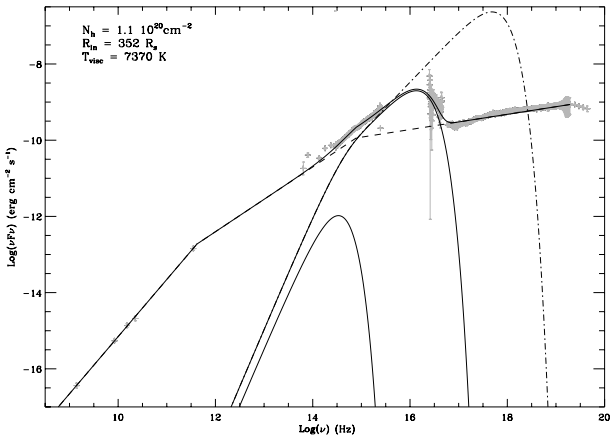

Figure 9. Spectral energy distribution for epoch 2 corrected with $N_H = 1.10 \times 10^{20}$ cm^{-2}. $R_{\rm in}$ and $T_{\rm visc}$ given in the figure are those derived by our fits. The lower solid thick curve is the emission representing the near-quiescent system, the intermediate solid thin curve is the multicolour blackbody disc in the low state, and the upper dash dot thin curve is the multicolour blackbody disc in the high state. The straight dashed lines are the three different power laws, as described in Section 3.4. The solid curve following the data is the sum of the contributions from the near-quiescent system, the accretion disc in the low state, and the three power laws. This figure can be seen in colour in the on-line version of the journal on *Synergy*.

Table 9. Results of different fits according to N_H. The N_H is fixed, R_{in} and T_{visc} are free parameters. Although it is not an independent parameter in the fits, we give T_{in} for information. The tolerance used in the fits was 1×10^{-2} (except where an asterisk is written, where the tolerance was between 0.1 and 1). Reasonable fits appear to be with N_H between 0.8 and 1.3×10^{20} cm^{-2}, and by inspecting the figures 1.1×10^{20} cm^{-2} seems to be the best value, and we will keep it for the rest of the paper (see the text for a discussion of this).

N_H ($\times 10^{20}$)	R_{in} (R_S)	T_{visc} (K)	T_{in} (eV)	χ^2
0.70*	1369	7373	8.53	65
0.75*	970	7320	10.97	58
0.80	450	7246	19.32	54
0.85	427	7266	20.15	54
0.90	407	7286	20.94	54
0.95	389	7306	21.72	55
1.00	374	7327	22.44	55
1.05	362	7348	23.06	56
1.10	**352**	**7370**	**23.62**	**56**
1.15	354	7394	23.60	57
1.20	354	7418	23.67	57
1.25	356	7442	23.65	58
1.30	326	7460	25.27	58
1.35	310	7480	26.37	59
1.40	316	7505	26.08	60
1.45	313	7528	26.35	60
1.50	310	7551	26.62	61
1.55	307	7575	26.90	62
1.60	308	7599	26.92	62
1.65	306	7622	27.13	63
1.75	302	7669	27.57	65
1.90	296	7739	28.25	67
2.05	292	7810	28.80	70

a very low low/hard state (Hynes et al. 2000); secondly, there is a strong non-thermal contribution in the radio domain with an inverted spectrum, extending up to the UV wavelengths, and even in the X-rays. We will develop this later.

In most of our fits the typical values of the inner disc temperature, T_{in} are between 20 and 30 eV and those of the inner disc radius R_{in} are between 300 and $450R_S$ (see Section 3.5 below and Table 9). These values are consistent with those derived by McClintock et al. (2001b), but the inner radii are higher than that derived by Esin et al. (2001), consistent with their model, including a significant advection-dominated accretion flow (ADAF) contribution to the EUV.

3.5 The hydrogen column density, N_H

We now try to better constrain the value of N_H by fitting the whole SED corrected with different values of N_H, with the inner radius of the accretion disc and the outer temperature as free parameters. All the other parameters are taken as described in previous sections. The results are reported in Table 9. The best fits had a reduced χ^2 of 54, with 728 degrees of freedom. This high value of the reduced χ^2 just shows how illustrative the fits are, because detailed spectral features such as the Balmer jump and the dip in the *Chandra* spectrum are not fitted. From the χ^2 values obtained and inspection of corresponding figures, reasonable fits appear to be with N_H between 0.8 and 1.3×10^{20} cm^{-2}.

With $N_H = 1.45 \times 10^{20}$ cm^{-2} ($R_{in} = 313R_S$) no accretion disc models are simultaneously consistent with the very different slopes in the UV and the EUV. With $N_H = 0.75 \times 10^{20}$ ($R_{in} = 970R_S$) the

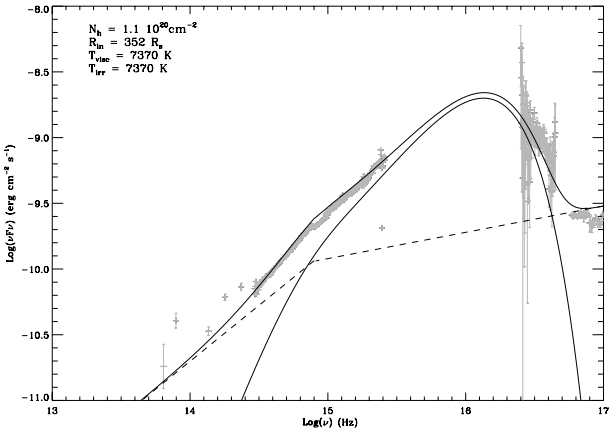

Figure 10. Spectral energy distribution for epoch 2 corrected with $N_H = 1.1 \times 10^{20}$ cm^{-2}, $R_{in} = 352R_S$ and with an irradiation of $T_{irr}(R_{out}) = 7370$ K (see Section 3.4.1). This figure can be seen in colour in the on-line version of the journal on *Synergy*.

presence of the X-ray power law makes it impossible to reconcile both high UV and low EUV fluxes. $N_H = 1.1 \times 10^{20}$ cm^{-2} is the only one of the values considered here which is consistent with both accretion disc models and the UV/EUV fluxes and slopes. We present the epoch 2 SED corrected with the column density $N_H = 1.1 \times 10^{20}$ cm^{-2} in Fig. 9.

Therefore, from the results of the fits, and also by plotting these results on the observations, $N_H = 0.8$–1.3×10^{20} cm^{-2} seems to be the preferred value. In the following we will consider the value of $N_H \sim 1.1 \times 10^{20}$ cm^{-2} as the most likely, and we will draw all the figures with this value.

3.6 Irradiation

In Fig. 10 we present the epoch 2 SED corrected with the column densities 1.10×10^{20} cm^{-2}, taking into account an irradiation with $T_{irr}(R_{out}) = 7370$ K, as described in Section 3.4.1. Fig. 9 shows the same SED without any irradiation. We can see that the slopes in the optical/UV parts of the spectrum are not consistent with the presence of irradiation. However, the irradiation component in our fit presents lots of assumptions, mainly concerning the geometry of the irradiating/irradiated region. Therefore, in view of the uncertainties in the irradiation function, although it is not required by our characterization of the data (which is also very crude), some irradiation of the disc cannot be ruled out.

3.7 Contributions to L_{bol}

The luminosity due to thermal–viscous dissipation in the accretion disc is given by integrating the luminosity σT^4 between R_{in} and R_{out}, for the two faces of the disc:

$$L_{disc} = 2 \times 2\pi\sigma T_{out}^4 R_{out}^3 \left(\frac{1}{R_{in}} - \frac{1}{R_{out}} \right).$$

Adopting values typical of the fits in previous sections, i.e. $R_{in} = 352R_S$ (corresponding to $T_{in} = 23.6$ eV) and $T_{visc} = 7370$ K, we obtain $L_{disc} = 2.2 \times 10^{36}$ erg s^{-1}.

In the three power laws corresponding, respectively, to the radio, NIR and X-ray domains, we integrate $F_\nu \propto \nu^\alpha$ in the frequency range given in Table 10, and multiply it by $4\pi D^2$ (i.e. assuming isotropic emission). The corresponding luminosities are given in Table 10. Therefore, assuming that L_{X-rays} is representative of the

Table 10. Contributions L_{bol} in different parts of the SED (called radio, NIR and X-rays following the convention given in Section 3.4.1). The frequency is given in $\log_{10}(\nu/\mathrm{Hz})$ and the luminosity in erg s^{-1}.

	Radio	NIR	X-rays
Frequency	[9–11.6]	[11.6–14.9]	[14.9–19.3]
Luminosity	4.6×10^{31}	5.3×10^{34}	1.5×10^{36}

contribution from the corona, we have $L_{\rm disc} \gtrsim L_{\rm corona}$, and we will discuss this result later in Section 4.3.1. This is consistent with the fact that in the case where all the gravitational power is dissipated in a static corona, nearly half of the coronal luminosity intercepts the disc and is reprocessed/reflected so $L_{\rm disc} \sim L_{\rm corona}/2$. Similarly if a fraction of the gravitational power is released in the disc (instead of the corona) $L_{\rm disc} \geqslant L_{\rm corona}/2$ (Haardt & Maraschi 1993).

3.8 The other epochs: evolution of the SED

There were no gross changes in the SED between epochs 1 and 6, so we overplot the fit to epoch 2 with the data from all epochs in Fig. 11. The SED did evolve a little during the outburst, and the best way to characterize this evolution is to quantify the change of the spectral index (defined as in equation 1) between optical ($10^{14.6}$ Hz) and X-ray (10^{18} Hz) domains. These domains are chosen because both show power-law spectra and we have simultaneous coverage during the six epochs of observations. This, reproduced in Fig. 12, shows that the electron energy distribution remains the same during the whole outburst. From Figs 5–7 it appears that the fluxes decrease slightly, however, the slopes do not change much. This suggests that the energy injected in the outflow decreases during the outburst.

We tried to reproduce this evolution of the SED by modifying some parameters of our simple model. One way to do this is by decreasing the outer (viscous) temperature. However, changing this temperature modifies the slope of the UV part of the SED, and as we can see in Fig. 6, this slope remains the same during the entire

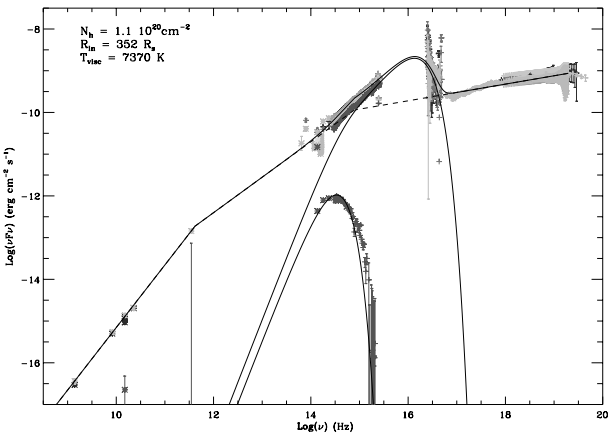

Figure 11. Spectral energy distribution: the fluxes are corrected with $N_H = 1.1 \times 10^{20}$ cm^{-2}. The overall fit is a multicolour blackbody disc model with an outer disc temperature of 7370 K and inner disc radius of $352R_S$. Straight lines: different power laws, with spectral indices of 0.5, and −0.8 (similar to Hynes et al. 2000). The lower curve corresponds to the blackbody emission from the companion star. This figure can be seen in colour in the on-line version of the journal on *Synergy*.

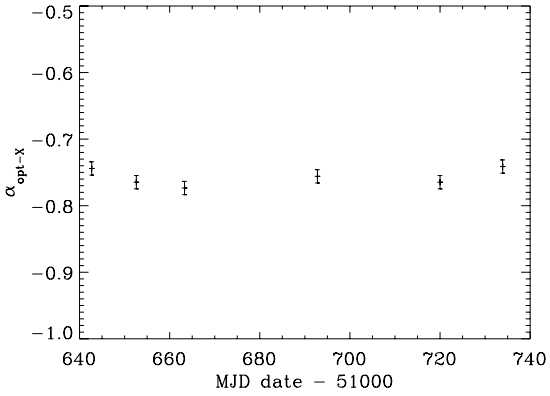

Figure 12. Evolution during the outburst of the spectral index linking the optical ($10^{14.6}$ Hz) and X-ray (10^{18} Hz) domains.

outburst. The other way to act on the multicolour blackbody disc would be to modify the inner radius, but this will only modify the EUV part of the SED. Therefore, the only way to reproduce this SED evolution is to act on the power laws, and we can indeed do this just by changing the constant of the power law (and not changing its exponent). This is consistent with a non-thermal contribution, which would have a decreasing energy during the outburst, but the same particle energy distribution. It is also suggestive of an outflow constrained to the central part of the accretion disc, the size of which would decrease during the outburst, which could be correlated with the increase in QPO frequency during the outburst (Wood et al. 2000).

This evolution is very interesting in the sense that it is different from what we see in other SXTs, and particularly in other states. For instance, in XTE J1859+226, Hynes et al. (2002) observed a change in the NIR–optical SED that they modelled as a change in viscous and irradiation temperature (as described in Section 3.4.1). In contrast, the evolution in XTE J1118+480 is mostly due to a change in the non-thermal (outflow) emission, compared with the thermal (disc) emission.

The lack of pronounced evolution of the SED during 3 months is also reminiscent of the behaviour of jet sources such as GRS 1915+105 and GX 339−4, in the so-called 'plateau state', where only small changes occur in the light curves. This, again, supports the idea of a steady outflow emanating from the source XTE J1118+480, as we will discuss in Section 4.2.

4 DISCUSSION

4.1 Variability and non-thermal contribution

A comprehensive discussion concerning the short time-scale variability of XTE J1118+480 during all the epochs of observations in the different wavebands (including NIR, UV and X-rays) can be found in Hynes et al. (2003). Here we just summarize the facts most relevant to our current analysis by combining our results on the SED and their results on the variability. Hynes et al. (2003) show that the XTE data exhibit a Poisson-subtracted fractional rms of approximately 35–37 per cent for the first observations decreasing to 26–28 per cent for the later ones. The UV variability is weaker than the optical or NIR, and stronger at longer wavelengths, with typical rms variability ∼3–4 per cent in the far-UV and ∼4–5 per cent in the near-UV. This suggests that at least some of the UV variability may be associated with the non-thermal component.

The ∼10-s QPO was seen in the optical, UV and X-rays, implying a common origin for this QPO throughout the spectrum. The sampling time of Hynes et al.'s (2003) NIR observations was insufficient to search for the QPO, however, they did detect flickering at NIR wavelengths, of larger amplitude (∼0.8 mag) than in the optical (∼0.4 mag). This NIR variability, up to 50 per cent, is consistent with a dominant non-thermal emission (Hynes et al. 2003). Furthermore, the featureless NIR spectrum we took in 2000 June (see data plotted in yellow in Fig. 3) is also consistent with the fact that the disc is not the only source of emission in this part of the spectrum (for more details concerning the NIR see Chaty et al. 2001b, in preparation). Hence both the SED and temporal behaviour suggest a strong non-thermal (probably synchrotron) emission at radio–UV wavelengths. Finally, it also shows that the cut-off frequency characteristic of the synchrotron radiation might be in the optical domain or even at higher frequencies.

4.2 How common is XTE J1118+480?

4.2.1 SED: comparison with other galactic sources

Several aspects of the broad-band spectrum of this source appear to be very similar to those of the other well-studied black hole binaries in the low state. The hard X-ray spectrum with a spectral index $\alpha \sim -0.8$ and a cut-off around 100 keV is typical of low/hard state spectra observed in Cygnus X-1 (e.g. Frontera et al. 2001b) or GX 339−4 (e.g. Zdziarski et al. 1998). The X-ray PDS spectrum of XTE J1118+480 is very similar to those of other black hole sources (Revnivtsev et al. 2000). However, the characteristic features are significantly shifted towards lower frequencies relative to other black hole sources with similar masses (cf. fig. 2 of Revnivtsev et al. 2000 and fig. 1 of Sunyaev & Revnivtsev 2000). This suggests that the X-ray-emitting region is larger in XTE J1118+480. Therefore, this hard X-ray variability, which is slower than in other SXTs, seems in turn to be consistent with a particularly large disc inner radius in this source. However, such 'slow and ubiquitous' QPOs have already been seen in other black hole candidates in the low state. For instance, QPOs at $P \sim 20$ s have been observed both in the X-ray and the optical bandes in the source GX 339−4 (Motch et al. 1983).

Another significant difference with other hard state sources is the low inner disc temperature inferred from our data. In the case of Cygnus X-1 in the hard state the inner temperature is $kT_{\rm in} \sim 150$ eV (see e.g. Balucinska-Church et al. 1995; Frontera et al. 2001b) contrasting with our derived value $kT_{\rm in} \sim 25$ eV (Table 9) for XTE J1118+480. This is consistent with a 'very low' low/hard state (Hynes et al. 2000). According to the multicolour blackbody disc model, this lower temperature implies a larger disc truncation radius than in typical sources (a few hundred $R_{\rm S}$ instead of a few tens). This can also simply be expressed in terms of $r_{\rm in}/r_{\rm out}$: this ratio is $4–7 \times 10^{-5}$ for a typical SXT such as XTE J1859+226, which we also observed with similar intensive coverage (Hynes et al. 2002). The $r_{\rm in}/r_{\rm out}$ ratio lies between 7×10^{-3} and 2×10^{-2} in the case of XTE J1118+480 (depending mainly on the value of the inner radius as derived with our fits). We also point out that the better energy coverage of the data available for XTE J1118+480 helped us to obtain accurate parameters, since the inner disc temperature of hard state sources is usually poorly determined due to strong interstellar absorption.

Finally, XTE J1118+480 differs from other transient sources by its exceptionally low X-ray to optical flux ratio (Tanaka & Shibazaki 1996) and its plateau-like light curve which contrasts with the exponential decay observed in many transients. However, once again in order to be consistent we have to compare XTE J1118+480 with other sources in the low/hard state, and when this is done it becomes less peculiar. For instance, the X-ray to optical flux ratio in the case of GX 339−4 can be as low as 2.5–3 (Motch et al. 1983), very similar to the value of 5 in the case of XTE J1118+480. Also, its plateau-like light curve is common in the jet source GRS 1915+105 (see e.g. Tanaka & Shibazaki 1996).

Therefore, the main difference with other sources is the prominence of the non-thermal contribution. Indeed, the radio–NIR spectrum presents an inverted spectrum, typical of non-thermal optically thick synchrotron emission. This combined with a lack of pronounced evolution of the SED strongly represents the signature of a jet. As a counterpoint, the radio spectral index during the 1999 outburst of XTE J1859+226 was negative most of the time, and the interval when it was positive was less than 4 d; its maximum value was 0.143 ± 0.180 (Brocksopp et al. 2002), cf. the steady 0.5 value in the 2000 outburst of XTE J1118+480. The radio–NIR component is much stronger in XTE J1118+480, exhibiting a low/hard state: in contrast the radio–NIR component was relatively weak in the high/soft state outburst of XTE J1859+226. This is consistent with the presence of an outflow (see e.g. Fender 2001).

This signature of a jet has been observed many times in GRS 1915+105 (see recent multiwavelength observations by Ueda et al. 2002), Cygnus X-1 (see Fender et al. 2000; Stirling et al. 2001) or GX 339−4 (Corbel et al. 2000). It is usually correlated with the appearance of the low/hard X-ray state spectrum, which is believed to be the result of a coupling between the Comptonizing corona and a compact jet (see, e.g., Corbel et al. 2000; Fender 2001). We will discuss this in more detail in Sections 4.2.2 and 4.3.2.

4.2.2 Comparison with galactic and extragalactic jet sources

The strong non-thermal contribution attributed to an outflow, implies that XTE J1118+480 is a *microquasar*. We therefore compare it with GRS 1915+105, the archetype of the microquasars. We can also compare the SED of XTE J1118+480 with typical SEDs of *quasars* given in Elvis et al. (1994), following the analysis of Ueda et al. (2002) in comparing GRS 1915+105 with typical quasars.

To compare the ratio of energy of the outflow with the accretion energy, we need estimates of both. The outflow energy can be estimated by taking the value νF_ν in the radio band ($\nu = 10^{10}$ Hz) for XTE J1118+480, GRS 1915+105 and quasars. However, for the measure of the accretion power, we have to take the wavelength where an optically thick thermal emission from the accretion disc presents a peak, therefore in the X-ray range ($\nu = 10^{18}$ Hz) in the case of GRS 1915+105, in the EUV ($\nu = 10^{16}$ Hz) in the case of XTE J1118+480 and in the UV ($\nu = 10^{15.2}$ Hz) in the case of quasars. Then we compare thereafter the ratio of νF_ν between the radio and X-rays for XTE J1118+480 and GRS 1915+105 with the ratio between radio and UV for quasars.

This outflow/accretion ratio is typically 10^{-6} for XTE J1118+480, when it is between 10^{-7} and 10^{-5} for GRS 1915+105, respectively, when this source is in a plateau state or exhibiting large radio flares. The value in XTE J1118+480 is intermediate between the two different values exhibited by GRS 1915+105. The main difference is that the ratio of XTE J1118+480 is stable, instead the ratio of GRS 1915+105 is varying on shorter time-scales between the two extreme values. This suggests that even if the contribution

of the outflow to the total energy budget in the two sources is comparable, there is a large difference in their behaviour, which is probably due to the fact that XTE J1118+480 is exhibiting a continuous outflow, and instead GRS 1915+105 shows energetic but sporadic ejections on short time-scales. Calculations of energy budget, taking into account different ejection behaviours are given in Chaty et al. (2001) by comparing GRS 1915+105 and SS 433.

For the quasars the outflow/accretion ratio is typically 10^{-2} and 10^{-6}, respectively, for radio-loud and radio-quiet quasars (Ueda et al. 2002). This suggests that XTE J1118+480 (and the microquasars) fall into the regime of radio-quiet quasars. The inverted radio spectrum resembles that of radio-quiet quasars, and the analogue of the millimetre break, around 10^{13} Hz, exhibited by the radio-quiet quasars and related to self-absorption, seems to be the submillimetre excess, around 10^{12} Hz, in XTE J1118+480. On the other hand, if the emission from the outflow also contributes substantially to the high-energy domain, then the outflow/accretion ratio becomes even bigger, up to the typical values of radio-loud quasars. If this analogy is real, then the intrinsic luminosity of the jet could dominate the energetics of XTE J1118+480, as in the case of the quasars (see Table 10).

Therefore, although the high-energy spectrum of XTE J1118+480 is very similar to what is observed in Seyfert galaxies, its phenomenology differs widely from that of strong extragalactic jet sources such as blazars. This is because blazars are dominated by relativistic beaming phenomena while the inclination in the case of XTE J1118+480 precludes this.

4.3 Accretion models

The low X-ray luminosity and the relatively large inner disc radius inferred from the comparisons with the multicolour blackbody disc model suggests that either the inner part of the accretion flow (i.e. at radii below $R_{\rm in}$) is radiatively inefficient [efficiency $L_{\rm bol}/(\dot{M}\times c^2) \sim 5\times10^{-4}$], or that a large fraction of material is ejected in an outflow, or both.

The ADAF model advocated by Ichimaru (1977) and Narayan & Yi (1994) explains low accretion efficiency as a consequence of the inner part of the flow advected into the black hole. The ADAF model was applied to XTE J1118+480 by Esin et al. (2001) who found a good fit to the optical–hard X-ray spectrum. Another possibility could be that the accretion power is advected into a jet or outflow, i.e. that a significant fraction of the energy could be used to power the jet. Indeed, ADAF solutions imply the flow is not bound (cf. Blandford & Begelman 1999). This outflow is indeed inferred from the flat radio spectrum and analogy with other sources in the hard state, where evidence for jets exists, as we discussed in Section 4.2. The most striking example of such sources is Cygnus X-1, which presents radio and X-ray spectra very similar to that of XTE J1118+480 and where a milliarcsec radio jet could be resolved (Stirling et al. 2001). However, since in XTE J1118+480 the fraction of the luminosity that can be firmly attributed to the jet represents only a few per cent of the total luminosity (see Section 3.7), the jet would have to be radiatively inefficient.

Actually the standard two-dimensional ADAF solution is likely to be strongly affected by the presence of the outflow and, more generally by the development of convective instabilities that only appear in two-dimensional solutions (see e.g. Stone, Pringle & Begelman 1999; Abramowicz, Lasota & Igumenshchev 2000; Igumenshchev, Abramowicz & Narayan 2000; Narayan, Igumenshchev & Abramowicz 2000; Quataert & Gruzinov 2000). As a consequence of the large theoretical uncertainties, we prefer to illustrate the possible presence of a hot optically thin geometrically thick component at the centre of the cold outer disc using a more phenomenological approach based on the constraints given by the observations and energy balance conditions as described below.

4.3.1 The hot disc model

We will now model the optical–hard X-ray spectrum, by assuming that the hot component comprises a sphere with radius equal to the cold disc truncation radius. The geometry is very similar to that of the sphere+disc geometry detailed in Dove et al. (1997).

To limit the number of parameters, and to avoid the uncertainties concerning the strength of the magnetic field, we further assume that the dominant cooling mechanism in the hot plasma is Compton cooling by the soft photons produced in the external disc. Other possible cooling mechanisms (bremsstrahlung, thermal synchrotron) are assumed to be negligible. This is a good approximation for luminous accreting black hole sources (Wardziński & Zdziarski 2000). In the case of XTE J1118+480, however, cyclotron/synchrotron and bremsstrahlung could be important cooling mechanisms (cf. Frontera et al. 2001a), but are not necessarily. We will discuss this further below, and will show how our assumption turns out to be consistent with the data.

We therefore used the non-linear Monte Carlo code of Malzac & Jourdain (2000) to compute the Comptonized spectrum emitted by the hot phase (the inner accretion flow) radiatively coupled in energy balance with the outer cold standard disc. In practice, we assume a homogeneous density, dissipation and heating rate inside the hot sphere. For a fixed Thomson optical depth, the hot plasma temperature is computed by balancing the heating and cooling. Possible temperature gradients due to the unavoidable inhomogeneity of the Compton cooling are accounted for by dividing the hot sphere into 10 homogeneous zones with equal volumes where the energy balance is computed locally. We neglect the effects of irradiation on the disc temperature profile, i.e. we assume the standard viscously heated multicolour blackbody disc ($T \propto R^{-3/4}$). The reprocessed emission is accounted for by re-emitting the absorbed energy, at the point it impinged on the external disc, with a blackbody spectrum at the local disc temperature.

The escaping X-ray spectrum is controlled mainly by the ratio of the volume-averaged dissipation rate in the hot phase (electron heating) to the soft flux from the disc that enters the cold phase (controlling the cooling). This ratio defining the energy balance of the hot component depends both on the assumed geometry and the fraction of radiated power dissipated in the hot phase:

$$f = L_{\rm c}/(L_{\rm v} + L_{\rm c}), \tag{2}$$

where $L_{\rm c}$ is the power radiated in the hot phase, $L_{\rm c} \sim L_{\rm X}$. $L_{\rm v}$ is the power viscously dissipated in the outer disc. The cold disc emission arises from both internal viscous dissipation $L_{\rm v}$, but also from reprocessing of the Comptonized hard X-rays irradiating the external disc. For our assumed geometry approximately one-third of the hard X-ray luminosity is intercepted by the disc. The observed disc luminosity is thus

$$L_{\rm disc} = [(1-f) + f/3](L_{\rm v} + L_{\rm c}) \tag{3}$$

and in the case of XTE J1118+480, f can be determined observationally

$$f \sim 1 \Big/ \left(\frac{2}{3} + \frac{L_{\rm disc}}{L_{\rm X}}\right) \sim 0.33. \tag{4}$$

The fraction of disc luminosity due to reprocessing is small, $\sim f/(3-2f) = 0.14$ and irradiation is unlikely to affect the outer disc structure. In particular, the local temperature depends only weakly on the total flux ($T \propto F^{1/4}$), thus for a local irradiating flux of 20 per cent of that of the local viscous flux, the disc temperature increases by less than 5 per cent. We note that this is perfectly in agreement with our observations, suggesting that effects of disc irradiation on the temperature profile should be weak (if any, see Section 3.6). Within the framework of the sphere+disc model, this 'weak irradiation' hypothesis is corroborated by the relatively low observed ratio of Comptonized to thermal emission. Therefore, our simple multicolour blackbody and power-law fits are consistent with our more sophisticated model assumptions. We also note that this geometry predicts an amplitude for the reflection component $R \sim 0.3$, which is slightly above the upper limits obtained by Frontera et al. (2001a) for their fits assuming low metallicity abundances in the disc (but see also Miller et al. 2002). However, even if such low-Z abundances might be related to a possible halo origin, as argued for by Wagner et al. (2001) and Mirabel et al. (2001), we point out that the metallicity should be higher than expected for a halo object, since the mass donor star is probably a CNO processed core (Haswell et al. 2002).

The spectral shape depends on five parameters: the disc outer temperature $T_{\rm out}$ and radius $R_{\rm out}$, the disc inner radius $R_{\rm in}$, and the fraction of accretion energy dissipated in the hot sphere to that dissipated in the accretion disc f, the hot sphere optical Thomson depth τ with respect to the sphere radius. The unique broad-band coverage in XTE J1118+480 constrains all the parameters relatively well.

In the simulation shown in Fig. 13 the cold disc parameters (and especially the locally emitted blackbody spectrum at its surface corresponding to the standard temperature dependence) have been set to values close to that assumed or derived from the fits of Section 3.4, namely $R_{\rm out} = 12 \times 10^3 R_{\rm s}$ (80 per cent of the Roche lobe radius), $R_{\rm in} = 300 R_{\rm s}$, $T_{\rm out} = 8000$ K. The Thomson optical depth along the sphere radius was fixed at $\tau = 1$ as indicated by the fit of Frontera et al. (2001a) for a spherical geometry, and $f = 0.33$ as discussed above. We did not include in the model any absorption as seen at $\log(\nu) \sim 17$, which was attributed to a warm absorber by Esin et al. (2001).

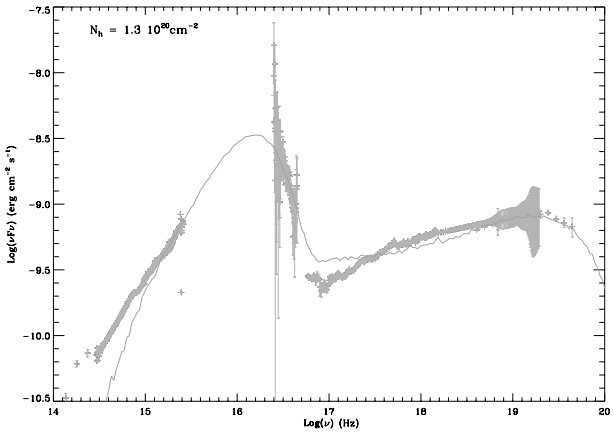

Figure 13. Modelling the optical to hard X-ray spectrum. The hot disc scheme is illustrated here, where we compare the non-linear Monte Carlo simulation for a central spherical hot plasma which radiates through Comptonization of the soft photons emitted by the outer cold disc both through internal viscous dissipation and reprocessing of the Comptonized hard X-rays (the latter being ≈20 per cent of the disc emission). See Section 3.1. This figure can be seen in colour in the on-line version of the journal on *Synergy*.

The most important parameters for the X-ray emission are f and τ. f controls the Compton y parameter of the plasma at equilibrium $y \propto \tau T_{\rm e}$ and thus the X-ray photon index Γ is very sensitive to f. With the f value independently provided by the observed luminosity of the cold and hot components, the model produces $\Gamma = 1.82$ (2–10 keV), in agreement with the results from spectral fits of the *SAX* data (Frontera et al. 2001a). Since all the parameters determining the X-ray slope are independently constrained, such an agreement is very remarkable. At fixed f, the parameter τ controls mainly the temperature of the hot phase. From energy balance we obtain a volume-averaged equilibrium temperature of the sphere of $kT_{\rm e} = 109$ keV in agreement with the value inferred from the fits of *SAX* data (Frontera et al. 2001a). Consequently, the shape of the high-energy cut-off is well reproduced.

Note that this model differs from the ADAF model of Esin et al. (2001) who considered cyclo-synchrotron radiation as the main source of soft photons for Comptonization and neglected the soft photons from the disc. We did precisely the opposite. In our model, if the bremsstrahlung and cyclo-synchrotron radiation were to constitute a significant additional source of soft photons, this would increase the cooling rate in the hot plasma, and, as a result we would obtain a much softer spectrum than was observed. The observations would then require a different geometry, reducing the soft photon input from the outer disc. For example, an oblate geometry for the central hot region could satisfy this requirement. In the extreme limit where the hot phase is geometrically thin along the disc axis we would be in the situation considered by Esin et al. (2001), dominated by cyclo-synchrotron radiation. Note that the correlated variability between the optical and X-rays suggests a causal connection, and that the synchrotron radiation emanating from the same region that produces the X-rays can contribute in the optical band (Merloni, Di Matteo & Fabian 2000), but not necessarily as a significant source of soft cooling photons. Therefore, this process is not inconsistent with our model where we neglected the synchrotron emission.

4.3.2 Jet corona models

If the X-ray emission is produced in the central part of the accretion flow, the ∼0.1 Hz QPO observed both in the X-ray and optical is difficult to explain (Merloni et al. 2000). On the other hand, it may be explained simply by a flux modulation at the Kepler frequency of the disc at $R_{\rm in}$. This suggests that a non-negligible fraction of the flux would be produced in a transition region where both the hot plasma and cold thin disc coexist.

This transition region could consist of a hot corona atop the external disc. The generation of magnetic field in the disc through magnetorotational instability and the subsequent buoyancy of the magnetic field (Tout & Pringle 1992; Miller & Stone 2000) is generally invoked as an efficient mechanism for the transfer of magnetic energy from the disc to a corona where it is dissipated through magnetic flares. This scenario for energy dissipation in the corona was built to explain a strong coronal emission in the innermost part of the accretion flow. At the large distances we infer for the disc truncation radius, it is expected to be less efficient.

Therefore, if $R_{\rm in}$ is as large as we infer, alternative dissipation processes such as transport and heating through Alfvén waves (Tagger & Pellat 1999) or viscous dissipation in a fast accreting corona (Różańska & Czerny 2000) may appear preferable. Actually, if the inner flow was very inefficient (or even non-existent), the X-ray

emission could be fully dominated by the coronal emission. In this context, mildly relativistic ejections of coronal plasma are likely to be important in hard state sources (Beloborodov 1999; Malzac, Beloborodov & Poutanen 2001). In particular, it may explain the relatively hard X-ray spectrum and absence of reflection observed in XTE J1118+480 together with being consistent with the presence of an outflow. From the theoretical side relativistic outflow models often require an accretion disc corona as the place where the flow is initially powered (see Tagger & Pellat 1999; Merloni & Fabian 2001). The accretion disc corona picture would thus be physically compatible with the presence of a jet inferred from the flat radio spectrum.

In accretion disc corona models a substantial part of the disc emission is due to reprocessing of the hard X-rays impinging on the disc. As the optical, near-UV and far-UV variability indicates that reprocessing is weaker than the extremely strong synchrotron component (Hynes et al. 2003), this constrains the corona to be active only in the innermost part of the disc. The X-ray luminosity should then come from a region of the disc forming a thin ring with inner radius $R_{\rm in}$ and outer radius $R_{\rm c}$.

One can obtain an estimate of $R_{\rm c}$ by assuming that at distances lower than $R_{\rm c}$, all the accretion power goes to the corona while at larger distance it is dissipated viscously in the disc. Since the estimated X-ray luminosity is approximately half of that of the disc and approximately half of the coronal emission is intercepted by the disc, we can conclude that approximately half of the disc luminosity could be due to the reprocessing. Assuming that the reprocessed luminosity is half of that of the disc one obtains $r_{\rm c} \sim 2R_{\rm in}$.

We point out that our results are perfectly consistent with the accretion–ejection instability (AEI) model (Tagger & Pellat 1999), which predicts that Alfvén waves efficiently power the corona and the jet in a range of distance comprised between $R_{\rm in}$ and the corotation radius of the Rossby vortex at a few $R_{\rm in}$ (Varnière & Tagger 2002). Particularly, from the value of the inner radius that we derive with our fits, the AEI predicts a QPO which is well in agreement (Varnière, Rodriguez & Tagger 2002) with the values observed in UV, optical and X-rays during the outburst at Fourier frequencies ~0.1 Hz. The prediction on the QPO frequency evolution would also be consistent with the observations by Wood et al. (2000). The AEI context, by assuming equipartition between magnetic field and gas pressure, would exclude a Schwarzschild black hole, and favour a Kerr black hole rotating at a spin between 0.90 and 0.99 (P. Varnière, private communication). This QPO may be explained simply by a flux modulation due to the Keplerian rotation of the disc or, in the Tagger & Pellat (1999) framework, the presence of the spiral wave (P. Varnière, private communication).

We also note that in addition to the Comptonized emission from the hot disc and/or corona, a synchrotron component from the jet could also contribute in the X-rays. Such a non-thermal component was seemingly detected in GRS 1915+105 in a low/hard state (Vadawale, Rao & Chakrabarti 2001). In fact, the whole X-ray emission could even arise from pure synchrotron from the jet as demonstrated by Markoff, Falcke & Fender (2001). This model attributes all the X-ray luminosity of XTE J1118+480 to synchrotron emission from the jet. A potential problem for this model is that it predicts essentially no reflection component. This makes it difficult to transpose to other similar jet sources such as Cygnus X-1, where a significant reflection component is clearly observed and correlated with other X-ray spectral characteristics such as the photon index (Gilfanov, Churazov & Revnivtsev 1999). However, the pure synchrotron model cannot be formally ruled out, and we could also have both mechanisms acting at the same time.

5 CONCLUSIONS

We reported multiwavelength observations of XTE J1118+480 during its outburst, assembling the most complete spectral energy distribution of this source yet published, including our observations with UKIRT, *HST*, *RXTE*, *EUVE*, and adding observations from the literature: Ryle Telescope, VLA, JCMT, *Chandra* and *SAX*. We followed the source for 6 months, and show its evolution during the outburst. The main results of our broad-band multi-epoch coverage are given below.

(i) The source XTE J1118+480 was in a very low state throughout the outburst (estimated inner radius at $350R_{\rm S}$).

(ii) The column density is low, between 0.80 and 1.30 $\times$ 10^{20} cm^{-2}.

(iii) The accretion disc seems to be heated mainly by viscosity throughout the outburst, without a strong irradiation contribution.

(iv) It exhibited an inverted spectrum from radio to at least optical wavelengths, characteristic of a strong non-thermal (likely synchrotron) contribution, usually attributed to an outflow.

(v) By examining the near-quiescent system we found that the best-fitting parameters were a fractional mass donor star contribution of 25 ± 2 per cent, a remnant accretion disc at 6000 ± 50 K and a distance of 1.71 ± 0.05 kpc.

(vi) The quasi-absence of variation of the SED during 3 months is consistent with a steady outflow emanating from the source, similarly to other 'microquasars' in the 'plateau' state.

(vii) The ratio between radio and EUV energy, indicative of the outflow to accretion energy ratio, suggests that the source falls into the regime of radio-quiet quasars, and is also consistent with a steady outflow.

(viii) The small change of the SED in the optical–UV part, along with the constant power-law slopes during the whole outburst, is consistent with a continuous, gradual decrease of the outflow energy.

(ix) We modelled the emission from the optical to the hard X-rays with a hot disc model, showing that the high-energy part of the spectrum can emanate from the accretion flow. We therefore have to take into account the possibility that the high-energy emission from this source comes from (a) Comptonization, (b) pure synchrotron or (c) a mixture of both.

Although this object exhibits peculiar characteristics, e.g. a large inner disc radius and a likely origin in the halo, some of its characteristics are very similar to other sources, particularly in the low–hard state and exhibiting jets or outflows. This object is particularly important because its very low absorption reveals phenomena that until now were difficult to study. XTE J1118+480 facilitates testing and refinement of models for variability and emission in black hole accretors.

ACKNOWLEDGMENTS

We thank Christopher W. Mauche for fruitful discussions concerning absorption in the EUV, and for giving us the *EUVE* data. We are grateful to Mike Garcia for useful discussions concerning the evolution of the SED, to him and Jeff McClintock for giving us the *Chandra* data, and to Filippo Frontera for the *SAX* data. We thank Tom R. Geballe who obtained the NIR spectrum of XTE J1118+480 on 2000 June 26. We thank Guy Pooley for the Ryle Telescope data also used in this figure, and VSNET for all their alerts on XTE J1118+480 and their optical data used in Fig. 1. SC and JM thank Michel Tagger, Peggy Varnière and Josep Martí. SC, CAH and RIH

gratefully acknowledge support from grant F/00–180/A from the Leverhulme Trust. SC and JM acknowledge a travel grant from the Groupe de Recherche *Phénomènes Cosmiques de Haute Énergie* of the French Centre National de la Recherche Scientifique. JM acknowledges a grant from the European Commission (contract number ERBFMRX-CT98-0195, TMR network 'Accretion on to black holes, compact stars and protostars'). WC also acknowledges support from HST-GO-08647.10-A.

The United Kingdom Infrared Telescope is operated by the Joint Astronomy Centre on behalf of the UK Particle Physics and Astronomy Research Council. UKIRT Service observations of XTE J1118+480 through the year 2000 were obtained thanks to override time which was pre-approved in the case of outbursting transients (U/00A/45, PI SC), to be coordinated with our *HST* and *RXTE* observations. SC is grateful to the UKIRT staff for these override service observations, and in particular to Andy Adamson, John K. Davies, Sandy K. Leggett and Chris Davis.

Based on observations made with NASA/ESA *HST*, associated with proposal GO 8647. Support was provided by NASA through a grant from the Space Telescope Science Institute, which is operated by the Association of Universities for Research in Astronomy, Inc, under NASA contract NAS 5-26555. We finally thank the *HST/STScI* and *RXTE* support staff for ongoing efficient effort in these multi-epoch campaigns. This research has made use of NASA's Astrophysics Data System Bibliographic Services and quick-look results provided by the ASM/RXTE team.

REFERENCES

Abramowicz M.A., Lasota J., Igumenshchev I.V., 2000, MNRAS, 314, 775
Balucinska-Church M., Belloni T., Church M.J., Hasinger G., 1995, A&A, 302, L5
Beloborodov A.M., 1999, MNRAS, 305, 181
Bessell M.S., Castelli F., Plez B., 1998, A&A, 333, 231
Blandford R.D., Begelman M.C., 1999, MNRAS, 303, L1
Bohlin R.C., Savage B.D., Drake J.F., 1978, ApJ, 224, 132
Brocksopp C. et al., 2002, MNRAS, 331, 765
Cardelli J.A., Clayton G.C., Mathis J.S., 1989, ApJ, 345, 245
Charles P., 1998, in Abramowicz M.A., Bjomsson G., Pringle J.E., eds, Theory of Black Hole Accretion Disks 'Black Holes in our Galaxy: Observations'. Cambridge Univ. Press, Cambridge, p. 1
Chaty S., Haswell C.A., Smith G.P., Smail I., Hynes R.I., 2000, IAU Circ., 7394, 3
Chaty S., Haswell C., Hynes R., Shrader C., Cui W., 2001a, in Combes F., Barret D., Thévenin F., eds, SF2A-2001: Semaine de l'Astrophysique Francaise. EdP-Sciences, p. 349 (astro-ph/0108242)
Chaty S., Haswell C., Hynes R., Shrader C., Cui W., 2001b, in Gimenez A., Reglero V., Winkler C., eds, Proc. 4th INTEGRAL workshop. ESA Publications, Noordwijk, p. 491 (astro-ph/0102103)
Chaty S., Rodríguez L.F., Mirabel I.F., Geballe T., Fuchs Y., 2001, A&A, 366, 1041
Cook L., Patterson J., Buczynski D., Fried R., 2000, IAU Circ., 7397, 2
Corbel S., Fender R.P., Tzioumis A.K., Nowak M., McIntyre V., Durouchoux P., Sood R., 2000, A&A, 359, 251
Cunningham C., 1976, ApJ, 208, 534
Dhawan V., Pooley G.G., Ogley R.N., Mirabel I.F., 2000, IAU Circ., 7395, 2
Dove J.B., Wilms J., Maisack M., Begelman M.C., 1997, ApJ, 487, 759
Dubus G., Lasota J., Hameury J., Charles P., 1999, MNRAS, 303, 139
Dubus G., Kim R.S.J., Menou K., Szkody P., Bowen D.V., 2001, ApJ, 553, 307
Eggleton P.P., 1983, ApJ, 268, 368
Elvis M. et al., 1994, ApJS, 95, 1
Esin A.A., McClintock J.E., Drake J.J., Garcia M.R., Haswell C.A., Hynes R.I., Muno M.P., 2001, ApJ, 555, 483
Fender R.P., 2001, MNRAS, 322, 31
Fender R.P., Pooley G.G., Durouchoux P., Tilanus R.P.J., Brocksopp C., 2000, MNRAS, 312, 853
Fender R.P., Hjellming R.M., Tilanus R.P.J., Pooley G.G., Deane J.R., Ogley R.N., Spencer R.E., 2001, MNRAS, 322, L23
Frank J., King A., Raine D., 1992, Accretion Power in Astrophysics. Cambridge Univ. Press, Cambridge
Frontera F. et al., 2001a, ApJ, 561, 1006
Frontera F. et al., 2001b, ApJ, 546, 1027
Garcia M., Brown W., Pahre M., McClintock J., Callanan P., Garnavich P., 2000, IAU Circ., 7392, 2
Gilfanov M., Churazov E., Revnivtsev M., 1999, A&A, 352, 182
Haardt F., Maraschi L., 1993, ApJ, 413, 507
Haswell C.A., Skillman D., Patterson J., Hynes R.I., Cui W., 2000, IAU Circ., 7427, 1
Haswell C.A., Hynes R.I., King A.R., Schenker K., 2002, MNRAS, 332, 928
Hynes R., Mauche C., Haswell C., Shrader C., Cui W., Chaty S., 2000, ApJ, 539, L37
Hynes R.I., Haswell C.A., Chaty S., Shrader C.R., Cui W., 2002, MNRAS, 331, 169
Hynes R.I. et al., 2003, MNRAS, 345, 292
Ichimaru S., 1977, ApJ, 214, 840
Igumenshchev I.V., Abramowicz M.A., Narayan R., 2000, ApJ, 537, L27
Leitherer C. et al., 2001, STIS Instrument Handbook, Version 5.0. STScI, Baltimore
McClintock J.E., Garcia M.R., Caldwell N., Falco E.E., Garnavich P.M., Zhao P., 2001a, ApJ, 551, L147
McClintock J.E. et al., 2001b, ApJ, 555, 477
Malzac J., Jourdain E., 2000, A&A, 359, 843
Malzac J., Beloborodov A.M., Poutanen J., 2001, MNRAS, 326, 417
Markoff S., Falcke H., Fender R., 2001, A&A, 372, L25
Mauche C., Hynes R., Charles P., Haswell C., 2000, IAU Circ., 7401, 2
Merloni A., Fabian A.C., 2001, MNRAS, 332, 165
Merloni A., Di Matteo T., Fabian A.C., 2000, MNRAS, 318, L15
Miller K.A., Stone J.M., 2000, ApJ, 534, 398
Miller J., Ballantyne D.R., Fabian A.C., Lewin W.H.G., 2002, MNRAS, 335, 865
Mirabel I.F., Dhawan V., Mignani R.P., Rodrigues I., Guglielmetti F., 2001, Nat, 413, 139
Motch C., Ricketts M.J., Page C.G., Ilovaisky S.A., Chevalier C., 1983, A&A, 119, 171
Narayan R., Yi I., 1994, ApJ, 428, L13
Narayan R., Igumenshchev I.V., Abramowicz M.A., 2000, ApJ, 539, 798
Orosz J.A., 2001, The Astronomer's Telegram, 67, 1
Paczyński B., 1971, ARA&A, 9, 183
Pooley G.G., Waldram E.M., 2000, IAU Circ., 7390, 2
Quataert E., Gruzinov A., 2000, ApJ, 539, 809
Remillard R., Morgan E., Smith D., Smith E., 2000, IAU Circ., 7389, 2
Revnivtsev M., Sunyaev R., Borozdin K., 2000, A&A, 361, L37
Różańska A., Czerny B., 2000, A&A, 360, 1170
Rumph T., Bowyer S., Vennes S., 1994, AJ, 107, 2108
Shakura N.I., Sunyaev R.A., 1973, A&A, 24, 337
Stirling A.M., Spencer R.E., de la Force C.J., Garrett M.A., Fender R.P., Ogley R.N., 2001, MNRAS, 327, 1273
Stone J.M., Pringle J.E., Begelman M.C., 1999, MNRAS, 310, 1002
Sunyaev R., Revnivtsev M., 2000, A&A, 358, 617
Sunyaev R.A., Titarchuk L.G., 1980, A&A, 86, 121
Tagger M., Pellat R., 1999, A&A, 349, 1003
Tanaka Y., Shibazaki N., 1996, Annu. Rev. A&A, 34, 607
Taranova O., Shenavrin V., 2000, IAU Circ., 7407, 2
Tout C.A., Pringle J.E., 1992, MNRAS, 259, 604
Ueda Y. et al., 2002, ApJ, 571, 918
Uemura M. et al., 2000, Publ. Astron. Soc. Japan, 52, L15

Vadawale S.V., Rao A.R., Chakrabarti S.K., 2001, A&A, 372, 793
Varnière P., Tagger M., 2002, A&A, 394, 329
Varnière P., Rodriguez J., Tagger M., 2002, A&A, 387, 497
Vrtilek S.D., Raymond J.C., Garcia M.R., Verbunt F., Hasinger G., Kurster M., 1990, A&A, 235, 162
Wagner R.M., Foltz C.B., Shahbaz T., Casares J., Charles P.A., Starrfield S.G., Hewett P., 2001, ApJ, 556, 42
Wardziński G., Zdziarski A.A., 2000, MNRAS, 314, 183
Whitehurst R., King A., 1991, MNRAS, 249, 25
Wood K.S. et al., 2000, ApJ, 544, L45
Zdziarski A.A., Poutanen J., Mikolajewska J., Gierlinski M., Ebisawa K., Johnson W.N., 1998, MNRAS, 301, 435
Zurita C. et al., 2002, MNRAS, 333, 791

This paper has been typeset from a TEX/LATEX file prepared by the author.

2.9.5 Observations en optique et infrarouge proche du candidat trou noir XTE J1720-318 : de l'état haut-mou à l'état bas-dur

"Optical/near-infrared observations of the black hole candidate XTE J1720-318 : from high-soft to low-hard state" par S. Chaty & N. Bessolaz, 2006, A&A, 455, 639

Cet article rassemble des observations en optique et infrarouge proche du candidat trou noir et microquasar XTE J1720-318, lors d'un sursaut. Ces observations ont eu lieu à deux époques distinctes, permettant d'étudier la source dans deux états différents : de l'état haut-mou à l'état bas-dur, et d'étudier l'évolution des différentes contributions (émission thermique du disque, non-thermique de la couronne, du jet...) dans ces deux états (voir le paragraphe 2.4.1 pour plus de détails).

A&A 455, 639–644 (2006)
DOI: 10.1051/0004-6361:20054735
© ESO 2006

Astronomy & Astrophysics

Optical/near-infrared observations of the black hole candidate XTE J1720-318: from high-soft to low-hard state⋆

S. Chaty[1] and N. Bessolaz[2]

[1] AIM – Astrophysique Interactions Multi-échelles (UMR 7158 CEA/CNRS/Université Paris 7 Denis Diderot), CEA Saclay, DSM/DAPNIA/Service d'Astrophysique, Bât. 709, L'Orme des Merisiers, 91191 Gif-sur-Yvette Cedex, France
e-mail: chaty@cea.fr
[2] Laboratoire d'Astrophysique, Observatoire de Grenoble, BP 53, 38041 Grenoble Cedex 9, France

Received 20 December 2005 / Accepted 6 April 2006

ABSTRACT

Aims. To gain a better understanding of high-energy Galactic sources, we observed the Galactic X-ray binary and black hole candidate XTE J1720-318 in the optical and near-infrared, just after the onset of its X-ray outburst in January, 2003. These observations were obtained with the ESO/NTT as the Target of Opportunity, in February and April 2003.
Methods. We performed an accurate astrometry and analysed photometrical and spectroscopic observations. We then produced a colour-magnitude diagram, looked at the overall evolution of the multi-wavelength light curve, and analysed the spectral energy distribution.
Results. We discovered the optical counterpart in the *R*-band ($R \sim 21.5$) and confirmed the near-infrared counterpart. We show that, for an absorption between 6 and 8 mag, XTE J1720-318 is likely to be an intermediate mass X-ray binary located at a distance between 3 and 10 kpc, hosting a main sequence star of spectral type between late B and early G. Our second set of observations took place simultaneously with the third secondary outburst present in X-ray and near-infrared light curves. The evolution of its spectral energy distribution shows that XTE J1720-318 entered a transition from a high-soft to a low-hard state in-between the two observations.

Key words. stars: binaries: close – stars: Hertzsprung-Russell (HR) and C-M diagrams – infrared: stars – X-rays: binaries – X-rays: individuals: XTE J1720-318

1. Introduction

X-ray binaries are constituted of a compact object and a companion star, the former attracting matter from the latter, either through an accretion disc or the wind. They are usually divided in 2 sub-classes: high mass X-ray binaries and low mass X-ray binaries, hosting early-type and late-type stars, respectively. Since accretion and ejection phenomena usually occur in these objects, they are ideal laboratories for studying relativistic phenomena and the formation and evolution of compact objects in binaries. However, to study them, we first have to derive the important parameters related to the nature of these systems, i.e. the distance, nature of the compact object, spectral type of the companion star, type of accretion, orbital parameters, etc. Because of the way they are formed, most of the observed Galactic X-ray binaries are located in the Galactic plane or even towards the Galactic centre, and therefore associated with very high absorption (up to $A_v \sim 50$ mag) because of the presence of gas and dust in this region. In this case, near-infrared (NIR) observations prove to be particularly useful, since the radiation is less absorbed at NIR wavelengths than at optical ones (see, e.g., Chaty et al. 2002). Furthermore, X-ray binaries have to be studied in a multi-wavelength context to disentangle all parts of the system emitting at various wavelengths: the accretion disc from high-energies to NIR, the companion star from ultra-violet to NIR, the jets from radio to X-rays, etc. (see, e.g., Chaty 2005).

On January 9, 2003, the All Sky Monitor (*ASM*) of the *Rossi-XTE* satellite discovered a new source in the X-ray sky: XTE J1720-318, in the direction of the Galactic bulge (Remillard et al. 2003). The 2–12 keV flux was initially ∼130 mCrab and reached ∼430 mCrab on January 10, 2003. Spectroscopic observations with *XMM-Newton* were carried out on February 20, 2003, allowing Markwardt (2003) to estimate the column density of hydrogen on the line of sight: $N_{\rm H} = 1.33{\times}10^{22}$ cm^{-2}. An iron line was detected at 6.2 keV with 95 eV equivalent width, and no low or high frequency oscillation was detected (Markwardt 2003). The 2–10 keV flux was estimated to be 1.6×10^{-9} erg cm^{-2} s^{-1} (Gonzalez-Riestra et al. 2003). The source was not detected during *INTEGRAL/IBIS* observations on February 28, 2003, but became visible at the end of the burst during *IBIS* surveys of the Galactic centre from the end of March 2003 (Goldoni et al. 2003). The source reached ∼25 mCrab in the 15–40 keV band and became detected in the 40–100 keV energy band at ∼30 mCrab on April 6 and 7, 2003, indicating that the source had undergone a change of state, as suggested by Goldoni et al. (2003). The high-energy observations suggest that the compact object is a black hole, first because of its early spectral evolution that was very similar to black hole X-ray transients (Remillard et al. 2003), and also because of X-ray spectral parameters (Cadolle Bel et al. 2004) and the presence of an iron line (Markwardt 2003).

A radio counterpart was discovered with the VLA on January 15, 2003, and confirmed with ATCA on January 16, 2003: only one radio source included in the *Rossi-XTE* error box

⋆ Based on ESO observations through programme # 070.D-0340.

Article published by EDP Sciences and available at http://www.edpsciences.org/aa or http://dx.doi.org/10.1051/0004-6361:20054735

significantly varied from 0.32 ± 0.04 to 4.9 ± 0.1 mJy at 4.9 GHz (Rupen et al. 2003). Radio observations took place from January to August 2003, allowing Brocksopp et al. (2005) to study the correlation between radio and X-ray fluxes.

A NIR counterpart was discovered then by Nagata et al. (2003) on January 18, 2003. Thirteen observations in J, H, and K_s, until May 21, 2003, allowed them to measure the exponential decay following the burst, which was equal to 60 days.

In this paper, we will first describe our optical and NIR observations and data reduction in Sect. 2, then report on our astrometry, photometry, and spectroscopy results in Sect. 3. We will then focus on constraining the companion star spectral type in Sect. 4, and finally we will analyse the evolution of the XTE J1720-318 light curve and spectral energy distribution (SED) in Sect. 5.

2. Observations and data reduction

Our observations were carried out as part of the Target of Opportunity (ToO) programme 070.D-0340 (PI: S. Chaty) dedicated to the study of new Galactic high-energy sources and jet sources. They were triggered so as to be conducted at the same time as *INTEGRAL* ToO observations, and we asked for two periods of observations. The first set of observations took place on February 28, 2003, and the second one on April 24, 2003. On February 28, 2003, we obtained NIR photometry in J-, H-, and K_s-bands with the spectra-imager SofI, and optical photometry in B-, V-, R-, and I-bands with EMMI, both installed on the NTT. On April 24, 2003, in addition to optical and NIR photometry, we also carried out NIR spectroscopy with SofI between 0.9 and 1.6 μm. We used the large field imaging of SofI's detector, giving an image scale of $0.288''$ pixel^{-1} and a field of view of $4.94' \times 4.94'$, and the EMMI detector with an image scale of $0.32''$ pixel^{-1} and a binning 2×2, giving a field of view of $9.9' \times 9.1'$.

Concerning the NIR observations, we repeated one set of observations for each filter with 9 different $30''$ offset positions, including XTE J1720-318, with an integration time of 90 s for each exposure, following the standard jitter procedure that allows us to cleanly subtract the blank NIR sky emission. We observed two photometrical standard stars of the faint NIR standard star catalogue of Persson et al. (1998): sj9157 on February 28, 2003, and sj9172 on April 24, 2003. We also performed rapid photometry in the K_s-band for half an hour to detect rapid variations of magnitude by taking a set of 90 images with 2 s integration time each. We binned the images by three using a median filter, and we carried out aperture photometry.

Concerning the optical observations, we acquired 300 s exposures in each filter, except for the B-band (200 s), using a 2×2 binning to increase the sensitivity. We observed the standard star RU152 in R- and I-bands. Since we did not have any standard star observations in the B and V filters, we used mean zero-points taken from the EMMI website[1].

We used the Image Reduction and Analysis Facility (IRAF) suite to perform data reduction, carrying out standard procedures of optical and NIR image reduction, including flat-fielding and NIR sky subtraction. The zero-points we obtained are reported in Table 1. As we had only one standard star observation available for each night, we used characteristic extinction coefficients at la Silla: $\mathrm{ext}_B = 0.214$, $\mathrm{ext}_V = 0.125$, $\mathrm{ext}_R = 0.091$, $\mathrm{ext}_I = 0.051$, $\mathrm{ext}_J = 0.08$, $\mathrm{ext}_H = 0.03$, and $\mathrm{ext}_{K\mathrm{s}} = 0.05$, to transform instrumental magnitudes into apparent magnitudes. The observations were performed through an airmass between 1 and 1.4.

[1] www.ls.eso.org/lasilla/sciops/ntt/emmi/

Table 1. Zero-points derived from SofI and EMMI observations. MJD = JD – 2 400 000.5.

	SofI observations	Emmi observations
February 28, 2003	$Z_J = 2.229 \pm 0.009$	
MJD 52 698	$Z_h = 2.259 \pm 0.007$	
	$Z_{k_s} = 2.862 \pm 0.006$	
April 24, 2003	$Z_J = 2.268 \pm 0.007$	$Z_b = 25.27 \pm 0.03$
MJD 52 753	$Z_h = 2.451 \pm 0.009$	$Z_v = 25.98 \pm 0.01$
	$Z_{k_s} = 2.999 \pm 0.011$	$Z_r = 26.21 \pm 0.02$
		$Z_i = 25.57 \pm 0.03$

Concerning the NIR spectroscopy, we took 12 spectra, half of them with an offset of $30''$ from the other half, to subtract the blank NIR sky, giving a total integration time of 180 s. To extract spectra and perform wavelength and flux calibrations, we used the *IRAF noao.twodspec* package. We used the standard star sj9157 already mentioned above to perform flux calibration. Since the spectral type of this star is unknown, we used the calibrated J, H, and K_s magnitudes of Persson et al. (1998) to deduce its spectral type by using a colour-colour diagram taken from Cox (2000) and assuming a main sequence star with negligible interstellar absorption on the line of sight. We then synthesised a blackbody spectrum with effective temperature, corresponding to the determined spectral type. This flux calibration is quite crude, since NIR stellar spectra often present broad absorption features; however, it gives a good indication of the flux.

3. Astrometry, photometry, and spectroscopy results

We used the K_s image of the XTE J1720-318 field taken on January 21, 2003 (O'Brien et al. 2003) to identify XTE J1720-318 in our NTT images. We then determined the position of the XTE J1720-318 NIR counterpart by deriving the astrometric solution, using ~12 stars taken from the GSC2 catalogue: the position we measured was: $\alpha = 17^{\mathrm{h}}19^{\mathrm{m}}58\overset{\mathrm{s}}{.}988 \pm 0\overset{\mathrm{s}}{.}008$; $\delta = -31°45'01\overset{''}{.}21 \pm 0\overset{''}{.}15$ (equinox J2000). This position is consistent with other determinations (Table 2).

We discovered the optical counterpart in the R- and I-bands at $\alpha = 17^{\mathrm{h}}19^{\mathrm{m}}58\overset{\mathrm{s}}{.}994 \pm 0\overset{\mathrm{s}}{.}007$, $\delta = -31°45'01\overset{''}{.}46 \pm 0\overset{''}{.}15$ (equinox J2000), a position that is consistent with the NIR counterpart. We present *BVRI* magnitudes in Table 3. The R and I magnitudes are consistent with detection limits given by Nagata et al. (2003): $R > 18$ and $I > 16.5$. We give a lower limit for the B- and V-bands, as we did not detect any counterpart in these bands.

Since XTE J1720-318 is located close to the Galactic centre, we had to perform crowded field photometry to obtain precise NIR magnitudes, using the *noao.daophot* package. This procedure, described in Massey & Davis (1992), consists of creating an empirical point-spread function with isolated bright stars, applying this model to the whole field, cancelling the contributions of neighbour stars, measuring the flux of the object itself, and then applying aperture correction (due to the use of a smaller aperture for measuring XTE J1720-318 magnitude than for standard stars). This procedure allows us to get photometry with better than 1% accuracy. We present the apparent J, H, and K_s magnitudes measured in February and April 2003 in Table 3. Uncertainties were determined from CCD readout and signal

Table 2. Summary of astrometry results (equinox J2000) for the XTE J1720-318 NIR counterpart.

	This paper	Nagata et al. (2003)	O'Brien et al. (2003)
α	$17^h19^m58\overset{s}{.}988 \pm 0\overset{s}{.}008$	$17^h19^m59\overset{s}{.}000 \pm 0\overset{s}{.}014$	$17^h19^m58\overset{s}{.}994 \pm 0\overset{s}{.}004$
δ	$-31°45'01\overset{''}{.}21 \pm 0\overset{''}{.}15$	$-31°45'01\overset{''}{.}2 \pm 0\overset{''}{.}2$	$-31°45'01\overset{''}{.}25 \pm 0.05$

Table 3. Apparent B, V, R, I, J, H, and K_s magnitudes of XTE J1720-318 (MJD = JD – 2 400 000.5).

Date	MJD	B	V	R	I	J	H	K_s
2003 02 28	52 698					17.47 ± 0.05	–	16.00 ± 0.06
2003 04 24	52 753	>23.2 ± 0.4	>23.1 ± 0.4	21.5 ± 0.3	20.6 ± 0.1	17.66 ± 0.05	16.99 ± 0.07	16.34 ± 0.05

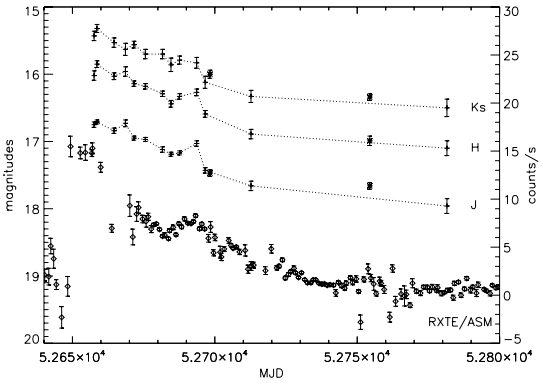

Fig. 1. Multi-wavelength XTE J1720-318 light curve. From bottom to top: *Rossi-XTE* X-ray light curve (indicated by diamonds); NIR J, H, and K_s light curves, respectively. NIR data taken from Nagata et al. (2003) are reported with "+", and data from this paper with "*". MJD = JD – 2 400 000.5.

noise. We note that we do not include the H-band observation of February 28, 2003, here because of bad sky subtraction.

Our NIR photometrical observations are reported in Fig. 1, where we also included results from Nagata et al. (2003). Our magnitudes, indicated by "*", are consistent with measures from Nagata et al. (2003). We notice the similar behaviour of X-ray and NIR light curves, particularly during the first maximum when the coverage is more complete, and we point out that we observed an increase in NIR on April 24, 2003 (MJD 52 753), observed by chance at exactly the same time as an X-ray increase seen on the light curve.

To analyse the rapid K_s photometry, we performed aperture photometry of XTE J1720-318 and three other stars of different magnitudes in the field. We show the results in the left panel of Fig. 2: we see the same type of variability for XTE J1720-318 as for comparison stars, showing that this variability is more likely due to sky variations than to the X-ray binary itself. Dividing XTE J1720-318 flux by the means of comparison star fluxes, we corrected the NIR light curve of XTE J1720-318 from this sky variability, to detect XTE J1720-318 intrinsic variations, if any. The corrected light curve is presented in the right panel of Fig. 2. The mean instrumental K_s magnitude, obtained by median-filtering all images, is 18.93±0.04 mag, and the standard deviation of all measures is ~0.11 mag. We can see a periodicity of ~600 s in Fig. 2; however, since the interval of magnitude variation is around 0.3 (3σ), it is not significant enough to interpret it as XTE J1720-318 intrinsic variations. Furthermore, a discrete Fourier analysis of these data does not give significant evidence of periodicity. Absence of significant variability at the level of +/–0.1 mag is consistent with the similar analysis done earlier in the outburst by O'Brien et al. (2003).

Finally, concerning the spectroscopy, we show the flux and wavelength calibrated spectrum we obtained in Fig. 3. Although the signal-to-noise ratio was too small to detect any line, the spectrum allowed us to estimate an upper limit to XTE J1720-318 flux: $\sim 2 \times 10^{-16}$ erg cm^{-2} s^{-1} Å^{-1}.

4. Constraints on the companion star spectral type

We will now try to constrain the nature of the companion star, first with a colour-magnitude diagram, then by modelling the optical and NIR spectral energy distribution (SED).

4.1. Colour–magnitude diagram

XTE J1720-318 optical and NIR magnitudes allow us to constrain the nature of the binary system by comparing its absolute magnitudes with those of well-determined spectral type stars (see, e.g., Chaty et al. 2002). For this purpose, we use template absolute magnitudes related to spectral types (taken from Ruelas-Mayorga 1991 for the NIR and Cox 2000 for the optical, respectively). The conversion of apparent magnitudes m to absolute magnitudes M depends on both distance d and interstellar absorption A_V, via: $M = m + 5 - 5\log d(pc) - A_V$. Concerning the interstellar absorption, we have three different estimates: First, *XMM-Newton* spectroscopy obtained in February 2003 gave $N_H = 1.24 \pm 0.02 \times 10^{22}$ cm^{-2} (Cadolle Bel et al. 2004). This column density corresponds to an absorption of $A_V = 6.9$ mag using the relation $A_V = 5.59 \times 10^{-22}\ N_H$ (Predehl & Schmitt 1995). Second, Nagata et al. (2003) obtained $A_V = 8$ by assuming a high temperature blackbody emission just after the X-ray burst. They also noted that extinction derived from the 2MASS survey is $A_V \sim 6$.

Here, we will use only one observing epoch, on April 24, 2003, when the source is fainter, to minimise the accretion disc contribution in the observed NIR flux. Even if the object was still far from quiescence, in this way, we determine a lower limit for the companion star spectral type by assuming that the accretion disc emission reddens the NIR flux.

To derive the possible spectral types, we computed the absolute magnitudes of XTE J1720-318, taking various distances d and absorption in the visible A_V. The results are reported with "*" in the ($J - K_s$, K_s) colour–magnitude diagram (CMD) presented in Fig. 4. The distance was computed between 1 and 10 kpc (from bottom to top, respectively) and the absorption between 6 and 8 magnitudes (from right to left, respectively).

From this CMD, we first derive that, in any case, the companion star must belong to the main sequence. Furthermore, if the interstellar absorption is high, $A_V \sim 8$ mag, the spectral type

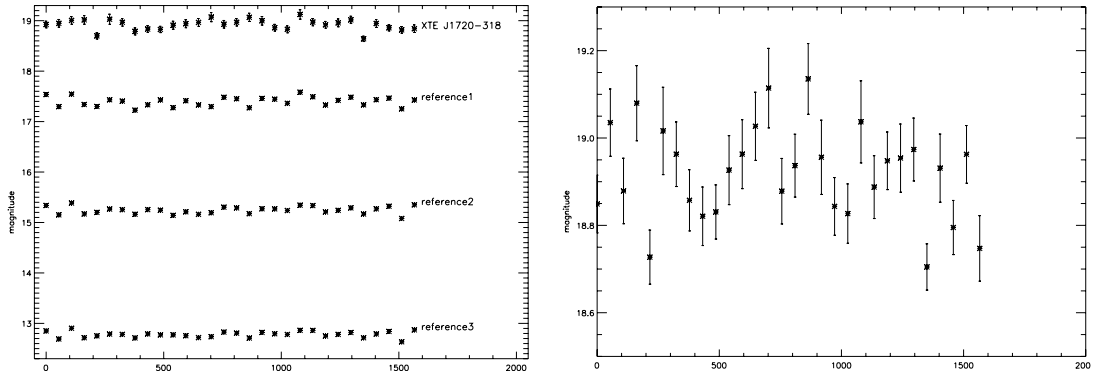

Fig. 2. *Left panel*: K_S light curve of XTE J1720-318 and three comparison stars of the field. *Right panel*: K_S light curve of XTE J1720-318 corrected from sky variations (the *y*-axis is in instrumental magnitude).

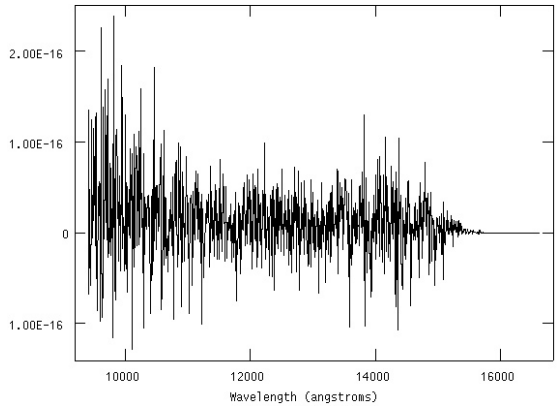

Fig. 3. NIR K_S-band spectrum of XTE J1720-318. The flux is given in erg cm^{-2} s^{-1} Å^{-1}.

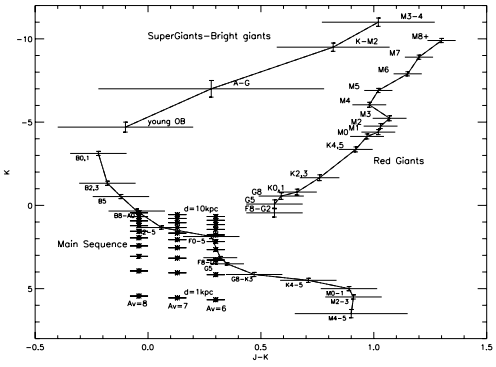

Fig. 4. Colour–magnitude diagram showing characteristic absolute magnitudes of various spectral types and XTE J1720-318 absolute magnitudes computed for interstellar absorption A_v between 6 and 8 mag ("*" *from right to left*) and distance between 1 and 10 kpc ("*" *from bottom to top*). We used the April 24, 2003, observations, when the object was fainter, to reduce the accretion disc contribution in the NIR flux. From this CMD we can conclude that XTE J1720-318 is an intermediate mass X-ray binary located at a distance between 3 and 10 kpc, and that the companion star is a main sequence star of spectral type between late B and early G (see text for more details).

would be between late B and early A, and the source far away, between 6 and 10 kpc. With an intermediate value of the interstellar absorption, $A_V \sim 7$ mag, the spectral type would be between late A and early F, and the distance between 5 and 7 kpc. Finally, with a small interstellar absorption, $A_V \sim 6$ mag, the spectral type would be between late F to early G, and the distance between 3 and 6 kpc. Therefore, we can conclude that, for an absorption between 6 and 8 mag, the XTE J1720-318 companion star is a main sequence star of spectral type between late B and early G, located at a distance between 3 and 10 kpc. This estimate of distance makes the source closer than suggested by Nagata et al. (2003): it is therefore possible that the source is not located in the Galactic bulge. We point out that from this analysis, XTE J1720-318 can be added to the list of intermediate mass X-ray binaries, like, e.g., V4641 Sgr (Chaty et al. 2003a).

4.2. Temperature and interstellar absorption

We now try to further constrain the absorption and spectral types by modelling XTE J1720-318's SED by an absorbed blackbody corrected from interstellar absorption. For each temperature, we calculate the associated blackbody spectrum that we multiply by the transmittance filter. Taking the interstellar absorption in the visible, we then derive absorption values for each wavelength, using Cardelli et al. (1989), and compute the magnitudes in each band.

We now want to compare these *RIJHK* magnitudes, computed for different effective temperatures and interstellar absorption, with apparent magnitudes. To do this, we calculate the discrepancy in each band by taking the K_S apparent magnitude and computing the quantity

$$S = (R - R_{obs})^2 + (I - I_{obs})^2 + (J - J_{obs})^2 + (H - H_{obs})^2$$

for the *R*-, *I*-, *J*-, and *H*-bands, for all considered temperatures and absorptions. In Fig. 5, we show the various curves of S versus effective temperatures T (varying between 3300 and 9300 K) parameterized by absorption A_V (varying between 5.5 and 8.5 mag).

We find that the best convergence, minimizing S, is found towards the values of the parameters ($A_V \sim 6$, $T \sim 4300$ K), corresponding to an XTE J1720-318 companion star spectral type of late F – early G; ($A_V \sim 7$, $T \sim 5600$ K), corresponding to late A – early F; and finally ($A_V \sim 8$, $T \sim 8100$ K), corresponding to late B and early A. This is, therefore, consistent with the results given by the CMD.

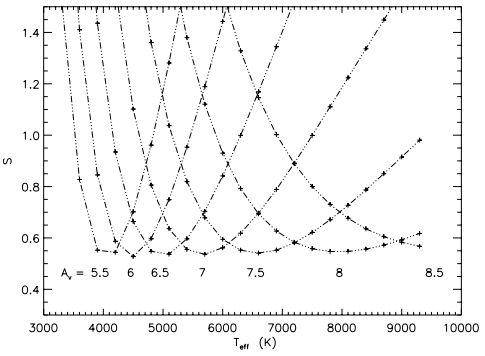

Fig. 5. Minimisation of the discrepancy between apparent and computed magnitudes, versus the blackbody effective temperature and interstellar absorption in the visible, given in magnitudes below each curve.

5. Evolution of XTE J1720-318 SED

In Fig. 6, we show the overall light curve of XTE J1720-318 from mid-January to the end of August 2003. First we can see that the light curve grossly has the form of a Fast-Rise Exponential-Decay light curve (so-called FRED), but superimposed on this FRED, the source exhibits a complex behaviour: after the main outburst on January 16 (MJD 52 656), we can see both in X-rays and in NIR a secondary outburst on January 29 (MJD 52 669), then a second one on February 22 (MJD 52 693), and finally a third one on April 24, 2003 (MJD 52 753), exactly at the time of our second epoch NIR observations. The main outburst and the last event are also associated with radio outbursts, and therefore with ejection events. We indicate the time of these events in Fig. 6 by O, 1, 2, and 3, respectively. There are other sources that exhibit clear secondary maxima in their X-ray light curves, such as A0620-00, GS 1124-68, GRO J0422+32 (Chen et al. 1997), 4U 1543-47 (Buxton & Bailyn 2004), and XTE J1550-564 (Jain et al. 2001). However, XTE J1720-318 seems to be the second source after A0620-00 to exhibit clear multi-secondary maxima in the optical/NIR, correlated with the X-rays, as seen in Fig. 6.

We also report the SED of XTE J1720-318 in Fig. 7 for the two observing epochs ("+" for February 28, 2003, and "∗" for April 24, 2003, respectively), where we put together ESO/NTT optical/NIR observations from this paper, *INTEGRAL/IBIS* high-energy observations (Cadolle Bel et al. 2004), and ATCA/VLA radio data (Brocksopp et al. 2005). We will now describe the light curve and both SEDs and analyse XTE J1720-318's evolution between these two observing epochs.

5.1. The February 2003 epoch: high-soft state

Observations obtained with *XMM-Newton*, *INTEGRAL/IBIS*, and *Rossi-XTE* in February 2003 showed that the source spectrum was very soft (power law index of $\Gamma = 2.7$): while the 2–12 keV flux was ∼100 mCrab, *IBIS* detected a source at only ∼2.1 mCrab in the 20–120 keV band (Cadolle Bel et al. 2004). XTE J1720-318 was not detected in radio (≤0.27 mJy at 4.8 GHz, Brocksopp et al. 2005), which is consistent with typical high-soft state (see, e.g., Chaty et al. 2003b). This is corroborated by the analysis of XTE J1720-318 SED from February 28, to March 2, 2003 (reported with "+" in Fig. 7), where we notice the characteristic shape of the accretion disc emission in X-rays (strong flux and soft spectrum), and the absence of radio emission.

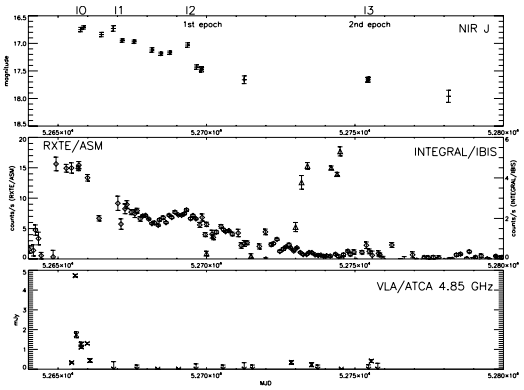

Fig. 6. Multi-wavelength light curve showing the outburst of XTE J1720-318 and its transition from high-soft to low-hard state. Top panel: NIR observations ("+": Nagata et al. 2003, "∗": this paper); Middle panel: high-energy observations ("◇": *RXTE/ASM*, "△": *INTEGRAL/IBIS* Cadolle Bel et al. 2004); Bottom panel: radio VLA/ATCA observations ("x": Brocksopp et al. 2005). We indicated at the top the times when the main outburst (O) and the three secondary outbursts (1, 2, 3 respectively) occurred. MJD = JD – 2 400 000.5.

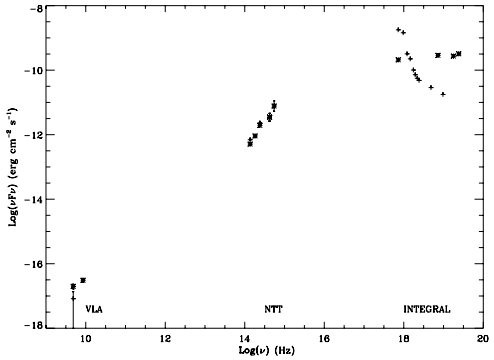

Fig. 7. Spectral Energy Distribution of XTE J1720-318 during the two observing epochs: the February 28, 2003, data are represented by "+", and the April 24, 2003, by "∗". The observations were taken nearly simultaneously with the VLA in the radio (Brocksopp et al. 2005), the NTT/EMMI and SOFI in the optical and NIR (this paper), and *INTEGRAL/IBIS* in the high-energy (Cadolle Bel et al. 2004). For the first epoch, the VLA data were taken on February 26, 2003, NTT/SOFI data on February 28, 2003, and *INTEGRAL/IBIS* data on February 28 – March 2, 2003. For the second epoch, VLA data were taken on April 26, 2003, NTT/SOFI data on April 24, 2003, NTT/EMMI on April 27, 2003, and *INTEGRAL/IBIS* data on February 28 – March 2, 2003. The February 28, 2003, observations correspond to the high-soft state: high and soft X-ray flux and no radio emission. On the contrary, the April 24, 2003, observations correspond to the low-hard state: low and hard X-ray flux and detection of radio emission. Optical and NIR fluxes were de-reddened, assuming an interstellar absorption in the visible of $A_V = 7$ mag. It is remarkable that they remain the same in both states.

5.2. The April 2003 epoch: low-hard state

On the other hand, after March 25, 2003 (MJD 52 723), XTE J1720-318 hard X-ray flux as seen by *INTEGRAL/IBIS* increased by a factor of 100 with respect to the high-soft state (Cadolle Bel et al. 2004), while the soft X-ray flux (*RXTE/ASM*) remained constant, as seen on the light curve of Fig. 6. Besides, we also observed a radio burst (Brocksopp et al. 2005),

simultaneous with an X-ray burst and an increase in the NIR flux. Therefore, XTE J1720-318 seems to have entered a transition towards a low-hard state in-between these 2 observing epochs, as suggested by Goldoni et al. (2003). This is confirmed by the analysis of the SED (data of this second epoch are reported with "∗" in Fig. 7): the source shows all the usual signs of the low-hard state. Firstly, we immediately notice that the source hardened in the high-energy domain with a high-energy power law index of $\Gamma = 1.8$. Secondly, the radio emission is usually interpreted in this state as synchrotron emission emanating from a jet. From the SED, we can derive the power law index α (in $S_\nu \propto \nu^\alpha$): ~ -0.3 in the radio and ~ 1.6 in the optical/NIR. Therefore, the extrapolation of the radio flux towards the optical/NIR domain is significantly fainter than the observed optical/NIR flux. This strongly suggests that the synchrotron emission from the jet is contributing only for a small part, if any, in the NIR emission. It seems also likely that there is no contribution from the accretion disk in the optical/NIR domain, since the slope in the NIR and optical remarkably remains the same in both observing epochs, while the X-ray decreased at the same time. Therefore, the NIR emission is dominated by the contribution of the companion star, which is consistent with XTE J1720-318 being an intermediate mass X-ray binary.

To further understand this source, it would be useful i) to get spectroscopic observations of XTE J1720-318 in quiescence to better characterise the companion star when the photospheric flux of the star dominates and ii) to observe the radial velocity of the binary system to derive the mass function and orbital parameters. With these parameters we will be able to further analyse its SED (as in, e.g., Chaty et al. 2003b, with the source XTE J1118+480).

6. Conclusions

We have reported optical and NIR observations of the X-ray binary XTE J1720-318, taken as Target of Opportunity observations following the January 2003 outburst of this source. By performing accurate astrometry, we discovered the optical counterpart in the *R*-band ($R \sim 21.5$) and confirmed the near-infrared counterpart. From photometric observations, analysis of a colour-magnitude diagram, and a basic modelling of its SED, we found that, for an absorption between 6 and 8 mag, XTE J1720-318 is likely to be an intermediate mass X-ray binary, hosting a black hole and a main sequence star of spectral type between late B and early G, located at a distance between 3 and 10 kpc. We also analysed the XTE J1720-318 X-ray and near-infrared light curves: this source exhibited three secondary outbursts, and our second set of observations took place simultaneously with the third one. Comparing the SEDs during and after its outburst, we confirm the change of state of this source, from high-soft to low-hard state.

Acknowledgements. S.C. thanks the ESO staff and especially Malvina Billères, Cédric Foellmi, Lisa Germany, Olivier Hainaut, Gaspare Lo-Curto, and Emanuela Pompei for performing the ToO observations. We are grateful to Marion Cadolle-Bel and Stéphane Corbel for making IBIS and ATCA data, respectively, available to us prior to publication. IRAF is distributed by the National Optical Astronomy Observatories, which are operated by the Association of Universities for Research in Astronomy, Inc., under a cooperative agreement with the National Science Foundation. This research has made use of NASA's Astrophysics Data System Bibliographic Services. *XTE* Results were provided by the ASM/RXTE teams at MIT and at the RXTE SOF and GOF at NASA's GSFC.

References

Brocksopp, C., Corbel, S., Fender, R., et al. 2005, MNRAS, 356, 125
Buxton, M. M., & Bailyn, C. D. 2004, ApJ, 615, 880
Cadolle Bel, M., Rodriguez, J., Sizun, P., et al. 2004, A&A, 426, 659
Cardelli, J. A., Clayton, G. C., & Mathis, J. S. 1989, ApJ, 345, 245
Chaty, S. 2005, in 2005 Very High Energy Phenomena in the Universe; Proceedings of the XLth Rencontres de Moriond
Chaty, S., Mirabel, I. F., Goldoni, P., et al. 2002, MNRAS, 331, 1065
Chaty, S., Charles, P. A., Martí, J., et al. 2003a, MNRAS, 343, 169
Chaty, S., Haswell, C. A., Malzac, J., et al. 2003b, MNRAS, 346, 689
Chen, W., Shrader, C. R., & Livio, M. 1997, ApJ, 491, 312
Cox, A. N. 2000, Allen's astrophysical quantities (Allen's astrophysical quantities, 4th ed., ed. A. N. Cox (New York: AIP Press; Springer)
Goldoni, P., Goldwurm, A., Kuulkers, E., et al. 2003, The Astronomer's Telegram, 153
Gonzalez-Riestra, R., Rodriguez-Pascual, P. M., Santos-Lleo, M., et al. 2003, IAU Circ., 8080, 1
Jain, R. K., Bailyn, C. D., Orosz, J. A., McClintock, J. E., & Remillard, R. A. 2001, ApJ, 554, L181
Markwardt, C. B. 2003, The Astronomer's Telegram, 115, 1
Massey, P., & Davis, L. 1992, A User's Guide to Stellar CCD Photometry with IRAF
Nagata, T., Kato, D., Baba, D., et al. 2003, PASJ, 55, L73
O'Brien, K., Clarke, F., Fender, R., et al. 2003, The Astronomer's Telegram, 117
Persson, S. E., Murphy, D. C., Krzeminski, W., Roth, M., & Rieke, M. J. 1998, AJ, 116, 2475
Predehl, P., & Schmitt, J. 1995, A&A, 293, 889
Remillard, R. A., Levine, A. M., Morgan, E. H., Smith, E., & Swank, J. 2003, IAU Circ., 8050
Ruelas-Mayorga, R. A. 1991, Rev. Mex. Astron. Astrofis., 22, 27
Rupen, M. P., Brocksopp, C., Mioduszewski, A. J., et al. 2003, IAU Circ., 8054

Chapitre 3

Astres binaires de grande masse

Ou comment les observations en optique et infrarouge permettent de révéler au jour les astres de haute énergie les plus obscurcis de notre Galaxie.

Sommaire

3.1 Introduction 107
3.2 Localisation des sources *INTEGRAL* dans le plan Galactique 110
3.3 Observations multi-longueurs d'onde de sources *INTEGRAL* 111
3.3.1 IGR J16318-4848 : représentant extrême des astres de haute énergie obscurcis 112
3.3.2 IGR J17544-2619 : archétype des supergéantes transitoires rapides de rayons X 116
3.3.3 Étude d'un échantillon de sources *INTEGRAL* en optique et infrarouge proche 121
3.3.4 Étude d'un échantillon de sources *INTEGRAL* en infrarouge moyen . . 122
3.4 Discussion et conclusions 125
3.5 Quelques articles publiés parmi les plus significatifs 133
3.5.1 La contrepartie optique/infrarouge proche de la source *INTEGRAL* obscurcie IGR J16318-4848 : une sgB[e] dans une binaire de rayons X de grande masse ? 135
3.5.2 Identifications de quatre sources *INTEGRAL* dans le plan Galactique à partir de localisations *Chandra* 153
3.5.3 IGR J17544-2619 : Une nouvelle transitoire rapide de rayons X à supergéante révélée par des observations en optique/infrarouge 169
3.5.4 Sources Galactiques de rayons X durs découvertes par *INTEGRAL* révélées par des observations multi-longueurs d'onde : I. Nature de l'étoile compagnon 177
3.5.5 Sources Galactiques de rayons X durs découvertes par *INTEGRAL* révélées par des observations multi-longueurs d'onde : II. Environnement de l'étoile compagnon 205

Mots clés : *INTEGRAL* ; IGR J16195-4945 ; IGR J16318-4848 ; IGR J17544-2619 ; infrarouge proche, infrarouge moyen

Abstract :

A new type of X-ray sources has been discovered by *INTEGRAL*, and their nature is revealed by means of multi-wavelength observations. Among these high-energy binary sources, two distinct classes are appearing. The first class is constituted of intrinsically obscured high-energy sources, of which IGR J16318-4848 seems to be an extreme representant. The second class is populated by the so-called supergiant fast X-ray transients, with IGR J17544-2619 being the archetype. I first report here on X-ray observations allowing an accurate localization of *INTEGRAL* sources, before describing a multi-wavelength study, from optical to mid-infrared wavelengths, of a sample of 20 *INTEGRAL* sources, including IGR J16318-4848 and IGR J17544-2619. This study first consists in an accurate astrometry, a photometry and a spectroscopy of these objects in optical and NIR, showing the predominance of high mass X-ray binary systems, hosting supergiant stars. Then, I show that in the case of the obscured sources IGR J16318-4848, IGR J16195-4945 and IGR J16358-4726, these observations suggest the presence of absorbing material (dust and/or cold gas) enshrouding the whole binary system. This chapter ends with a discussion about the nature of *INTEGRAL* sources in general, and the distinction between obscured sources and SFXTs.

Résumé :

Un nouveau type de sources de rayons X a été découvert par l'observatoire *INTEGRAL*, dont la nature est révélée par des observations multi-longueurs d'onde. Parmi ces systèmes binaires de haute énergie, deux classes distinctes apparaissent. La première classe est constituée d'astres de haute énergie intrinsèquement obscurcis, dont IGR J16318-4848 semble être un représentant extrême. La seconde classe est peuplée d'astres nommés "Transitoires rapides de rayons X à supergéante" ("Supergiant Fast X-ray Transients", SFXTs), dont IGR J17544-2619 semble être l'archétype. Je décris d'abord dans ce chapitre des observations en rayons X permettant une localisation précise de sources *INTEGRAL*, avant de présenter une étude multi-longueurs d'onde, en me focalisant sur les observations de l'optique à l'infrarouge moyen, d'un échantillon d'une vingtaine de sources *INTEGRAL*, incluant IGR J16318-4848 et IGR J17544-2619. Cette étude consiste tout d'abord en une astrométrie précise, une photométrie et une spectroscopie en optique et en infrarouge proche de ces objets, montrant la prédominance des systèmes binaires de grande masse contenant des supergéantes. Puis, je montre que dans le cas des sources obscurcies IGR J16318-4848, IGR J16195-4945 et IGR J16358-4726, les observations en infrarouge moyen suggèrent la présence de matériau absorbant (poussière et/ou gaz froid) entourant le système binaire dans son ensemble. Ce chapitre se termine par une discussion sur la nature des sources *INTEGRAL* en général, et de la distinction entre sources absorbées et SFXTs.

3.1 Introduction

L'observatoire INTErnational Gamma-Ray Astrophysics Laboratory (*INTEGRAL*) a effectué un relevé détaillé du plan galactique, et le détecteur ISGRI, de l'imageur IBIS, a découvert beaucoup de nouvelles sources, la plupart rapportées dans Bird et al. (2006), et montrées dans les figures 3.1 et 3.2[1]. Sur 214 sources *INTEGRAL* au total, les sources identifiées incluent 50 Noyaux Actifs de Galaxie (AGN), 32 binaires X de grande masse (HMXBs), 9 binaires X de faible masse (LMXBs), 9 variables cataclysmiques (CVs) et 6 sources d'autres types (Bird et al. 2006 ; Bodaghee et al. 2007). Les objets extragalactiques représentent donc 23% du total, les binaires galactiques 18% et les sources diverses 7%. La distribution des périodes orbitales des sources *INTEGRAL* suit la tendance bimodale des sources connues précédemment (Bodaghee et al., 2007), c'est-à-dire un pic aux courtes périodes orbitales (CVs, LMXBs) et un pic aux longues périodes orbitales (HMXBs). Beaucoup de ces nouveaux astres sont concentrés dans une direction tangentielle au bras de Norma de notre Galaxie (voir par exemple Chaty & Filliatre 2005 et Tomsick et al. 2004, et la figure 3.3 pour la localisation de ce bras), une région de notre Galaxie riche en régions de formation d'étoiles (Bronfman et al., 1996). Le résultat le plus important à ce jour de l'observatoire *INTEGRAL* est probablement la découverte de plusieurs astres nouveaux émettant dans les hautes énergies, caractérisés par des propriétés communes qui avaient rarement été vues jusqu'à maintenant. La plupart sont des binaires X de grande masse (HMXBs d'après l'acronyme anglais "High Mass X-ray binaries") abritant une étoile à neutron orbitant autour d'un compagnon O/B, et dans certains cas une étoile supergéante. Ces nouveaux astres se divisent alors en deux classes. Certains sont très obscurcis, caractérisés par une énorme extinction intrinsèque et locale. Le représentant certainement le plus extrême de cette classe est la source hautement absorbée IGR J16318-4848 (Filliatre & Chaty, 2004). Les autres astres sont des binaires X de grande masse contenant une étoile supergéante, caractérisés par des sursauts rapides et transitoires : une propriété inhabituelle au sein des binaires X de grande masse. Ils sont donc appelés "Supergéantes transitoires rapides de rayons X" (ou "Supergiant Fast X-ray Transients, SFXTs", en anglais ; Negueruela et al., 2006b), l'archétype de cette classe étant IGR J17544-2619.

Les observations dans les hautes énergies ne sont pas suffisantes pour révéler la nature de ces astres nouvellement découverts, car même si *INTEGRAL* peut fournir une localisation de ces sources qui est déjà très précise pour cette gamme d'énergie ($\sim 2'$), elle ne l'est pas assez pour repérer leur contrepartie à d'autres longueurs d'onde. Il est donc nécessaire d'entreprendre des observations multi-longueurs d'onde. Ainsi, la première étape est d'observer dans la partie basse énergie du domaine des hautes énergies, par exemple avec *XMM-Newton* ou *Chandra* ou même *Swift*. Ces satellites peuvent fournir une précision de localisation d'un astre émettant dans les hautes énergies à la seconde d'arc près. À ce stade, la chasse à la contrepartie optique de l'astre est ouverte. Cependant, encore une fois, apparaît une difficulté, due au niveau élevé d'absorption dans cette région de la Galaxie, proche du plan galactique. Il faut alors observer dans le domaine de l'infrarouge proche afin de commencer à révéler ces astres au grand jour. Enfin, puisque

[1]Il existe un site regroupant les informations mises à jour sur ces nouveaux astres *INTEGRAL* : http ://isdc.unige.ch/∼rodrigue/html/igrsources.html

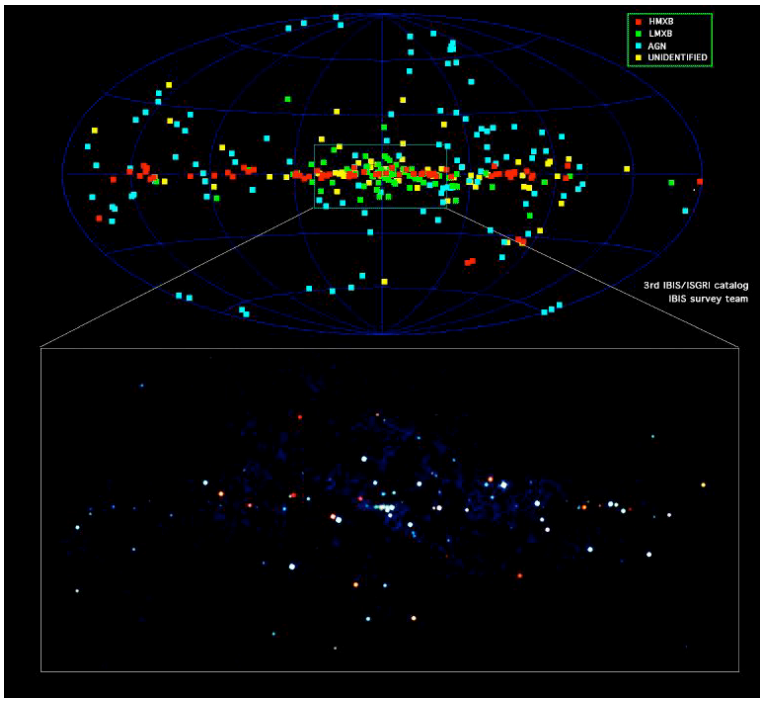

FIG. 3.1 – Répartition sur la voûte céleste des objets détectés par la caméra IBIS/ISGRI entre 17 et 100 keV. Le code de couleur sur l'image du haut indique le type de la source. L'image du bas est un zoom sur les régions centrales de la Galaxie, particulièrement bien exposées durant ce sondage. Dans ce dernier cas, le code des couleurs décrit des sources émettant préférentiellement à basse énergie (en-dessous de 30 keV, en rouge) ou à haute énergie (au-dessus de 40 keV, en bleu) (Crédit IBIS Survey Team ; Bird et al. 2006).

ces astres présentent une absorption élevée, il doit évidemment y avoir du matériau absorbant... C'est uniquement en observant aux longueurs d'onde de l'infrarouge moyen qu'il est possible de caractériser la nature de cette matière absorbante, et de déterminer si elle est constituée de gaz froid, ou de poussière, ou d'autre chose...

Je décris d'abord la recherche de contreparties dans les rayons X des sources *INTEGRAL* dans le paragraphe 3.2, avant d'aborder, dans le paragraphe 3.3, les observations multi-longueurs d'onde des deux astres archétypes décris ci-dessus, puis de livrer les résultats sur les observations en optique, infrarouge proche et moyen concernant une vingtaine de ces astres nouvellement découverts par l'observatoire *INTEGRAL*, et appartenant aux deux classes distinctes. Je discute ces résultats et conclus dans le paragraphe 3.4.

FIG. 3.2 – Image du bulbe de la Galaxie (Lebrun et al., 2004).

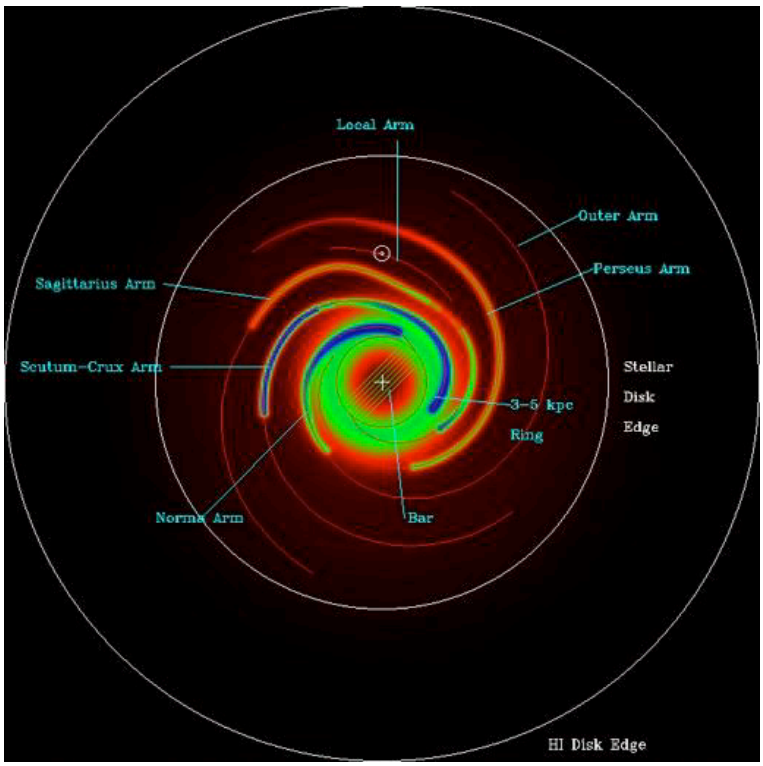

FIG. 3.3 – Diagramme HI de notre Galaxie, avec indication des différents bras.

3.2 Localisation des sources *INTEGRAL* dans le plan Galactique

L'imagerie en rayons X durs du plan Galactique par le satellite *INTEGRAL* a permis de révéler un grand nombre de sources nouvelles ou auparavant peu étudiées. Alors qu'*INTEGRAL* excelle dans la détection de sources dans la bande 20-50 keV, il ne localise les sources qu'à $1' - 5'$ près, ce qui n'est pas adéquat pour identifier les contreparties en optique et infrarouge. De plus, la plupart des sources *INTEGRAL* ne sont pas assez brillantes pour être bien étudiées (ou souvent même détectées) avec l'instrument à basse énergie d'*INTEGRAL*, JEM-X, qui a une bande d'énergie de 5 à 35 keV. De courtes expositions de sources *INTEGRAL*, obtenues avec le satellite de rayons X *Chandra*, permettent une grande avancée dans la compréhension de la nature de ces sources, en fournissant des positions plus précises que la seconde d'arc, conduisant à des contreparties optiques/NIR uniques, ainsi qu'à des spectres 0.3-10 keV qui peuvent être utilisés pour mesurer les densités de colonne et les formes de continuum. Nos programmes d'étude utilisant le satellite *Chandra* ont donc avec succès atteint les buts observationnels que je vais maintenant décrire.

Les positions *Chandra* fournissent des identifications optiques/IR, et permettent de conduire ensuite des observations photométriques et/ou spectroscopiques afin de déterminer les types spectraux des compagnons, qui sont aussi la clé pour obtenir des estimations de distance et de luminosité. De plus, les spectres *Chandra* fournissent des mesures de densité de colonne, indiquant si les sources présentent des absorptions intrinsèques. Alors que dans certains cas les observations X peuvent fournir une détermination de la période orbitale (Corbet et al. 2005 ; Thompson et al. 2006), des observations de vitesse radiale en optique ou IR sont nécessaires, et de telles études seront nécessaires pour prouver que des systèmes contiennent des trous noirs.

Notre programme d'étude avec *Chandra* consiste à acquérir des observations de 5 ks sur chaque source, afin d'identifier les sources *INTEGRAL* dans le plan Galactique. Dans le cycle 6, nous avons obtenu des identifications pour 4 sources (Tomsick et al., 2006a), et montré que deux de ces sources, IGR J16207-5129 et IGR J16195-4945, au vu des températures élevées du corps noir stellaire de l'étoile compagnon (T$>$ 9400 K et T$>$ 18000 K respectivement), sont vraisemblablement des systèmes binaires X de grande masse. Les deux autres sources, IGR J16167-4957 et IGR J17195-4100, au vu de l'extinction faible et des basses températures de leur corps noir stellaire, sont probablement des systèmes binaires X de faible masse. Bien que nos observations du cycle 8 ne font que commencer, nous avons déjà identifié une HMXB (Tomsick et al., 2006b) et nous avons observé en IR un autre candidat HMXB (Tomsick et al., 2007). La figure 3.4 montre les six images *Chandra* avec des sources brillantes uniques à l'intérieur des cercles d'erreur *INTEGRAL* dans chaque cas. Nous obtiendrons d'autres observations *Chandra* dans un futur proche. Nous n'avons pas détecté IGR J18539+0727, ce qui confirme qu'il s'agit d'une source transitoire (Bodaghee et al., 2007).

Nos analyses détaillées des quatre sources du cycle 6 de *Chandra* sont présentées dans Tomsick et al. (2006a)[2]. Bien qu'il y ait un pile-up modéré dans certains cas, les ajustements de loi de puissance absorbée fournissent une description adéquate des données, et nous avons obtenu de

[2]cf l'article présenté dans la sous-section 3.5.2

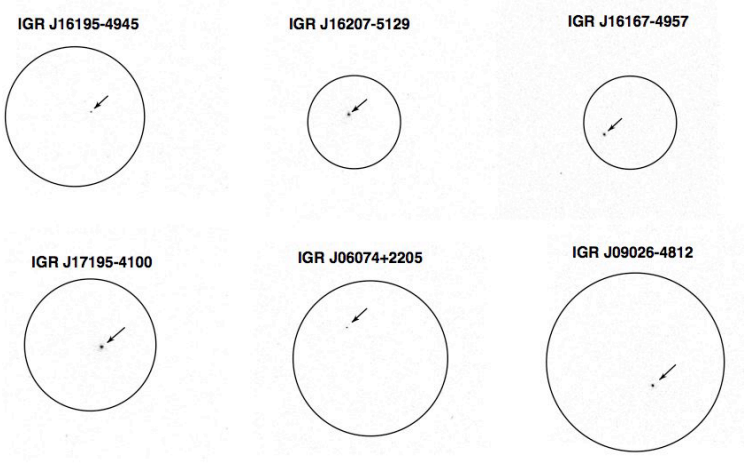

FIG. 3.4 – Images *Chandra* 0.3–10 keV, obtenues en 5 ks, de 6 sources *INTEGRAL*. Les cercles représentent les cercles d'erreur *INTEGRAL*, à 90% de confiance, et leur rayon varie de $1.2'$ (pour IGR J16207–5129) à $2.3'$ (pour IGR J09026–4812). Pour chacune de ces sources, nous avons détecté les contreparties X avec *Chandra* (Tomsick et al. 2006a ; Tomsick et al. 2006b ; Tomsick et al. 2007).

bonnes contraintes pour les paramètres spectraux. Nous avons trouvé des indices de photon durs de γ = 0.5-1.1 et que l'une des HMXBs (IGR J16195–4945) avait une densité de colonne qui pouvait être aussi grande que 10^{23} cm^{-2}. En utilisant notre propre photométrie optique et IR acquise à l'ESO/NTT, décrite dans le paragraphe 3.3, ainsi que les catalogues célestes disponibles (USNO, DENIS, 2MASS, et GLIMPSE), nous avons trouvé les contreparties IR et/ou optiques pour l'ensemble des 4 sources, avec des magnitudes J comprises entre 14.1 and 10.4. Ce qui est important, c'est que les positions *Chandra* ont permis une identification unique dans chaque cas, alors que, pour IGR J16167–4957 et IGR J17195–4100, d'autres sources optiques/IR de brillance comparable sont présentes dans un rayon de $\sim 2''$. Ainsi, *Chandra*, avec sa précision de localisation inférieure à la seconde d'arc, est le seul satellite qui pouvait fournir une identification unique. La distribution spectrale d'énergie (SED) pour la source la plus brillante est montrée dans la Figure 3.5. La photométrie optique/IR nous permet de déterminer que la température de corps noir du compagnon est supérieure à 18 000 K, ce qui montre que la source est une HMXB, ce qui a été confirmé par de la spectroscopie optique (Masetti et al., 2006). Ainsi, en résumé, nos résultats démontrent que nous sommes en mesure d'en apprendre significativement sur chaque source *INTEGRAL* à partir d'expositions courtes avec un satellite tel que *Chandra*, permettant une localisation précise, et finalement, que l'obtention de ces positions précises constituent une étape essentielle afin de progresser dans la compréhension de ces systèmes.

3.3 Observations multi-longueurs d'onde de sources *INTEGRAL*

Afin d'étudier les astres *INTEGRAL* nouvellement découverts, et pour lesquels une position précise ($\sim$ seconde d'arc) est disponible, il est nécessaire d'entreprendre des observations

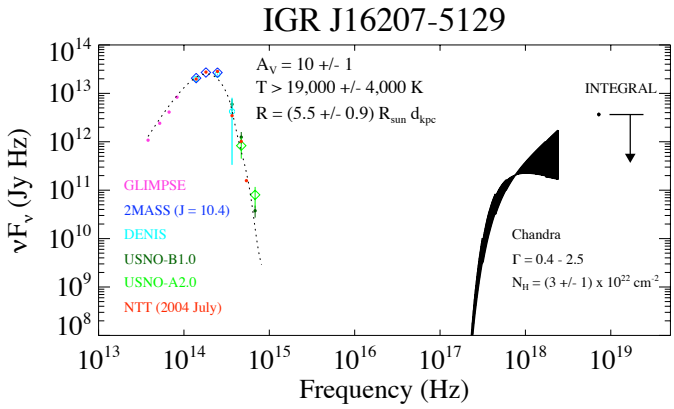

FIG. 3.5 – Distribution spectrale d'énergie de IGR J16207–5129. La partie optique/IR du spectre est ajustée avec un corps noir modifié par les effets de l'extinction (adapté de Tomsick et al. 2006a).

multi-longueurs d'onde dans les domaines optique, infrarouge proche et infrarouge moyen. Les observations multi-longueurs d'onde que je décris ici ont été acquises à l'Observatoire Européen Austral (ESO), dans ces trois domaines :

- • en optique ($400 - 800$ nm) avec l'instrument EMMI, au foyer du télescope de 3.5m New Technology Telescope (NTT) à l'observatoire de La Silla,
- • en infrarouge proche ($1 - 2.5$ μm) avec l'instrument SOFI au foyer du NTT,
- • et en infrarouge moyen ($5 - 20$ μm) avec l'instrument VISIR au foyer de Melipal, le troisième télescope de 8m (UT3) du Very Large Telescope (VLT) de l'observatoire de Paranal.

Ces observations ont été acquises en utilisant deux modes distincts : le mode "Cible d'Opportunité" (appelé dans la suite ToO, acronyme anglais de "Target of Opportunity") et "Visiteur". Ces observations incluent de la photométrie et de la spectroscopie sur une vingtaine d'astres *INTEGRAL*, ayant pour but d'identifier leur contrepartie par une astrométrie précise, la nature de l'étoile compagnon, d'en déduire leur distance, et finalement de caractériser la présence d'un milieu circumstellaire, sa température et sa composition.

3.3.1 IGR J16318-4848 : représentant extrême des astres de haute énergie obscurcis

Je vais commencer par rappeler les caractéristiques principales de cette source dans le domaine des hautes énergies (principalement rapportées dans Matt & Guainazzi 2003 et Walter et al. 2003), avant de décrire les observations en optique et infrarouge proche de cet astre. IGR J16318-4848 fut la première source découverte par le détecteur ISGRI de l'imageur IBIS, à bord d'*INTEGRAL*, le 29 janvier 2003, aux coordonnées galactiques $(l, b) \sim (336°, 0.5°)$, avec une incertitude de localisation d'un rayon de $2'$ (Courvoisier et al., 2003). Des observations en cible d'opportunité furent alors déclenchées avec *XMM-Newton*, qui permirent une localisation

plus précise à $4''$. Les observations avec *XMM-Newton* montrèrent que la source présentait une absorption élevée de $N_{\rm H} \sim 2 \times 10^{24}$ cm^{-2}, une température de kT $= 9$ keV, et un indice photonique ~ 2. Un "bord" d'absorption du Fer était visible de façon très prononcée dans son spectre de haute énergie, en plus de raies de fluorescence en émission du Fe Kα, Kβ et Ni Kα. Le flux dans la bande 15-40 keV était de 50-100 mCrab, la luminosité (en supposant que la source était située à une distance de 5 kpc) était $L_{5kpc} = 1 - 20 \times 10^{36}$ erg s^{-1}. Le flux était hautement variable (d'un facteur 20), et aucune oscillation n'était détectée. Il s'écoulait habituellement 10 heures entre les sursauts, et il n'était pas rare d'observer 2 à 3 jours d'inactivité. Les raies et le continuum variaient sur une échelle de temps du millier de secondes : ceci permit de contraindre la taille de la région émettrice à une limite supérieure de 3×10^{13} cm. Ces propriétés dans les rayons X, signatures d'une accrétion sous forme de vent, rappelaient d'autres astres spéciaux, comme par exemple CI Cam et GX 301-2.

La localisation précise nous a permis de rechercher la contrepartie de cet astre à d'autres longueurs d'onde ; et les résultats que je vais maintenant décrire proviennent principalement de Filliatre & Chaty (2004)[3], et je renvoie à la lecture de ce papier pour plus de détails. Des observations photométriques et spectroscopiques, en optique et infrarouge proche, ont été déclenchées en cible d'opportunité juste après la découverte de cet astre, mais les observations n'ont pas pu être réalisées avant les 23-25 février 2003. Walter et al. (2003) avaient rapporté la découverte des contreparties optiques et infrarouge proche, cependant, après une astrométrie améliorée basée sur ces nouvelles observations optiques/infrarouge proche, Filliatre & Chaty (2004) montrèrent que ces derniers avaient mal identifié la contrepartie optique. De plus, deux astres étaient présents en optique à l'intérieur du cercle d'incertitude de $4''$ fourni par l'instrument EPIC sur *XMM-Newton*, mais la comparaison avec la plaque USNO B1.0 en bande R montra qu'un seul des deux astres avait varié. Cette astrométrie indépendante et améliorée permis donc à Filliatre & Chaty (2004) de découvrir la vraie contrepartie optique, et de confirmer la contrepartie infrarouge proche proposée par Walter et al. (2003). La contrepartie optique de l'astre n'est pas détectée dans les filtres B et V (B $> 25.4 \pm 1.0$; V $> 21.1 \pm 0.1$), et apparaît dans les filtres R, I et Z (R $= 17.72 \pm 0.12$; I $= 16.05 \pm 0.54$). La première surprise apportée par les observations en optique et infrarouge proche est l'extrême brillance de cet astre en infrarouge proche : les magnitudes de la contrepartie infrarouge proche étaient J $= 10.33 \pm 0.14$; H $= 8.33 \pm 0.10$ et Ks $= 7.20 \pm 0.05$. Cet astre est trop brillant pour effectuer des observations photométriques avec un télescope de 4 mètres de diamètre[4], même avec un temps d'intégration de 1s !

La deuxième surprise apportée par les observations optiques et infrarouge proche est l'extrême absorption que présente cet astre en optique. En examinant la magnitude en fonction des longueurs d'onde optique/infrarouge proche (B, V, R, I, J, H, Ks) de IGR J16318-4848 et d'astres voisins présents dans le champ de vue, il est évident que l'astre de haute énergie présente une absorption intrinsèque inhabituellement élevée en optique, de $A_v = 17.4$ magnitudes, bien plus élevée que l'absorption le long de la ligne de visée que présentent les astres voisins (absorption de $A_v = 11.4$ magnitudes), mais encore cent fois plus faible que l'absorption dans les rayons X ! Ceci a conduit Filliatre & Chaty (2004) à suggérer que le matériau absorbant les rayons X de-

[3] cf l'article présenté dans la sous-section 3.5.1

[4] Ceci montre au passage la nécessité de maintenir de petites télescopes afin d'effectuer de telles observations.

vait être concentré autour de l'objet compact, alors que le matériau absorbant les rayonnements optique et infrarouge proche devait être lui concentré autour de l'ensemble du système binaire.

La spectroscopie en infrarouge proche, dans le domaine $0.95 - 2.5\ \mu$m, montrée dans la figure 3.6, a révélé la troisième surprise apportée par les observations en optique et infrarouge proche : l'astre de haute énergie présente un spectre inhabituel en infrarouge proche, très riche en raies d'émission de grande amplitude. Toutes ces raies nous permettent de caractériser le milieu entourant cet objet. Nous en rappelons ici les principales caractéristiques :

- • les raies de grande amplitude d'H (Brackett, Paschen, Pfund) et d'He I (avec profils P-Cygni) proviennent d'un vent dense et ionisé,
- • les raies d'He II viennent d'une région hautement excitée, proche de l'objet compact,
- • les raies interdites de [FeII] indiquent la présence de matériau chauffé par un choc,
- • les raies permises de FeII impliquent un milieu aux densités supérieures à $10^5 - 10^6$ cm^{-3},
- • les raies de NaI sont créées dans des régions froides et denses, protégées à la fois des rayonnements de l'étoile et de l'objet compact.

Il est donc clair à partir de ces caractéristiques ques ces raies proviennent de milieux différents (présentant des densités et des températures variées), suggérant la présence dans cet astre de haute énergie d'un environnement circumstellaire hautement complexe et stratifié, ainsi que la présence d'une enveloppe et d'un vent. Seules des étoiles lumineuses post séquence principale montrent de tels environnement extrêmes, et ainsi l'étoile compagnon est probablement une étoile supergéante de type spectral sgB[e] (ou même une étoile de type spectral non classifié uncl/sgB[e] à cause de sa luminosité élevée). Le système est donc un système binaire de rayons X de grande masse. Comme c'était le cas dans les rayons X, les propriétés en infrarouge proche sont similaires à celles d'un autre astre de haute énergie aux caractéristiques spéciales : CI Cam.

Filliatre & Chaty (2004) ont ensuite construit la distribution spectrale d'énergie multi-longueur d'onde de cet astre, depuis la radio jusqu'aux rayons X, en incluant les domaines optique et infrarouge proche. Ils ont ajusté à ces observations un corps noir représentant l'émission de l'étoile compagnon, et en ont déduit les paramètres suivants : $A_v = 17.5$ magnitudes, $L \sim 10^6 D^2_{6kpc} \times L_\odot$, $T = 20250$ K, $M = 30 M_\odot$ et $r/D = 5 \times 10^{-10}$, où A_v est l'absorption dans la bande V et L, T, M, r et D sont respectivement la luminosité, la température, la masse, le rayon et la distance de l'étoile compagnon. Ces paramètres impliquent une étoile de luminosité, de température et de masse élevées, probablement donc une supergéante, située à une distance de 6 kpc. La photométrie, la spectroscopie et l'ajustement de la distribution spectrale d'énergie donnent donc des résultats cohérents entre eux. De plus, en plaçant ces paramètres sur un diagramme Hertzsprung-Russell (ou température–luminosité, voir la figure 1.3), on remarque que cette étoile compagnon est située au bord du domaine des supergéantes bleues, indiquant qu'il s'agit d'un objet extrême même parmi ces déjà extrêmes étoiles supergéantes bleues !

La distribution spectrale d'énergie peut aussi nous permettre d'essayer d'en déduire la nature de l'objet compact. En effet, une corrélation entre densités de flux de rayons X et de radio a été trouvée au sein des systèmes de trous noirs, associés à une émission de rayons X dans l'état bas/dur (Gallo et al., 2003). Si l'objet compact de IGR J16318-4848 était un trou noir, son flux de rayons X, d'un niveau de 50-100 mCrab, et dans l'état bas/dur conduirait à un flux radio de 10 mJy. Cependant, une observation radio effectuée avec ATCA le 9 février 2003 n'a détecté aucun astre jusqu'à 0.1 mJy, ce qui suggère que l'objet compact est une étoile à neutron. Mais je sou-

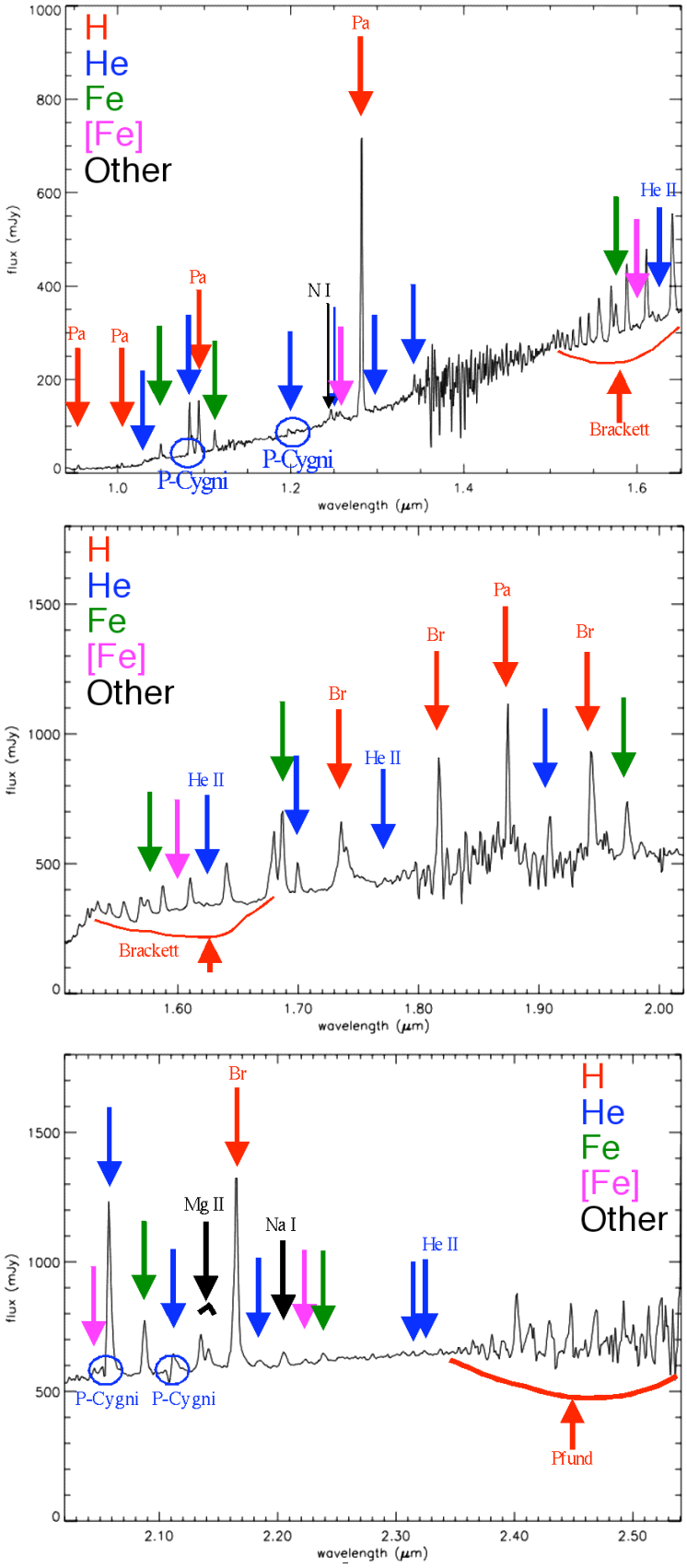

FIG. 3.6 – Spectres en infrarouge proche (0.95-1.65 μm en haut, 1.5-2.05 μm au milieu et 2.0-2.55 μm en bas) de IGR J16318-4848 acquis à l'ESO/NTT (Filliatre & Chaty, 2004).

ligne qu'il faut être prudent, puisque cette corrélation pourrait s'avérer ne pas être si universelle, comme l'atteste par exemple Cadolle Bel et al. (2007)[5].

Maintenant, la question qui reste en suspens est : quelle est la cause de cette absorption inhabituelle dans les domaines optique et infrarouge proche ? Afin de répondre à cette question, j'ai récemment obtenu des observations en infrarouge moyen avec l'instrument VISIR installé au foyer Cassegrain du télescope UT3 du VLT. J'étais donc en possession de la distribution spectrale d'énergie de IGR J16318-4848 des longueurs d'onde allant de l'optique à l'infrarouge moyen, et incluant des données du NTT de l'ESO, du satellite *Spitzer* (relevé GLIMPSE) et de VISIR sur le VLT (voir figure 3.7). J'ai ajusté les observations avec un modèle d'étoile compagnon (en prenant les paramètres habituels d'une étoile sgB[e]) et une simple composante sphérique de poussière. Plus de détails sur cette procédure d'ajustement sont donnés dans le paragraphe 3.3.4. Les paramètres obtenus concernant l'étoile compagnon sont une température T $= 23500$ K, un rayon R$_{star}$ $= 20.5 R_{\odot} = 15 \times 10^6$ km, et ceux concernant la composante de poussière sont : une température T $= 900$ K, un rayon R $= 11.9 R_{star} = 171 \times 10^6$ km et une absorption A$_v$ $= 17.4$ magnitudes. La distance de l'astre dérivée à partir de l'ajustement est de D $= 1.2$ kpc. Le χ^2 réduit (χ^2/degré de liberté ou χ^2/dof) de l'ajustement est de 35/33, (plus de détails sur ce travail sont donnés dans Rahoui et al. (2008). Ce qui est important dans ce résultat est que dans le cas de IGR J16318-4848 il est nécessaire d'ajouter une composante additionnelle (probablement due à l'émission de la poussière). L'extension de cette composante de poussière semble suggérer qu'elle entoure l'ensemble du système binaire, ainsi que le ferait un cocon de poussière.

Résumons maintenant brièvement la nature de IGR J16318-4848. Nous faisons face à un système binaire de haute énergie de grande masse, situé à une distance entre 1 et 6 kpc, hébergeant (probablement) une étoile à neutron et une étoile supergéante de type spectral précoce sgB[e]. Il s'agit du deuxième système binaire de haute énergie de grande masse comportant une étoile supergéante sgB[e], après CI Cam. Les faits les plus surprenants sont i) l'objet compact semble être entouré d'un matériau absorbant et ii) l'ensemble du système binaire lui-même semble être entouré d'un matériau circumstellaire dense et absorbant, peut-être une enveloppe ou un cocon de poussière, où on détecte la présence à la fois de composantes de vent stellaire froid et chaud. IGR J16318-4848 semble donc être un représentant extrême de cette nouvelle classe de sources obscurcies dont nous reparlerons dans la suite.

3.3.2 IGR J17544-2619 : archétype des supergéantes transitoires rapides de rayons X

Les supergéantes transitoires rapides de rayons X (Supergiant Fast X-ray Transients, SFXTs) constituent une classe d'astres récemment identifiée parmi les sources découvertes par *INTEGRAL*. Comme son nom l'indique, cette classe est constituée de sources transitoires de haute énergie, dont les caractéristiques communes sont : elles présentent des sursauts rapides qui ne durent que quelques heures, leur émission en quiescence est faible, leur spectre dans les hautes énergies requiert comme accréteur un objet compact –trou noir ou étoile à neutron–, et elles hé-

[5]Sur cet aspect de la corrélation et des sources qui ne la suivent pas, voir une discussion plus complète dans le paragraphe 2.4.2

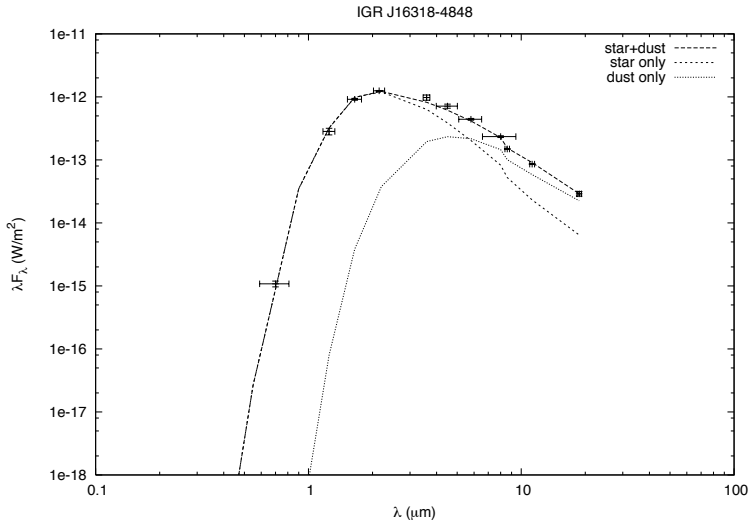

FIG. 3.7 – Distribution spectrale d'énergie de l'optique à l'infrarouge moyen de IGR J16318-4848 incluant des données du NTT de l'ESO, de VISIR sur l'UT3 du VLT et du satellite *Spitzer* (relevé GLIMPSE). Sur ce graphe sont indiquées les observations, ajustées avec un modèle comprenant une étoile compagnon (en prenant les paramètres habituels d'une sgB[e]) et une simple composante sphérique de poussière. Le modèle de l'étoile est en pointillés-traits fins, celui de la poussière en pointillés-points, et l'ajustement total est en pointillés-traits gras. Cet ajustement a permis de déduire les paramètres suivants : i) concernant l'étoile compagnon star : température T $= 23500K$ et rayon $R_{star} = 20.5R_{\odot} = 15 \times 10^6$ km ; ii) concernant la composante de poussière : température T $= 900K$, rayon R $= 11.9R_{star} = 171 \times 10^6$ km. L'absorption dérivée de l'ajustement est de $A_v = 17.4$ magnitudes, et la distance D $= 1.2$ kpc. La valeur du χ^2 réduit (χ^2/dof) de l'ajustement est 35/33. Le résultat principal fourni par cette distribution spectrale d'énergie est que dans le cas de IGR J16318-4848 il est nécessaire d'ajouter une composante additionnelle (par exemple de poussière) afin de pouvoir l'ajuster aux observations multi-longueurs d'onde.

bergent une étoile compagnon de type spectral supergéante O/B. Parmi ces astres, IGR J17544-2619 semble en être l'archétype, puisqu'il présente toutes les caractéristiques communes aux astres appartenant à cette classe de SFXTs. Je vais maintenant rappeler les propriétés dans les hautes énergies de IGR J17544-2619, avant de décrire les observations en optique et infrarouge proche.

IGR J17544-2619 est un astre transitoire et brillant dans les rayons X, découvert par *INTEGRAL* le 17 septembre 2003, à 3° du centre Galactique centre (Sunyaev et al., 2003). *XMM-Newton* a observé le champ de vue de cet astre, et EPIC a détecté une contrepartie dans les rayons X avec une luminosité variable non absorbée d'une valeur moyenne de $1.1 - 5.7 \times 10^{35}$ erg s^{-1} dans la bande d'énergie 0.5-10 keV, en supposant une distance de 8 kpc (cf par exemple González-Riestra et al. 2004). Les spectres EPIC peuvent être représentés par un modèle de loi de puissance avec des indices de photon variables de $1.42 - 2.25 \pm 0.15$. Le spectre dans la bande d'énergie 0.5-10 keV durcit lorsque l'intensité croît. Cet astre a ainsi un spectre de rayons X très dur, et présente une faible absorption intrinsèque ($\sim 10^{22}$ cm^{-2}). Ses sursauts durent

quelques heures, entre deux sursauts il présente de longues périodes de quiescence, et il semble qu'il existe une longue période de sursauts d'activité de 165 days (Negueruela et al., 2006b). De plus, aucune émission radio n'a été détectée jusqu'à une limite supérieure de 7.35 mJy à 0.61 GHz (Pandey et al., 2006). L'objet compact est probablement une étoile à neutron, ainsi que l'a suggéré in't Zand (2005). Certaines propriétés à haute énergie de cet astre étaient similaires à d'autres astres *INTEGRAL* (tels que IGR J16318-4848, IGR J16320-4851, IGR J16358-4726, cf par exemple Chaty & Filliatre 2005). La question qui a rapidement surgi concernant cet astre est donc : est-ce une autre binaire X galactique hautement absorbée ? Mais les sursauts rapides d'activité de cet astre, plutôt inhabituels au sein des binaires X de grande masse, pouvaient même suggérer qu'il appartenait à un nouveau type de binaires de rayons X. Il était donc important d'établir sa nature, et encore une fois, les observations en optique et en infrarouge vont jouer ici un rôle crucial sur la quête permettant de révéler la nature de cet astre.

Pellizza et al. (2006) ont réussi à obtenir des observations optique et infrarouge proche en cible d'opportunité un jour seulement après la découverte de cet astre. Je décris ici les principaux résultats, et renvoie à Pellizza et al. (2006)[6] pour obtenir plus de détails sur l'étude de la contrepartie optique et infrarouge proche de cette source. À l'intérieur du cercle d'incertitude de rayon $2'$ fourni par *INTEGRAL* de l'astre IGR J17544-2619, se trouve une source *ROSAT* (1RXS J175428, localisée avec un rayon d'incertitude de $23''$) qui n'a en fait aucun lien avec IGR J17544-2619. Les observations de *XMM-Newton* ont permis de localiser avec précision l'astre avec un cercle d'incertitude de rayon $4''$. Mais même dans un cercle aussi petit, se trouvaient à l'intérieur cinq candidats à la contrepartie optique : un candidat brillant (appelé C1 dans Pellizza et al. 2006) et catalogué dans USNO et 2MASS, trois candidats très faibles (C2, C3 et C5), probablement des étoiles naines situées en premier plan, et finalement un objet étendu (C4), vraisemblablement une galaxie à grand décalage vers le rouge. Pellizza et al. (2006) ont montré que le candidat C1 devait être la contrepartie de IGR J17544-2619, et l'ont confirmé par une astrométrie incluant des observations du satellite *Chandra*. En effet, ces observations ont permis de localiser cet astre encore plus précisément, avec un cercle d'incertitude de rayon $0.4''$.

Pellizza et al. (2006) ont aussi effectué de la spectroscopie sur le candidat C1, dont le spectre, montré dans la figure 3.8, est caractéristique d'une étoile supergéante bleue de type spectral O9Ib, de masse $25 - 28 M_{\odot}$ et de température T $\sim$ 31000 K : il s'agit donc d'un système binaire de grande masse. Le spectre présente aussi des profils $H\alpha$ P-Cygni, suggérant la présence d'un vent stellaire à une vitesse de 265 ± 20 km/s. Si la vitesse de ce vent est confirmée, elle est inhabituellement faible pour des étoiles de type spectral O (cette valeur est par exemple inférieure à la vitesse du vent de 400 km/s présent dans IGR J16318-4848, et rapportée dans Filliatre & Chaty 2004). La distance déduite de ces observations est de 3-4 kpc.

Afin de mieux caractériser la nature de l'émission de cet astre, et pour répondre à la question sur la présence de poussière autour de ce type d'astres, j'ai obtenu récemment des observations en infrarouge moyen avec VISIR sur le VLT/UT3. Ces observations m'ont ainsi permis d'ajuster la distribution spectrale d'énergie de IGR J17544-2619 de l'optique à l'infrarouge moyen, incluant des données du NTT de l'ESO, du satellite *Spitzer* (relevé GLIMPSE) et de l'instrument VISIR sur le VLT/UT3 (cf Figure 3.9). Les observations ajustées avec un modèle d'étoile compagnon

[6] cf l'article présenté dans la sous-section 3.5.3

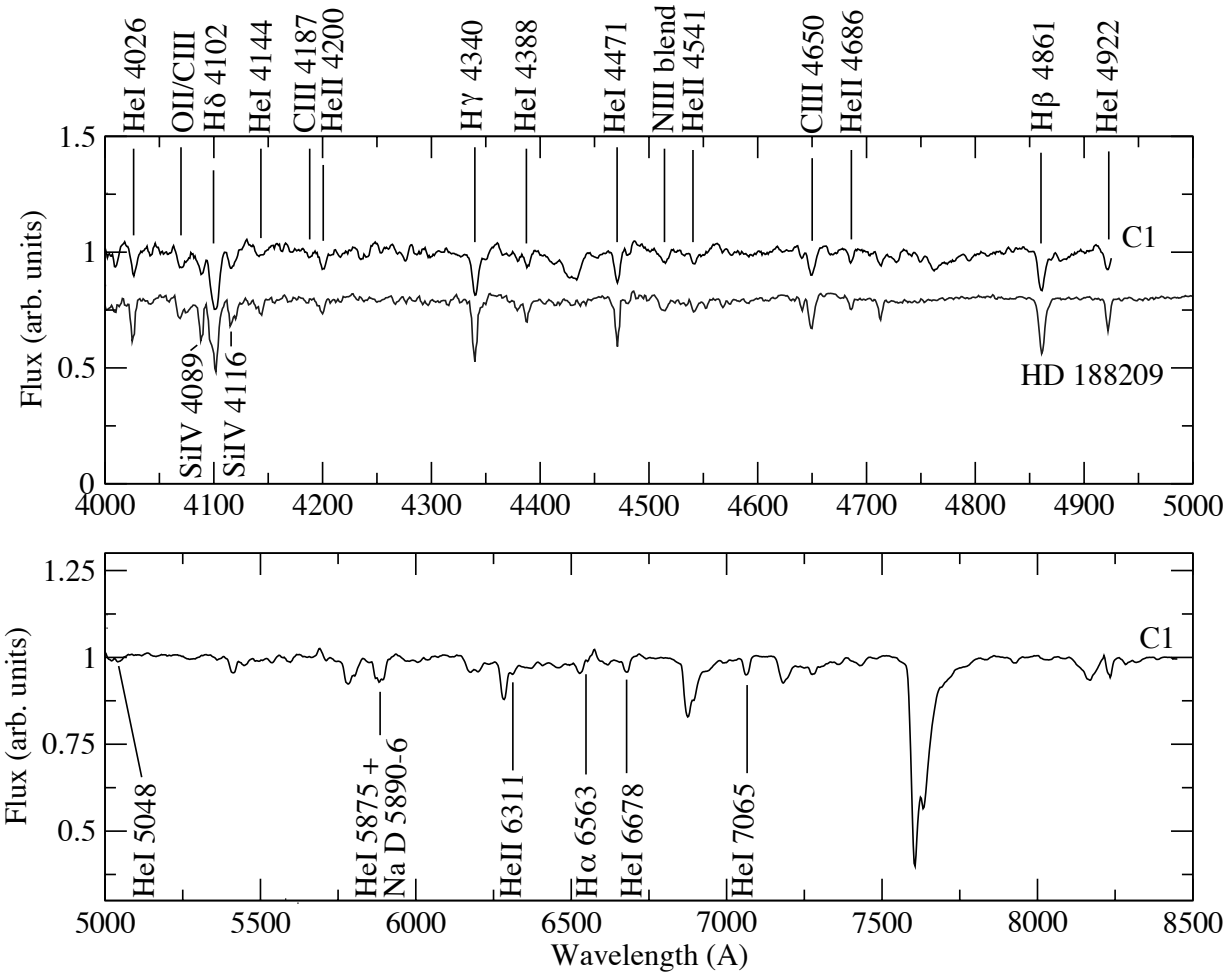

FIG. 3.8 – Spectre optique de IGR J17544-2619 montrant les raies identifiées, parmi lesquelles Pellizza et al. (2006) ont trouvé des raies HI, HeI et HeII de grande amplitude, typiques d'étoiles de type O.

Panneau supérieur : spectre bleu de IGR J17544-2619 (courbe supérieure) et de l'étoile standard HD 188209 de type spectral O9Ib. Le degré élevé de similarité entre ces deux spectres justifie la classification de l'étoile compagnon de IGR J17544-2619 comme étoile de type spectral O9Ib.

Panneau inférieur : Spectre de IGR J17544-2619 entre 5000 Å et 8500 Å.

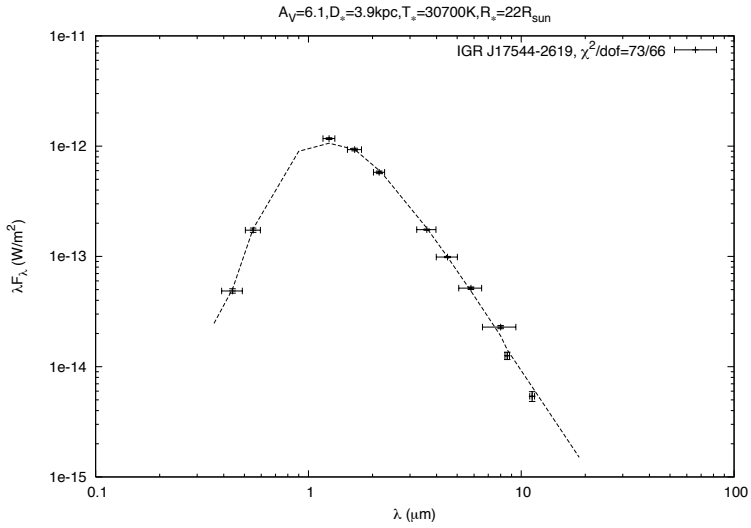

FIG. 3.9 – Distribution d'énergie spectrale de l'optique à l'infrarouge moyen de IGR J17544-2619 incluant des données du NTT de l'ESO, de l'instrument VISIR sur le VLT/UT3, du satellite *Spitzer* (relevé GLIMPSE). Les observations ajustées avec un modèle d'étoile compagnon (en prenant les paramètres habituels d'une étoile O9Ib) ont permis de dériver les paramètres suivants concernant l'étoile compagnon : température T $= 30700$ K et rayon $R_{star} = 22R_{\odot} = 15 \times 10^6$ km. L'absorption dérivée de l'ajustement est $A_v = 6.1$ magnitudes, et la distance D $= 3.9$ kpc. La valeur du χ^2 réduit (χ^2/dof) de l'ajustement est 19/33 (plus de détails sur ce travail sont donnés dans Rahoui et al. (2008). Le résultat principal apporté par cet ajustement de distribution spectrale d'énergie est que dans le cas de IGR J17544-2619 il n'est pas nécessaire d'ajouter une composante additionnelle (par exemple de poussière) afin d'ajuster sa distribution spectrale d'énergie, seule une composante stellaire étant nécessaire.

(en prenant les paramètres habituels d'une étoile O9Ib) ont permis de déduire les paramètres suivants concernant l'étoile compagnon : température T $= 30700$ K et rayon $R_{star} = 22R_{\odot} = 15 \times 10^6$ km. L'absorption dérivée de l'ajustement est $A_v = 6.1$ magnitudes, et la distance D $= 3.9$ kpc. La valeur du χ^2 réduit (χ^2/dof) de l'ajustement est 19/33 (plus de détails sur ce travail sont donnés dans Rahoui et al. 2008). Le résultat principal apporté par cet ajustement de distribution spectrale d'énergie est que dans le cas de IGR J17544-2619 il n'est pas nécessaire d'ajouter une composante additionnelle (par exemple de poussière) afin d'ajuster la distribution spectrale d'énergie, seule une composante stellaire étant nécessaire.

Résumons maintenant la nature de IGR J17544-2619. Il s'agit d'une binaire X de grande masse située à une distance de 3-4 kpc, constituée d'une supergéante de type spectral O9Ib (masse de $25 - 28M_{\odot}$), avec un vent stellaire de faible vitesse et un objet compact qui est probablement une étoile à neutron, sans aucun matériau absorbant autour du système binaire.

3.3.3 Étude d'un échantillon de sources *INTEGRAL* en optique et infrarouge proche

En plus des deux sources décrites ci-dessus, j'ai observé une vingtaine de sources récemment découvertes par le satellite *INTEGRAL*. La méthode est similaire : après la découverte d'une nouvelle source par *INTEGRAL*, sa localisation plus précise par *XMM-Newton*, *Chandra* ou même *Swift*, il est possible d'effectuer une astrométrie précise afin de tenter d'identifier la contrepartie de la source, puis, une fois qu'elle est identifiée, d'en effectuer une étude photométrique et spectroscopique dans les domaines optique et infrarouge proche. Les résultats concernant l'ensemble des sources étudiées sont donnés dans le tableau 3.1. Je vais dans la suite décrire succinctement les résultats obtenus en optique et infrarouge proche sur ces sources *INTEGRAL*.

Quatre sources *INTEGRAL*, IGR J16195-4945, IGR J16207-5129, IGR J16167-4957 (situées dans le bras de Norma) et IGR J17195-4100 (dans le centre galactique) ont ainsi été étudiées en optique et infrarouge après une localisation précise dans les rayons X par *Chandra*. Les résultats sur ces quatre sources, publiés dans Tomsick et al. (2006a)[7], ont déjà été décrits dans le paragraphe 3.2.

Treize autres sources *INTEGRAL* ont été étudiées en optique et infrarouge proche, grâce à la localisation par différents satellites, dont *ROSAT*, *XMM-Newton*, *Chandra*, ainsi qu'en radio au VLA pour une source. Il s'agit des sources *INTEGRAL* IGR J16320-4751, IGR J16358-4726, IGR J16393-4643, IGR J16418-4532, IGR J16479-4514, IGR J16558-5203, IGR J17091-3624, IGR J17252-3616, IGR J17391-3021, IGR J17597-2201, IGR J18027-2016, IGR J18483-0311, IGR J19140+0951. Les résultats obtenus en optique et infrarouge proche au sujet de ces sources sont présentés dans Chaty et al. (2008)[8]. Dans la plupart des cas, les cercles d'erreur fournis par les satellites X ne sont pas assez contraignants pour isoler une seule contrepartie candidate. Il subsiste alors une ambigüité sur l'identification de la vraie contrepartie, ce qui justifie le besoin d'une position précise à moins d'une seconde d'arc, telle qu'elle est fournie par *Chandra*. Après avoir effectué l'astrométrie précise à partir des images infrarouges, la photométrie et la spectroscopie des contreparties candidates permettent alors de distinguer les contreparties les plus probables. L'analyse spectroscopique de la contrepartie candidate, souvent l'étoile la plus brillante présente dans le cercle d'erreur, a permis de déterminer les types spectraux des sources IGR J16320-4751, IGR J16358-4726, IGR J16479-4514, IGR J17252-3616 et IGR J18027-2016 : elles abritent toutes une étoile compagnon de type spectral supergéante OB, IGR J16358-4726 contenant probablement une étoile sgB[e]. Cette étude a aussi permis de confimer la nature de supergéante O et B de IGR J17391-3021 et IGR J19140+0951 respectivement. En outre, l'analyse des distributions spectrales d'énergie des contreparties candidates de chaque source a montré que IGR J16418-4532 contient aussi une étoile compagnon supergéante O/B, que IGR J16393-4643 abrite probablement une étoile BeV, et que IGR J18483-0311 est un système binaire de grande masse. Une astrométrie précise a permis de rejeter les contreparties qui avaient été suggérées pour IGR J17091-3624 et IGR J17597-2201, et de proposer, à partir de l'ajustement de leur SED, deux nouvelles contreparties candidates pour chaque source, les étoiles compagnons

[7] cf l'article présenté dans la sous-section 3.5.2

[8] cf l'article présenté dans la sous-section 3.5.4

étant probablement une BeV dans le premier cas, et de faible masse dans le second. La nature AGN de IGR J16558-5203 est aussi confirmée. Ainsi, toutes ces sources, à part l'exception de la source extragalactique, sont des systèmes binaires X de grande masse avec supergéante de type spectral O/B pour la plupart, ou étoile de la séquence principale de type Be. Ceci montre encore une fois la prédominance de ce type d'objets dans l'ensemble des sources détectées par le satellite *INTEGRAL*.

Finalement, j'ai découvert que certaines des images en infrarouge proche de ces sources présentent des régions d'absorption intenses s'étendant sur de grandes échelles, sur la ligne de visée de quatre de ces sources *INTEGRAL*. Ceci indiquerait donc qu'il y a quelque chose de spécial dans la direction de ces sources, et donc peut-être dans l'environnement de ces sources. Ceci est cohérent avec le fait que la région de Norma, dans la direction de laquelle sont localisées ces sources, est une région de notre Galaxie très riche en régions de formation d'étoiles (Bronfman et al., 1996), et donc propice à la formation d'une population d'étoiles massives, telles que les supergéantes trouvées dans ces systèmes. Nous en reparlerons dans le chapitre 4.

3.3.4 Étude d'un échantillon de sources *INTEGRAL* en infrarouge moyen

Je décris ici les résultats principaux des observations en infrarouge moyen (plus de détails sur ce travail sont donnés dans Rahoui et al. (2008)[9]). Les observations en infrarouge moyen ont été effectuées en 2005/2006 à l'observatoire de Paranal avec l'instrument VISIR installé au foyer Cassegrain de UT3. Les résultats sur les 9 sources *INTEGRAL* sur 14, qui ont été détectées dans le domaine infrarouge moyen, sont présentés dans le tableau 3.2. J'ai ensuite ajusté l'émission de ces sources, de l'optique à l'infrarouge moyen, par un corps noir absorbé représentant l'émission stellaire. Les paramètres libres de cet ajustement étaient l'absorption dans la bande V, la distance du système binaire, la température et le rayon du corps noir représentant l'émission de l'étoile compagnon. L'absorption à la longueur d'onde λ est calculée en utilisant le rapport $\frac{A_\lambda}{A_V}$ donné dans Rieke & Lebofsky (1985) pour les longueurs d'onde optique et infrarouge moyen au-dessus de $8\ \mu$m. Pour les longueurs d'onde de 1.25 à $8\ \mu$m, l'expression analytique utilisée est celle donnée dans Indebetouw et al. (2005). Les ajustements ont été optimisés en minimisant le χ^2.

Pour la plupart des sources les distributions spectrales d'énergie ont pu être précisément ajustées, ce qui montre que l'émission en infrarouge moyen a une origine stellaire, et correspond à la queue Rayleigh-Jeans du spectre stellaire de corps noir. Cependant, dans le cas de IGR J16318-4848 (ainsi que décrit ci-dessus), de IGR J16195-4945 et de IGR J16358-4726, les flux ajustés étaient trop faibles comparés aux flux observés en infrarouge moyen. Il fallait donc ajouter l'émission corps noir d'un nuage sphérique de poussière centré sur l'étoile compagnon, afin d'améliorer les ajustements dans le domaine infrarouge moyen, en considérant leurs flux élevés à ces longueurs d'onde. Uniquement dans ces deux cas, ont été ajoutés aux paramètres libres d'ajustement la température et le rayon d'un corps noir représentant l'émission d'un nuage de poussière.

L'ajustement de IGR J16318-4848 a déjà été montré dans la figure 3.7. Les ajustements des distributions spectrales d'énergie de IGR J16195-4945 et IGR J16358-4726 depuis l'infrarouge

[9] cf l'article présenté dans la sous-section 3.5.5

TAB. 3.1 – Résumé des caractéristiques des sources *INTEGRAL* étudiées : nom, région (GC : centre galactique, No : Norma), période de spin et orbitale, densités de colonne interstellaire, IR et X, type spectral, type de source et référence du type spectral. Acronymes des types : AGN = "Active Galactic Nucleus", B = "Burster", BHC = "Black Hole Candidate", CV = "Cataclysmic Variable", D = "Dipping source", G = GXB "Galactic X-ray Binary", L = LMXB "Low Mass X-ray Binary", H = HMXB "High Mass X-ray Binary System", IP = "Intermediate polar", O = OBS "Obscured source", P = "Persistent source", S = SFXT "Supergiant Fast X-ray Transient", T = "Transient source", XP = "X-ray Pulsar". La classification en tant que SFXT est préliminaire, par manque d'observations sur une grande échelle de temps. Les types spectraux proviennent de spectroscopie optique/NIR : c : Chaty et al. (2008), co : Combi et al. (2006), f : Filliatre & Chaty (2004), i : in't Zand et al. (2006), m : Masetti et al. (2006) n1 : Negueruela et al. (2005), n2 : Negueruela et al. (2006b), n3 : Nespoli et al. (2007), p : Pellizza et al. (2006), t : Tomsick et al. (2006a).

Source	Reg	P_s(s)	P_o(d)	Nh_{is}	Nh_{IR}	Nh_X	SpT	Type	Ref
IGR J16167-4957	No							CV/IP	t
IGR J16195-4945	No			2.18	2.9	7	OB	H ?/S ?/O	t
IGR J16207-5129	No			1.73	2.0	3.7	BOI	H/O	t
IGR J16318-4848	No			2.06	3.3	200	sgB[e]	H/O/P	f
IGR J16320-4751	No	1250	9	2.14	6.6	21	sgOB	H/XP/T/O	c
IGR J16358-4726	No	5880		2.20	3.3	33	sgB[e] ?	H/XP/T/O	c
IGR J16393-4643	No	912	3.6875	2.19	2.19	24.98	BeV	H ?/XP/T	c
IGR J16418-4532	No	965	3.75	1.88	2.7	10	sgOB	H/XP/S	c
IGR J16465-4507	No	228		2.12	1.1	60	B0.5I	H/S	n1
IGR J16479-4514	No			2.14	3.4	7.7	sgOB	H/S ?	c
IGR J16558-5203	No						Sey1.2	AGN	m
IGR J17091-3624	GC			0.77	1.03	1.0	BeV	L/BHC	c
IGR J17195-4100	GC							CV/IP	t
IGR J17252-3616	GC	413	9.7	1.56	3.8	15	sgOB	H/XP/O	c
IGR J17391-3021	GC			1.37	1.7	29.98	O8Iab(f)	H/S/O	n2
IGR J17544-2619	GC	NS	165 ?	1.44	1.1	1.4	O9Ib	S	p
IGR J17597-2201	GC			1.17	2.84	4.50	LMXB	L/B/D/P	c
IGR J18027-1455	GC						Sey1	AGN	co
IGR J18027-2016	GC	139	4.6	1.04	1.53	9.05	sgOB	H/XP/T	c
IGR J18483-0311	GC			1.62	2.45	27.69	HMXB	H	c
IGR J19140+0951			13.55	1.68	2.9	6	sgB0.5I	H/O	n3

proche jusqu'à l'infrarouge moyen, incluant des données du NTT de l'ESO et du satellite *Spitzer* (relevé GLIMPSE) sont montrés respectivement en haut et en bas de la Figure 3.10. Décrivons le cas de IGR J16195-4945. Les observations, ajustées avec un modèle comprenant une étoile compagnon (en prenant les paramètres habituels d'une étoile O/B) et une simple composante sphérique de poussière, ont permis de déduire les paramètres suivants : i) concernant l'étoile compagnon : température T $= 23100$ K et rayon R$_{star} = 22.6 R_{\odot} = 15 \times 10^6$ km ; ii) concernant la composante de poussière : température T $= 950$K, rayon R $= 6.1 R_{star} = 95 \times 10^6$ km. L'absorption dérivée de l'ajustement est de A$_v = 15.4$ magnitudes, et la distance D $= 8.4$ kpc. La valeur du χ^2 réduit (χ^2/dof) de l'ajustement est de =17/42. Le résultat principal fourni par l'ajustement de cette distribution spectrale d'énergie est que dans le cas de IGR J16195-4945, comme pour IGR J16318-4848 il est nécessaire d'ajouter une composante additionnelle (par exemple de poussière) afin de pouvoir l'ajuster aux observations multi-longueurs d'onde. De nouveau, comme pour IGR J16318-4848, l'extension de cette composante de poussière semble suggérer qu'elle entoure le système binaire dans son ensemble, comme le ferait probablement un cocon de poussière.

Je souligne le fait qu'il faut être plus prudent dans les conclusions concernant IGR J16195-4945 que celles sur IGR J16318-4848, puisque IGR J16195-4945 i) n'était pas détectée avec VISIR, mais seulement avec SPITZER, et ii) les magnitudes optiques acquises avec le NTT de l'ESO semblent être celles d'un objet contaminé par un autre astre (cf Tomsick et al. 2006a et Tovmassian et al. 2006). Cependant, ces deux sources semblent être très similaires, puisqu'elles présentent la même température (~ 23000 K) et sont grandement obscurcies : elles présentent toutes deux une absorption A$_V \sim 17$ magnitudes en optique, et leur densité de colonne déduite des observations en rayons X est respectivement $N_{\rm H} = 2.1 \times 10^{24}$ cm^{-2} pour IGR J16318-4848 et $N_{\rm H} \sim 10^{23}$ cm^{-2} pour IGR J16195-4945. En fait, le cas de IGR J16195-4945 est extrêmement intéressant, puisque cet astre ressemblerait fort à IGR J16318-4848 s'il était situé à la même distance (nos ajustements suggèrent que IGR J16195-4945 est 7 fois plus distant que IGR J16318-4848). Ainsi, les paramètres déduits de nos ajustements suggèrent que IGR J16195-4945 ne devrait pas être visible en optique, et ce résultat est cohérent avec la conclusion apportée par Tovmassian et al. (2006), proposant que l'astre optique observé dans Tomsick et al. (2006a) n'est pas l'astre *INTEGRAL* mais un astre en premier plan.

Un autre point important est que les ajustements sont très dépendants de la correction d'absorption utilisée, et les astres qui présentent une absorption élevée semblent être mieux ajustés avec la correction d'absorption donnée dans Indebetouw et al. (2005) que celle de Rieke & Lebofsky (1985), probablement parce que la première a été calibrée en utilisant des données en infrarouge moyen plus récentes, obtenues à partir des observations *Spitzer*. En résumé, si les observations et les ajustements ne laissent la place à aucun doute au sujet de la présence de poussière autour de IGR J16318-4848, la situation est moins claire pour IGR J16195-4945 et IGR J16358-4726, même si les paramètres déduits en ajustant les observations suggèrent la présence de poussière.

Ainsi, dans trois cas uniquement, concernant les astres IGR J16318-4848, IGR J16195-4945 et IGR J16358-4726, la présence de poussière froide est exigée par les ajustements. Dans ce contexte, IGR J16318-4848 prouve encore une fois qu'il s'agit d'une source extraordinaire parmi les autres sources *INTEGRAL*, et qu'il existe beaucoup plus de matériau absorbant autour de cette

TAB. 3.2 – Résumé des résultats en infrarouge moyen sur les astres *INTEGRAL* étudiés : paramètres utilisés pour ajuster les SEDs des sources. Dans ce tableau sont donnés le nom des sources, l'extinction interstellaire (A_i en magnitudes), l'extinction en X (A_X en magnitudes), l'extinction en optique (A_V en magnitudes), la distance, la température et le rayon de l'étoile compagnon (D_* en kpc, T_* en K et R_* en $R_\odot$), et la température et le rayon de la composante de poussière (T_D en K et R_D en $R_\odot$) –lorsqu'il s'avérait nécessaire de l'ajouter afin d'ajuster les observations– et le χ^2/dof.

Sources	A_i	A_X	A_V	$D_*(kpc)$	$T_*(K)$	$R_*(R_\odot)$	$T_D(K)$	$R_D(R_*)$	χ^2/dof
IGR J16195-4945	11.65	37.41	15.4	8.4	23100	22.6	950	6.1	17/42
IGR J16207-5129	9.25	19.77	10.7	4.8	32500	21.2			173/72
IGR J16318-4848	11.01	1069.52	17.4	1.2	23500	20.5	900	11.9	35/33
IGR J16320-4751	11.44	112.24	35.1	3.7	32600	22.6			14.7/54
IGR J16358-4726	11.76	176.38	17.5	14.6	24800	20.5	820	10	3/13
IGR J16418-4532	10.05	53.45	14.3	10.9	27000	20.2			1.42/42
IGR J16465-4507	11.33	320.69	5.4	8.8	27500	22.9			55/33
IGR J16479-4514	11.44	41.16	18.2	4.6	32000	20.3			11/18
IGR J17252-3616	8.34	80.17	20.2	6.2	30000	20.6			1/6
IGR J17391-3021	7.32	160.35	9.3	2.9	32100	22.9			19/26
IGR J17544-2619	7.70	7.70	6.1	3.9	30700	22			19/33
IGR J19140+0951	8.98	32.07	15.7	2.5	20000	21.2			43/27

source qu'autour des autres. Ainsi IGR J16318-4848, et probablement aussi IGR J16195-4945 et IGR J16358-4726, restent des cas exceptionnels, qui méritent probablement de constituer une classe à eux seuls !

3.4 Discussion et conclusions

Maintenant, la question qui reste en suspens est : "Que sont ces sources ?". 80% de ces sources *INTEGRAL* nouvellement découvertes dans la direction du bras de Norma sont des binaires X de grande masse, abritant des objets compacts (probablement des étoiles à neutron) orbitant autour de secondaires supergéantes O/B. Ces systèmes accrètent de la matière sous forme de vent sphérique, et présentent une composante d'absorption additionnelle supérieure à la moyenne d'un facteur ~ 4. Ce sont des pulsars de rayons X, avec des périodes de pulsations (~ 1 ks) plus longues que celles des sources connues jusqu'ici (Bodaghee et al., 2007). Pour aller plus loin dans la compréhension de ces sources, nous pouvons utiliser le diagramme de Corbet déjà évoqué dans le chapitre 1, et montré dans la figure 1.5. À peu près toutes les HMXBs *INTEGRAL* pour lesquelles à la fois les périodes de spin et d'orbite ont été mesurées sont situées parmi les autres accréteurs par vent dans le diagramme de Corbet. Ces systèmes se trouvent dans la partie

supérieure de ce diagramme, comme indiqué dans la figure 3.11, et sont donc des systèmes binaires de grande masse avec supergéantes, et accrétant par vent. Reportons-nous maintenant au diagramme montré dans la figure 3.12, illustrant les relations entre période orbitale, période de spin et masse du système binaire. Ce diagramme montre que si le système présente une période orbitale de 10 jours, et que l'étoile donneur a une masse de $20\ M_{\odot}$, alors la séparation orbitale est de $50\ R_{\odot}$. Ce qui signifie que cette séparation est inférieure au rayon du cocon de poussière, car ce rayon s'élève à $240\ R_{\odot}$ par exemple pour IGR J16318-4848.

Les sources obscurcies et les SFXTs partagent des propriétés similaires, cependant, elles ne font pas partie du même type d'astres, principalement parce que l'excès d'absorption, lorsqu'il existe, ne semble pas avoir la même origine dans les deux classes d'objet. Par exemple, l'excès d'absorption a deux origines distinctes dans le cas des sources hautement obscurcies, telles que IGR J16318-4848. Dans le cas de cette source, les observations des hautes énergies jusqu'au domaine de l'infrarouge moyen suggèrent qu'il existe du matériau absorbant concentré autour de l'objet compact, et aussi la présence de poussière, de gaz froid, ou même un cocon de poussière, entourant l'ensemble du système binaire. Au contraire, dans le cas des SFXTs, telles que IGR J17544-2619, la présence de matériau absorbant, lorsqu'il y en a, semble concentrée uniquement autour de l'objet compact, et les observations en infrarouge moyen montrent qu'il n'est pas nécessaire d'ajouter la présence de matériau absorbant autour de l'ensemble du système binaire pour reproduire les observations. Nous pouvons dès lors essayer d'expliquer les différentes caractéristiques de ces deux types d'astres, et donc de distinguer la nature de ces sources, en spéculant sur la géométrie de ces systèmes :

- • Les sources hautement absorbées (dont le représentant extrême est IGR J16318-4848) se caractérisent par la présence de matériau absorbant à la fois autour de l'objet compact et de l'ensemble du système binaire, à des niveaux différents d'absorption. Ces propriétés semblent pouvoir s'expliquer par la présence d'un vent équatorial de faible vitesse et de grande densité s'échappant des supergéantes sgB[e], et formant peu à peu un cocon de poussière en s'accumulant autour de l'étoile. Ces sources se caractériseraient alors par la présence d'un objet compact (étoile à neutron ou trou noir) orbitant sur une orbite circulaire, à l'intérieur d'un cocon dense composé de gaz froid et de poussière et entourant l'étoile compagnon. Pour qu'il y ait accrétion de matière par vent, il suffit que le cocon de gaz et de poussière atteigne une densité de 10^{11-12} cm^{-3}, une épaisseur de 10^{12-13} cm (c'est-à-dire $10-100\ R_{\odot}$), et un rayon de 10^{13-14} cm (soit 1-10 u.a.). Les résultats obtenus sur les tailles de cocon de poussière entourant les systèmes absorbés sont cohérents avec ces tailles (Rahoui et al., 2008).

- • Les SFXTs (dont l'archétype est IGR J17544-2619) se caractérisent par des sursauts rapides d'activité dans les rayons X, et la présence d'une étoile compagnon supergéante. Leurs propriétés semblent pouvoir être expliquées par la présence d'un objet compact (étoile à neutron ou trou noir) situé sur une grande orbite excentrique autour de l'étoile compagnon, et c'est probablement lorsque l'objet compact pénètre dans l'enveloppe de l'étoile supergéante que les sursauts se produisent (Chaty & Rahoui, 2006).

Ainsi la nature transitoire ou persistante dans les rayons X de ces astres semble être reliée à la géométrie de ces systèmes. Des schémas représentant ces deux configurations de source sont montrés dans la figure 3.13[10]. Évidemment la confirmation de cette suggestion, donc la réponse à ces questions, et en particulier la distinction entre ces deux classes d'objets, sera probablement fournie par la connaissance de la période orbitale, et donc de la géométrie du système.

Hormis la géométrie de ces systèmes, plusieurs questions restent encore en suspens, la plupart étant reliées à la présence de l'excès en infrarouge moyen dans ces sources. Par exemple, aucune émission radio n'a été détectée en provenance de ces sources, alors qu'une émission radio est habituellement détectée au sein de l'ensemble des systèmes binaires de haute énergie, il semble donc qu'il y ait de nouveau quelque chose de spécial concernant ces sources. Il y a au moins deux explications possibles : soit l'accrétion se fait uniquement par vent, et donc aucun disque d'accrétion ne se forme, empêchant du même coup la formation du disque d'accrétion (cf chapitre 2 sur les microquasars), soit la poussière englobant l'ensemble du système binaire empêche le déclenchement de la formation de jets. Mais la question la plus importante est probablement celle-ci : cet environnement cicumstellaire inhabituel est-il dû à l'évolution stellaire ou au système binaire lui-même ? Autrement dit, est-ce que la présence de l'objet compact autour de l'étoile supergéante joue un rôle sur les caractéristiques extraordinaires de ces astres ? Afin de répondre à cette question, il sera nécessaire de mieux caractériser le cocon de gaz froid et de poussière qui entoure ces systèmes, afin de connaître sa température, sa composition, sa géométrie, son extension autour de l'ensemble du système binaire, etc... C'est uniquement une fois que ces données seront connues, que nous aurons des indices sur la provenance de cette poussière et de ce gaz froid[11].

Nous faisons donc maintenant face à une population majoritaire de systèmes binaires de haute énergie nés avec deux composantes très massives. Cette population remet en question la plupart des modèles de synthèse de population, qui prévoyaient moins de systèmes binaires de grande masse que ce que le satellite *INTEGRAL* a détecté. En outre, il apparaît que ces systèmes comprenant une supergéante et un objet compact (étoile à neutron ou trou noir) ont une durée de vie courte, puisque la durée entre les deux supernovæne doit pas dépasser une dizaine de millions d'années. Ces systèmes sont probablement les progéniteurs primaires de coalescences entre deux étoiles à neutron, ou entre une étoile à neutron et un trou noir, après émission d'ondes gravitationnelles. Il existe donc la possibilité qu'ils soient reliés aux sursauts de rayons gamma courts et durs, et aussi qu'ils soient de bons candidats à la détection d'ondes gravitationnelles. Je développerai ces deux points, sur les modèles de synthèse de population et la coalescence de ces systèmes, dans le chapitre 4.

En résumé, une nouvelle population d'astres a été récemment révélée par le satellite *INTEGRAL*, et il apparaît qu'une étude attentive de cette nouvelle population pourrait apporter des contraintes sur la géométrie des systèmes binaires de haute énergie, ainsi qu'une meilleure compréhension de la formation, de l'évolution et de la fin de vie de ces systèmes. Mon mot de la fin sera que, parce que ces sources sont pour la plupart obscurcies, les "astres du bras de Norma"

[10]Une animation de ces sources est disponible sur le site http ://www.aim.univ-paris7.fr/CHATY/Research/hidden.html

[11]Des observations de IGR J16318-4848, en infrarouge moyen avec VISIR sur le VLT, sont prévues pour analyser et caractériser le milieu circumstellaire de cet astre, représentant extrême des sources *INTEGRAL* obscurcies.

peuvent être étudiés uniquement dans les domaines des hautes énergies et de l'infrarouge. Il est donc nécessaire d'entreprendre une étude commune basée sur des observations multi-longueurs d'onde dans les hautes énergies, l'optique, l'infrarouge proche et l'infrarouge moyen (et même le sub-millimétrique et la radio), pendant les périodes de sursaut d'activité et les périodes d'inactivité, afin de comprendre ces astres, et révéler leurs secrets.

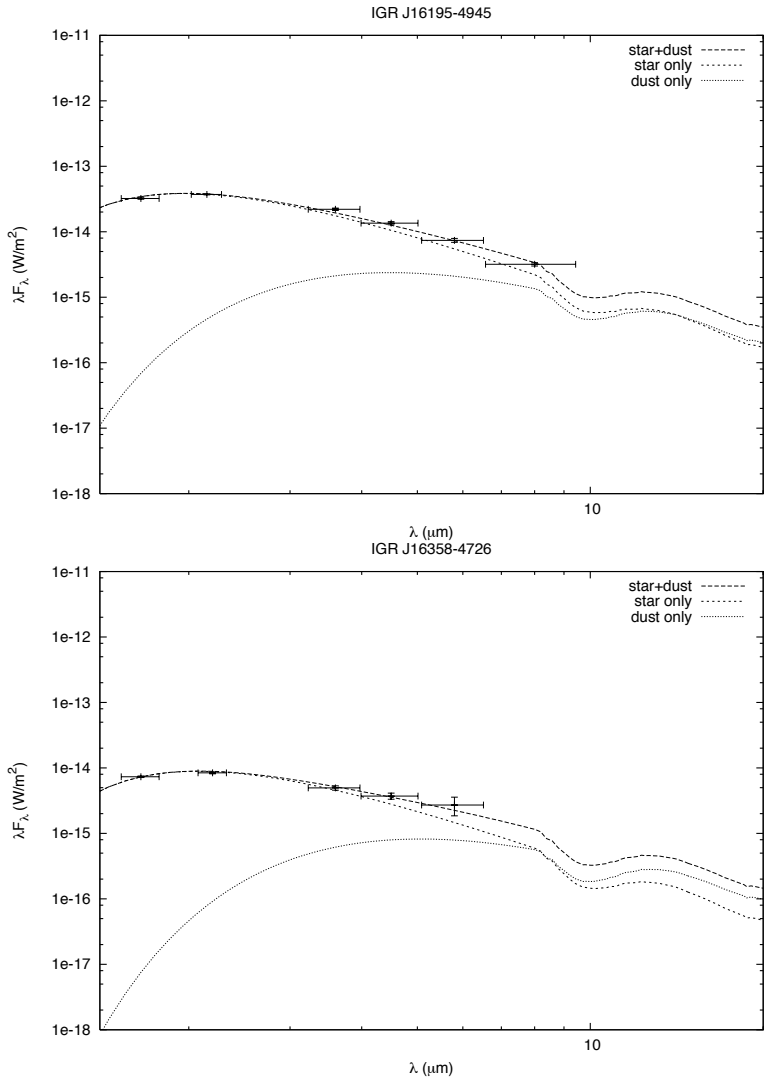

FIG. 3.10 – Distributions spectrales d'énergie de IGR J16195-4945 et IGR J16358-4726 depuis l'infrarouge proche jusqu'à l'infrarouge moyen, incluant des données du NTT de l'ESO et du satellite *Spitzer* (relevé GLIMPSE). Le modèle de l'étoile est en pointillés-traits fins, celui de la poussière en pointillés-points, et l'ajustement total est en pointillés-traits gras. Dans le cas de IGR J16195-4945 et IGR J16358-4527, comme pour IGR J16318-4848, il est nécessaire d'ajouter une composante additionnelle (par exemple de poussière) afin de pouvoir ajuster le modèle d'émission aux observations multi-longueurs d'onde (cf texte pour les paramètres de l'ajustement). De nouveau, l'extension de cette composante de poussière semble suggérer qu'elle entoure le système binaire dans son ensemble, comme le ferait probablement un cocon de poussière.

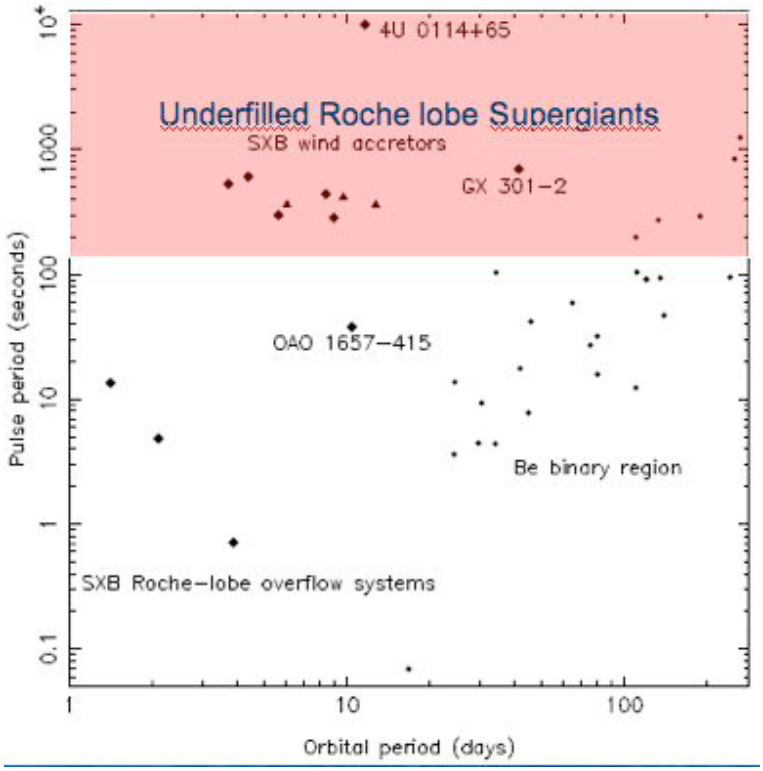

FIG. 3.11 – Diagramme de Corbet : Période de spin des étoiles à neutron accrétantes en fonction de la période du système binaire. Les différents symboles indiquent les différents types de systèmes binaires (Corbet, 1986). Les nouvelles sources *INTEGRAL* détectées sont rassemblées dans la partie supérieure –rose– de ce diagramme.

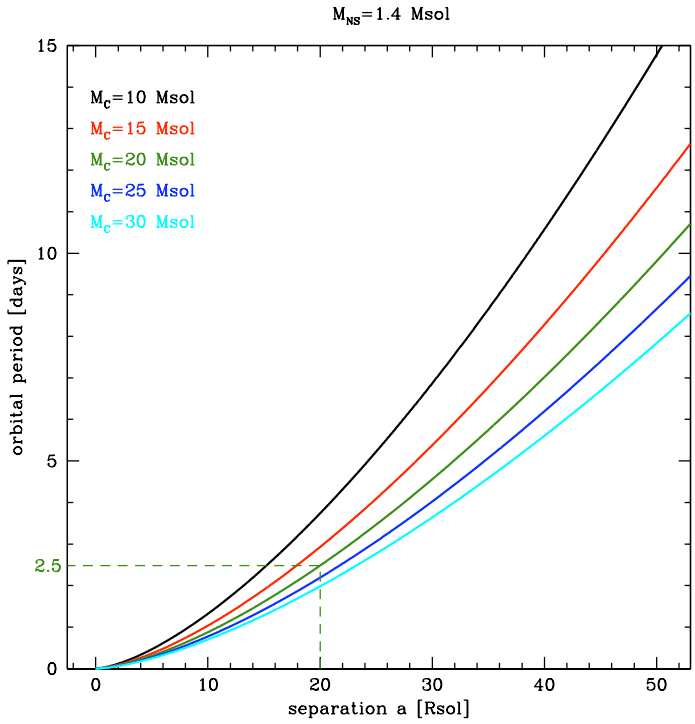

FIG. 3.12 – Diagramme de la période orbitale (en jours) en fonction de la séparation a, illustrant les relations entre période orbitale, période de spin et masse du système binaire (aimablement fourni par J.A. Zurita Heras).

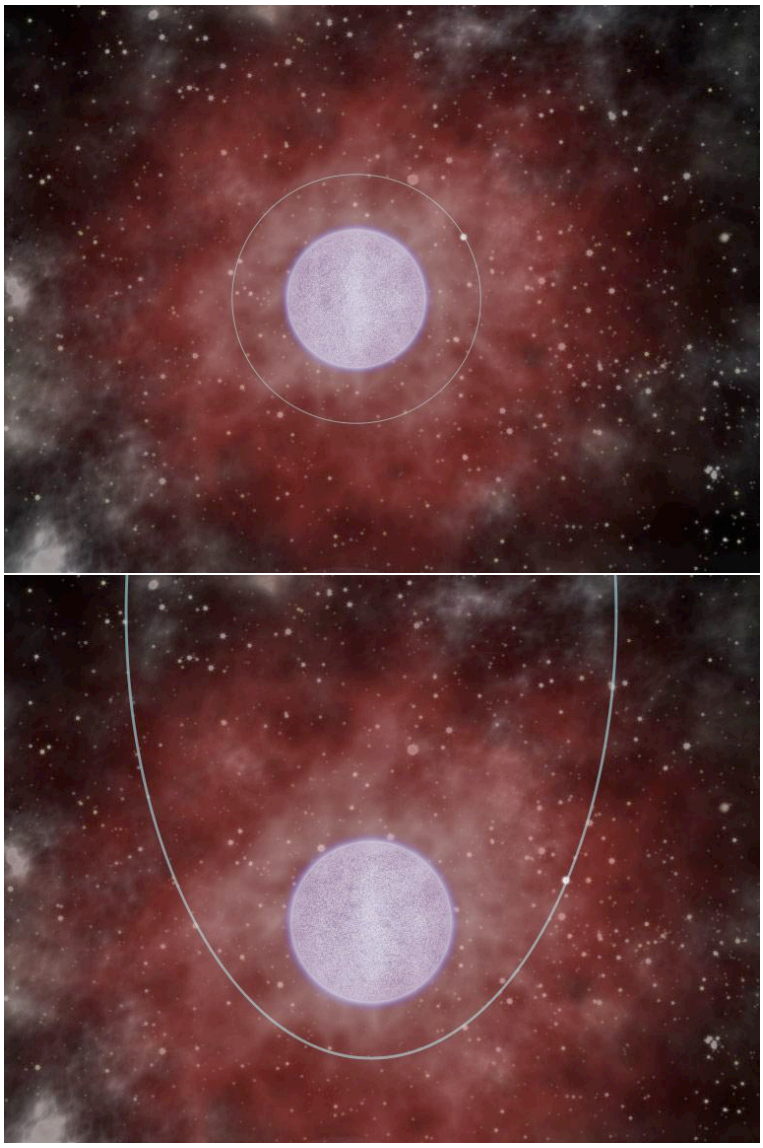

FIG. 3.13 – Schémas illustrant les 2 types de sources *INTEGRAL* : sources obscurcies en haut, et SFXTs en bas. L'accrétion de matière est permanente dans le cas des sources obscurcies, correspondant à un objet compact sur une orbite circulaire autour de l'étoile supergéante. Dans ce cas, l'objet compact est constamment à l'intérieur du cocon de poussière entourant l'ensemble du système. Par contre, l'accrétion est intermittente dans le cas des SFXTs, correspondant à un objet compact sur une orbite excentrique. Dans ce cas, l'accrétion se produit lorsque l'objet compact est proche de l'étoile compagnon, accrétant à partir de son vent stellaire. Une animation de ces sources est disponible sur le site http ://www.aim.univ-paris7.fr/CHATY/Research/hidden.html

3.5 Quelques articles publiés parmi les plus significatifs

3.5.1 La contrepartie optique/infrarouge proche de la source *INTEGRAL* obscurcie IGR J16318-4848 : une sgB[e] dans une binaire de rayons X de grande masse ?

"The optical/near-infrared counterpart of the *INTEGRAL* obscured source IGR J16318-4848 : an sgB[e] in a high-mass X-ray binary ?" par P. Filliatre & S. Chaty, 2004, ApJ, 616, 469

Dans cet article est présenté un ensemble d'observations en optique et en infrarouge proche de la contrepartie de la première source détectée par *INTEGRAL* : IGR J16318-4848. Ces observations ont montré le caractère extraordinaire de cette source : très absorbée en optique, devenant un phare en infrarouge, avec une absorption cent fois plus importante sur la source elle-même que sur la ligne de visée. Les spectres de cette source sont encore plus étonnants, le continuum étant quasiment caché par de nombreuses raies d'émission intenses. La conclusion de ces observations est que l'étoile compagnon est une supergéante de type B avec raies d'émission interdites, une sgB[e], le système est donc un système binaire de grande masse, et cette source est devenue le représentant extrême du nouveau type d'astres révélé par *INTEGRAL* : des systèmes binaires de grande masse à supergéante, très absorbés (voir le paragraphe 3.3.1 pour plus de détails).

The Astrophysical Journal, 616:469–484, 2004 November 20
© 2004. The American Astronomical Society. All rights reserved. Printed in U.S.A.

THE OPTICAL/NEAR-INFRARED COUNTERPART OF THE *INTEGRAL* OBSCURED SOURCE IGR J16318−4848: AN sgB[e] IN A HIGH-MASS X-RAY BINARY?[1]

P. Filliatre
Service d'Astrophysique, CEA/DSM/DAPNIA/SAp, Centre d'Etudes de Saclay, Orme des Merisiers, Bâtiment 709, F-91191 Gif-sur-Yvette Cedex, France; and Fédération Astroparticule et Cosmologie, Paris, France; filliatr@cea.fr

and

S. Chaty
Université Paris 7, 2 Place Jussieu, F-75005 Paris; and Service d'Astrophysique, CEA/DSM/DAPNIA/SAp, Centre d'Etudes de Saclay, Orme des Merisiers, Bâtiment 709, F-91191 Gif-sur-Yvette Cedex, France; chaty@cea.fr
Received 2004 March 24; accepted 2004 July 30

ABSTRACT

The X-ray source IGR J16318−4848 was the first source discovered by *INTEGRAL* on 2003 January 29. The high-energy spectrum exhibits such a high column density that the source is undetectable in X-rays below 2 keV. On 2003 February 23–25, we triggered our Target of Opportunity (ToO) program using the EMMI and SOFI instruments on the New Technology Telescope of the European Southern Observatory (La Silla) to obtain optical and near-infrared (NIR) observations. We confirm the already proposed NIR counterpart and for the first time extended detection into optical. We report here photometric measurements in the *R*, *I*, and *J* bands, upper flux limits in the *Bb* and *V* bands, and lower flux limits in the *H* and K_s bands. We also obtain NIR spectroscopy between 0.95 and 2.52 μm, revealing a large number of emission lines, including forbidden iron lines and P Cygni profiles, and showing a strong similarity with CI Cam, another strongly absorbed source. Together with the spectral energy distribution (SED), these data point to a high-luminosity, high-temperature source, with an intrinsic optical/NIR absorption greater than the interstellar absorption but 2 orders of magnitude below the X-ray absorption. We propose the following picture to match the data: the source is a high-mass X-ray binary (HMXB) at a distance between 0.9 and 6.2 kpc, and the optical/NIR counterpart corresponds to the mass donor, which is an early-type star, maybe an sgB[e] star, surrounded by a dense and absorbing circumstellar material. This would make the second HMXB with an sgB[e] star as the mass donor after CI Cam. Such sources may represent a different evolutionary state of X-ray binaries previously undetected with the lower energy space telescopes; if so, a new class of strongly absorbed X-ray binaries is being unveiled by *INTEGRAL*.

Subject headings: circumstellar matter — stars: emission-line, Be — X-rays: binaries

1. INTRODUCTION

IGR J16318−4848 was the first new source discovered by the *INTEGRAL* IBIS/ISGRI imager (Ubertini et al. 2003; Lebrun et al. 2003). The source was first detected on 2003 January 29 (Courvoisier et al. 2003) in the energy band 15–40 keV with a mean 20–50 keV flux of 6×10^{11} ergs cm^{-2} s^{-1}. The source was thereafter regularly observed for 2 months. No X-ray counterpart could be found in the *ROSAT* All Sky Survey (Voges et al. 1999). The source was observed by *XMM-Newton* on 2003 February 10, which detected a single X-ray source within the *INTEGRAL* error box using the EPIC PN and MOS cameras (Strüder et al. 2001; Turner et al. 2001), giving the most precise position to date: $\alpha = 16^{\rm h}31^{\rm m}48\overset{\rm s}{.}6$, $\delta = -48^\circ 49' 00''$ with a $4''$ error box (a circle with a radius of $4''$; Schartel et al. 2003). X-ray spectroscopy revealed a very high absorption column density: $N_{\rm H} > 10^{24}$ cm^{-2} (Matt & Guainazzi 2003; Walter et al. 2003), which renders the source invisible below 2 keV. This amount of absorption is unusual in Galactic sources. This could explain the nondetection by *ROSAT*, although the source was discovered at a similar flux level in archival *ASCA* observations in 1994 (Murakami et al. 2003; Revnivtsev et al. 2003) on both GIS and SIS instruments (between 0.4 and 10 keV). Relatively bright and highly absorbed sources like IGR J16318−4848 could have escaped detection in past X-ray surveys and could still contribute significantly to the Galactic hard X-ray background in the 10–200 keV band.

The high column density prompted a counterpart research in the near-infrared (NIR): in the EPIC error box, a possible counterpart was proposed by Foschini et al. (2003) using the Two Micron All Sky Survey (2MASS) with the following magnitudes: $J = 10.162 \pm 0.018$, $H = 8.328 \pm 0.037$, $K_s = 7.187 \pm 0.015$ (Walter et al. 2003). On the other hand, no radio emission at the position of the source could be detected. These broad characteristics suggest that it is an X-ray binary, the nature of the compact object (neutron star or black hole) being subject to debate.

In the course of a Target of Opportunity (ToO) program at the European Southern Observatory (ESO) dedicated to look for counterparts of high-energy sources newly discovered by satellites including *INTEGRAL* (PI: S. Chaty), we carried out photometric observations in the optical and NIR and spectroscopic observations in the NIR. The goals were to search for likely counterparts within the EPIC error box and to obtain information about the environment and the nature of the source, especially about the mass donor.

The main results of this paper have been already presented in a very condensed way in Chaty & Filliatre (2004). In § 2 we

[1] Based on observations collected at the European Southern Observatory, Chile (observing proposal ESO N 70.D-0340).

TABLE 1
TERMS OF COLOR EQUATION

Band	Zero-Point Magnitude	Color Term	Extinction Coefficient
Bb	25.03 ± 0.03	−0.03 ± 0.01(*B* − *V*)	0.214[a]
V	25.59 ± 0.02	0.08 ± 0.01(*V* − *R*)	0.125[a]
R	25.90 ± 0.03	−0.005 ± 0.2(*R* − *I*)	0.091[a]
I	25.42 ± 0.04	0.04 ± 0.29(*R* − *I*)	0.051[a]
J	23.34 ± 0.06	−0.007(*J* − *K*)[b]	0.40 ± 0.05
H	23.17 ± 0.06	−0.022(*J* − *K*)[b]	0.31 ± 0.05
K_s	22.39 ± 0.06	0.023(*J* − *K*)[b]	0.15 ± 0.05

NOTE.—The extinction coefficients for the optical bands are taken from Gonzalez et al. (2002), the color terms for the NIR are taken from Lidman et al. (2002), and the other coefficients are measured values.
[a] Not measured, taken from Gonzalez et al. (2002).
[b] Not measured, taken from Lidman et al. (2002).

describe briefly our observations and their reduction; in § 3 we report on astrometry and photometry of all possible counterparts of the source and give the most likely candidate; for the latter, we give in § 4 the spectral energy distribution, putting our data together with the survey archives and published data, and derive absorption and temperature estimates; in § 5 we study the spectral lines; in § 6 we discuss the distance to the source, its nature, and the nature of its components; then, in § 7, we conclude.

2. THE OBSERVATIONS

The observations were carried out using the New Technology Telescope (NTT) of the ESO at La Silla (Chile) on 2003 February 23–25. We used the EMMI (optical) and SOFI (NIR) instruments. For astrometry and photometry, we had a total of eight broad bands: *Bb*, *V*, *R*, *I*, *Z*, *J*, *H*, K_s. For spectroscopy, we used two bands: Grism Blue Filter (GBF; range 0.95–1.64 μm, resolution 930) and Grism Red Filter (GRF; range 1.53–2.52 μm, resolution 980).

All the data were reduced using the IRAF suite.[2]

2.1. *Optical Photometric Data*

The optical data have been taken on 2003 February 24 with EMMI between UT 7:30 and 8:30. The seeing was typically 0.″9, and the air mass on the source was between 1.225 and 1.277. We acquired one 180 s exposure for each band (*Bb*, *V*, *R*, *I*, *Z*) and an extra 60 s exposure for *Bb*. The data analysis involved subtraction of the bias and division by the flat field. For calibration, we obtained an exposure of 30, 15, 10, 10, and 10 s, respectively, of the five stars of PG 1633+099 from the Landolt catalog (Landolt 1992). The EMMI detector is a mosaic of two arrays, each with two readouts, resulting in a 4152×4110 array with a pixel scale of 0.″166 pixel^{-1}. This makes four parts with slightly different characteristics. The source fell into the second readout of the first array, as did three of the standard stars; therefore, we used these three stars to compute the color equation for *BbVRI*. These stars were PG 1633+099 B, C, and D. As the air mass was identical for these three stars, it was then not possible to determine the extinction coefficient with them, and we adopted the values reported in the EMMI manual (Gonzalez et al. 2002). We found the zero point and the color coefficient by a linear regression. The results are given in Table 1. The zero-point magnitude is in good agreement with data given in Gonzalez et al. (2002; converted for 1 ADU s^{-1} to be directly comparable with our results): 24.98 ± 0.03, 25.69 ± 0.01, 25.98 ± 0.02, and 25.28 ± 0.03 for *Bb*, *V*, *R*, and *I*, respectively.

2.2. *NIR Photometric Data*

The NIR photometric data have been taken with SOFI on the NTT between UT 7:00 and 10:00 on 2003 February 23. The SOFI detector is a 1024×1024 CCD with a pixel scale of 0.″288 pixel^{-1}. The seeing was typically 1″, and the air mass on the source was between 1.088 and 1.388. We obtained nine exposures of 10 s and 11 exposures of 5 s in the *J* band. We obtained five exposures of 10 s and nine exposures of 2 s in the *H* band. We acquired 245 exposures of 2 s in the K_s band. In order to correct for the bright NIR sky, following the standard procedure, the pointings of all these frames were dithered. This allowed us to obtain a sky template by median filtering the frames. This template was then subtracted from the flat-fielded frames. The alignment of the frames was performed using ∼2000 common stars. Within each band, frames with different exposure times were averaged separately. For calibration, five exposures for each band of standard stars sj9157 (integration time 2 s) and sj9170 (1.2 s) of Persson et al. (1998) were done. The color term was taken from Lidman et al. (2002) because we had three bands and only two standard stars. We found the zero point and the extinction coefficient by a linear regression. The results are reported in Table 1. The zero-point magnitude is in good agreement with data given in Lidman et al. (2002): 23.2, 23.1, and 22.5 ± 0.01 for *J*, *H*, and K_s, respectively.

2.3. *NIR Spectroscopy*

The NIR spectroscopic data have been taken with the SOFI low-resolution grism on the NTT between UT 8:00 and 9:00 on 2003 February 25 with the GBF and GRF. The seeing was typically 0.″9, and the air mass on the object varied between 1.160 and 1.260. For each GBF and GRF band, we obtained 24 exposures of 6 s. After subtraction of the bias, the exposures were divided by the response of the flat field along the dispersion line. The resulting individual rough spectra show a dispersion of around 20%, which seems to be random and not associated with a short time variation of the source. Therefore, the two averaged spectra have a relative precision of 4% in flux. Given the seeing and the slit width of 1″, we expect to collect around 75% of the flux; however, as we will scale the spectra to match the broadband magnitudes, absolute calibration is not an issue. Wavelength calibration was done by observing a xenon arc. We obtained 16 exposures of 5 s for

[2] IRAF is distributed by the National Optical Astronomy Observatory, which is operated by the Association of Universities for Research in Astronomy, Inc., under cooperative agreement with the National Science Foundation.

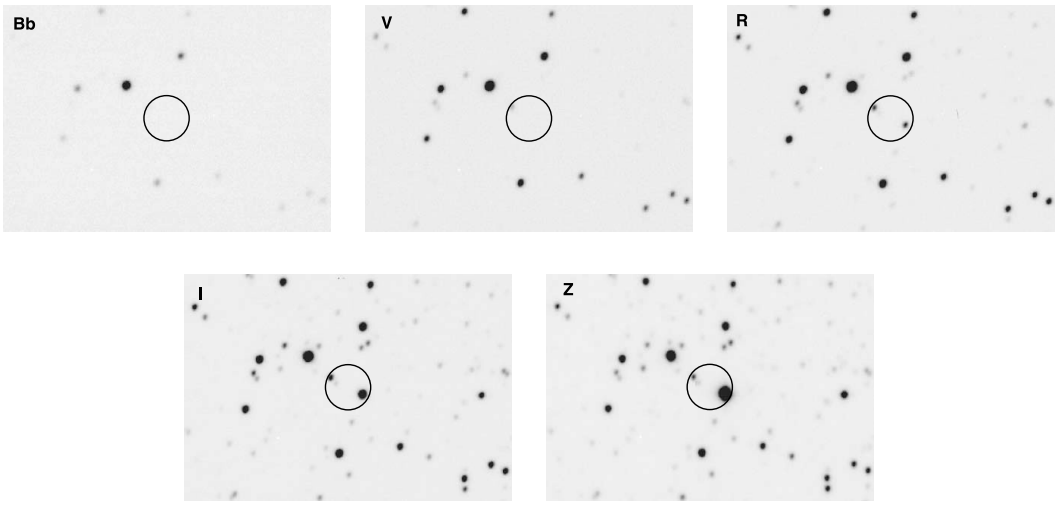

FIG. 1.—Error box of 4″ shown on the *BbVRIZ* frames of EMMI. North is up, east is to the left. The scale is given by the error box. Candidate 1 is at the southwest border of the circle, and candidates 2 and 3 are at the northeast border (see Fig. 2 for identification).

standard star hip80456 ($m_V = 7.74$, spectral type F5 V) and eight exposures of 10 s for standard star hip83612 ($m_V = 8.38$, spectral type G1 V). With these stars we made a telluric correction, followed by a flux calibration using a blackbody spectrum extrapolated from the magnitude and spectral type of the standard star. Some absorption lines, especially Brγ, were seen on the standard stars: we removed the lines and replaced them by a linear interpolation, as the continuum was smooth enough. As for the object, the two bands did not match in continuum flux in the overlap region, and the continuum was extracted and scaled to match the J and K_s broadband values, giving a good agreement with the H broadband value (see § 3.2). In two regions, between 1.35 and 1.45 μm and between 1.8 and 2.0 μm, there is a strong absorption and the flux calibration did not work successfully. The spectrum is also very noisy above 2.35 μm.

3. IDENTIFICATION OF THE COUNTERPART

3.1. *Astrometry of the Candidates*

The EMMI pixel scale is 0.″166. Therefore, the error box of 4″ reported by EPIC (Schartel et al. 2003) corresponds to a circle with a radius of 24 pixels, noticeably greater than the FWHM $\sim$5 pixels measured on the stars on the processed *BbVRIZ* frames and corresponding to the 0.″9 seeing. To find the pixel coordinates of the center of the EPIC error box, we proceed as follows:

1. We use the Guide Star Catalogue[3] (GSC) to find the astrometric coordinates of 15 stars in the field with a precision compatible with the EMMI pixel scale.
2. We use the relevant frame of the Digitized Sky Survey (DSS) catalog[4] to find visually these stars and mark them on the EMMI frames; this DSS frame is not actually used for astrometry, only for visual identification.
3. We compute the transformation matrix to go from the astrometric coordinates to EMMI pixel coordinates; the residuals are well below the error box, at the 0.″2 level, compatible with the EMMI pixel scale and the 0.″5 error reported for GSC.[5]
4. We use this matrix to compute the pixel coordinates of the center of the error box.

We show the position of the source with the EPIC error box of 4″ superimposed, on EMMI and SOFI frames, respectively, in Figures 1 and 2.

[3] See http://archive.eso.org/gsc/gsc.
[4] See http://archive.eso.org/dss/dss.
[5] See http://www-gsss.stsci.edu/gsc/gsc2/GSC2home.htm.

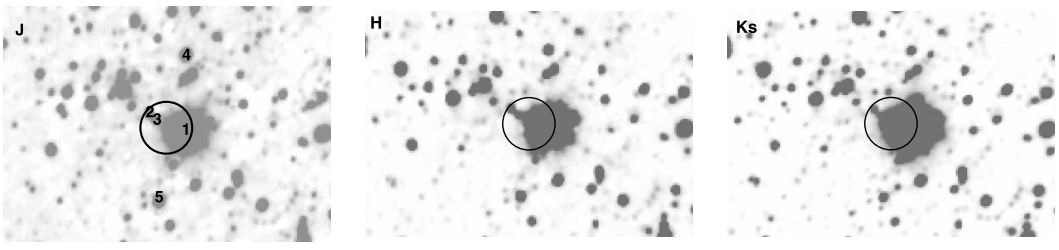

FIG. 2.—Error box of 4″ shown on the J (shortest exposures), H (shortest exposures), and K_s frames obtained with SOFI. North is up, east is to the left. Star labels are given on the J frame.

TABLE 2
ASTROMETRY OF THE THREE CANDIDATES, WITH AN UNCERTAINTY OF ±0.″2

Candidate	α	δ
1	16 31 48.31	−48 49 00.7
2	16 31 48.89	−48 48 57.7
3	16 31 48.78	−48 48 58.7

NOTE.—Units of right ascension are hours, minutes, and seconds, and units of declination are degrees, arcminutes, and arcseconds.

Given the SOFI pixel scale, the uncertainty of 4″ reported by EPIC corresponds to a circle with a radius of 13.9 pixels, noticeably greater than the FWHM ∼3 pixels measured on the stars on the processed JHK_s frames. We use a similar method to find the pixel coordinates of the center of the EPIC error box, but we use 2MASS[6] as the catalog. Again, the residuals in the construction of the transformation matrix are about a pixel size, e.g., 0.″3, with an uncertainty for the 2MASS catalog of about 0.″09.

On Figures 1 and 2, the scale is nearly the same and given by the size of the 4″ error box, to allow for visual comparisons. The astrometry is consistent within the errors in both optical and NIR image sets. Three candidates appear within the error box. For further reference, we label them 1, 2, and 3 in the left panel of Figure 2. The position of the center of each candidate with respect to the center of the circle is, on frame *J*, 3″ southwest, 3.″6 northeast, and 2.″2 northeast, respectively. Figure 2 also labels two field stars (4 and 5) for comparison.

We give in Table 2 the astrometry of the three candidates, computed by inverting the transformation matrix from GSC coordinates to pixels on frames *R*, *I*, *J* and averaging, putting statistical weight according to the uncertainties on the catalogs; the dispersion being below 0.″1, and given the uncertainties in GSC and 2MASS, we take the residual value of 0.″5 as the error estimate.

3.2. *Broadband Magnitudes of the Candidates*

We performed photometry in the $BbVRIJHK_s$ bands using the daophot package of IRAF, for the three candidates reported in Figure 2. For *Bb* and *V* frames, we indicate for candidates 1 and 3 the magnitude of the faintest star as an upper limit for the flux. The results are given in Table 3. Table 4 is a summary of archival observations of candidate 1.

Candidate 2 is barely detectable in *Bb*, more clearly in *V*. Candidates 1 and 3 are detected in the other bands. Candidate 1 is also found in the 2MASS catalog and was suggested as an infrared counterpart by Foschini et al. (2003); it is saturating the EMMI detector in *Z*. It is also one of the brightest stars in the NIR field. It saturates in *H* and K_s (even with the shortest exposure time), and in *J* (shortest exposures) it peaks to 32,000 ADU, above the limit of linearity of 10,000 ADU of SOFI (Lidman et al. 2002). The position is taken near the maximum, before saturation. Therefore, magnitudes for this star reported in Table 3 are upper limits in *H* and K_s, and there is a possible bias in *J*; note also that the optical frames show that there is no neighbor in the glare of the star, so it is likely that there is no significant contamination in NIR.

Candidate 1 has been seen in the DENIS[7] catalog, with magnitudes in agreement with our results. It has been seen in the DSS2[8] infrared plate (1980), but not seen in the DSS2 red plate (1992). However, as stated by Foschini et al. (2003), this candidate is not visible on the USNO-B1.0 plates[9] taken with IIIaF emulsion, filter RG 630 (see Fig. 3) and OG 590, corresponding to the *R* band, obtained, respectively, in 1982 and 1992. This is in contradiction with Walter et al. (2003), who identified a counterpart in the USNO-B1.0 catalog; however, it appears in light of our data that their identification corresponds to our candidate 2, whereas their identification with 2MASS is

[6] See http://irsa.ipac.caltech.edu.

TABLE 3
PHOTOMETRY OF THE STARS LABELED IN FIGURE 2

Band	1	2	3
Bb	>25.4 ± 1	22.70 ± 0.12	>25.4 ± 1
V	>21.1 ± 0.1	19.67 ± 0.03	>21.1 ± 0.1
R	17.72 ± 0.12	17.86 ± 0.05	20.25 ± 0.14
I	16.05 ± 0.54	17.71 ± 0.06	19.74 ± 0.17
J	10.33 ± 0.14	16.42 ± 0.14	16.97 ± 0.14
H	<10.35 ± 0.15	16.43 ± 0.16	16.93 ± 0.16
K_s	<9.13 ± 0.10	15.22 ± 0.20	14.86 ± 0.17

TABLE 4
ARCHIVAL DATA ON CANDIDATE 1

Name	Year	Band	Result
DSS2	1980	Infrared plate	Seen
	1992	Red plate	Unseen
USNO-B1.0	1982	RG 630	Unseen
	1992	OG 590	Unseen
2MASS	1999	*J*	10.162 ± 0.018
		H	8.328 ± 0.037
		K_s	7.187 ± 0.015
DENIS	2003	*I*	16.217 ± 0.06
		J	10.239 ± 0.05
		K	7.255 ± 0.07
IRAS	1983	12 μm	<0.9 Jy
		25 μm	<0.7 Jy
		60 μm	<4 Jy
		100 μm	<40 Jy
ATCA	2003	8.6 GHz	<0.1 mJy
		4.8 GHz	<0.1 mJy

[7] See http://cdsweb.u-strasbg.fr/denis.html.
[8] See http://archive.eso.org/dss/dss.
[9] See http://www.nofs.navy.mil/data/fchpix.

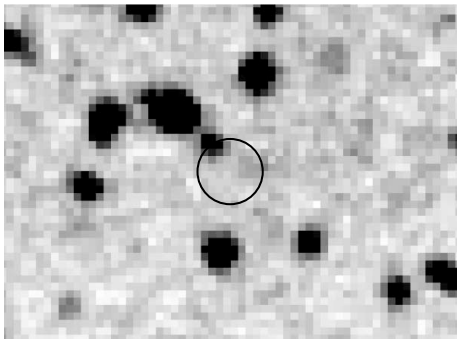

FIG. 3.—USNO-B1.0 plate, IIIaF emulsion, filter RG 630. The EPIC error box is reported. North is up, east is to the left.

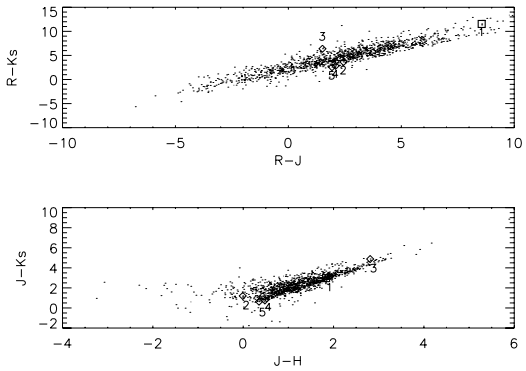

FIG. 4.—Color of stars of the field, detected together in R, J, H, and K_s. 2MASS magnitudes were used in H and K_s for candidate 1. The numbers 1–5 refer to stars labeled in Fig. 2.

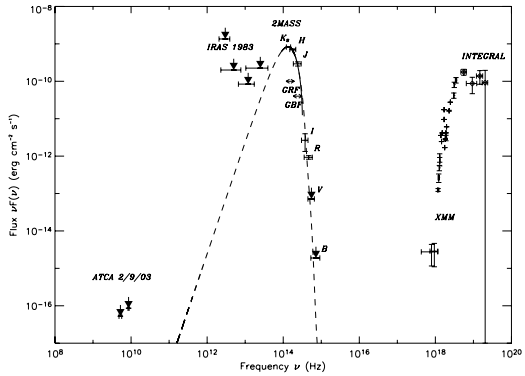

FIG. 5.—Observed SED in [ν, $\nu F(\nu)$] units, including the results of Table 3 and the archival data of Table 4. At this stage, the rescaled continuum spectra in GBF and GRF and literature data are given. The B and V data are upper limit only. The dashed line corresponds to the fit discussed in § 4.2: an absorbed blackbody, representing well the data. The results of *INTEGRAL*, *XMM*, *IRAS*, and ATCA are also shown.

actually our candidate 1. This mistake was probably due to the fact that candidates 1 and 2 have nearly the same magnitude in R in our results and that candidate 2 is reported to vary 1 magnitude over an interval of 50 yr (between the two epochs of the USNO catalog). Our observation of candidate 1 in the R band is therefore, to the extent of our knowledge, a discovery. As the magnitude limit on the USNO-B1.0 catalog is around 20, our detection seems to imply a variability in R band of more than 2 mag, whereas there is no variability on J between 2003 (our data) and 1999 (2MASS). Such a strong variability in the optical (although comparisons with photographic measurements of objects of such unusual colors may be rather uncertain because of slightly different bandpasses), associated with the high variability of IGR J16318−4848 in the X-rays, would suggest that candidate 1 is the genuine counterpart of IGR J16318−4848.

We also search for the source in the *IRAS* Point Source Catalog[10] version 2.1 and find no source closer than 230″. We found 1900 *IRAS* sources in a 3° radius around the EPIC position. We choose as a robust upper limit for Table 4 the flux such as 90% of the *IRAS* sources have greater fluxes: indeed, the flux distribution shows an obvious deficit of fainter sources.

Radio observations were performed with the Australia Telescope Compact Array (ATCA) at 4.8 and 8.6 GHz (Walter et al. 2003) on 2003 February 9 and show no detection with a 1 σ upper limit of 0.1 mJy.

The differences in magnitude $R-J$, $R-K_s$, $J-H$, $J-K_s$ of the stars of the field are shown in Figure 4. The unusual colors of candidate 1 are obvious, suggesting a reddening by absorption: the star is within the bulk of the distribution in the ($J-H$, $J-K_s$)-plane but is a clear outlier in the ($R-J$, $R-K_s$)-plane, where absorption is more critical. Since being brighter at longer wavelength is expected for a highly obscured source, this suggests that candidates 2 and 3 may be field stars, and candidate 1 is therefore the most likely candidate for the IGR J16318−4848 counterpart.

3.3. *Summary*

In the two previous subsections we have shown that three sources have positions compatible with the error box given by EPIC. Candidate 1 is seen in 2MASS, and we confirm its photometry in the J band. We discovered this candidate in the R band, since it is not detected in the USNO-B1.0 catalog. The dependence of its magnitudes on the wavelength shows a strong brightening at longer wavelengths, which indicates that it is strongly absorbed, whereas the two other candidates have behaviors comparable to the field stars. Therefore, in the rest of this paper we consider candidate 1 as the genuine counterpart of IGR J16318−4848.

4. THE SPECTRAL ENERGY DISTRIBUTION

4.1. *Spectral Continuum*

The continua of both GBF and GRF spectra were extracted and scaled to match our J magnitude and the 2MASS K_s magnitude for candidate 1. This method is approximate, given the unusual colors of the object; nevertheless, this leads to a very good agreement in the overlapping region and with the corresponding 2MASS H magnitude. This approach assumes that the observed magnitudes are mainly due to the continua; indeed, in both GRF and GBF, the power of the continua represents about 95% of the total power. In Figure 5 we show the spectral energy distribution (SED) in [ν, $\nu F(\nu)$] units, including the two continua, with results from Table 3 and the archival data of Table 4. At this stage, no dereddening is done. We have also included in the SED a compilation of several observations of the source, covering a very wide range of wavelengths, going from centimeter (ATCA) to X-rays (*XMM*, *INTEGRAL*), over 10 decades in wavelength. Data confirming our observations, such as, for instance, the DENIS catalog, are not reported on the SED. However, two caveats have to be mentioned:

1. The data were taken at different dates, and the source is variable (see Walter et al. 2003 and our comment on the nondetection of the source in the USNO-B1.0 catalog).
2. The emissions at different wavelengths can come from different components of the system, since the source is likely to be a complex system involving a compact object, a companion star of an early type, and dust (see below).

[10] See http://irsa.ipac.caltech.edu/IRASdocs/iras.html.

Therefore, throughout the discussion we emphasize our optical/NIR data and use the other data mainly for completion or confirmation.

4.2. *Absorption and Temperature Estimates*

We suppose that our NIR (photometry and spectroscopy) and optical data are measurements of a blackbody at temperature T with absorption A_V. If the emitting region is spherical of radius r at a distance D from Earth, then the measured flux in mJy is given by

$$f(\nu) = \frac{2\times10^{29}\pi h}{c^2}\frac{r^2}{D^2}\frac{\nu^3}{\exp(h\nu/kT)-1}A_\nu, \qquad (1)$$

where A_ν is the absorption at frequency ν, given A_V, and is computed according to the formulae of Cardelli et al. (1989). We fit our R, I, GBF, and GRF fluxes for parameters r/D, T, and A_V using a gradient minimization method. The fit shown in Figure 5 has $r/D = 5\times10^{-10}$, $T = 20{,}250$ K, $A_V = 17.5$, but because of a strong degeneracy, this is not the sole choice for these parameters.

This fit reproduces our data well, rendering plausible the hypothesis that an absorbed blackbody is the origin of the continuum emission. Note that the absorption law is unknown for wavelengths above 3.3 μm (9×10^{13} Hz; Cardelli et al. 1989), and we assume that the expression is still valid for longer wavelengths. The value of the fit is quickly decreasing at frequencies lower than the K_s band, rendering likely the nondetection of the source by *IRAS* and ATCA: at 2.5×10^{13} Hz, the average flux of the fit is only 16% of the upper limit of *IRAS*.

However, the parameters of the fit are strongly degenerate, and therefore the parameter estimates returned by the minimization method depend strongly on the first guess. Physically, it means that a cool, close source with low absorption can fit the data, as well as a hot, distant, and absorbed one. By analogy to chaotic mechanic systems, we call "attractor" the locus in the parameter space of the various minimum χ^2 we can get by varying the first guess. To trace this attractor, we use the minimization method 5000 times, with uniformly distributed parameters over $r/D = 10^{-12}$ to 10^{-8}, $T = 1000$–$61{,}000$ K, $A_V = 0$–25. The result is shown in Figure 6. There is a clear attractor solution, with all individual points corresponding to indistinguishable fits with nearly identical χ^2. In the temperature/absorption plane, almost all points converged toward a line well fitted by

$$\frac{A_V}{A_{V0}} = 1 - \frac{T_0}{T}, \qquad (2)$$

with $A_{V0} = 18.68$, $T_0 = 1200$ K. Note that there is a slight discrepancy for high temperatures, indicating that this simple empirical model is not fully satisfying. The T_0 parameter corresponds to the blackbody temperature that fitted our data if there is no absorption. The A_{V0} parameter is the absorption limit when $T \to \infty$, i.e., the maximum absorption compatible with our data, and the convergence toward this limit is rather quick. Two regions can be loosely distinguished, corresponding to two different physical situations:

1. A low temperature (below ~6000 K) where the absorption is very badly constrained between $A_V = 5$ and 15. This temperature is compatible with a main-sequence dwarf star photosphere, a cool red giant, or even hot dust if the temperature is not too much above 1000 K. On the other hand, the heating of dust can be nonthermal (free-free, for instance). This case corresponds also to a higher r/D ratio, indicating a rather close and/or large source.

2. A high temperature (above ~10,000 K), where the absorption is rather strongly constrained between $A_V = 16$ and 18.7. This temperature is compatible with an early-type star photosphere. However, because the NIR corresponds to the Rayleigh-Jeans region of the spectrum, the temperature has almost no effect on the shape of the spectrum and is therefore very weakly constrained.

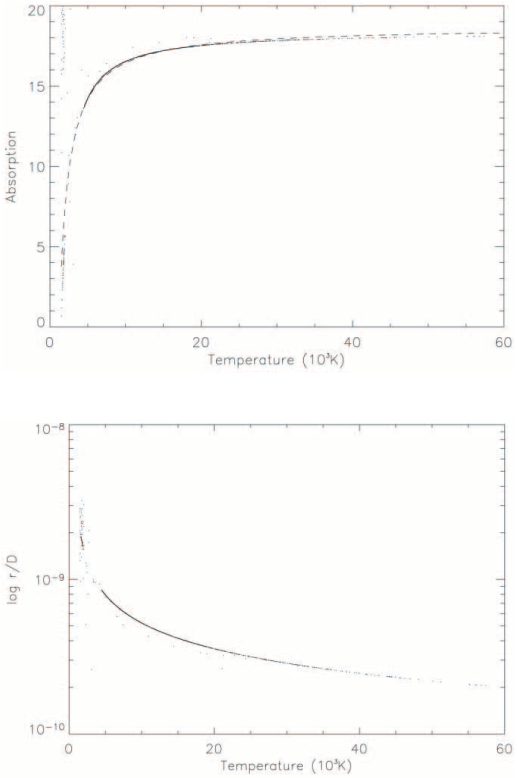

FIG. 6.—Attractor solution for the minimization procedure to fit an absorbed blackbody to data plotted in Fig. 5. The top panel is for absorption, while the bottom panel is for r/D. The points converge toward an attractor, which is fitted by a dashed line in the top panel. The remaining scattered points indicate that the 1% tolerance criterion required for convergence has not been reached in 50 iterations. See text for a discussion of the fit.

This ambiguity of fitting with an absorbed blackbody had been already noted by Revnivtsev et al. (2003), using archival observations. We essentially agree with their results.

The absorption can be intrinsic, or along the line of sight (interstellar absorption), or both. In the case of interstellar absorption, an upper limit (valid for a source not too close) can be obtained with the N_H tool of HEASARC,[11] using the

[11] See http://heasarc.gsfc.nasa.gov/cgi-bin/Tools/w3nh/w3nh.pl.

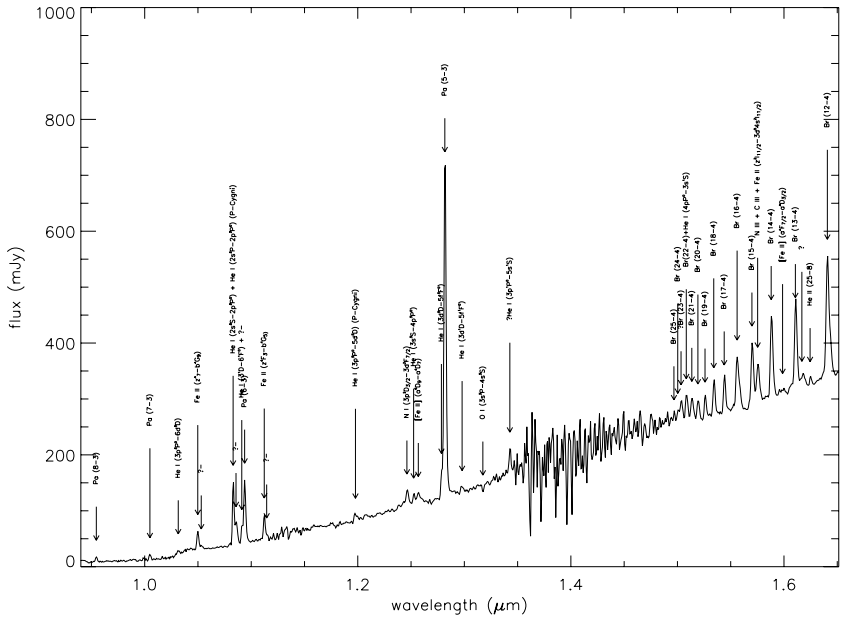

FIG. 7.—GBF spectrum for the object. Indicated lines refer to Table 5.

results of Dickey & Lockman (1990). Within 1° around the position of the source, seven data points are available, well distributed and well centered. By averaging and putting weight in order to favor closer points of the source, we obtain an estimate of the H I column density of $(2.11 \pm 0.3) \times 10^{22}$ cm^{-2}. Using the relation of Predehl & Schmitt (1995), we get an estimate for the interstellar absorption of $A_V = 11.8 \pm 1.6$. If the temperature is above ~10,000 K (the "high-temperature case" above), this seems to point to an absorption more than 3 σ above interstellar absorption and hence is an indication of a strong intrinsic absorption and that if the star responsible for optical/NIR radiation is this hot, we see it through a rather dense circumstellar material. This indication is in agreement with the fact that the source, if it is the candidate 1 reported in Figure 4, exhibits unusual colors, whereas the neighbor stars labeled 2–5 have color not different from those of field stars. However, given the proximity of the source to the Galactic plane, the interstellar medium may be patchy; hence, the derived value of interstellar absorption must be taken only as an estimate.

A more detailed modelization of the SED should include the contribution of the dust, taking into account the distribution of the material and its physical properties. However, valuable constraints would come from data in the mid-infrared range, where the dust contribution is expected to be noticeable. In the K_s band, the contribution of the dust is likely to be hard to distinguish, and indeed our fit is satisfactory in this band. That is the reason why we choose to keep a simple absorbed blackbody model, being not in contradiction with the possible presence of dust.

5. THE SPECTROSCOPY

In this section we focus on the spectroscopic lines in order to distinguish between the "low-temperature" and the "high-temperature" case of Figure 6. We also gather key information to assign a spectral type to the mass donor of the source.

5.1. *Line Identification*

The full GBF and GRF spectra are presented in Figures 7, 8, and 9. The GRF spectrum is cut into two parts for a clearer view. The spectra display around 80 lines, most of them being emission lines. All lines selected here are detected above the 2 σ level, and the relative uncertainty in flux is roughly 12%.

Line fitting is performed with the splot routine of IRAF, assuming a Gaussian shape. Tables 5, 6, and 7 (corresponding to Figs. 7, 8, and 9, respectively) report the central wavelength for the identification and for the fit, peak flux, equivalent width, and FWHM. A negative figure for width indicates that it is an emission feature, while a positive figure indicates an absorption feature. To assess if the lines are real features of the object, we also extracted the spectrum on a different aperture (for GBF only). This spectrum is an order of magnitude below the object spectrum and clearly featureless (except in the strongly absorbed region between 1.35 and 1.45 μm), proving that the sky subtraction worked successfully in order to remove the sky lines.

Identification is done using the UKIRT[12] catalog and the works of Morris et al. (1996), Clark et al. (1999), and Bandyopadhyay et al. (1997). Only the strongest lines are fitted in the noisiest regions. A question mark indicates that the identification is not certain or that the fitted value is very sensitive to continuum parameters given in input to splot and therefore highly uncertain. Several identifications were often possible, given our resolution. Note that there is always an ambiguity between hydrogen and He II lines, i.e., a transition He II

[12] See http://www.jach.hawaii.edu/JACpublic/UKIRT/astronomy.

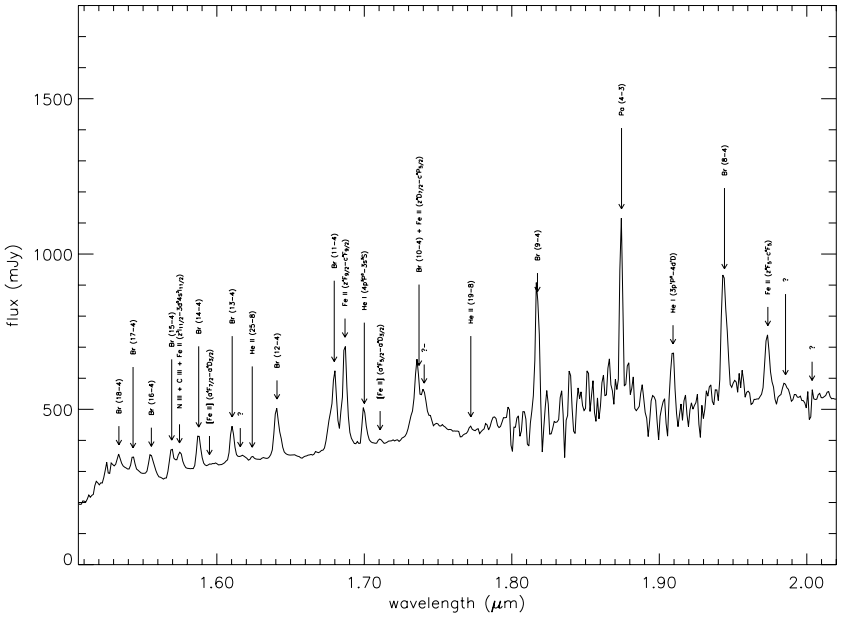

FIG. 8.—GRF spectrum for the object, first part. Indicated lines refer to Table 6.

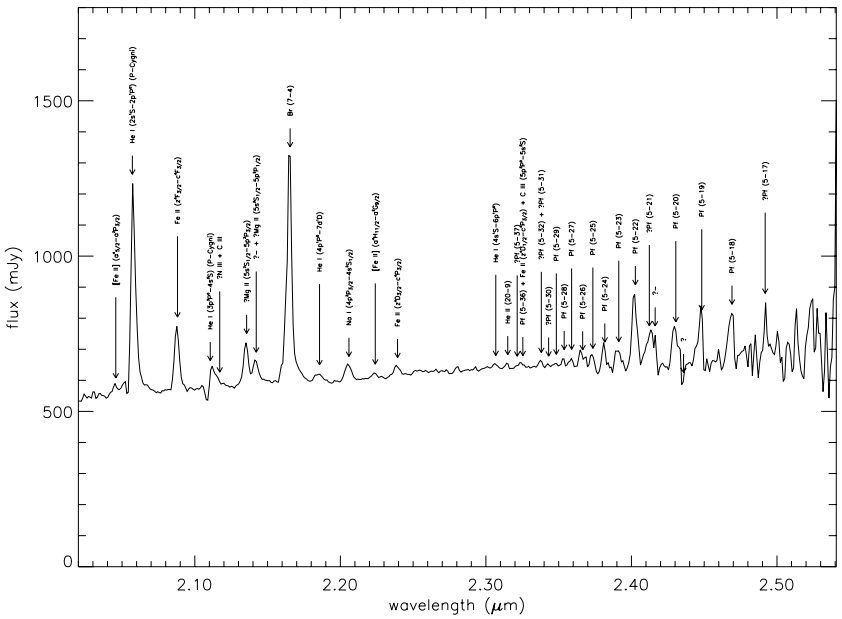

FIG. 9.—GRF spectrum for the object, second part. Indicated lines refer to Table 7.

TABLE 5
IDENTIFICATION OF LINES ON THE GBF SPECTRUM

Identification	λ (μm)	$\lambda_{\rm fit}$ (μm)	Flux (mJy)	EW (Å)	FWHM (Å)
Pa (8–3)	0.9549	0.9546	9	−21	19
Pa (7–3)	1.0052	1.0049	10	−15	18
He I (74)($3p\ ^3P^0$–$6d\ ^3D$)	10314	1.0315	4	−2	15
Fe II ($z\ ^4F_7$–$b\ ^4G_9$)	1.0501	1.0498	34	−24	20
?−	?−	1.0531	6	−6	30
He I ($2s\ ^3S$–$2p\ ^3P^0$)	1.0832	1.0830	119	−47	15
+He I ($2s\ ^3P$–$2p\ ^3P^0$)	1.0833				
?−	?−	1.0857	40	−30	29
He I ($3\ ^1D$–$6\ ^1F^0$)	1.0917	1.0911	34	−10	12
+?−	?−	1.0911	34	−10	12
Pa (6–3)	1.0941	1.0938	110	−59	22
Fe II ($z\ ^4F_3$–$b\ ^4G_5$)	1.1126	1.1122	46	−17	17
?−	?−	1.1145	7	−3	19
He I ($3p\ ^3P^0$–$5d\ ^3D$)	1.1970	1.1970	10	−3	27
N I (36)($3p\ ^2D_{3/2}$–$3d\ ^2F_{7/2}$)	1.2469	1.2461	25	−11	43
He I ($3s\ ^3S$–$4p\ ^3P^0$)	1.2528	1.2524	19	−3	18
[Fe II] ($a\ ^6D_9$–$a\ ^4D_7$)	1.2567	1.2568	17	−7	47
He I ($3d\ ^3D$–$5f\ ^3F^0$)	1.2789	1.2785	49	?−6	14
Pa (5–3)	1.2822	1.2817	634	−117	22
He I ($3d\ ^1D$–$5f\ ^1F^0$)	1.2976	1.2979	7	?−1	18
O I ($3s\ ^3P$–$4s\ ^3S$)	1.3165	1.3174	−15	2	20
?He I ($3p\ ^1P^0$–$5s\ ^1S$)	1.3415	1.3427	48	−6	21
Br (25–4)	1.4971	1.4967	21	−1	14
Br (24–4)	1.5005	1.5003	21	−2	21
?Br (23–4)	1.5043	1.5034	38	−4	26
Br (22–4)	1.5087	1.5083	49	−5	25
+He I ($4p\ ^1P^0$–$3s\ ^1S$)	1.5088				
Br (21–4)	1.5137	1.5135	40	−5	29
Br (20–4)	1.5196	1.5192	36	−4	25
Br (19–4)	1.5265	1.5259	38	−16	21
Br (18–4)	1.5346	1.5341	65	−6	23
Br (17–4)	1.5443	1.5439	68	−6	22
Br (16–4)	1.5561	1.5560	87	−12	36
Br (15–4)	1.5705	1.5699	110	−10	25
N III+C III 13–9	1.575	1.5753	65	−8	33
+Fe II ($z\ ^2I_{11/2}$–$3d^5 4s\ ^2I_{11/2}$)	1.576				
Br (14–4)	1.5885	1.5880	147	−14	27
[Fe II] ($a\ ^4F_{7/2}$–$a\ ^4D_{3/2}$)	1.598	1.5987	5	−1	28
Br (13–4)	1.6114	1.6107	158	−14	27
?	?	1.6168	18	−3	51
He II (25–8)	1.6241	1.6245	12	−1	13
Br (12–4)	1.6412	1.6407	203	−23	37

($2n$–$2m$) has nearly identical wavelength as the (n–m) hydrogen transition. In any case, there are only two very weak He II transitions with odd levels (25–8 and 20–9), suggesting that the contribution of even levels to hydrogen lines is negligible. Therefore, this ambiguity is not indicated in the tables.

In very few cases, there seems to be a double-peak structure, in which case the lower peak is then indicated by a "?−" in the tables [for instance, the Pa (6–3) at 1.0941 μm is preceded by a peak at 1.0911 μm]. The separation is around 400 km s^{-1}, similar to the value reported for Ci Cam (Clark et al. 1999), but the result is by far too dubious to lead to any firm conclusion. The FWHM values for the lines of xenon arcs are 21 and 29 Å, and we found that line broadening is not significant for the well-defined lines. The gap between the wavelength of the identified transitions and the fitted values is consistent within the 1 σ level with no systemic velocity of the object: $c\Delta\lambda/\lambda = -110 \pm 130$ km s^{-1}.

Four lines show a P Cygni profile, indicating that there is a stellar wind of circumstellar material. All four are He I: $2s\ ^3S$–$2p\ ^3P^0$ (1.0832 μm), $3p\ ^3P^0$–$5d\ ^3D$ (1.1970 μm), $2s\ ^1S$–$2p\ ^1P^0$ (2.0587 μm), and $3p\ ^3P^0$–$4s\ ^3S$ (2.1126 μm). The P Cygni profile is evident in the two latter cases, more dubious in the former two. Putting more statistical weight on the two last lines, we infer a wind velocity of 410 ± 40 km s^{-1}, the uncertainty corresponding to the dispersion of the result using the four lines. No other line shows any clear P Cygni profile.

No significant time variation of the lines (in flux or in wavelength) was found, but we cannot give constraints on this because of the short total duration of the observations (10 minutes between the first and the last GBF spectrum).

Many spectral lines are common to IGR J16318−4848 and CI Cam (Clark et al. 1999): 47 lines out of the 57 identified lines of IGR J16318−4848 are seen in CI Cam between 1 and 2.35 μm (Clark et al. 1999), and conversely 42 out of

TABLE 6
IDENTIFICATION OF LINES ON THE GRF SPECTRUM, PART 1

Identification	λ (μm)	λ_{fit} (μm)	Flux (mJy)	EW (Å)	FWHM (Å)
Br (18–4)	1.5346	1.5336	39	−4	26
Br (17–4)	1.5443	1.5432	47	−4	25
Br (16–4)	1.5561	1.5556	66	−10	40
Br (15–4)	1.5705	1.5694	79	−8	27
N III+C III 13–9	1.575	1.5747	59	−10	48
+Fe II ($z\ ^2I^0_{11/2}$–$3d^5 4s\ ^2I_{11/2}$)	1.576				
Br (14–4)	1.5885	1.5877	108	−11	30
[Fe II] ($a\ ^4F_{7/2}$–$a\ ^4D_{3/2}$)	1.598	1.5950	9	?−6	?58
Br (13–4)	1.6114	1.6104	118	−12	32
?	?	1.6159	21	−5	70
He II (25–8)	1.6241	1.6240	9	−3?	85?
Br (12–4)	1.6412	1.6408	150	−21	44
Br (11–4)	1.6811	1.6796	217	−33	52
Fe II ($z\ ^4F_{9/2}$–$c\ ^4F_{9/2}$)	1.688	1.6869	328	−32	34
He I ($4p\ ^3P^0$–$3s\ ^3S$)	1.7007	1.7000	118	−9	29
[Fe II] ($a\ ^4F_{5/2}$–$a\ ^4D_{3/2}$)	1.711	1.7107	?15	?−1	?27
Br (10–4)	1.7367	1.7371	179	−45	90
+Fe II ($z\ ^4D_{7/2}$–$c\ ^4P_{5/2}$)					
?–	?–	?17406	?160	?−15	?48
He II (19–8)	1.7717	1.7722	?17	?−2	?32
Br (9–4)	1.8181	1.8174	473	−36	30
Pa (4–3)	1.8756	1.8744	597	−22	20
He I ($3p\ ^1P^0$–$4d\ ^1D$)	1.9094	1.9093	247	−18	31
Br (8–4)	1.9451	1.9442	386	−29	39
Fe II ($z\ ^4F_5$–$c\ ^4F_5$)	1.9746	1.9736	196	−14	36
?	?	1.9856	42	−3	35
?	?	2.0026	−156	2	8

68 identified lines of CI Cam are seen in IGR J16318−4848; lines after 2.35 μm were not listed by Clark et al. (1999), and the CO bands are not seen in the source, but Pfund lines are common with CI Cam; an unidentified feature at 1.9855 μm is common to both sources; the 2–10 keV X-ray spectrum of IGR J16318−4848 (Matt & Guainazzi 2003) is very similar to the X-ray spectrum of CI Cam (Boirin et al. 2002). These are hints that the two systems are physically similar.

5.2. *Hydrogen Lines*

The Paschen, Brackett, and Pfund series are obvious on the spectra. They allow us to possibly estimate the absorption, using the Brackett decrement, independently of the SED fitting. The relative intensities of the hydrogen recombination lines have been calculated by Hummer & Storey (1987) for an electron temperature of 10^4 K and an electron density of 10^4 cm^{-3} and considering case B recombination. We compute the integrated fluxes of our Brackett and Paschen lines and divide by these relative intensities to obtain the absorption law. We fit separately the Brackett GBF lines and the Brackett GRF lines (all the lines) for the absorption A_V and put a very low statistical weight on lines for which the intensity is uncertain, e.g., those at the edges of the GBF and GRF spectra, or within the noisiest regions. Results are given in Figure 10. GBF and GRF lines, considered separately, give somewhat different absorption values, 25.4 and 18.1; the joint fit gives a value of $A_V = 18.2$. However, in the fitting procedure, the minimum value of absorption is not very sharply defined. Note also that Br (7–4) (or Brγ) has a smaller flux than expected with respect to the higher order Brackett lines, suggesting that the lines are optically thick or self-absorbed. Nevertheless, this method clearly favors the high-temperature part of Figure 6 because it indicates that absorption is higher than 16. Therefore, it is likely that we are actually observing an early-type hot star through a dense absorbing column, rather than a cool late star with lower absorption.

5.3. *Helium Lines*

The upper state of the He I 1.0832 μm doublet, a strong line on our spectrum, can be populated by recombination or can be collisionally excited from the metastable $2s\ ^3S$ state; hence, its flux can be large even when the ionized fraction of helium is low (McGregor et al. 1988). Therefore, this line can come from either ionized or neutral regions. The 2.0581 μm transition is among the strongest in our spectrum: this could be a hint of the presence of a high-density region close to the star; in this case the 584 Å transition would be optically thick (McGregor et al. 1988), but because of the strong absorption, this transition will be very difficult to observe. Because two mechanisms can populate these transitions, the 1.0832 and 2.0581 μm lines are not reliable indicators of circumstellar conditions.

We may estimate abundance of helium from the intensity ratios of He I 1.197 and 1.7007 μm to Br (7–4). This is a lower limit for the helium abundance because, as the ionization energy of helium is greater than the one of hydrogen, we have $N(\mathrm{He}^+)/N(\mathrm{H}^+) < N(\mathrm{He})/N(\mathrm{H})$ and because He I will not arise in the shielded Fe^+ zones. According to Allen et al. (1985), we have

$$\frac{N(\mathrm{He}^+)}{N(\mathrm{H}^+)} = 0.79\frac{I(1.7007\ \mu\mathrm{m})}{I(\mathrm{Br}(7\text{–}4))} = 1.15\frac{I(1.197\ \mu\mathrm{m})}{I(\mathrm{Br}(7\text{–}4))}. \quad (3)$$

TABLE 7
IDENTIFICATION OF LINES ON THE GRF SPECTRUM, PART 2

Identification	λ (μm)	$\lambda_{\rm fit}$ (μm)	Flux (mJy)	EW (Å)	FWHM (Å)
[Fe II] ($a^4_{5/2}$–$a\ ^2P_{3/2}$)	2.046	2.0457	24	−1	26
He I ($2s\ ^1S$–$2p\ ^1P^0$)	2.0587	2.0581	628	−42	35
Fe II ($z\ ^4F_{3/2}$–$c\ ^4F_{3/2}$)	2.089	2.0881	201	−13	36
He I ($3p\ ^3P^0$–$4s\ ^3S$)	2.1126	2.1116	63	−5	43
?N III + C III	2.116	?2.1151	? 42	? −4	? 44
?Mg II ($5s\ ^2S_{1/2}$–$5p\ ^2P^0_{3/2}$)	2.138	2.1356	135	−8	35
?–	?–	2.1422	71	−6	47
+?Mg II ($5s\ ^2S_{1/2}$–$5p\ ^2P^0_{1/2}$)	2.144				
Br (7–4)	2.1661	2.1655	698	−45	36
He I ($4p\ ^1P^0$–$7d\ ^1D$)	2.1847	?2.1857	?55	?−7	50
Na I ($4p\ ^2P^0_{3/2}$–$4s\ ^2S_{1/2}$)	2.2056,2.209	2.2059	45	−3	40
[Fe II] ($a\ ^4H_{11/2}$–$a\ ^2G_{9/2}$)	2.224	2.2240	12	−0	21
Fe II ($z\ ^4D_{3/2}$–$c\ ^4P_{3/2}$)	2.240	2.2393	30	−2	40
He I ($4s\ ^1S$–$6p\ ^1P^0$)	2.3069	2.3068	17	−1	40
He II (20–9)	2.314	2.3150	20	−1	22
?Pf (5–37)	2.3218	?2.3215	?8	?−0	?12
Pf (5–36)	2.3242	2.3244	15	−1	35
+Fe II ($z\ ^4D^0_{1/2}$–$c\ ^4P_{3/2}$)	2.3247				
+C III ($5p\ ^3P^0$–$5s\ ^3S$)	2.324				
?Pf (5–32)	2.3365	2.3381	25	−1	29
+?Pf (5–31)	2.3404				
?Pf (5–30)	2.3445	2.3431	14	?−1	19
Pf (5–29)	2.3492	2.3484	14	−1	50
Pf (5–28)	2.3545	2.3538	35	−1	20
Pf (5–27)	2.3604	2.3589	30	−2	33
Pf (5–26)	2.3669	2.3665	50	−4	49
Pf (5–25)	2.3744	2.3735	47	−2	27
Pf (5–24)	2.3828	2.3817	81	−3	22
Pf (5–23)	2.3925	2.3913	319	−19	36
Pf (5–22)	2.4036	2.4027	231	−14	36
?Pf (5–21)	2.4164	2.4123	67	−6	53
?–	?–	2.4153	65	−4	39
Pf (5–20)	2.4314	2.4305	115	−7	39
?	?	2.4358	−114	3	14
Pf (5–19)	2.4490	2.4483	182	−7	24
Pf (5–18)	2.4670	2.4691	152	−8	34
?Pf (5–17)	2.4953	2.4929	172	−4	17

The result depends on the absorption A_V we choose to deredden the lines, as the line wavelengths are remote from each other. The impact of absorption on the second ratio is higher because of a greater distance between the two wavelengths, and because the line at 1.197 μm has an absorbed flux much weaker than the one at 1.7007 μm, there must exist an absorption value for which the two ratios are equal. This happens for $A_V = 17.4 \pm 2.5$, the uncertainty coming from a relative uncertainty of 4% on the flux lines. It is remarkable that this value is within the attractor values in the high-temperature region of Figure 6 (the value of 17.4 is associated with a temperature of 18,000 K; however, the constraint on temperature is very loose, as can be seen in Fig. 6). The corresponding value is $N(\mathrm{He}^+/\mathrm{H}^+) = 0.32 \pm 0.04$. The first ratio is less subject to absorption and gives $N(\mathrm{He}^+/\mathrm{H}^+)$ values ranging from 0.2 to 0.5 for A_V going from 10 to 25. In any case, this is a value far higher than the solar value of $N(\mathrm{He})/N(\mathrm{H}) = 0.067$, indicating an evolved star. Note, however, that Br (7–4) is smaller than expected considering the higher order Brackett series and that its intensity, according to Figure 10, may be underestimated up to a factor of 10, causing an equivalent overestimation of the $N(\mathrm{He}^+/\mathrm{H}^+)$ ratio.

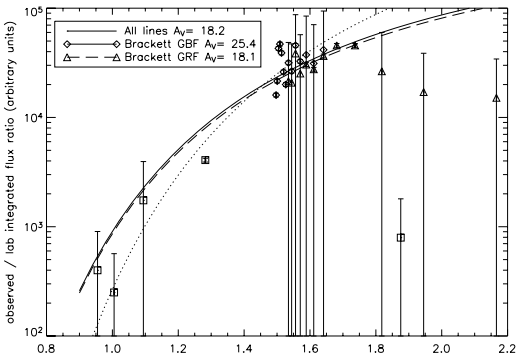

FIG. 10.—Observed integrated fluxes of hydrogen lines divided by the relative intensities from Hummer & Storey (1987). The lines indicate the best-fit absorption model for the Brackett lines in the GBF spectrum (*diamonds*: data; *short-dashed line*: fit), in the GRF spectrum (*triangles*, *long-dashed line*), and all lines including Paschen (*squares*, *solid lines*). Error bars are 4% relative in flux, except for the lines at the edges and in the noisiest regions.

TABLE 8
HELIUM LINE COMPARISONS

Wavelength (μm)	Dereddened Intensity (mJy)	Predicted Intensity (1.700 μm = 1)	Observed/Predicted (1.700 μm = 1)
1.0832.....	35280	71.4	0.27
1.1970.....	1274	0.69	1
1.7007.....	1852	1	1
2.0587.....	4754	0.01	257

We also consider the relative intensities of lines at 1.0832 (doublet), 1.1970, 1.7007, and 2.0587 μm and compare to predicted recombination intensities (see, e.g., Allen et al. 1985). The results are given in Table 8. For dereddening, we take $A_V = 17.4$. Note the concordance (better than 1%) between the 1.1970 and 1.7007 μm, another indication that dereddening is correct. We are in a case very similar to the one of η Carinae, discussed in Allen et al. (1985), with a line at 1.0832 μm about 4 times weaker than expected and the prominence of the line at 2.0587 μm. Very interestingly, the ratios for CI Cam show a similar behavior (Clark et al. 1999), with a line at 1.0832 μm about 3 times weaker than expected and with a 2.0587 μm line 7 times relatively more prominent than in our data. In the case of η Carinae, these facts were explained by invoking a large optical depth for 1.0832 μm and a significant optical thickness in the $1\ ^1S$–$1\ ^1P$ 584.3 μm transition of He for 2.0587 μm.

Two He II transitions, at 1.6241 and 1.7717 μm, are present, although very weak. The first one was also seen in CI Cam (Clark et al. 1999). They indicate a high temperature able to ionize helium. Rough flux ratio with Fe II lines, using the solar abundances, leads to flux of photons able to ionize helium and iron in agreement with a temperature between 10^4 and 2×10^4 K.

5.4. *Metallic Lines*

Several Fe II lines can be seen in our spectra. Among the strongest, 1.1126 and 2.089 μm are also seen in early-type high-luminosity stars (McGregor et al. 1988) and arise in highly excited levels that are probably populated by UV fluorescence.

A peculiar emphasis must be put on the presence of six forbidden iron lines. Although they are rather weak, the 1.1567 μm line being, for instance, weaker than its neighbors of He I and N I, they provide a very important clue for the identification of the star.

The doublet emission of Na I $4s\ ^2S$–$4p\ ^2P^0$ is seen, although not separated. The emission is most likely fluorescent, being pumped by 0.3303 μm photons. The ionization potential is low (5.1 eV), so that sodium will be largely ionized around the star. Therefore, the sodium emission comes from regions that are not exposed directly to the radiation of the star or of the compact object. This suggests the presence of matter surrounding both objects. The other lines of Na I, such as 1.1385 and 1.1407 μm, are not seen.

The Mg II doublet at 2.138 and 2.144 μm is clearly seen. It can be excited by Lβ fluorescence. In our case, the 2.138 μm line is twice more intense than the 2.144 μm line, in agreement with the higher statistical weight of the $5P_{3/2}$ transition and also its shorter distance to Lβ.

5.5. *Molecular Lines*

No lines from H_2 have been found, suggesting either that shock heating is relatively unimportant or that temperature is sufficiently high to dissociate the molecules. Molecular hydrogen has not been seen in either CI Cam (Clark et al. 1999) or the massive stars in transition studied by Morris et al. (1996). Emission lines of H_2 are more usual in massive young stellar objects (Kumar et al. 2002), suggesting that there is no such radiation-protected medium in the environment of this source.

No CO bands have been found, although a strong 8 bin rebinning of the GRF spectrum shows a step of $\sim$10 mJy over 0.1 μm at 2.295 μm, locus of the (2–0) band head. However, this is too weak and too uncertain. The CO flux, if present, is therefore lower than $\sim$10 mJy (with no dereddening).

5.6. *Summary*

This study on the spectroscopic lines has shown that there is a dense circumstellar material around the source, possibly enshrouding both the mass donor and the compact object, and with a stellar wind component. This points to a high absorption, and we have seen that the value of $A_V = 17.4$ is favored from the data. The line ratios favor a high temperature; along with the high absorption, this is consistent with the high-temperature case of Figure 6 and points to a hot early-type star observed through a dense absorbing material. Moreover, the presence of forbidden lines and the fact that almost all the lines are in emission point toward an "[e]" star, e.g., a B[e], with a striking similarity to the companion star in CI Cam.

6. DISCUSSION

6.1. *Distance Estimate*

Simple qualitative arguments show that the source is likely to be Galactic and is not an outer galaxy:

1. The Galactic latitude is $-27'$; usually absorption prevents observations of extragalactic objects so close to the Galactic plane (see, however, Martí et al. 1998 and Ribó et al. 2004 for two counterexamples); however, as *INTEGRAL* is aimed primarily within the Galactic plane, a selection effect of unusual extragalactic objects is possible.
2. The lines in the spectrum show no cosmological redshift; relatively nearby objects (up to a few megaparsecs) would show no redshift, but we can exclude the possibility of a quasar. On the other hand, the source is pointlike, with a seeing better than $1''$, in disagreement with the possibility of a nearby active galactic nucleus.
3. In the X-rays, given the variability timescale, which leads to a limit of the distance between the X-ray source and the fluorescent emission region, the width of the Fe Kα fluorescent line is too small to come from a Seyfert II galaxy or an ultraluminous infrared galaxy (Revnivtsev et al. 2003; Walter et al. 2003).

Estimating the distance from the r/D ratio of the SED fit of Figures 5 and 6 requires making some assumptions about the source. We assume that our source is an sgB[e] star, as we discuss in § 6.3, and take the list of Lamers et al. (1998), giving the bolometric luminosity and the temperature for known sgB[e] stars. Using Stefan's law, we compute a star radius and use it to break the degeneracy of our fit. This gives a distance between 0.9 (Hen S35 in LMC, type B1Iab) and 6.2 kpc (R66 in LMC, type B8). As high-mass stars remain usually close to star-forming regions, we assume that our source is in a Galactic arm. It can be then in the Sagittarius-Carina arm (0.7 kpc), the inner Scutum-Crux arm (3.2 kpc), the Norma-Cygnus arm (4.8 kpc), and a star-forming complex

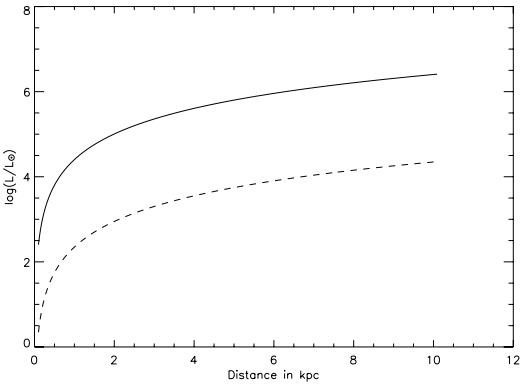

FIG. 11.—Relation between distance and luminosity assuming $A_V = 17.4$ (*solid line*) and 11.8 (*dashed line*).

at 7 kpc, where features and distances are taken from Russeil (2003). The next intercept between the direction of the source and a Galactic arm, which is the Perseus arm at 10.8 kpc, is slightly too far. Conversely, all the stars of the list give a spectrum indistinguishable from the absorbed blackbody fit when put at the distance and absorption of our source, but it is only a simple consistency test of the method, not a clue that our source is really an sgB[e]. However, errors are difficult to assess because of the various parameters involved, often in a nonlinear way, and also because the characteristics of the sgB[e] stars show too much dispersion (with a possible existence of two subgroups; see Lamers et al. 1998) to be considered as standard candles.

Using the results of § 4.2 and fixing the distance and the absorption, we can have an estimate of the luminosity. This is shown in Figure 11. For $A_V = 17.4$ (hence $T = 18{,}000$ K), we have $\log(L/L_\odot) > 4$ for $D > 1$ kpc. The corresponding radius is $R_* > 10\ R_\odot$. These characteristics are compatible with a B0- to B5-type giant star, or B or A supergiant star. For $A_V = 11.8$, for instance (hence $T = 4000$ K), we have $\log(L/L_\odot) > 2$ for $D > 1$ kpc. The corresponding radius is $R_* > 30\ R_\odot$. These characteristics are compatible with a G- to M-type supergiant star. However, we have seen that a higher absorption value is preferred by the data.

A consistency check can be made by putting the source on a color-color H-R diagram. This is done in Figure 12, using an H-R diagram computed from template stars of Ruelas-Mayorga (1991), for the two absorption values considered above. The low-absorption value is compatible with a distant red supergiant or a close red giant. The high-absorption case is compatible with an early-type supergiant, an OB, or a B, provided that the distance is not greater than 4 kpc; this suggests a location in the Scutum-Crux arm. The absorption cannot be substantially higher to be compatible with this figure; this is consistent with Figure 6, showing that absorption is always below 18 for temperatures below 60,000 K.

6.2. *Nature of the Source*

The fact that IGR J16318−4848 was detected during an outburst of X-ray emission and that a previous outburst was found in the *ASCA* archival data of 1994 (Murakami et al. 2003) strongly points toward a binary system, including a compact object such as a neutron star or a black hole. A correlation between the X-ray and the radio emission in low/hard-state black hole binaries is proposed in Gallo et al. (2003). According to this correlation, and given the *XMM* flux and absorption in the 2–10 keV band (Matt & Guainazzi 2003), a

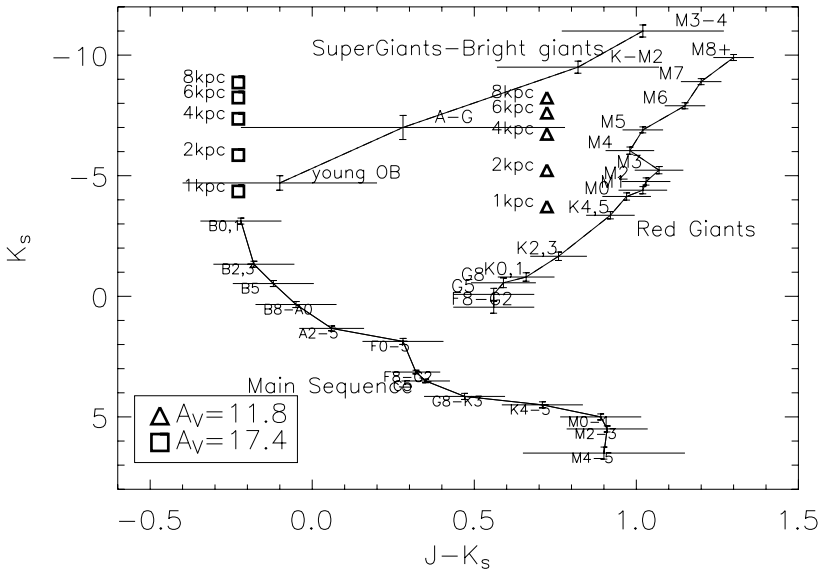

FIG. 12.—Position on the color-color H-R diagram computed from template stars of Ruelas-Mayorga (1991), for distance from 1 to 8 kpc, and for two absorption values: $A_V = 17.4$ and 11.8.

radio flux of 43 ± 30 mJy is expected (where the error bar comes from the uncertainties given in Gallo et al. 2003 for the parameters of their fit), more than 1 order of magnitude above the upper limit given by ATCA (Walter et al. 2003). This is a hint that the compact object is a neutron star instead of a black hole, but given that the environment is so unique, one has to be cautious about applying this X-ray/radio relationship. Note that, similarly, the flux of CI Cam (12 mJy at 1.4 GHz according to Hjellming & Mioduszewski 1998) is somewhat smaller than the expected flux (52 ± 30 mJy) given the ~65 mcrab flux during the outbursts (Frontera et al. 1998) if the correlation of Gallo et al. (2003) holds.

We detect no significant variation of the lines in wavelength, but given the short duration of the observations (10 minutes between the first and the last spectrum in each GBF and GRF band), this is not surprising. Long-duration observations would be useful in order to detect such a variation, if any, and to infer constraints on the masses of the system.

Using the X-ray observations by *XMM* and *INTEGRAL*, Matt & Guainazzi (2003) and Walter et al. (2003) infer the following unabsorbed luminosities at 1 kpc: 1.3×10^{35} ergs s^{-1} between 2 and 10 keV and 3×10^{34} ergs s^{-1} between 20 and 50 keV. As the photon index is very close to 2, the bolometric luminosity is somewhat difficult to estimate accurately because it is strongly model dependent, in particular on the cutoff energies. Assuming that the X-ray emission is dominating the SED of the compact object, we choose the sum of the two quoted values to be a good estimator of the luminosity (indeed it is a lower limit). Using the above estimation of the distance, this leads to a luminosity ranging from 1.3×10^{35} (0.9 kpc) to 6.2×10^{36} ergs s^{-1} (6.2 kpc), at least 30 times lower than the Eddington limit of 1.8×10^{38} ergs s^{-1} for a neutron star of 1.4 $M_{\odot}$. That suggests that moderate accretion is taking place, but given that the environment is so unique, one has to be cautious about applying this relationship. Note that the luminosity in the X-rays during the outburst is compatible with the common values for Be/X-ray binaries, where the compact object is a neutron star (Negueruela 1998).

The huge difference in the absorption between the X-ray and our optical/NIR observations (the H I column density is 100 times higher in the X-rays than in our observations; see Walter et al. 2003) indicates that the X-ray absorption is intrinsic to the compact object (Revnivtsev et al. 2003). It is probably due to mass loss from the companion star enshrouding the compact object, thereby absorbing the X-ray emission. Using the variability timescale of the X-ray emission and the maximum delay observed between the Fe Kα line and the continuum variations, Walter et al. (2003) deduce that the distance r between the zone in which fluorescent emission takes place and the X-ray source is constrained by $r < 10^{13}$ cm $=$ 140 $R_{\odot}$. We suppose that the distance between the source of the NIR emission and the source of the X-ray emission is at least r; a hint for this hypothesis is that the absorption in the X-rays is much higher than in the NIR, although one has to be cautious because the nature of the absorbing material might not be the same in both wavelength domains. Unless the donor is a red giant of type K or later, this excludes a symbiotic binary system; however, we have seen that our data prefer hot stars and therefore that a high-mass X-ray binary (HMXB) is preferred. Assuming that we have a neutron star of 1.4 $M_{\odot}$ orbiting a B-type star with $1.4 \lesssim \log(M/M_{\odot}) \lesssim 1.7$ and that we have $r = 10^{13}$ cm, we obtain a lower limit for the period between 28 and 38 days. With $r = 10^{12}$ cm, the minimum period is shortened to 0.9–1.2 days. In both cases, the period is far too long to have been detected by our observations. This point needs further observations to detect and measure an orbital period and would increase noticeably our knowledge of IGR J16318−4848. It is possible that the X-ray outburst is close to the passage of the compact companion at the periastron, as is the case in type I Be/X-ray binaries (Negueruela 1998).

6.3. *About the Mass Donor*

The probably high absorption (we have seen that $A_V = 17.4$ is favored by our data) points to a massive supergiant star, with a luminosity higher than $10^{4.4}$ $L_{\odot}$ for a distance greater than 1 kpc and 10^5 $L_{\odot}$ for a distance greater than 2 kpc. The hypothesis of binarity leads to an HMXB, the traditional mass donors of which are classical Be and OB supergiant stars. The latter, favored by the high luminosity, is not probable because it generally leads to persistent X-ray emission.

The fact that the lines of the spectrum are nearly all emission lines and the fact that among them we have forbidden lines are key constraints for the identification of the spectral type of the mass donor. Usual stars have absorption lines. The P Cygni profiles seem to be not numerous enough to make a classification as a P Cygni star as HDE 316285 (Hillier et al. 1998). Bright infrared [Fe II] emission appears to be a common property among LBVs with prominent nebulae (Smith 2002); however, the line at 1.643 μm is very bright in these cases, whereas we do not observe this line, and the other forbidden lines are weak. Among the class of massive stars in transition, the spectral properties around 2 μm are in good agreement with both B[e] and Of/WN stars (Morris et al. 1996). The other star types (O, B0) considered in Morris et al. (1996) are disfavored because the Brγ line is in absorption in these types, but as noted in this article, there is always at least one example from each group that can be easily associated with another one, and therefore robust conclusions are difficult to infer from the infrared spectrum alone. However, Wolf-Rayet stars can be ruled out, as these stars are usually very poor in hydrogen.

The NIR spectrum of IGR J16318−4848 shows strong hydrogen Paschen, Brackett, and Pfund emission lines. Although we have no spectroscopic data in the visible region, we can assume that Balmer emission lines are probably present at a strong level. The spectrum shows also emission lines of Fe II, both allowed and forbidden transitions. The absorption seems to be higher than the estimated interstellar absorption along the line of sight (considering $A_V = 11.8 \pm 1.6$ for interstellar absorption, or considering the very unusual colors of the source with respect to the field stars, as seen in Fig. 4); moreover, the presence of Na I lines indicates the presence of circumstellar regions shielded from direct stellar radiation, but the absence of molecular H_2 suggests a rather hot temperature. All this seems to converge toward the existence of hot circumstellar dust, although the lack of observations in the optical range makes it difficult to assess an excess of IR emission. These points are the characteristics of the "B[e] phenomenon," according to the classification of Lamers et al. (1998).

The fact that the luminosity is high suggests a supergiant B[e] (sgB[e]). Some of the secondary criteria for an sgB[e] classification according to Lamers et al. (1998) are fulfilled: some lines show a P Cygni profile indicating mass loss (criterion B1 of Lamers et al. 1998), and the possibly high He/H ratio indicates an evolved star (criterion B3), although this ratio is not very firmly constrained by our data, and a high extinction (criterion B4). However, we did not see any hybrid

spectrum (there is no broad absorption feature) or strong interstellar bands (contradicting criteria B2 and B4), but the latter feature is only reported as "usual." The nondetection of the source in the USNO-B1.0 catalog suggests that photometric variations can be higher than 2 mag in the *R* band (contradicting criterion B5, saying that the variation is on the order of 0.1–0.2 mag); however, the 2MASS magnitude in the *J* band (in 1999) is in agreement with our own measurements (2003). The criteria for the other B[e] subtypes (pre–main-sequence stars, compact planetary nebulae, or symbiotic binaries) are clearly not satisfied. In addition, as already stated, the spectrum is very similar to that of CI Cam, in both the X-ray domain (Boirin et al. 2002) and the NIR domain (Clark et al. 1999). CI Cam has been classified as an sgB[e] in the optical domain by Robinson et al. (2002) and Hynes et al. (2002), as the first sgB[e] associated with an HMXB. The lack of *IRAS* detection is a concern with this hypothesis, as CI Cam is a significant *IRAS* source. However, CI Cam is also much brighter than IGR J16318−4848 in the NIR and visible wavelength. By comparing the fluxes in the *K* band of both sources, we expect a flux at 12 μm about 1 Jy or less for IGR J16318−4848, around the upper limit we estimated for *IRAS*. Therefore, the lack of detection is not really conclusive. A classification as sgB[e] appears to be a reasonable choice, even if a classification as unclB[e]/sgB[e] may be more secure because of the problematic fulfillment of some secondary criteria.

Therefore, we propose sgB[e] as a tentative identification for the massive companion of IGR J16318−4848, making this source the second HMXB with an sgB[e] after CI Cam. There is evidence that the circumstellar material of an sgB[e] is concentrated in a disk (Hubert & Jaschek 1998), with a rarefied polar wind. As already proposed by Hynes et al. (2002) in the case of CI Cam, it is possible that the X-ray outburst is caused by the passage of the compact object in the disk, perhaps near the periastron. In this case, the burst should be periodic, as the *ASCA* observations in 1994 suggest (Murakami et al. 2003).

7. CONCLUSIONS

The source IGR J16318−4848 was the first source discovered by *INTEGRAL*. In the course of a ToO program using the NTT, we performed photometric and spectroscopic observations less than 1 month after its discovery in the optical and NIR domains. We list here our main results:

1. We discovered the optical counterpart and confirmed an already proposed NIR candidate.
2. We performed an independent astrometry for this candidate.
3. We obtained photometric measurements for the *R*, *I*, and *J* bands, flux upper limits for *B* and *V*, and flux lower limits for *H* and K_s.
4. With the continua of our GBF and GRF spectra, these photometric measurements, and X-ray, radio, and archival data, we constructed an SED covering 10 decades in wavelength.
5. On the spectrum we identified 72 emission lines, including forbidden lines, of which 80% of these lines have been detected in CI Cam, suggesting a similar nature.
6. The data favor an absorption of $A_V = 17.4$, greater than the interstellar absorption, and a temperature above 10,000 K.
7. The data favor the existence of a dense circumstellar material, with stellar wind.
8. The distance is between ~0.9 and 6.2 kpc.
9. We propose as the most likely hypothesis that the source is an HMXB with an sgB[e] star as the mass donor; it would be the second case after CI Cam.

Complementary observations are needed in order to confirm our results; among them we propose the following:

1. High-resolution NIR spectroscopy, if possible extended to optical, in order to (1) extend the SED in the optical and in the mid-infrared to directly see an NIR excess, (2) check if the similarity with CI Cam as observed in the NIR is still valid in the optical, and (3) improve our results concerning P Cygni profiles and line broadening.
2. Long-term follow-up spectroscopy and photometry, in order to (1) search for line variability and (2) search for a periodic behavior to infer the orbital elements.

This source shows many unusual features; the first is its strong intrinsic absorption. Interestingly, among the 10 sources that *INTEGRAL* has discovered in this region, this feature is common (at least in the X-rays) to the three sources discussed by Revnivtsev (2003), IGR J16318−4848, IGR J16320−4751, and IGR J16358−4726, although the $N_{\rm H}$ column density is lower by an order of magnitude in the two latter systems (Rodriguez et al. 2003; Patel et al. 2004). However, a clear identification for the optical/NIR counterpart has been made only for IGR J16318−4848. Moreover, the type of the mass donor, as inferred from our study, has been considered up to now as very rare. There is therefore the possibility that *INTEGRAL*, with the discovery of IGR J16318−4848, has unveiled a new class of binaries that will deserve much attention in the future.

This work uses observations made at the ESO NTT upon detection and localization made by *INTEGRAL* and *XMM*. We are very grateful to the ESO staff for their availability and skills for performing override programs, and special thanks go to Malvina Billeres for having performed these service ToO observations. We use the 2MASS, DENIS, USNO, GSC, and DSS catalogs for astrometry and photometry. We acknowledge P. Ferrando, P. Goldoni, F. Lebrun, M. Ribó, and J. Rodriguez for useful discussions and careful reading of the manuscript. S. C. thanks R. Hynes, I. Negueruela, and M. Ribó for useful discussions on the nature of the source and R. Walter for useful discussions. We thank the referee for a careful reading of the manuscript and useful suggestions. P. F. also acknowledge the CNRS/Fédération de Recherche APC for funding.

REFERENCES

Allen, D. A., Jones, T. J., & Hyland, A. R. 1985, ApJ, 291, 280
Bandyopadhyay, R., Shahbaz, T., Charles, P. A., van Kerkwijk, M. H., & Naylor, T. 1997, MNRAS, 285, 718
Boirin, L., et al. 2002, A&A, 394, 205
Cardelli, J. A., Clayton, G. C., & Mathis, J. S. 1989, ApJ, 345, 245
Chaty, S., & Filliatre, P. 2004, Rev. Mex. AA Conf. Ser., 20, 65
Clark, J. S., Steele, I. A., Fender, R. P., & Coe, M. J. 1999, A&A, 348, 888
Courvoisier, T., Walter, R., Rodriguez, J., Bouchet, L., & Lutovinov, A. A. 2003, IAU Circ., 8063, 3
Dickey, J. M., & Lockman, F. J. 1990, ARA&A, 28, 215
Foschini, L., Rodriguez, J., & Walter, R. 2003, IAU Circ., 8076, 2
Frontera, F., et al. 1998, A&A, 339, L69
Gallo, E., Fender, R. P., & Pooley, G. G. 2003, MNRAS, 344, 60
Gonzalez, J.-F., Brillant, S., Pompei, E., & Hainaut, O. R. 2002, EMMI User's Manual, http://www.ls.eso.org/lasilla/sciops/ntt/emmi/emmiManual.html

Hillier, D. J., Crowther, P. A., Najarro, F., & Fullerton, A. W. 1998, A&A, 340, 483
Hjellming, R. M., & Mioduszewski, A. J. 1998, IAU Circ., 6857, 1
Hubert, A. M., & Jaschek, C. 1998, B[e] Stars (Dordrecht: Kluwer)
Hummer, D. G., & Storey, P. J. 1987, MNRAS, 224, 801
Hynes, R. I., et al. 2002, A&A, 392, 991
Kumar, M. S. N., Bachiller, R., & Davis, C. J. 2002, ApJ, 576, 313
Lamers, H. J. G. L. M., Zickgraf, F.-J., de Winter, D., Houziaux, L., & Zorec, J. 1998, A&A, 340, 117
Landolt, A. U. 1992, AJ, 104, 340
Lebrun, F., et al. 2003, A&A, 411, L141
Lidman, G., Cuby, J.-G., Vanzi, L., Billières, M., Hainaut, O. R., & Pompei, P. 2002, SOFI User's Manual, http://www.ls.eso.org/lasilla/sciops/ntt/sofi
Martí, J., Mirabel, I. F., Chaty, S., & Rodríguez, L. F. 1998, A&A, 330, 72
Matt, G., & Guainazzi, M. 2003, MNRAS, 341, L13
McGregor, P. J., Hyland, A. R., & Hillier, D. J. 1988, ApJ, 324, 1071
Morris, P. W., Eenens, P. R. J., Hanson, M. M., Conti, P. S., & Blum, R. D. 1996, ApJ, 470, 597
Murakami, H., Dotani, T., & Wijnands, R. 2003, IAU Circ., 8070, 3
Negueruela, I. 1998, A&A, 338, 505
Patel, S. K., et al. 2004, ApJ, 602, L45
Persson, S. E., Murphy, D. C., Krzeminski, W., Roth, M., & Rieke, M. J. 1998, AJ, 116, 2475
Predehl, P., & Schmitt, J. H. M. M. 1995, A&A, 293, 889
Revnivtsev, M. G. 2003, Astron. Lett., 29, 644
Revnivtsev, M. G., Sazonov, S. Y., Gilfanov, M. R., & Sunyaev, R. A. 2003, Astron. Lett., 29, 587
Ribó, M., Combi, J. A., & Mirabel, I. F. 2004, ATel, 235, 1
Robinson, E. L., Ivans, I. I., & Welsh, W. F. 2002, ApJ, 565, 1169
Rodriguez, J., Tomsick, J. A., Foschini, L., Walter, R., Goldwurm, A., Corbel, S., & Kaaret, P. 2003, A&A, 407, L41
Ruelas-Mayorga, R. A. 1991, Rev. Mex. AA, 22, 27
Russeil, D. 2003, A&A, 397, 133
Schartel, N., et al. 2003, IAU Circ., 8072, 3
Smith, N. 2002, MNRAS, 336, L22
Strüder, L., et al. 2001, A&A, 365, L18
Turner, M. J. L., et al. 2001, A&A, 365, L27
Ubertini, P., et al. 2003, A&A, 411, L131
Voges, W., et al. 1999, A&A, 349, 389
Walter, R., et al. 2003, A&A, 411, L427

3.5.2 Identifications de quatre sources *INTEGRAL* dans le plan Galactique à partir de localisations *Chandra*

"Identifications of four *INTEGRAL* sources in the Galactic plane via *Chandra* localizations" par J.A. Tomsick, S. Chaty, J. Rodriguez, L. Foschini, R. Walter and P. Kaaret, 2006, ApJ, 647, 1309

Dans cet article sont compilées des observations optique et infrarouge proche de quatre nouvelles sources *INTEGRAL* localisées précisément avec le satellite Chandra, permettant ainsi de répérer la contrepartie optique/infrarouge de la source, et de contraindre la nature des étoiles compagnons, et donc des systèmes binaires. Cet article montre que deux de ces sources sont des systèmes binaires de grande masse (voir le paragraphe 3.2 pour plus de détails).

The Astrophysical Journal, 647:1309–1322, 2006 August 20
© 2006. The American Astronomical Society. All rights reserved. Printed in U.S.A.

IDENTIFICATIONS OF FOUR *INTEGRAL* SOURCES IN THE GALACTIC PLANE VIA *CHANDRA* LOCALIZATIONS

John A. Tomsick,[1] Sylvain Chaty,[2] Jerome Rodriguez,[2] Luigi Foschini,[3] Roland Walter,[4] and Philip Kaaret[5]
Received 2006 March 18; accepted 2006 May 3

ABSTRACT

Hard X-ray imaging of the Galactic plane by the *INTEGRAL* satellite is uncovering large numbers of 20–100 keV "IGR" sources. We present results from *Chandra*, *INTEGRAL*, optical, and IR observations of four IGR sources: three sources in the Norma region of the Galaxy (IGR J16195−4945, IGR J16207−5129, and IGR J16167−4957) and one that is closer to the Galactic center (IGR J17195−4100). In all four cases, one relatively bright *Chandra* source is seen in the *INTEGRAL* error circle, and these are likely to be the soft X-ray counterparts of the IGR sources. They have hard 0.3–10 keV spectra with power-law photon indices of $\Gamma = 0.5$–1.1. While many previously studied IGR sources show high column densities ($N_{\rm H} \sim 10^{23}$–10^{24} cm^{-2}), only IGR J16195−4945 has a column density that could be as high as 10^{23} cm^{-2}. Using optical and IR sky survey catalogs and our own photometry, we have obtained identifications for all four sources. The *J*-band magnitudes are in the range 14.9–10.4, and we have used the optical/IR spectral energy distributions (SEDs) to constrain the nature of the sources. Blackbody components with temperature lower limits of >9400 K for IGR J16195−4945 and >18,000 K for IGR J16207−5129 indicate that these are very likely high-mass X-ray binaries (HMXBs). However, for IGR J16167−4957 and IGR J17195−4100, low extinction and the SEDs indicate later spectral types for the putative companions, suggesting that these are not HMXBs.

Subject headings: infrared: stars — stars: individual (IGR J16195−4945, IGR J16207−5129, IGR J16167−4957, IGR J17195−4100) — stars: neutron — X-rays: stars

1. INTRODUCTION

The hard X-ray imaging of the Galactic plane by the *International Gamma-Ray Astrophysics Laboratory* (*INTEGRAL*; Winkler et al. 2003) is uncovering a large number of new or previously poorly studied high-energy sources. During the first two years of *INTEGRAL* operations (2002 October–2004 September), 56 new "IGR" sources were discovered (Bird et al. 2006), and many more IGR sources have been discovered to date. *INTEGRAL* is also detecting many sources that are present in other X-ray catalogs but were not targets of focused studies until they were shown to be strong emitters of hard X-rays by *INTEGRAL*. If these sources are included, well over 100 IGR sources have been found.[6] All or nearly all of the IGR sources have been found in the 20–50 keV band with the Imager on Board the *INTEGRAL* Satellite (IBIS) coded aperture mask instrument (Ubertini et al. 2003; Lebrun et al. 2003). Large numbers of IGR sources have been found because of the combination of hard X-ray imaging with 12′ angular resolution, a large field of view (9° by 9° fully coded field of view for IBIS), and the *INTEGRAL* observing plan, which emphasizes observations of the Galactic plane.

Follow-up observations of the IGR sources have shown a diversity of source types, including low-mass X-ray binaries (LMXBs), high-mass X-ray binaries (HMXBs), active galactic nuclei, and cataclysmic variables, as well as other source types. While some of the sources have proved to be transient, others have been consistently detected in X-rays in multiple *INTEGRAL* observations as well as by other current and previous X-ray instruments, suggesting that they are persistent. One subgroup of IGR sources exhibits persistent but highly variable X-ray emission. These sources lie within a few degrees of the Galactic plane and show some evidence for clustering near Galactic spiral arms (Lutovinov et al. 2005a). Their X-ray fluxes are typically ∼1–10 millicrab in the hard X-ray band (Dean et al. 2005), and their luminosities are mostly unknown due to large uncertainties on their distances, but they may have luminosities of 10^{33}–10^{36} ergs s^{-1} if they are at typical 1–10 kpc Galactic distances.

Although X-ray, optical, and infrared (IR) observations of this group of persistent Galactic IGR sources show that they do not have uniform properties, some trends have been identified. For many of these sources, their X-ray spectra show high column densities with values of $N_{\rm H}$ well in excess of the levels expected due to interstellar material. The most extreme example is IGR J16318−4848, for which $N_{\rm H} \sim 2 \times 10^{24}$ cm^{-2} (Matt & Guainazzi 2003; Walter et al. 2003), and there are also several other sources with values of $N_{\rm H}$ in the 10^{23}–10^{24} cm^{-2} range (e.g., Rodriguez et al. 2003; Combi et al. 2004; Beckmann et al. 2005). Many of the Galactic IGR sources also exhibit X-ray pulsations, indicating the presence of a neutron star. Pulsations are detected for at least five of the persistent IGR sources with periods of 139–1303 s (e.g., Lutovinov et al. 2005b; Bodaghee et al. 2006). Finally, in some cases for which optical or IR spectra of IGR sources have been obtained, high-mass stellar companions have been found. IGR J16318−4848 harbors an unusual supergiant B[e] star, and the IR spectra also show P Cygni profiles, suggesting the presence of a

[1] Center for Astrophysics and Space Sciences, Code 0424, University of California at San Diego, La Jolla, CA 92093; jtomsick@ucsd.edu.
[2] AIM–Astrophysique Interactions Multiéchelles (UMR 7158 CEA/CNRS/Université Paris 7 Denis Diderot), CEA Saclay, DSM/DAPNIA/Service d'Astrophysique, Bât. 709, L'Orme des Merisiers, FR-91 191 Gif-sur-Yvette Cedex, France.
[3] INAF/Istituto di Astrofisica Spaziale e Fisica Cosmica–Bologna, Via Gobetti 101, 40129 Bologna, Italy.
[4] *INTEGRAL* Science Data Centre, Chemin d'Ecogia, 16, 1290 Versoix, Switzerland.
[5] Department of Physics and Astronomy, University of Iowa, Iowa City, IA 52242.
[6] A current list of IGR sources is available at http://isdc.unige.ch/~rodrigue/html/igrsources.html.

TABLE 1
Chandra Observations

ObsID	Target	l (deg)	b (deg)	Start Time	Exposure Time (s)
5471.....	IGR J16195−4945	333.56	+0.34	2005 Apr 29, UT 17:25	4752
5472.....	IGR J16207−5129	332.46	−1.05	2005 Jun 25, UT 03:17	5109
5473.....	IGR J16167−4957	333.06	+0.50	2005 Jun 13, UT 19:14	4979
5474.....	IGR J17195−4100	346.98	−2.14	2005 Jul 25, UT 12:57	4701

strong stellar outflow (Filliatre & Chaty 2004). Another example is IGR J17391−3021 (= XTE J1739−302), which also contains a supergiant (Smith et al. 2006; Negueruela et al. 2006).

Here, we present results for X-ray, optical, and IR follow-up studies of four IGR sources that are in the Galactic plane. Three of the sources (IGR J16195−4945, IGR J16207−5129, and IGR J16167−4957) are in the Norma region of the Galaxy (i.e., close to the tangent to the Norma spiral arm) at $332^\circ < l < 334^\circ$, and the fourth (IGR J17195−4100) is about halfway between the Norma region and the Galactic center at $l = 347^\circ$. Although none of the sources have been previously well studied, it has been pointed out that IGR J16195−4945 is probably the *Advanced Satellite for Cosmology and Astrophysics* (*ASCA*) source AX J161929−4945 (Sugizaki et al. 2001; Sidoli et al. 2005). The 2–10 keV *ASCA* spectrum of this source is well described by a very hard power law with a photon index of $\Gamma = 0.6^{+0.8}_{-0.5}$ and a relatively high column density of $N_{\rm H} = (12^{+8}_{-4}) \times 10^{22}$ cm^{-2}. Based on its X-ray properties, it has been suggested that the source is a neutron star HMXB (Sidoli et al. 2005; Bird et al. 2006). IGR J16167−4957 and IGR J17195−4100 have been tentatively identified with *ROSAT* (*Röntgensatellit*) sources (Stephen et al. 2005), but it appears that *INTEGRAL* is the first X-ray satellite to detect IGR J16207−5129. The nature of these three sources is completely uncertain (Bird et al. 2006).

In this work, we use observations with the *Chandra X-Ray Observatory* (Weisskopf et al. 2002) to obtain subarcsecond X-ray positions for the four sources (§ 2) and to determine whether the sources are associated with known sources (§ 3). In §§ 4 and 5 we present a study of the *Chandra* and *INTEGRAL* spectra. In § 6 we report on optical and IR photometry of these sources we obtained at ESO's New Technology Telescope (NTT), and we combine these measurements with those available in optical and IR catalogs in order to constrain the optical and IR spectral energy distributions (§ 7). In §§ 8 and 9 we discuss our results and present our conclusions.

2. *CHANDRA* OBSERVATIONS AND SOURCE DETECTION

We obtained short, ∼5 ks *Chandra* observations of the fields of IGR J16195−4945, IGR J16207−5129, IGR J16167−4957, and IGR J17195−4100 with the primary goal of localizing the sources to facilitate IR and optical identifications. We chose targets located close to the Galactic plane that were detected in the 20–40 keV band during our 2003 February *INTEGRAL* observation of the black hole transient 4U 1630−47 (Tomsick et al. 2004, 2005) and that were also reported in the first and second catalogs of *INTEGRAL* sources (Bird et al. 2004, 2006). Consistent hard X-ray detections gave us reason to believe that these were persistent sources and that the probability of detection with *Chandra* was high.

Table 1 shows the Observation IDs (ObsIDs) and times of our *Chandra* observations of the four IGR sources, which took place between 2005 April and July. We used the Advanced CCD Imaging Spectrometer (ACIS; Garmire et al. 2003) with the center of the 3′ *INTEGRAL* error circle placed at the nominal aim point for the ACIS-I (Imager) array. Although the effective exposure times are lower in the gaps between ACIS-I chips, we used a dithering pattern with an amplitude twice as large as the standard pattern to achieve a more uniform sensitivity over the *INTEGRAL* error circle. In processing the data, we started with the level 1 event list produced by the standard data processing with ASCDS versions between 7.5.3 and 7.6.2. For further processing, we used the *Chandra* Interactive Analysis of Observations (CIAO) version 3.3.0.1 software and Calibration Database (CALDB) version 3.2.1. We used the CIAO routine `acis_process_events` to obtain a level 2 event list and image.

The *Chandra* images are shown in Figure 1. For each target, we searched for sources in a 7×7 arcmin^2 region that includes the full *INTEGRAL* error circle. We restricted the energy range to 0.3–10 keV and used the CIAO routine `wavdetect` (Freeman et al. 2002). Based on the image size of 854×854 pixels and our detection threshold of 10^{-6} (see Freeman et al. 2002 for a precise definition), we would expect to detect $\lesssim$1 spurious source. For ObsIDs 5471, 5472, 5473, and 5474, we detected 4, 7, 4, and 7 sources, respectively. The brightest sources for these four ObsIDs have 183, 678, 866, and 676 counts, respectively, while the remaining sources have between 3 and 24 counts. In addition, each of these four brightest sources is located within the respective *INTEGRAL* error circle (see Fig. 1), making it very likely that these sources are, in fact, the soft X-ray counterparts of the IGR sources. In the following, we focus on the properties of these four sources and primarily refer to them by their IGR names (even though *Chandra* names are also given to the sources).

3. *CHANDRA* POSITIONS AND ASSOCIATIONS WITH KNOWN SOURCES

Table 2 provides the *Chandra* positions for the four sources. The positions come from the `wavdetect` analysis described above, and the position uncertainties are 0.″6. This value is the nominal *Chandra* pointing accuracy, and the statistical errors calculated by `wavdetect` are negligible in comparison. Here, we use the SIMBAD database to determine whether the *Chandra* sources are associated with previously known sources.

For IGR J16195−4945, the *Chandra* source CXOU J161932.2−494430 lies 1.″1 from the best *ASCA* position for AX J161929−4945, which is just outside the 1′ *ASCA* error circle (see Fig. 1). While Sugizaki et al. (2001) quote *ASCA* position uncertainties of 1′, a careful analysis by Ueda et al. (1999) shows that the 90% confidence error radii for *ASCA* sources are in the range 0.″6–0.″8, depending on the detection significance. Thus, the 1′ error circle can be considered to be slightly larger than a 90% confidence error circle. Still, CXOU J161932.2−494430 and AX J161929−4945 are close enough that we consider the association likely. An association between IGR J16195−4945, AX J161929−4945, and the B1/B2 Ia supergiant HD 146628 has also been suggested (Sidoli et al. 2005; Tomsick et al. 2004;

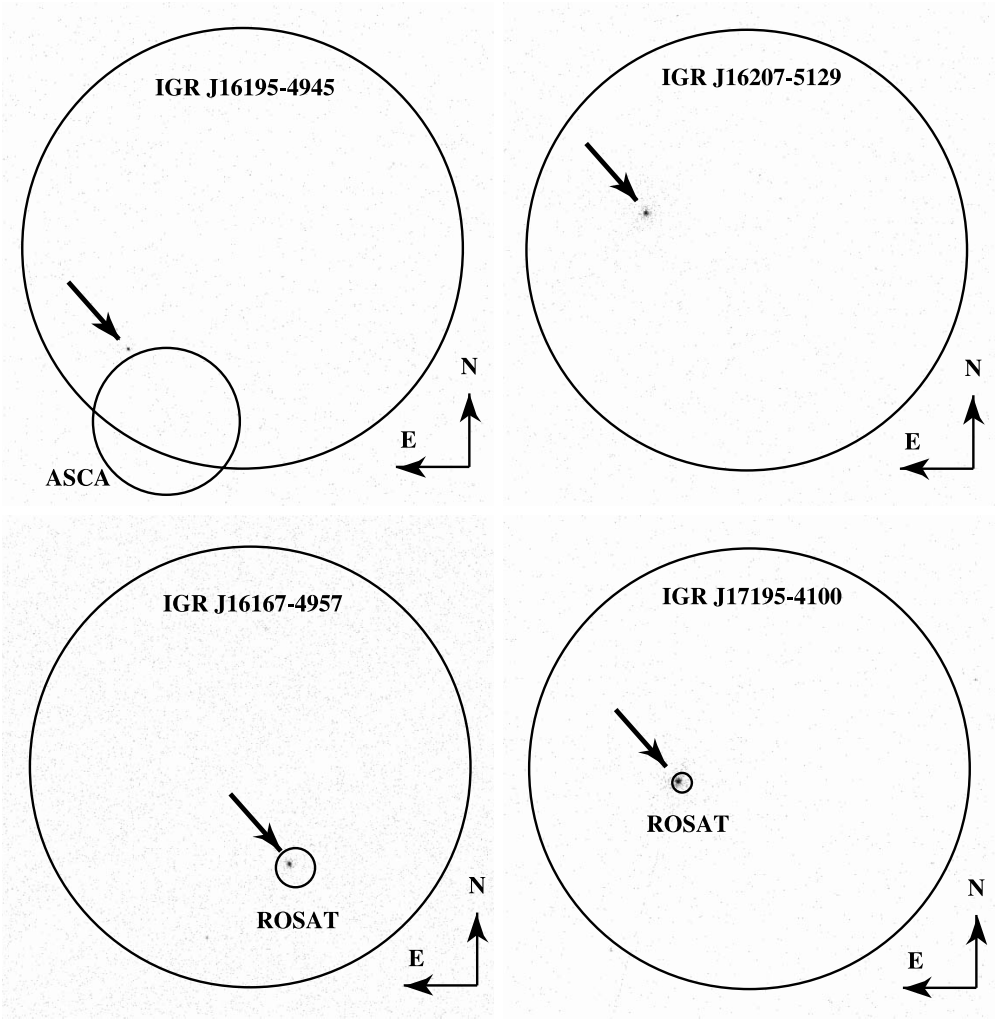

FIG. 1.—*Chandra* 0.3–10 keV images of the four IGR sources. The large circles are the 3′ *INTEGRAL* error circles. In three cases, *ASCA* or *ROSAT* counterparts have been suggested, and their error circles are also shown. Arrows point to the brightest *Chandra* source detected in each observation, and these are very likely the soft X-ray counterparts to the IGR sources. The lengths of the north and east arrows are 1′.

Sugizaki et al. 2001). However, the *Chandra* position is 1.′2 away from HD 146628, clearly ruling out this association. There are no sources in the SIMBAD database within 1′ of the *Chandra* position.

There is no evidence that IGR J16207−5129 was previously detected in the X-ray band. While the source is bright enough to be seen in the *ASCA* Galactic plane scans, it lies just outside of the region that was observed, at a Galactic latitude of $b = -1.^{\circ}05$. A possible association between IGR J16207−5129 and the A1 IVe star HD 146803 was suggested (Tomsick et al. 2004; Masetti et al. 2006b); however, this is ruled out by the fact that the positions for HD 146803 and CXOU J162046.2−513006 are not compatible. There are no sources in the SIMBAD database within 1′ of the *Chandra* position.

TABLE 2
Chandra COUNT RATES AND POSITIONS

IGR Name	CXOU Name	ACIS Rate[a]	R.A.[b]	Decl.[c]	X-Ray Identification
J16195−4945.....	J161932.2−494430	0.039	16 19 32.20	−49 44 30.7	AX J161929−4945(?)
J16207−5129.....	J162046.2−513006	0.13	16 20 46.26	−51 30 06.0	...
J16167−4957.....	J161637.7−495844	0.18	16 16 37.74	−49 58 44.5	1RXS J161637.2−495847
J17195−4100.....	J171935.8−410053	0.15	17 19 35.88	−41 00 53.6	1RXS J171935.6−410054

[a] Count rate detected by the ACIS-I instrument in the 0.3–10 keV bandpass.
[b] Right ascension (equinox J2000.0). Units of right ascension are hours, minutes, and seconds, and units of declination are degrees, arcminutes, and arcseconds. The radius of the error circle is 0.″6.
[c] Declination (equinox J2000.0). The radius of the error circle is 0.″6.

For IGR J16167−4957 and IGR J17195−4100, the *Chandra* positions confirm associations with 1RXS J161637.2−495847 and 1RXS J171935.6−410054, respectively (see Fig. 1). A SIMBAD search at the *Chandra* position of CXOU J161637.7−495844 reveals only IGR J16167−4957 and the *ROSAT* source within 1′. For IGR J17195−4100, the only other SIMBAD source within 1′ of CXOU J171935.8−410053 is USNO-B1.0 0489-0511283. This USNO source is 0.″70 from the *Chandra* position and must be considered as a possible optical counterpart. We investigate this possibility further in § 6.

4. *CHANDRA* ENERGY SPECTRA AND LIGHT CURVES

We produced 0.3−10 keV energy spectra for each of the four bright *Chandra* sources using the CIAO tool `dmextract` to produce the spectrum and the tools `mkacisrmf` and `mkarf` to produce the files needed to characterize the instrument response. We used a circular source extraction region with a radius of 2.″5 and an annular background region centered on the source with inner and outer radii of 10″ and 60″, respectively. Given that two of the sources are close to the gaps between the ACIS chips, we produced exposure maps to determine the effective exposure time for each source. The sources IGR J16207−5129 and IGR J17195−4100 (ObsIDs 5472 and 5474) received the full exposure time, but IGR J16195−4945 (ObsID 5471) and IGR J16167−4957 (ObsID 5473) received 70% and 67% of the full exposure time, respectively. The CIAO tool `mkarf` automatically accounts for the reduced instrument response near chip boundaries.

We fitted the spectra using the software package XSPEC 11.3.2o. Originally, we rebinned the spectra and fitted them using χ^2 minimization. After rebinning, the spectrum for the lowest count rate source (IGR J16195−4945) had nine bins with an average of 20 counts per bin, while we used 12 bin spectra for the other three sources. We fitted the spectra using a model consisting of an absorbed power law, and, based on the results for other IGR sources, it would not be surprising if the column density has intrinsic and interstellar contributions (e.g., Walter et al. 2003; Revnivtsev 2003). The absorbed power-law fit is acceptable ($\chi^2/\nu = 4.0/6$) for IGR J16195−4945, but we obtained very poor fits for the other three sources with values of χ^2 between 46 and 83 for 9 degrees of freedom (dof). Large positive residuals above ∼6 keV are the main reason for the poor fits. This suggests that photon pileup (Davis 2001) is affecting these three spectra, and, indeed, one expects pileup to significantly impact the spectral shape for sources with count rates as high as we observe for the three brighter sources (0.13−0.18 s^{-1}). We refitted the three affected spectra after including the XSPEC `pileup` model (Davis 2001), and the quality of the fits improves enormously with χ^2 values of 3.7, 8.7, and 9.2 (8 dof) for IGR J16207−5129, IGR J16167−4957, and IGR J17195−4100, respectively. Comptonization models (e.g., `comptt` in XSPEC) approximate a power-law shape in the 0.3−10 keV band and provide fits of similar quality to the power-law fits. While a thermal blackbody model can adequately describe the spectrum of the fainter source, such a model provides very poor fits to the spectra of the three brighter sources. Even if the pileup correction is included, an absorbed blackbody model gives χ^2 values between 32 and 98 for 8 dof. We conclude that these three spectra are nonthermal, and we focus on the power-law model below.

Another signature of photon pileup is the flattening of the point-spread function (PSF), and this causes the three brighter sources to appear extended when their radial profiles (i.e., surface brightness vs. angle from the source position) are compared to the profiles of point sources that are unaffected by pileup. We studied the radial profiles of the four IGR sources as a check of the pileup correction, and we conclude that the PSF distortions are well explained by pileup only and that the pileup corrections we apply in performing the spectral fits are correct.

Figure 2 shows the 0.3−10 keV spectra and residuals for the absorbed power-law fits (with the pileup correction), and Table 3 provides the values of the spectral parameters. To obtain these values, we refitted the spectra by minimizing the Cash *C*-statistic (Cash 1979), which is an improvement over χ^2 minimization for spectra with small numbers of counts, as the Cash analysis does not require discarding information by rebinning the spectra. While none of the sources show the extremely high column densities that have been seen for some of the IGR sources, the measured values of $N_{\rm H}$ for IGR J16195−4945 and IGR J16207−5129 are $7^{+5}_{-3} \times 10^{22}$ and $3.7^{+1.4}_{-1.2} \times 10^{22}$ $\rm cm^{-2}$ (90% confidence errors), placing them somewhat above their respective Galactic column densities of 2.2×10^{22} and 1.7×10^{22} $\rm cm^{-2}$ (Dickey & Lockman 1990). IGR J16167−4957 and IGR J17195−4100 have values of $N_{\rm H}$ that are significantly lower than their Galactic column densities.

All the sources are intrinsically hard in the 0.3−10 keV band based on the measured values of the power-law photon index. As shown in Table 3, the best-fit values of Γ range from 0.5 to 1.1, and in all cases the spectra are constrained so that $\Gamma < 1.6$ based on the 90% confidence ($\Delta C = 2.7$) error bars. While the errors on the individual parameters indicate very hard spectra, we also calculated error contours to account for possible correlations between $N_{\rm H}$ and Γ. The contour plots in Figure 3 show the 68% ($\Delta C = 2.3$) and 90% ($\Delta C = 4.6$) confidence error contours, and it is clear that these parameters are significantly correlated for all four spectra. While this analysis shows that the error regions are somewhat larger than indicated by the individual parameter values given in Table 3, the spectra are still constrained to be quite hard, with $\Gamma < 1.8$ (90% confidence), and it is still the case that IGR J16195−4945 and IGR J16207−5129 have column densities that are higher than the Galactic values, while $N_{\rm H}$ is significantly less than the Galactic values for the other two sources.

We produced 0.3−10 keV light curves with 64 s time bins for all four sources. The light curves for IGR J16195−4945 and IGR J16167−4957 are strongly affected by the dithering over gaps between the ACIS chips. In both cases, the count rates drop to zero several times during the observation. In all, about 30% of the time bins are affected, and we do not study the light curves for these two sources further. On the other hand, there are no problems with the light curves for IGR J16207−5129 and IGR J17195−4100, and these are shown in Figure 4. The clearest variability is seen for IGR J16207−5129. In the middle of the observation, the count rate drops to about a third of its average level, remains there for ∼500 s, and then recovers. We formally tested for variability by fitting each light curve with a constant and obtained $\chi^2/\nu = 163/78$ and $\chi^2/\nu = 100/72$ for IGR J16207−5129 and IGR J17195−4100, respectively. Thus, it is likely that both sources exhibit some variability.

5. *INTEGRAL* ENERGY SPECTRA

We also produced >22 keV spectra from the IBIS ISGRI (*INTEGRAL* Soft Gamma-Ray Imager) instrument on *INTEGRAL*. The observations used to produce the spectra include all public data available from *INTEGRAL* revolutions 46 to 235 (2003 February 27 to 2004 September 15). We made sky images and mosaics with the Offline Analysis Software version 5.1 in 10 energy bands between 22 and 250 keV, and we derived average source spectra from the mosaic images. After making vignetting,

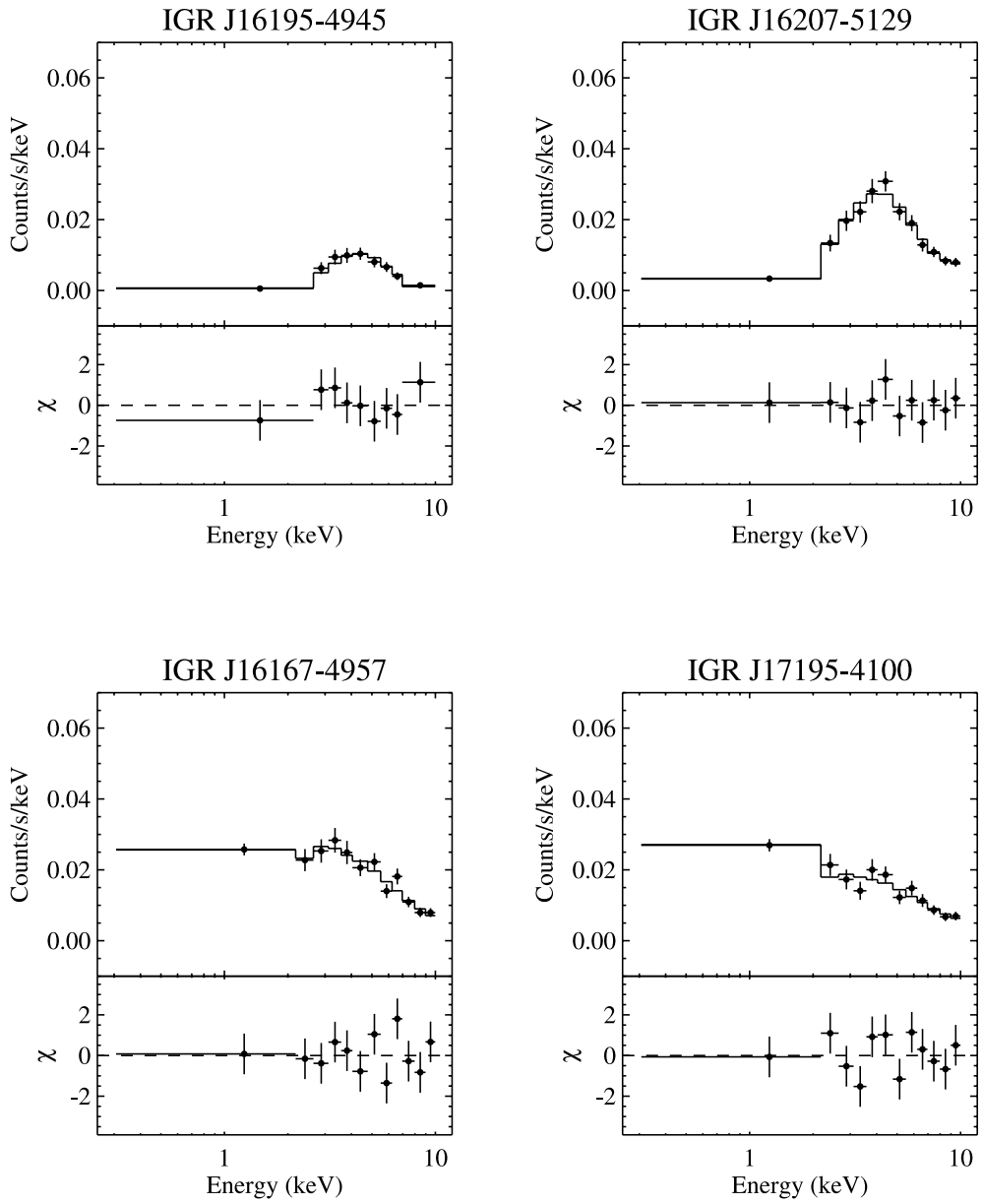

FIG. 2.—*Chandra* energy spectra and residuals for the four IGR sources fitted with an absorbed power-law model. For IGR J16207−5129, IGR J16167−4957, and IGR J17195−4100, a pileup correction is included in the model.

TABLE 3
Chandra SPECTRAL RESULTS

IGR Name	N_H ($\times 10^{22}$ cm^{-2})	Γ	Flux[a]	α[b]	Fit Statistic[c]	Galactic N_H[d] ($\times 10^{22}$ cm^{-2})
J16195−4945.....	7^{+5}_{-3}	$0.5^{+0.9}_{-0.7}$	$4.6^{+2.1}_{-0.8}$	...	453	2.2
J16207−5129.....	$3.7^{+1.4}_{-1.2}$	$0.5^{+0.6}_{-0.5}$	42^{+9}_{-7}	$0.43^{+0.10}_{-0.09}$	667	1.7
J16167−4957.....	$0.5^{+0.3}_{-0.2}$	$1.1^{+0.5}_{-0.4}$	44^{+11}_{-10}	$0.62^{+0.06}_{-0.07}$	701	2.2
J17195−4100.....	$0.08^{+0.13}_{-0.08}$	1.1 ± 0.3	25^{+9}_{-4}	$0.64^{+0.09}_{-0.10}$	743	0.77

NOTE.—Errors in this table are at the 90% confidence level ($\Delta C = 2.7$).
[a] Unabsorbed 0.3–10 keV flux in units of 10^{-12} ergs cm^{-2} s^{-1}.
[b] The grade migration parameter in the pileup model (Davis 2001). The probability that n events will be piled together but will still be retained after data filtering is α^{n-1}.
[c] The Cash statistic for the best-fit model. In each case, the spectra include 663 energy bins.
[d] The column density through the Galaxy from Dickey & Lockman (1990).

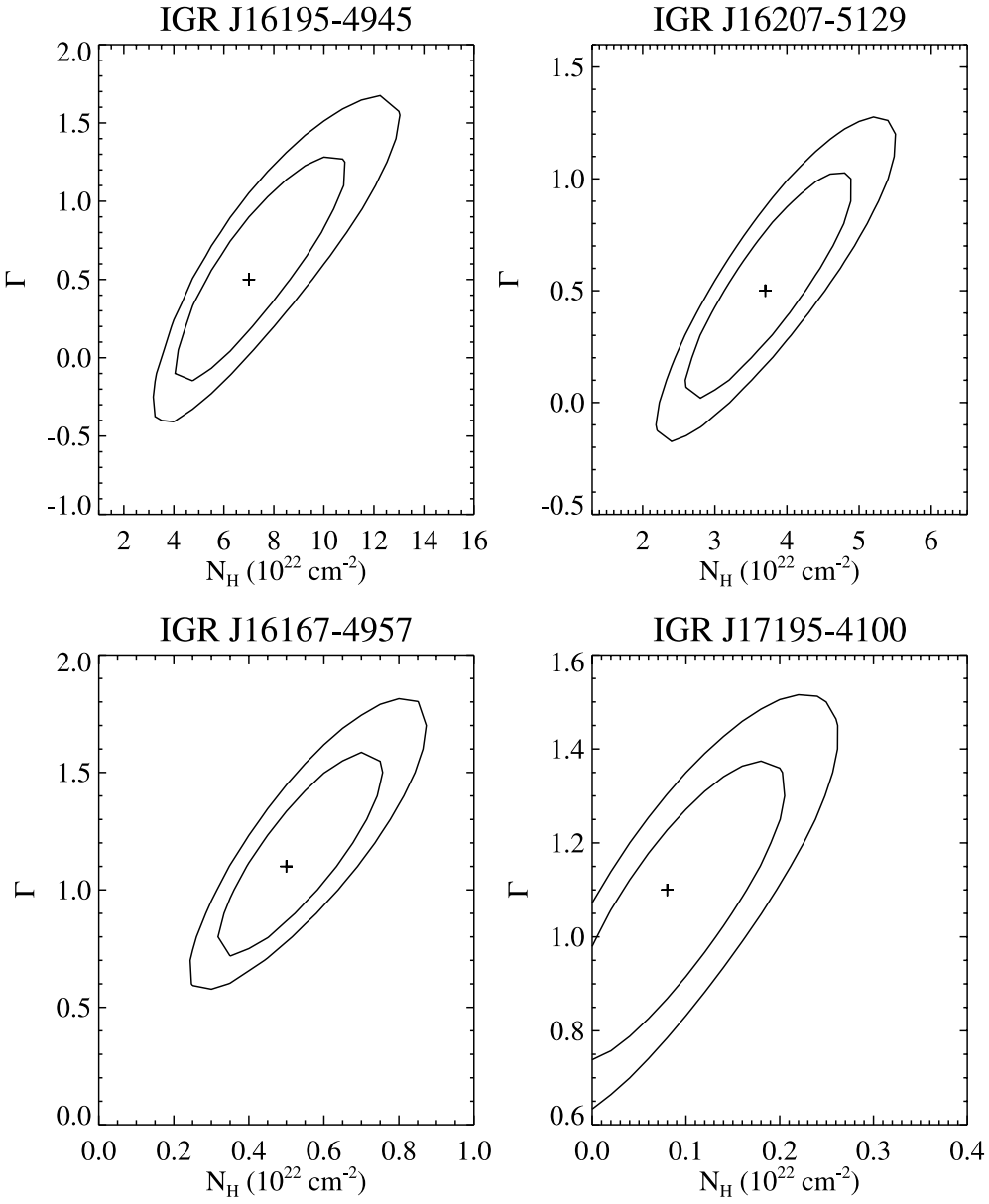

FIG. 3.—Error contours for the parameters N_H and Γ from the fits to the *Chandra* spectra. The inner contour is 68% confidence ($\Delta C = 2.3$), and the outer contour is 90% confidence ($\Delta C = 4.6$).

off-axis, and dead-time corrections, the effective exposure time is 495 ks for IGR J17195−4100 and ∼165 ks per source for the other three sources (see Table 4). Despite the relatively long exposure times, these sources are rather faint for *INTEGRAL*, with 20–50 keV ISGRI count rates between 0.18 ± 0.03 and 0.35 ± 0.03 s^{-1} (compared to, e.g., a 20–60 keV count rate of 160 s^{-1} for the Crab pulsar and Nebula). Thus, the spectra of the IGR sources consist of a relatively small number of energy bins. For IGR J16195−4945, IGR J16207−5129, and IGR J17195−4100, we are able to obtain four energy bins in which the source is detected at a significance of at least 4 σ, and for IGR J16167−4957, the source is only detected in two energy bins.

We fitted the ISGRI spectra with a power-law model, and the results of these fits are given in Table 4. For IGR J16195−4945, IGR J16207−5129, and IGR J17195−4100, acceptable fits are obtained with the power-law model with values of Γ equal to 1.7 ± 0.8, 1.9 ± 0.5, and 2.8 ± 0.8, respectively. While for IGR J16195−4945 the 90% confidence error region for Γ overlaps with the error region determined using the *Chandra* spectrum, the spectra for IGR J16207−5129 and IGR J17195−4100 are significantly steeper in the 20–50 keV band than in the 0.3–10 keV *Chandra* band. Although the spectrum for IGR J16167−4947 only has two energy bins, it is still possible to calculate the value for Γ, and we obtain $4.3^{+1.6}_{-1.4}$, which is significantly steeper than the *Chandra* measurement.

The fact that the spectra are steeper in the ISGRI 20–50 keV band when compared to the *Chandra* 0.3–10 keV band suggests that there is a high-energy cutoff. To investigate the cutoff

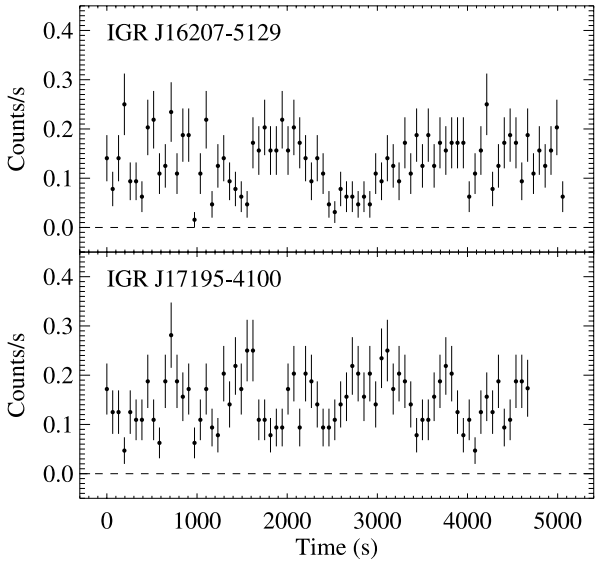

FIG. 4.—*Chandra* 0.3–10 keV light curves with 64 s time bins for two of the IGR sources. IGR J16207−5129 is clearly variable, and there is evidence that IGR J17195−4100 is also variable (see text). The light curves for the other two IGR sources are significantly affected by dithering over the gap between ACIS chips and are not shown.

and to compare the flux levels measured by the two instruments, we performed combined fits for the *Chandra* plus ISGRI spectra. As there is evidence that these sources are variable, and the *Chandra* and ISGRI spectra were not taken simultaneously, it is essential to leave the overall normalization between the two instruments as a free parameter. Leaving all parameters free, we fitted the spectrum for each source with and without an exponential cutoff (`highecut` in XSPEC). The cutoff is detected at the highest level of significance for IGR J16207−5129 with an improvement in the fit from $\chi^2/\nu = 19.6/11$ to 5.3/9, corresponding to an F-test significance of 99.7%. The cutoff is also marginally statistically significant for IGR J16167−4957, with a 98.4% chance that the cutoff is required. The spectra for IGR J16195−4945 and IGR J17195−4100 allow for the possibility that there is a cutoff in the ISGRI energy range, but the cutoff is not required.

While we allowed the $N_{\rm H}$, the power-law parameters, α in the pileup model (for the three brighter sources), the cutoff parameters ($E_{\rm cut}$ and $E_{\rm fold}$), and the overall normalization between the two instruments to be free for the fits described in the previous paragraph, with so many free parameters, the parameter values are very poorly constrained. Thus, we fixed the $N_{\rm H}$, power-law, and pileup parameters to the values measured by *Chandra* and left just the normalization between instruments and the exponential folding energy ($E_{\rm fold}$) as free parameters in the fit. We fixed the energy at which the exponential cutoff begins ($E_{\rm cut}$) to 10 keV, just above the *Chandra* bandpass. However, it should be noted that while the *Chandra* spectra do not show any evidence for a spectral cutoff, the quality of the spectra and the distortion of the spectra due to pileup do not allow us to rule out the possibility that the cutoff starts at a lower energy. For IGR J16195−4945, IGR J16207−5129, IGR J16167−4957, and IGR J17195−4100, respectively, we obtained ISGRI relative normalizations of $1.1^{+0.9}_{-0.6}$, $0.23^{+0.10}_{-0.08}$, $1.4^{+2.5}_{-0.9}$, and $0.9^{+0.7}_{-0.4}$, as well as the following values for $E_{\rm fold}$: 32^{+110}_{-14}, 23^{+13}_{-6}, 9^{+7}_{-3}, and 20^{+18}_{-7} keV (90% confidence errors). These values indicate that IGR J16207−5129 was relatively bright during the *Chandra* observation compared to the brightness detected by ISGRI in 2003–2004, while the other sources were consistent with a relative normalization of 1.0. In addition, it is notable that the range of values we measure for $E_{\rm fold}$, 9–32 keV, is similar to the values that have been measured for HMXB pulsars (Coburn et al. 2002).

6. IR AND OPTICAL IDENTIFICATIONS

With the 0.″6 *Chandra* positions for the four IGR sources, we are able to search for counterparts to these sources at other wavelengths. We searched the following catalogs: United States Naval Observatory (USNO-B1.0 and USNO-A2.0), Deep Near-Infrared Survey of the Southern Sky (DENIS), Two Micron All-Sky Survey (2MASS), and *Spitzer*'s Galactic Legacy Infrared Midplane Survey Extraordinaire (GLIMPSE). We also performed optical and IR photometry at ESO's New Technology Telescope, and the NTT observations and results are described below.

The USNO catalogs are from optical surveys that cover most of the sky. For the USNO-B1.0, the position accuracies are 0.″2 and the photometry is good to ±0.3 mag in B, R, and I. USNO-A2.0 provides 0.″25 positions and B and R measurements that are generally accurate to ±0.5 mag but may be somewhat worse than this in the southern hemisphere. DENIS[7] is an optical and IR survey, concentrating on the southern hemisphere. The position accuracies are 1″, and accurate photometry is available in the I, J, and K_s bands. 2MASS[8] is an all-sky IR survey. The catalog provides very good positions (0.″2 accuracy) and accurate photometry in the J, H, and K_s bands. GLIMPSE uses the Infrared Array Camera (IRAC) on *Spitzer* to obtain short exposures of the Galactic plane, covering the Galactic longitude range between 10° and 65° on both sides of the Galactic center and Galactic latitudes within 1° of the plane. Images are obtained in four bands centered at wavelengths of 3.6, 4.5, 5.8, and 8.0 μm. The GLIMPSE team has compiled an online

[7] See http://cdsweb.u-strasbg.fr/denis.html.
[8] See http://www.ipac.caltech.edu/2mass/releases/second/doc/.

TABLE 4
INTEGRAL SPECTRAL RESULTS

IGR Name	Exposure Time (ks)	Count Rate[a]	Γ	Flux[b]	χ^2/ν
J16195−4945.....	167	0.24 ± 0.03	1.7 ± 0.8	19 ± 3	1.3/2
J16207−5129.....	165	0.35 ± 0.03	1.9 ± 0.5	28 ± 3	2.5/2
J16167−4957.....	167	0.18 ± 0.03	$4.3^{+1.6}_{-1.4}$	16^{+3}_{-4}	0/0
J17195−4100.....	495	0.23 ± 0.02	2.8 ± 0.8	19 ± 3	1.1/2

[a] 20–50 keV ISGRI count rate.
[b] 20–50 keV flux in units of 10^{-12} ergs cm^{-2} s^{-1}.

TABLE 5
OPTICAL AND IR MAGNITUDES OR FLUXES

Parameter	IGR J16195−4945	IGR J16207−5129	IGR J16167−4957	IGR J17195−4100
		USNO-B1.0		
Name[a]	0402-0529810	0384-0560875	0400-0527262	0489-0511283
Separation[b]	1.″03	0.″81	0.″53	0.″70
B	16.5 ± 0.3	19.7 ± 0.3	16.8 ± 0.3	15.1 ± 0.3
R	15.3 ± 0.3	15.2 ± 0.3	15.8 ± 0.3	14.4 ± 0.3
I	15.6 ± 0.3	13.0 ± 0.3	14.5 ± 0.3	14.3 ± 0.3
		USNO-A2.0		
Name[a]	0375-27014824	0375-27093111	0375-26829054	0450-27095307
Separation[b]	0.″72	0.″31	0.″45	0.″31
B	17.4 ± 0.5	18.9 ± 0.5	16.8 ± 0.5	15.2 ± 0.5
R	16.2 ± 0.5	15.6 ± 0.5	16.2 ± 0.5	14.3 ± 0.5
		DENIS		
Name[a]	J161932.1−494430	J162046.2−513006	...	J171935.8−410053
Separation[b]	0.″42	0.″29	...	0.″10
I	15.38 ± 0.05	13.4 ± 1.0	...	14.81 ± 0.04
J	13.55 ± 0.08	10.54 ± 0.05	...	...
K_s	10.92 ± 0.06	9.17 ± 0.06	...	...
		2MASS		
Name[a]	J16193220−4944305	J16204627−5130060	J16163776−4958445	J17193608−4100548
Separation[b]	0.″14	0.″11	0.″26	2.″6
J	13.57 ± 0.03	10.44 ± 0.02	14.86 ± 0.06	...[c]
H	11.96 ± 0.03	9.62 ± 0.02	14.28 ± 0.09	...[c]
K_s	11.00 ± 0.02	9.13 ± 0.02	13.76 ± 0.10	...[c]
		GLIMPSE		
Name[a]	G333.5571+00.3390	G332.4590−01.0501	G333.0560+00.4962	...
Separation[b]	0.″21	0.″07	0.″34	...
3.6 μm	26.5 ± 1.1 mJy	100 ± 3 mJy	1.79 ± 0.16 mJy	...
4.5 μm	20.3 ± 1.1 mJy	61 ± 3 mJy	1.40 ± 0.16 mJy	...
5.8 μm	14.3 ± 1.0 mJy	46 ± 2 mJy	...	...
8.0 μm	8.5 ± 0.5 mJy	28.4 ± 0.9 mJy	...	...
		New Technology Telescope		
B	18.14 ± 0.06	19.8 ± 0.1	...	...
V	17.22 ± 0.05	17.74 ± 0.06	...	...
R	16.42 ± 0.05	15.38 ± 0.03	...	...
I	15.54 ± 0.03	13.58 ± 0.02	...	...
J	...	10.38 ± 0.02	15.0 ± 0.1	14.1 ± 0.1
H	...	9.60 ± 0.02	14.4 ± 0.1	13.65 ± 0.07
K_s	...	9.18 ± 0.04	13.8 ± 0.1	13.2 ± 0.1

[a] Name of the nearest star in the catalog.
[b] Separation between the *Chandra* position and the nearest star in the catalog.
[c] This 2MASS source is too far from the *Chandra* position to be associated.

catalog[9] with lists of detected sources, including fluxes and positions accurate to 0.″3.

On 2004 July 10 between UT 0 and 1 hr, we obtained optical photometry in B, V, R, and I bands of the fields of IGR J16195−4945 and IGR J16207−5129 with the spectro-imager EMMI (ESO Multi-Mode Instrument) installed on the NTT. We used the large field imaging of EMMI's detector, giving, after 2×2 rebinning, a pixel size of 0.″333 and a field of view of $9.'9 \times 9.'0$. We used an integration time of 1 s per exposure. We observed five photometric standard stars from the optical standard star catalog of Landolt (1992): PG 1633+099, PG 1633+099A, PG 1633+099B, PG 1633+099C, and PG 1633+099D. We also obtained IR photometry in J, H, and K_s bands of IGR J16207−5129 (on 2004 July 8 at UT 4.67 hr), of IGR J16167−4957 (on July 11 at UT 5.67 hr), and of IGR J17195−4100 (on July 11 at UT 6.83 hr) with the spectro-imager SofI (Son of ISAAC) installed on the NTT. We used the large field imaging of SofI's detector, giving a pixel size of 0.″288 and a field of view of $4.'94 \times 4.'94$. These photometric observations were obtained by repeating a set of images for each filter with nine different 30″ offset positions, including the targets, with an integration time of 60 s for each exposure, following the standard jitter procedure

[9] See http://www.astro.wisc.edu/sirtf/.

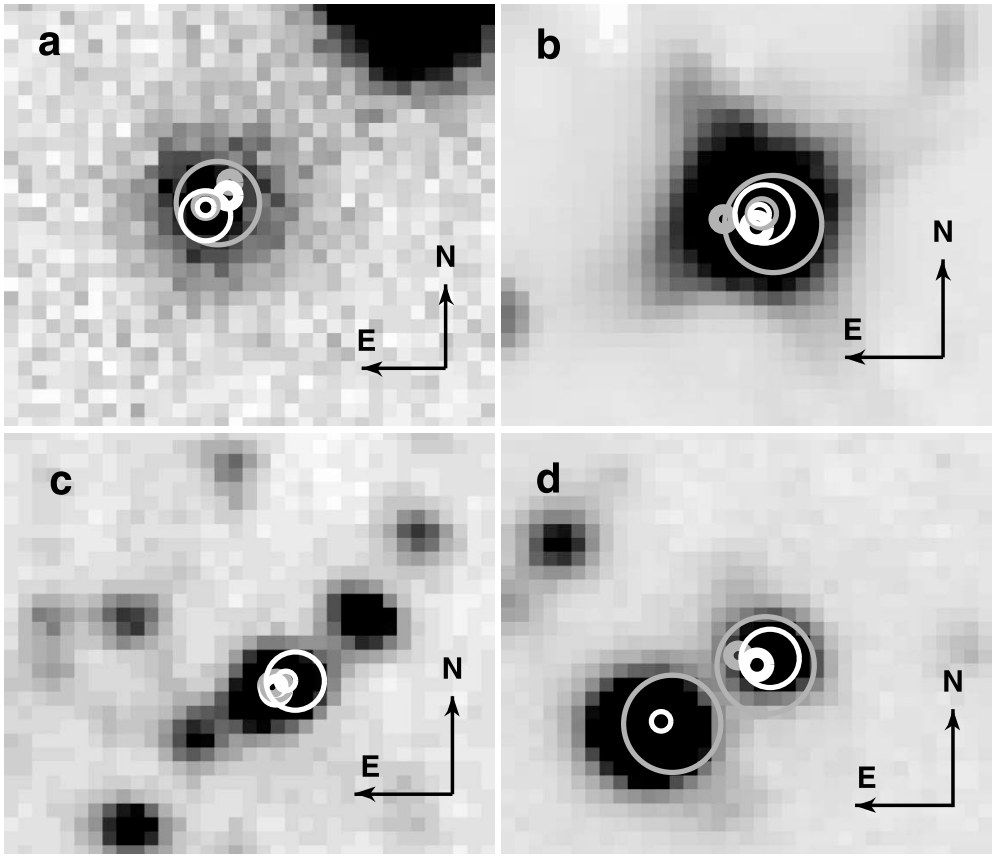

FIG. 5.—NTT images for (*a*) IGR J16195−4945 (*I* band), (*b*) IGR J16207−5129 (K_s band), (*c*) IGR J16167−4957 (K_s band), and (*d*) IGR J17195−4100 (K_s band). The lengths of the north and east arrows are 2″. From smallest to largest, the error circles are 2MASS (*thin white* 0.″2 *radius error circle*), USNO-B1.0 (*thick gray* 0.″2 *circle*), USNO-A2.0 (*thick white* 0.″25 *circle*), GLIMPSE (*thin gray* 0.″3 *circle*), *Chandra* (*thin white* 0.″6 *circle*), and DENIS (*thin gray* 1″ *circle*).

allowing for clean subtraction of the blank sky emission in IR. On several occasions, we observed three photometric standard stars from the faint IR standard star catalog of Persson et al. (1998): [PMK98] 9157, [PMK98] 9172, and [PMK98] 9181. We used the Image Reduction and Analysis Facility (IRAF) suite to perform data reduction, carrying out standard procedures of optical and NIR image reduction, including flat-fielding and NIR sky subtraction. We carried out aperture photometry, and we then transformed instrumental magnitudes into apparent magnitudes. The targets were close to the zenith during the observations.

Table 5 provides the results of our search of the catalogs, and also the results of our NTT observations. For each of the five catalogs, we list the closest source to the *Chandra* position and the measured magnitudes. In Figure 5, we show an *I*-band NTT image for IGR J16195−4945 and K_s-band images for the other three sources. The *Chandra* positions and the positions obtained from the catalogs are plotted on these images.

For IGR J16195−4945, the *Chandra* position lies on an apparently stellar IR source (based on an inspection of the 2MASS images) with a magnitude of $J = 13.57 \pm 0.03$. The 2MASS and GLIMPSE positions lie inside the *Chandra* error circle, indicating a good association between the X-ray and IR sources (see Fig. 5*a*). However, the USNO-A2.0 position lies on the edge of the *Chandra* error circle, and the USNO-B1.0 position lies slightly outside. This may indicate the presence of a second optical source blended with the counterpart. Due to the faintness of the source (or sources), it is not clear from the NTT *I*-band image whether there are two blended sources or not. However, we present analysis of the spectral energy distributions (SEDs) below, and the IGR J16195−4945 SED (see Fig. 6, *top left*) supports the possibility that there are two blended sources.

For IGR J16207−5129, the *Chandra* position lies on a bright IR source with $J = 10.44 \pm 0.02$. This source is present in all five catalogs, and all the positions are consistent with the *Chandra* source except for the USNO-B1.0 position, which lies just outside the *Chandra* error circle (see Fig. 5*b*). While this could indicate the presence of an interloper, the SED does not suggest any contamination by other sources (see Fig. 6, *top right*).

For IGR J16167−4957, the *Chandra* position lies on a source with $J = 14.86 \pm 0.06$. The source appears in the GLIMPSE, 2MASS, and USNO catalogs, and all positions lie within the *Chandra* error circle (see Fig. 5*c*). Although the 2MASS images suggest that the source is extended to the southeast, the NTT K_s-band image shows that there is actually a blend of at least three sources. The IGR J16167−4957 *Chandra* position is consistent with the brightest of the blended IR sources, but there is some suggestion in the NTT image that the brightest "source" may also be a blend.

For IGR J17195−4100, the *Chandra* position is near two sources that are clearly blended in the 2MASS images. The position of the 2MASS source is 2.″6 away from the *Chandra* position, indicating that the bright IR source is not IGR J17195−4100.

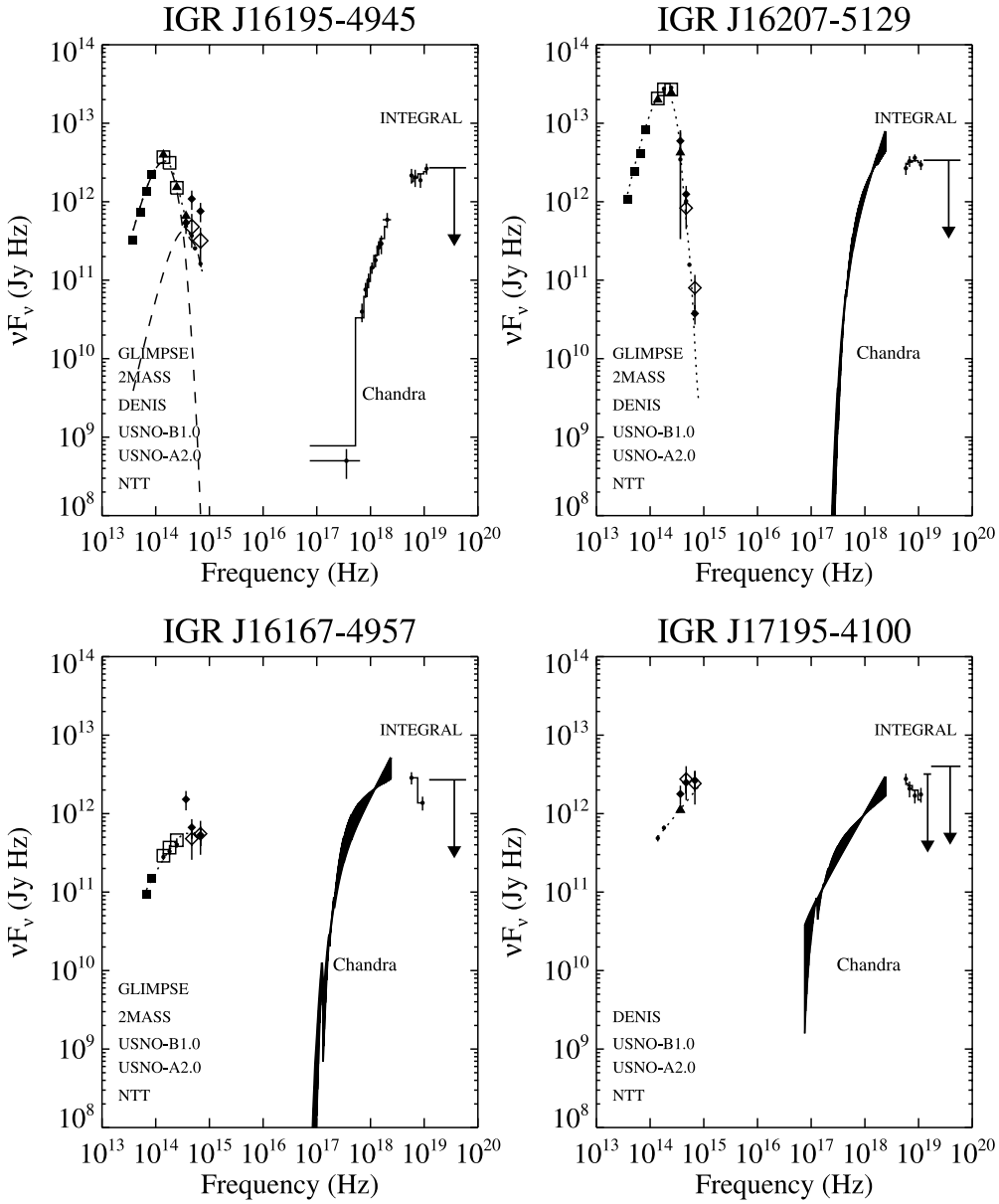

FIG. 6.—Spectral energy distributions (SEDs) for the four IGR sources. The IR and optical fluxes come from the measurements given in Table 5, and this part of the spectrum has been fitted with a blackbody model modified by the effects of extinction. The dotted line indicates the best fit (see text). *Chandra* and *INTEGRAL* measurements are also shown. For IGR J16207−5129, IGR J16167−4957, and IGR J17195−4100, our best estimate of the spectrum in the *Chandra* energy range is the model (*solid line*). For the optical/IR data, the different symbols are GLIMPSE (*filled squares*), 2MASS (*open squares*), DENIS (*filled triangles*), USNO-B1.0 (*filled diamonds*), USNO-A2.0 (*open diamonds*), and NTT (*filled circles*).

With *I*-band and IR coverage, both sources appear in the DENIS survey, and the optically brighter northwest source is the one that is consistent with the *Chandra* position. Our results confirm the association between IGR J17195−4100 and USNO-B1.0 0489-0511283.

7. SPECTRAL ENERGY DISTRIBUTIONS

Figure 6 shows the spectral energy distributions (SEDs) for the four sources. These include the optical and IR measurements given in Table 5, the spectrum in the *Chandra* bandpass, and *INTEGRAL* measurements. It should be noted that the optical and IR fluxes are not dereddened, and absorption is not removed from the *Chandra* spectra. The SED measurements are spread over a period of years, so discontinuities in the SED may be due to source variability. For the IR and optical parts of the SED, a check on variability is provided by the fact that we have multiple measurements for many of the photometric bands. A comparison shows that the IR fluxes are quite stable for IGR J16195−4945, IGR J16207−5129, and IGR J16167−4957. For IGR J16195−4945, the 1 σ error regions overlap for the *J*- and K_s-band measurements from DENIS and 2MASS. For IGR J16207−5129, the DENIS, 2MASS, and NTT *J*- and K_s-band measurements only

TABLE 6
IR/Optical SED Fits

Parameter	IGR J16195−4945	IGR J16207−5129	IGR J16167−4957	IGR J17195−4100
		Blackbody		
A_V	<0.16	$10.8^{+0.3}_{-0.8}$	<1.16	<2.84
T (K)	1944^{+39}_{-42}	>18000	2790^{+350}_{-70}	4100^{+5500}_{-200}
R/d ($R_\odot$ kpc^{-1})[a]	10.3 ± 0.6	<5.53	1.84 ± 0.21	$1.40^{+0.14}_{-0.62}$
χ^2/ν	269/16	23/19	54/10	26/6
		Power Law		
A_V	7.1 ± 0.6	$11.6^{+0.8}_{-0.7}$	$1.3^{+0.6}_{-0.5}$	<0.96
α[b]	−0.73 ± 0.13	$-2.29^{+0.24}_{-0.28}$	$-0.36^{+0.17}_{-0.18}$	$0.17^{+0.12}_{-0.47}$
$N_{\rm pl}$[c]	0.030 ± 0.003	0.27 ± 0.03	0.00191 ± 0.00015	0.0039 ± 0.0006
χ^2/ν	300/16	19/19	12/10	9/6
		Two Blackbodies		
$A_{V,1}$	$17.5^{+0.8}_{-2.3}$	...	...	...
T_1 (K)	>9400	...	...	...
R_1/d ($R_\odot$ kpc^{-1})	<4.36	...	...	...
$A_{V,2}$	<4.89	...	...	...
T_2 (K)	>3800	...	...	...
R_2/d ($R_\odot$ kpc^{-1})	<1.13	...	...	...
χ^2/ν	12/14	23/17	8/7	7/3
		Blackbody + Power Law		
$A_{V,\rm bb}$	$17.5^{+0.8}_{-2.1}$	...	...	...
T (K)	>9500	...	...	...
R/d ($R_\odot$ kpc^{-1})	<4.25	...	...	...
$A_{V,\rm pl}$	$4.3^{+2.8}_{-1.1}$	...	...	...
α[b]	$-1.7^{+1.0}_{-2.9}$	...	...	...
$N_{\rm pl}$[c]	$0.0015^{+0.0020}_{-0.0013}$	...	...	...
χ^2/ν	12/14	18/17	8/7	5/3

[a] R/d is the ratio of the radius of the spherical blackbody (in $R_\odot$) to the distance to the source (in kpc).
[b] The power-law index, defined according to $F_\nu \propto \nu^{-\alpha}$.
[c] The power-law normalization, corresponding to the flux in Jy at a reference frequency of 10^{14} Hz.

range from 10.38 to 10.54 and from 9.13 to 9.18, respectively. For IGR J16167−4957, the 2MASS and NTT measurements are consistent at the 1 σ level for J, H, and K_s. For IGR J16207−5129, the optical flux also appears to be rather stable, but for IGR J16195−4945 and IGR J16167−4957, the agreement between the various optical measurements is not as good (see Fig. 6). For IGR J17195−4100, the agreement in the optical bands is relatively good, but this source has the sparsest optical/IR measurements.

For IGR J16195−4945, we simply show in the top left panel of Figure 6 the data and the best-fit model for *Chandra*; however, for the other three sources the spectrum is significantly distorted by pileup, and we show the range of flux measurements based on the error ranges for the model parameters. For IGR J16207−5129, the flux range shown reflects the 90% confidence error range on Γ, which is 0.0–1.1. For IGR J16167−4957 and IGR J17195−4100, the Γ ranges are 0.7–1.6 and 0.8–1.4, respectively. The *INTEGRAL* 20–50 keV measurements and 50–250 keV upper limits are shown. As described in § 5, the fits shown include a high-energy cutoff and a free normalization between *Chandra* and ISGRI. IGR J16207−5129 is the only source for which the normalization for ISGRI relative to *Chandra* is required to be less than 1.0, and this is apparent in Figure 6.

To characterize the shape of the optical and IR continuum, we fitted each of the SEDs with four models: a single blackbody, a single power law, the sum of two blackbodies, and a blackbody plus a power law. Presumably, blackbody components could be indicative of thermal components from a star, but we consider the power law to be a phenomenological component. The models also account for interstellar extinction using the analytical approximation of Cardelli et al. (1989). This adds a single free parameter, A_V, to the single-component models, while for the two-component models we allow the components to have different extinctions. We used χ^2 minimization when fitting the SEDs, and for IGR J16195−4945 and IGR J16207−5129, all of the models resulted in formally very poor fits, with the best models leading to $\chi^2/\nu = 128/14$ and $\chi^2/\nu = 684/16$ for the two sources, respectively. Such poor fits may indicate inadequacies of our models, but they are also at least in part due to systematic errors, which may be related to the variability discussed above or possibly due to, e.g., uncertainties in magnitude/flux conversion. While it is clear that systematic errors must be included for these two sources, it is not clear which data points are the most suspect. Thus, we included systematic errors by simply multiplying the existing errors on all of the optical and IR data points by a constant factor. We adjusted the constant factor until we achieved a reduced χ^2 of 1.0 for at least one of the models. For IGR J16195−4945 and IGR J16207−5129, the constant factors are 2.2 and 6.5, respectively. For the other two sources, IGR J16167−4957 and IGR J17195−4100, we did not need to include any systematic errors. The SED fit results are presented in Table 6, and here we describe the results for each source in turn.

For IGR J16195−4945, neither of the single-component models provide an acceptable fit to the optical/IR SED, and a two-component model is required at high significance. The two-blackbody and blackbody plus power-law models provide acceptable fits, and both imply that the IR flux is dominated by a high-temperature star (>9400 K) with high extinction ($A_V \sim 18$). In addition, both models imply that the component that dominates the optical flux has a significantly lower extinction ($A_V < 7.1$). This SED and the shift between the optical and IR source positions reported in § 6 provide evidence that the optical component comes from an interloping star, while the IR component likely comes from IGR J16195−4945.

Our highest quality optical/IR SED is the one for IGR J16207−5129. For this SED, two-component models do not provide any improvement over the single-component models, and the blackbody and power-law models provide fits of roughly the same quality. The power-law index is $\alpha = -2.29^{+0.24}_{-0.28}$, which is nearly consistent with the value of $\alpha = -2$ expected for a blackbody. The fits strongly suggest that the spectrum is thermal, as would be expected for stellar emission. From the blackbody fit, the value obtained for the extinction, $A_V = 10.8^{+0.3}_{-0.8}$, is very close to the value of $A_V = 9.5$ obtained by converting the Galactic column density of $N_{\rm H} = 1.7 \times 10^{22}$ cm^{-2} to optical extinction using the Predehl & Schmitt (1995) relationship.

A blackbody model does not provide a good fit to the IGR J16167−4957 and IGR J17195−4100 SEDs with values of χ^2/ν of 54/10 and 26/6, respectively. However, both SEDs are adequately described by a power-law model with indices of $\alpha = -0.36^{+0.17}_{-0.18}$ and $\alpha = 0.17^{+0.12}_{-0.47}$, respectively. The power-law fits for both sources imply low extinction, which is consistent with the values of $N_{\rm H}$ measured via fits to the X-ray spectrum. Although we fitted the SEDs for these two sources with the two-component models, the improvements in χ^2 do not justify the addition of another component, and the parameters for the two-component fits are very poorly constrained.

8. DISCUSSION

In the following sections, we discuss the detailed constraints on the nature of each source, considering the information we have obtained from *Chandra*, *INTEGRAL*, and the optical/IR SEDs.

8.1. *IGR J16195−4945*

Of our four sources, IGR J16195−4945 is the most similar to the class of obscured IGR sources. At $N_{\rm H} = (7^{+5}_{-3}) \times 10^{22}$ cm^{-2}, the X-ray-measured column density is higher than the Galactic value of 2.2×10^{22} cm^{-2}, suggesting the possibility that the X-ray source is intrinsically absorbed. Due to the possibility of intrinsic absorption, we cannot use the X-ray-measured $N_{\rm H}$ to constrain the distance to the source; however, because the optical and IR emission from the system is likely to predominantly come from regions that are not as affected by intrinsic absorption, such as the companion star, we expect that the optical extinction is dominated by interstellar material. Thus, the fact that $A_V = 17.5^{+0.8}_{-2.3}$ for the extinction on the blackbody component is as large or larger than the value obtained by converting the Galactic $N_{\rm H}$ to optical extinction ($A_V = 12.3$) is likely to indicate that we are looking at the source through much of the Galaxy. The distance to the Norma-Cygnus arm along this line of sight is ∼5 kpc (Russeil 2003), and although we cannot formally constrain the distance to the source, we assume a fiducial value of 5 kpc. From the unabsorbed fluxes reported in Tables 3 and 4, the implied X-ray luminosities are $1.4 \times 10^{34} (d/5\ {\rm kpc})^2$ ergs s^{-1} (0.3–10 keV) and $5.8 \times 10^{34} (d/5\ {\rm kpc})^2$ ergs s^{-1} (20–50 keV).

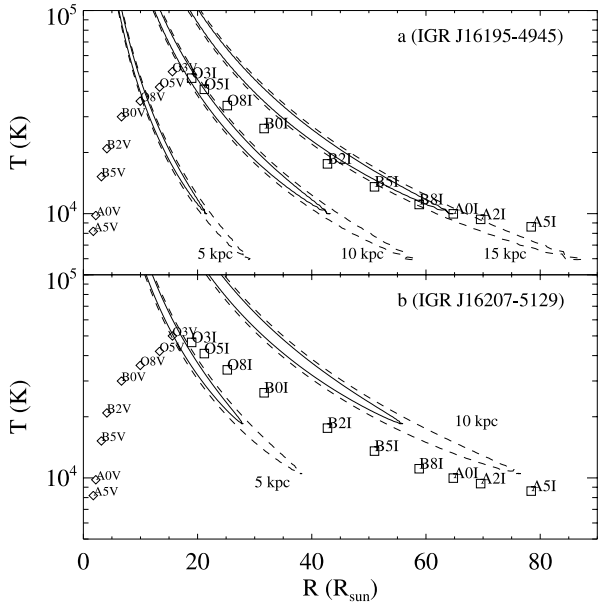

FIG. 7.—Error contours for (*a*) IGR J16195−4945 and (*b*) IGR J16207−5129 for the blackbody parameters in the optical/IR SEDs. Contours are shown for the stellar radius (R) and temperature (T), assuming various distances. The solid contours are 68% confidence ($\Delta\chi^2 = 2.3$), and the dashed contours are 90% confidence ($\Delta\chi^2 = 4.6$). Radii and temperatures for various spectral types from de Jager & Nieuwenhuijzen (1987) are overplotted, allowing us to constrain the likely spectral types of the companions in these systems.

The IR portion of the SED is consistent with a single-temperature blackbody, suggesting that it is more likely that the IR emission comes from a stellar companion than from, e.g., an accretion disk. The lack of variability in the IR emission discussed in § 7 also provides evidence that the emission comes from a star. The fit to the SED gives a lower limit on the blackbody temperature of $T > 9400$ K, and this indicates a spectral type earlier than A1–A2 regardless of whether the star is a main-sequence star or a supergiant (de Jager & Nieuwenhuijzen 1987; Cox 2000). The question of whether the companion is a main-sequence star or a supergiant depends sensitively on the distance to the source. In the fit to the SED, the parameters T and R/d have a significant level of degeneracy, and in Figure 7*a* we show 68% and 90% confidence error contours for T and R for assumed distances of 5, 10, and 15 kpc along with temperatures and radii for stars with various spectral types. If the distance is ∼3–9 kpc, the companion is a main-sequence B- or O-type star. If the distance is ∼9–15 kpc, a large range of supergiant A, B, and O spectral types are possible.

8.2. *IGR J16207−5129*

Like that of IGR J16195−4945, the IGR J16207−5129 $N_{\rm H}$ is somewhat (about a factor of 2) higher than the Galactic value, allowing for, but not requiring, some intrinsic absorption. From the optical/IR SED, $A_V = 10.8^{+0.3}_{-0.8}$, and this value suggests a relatively large distance for this source. Thus, it is reasonable to take 5 kpc, the distance to the Norma-Cygnus arm along the line of sight, as a fiducial distance. The implied 0.3–10 keV luminosity is $1.3 \times 10^{35} (d/5\ {\rm kpc})^2$ ergs s^{-1}, about an order of magnitude higher than that of IGR J16195−4945, and the 20–50 keV luminosity is $8.3 \times 10^{34} (d/5\ {\rm kpc})^2$ ergs s^{-1}.

In this case, the optical/IR SED consists of a single-temperature blackbody, and it is very likely that this emission comes from the

TABLE 7
SUMMARY OF RESULTS

IGR Name	d (kpc)	$d_{\rm fiducial}$ (kpc)	L(0.3–10 keV)[a]	L(20–50 keV)[b]	Spectral Type
J16195−4945.....	∼3–15	5 (Norma-Cygnus?)	1.4×10^{34}	5.8×10^{34}	OB V or supergiant
J16207−5129.....	∼3–10	5 (Norma-Cygnus?)	1.3×10^{35}	8.3×10^{34}	OB V or supergiant
J16167−4957.....	1.8–4.2	3 (Scutum-Crux?)	4.7×10^{34}	1.7×10^{34}	Later than A0 V
J17195−4100.....	<2.6	<2.6	$<2.0 \times 10^{34}$	$<1.6 \times 10^{34}$	Later than A3 V

[a] The X-ray luminosity in ergs s^{-1} measured by *Chandra* at the fiducial distance.
[b] The X-ray luminosity in ergs s^{-1} measured by *INTEGRAL* at the fiducial distance.

stellar companion. The lower limit on the stellar temperature is >18,000 K, indicating that this system harbors a very hot, and likely massive, star. Figure 7 shows the error contours for the parameters T and R assuming distances of 5 and 10 kpc. At ∼3–5 kpc, the companion is a main-sequence B- or O-type star. At ∼5–9 kpc, various supergiant types are possible. At 10 kpc, the ranges of possible temperatures and radii are not consistent with any known spectral type, indicating that this system is closer than 10 kpc.

8.3. *IGR J16167−4957*

Although this source is close to the Galactic plane at $b = +0.^\circ50$ and is within $0.^\circ5$ of IGR J16195−4945 and $1.^\circ7$ of IGR J16207−5129, its X-ray spectrum indicates a column density of $N_{\rm H} = (5^{+3}_{-2}) \times 10^{21}$ cm^{-2}, which is an order of magnitude lower than the value for IGR J16195−4945 and is also lower than the Galactic column density of 2.2×10^{22} cm^{-2} along this line of sight. The measured $N_{\rm H}$ corresponds to an extinction of $A_V = 2.8^{+1.7}_{-1.1}$, and although the optical/IR SED is fitted with a phenomenological power-law model, the implied extinction is even lower, $A_V = 1.3^{+0.6}_{-0.5}$. While the inhomogeneous distribution of gas and dust in the Galaxy makes it difficult to use extinction measurements to determine source distances in any rigorous way, here we make an estimate using the values from the Diplas & Savage (1994) study, which includes UV extinction measurements of nearly 400 early-type stars along various lines of sight through the Galaxy and with distances as large as 10 kpc. In that study, the average extinction per kpc is $A_V/d = 0.45$ mag kpc^{-1}. For IGR J16167−4957, the extinction inferred from the X-ray spectrum allows the distance to be anywhere from 2 to 10 kpc, but the optical/IR extinction implies a distance of $2.9^{+1.3}_{-1.1}$ kpc. This estimate is marginally consistent with the source being in the Norma-Cygnus arm at ∼5 kpc, but the line of sight also crosses the Scutum-Crux arm at ∼3 kpc. Given the lower extinction for this source compared to IGR J16195−4945 and IGR J16207−5129, which are likely in the Norma-Cygnus arm, we take 3 kpc as a fiducial distance for IGR J16167−4957, and the X-ray luminosities are $4.7 \times 10^{34} (d/3 \text{ kpc})^2$ ergs s^{-1} (0.3–10 keV) and $1.7 \times 10^{34} (d/3 \text{ kpc})^2$ ergs s^{-1} (20–50 keV).

The interpretation for the shape of the optical/IR SED is not immediately clear, but the fact that it is not consistent with a single-temperature blackbody suggests that the emission is not simply from a companion star. The power-law index of $-0.36^{+0.17}_{-0.18}$ is considerably flatter than a blackbody, and this could indicate a multitemperature blackbody, as might be expected from an accretion disk. Regardless of the dominant contributor to the optical/IR emission, we can take the measured magnitudes as an upper limit on the contribution from a putative optical companion. If we assume a distance and an extinction at the upper ends of the derived ranges, 4.2 kpc and $A_V = 2.8$, respectively, and interpolate between the measured B and R magnitudes to infer a V-band magnitude of 16.5, the limit on the absolute magnitude is $M_V > 0.6$. Unless the distance is very much larger than 4.2 kpc, this rules out a supergiant companion, and the companion's spectral type is later than A0 V. Thus, IGR J16167−4957 is not an HMXB.

8.4. *IGR J17195−4100*

At $l = 346.^\circ98$ and $b = -2.^\circ14$, this source is ∼14° from the other three sources and is slightly off the Galactic plane. The measured upper limit on the column density of $N_{\rm H} < 2 \times 10^{21}$ cm^{-2} is considerably lower than the Galactic value of 7.7×10^{21} cm^{-2}, indicating that the distance to the source may be relatively low. The $N_{\rm H}$ from the X-ray spectrum implies $A_V < 1.18$, and the optical/IR SED gives an upper limit of $A_V < 0.96$. Using the average value of A_V/d from Diplas & Savage (1994) indicates a distance upper limit in the range $d < 2.1$–2.6 kpc. The upper limit on the distance of 2.6 kpc implies upper limits on the X-ray luminosities of $<2.0 \times 10^{34}$ ergs s^{-1} (0.3–10 keV) and $<1.6 \times 10^{34}$ ergs s^{-1} (20–50 keV).

Like IGR J16167−4957, the physical interpretation for the power-law shape of the optical/IR SED is not clear. We can take the optical/IR magnitudes observed as upper limits on the contribution from a companion star. Interpolating between the B and R bands, we estimate that $V = 14.8$. This, along with the highest upper limits we measure for the extinction, $A_V < 1.18$, and distance, $d < 2.6$ kpc, implies an upper limit on the absolute magnitude of $M_V < 1.5$. This rules out a supergiant companion or an OB main-sequence star. The earliest spectral type possible is ∼A3 V.

9. SUMMARY OF THE NATURE OF THE FOUR IGR SOURCES

Table 7 contains a summary of the results described in § 8, including constraints on the source distances, X-ray luminosities, and possible spectral types. Our basic conclusion is that IGR J16195−4945 and IGR J16207−5129 are very likely HMXBs and are at distances consistent with the Norma-Cygnus arm (although the distances are not well enough constrained to say definitively that they are in this spiral arm), while the other two IGR sources (IGR J16167−4957 and IGR J17195−4100) are nearer and are not HMXBs. Assuming distances of 5 kpc for the two HMXBs, the 0.3–10 keV luminosities are 10^{34}–10^{35} ergs s^{-1}, which is, not surprisingly, significantly lower than the brightest HMXB pulsars (e.g., Vela X-1, Cen X-3), but the luminosities are not atypical when considering the full range of HMXB pulsar luminosities.

Of the four IGR sources, only IGR J16195−4945 has a column density that is consistent with the source having significant intrinsic absorption. While IGR J16207−5129 could conceivably also have some level of intrinsic absorption, comparing its column

density to the Galactic value suggests that the intrinsic N_H is not more than $\sim 1 \times 10^{22}$ cm^{-2}, while many IGR sources have $N_H \sim 10^{23}$–10^{24} cm^{-2}. From the perspective of IGR sources and HMXB evolution (Dean et al. 2005), the very high column density IGR sources may be in an evolutionary stage during which the neutron star is spiraling toward its companion, becoming embedded in the wind from the high-mass companion. In this picture, we may be seeing IGR J16207−5129 early in this evolutionary phase, so that the neutron star is still in a low-density portion of the wind. Source-to-source differences in N_H could also be indicative of variations in the strength of the stellar wind over time.

After submission of this work, two other reports provided further information about the HMXBs. Using *INTEGRAL*, Sguera et al. (2006) found a 1.5 hr X-ray outburst from IGR J16195−4945, indicating that this source may belong to the class of supergiant fast X-ray transients. In addition, for IGR J16207−5129, Masetti et al. (2006a) report on optical spectra of USNO-A2.0 0375−27093111 (i.e., the same star that we have determined to be the counterpart) and find that the spectrum includes Hα in emission and is consistent with that of an HMXB.

Masetti et al. (2006a) also report on the optical spectra of the stars that we have (independently) determined to be the optical counterparts of IGR J17195−4100 and IGR J16167−4957. These stars show hydrogen Balmer series emission lines as well as He I and He II emission lines. While this indicates that they are either cataclysmic variables (CVs) or LMXBs, the hard X-ray spectra would be very unusual for LMXBs (e.g., Muno et al. 2004). A CV interpretation is more likely, and Masetti et al. (2006a) also come to this conclusion.

J. A. T. acknowledges partial support from *Chandra* award GO5-6037X issued by the *Chandra X-Ray Observatory* Center, which is operated by the Smithsonian Astrophysical Observatory for and on behalf of the National Aeronautics and Space Administration (NASA), under contract NAS8-03060. J. A. T. acknowledges partial support from a NASA *INTEGRAL* Guest Observer grant NNG05GC49G. L. F. acknowledges partial funding from the Italian Space Agency (ASI) under contract I/R/046/04 and from MIUR under contract COFIN 2004-023189. We thank the referee for helpful comments that improved this manuscript. This work is based in part on ESO observations through program 073.D-0339. This publication makes use of data products from the Two Micron All-Sky Survey, which is a joint project of the University of Massachusetts and the Infrared Processing and Analysis Center, California Institute of Technology, funded by NASA and the National Science Foundation. This research has made use of the USNOFS Image and Catalogue Archive operated by the United States Naval Observatory, Flagstaff Station, as well as the SIMBAD database, operated at CDS, Strasbourg, France. We have also used data from *Spitzer*'s Galactic Legacy Infrared Midplane Survey Extraordinaire (GLIMPSE) as well as the Deep Near-Infrared Survey of the Southern Sky (DENIS).

REFERENCES

Beckmann, V., et al. 2005, ApJ, 631, 506
Bird, A. J., et al. 2004, ApJ, 607, L33
———. 2006, ApJ, 636, 765
Bodaghee, A., Walter, R., Zurita Heras, J. A., Bird, A. J., Courvoisier, T. J.-L., Malizia, A., Terrier, R., & Ubertini, P. 2006, A&A, 447, 1027
Cardelli, J. A., Clayton, G. C., & Mathis, J. S. 1989, ApJ, 345, 245
Cash, W. 1979, ApJ, 228, 939
Coburn, W., Heindl, W. A., Rothschild, R. E., Gruber, D. E., Kreykenbohm, I., Wilms, J., Kretschmar, P., & Staubert, R. 2002, ApJ, 580, 394
Combi, J. A., Ribó, M., Mirabel, I. F., & Sugizaki, M. 2004, A&A, 422, 1031
Cox, A. N., ed. 2000, Allen's Astrophysical Quantities (4th ed.; New York: AIP)
Davis, J. E. 2001, ApJ, 562, 575
Dean, A. J., et al. 2005, A&A, 443, 485
de Jager, C., & Nieuwenhuijzen, H. 1987, A&A, 177, 217
Dickey, J. M., & Lockman, F. J. 1990, ARA&A, 28, 215
Diplas, A., & Savage, B. D. 1994, ApJ, 427, 274
Filliatre, P., & Chaty, S. 2004, ApJ, 616, 469
Freeman, P. E., Kashyap, V., Rosner, R., & Lamb, D. Q. 2002, ApJS, 138, 185
Garmire, G. P., Bautz, M. W., Ford, P. G., Nousek, J. A., & Ricker, G. R. 2003, Proc. SPIE, 4851, 28
Landolt, A. U. 1992, AJ, 104, 340
Lebrun, F., et al. 2003, A&A, 411, L141
Lutovinov, A., Revnivtsev, M., Gilfanov, M., Shtykovskiy, P., Molkov, S., & Sunyaev, R. 2005a, A&A, 444, 821
Lutovinov, A., Rodriguez, J., Revnivtsev, M., & Shtykovskiy, P. 2005b, A&A, 433, L41
Masetti, N., Morelli, L., Palazzi, E., Stephen, J., Bazzano, A., Dean, A. J., Walter, R., & Minniti, D. 2006a, Astron. Tel., 783, 1
Masetti, N., et al. 2006b, A&A, 449, 1139
Matt, G., & Guainazzi, M. 2003, MNRAS, 341, L13
Muno, M. P., et al. 2004, ApJ, 613, 1179
Negueruela, I., Smith, D. M., Harrison, T. E., & Torrejón, J. M. 2006, ApJ, 638, 982
Persson, S. E., Murphy, D. C., Krzeminski, W., Roth, M., & Rieke, M. J. 1998, AJ, 116, 2475
Predehl, P., & Schmitt, J. H. M. M. 1995, A&A, 293, 889
Revnivtsev, M. G. 2003, Astron. Lett., 29, 644
Rodriguez, J., Tomsick, J. A., Foschini, L., Walter, R., Goldwurm, A., Corbel, S., & Kaaret, P. 2003, A&A, 407, L41
Russeil, D. 2003, A&A, 397, 133
Sguera, V., et al. 2006, ApJ, 646, 452
Sidoli, L., Vercellone, S., Mereghetti, S., & Tavani, M. 2005, A&A, 429, L47
Smith, D. M., Heindl, W. A., Markwardt, C. B., Swank, J. H., Negueruela, I., Harrison, T. E., & Huss, L. 2006, ApJ, 638, 974
Stephen, J. B., et al. 2005, A&A, 432, L49
Sugizaki, M., Mitsuda, K., Kaneda, H., Matsuzaki, K., Yamauchi, S., & Koyama, K. 2001, ApJS, 134, 77
Tomsick, J. A., Corbel, S., Goldwurm, A., & Kaaret, P. 2005, ApJ, 630, 413
Tomsick, J. A., Lingenfelter, R., Corbel, S., Goldwurm, A., & Kaaret, P. 2004, in The INTEGRAL Universe, ed. V. Schoenfelder, G. Lichti, & C. Winkler (ESA SP-552; Noordwijk: ESA), 413
Ubertini, P., et al. 2003, A&A, 411, L131
Ueda, Y., et al. 1999, ApJ, 518, 656
Walter, R., et al. 2003, A&A, 411, L427
Weisskopf, M. C., Brinkman, B., Canizares, C., Garmire, G., Murray, S., & Van Speybroeck, L. P. 2002, PASP, 114, 1
Winkler, C., et al. 2003, A&A, 411, L1

3.5.3 IGR J17544-2619 : Une nouvelle transitoire rapide de rayons X à supergéante révélée par des observations en optique/infrarouge

"IGR J17544-2619 : A new supergiant fast X-ray transient revealed by optical/infrared observations" par L.J. Pellizza, S. Chaty and I. Negueruela, 2006, A&A, 455, 653

Dans cet article est présenté un ensemble d'observations en optique et en infrarouge proche de la contrepartie d'une source détectée par *INTEGRAL* : IGR J17544-2619. Ces observations ont montré le caractère inhabituel de cette source : peu absorbée en optique/infrarouge, les spectres de cette source étant typiques d'une étoile supergéante de type spectral 0. La conclusion de ces observations est donc que l'étoile compagnon est une supergéante, et le système est donc un système binaire de grande masse. Ce qui confère à cet astre un côté inhabituel, c'est qu'il présente des sursauts d'activité transitoires et très rapides, durant moins d'une heure, alors que les systèmes binaires de grande masse présentent habituellement une émission permanente dans les X. Cette source est devenue l'archétype du deuxième nouveau type d'astres révélé par *INTEGRAL*, et appelé SFXT, pour *Supergiant Fast X-ray Transients* : des Supergéantes transitoires rapides de rayons X (voir le paragraphe 3.3.2 pour plus de détails).

A&A 455, 653–658 (2006)
DOI: 10.1051/0004-6361:20054436
© ESO 2006

Astronomy & Astrophysics

IGR J17544−2619: a new supergiant fast X-ray transient revealed by optical/infrared observations⋆

L. J. Pellizza[1], S. Chaty[1], and I. Negueruela[2]

[1] AIM – Astrophysique Interactions Multi-échelles (Unité Mixte de Recherche 7158 CEA/CNRS/Université Paris 7 Denis Diderot), CEA Saclay, DSM/DAPNIA/Service d'Astrophysique, Bât. 709, L'Orme des Merisiers, 91191 Gif-sur-Yvette Cedex, France
e-mail: lpellizz@discovery.saclay.cea.fr
[2] Dpto. de Física, Ingeniería de Sistemas y Teoría de la Señal, Universidad de Alicante, Apdo. 99, E03080 Alicante, Spain

Received 28 October 2005 / Accepted 10 May 2006

ABSTRACT

One of the most recent discoveries of the *INTEGRAL* observatory is the existence of a previously unknown population of X-ray sources in the inner arms of the Galaxy. IGR J17544−2619, IGR J16465−4507 and XTE J1739−302 are among these sources. Although the nature of these systems is still unexplained, the investigations of the optical/NIR counterparts of the two last sources, combined with high energy data, have provided evidence of them being highly absorbed high mass X-ray binaries with blue supergiant secondaries and displaying fast X-ray transient behaviour. In this work we present our optical/NIR observations of IGR J17544−2619, aimed at identifying and characterizing its counterpart. We show that the source is a high mass X-ray binary at a distance of 2–4 kpc with a strongly absorbed O9Ib secondary, and discuss the nature of the system.

Key words. X-rays: binaries – X-rays: individual: IGR J17544-2619

1. Introduction

In recent years, a set of new X-ray sources were discovered by *INTEGRAL* and *RXTE* observatories within a few tens of degrees of the direction to the galactic center (Negueruela 2004; Kuulkers 2005). These sources present hard X-ray spectra, usually interpreted as due to strong absoption by large hydrogen column densities arising from circumstellar material. Their continuum spectral parameters are typical of neutron stars or black holes. They are suspected to be high mass X-ray binaries (HMXBs) embedded in highly absorbing media, and for some of them massive companions were identified (e.g., Filliatre & Chaty 2004; Smith 2004; Masetti et al. 2006; Negueruela et al. 2005, 2006). Among these sources there are transient ones, characterized by very short outbursts (∼hours) separated by large quiescence periods (Smith et al. 2006; in't Zand 2005). IGR J16465−4507 and XTE J1739−302/IGR J17391−3021 are two of these transient sources, which have been shown to be HMXBs with highly reddened early type supergiant secondaries (Smith 2004; Negueruela et al. 2005, 2006), hence supporting the hypothesis of these sources being surrounded by large amounts of material.

IGR J17544−2619 is a fast transient source lying in the direction of the galactic center ($l = 3.24°$, $b = -0.34°$). It was discovered by the IBIS/ISGRI instruments onboard *INTEGRAL* on September 17, 2003 (Sunyaev et al. 2003), during an outburst which lasted around 2 h. A second outburst lasting for 8 h was observed the same day (Grebenev et al. 2003), and a third one lasting for 10 h was detected on March 8, 2004 (Grebenev et al. 2004), demonstrating that this is a recurrent transient source. An oscillation-like behaviour with a time scale of 1.5–2 h has also been detected in the March 2004 observation (Grebenev et al. 2004). The source has also been observed by *XMM-Newton* on March 17 and September 11 and 17, 2003 (González-Riestra et al. 2004) and by *Chandra* on July 3, 2004 (in't Zand 2005). *XMM-Newton* observations revealed a hard spectrum, that can be modelled by an absorbed power law with either variable absorption or variable spectral index, in both cases with a large hydrogen column density ($N_{\rm H} \sim 1.9–4.3 \times 10^{22}$ cm^{-2}). *Chandra* observations also showed a hard spectrum during bursts, but a softer one in quiescence, with similar absorption ($N_{\rm H} = 1.36 \pm 0.22 \times 10^{22}$ cm^{-2}). Assuming a distance of 8 kpc, total unabsorbed luminosities of the source in the 0.5–10 keV range are of the order of 10^{32} erg s^{-1} in quiescence and 10^{35}–10^{36} erg s^{-1} during activity. These values are typical of HMXBs containing either neutron stars or black holes. *XMM-Newton* and *Chandra* observations also allowed a precise positioning of the source (4″ and 0.6″ error boxes respectively), challenging its identification with the *ROSAT* source 1RXS J175428.3−2620 proposed by Wijnands (2004), and supporting the optical/NIR counterpart candidate (USNO-B1.0 0636-0620933/2MASS J17542527−2619526) suggested by Rodriguez (2003). The *XMM-Newton* ultraviolet magnitudes, combined with optical/NIR data are also consistent with IGR J17544−2619 having an early O-type companion (González-Riestra et al. 2004).

One day after the discovery of IGR J17544−2619, we triggered our ESO Target of Opportunity program to obtain optical and NIR images of the field of this source, and optical spectra of the counterpart candidate proposed by Rodriguez (2003), which is also the brightest object in the *XMM-Newton* error box. These measurements were aimed at confirming the optical/NIR

⋆ Based on observations collected at the European Southern Observatory, Chile, under proposal ESO 71.D-0073.

Article published by EDP Sciences and available at http://www.edpsciences.org/aa or http://dx.doi.org/10.1051/0004-6361:20054436

Table 1. Optical and NIR imaging log.

Filter	Exposure time (s)	# frames	Filter	Exposure time (s)	# frames
B	300	1	*J*	60	9
V	200	1	*H*	60	9
V	10	90	K_s	60	9
R	200	1	K_s	2	366

Table 2. Spectroscopy log.

Grating or grism	Exposure time (s)	Wavelength range (Å)	Resolution (Å)
#3	150	3600–8400	7.9
#5	400	3800–6700	4.5
#6	300	6180–6860	1.2
#12	700	4000–4920	2.6

counterpart and determining its properties. In this paper we present our observations (Sect. 2), their results (Sect. 3), and discuss the nature of the system (Sect. 4).

2. Observations

Our observations of IGR J17544−2619 were carried out on the nights of September 18, 2003 (imaging) and May 11, 2004 (spectroscopy), with the ESO 3.5-meter New Technology Telescope (NTT) at La Silla Observatory, Chile. Optical and NIR images of the field of the source were obtained with the ESO Multi-Mode Instrument (EMMI) and the Son Of Isaac (SOFI) instruments respectively, as part of a Target of Opportunity program (ESO 71.D-0073, P. I. Chaty). Intermediate resolution optical spectra of the counterpart candidate proposed by Rodriguez (2003) were also obtained with EMMI.

The red arm of EMMI, equipped with a mosaic of two 2048×4096 MIT CCD detectors, was used in the longslit REMD mode together with grating #6 and in RILD mode with grisms #3 and #5 for spectroscopy. The same arm of EMMI was used in RILD mode with *B*, *V* and *R* Bessel filters for imaging. The blue arm, equipped with a Textronik TK1034 thinned, back-illuminated 1024 × 1024 CCD, was also used for spectroscopy in the longslit BLMD mode with grating #12. SOFI, equipped with a Rockwell Hg:Cd:Te 1024 × 1024 Hawaii array, was used with the Large Field Objective and *J*, *H* and K_s filters for NIR imaging.

We took a set of very deep images in each filter in order to search for possible counterpart candidates not detected by previous surveys, and to perform accurate photometry of all candidates. Due to the nature of the high energy source, photometric variability is expected, hence two sets of short, contiguous exposures spanning 1–2 h were also taken to construct optical and NIR light curves respectively. We took also long exposure spectra of USNO-B1.0 0636-0620933 in order to cover the whole optical spectral range with a high S/N ratio. Tables 1 and 2 give the basic parameters used for the observations. The standard reduction procedures for optical and NIR images (sky/bias substraction and flat-fielding) were used to obtain the final science images. The reduction was performed using the IRAF package CCDRED (Tody 1993). The spectra were pre-processed with MIDAS and then reduced using the Starlink packages CCDPACK and FIGARO.

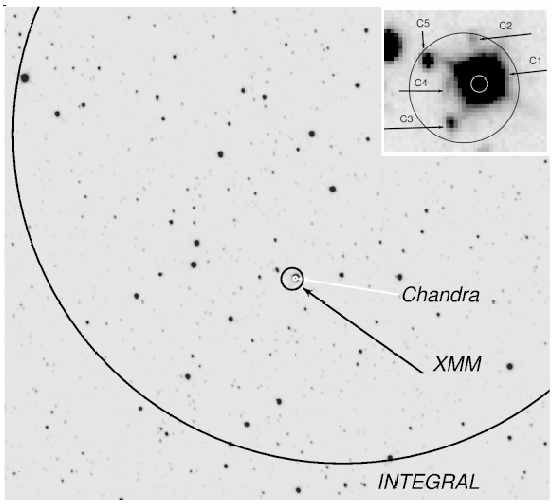

Fig. 1. K_s band image of the field of IGR J17544−2619. North is up and East is to the left. The large circular section is the *INTEGRAL* error circle (2′ radius) for the source, while the small circles are the *XMM-Newton* and *Chandra* error boxes (black, 4″ and white, 0.6″ radius respectively). *Inset*: the five counterpart candidates (C1–C5) found inside the *XMM-Newton* error box (black circle). The brightest candidate (C1), the only one allowed by the *Chandra* error box (white circle), is USNO-B1.0 0636-0620933/2MASS J17542527−2619526, the candidate proposed by Rodriguez (2003). The image was processed to unveil the faintest candidates, hence the intensity scale is nonlinear.

3. Data analysis and results

3.1. Astrometry

We performed the astrometry of our images to determine the position in our frames of the *XMM-Newton* and *Chandra* error boxes for IGR J17544−2619 and to search for optical/NIR counterparts within them. We chose the best frame in each band for this purpose, and selected from it a set of bright pointlike objects in uncrowded regions. We took the coordinates of these objects from the USNO B1.0 and the 2MASS catalogs (Monet et al. 2003; Cutri et al. 2003), and computed the plate solution for each frame using the IRAF CCMAP task, obtaining an rms error <0.15″, which is small enough for our purposes. In Fig. 1 we show the field of the source in the K_s band, together with the *INTEGRAL*, *XMM-Newton* and *Chandra* error circles. Inside the second one we found 5 counterpart candidates (C1–C5, their positions are given in Table 3). The brightest candidate (C1) is the one proposed by Rodriguez (2003), the other four (including one apparently extended object, C4) are only visible in the NIR and are extremely faint, close to our detection limit. The *Chandra* error box clearly excludes all the candidates but C1, hence we conclude that this is the correct counterpart of IGR J17544−2619. The three faint pointlike objects are probably foreground dwarf stars, while the extended one might be a background galaxy.

3.2. Spectroscopy

Spectroscopic observations of candidate C1 enabled us to determine for the first time its spectral type. In Fig. 2 we present the optical spectra of this object taken with grisms #12 and #3, while in Table 4 we list the spectral features identified in it. The presence of intense He II lines in the spectrum of C1 suggests an O spectral type. According to the

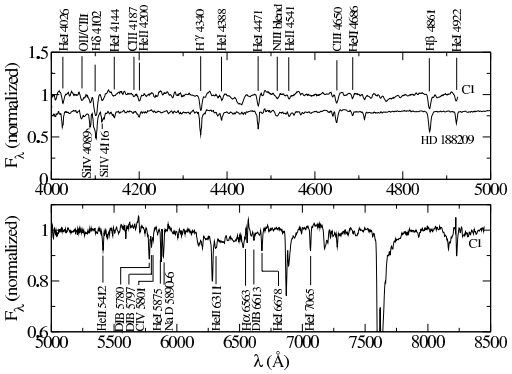

Fig. 2. Optical spectrum of USNO-B1.0 0636-0620933 showing the identified lines, among which we found strong He II lines typical of an O-type star. *Upper panel*: blue spectrum of C1 taken with grism #12 (upper curve), and the standard O9Ib star HD 188209 (lower curve). The high degree of similarity between them supports our classification of C1 as an O9Ib star. *Lower panel*: red spectrum of C1 between 5000 Å and 8500 Å, taken with grism #3. The features at 6850 Å and 7600 Å are of telluric origin.

Table 3. Positions of optical/NIR counterpart candidates of the high energy source IGR J17544−2619, and their distances to the brightest one.

Id.	α (J2000) (h m s)	δ (J2000) (° ′ ″)	Distance to C1 (″)	Notes
C1	17:54:25.27	−26:19:52.7	0.0	Bright
C2	17:54:25.32	−26:19:49.7	3.1	Faint, pointlike
C3	17:54:25.44	−26:19:55.8	3.9	Faint, pointlike
C4	17:54:25.46	−26:19:53.2	2.6	Faint, extended?
C5	17:54:25.57	−26:19:51.2	4.3	Faint, pointlike

classification criteria of Walborn & Fitzpatrick (1990), the ratio He II 4541 Å/He I 4471 Å indicates that C1 is an O9 star. The luminosity class of C1 could also be determined using the intensity of the He II 4686 Å as a luminosity indicator (Walborn & Fitzpatrick 1990). This line is very weak, but clearly visible in absorption in our object, indicating a Ib luminosity class. Due to the low S/N ratio of the spectrum, there is some uncertainty about this spectral classification, but the O9Ib spectral type is fully supported by the lower resolution, higher S/N ratio grism #5 spectrum. Figure 2 includes, for comparison, the spectrum of the O9Ib star HD 188209, showing that the general appearance of both spectra is similar. This classification confirms that C1 is a blue supergiant and, via the calibration of Drilling & Landolt (1999), provides the first determination of its mass, 25−28 $M_\odot$. Hence, we conclude that IGR J17544−2619 is a HMXB. Another interesting feature of the C1 spectrum is the Hα line, that shows a P-Cygni type profile. This is the signature of mass loss through a strong stellar wind, present in normal O-type stars.

The spectrum of C1 shows also several diffuse interstellar bands (DIBs), usually present in the spectra of sources with large extinction. The DIBs at 5780 Å, 5797 Å and 6613 Å correlate with the color excess $E(B-V)$ (e.g., Herbig 1993; Cox et al. 2005), hence we can use them to determine the latter. In our spectra, the DIB at 5797 Å is blended with the C IV 5801 Å line, but the other two DIBs are clearly resolved. The first one shows an equivalent width $W_{5780} = 1020 \pm 80$ mÅ implying, through the relationship given by Herbig (1993), a color excess

Table 4. Absorption lines identified in the spectrum of USNO-B1.0 0636-0620933, and the atomic species that produce them.

λ_{obs} (Å)	λ_{lab} (Å)	Species	λ_{obs} (Å)	λ_{lab} (Å)	Species
4027 ± 1	4026.189	He I	4542 ± 1	4541.590	He II
	4026.362	He I	4650 ± 1	4650.160	C III
4070 ± 1	4067.870	C III		4651.350	C III
	4068.970	C III	4685 ± 1	4685.682	He II
	4069.636	O II	4861 ± 1	4861.332	Hβ
	4069.897	O II	4921 ± 1	4921.929	He I
	4070.300	C III	5412 ± 3	5411.524	He II
4089 ± 1	4088.863	Si IV	5881 ± 3	5875.618	He I
4101 ± 1	4101.737	Hδ		5875.650	He I
4115 ± 1	4116.104	Si IV		5875.989	He I
4142 ± 1	4143.759	He I		5889.953	Na I
4187 ± 1	4187.050	C III		5895.923	Na I
4200 ± 1	4199.830	He II	6310 ± 3	6310.800	He II
4340 ± 1	4340.468	Hγ	6564 ± 1	6562.817	Hα
4388 ± 1	4387.928	He I	6679 ± 3	6678.149	He I
4471 ± 1	4471.477	He I	7062 ± 3	7065.188	He I
	4471.688	He I		7065.719	He I
4515 ± 1	4510.920	N III			
	4514.890	N III			

$E(B-V) = 1.97 \pm 0.15$. For the other one, our measured equivalent width ($W_{6613} = 300 \pm 50$ mÅ) is contained in the region where the relationship between W and $E(B-V)$ is nonlinear. Figure 4 of Cox et al. (2005) shows that this value is consistent with $E(B-V) > 1$, the flattening of the relationship preventing any other meaningful conclusion.

3.3. Photometry

Differential aperture photometry of C1 was made using the IRAF package APPHOT. For each frame, we measured its instrumental optical and NIR magnitudes m_B, m_V, m_R, m_J, m_H and m_{K_s}, together with those of 18 comparison stars with known USNO B1.0 and 2MASS magnitudes. The Johnson B, V and R magnitudes of the comparison stars were computed from their photographic IIIa-J (blue) and IIIa-F (red) magnitudes taken from the USNO B1.0 catalog and the transformations of Windhorst et al. (1991), while their J, H and K_s standard magnitudes were taken directly from the 2MASS catalog.

Linear fits of the standard optical magnitudes against corresponding instrumental magnitudes present slopes consistent with unity within errors of a few percent, showing that our instrumental magnitudes differ from the standard system only in the zero points for the different bands. These were computed by taking the mean of the differences $B - m_B$, $V - m_V$ and $R - m_R$ for the comparison stars. Their uncertainties were determined by assuming that these differences follow a normal distribution, and computing the error of the mean. The standard deviation of these differences is ~0.2 mag, consistent with the facts that USNO B1.0 uncertainties are around 0.3 mag in the worst cases (Monet et al. 2003) and that the transformations between photographic and Johnson systems add an error of ~0.1 mag in quadrature (Windhorst et al. 1991). Hence, our zero points have uncertainties of ~0.05 mag.

For NIR images, C1 was slightly in the nonlinear range of SOFI CCDs, hence quadratic fits of standard 2MASS magnitudes J, H and K_s against corresponding instrumental magnitudes m_J, m_H and m_{K_s} respectively were used to derive the NIR magnitudes of C1. The errors of the estimated magnitudes were

Table 5. Optical and NIR magnitudes of the counterpart candidates of the high energy source IGR J17544−2619. The lower limits stand for the combined magnitudes of the four faint candidates C2−C5.

Id.	B ±0.05 (mag)	V ±0.05 (mag)	R (mag)	J ±0.02 (mag)	H ±0.02 (mag)	K_s ±0.02 (mag)
C1	14.44	12.65	<11.9	8.71	8.03	7.99
C2–5	>19.5	>17.7	>16.2	>13.8	>13.1	>13.1

computed from the full covariance matrix of the fitted parameters, and take into account the uncertainties of the 2MASS magnitudes of the comparison stars, our instrumental magnitude errors being much smaller.

The optical and NIR magnitudes of C1 are shown in Table 5. The value of R is an upper limit as the image of C1 was slightly saturated in this band. We performed the photometry for different aperture diameters d from 1″ to 5″ in order to detect any flux contribution from the fainter candidates. In all cases, the constancy of the C1 instrumental magnitudes for $d > 2.5''$ up to an accuracy of 0.01 mag allows us to put conservative lower limits for the combined magnitude of all of them (see Table 5). The contribution of C2−C5 is thus negligible and we can ensure that it does not contaminate our results on C1 at the 0.01 mag accuracy level.

Our broad-band magnitudes are in accordance with those listed in Rodriguez (2003), and also with the B magnitude measured by *XMM-Newton* (González Riestra et al. 2004). We note that our J and H magnitudes differ (the first one marginally) from those given by 2MASS, our estimates being lower than catalog values; but our K_s value agrees well with 2MASS data ($J_{2MASS} = 8.791 \pm 0.021$, $H_{2MASS} = 8.310 \pm 0.031$, $K_{s,2MASS} = 8.018 \pm 0.026$). Because of the high accuracy of both 2MASS and our measurements, and the fact that our determinations are based on the 2MASS magnitudes of the comparison stars, we conclude that the differences might arise in a true variation in the NIR flux of C1, brighter in September 2003 than in the epoch of 2MASS observations (July 1998). This variation makes a stronger case for the identification of C1 as the correct counterpart of IGR J17544−2619. We suggest that it might be related to the X-ray activity of the source. A more detailed study through simultaneous multiwavelength campaigns both during quiescence and activity would be important to confirm these points.

The combination of the spectral type of C1 with its photometry gave us a deeper insight into the nature of the system. An O9Ib star has an intrinsic colour $(B-V)_0 = -0.28 \pm 0.01$ (Schmidt-Kaler 1982), whereas we measure $B-V = 1.79 \pm 0.10$, implying a reddening $E(B-V) = 2.07 \pm 0.11$. This value is consistent with that found using the DIBs observed in the spectra of C1. Hereafter we use the average of both, $E(B-V) = 2.02 \pm 0.13$. Assuming a standard extinction law ($R_V = 3.1$) gives a total visual extinction $A_V = 6.26 \pm 0.40$. There is no reliable absolute visual magnitude calibration for O9Ib stars alone, but as Ib stars are the least luminous objects of class I, we take the mean value for *all* O9I stars, $M_V = -6.29$ (Martins et al. 2005), as an upper limit for the luminosity of C1. On the other hand, the faintest O9I stars have $M_V \sim -5.6$ (Martins et al. 2005). With this interval for the absolute visual magnitude of C1, we derive a range of 2.1–4.2 kpc for the distance of the system, far smaller than the 8.5 kpc computed by Smith (2004) using USNO B1.0 photometry. The disagreement arises from the lack of accuracy of USNO magnitudes. This result is very robust,

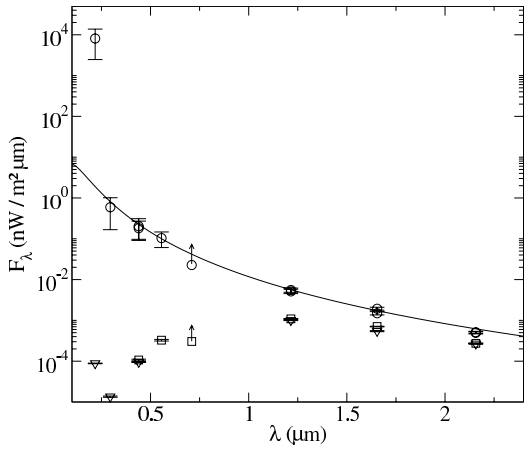

Fig. 3. Spectral energy distribution $F_\lambda(\lambda)$ of the source. Squares represent the fluxes observed by us and triangles those from *XMM-Newton* and 2MASS data. Circles correspond to extinction corrected fluxes. The solid line shows the SED of a blackbody at the effective temperature of an O9Ib star ($T_{eff} = 3.1 \times 10^4$ K), normalized to have the same unabsorbed V magnitude of the source.

even if C1 were among the brightest O9I stars, the distance would be still smaller than ∼5 kpc, and if a value $R_V > 3.1$ were used, the distance would decrease. Hence, the most probable localization of IGR J17544−2619 is between 2−4 kpc of the Sun, in the Scutum–Crux arm of the Milky Way (see Vallée 2005 for a model of the Milky Way spiral arms). We note that small distances were also obtained for XTE J1739−302 (1.8–2.9 kpc; Negueruela et al. 2006) and IGR J16318−4848 (<4 kpc; Filliatre & Chaty 2004).

The observed extinction implies a hydrogen column density $N_H = 1.2 \times 10^{22}$ cm^{-2}, close to the interstellar value (1.4×10^{22} cm^{-2}, Dickey & Lockman 1990). Our value is consistent with those obtained from *Chandra* observations ($1.36 \pm 0.22 \times 10^{22}$ cm^{-2}) and lower than *XMM-Newton* results ($1.9–4.3 \times 10^{22}$ cm^{-2}), showing that the higher N_H values are obtained during X-ray activity, N_H decreasing during quiescence. This suggests the existence of a highly variable circumstellar medium around the system, whose presence is related to the high energy activity of the source. We note that the possibility of the extinction being always completely interstellar is difficult to reconcile with the variable N_H suggested by the combination of X-ray and our observations.

The photometry obtained allowed us to construct for the first time a spectral energy distribution (SED) of the source, which we show in Fig. 3. Squares in this figure represent our measurements of the observed flux of the source F_λ as a function of wavelength λ, while triangles represent *XMM-Newton* and 2MASS data. Using the estimated visual extinction and its relationship to the extinction in other bands (Mathis 1999), we computed the latter and corrected the SED for its effects (circles in Fig. 3). We also constructed the SED of an O9Ib star normalized to have the same unabsorbed V magnitude of C1, using its intrinsic color indices (Drilling & Landolt 1999; Tokunaga 1999). We found that it is very well fitted by a blackbody with a temperature equal to the effective temperature of an O9I star ($T_{eff} = 3.1 \times 10^4$ K, Martins et al. 2005), normalized in the same way (solid line in Fig. 3). We note the very good agreement between the two unabsorbed SEDs in the optical, NIR and part of the UV, confirming our assumption of standard reddening. The lack of detection of C1 in the *UVM2* band ($\lambda = 0.234$ μm,

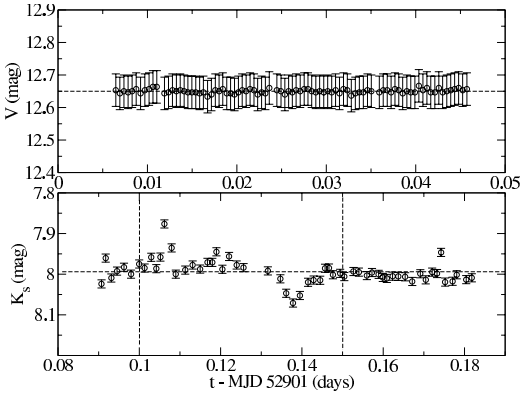

Fig. 4. Optical and NIR light curves of C1. Abscissas are given as Modified Julian Dates (MJD), MJD 52 901 being September 19, 2003, 0^h UT. *Upper panel*: the *V* band light curve is extremely flat, showing a constant contribution from the O star. *Lower panel*: the K_s band light curve shows erratic variations around t − MJD 52 901 ∼ 0.10−0.15 days (between the two dashed lines), note the two brightenings (∼0.10 mag at 0.105 days and ∼0.05 mag at 0.12 days) and the fading (∼0.10 mag at 0.14 days). The differences with the *V* band curve suggest that they are probing different parts of the system, and supports the picture of the existence of circumstellar material around the star.

González-Riestra et al. 2004) is consistent with the blackbody spectrum and the amount of extinction derived by us. However, the detection at 0.218 μm (*UVW*2 band) is puzzling, because the absorbed flux should be more than two magnitudes below the limiting magnitude of the *XMM-Newton* OM for this wavelength (there is a strong enhancement in the extinction curve at this wavelength, the 2175 Å bump). A peculiar value for the extinction at 0.218 μm (e.g., due to the depletion of the material that produces the 2175 Å bump) could be one solution, but it is improbable given the good agreement in other wavelengths and the fact that a reduction of ∼9 mag in the extinction in the *UVW*2 band is needed to restore the agreement with the blackbody spectrum. On the other hand, if the computed absorption is correct, the measured magnitude (m_{UVW2} = 14.49 ± 0.02) implies that the unabsorbed flux at this wavelength is more than three orders of magnitude greater than the blackbody estimate. This disagreement could be explained if the source were variable in the UV, because the observations in the *UVW*2 and *UVW*1 (λ = 0.295 μm) bands were separated by 6 days. If this is the case, it would be interesting also to determine if the variability is connected to the X-ray behaviour. Simultaneous multiwavelength campaigns are clearly needed to investigate this issue and determine the astrophysical processes which operate in this source.

3.4. Light curves

Using the 90 *V*-band and the 366 K_s-band short exposures (see Table 1), we constructed optical/NIR light curves of C1 spanning 3.4 ks and 8 ks respectively (Fig. 4). The NIR data were averaged in groups of 4, which results in a lower uncertainty of ∼0.01 mag. The *V* light curve is flat and completely featureless down to our accuracy level of 0.05 mag. The K_s light curve, instead, shows an erratic behaviour barely above our accuracy limits of 0.01 mag. A few sporadic events are seen around t − MJD 52 901 ∼ 0.10−0.15 days, including two short brightenings of approximately 0.05−0.10 mag and an abrupt fading of about 0.10 mag, reminiscent of an eclipse. No periodicity is apparent in our light curves.

Although the optical and NIR light curves are not simultaneous, they are close in time, hence their different behaviours suggest that they are probing different parts of the system. The extreme flatness of the optical light curve contrasts with the multiple short erratic variations found in the NIR light curve. The *V* light curve is probably reflecting the behaviour of the O9Ib star, as it is the brightest source in this spectral domain. We note that the constant light curve observed is not in contradiction with the fact that most O stars are microvariable in *V* (e.g., Balona 1992), because their amplitudes are <0.1 mag, lower than or of the same magnitude of our accuracy (±0.05 mag). The NIR variations, that occur on timescales of the order of hours, could be generated by a different component. A possible candidate is a variable amount of warm material (either circumstellar or in an accretion disc) emitting in the NIR. We note that IGR J17544−2619 was recently detected in the medium IR (8.59 μm and 11.26 μm) by the VISIR instrument on VLT (Chaty et al., in prep.). We also note that the erratic variability observed in K_s could explain the differences between our NIR magnitudes and 2MASS values. Longer light curves in several optical and IR bands together with optical/NIR spectra would be needed to address this issue.

4. Discussion

Using optical and NIR imaging of the field of IGR J17544−2619 we identified the optical/NIR counterpart of this high energy source to be USNO-B1.0 0636-0620933/2MASS J17542527−2619526. We have obtained strong evidence for IGR J17544−2619 being a high mass X-ray binary. Although our data do not give any clue about the accretor in the HMXB, they can be obtained from the X-ray data. The peak flux density scaled to 1 kpc (0.5−1.9 Crab, for our distance range of 2.1−4.2 kpc) and the spectral index obtained by *Chandra* are consistent with those of black holes in the hard state. Applying the relationship of Gallo et al. (2003), we obtain an expected radio flux of ∼10−35 mJy for this source if the accretor is a black hole. Hence, the lack of detection of IGR J17544−2619 in radio (3σ upper limit of 7 mJy at 0.61 GHz, Pandey et al. 2006) suggests that the compact object is rather a neutron star. This agrees with the results of in't Zand (2005), who shows that the X-ray spectrum of IGR J17544−2619 in quiescence can be satisfactorily fitted by a neutron star model with a luminosity of $\sim 5 \times 10^{32}$ erg s^{-1}.

For the mass donor, our results show that it is an O9Ib blue supergiant with a mass of 25−28 $M_\odot$. Hence, at its birth the object should have been an O+O binary, a rare system due to the high masses of its components and their short lifetimes (a 25 $M_\odot$ star lives only ∼7 Myr in the main sequence). This characteristic is consistent with the fact that we find IGR J17544−2619 in a star-forming region of the Galaxy (the Scutum-Crux arm at ∼3−4 kpc). It is not surprising then to find other systems with similar properties in nearby regions (Scutum-Crux and Norma arms). Although massive binaries undergo mass-transfer phases before the primary evolves into a compact object, recent results suggest that the maximum mass gained by the secondary could be as small as 10% of the mass transferred (e.g., Petrovic et al. 2005). This suggests that the mass of the primary should have been $\gtrsim$25 $M_\odot$, and hence that such massive stars are not necessarily constrained to evolve into black holes.

Our data, combined with X-ray observations, suggest that this system is embedded in circumstellar material. We derive a

moderately high hydrogen column density $N_H = 1.2\times10^{22}$ cm^{-2}, that agrees well with *Chandra* results and is lower than that derived from *XMM-Newton* data (González-Riestra et al. 2004; in't Zand 2005). This confirms that the extinction of the system is variable, and hence it can not be completely interstellar. The existence of NIR variability with no optical correlation shown by our light curves could be explained if we assume that optical and NIR emission arise in different regions of the system. The optical radiation comes from the blue supergiant, hence at least part of the NIR should come from another region, the circumstellar environment being a good candidate. This scenario is interesting regarding the recent detection of IGR J17544−2619 in the medium IR.

Our analysis, together with other recents studies (Smith 2004; in't Zand 2005; Negueruela et al. 2006; Smith et al. 2006) suggest that the group of the sources discovered by *INTEGRAL* and *RXTE* observatories close to the direction of the galactic center is not homogeneous, it rather shows two distinct subgroups. The first one comprises HMXBs with persistent X-ray emission, large circumstellar absorption and supergiant mass donors (e.g., IGR J16318−4848, Filliatre & Chaty 2004). The second group, dubbed *supergiant fast X-ray transients* (SFXT) by Negueruela et al. (2006) and Smith et al. (2006), includes also supergiant HMXBs, but with fast (∼hours) transient X-ray emission, very low quiescence X-ray luminosity ($\leq10^{34}$ erg s^{-1}), and moderate to high variable X-ray extinction originated in the circumstellar environment. IGR J17544−2619 belongs to this second group, together with XTE J1739−302 (the prototype of the group, Negueruela et al. 2006), IGR J16465−4507, AX 1845.0−0433 and possibly XTE J1901+014. SFXTs include also at least three other sources, SAX J1818.6−1703, AX J1749.1−2733 (in't Zand 2005) and IGR J11215-5952 (Sidoli et al. 2006).

As pointed out by in't Zand (2005) and Negueruela et al. (2006), the physical mechanism driving the fast outbursts in SFXTs would be related neither to the compact object, as the group includes both neutron star and black hole HMXBs, nor to the low luminosity, as fast outbursts were observed also in Vela X-1 and Cygnus X-1. The accretion mechanism is then the most probable cause of the short duration of the outbursts. As supergiant HMXBs are believed to be powered by accretion from the strong wind of the secondary, the variation of the mass flux of the wind is probably the cause of the outbursts. The changing distance of the mass donor in an excentric orbit is an attractive posibility for explaining this mass flux variation, as it could also explain the low quiescent luminosity and small duty cycle of the X-ray source if the O star spends most of the orbital period far away from the accretor. We point out that this is consistent with the fact that recurrent outbursts have been recently found in an SFXT (IGR J11215-5952), with a period of 329 days (Sidoli et al. 2006). On the other hand, local inhomogeinities (clumps) in the wind were proposed as an alternative to explain the fast outbursts, as they are individually accreted by the compact object (in't Zand 2005). We note that, if as we propose, the variability of the circumstellar medium and the X-ray activity are correlated, then individual clump accretion could not explain the whole phenomenology. A global wind density variation (whether it is composed of clumps or not) would be a better explanation for the outbursts, provided that it lasts for a time of the order of a few hours.

Finally, we point out that a more detailed monitoring of this system would be important to completely unveil its properties and hence improve our knowledge on this kind of high energy sources. Particularly, simultaneous multiwavelength campaigns would be needed to precisely measure the SED both in quiescence and during activity, establish the existence of circumstellar material beyond any doubt, and determine its properties. The analysis of both long and short-term variability (including the search for a binary period and wind velocity variability) and their connection to high energy activity would also shed light over the physical mechanisms involved in the behaviour of these systems.

Acknowledgements. We would like to thank Dr. Marc Ribó for useful discussions and a careful reading of the manuscript, and the anonymous referee for suggestions which greatly improved this paper. IN is a researcher of the program *Ramón y Cajal*, funded by the Spanish Ministerio de Ciencia y Tecnología and the University of Alicante, with partial support from the Generalitat Valenciana and the European Regional Development Fund (ERDF/FEDER). This research is partially supported by the Spanish MCyT under grant AYA2002-00814. This publication makes use of data products from the Two Micron All Sky Survey, which is a joint project of the University of Massachusetts and the Infrared Processing and Analysis Center/California Institute of Technology, funded by the National Aeronautics and Space Administration and the National Science Foundation. This research has made use of the SIMBAD database and VizieR Service operated at CDS, Strasbourg, France, and of NASA's Astrophysics Data System Bibliographic Services.

References

Balona, L. A. 1992, MNRAS, 254, 403
Cox, N. L. J., Kaper, L., Foing, B. H., & Ehrenfreund, P. 2005, A&A, 438, 187
Cutri, R. M., Skrutskie, M. F., van Dyk, S., et al. 2003, 2MASS All-Sky Catalog of Point Sources, University of Massachusetts and Infrared Processing and Analysis Center (IPAC/California Institute of Technology), Vizier online catalog II/246
Dickey, J. M., & Lockman, F. J. 1990, ARA&A, 28, 215
Drilling, J. S., & Landolt, A. U. 1999, in Allen's Astrophysical Quantities, ed. A. N. Cox (Springer), 381
Filliatre, P., & Chaty, S. 2004, ApJ, 616, 469
Gallo, E., Fender, R. P., & Pooley, G. G. 2003, MNRAS, 344, 60
Grebenev, S. A., Lutovinov, A. A., & Sunyaev, R. A. 2003, ATel, 192
Grebenev, S. A., Rodriguez, J., Westergaard, N. J., Sunyaev, R. A., & Oosterbrock, T. 2004, ATel, 252
González-Riestra, R., Oosterbroek, T., Kuulkers, E., Orr, A., & Parmar, A. N. 2004, A&A, 420, 589
Herbig, G. H. 1993, ApJ, 407, 142
in't Zand, J. J. M. 2005, A&A, 441, L1
Kuulkers, E. 2005, AIP Conf. Proc., 797, 402
Martins, F., Schaerer, D., & Hillier, D. J. 2005, A&A, 436, 1049
Masetti, N., Pretorius, M. L., Palazzi, E., et al. 2006, A&A, 449, 1139
Mathis, J. S. 1999, in Allen's Astrophysical Quantities, ed. A. N. Cox (Springer), 523
Monet, D. G., Levine, S. E., Canzian, B., et al. 2003, AJ, 125, 984
Negueruela, I. 2004, in The Many Scales of the Universe – JENAM 2004 Astrophysics Reviews, ed. J. C. del Toro Iniesta, et al., Proc of the Joint European and Spanish Astronomical Meeting, Granada, Spain, September 2004 [arXiv:astro-ph/0411759]
Negueruela, I., Smith, D. M., & Chaty, S. 2005, ATel, 429
Negueruela, I., Smith, D. M., Harrison, Th. E., & Torrejón, J. M. 2006, ApJ, 638, 982
Pandey, M., Manchanda, R., Rao, A. P., Durouchoux, P., & Ishwara-Chandra, C. H. 2006, A&A, 446, 471
Petrovic, J., Langer, N., & van der Hutch, K. A. 2005, A&A, 435, 1013
Rodriguez, J. 2003, ATel, 194
Schmidt-Kaler, Th. 1982, in Landolt-Börnstein New Series, Group VI, vol. 2b, ed. K. Schaifers, & H. H. Voigt (Springer-Verlag), 1
Sidoli, L., Paizis, A., & Mereghetti, S. 2006, A&A, 450, L9
Smith, D. M. 2004, ATel, 338
Smith, D. M., Heindl, W. A., Markwardt, C. B., et al. 2006, ApJ, 638, 974
Sunyaev, R. A., Grebenev, S. A., Lutovinov, A. A., et al. 2003, ATel, 190
Tody, D. 1993, in Astronomical Data Analysis Software and Systems II, ed. R. J. Hanisch, R. J. V. Brissenden, & J. Barnes, ASP Conf. Ser., 52, 173
Tokunaga, A. T. 1999, in Allen's Astrophysical Quantities, ed. A. N. Cox (Springer), 143
Vallée, J. P. 2005, AJ, 130, 569
Walborn, N. R., & Fitzpatrick, E. L. 1990, PASP, 102, 379
Wijnands, R. 2003, ATel, 191
Windhorst, R. A., Burstein, D., Mathis, D. F., et al. 1991, ApJ, 380, 362

3.5.4 Sources Galactiques de rayons X durs découvertes par *INTEGRAL* révélées par des observations multi-longueurs d'onde : I. Nature de l'étoile compagnon

"Galactic hard X-ray sources discovered by *INTEGRAL* brought to light by multiwavelength observations : I. The nature of the companion star" par S. Chaty et al., 2008, A&A in press

Dans cet article sont compilées des observations optique et infrarouge proche de quinze nouvelles sources *INTEGRAL* localisées précisément avec les satellites XMM ou Chandra pour la plupart, permettant ainsi de répérer dans la plupart des cas la contrepartie optique/infrarouge de la source, et de contraindre la nature des étoiles compagnons, et donc des systèmes binaires. Cet article montre que dans beaucoup de cas, une meilleure localisation de la source X est nécessaire afin de lever l'ambigüité sur la contrepartie optique/infrarouge. Cependant, l'astrométrie précise, la photométrie et la spectroscopie effectuées dans cet article sur ces quinze sources montrent que ces sources *INTEGRAL* sont des systèmes binaires de grande masse, contenant pour la plupart des supergéantes. Ceci confirme donc la prédominance des HMXBs à supergéantes au sein des sources *INTEGRAL*. De plus, certaines de ces sources sont associées à de grandes régions d'absorption, probablement liées à leur localisation dans des régions de la Galaxie riches en formation stellaire (voir le paragraphe 3.3.3 pour plus de détails).

Astronomy & Astrophysics manuscript no. integral
January 11, 2008
© ESO 2008

Galactic hard X-ray sources discovered by *INTEGRAL* brought to light by multi-wavelength observations. ⋆

I. The nature of the companion star

S. Chaty[1], F. Rahoui[2,1], C. Foellmi[3], J. A. Tomsick[4], J. Rodriguez[1], and R. Walter[5]

[1] Laboratoire AIM, CEA/DSM - CNRS - Université Paris Diderot, DAPNIA/Service d'Astrophysique, Bât. 709, CEA-Saclay, FR-91191 Gif-sur-Yvette Cedex, France, e-mail: chaty@cea.fr
[2] ESO, Alonso de Cordova 3107, Vitacura, Casilla 19001, Santiago 19, Chile
[3] Laboratoire d'Astrophysique, Observatoire de Grenoble, BP 53, F-38041 Grenoble Cedex 9, France
[4] Space Sciences Laboratory, 7 Gauss Way, University of California, Berkeley, CA 94720-7450, USA
[5] INTEGRAL Science Data Centre, Chemin d'Écogia 16, CH-1290 Versoix, Switzerland

Received January 11, 2008; accepted January 11, 2008

ABSTRACT

Context. The hard X-ray *INTEGRAL* observatory has brought to light an emerging population of highly obscured X-ray binary systems in the course of being unveiled by means of multi-wavelength observations. Previous studies have shown that many of these sources are high-mass X-ray binaries hosting neutron stars orbiting around luminous and evolved companion stars.
Aims. To better understand this newly-discovered population, we have selected a sample of sources for which an accurate localization is available to identify the stellar counterpart and reveal the nature of the companion star and of the binary system.
Methods. We performed an intensive study of a sample of thirteen *INTEGRAL* sources, through multi-wavelength optical to NIR photometric and spectroscopic observations, using EMMI and SofI instruments at the ESO NTT telescope. We performed accurate astrometry and identified candidate counterparts for which we give the optical and NIR magnitudes. We detected many spectral lines allowing to determine the spectral type of the companion star. We fitted with stellar black bodies the mid-infrared to optical spectral energy distributions of these sources. From the spectral analysis and SED fitting we identified the nature of the companion stars and of the binary systems.
Results. By spectroscopic analysis of the most likely candidates we found the spectral types of IGR J16320-4751, IGR J16358-4726, IGR J16479-4514, IGR J17252-3616, IGR J18027-2016: They all host OB type supergiant companion stars, with IGR J16358-4726 likely hosting a sgB[e]. Our spectra also confirm the supergiant O and B nature of IGR J17391-3021 and IGR J19140+0951 respectively. From SED fitting we found that IGR J16418-4532 is a (likely OB supergiant) HMXB, IGR J16393-4643 a (likely BIV-V star) HMXB, and IGR J18483-0311 a likely HMXB system. By accurate astrometry, we rejected the proposed counterparts of IGR J17091-3624 and IGR J17597-2201, and we discovered two new candidate counterparts for each source, both suggesting an LMXB from SED fitting. We confirm the AGN nature of IGR J16558-5203. Finally, we report that NIR fields of four sources of our sample exhibit large-scale regions of absorption.
Conclusions. By putting together all these results, we show that the majority of these systems are high-mass X-ray binaries hosting supergiant companion stars. We therefore confirm that *INTEGRAL* is revealing a dominant class of obscured and short-living high-energy binary systems, and we suggest an association of these systems with regions of the Galaxy exhibiting large-scale absorptions. Stellar population models must in the future take these systems into account in order to assess realistic estimates of high-energy binary systems in our Galaxy.

Key words. Infrared: stars – X-rays: binaries, individuals: IGR J16320-4751, IGR J16358-4726, IGR J16393-4643, IGR J16418-4532, IGR J16479-4514, IGR J16558-5203, IGR J17091-3624, IGR J17252-3616, IGR J17391-3021, IGR J17597-2201, IGR J18027-2016, IGR J18483-0311, IGR J19140+0951 – Stars: supergiants

1. Introduction

The hard X-ray *INTEGRAL* observatory was launched on the 17th of October 2002, and since then, it has performed a detailed survey of the Galactic plane. The ISGRI detector on the IBIS imager (Lebrun et al., 2003) has discovered many new hard X-ray sources[1], including binary systems, pulsars and AGNs, all these so-called IGR sources being reported in Bird et al. (2007) and Bodaghee et al. (2007). One of the most important achievements of the *INTEGRAL* observatory to date

Send offprint requests to: S. Chaty
⋆ Based on ESO observations through programme # 073.D-0339.

[1] An updated list of these sources is maintained at http://isdc.unige.ch/~rodrigue/html/igrsources.html.

is that it is revealing hard X-ray sources which were not easily detected in earlier soft X-ray (typically < 10 keV) observations, bringing to light a previously hidden part of a population of highly obscured high-energy binary systems in our Galaxy. These objects share characteristics which previously had rarely been seen (see Dean et al. 2005). They are high-mass X-ray binaries (HMXBs) hosting a neutron star orbiting around an O/B companion star, in some cases a supergiant star (see e.g. Filliatre & Chaty 2004 and Pellizza et al. 2006), some of them being possibly long-period X-ray pulsars. Many of these new sources are highly absorbed, exhibiting column densities higher than about 10^{23} cm^{-2}, and concentrated in directions tangential to Galactic arms, as for instance the Norma arm (see Chaty & Filliatre 2005, Tomsick et al. 2004a and Walter et al. 2004b), the richest arm of our Galaxy in high-mass star forming regions. This short-living population hosts the likely progenitors of extremely compact binary objects, which are good candidates of gravitational wave emitters, and might constitute a key sample in the understanding of the evolution of high-energy binary systems.

Among these HMXBs hosting an O/B supergiant companion star, two classes, which might overlap, seem to appear (Chaty & Rahoui, 2006). The first class is constituted of intrinsically highly obscured hard X-ray sources, exhibiting a huge local extinction. The most extreme example of these sources is the highly absorbed source IGR J16318-4848 (Filliatre & Chaty, 2004). The second class exhibits fast and transient outbursts, with peak fluxes of order 10^{-9} erg s^{-1}cm^{-2} in the $20 - 40$ keV band, and lasting only a few hours, this last characteristic is very unusual among HMXBs. For this reason they are called Supergiant Fast X-ray Transients (SFXTs, Negueruela et al., 2006b). These SFXTs exhibit faint quiescent emission, and their hard X-ray spectra require a black hole or neutron star accretor. Among these sources, IGR J17544-2619 (Pellizza et al., 2006) seems to be the archetype of this new class of HMXBs, exhibiting long quiescence periods (Zurita Heras et al. in prep.).

Even if the *INTEGRAL* observatory can provide a localisation which is already very accurate above 10 keV ($\sim 2'$), it is not accurate enough to pinpoint the source at other wavelengths, which is necessary to reveal the nature of these sources. So the first step in the study of these sources is to look for an accurate localization of the hard X-ray sources by X-ray satellites such as *XMM-Newton*, *Swift* or *Chandra*. While *XMM-Newton* and *Swift* provide positions which are good enough to restrict the list of possible counterparts to a small number, only *Chandra* gives unique identifications in most cases (see for instance the multi-wavelength study of four *INTEGRAL* sources in the direction of the Norma arm by Tomsick et al. 2006, via *Chandra* localisation). Once the source position is known to better than several arcseconds, the hunt for the optical counterpart of the source can begin. However, a difficulty persists, due to the high level of interstellar absorption in this region of the Galaxy, close to the Galactic plane. Near-infrared (NIR) observations, thanks to accurate astrometry, and photometric and spectroscopic analysis, allow for the nature of these sources to be revealed, constraining the spectral type of the companion star and the type of the binary system.

Finally, mid-infrared (MIR) observations are required to understand why these sources exhibit a strong local absorption, by characterizing the nature of the absorbing matter, and determining if it is made of cold gas or dust, or anything else. Based on optical/NIR observations we are reporting here, we have performed MIR observations with the VISIR instrument on ESO VLT/UT3. These observations, focusing on the characterization of the presence, temperature, extension and composition of the absorbing material constituting the circumstellar medium enshrouding the obscured sources, are described in a companion paper by Rahoui et al. (2008).

Here we report on an intensive multi-wavelength study of a sample of 13 *INTEGRAL* sources belonging to both obscured and SFXT classes, for which accurate X-ray localizations are available, aimed at identifying their counterparts and constraining the nature of the companion star and of the binary system. We first describe the ESO optical/NIR photometric and spectroscopic observations, and build the spectral energy distributions (SEDs) in Section 2. We then review hard X-ray properties of each source, and report the results of our optical/NIR observations in Section 3. We give general results and discuss them in Section 4, and we provide our conclusions in Section 5.

2. Observations

The multi-wavelength observations that we describe here are constituted of astrometry, photometry and spectroscopy on 13 *INTEGRAL* sources indicated in Table 1. They were performed at the European Southern Observatory (ESO, Chile), in 2 domains: in optical ($0.4 - 0.8\,\mu$m) with the EMMI instrument and in NIR ($1 - 2.5\,\mu$m) with the SofI instrument, both on the 3.5m New Technology Telescope (NTT) at La Silla Observatory. Our optical and NIR observations were carried out as part of the programme ESO # 073.D-0339, through visitor mode [2].

2.1. Optical observations

On 2004 July 10 between UT 0.0 and 11.0 we obtained optical photometry in *B*, *V R*, *I* and *Z* bands of the sources given in the Table 2 with the spectro-imager EMMI, installed on the NTT. We used the large field of EMMI's detector, with the images binned by a factor 2, giving an image scale of $0.332''$ pixel^{-1} and a field of view of $9.0' \times 10.0'$. The photometric observations were performed with an integration time between 1 and 30 s for each exposure, as reported in Table 2. We observed five photometric standard stars of the optical standard star catalogue of Landolt (1992): PG 1633+099, PG 1633+099A; PG 1633+099B; PG 1633+099C and PG 1633+099D.

We also carried out optical spectroscopy on 2004 July 9, taking 30 spectra of the source IGR J17391-3021 with the low-resolution grism #1 of EMMI, with a slit of $1.0''$ providing a resolution of about 350, and a spectral range between 4370 and 10270 Å with a dispersion of about 7.3 Å. Each individual spectrum had an exposure time between 60 and 120 s, giving a total integration time between 720 and 1440 s, as reported

[2] The reduced data are available for retrieval at http://wikimbad.org.

in Table 3. We observed the spectro-photometric standard star LTT 7379 taken with a similar airmass to flux calibrate the optical spectra.

Finally, we obtained through internal DDT time long-slit low-resolution spectra of 2 sources –IGR J17252-3616 and IGR J18027-2016– with the spectro-imager EFOSC2 installed at the 3.6 m of La Silla Observatory.

2.2. NIR observations

We performed NIR photometry in J, H and K_s bands of the sources given in Table 1 on 2004 July 08-11 with the spectro-imager SofI, installed on the NTT. We used the large field of SofI's detector, giving an image scale of $0.288''$ pixel^{-1} and a field of view of $4.92' \times 4.92'$. The photometric observations were obtained by repeating a set of images for each filter with 9 different $30''$ offset positions including the targets, following the standard jitter procedure allowing to cleanly subtract the sky emission in NIR. The integration time varied between 10 and 50 s for each individual exposure, giving a total exposure time between 108 and 450 s. The NIR photometry results are given in Table 4. We observed three photometric standard stars of the faint NIR standard star catalogue of Persson et al. (1998): sj9157, sj9172 and sj9181.

We also carried out NIR spectroscopy with SofI between 0.9 and 2.5 μm, taking 12 spectra using alternatively the low-resolution Blue and Red grisms respectively, half of them with the $1.0''$ slit on the source and the other half with an offset of $30''$, in order to subtract the NIR sky emission. Each individual spectrum has an exposure time between 60 and 180 s, giving a total integration time between 720 and 2160 s in each grism, as reported in Table 3.

2.3. Data reduction

We used the IRAF (Image Reduction and Analysis Facility) suite to perform data reduction, carrying out standard procedures of optical and NIR image reduction, including flat-fielding and NIR sky subtraction.

We performed accurate astrometry on each entire SofI $4.92' \times 4.92'$ field, using all stars from the 2MASS catalogue present in this field[3] (amounting to $\sim$ 1000 2MASS objects). The rms of astrometry fit is always less than $0.''5$, and we obtained a pixel scale in x,y axis of -0.28783 and $0.28801''$/pixel respectively. The finding charts including the results of our astrometry are shown in Figures 2 and 3 for all sources of our sample.

We carried out aperture photometry, and we then transformed instrumental magnitudes into apparent magnitudes using the standard relation: $mag_{app} = mag_{inst} - Zp - ext \times AM$ where mag_{app} and mag_{inst} are respectively the apparent and instrumental magnitudes, Zp is the zero-point, ext the extinction and AM the airmass. We used for the extinction $ext_J = 0.06$, $ext_H = 0.04$ and $ext_{Ks} = 0.10$ typical of La Silla observatory.

[3] The pixel size of 2MASS is $2.''0$ and the position reconstruction error is $\sim 0.''2$.

The log of the observations and the results of photometry are given in Tables 2 and 4 for the optical and NIR respectively.

We analyzed the optical spectra using standard IRAF tasks, subtracting bias and correcting for flat field, and we used the *IRAF noao.twodspec* package in order to extract spectra and perform wavelength and flux calibrations. The optical spectra have been reduced and flux-calibrated in "F-lambda" units - erg cm^{-2}s^{-1}Å.

NIR spectra have been reduced using IRAF by flat-fielding, correcting the geometrical distortion using the arc frame, shifting the individual images using the jitter offsets, combining these images and finally extracting the spectra. The analysis of SofI spectroscopic data, and more precisely the sky subtraction, was difficult due to a variable sky, mainly in the red part of the blue grism, causing some wave patterns. The target spectra were then corrected for the telluric lines using a median of various standard stars observed with the same configuration during the corresponding nights. All spectra, optical and NIR, are finally shifted to the heliocentric rest frame.

2.4. SEDs

Once the most likely counterpart was identified through astrometry, photometry and spectroscopy when available, we were able to build the optical/NIR SEDs of all sources of our sample, shown in Figure 1. While these SEDs are mainly based on optical and NIR photometry from this paper, we also add MIR observations ($5 - 20$ μm) obtained with the VISIR instrument on Melipal, the 8 m third Unit Telescope (UT3) of the ESO Very Large Telescope (VLT) at Paranal Observatory, reported in the companion paper by Rahoui et al. (2008). In addition, we also put MIR data taken from the *Spitzer* GLIMPSE survey, reported in Rahoui et al. (2008), and in Table 5 for the sources not included in this companion paper. Finally, we also include in these SEDs data from X-ray observations taken with *INTEGRAL*/IBIS for all the sources, *XMM* for IGR J16418-4532, IGR J17252-3616 and IGR J19140+0951, *RXTE* for IGR J16358-4726, IGR J17091-3624, IGR J17597-2201 and IGR J17391-3021, *ASCA* for IGR J16320-4751, IGR J16393-4643 and IGR J16479-4514, *BeppoSAX* for IGR J18027-2016, and finally *INTEGRAL*/JEM-X for IGR J18483-0311.

We fitted the optical to MIR observing data with a black body emission reproducing the stellar emission. The broad band SEDs of these sources were modelled using an absorbed black-body emission component, representing the companion star emission (D_* and R_* are respectively the distance and radius of the star):

$$\lambda F(\lambda) = \frac{2\pi hc^2}{{D_*}^2 \lambda^4} 10^{-0.4A_\lambda} \left[\frac{{R_*}^2}{e^{\frac{hc}{\lambda k T_*}} - 1} \right] \quad \text{in W.m}^{-2} \qquad (1)$$

The free parameters of the fits were the absorption in the V band A_V, the companion star black-body temperature T_* and its $\frac{R_*}{D_*}$ ratio. The fits were performed using a χ^2 minimization.

Best-fitting parameters for individual sources, as well as corresponding χ^2 and 90%–confidence ranges of parameters, are reported in Table 6 for the sources IGR J16393-4643, IGR J16418-4532, IGR J17091-3624, IGR J17597-2201,

IGR J18027-2016 and IGR J18483-0311, and in Rahoui et al. (2008) for the remaining sources. The IGR J16558-5203 SED has not been fitted, because of its AGN nature. In this Table we also give the interstellar extinction in magnitude, A_i, obtained from the neutral hydrogen column density $N_{\rm HI}$, and the X-ray extinction in magnitude, A_X, obtained from X-ray observations. Both extinctions were converted to magnitudes using the conversion between $N_{\rm H}$ and A_v given by Predehl & Schmitt (1995). $N_{\rm HI}$ has been computed using the nH tool from HEASARC[4] (Dickey & Lockman, 1990). Since $N_{\rm HI}$ is the total galactic column density along the line of sight, it is likely overestimated compared to the real value at the distance of the sources.

Finally, we overplot on the SEDs of Figure 1 the best-fitted model to our observations. The dip seen at $\sim 4 \times 10^{13}$ Hz is due to silicate absorption present in our extinction model (more details on this model are given in Rahoui et al. 2008).

3. Results on individual sources

All the sources studied in this paper have been discovered with the IBIS/ISGRI detector onboard the *INTEGRAL* observatory. The sample of 13 sources, along with their position, uncertainty, and references about their discovery and position are given in Table 1. We present in the following our results on each source, for which we followed the same strategy. We first observed the field in optical and NIR, we performed accurate astrometry, and we derived the photometry of the candidates inside the X-ray satellite error circle. We then analyzed the optical/NIR spectrum of the most likely candidate, when available. Finally, we give the results of the optical-MIR SED fitting.

3.1. IGR J16320-4751

IGR J16320-4751 was discovered on 2003 February by Tomsick et al. (2003) at the position RA = $16^h32\overset{m}{.}0$, Decl. = $-47°51'$ (equinox J2000.0; uncertainty $2'$). Follow-up *XMM-Newton* observations localized the source at $16^h32^m01\overset{s}{.}9$ $-47°52'27''$ with $3''$ accuracy (Rodriguez et al. 2003; Rodriguez et al. 2006). It is a heavily absorbed variable source with $\rm N_H \sim 2.1 \times 10^{23} cm^{-2}$, and a hard X-ray spectrum fitted by an absorbed power-law, with $\Gamma \sim 1.6$ (Rodriguez et al., 2006). Soft X-ray pulsations have been detected on this source at a period of P$\sim 1309 \pm 40$ s with *XMM-Newton* and P$\sim 1295 \pm 50$ s with *ASCA* observations, these pulsations being the signature of an X-ray pulsar (Lutovinov et al., 2005b). An orbital period of 8.96 ± 0.01 days was found from a *Swift*/BAT lightcurve extending from 2004 December 21 to 2005 September 17 (Corbet et al., 2005), and of 8.99 ± 0.05 days with *INTEGRAL* (Walter et al., 2006). We point out that putting the spin and orbital periods of this source on a Corbet diagram (Corbet, 1986) allows us to suggest a supergiant HMXB nature. IGR J16320-4751 might have been persistent for at least 8 years, since this source is in fact the rediscovery of a previously known *ASCA* source AX J1631.9-4752.

We performed accurate astrometry of the field (rms of fit = $0\overset{''}{.}49$), and overplot the $3''$ *XMM-Newton* error circle in the finding chart of Figure 2. We give the infrared magnitudes of all the candidate counterparts in Table 4. Two candidate counterparts had been proposed for this source (Rodriguez et al., 2003), however the *XMM-Newton* $3''$ error circle made the ambiguity disappear, accurately localizing the candidate labeled 1 in Figure 2, and making it the most likely counterpart (2MASS J16320215-4752289; Rodriguez et al. 2006). This result is in agreement with Negueruela & Schurch (2007) rejecting candidate 2 on the basis of 2MASS photometry. In addition, Candidate 1 is much more absorbed than Candidate 2, as can be seen from the optical and NIR magnitudes given for both candidate counterparts in Tables 2 and 4 respectively, since Candidate 1 is invisible in the optical, but becomes as bright as Candidate 2 in the Ks band. We point out that there are in addition at least two faint candidate counterparts (labeled 3 and 4) inside the error circle, therefore it would be useful to get a more accurate position to unambiguously pinpoint the right counterpart. However, the faintness of Candidates 3 and 4 tends to rule them out as candidate counterparts, and in the following we will consider Candidate 1 as the most likely counterpart of this source.

NIR spectra of candidate 1 of IGR J16320-4751 are shown in Figure 4. We report the detected lines in Table 8. There are only a few lines visible in the blue NIR spectrum, probably because it is very faint and absorbed. The red NIR spectrum exhibits a very red continuum, and the presence of absorption and emission lines: the Pa(7-3) emission line, the Brackett series with P-Cygni profiles between 1.5 and 2.17 μm, and HeI at 2.166 μm (perhaps with P-Cygni profile). The presence of these narrow and deep Paschen and HeI lines, associated with P-Cygni profiles, are typical of early-type stars, and more precisely of luminous supergiant OB stars (Caron et al. 2003, Munari & Tomasella 1999), which is therefore the likely spectral type of the companion star. We also took optical and NIR spectra of Candidate 2: they do not exhibit any emission lines, and seem typical of a late-type star. Such a spectral type would therefore be hard to reconcile with the wind accretion hard X-ray spectra and the localization of this source in the Corbet diagram. Therefore both astrometry and spectroscopy allow us to exclude Candidate 2 as a candidate counterpart. These results strengthen Candidate 1 as the real counterpart of IGR J16320-4751. From the nature of the companion star and of the compact object, we derive that this source belongs to the very obscured supergiant HMXB class, hosting a neutron star. Finally, this result is also in agreement with the fit of its SED, computed in Rahoui et al. (2008), and shown in Figure 1.

3.2. IGR J16358-4726

IGR J16358-4726 was discovered on 2003 March 19 by Revnivtsev et al. (2003b) at the position RA = $16^h35\overset{m}{.}8$, Decl. = $-47°26'$ (equinox J2000.0; position uncertainty $1\overset{'}{.}5$). This hard X-ray source was observed for 25700 s serendipitously with *Chandra* during a scheduled observation of SGR 1627-41 on 2003 March 24. *Chandra* localized the source at ($16^h35^m53\overset{s}{.}8$, $-47°25'41\overset{''}{.}1$) with $0\overset{''}{.}6$ accuracy (Kouveliotou et al., 2003). We point out however that the uncertainty may

[4] http://heasarc.gsfc.nasa.gov/cgi-bin/Tools/w3nh/w3nh.pl

Table 1. Sample of sources. We give in this Table the name and coordinates of the sources: position (RA, DEC, J2000.0), galactic longitude and latitude (l,b), uncertainty (Unc. in arcmin) and reference (Ref1) of the discovery of the source by *INTEGRAL*; and position (RA, DEC, J2000.0), uncertainty (Unc.) and reference (Ref2) of the most accurate position by the satellite indicated in parenthesis. References are b: Bodaghee et al. (2006), c: Chernyakova et al. (2003), h: Hannikainen et al. (2003), i: in't Zand et al. (2006), ke: Kennea & et al. (2007), ko: Kouveliotou et al. (2003), ku: Kuulkers et al. (2003), l3: Lutovinov et al. (2003), ma: Malizia et al. (2004), mo: Molkov et al. (2003), re2: Revnivtsev et al. (2003b), re4: Revnivtsev et al. (2004), ro: Rodriguez et al. (2006), sg: Sguera et al. (2007), sm: Smith et al. (2006), st: Stephen et al. (2005), su: Sunyaev et al. (2003), t3: Tomsick et al. (2003), t4: Tomsick et al. (2004b), w4: Walter et al. (2004a), w6: Walter et al. (2006), z: Zurita Heras et al. (2006).

Source	RA	DEC	l	b	Unc.	Ref1	RA	DEC	Unc.	Ref2
IGR J16320-4751	248.006	-47.875	336.3	0.169	0.4	t3	$16^h32^m01\overset{s}{.}9$	$-47°52'27''$	$3''$ (*XMM*)	ro
IGR J16358-4726	248.976	-47.425	337.01	-0.007	0.8	re2	$16^h35^m53\overset{s}{.}8$	$-47°25'41\overset{''}{.}1$	$0\overset{''}{.}6$ (*Chandra*)	ko
IGR J16393-4643	249.775	-46.706	338.015	0.100	0.7	ma	$16^h39^m05\overset{s}{.}4$	$-46°42'12''$	$4''$ (*XMM*)	b
IGR J16418-4532	250.468	-45.548	339.19	0.489	1.0	t4	$16^h41^m51\overset{s}{.}0$	$-45°32'25''$	$4''$ (*XMM*)	w6
IGR J16479-4514	252.015	-45.216	340.16	0.124	1.4	mo	$16^h48^m06\overset{s}{.}6$	$-45°12'08''$	$4''$ (*XMM*)	w6
IGR J16558-5203	254.010	-52.062	335.687	-05.493	2.0	w4	$16^h56^m05\overset{s}{.}73$	$-52°03'41\overset{''}{.}18$	$3\overset{''}{.}52$ (*Swift*)	st
IGR J17091-3624	257.280	-36.407	349.5	2.2	0.5	ku	$17^h09^m07\overset{s}{.}6$	$-36°24'24\overset{''}{.}9$	$3\overset{''}{.}6$ (*Swift*)	ke
IGR J17252-3616	261.299	-36.282	351.5	-0.354	0.5	w4	$17^h25^m11\overset{s}{.}4$	$-36°16'58\overset{''}{.}6$	$4''$ (*XMM*)	z
IGR J17391-3021	264.800	-30.349	358.07	0.445	1.2	su	$17^h39^m11\overset{s}{.}58$	$-30°20'37\overset{''}{.}6$	$\sim 1''$ (*Chandra*)	sm
IGR J17597-2201	269.935	-22.026	7.581	0.775	0.6	l3	$17^h59^m45\overset{s}{.}7$	$-22°01'39''$	$4''$ (*XMM*)	w6
IGR J18027-2016	270.661	-20.304	9.418	1.044	0.7	re4	$18^h02^m42\overset{s}{.}0$	$-20°17'18''$	$4''$ (*XMM*)	w6
IGR J18483-0311	282.068	-3.171	29.760	-0.744	0.8	c	$18^h48^m17\overset{s}{.}17$	$-03°10'15\overset{''}{.}54$	$3.3''$ (*Swift*)	sg
IGR J19140+0951	288.516	9.878	44.30	-0.469	0.5	h	$19^h14^m4\overset{s}{.}232$	$+09°52'58\overset{''}{.}29$	$0\overset{''}{.}6$ (*Chandra*)	i

Table 2. Results in Optical. We indicate the name of the source, the date and UT time of the observations, the airmass (AM), the exposure time in seconds (ET) and the B, V, R, I and Z magnitudes. Z-band magnitudes are instrumental.

Source	Date	AM	ET	B	V	R	I	Z
IGR J16320-4751 C1	2004-07-10T03:04	1.1	30	$> 22.79 \pm 0.27$	$> 24.70 \pm 0.46$	$> 22.10 \pm 0.26$	$> 22.31 \pm 0.25$	$> 21.67 \pm 0.42$
IGR J16320-4751 C2	2004-07-10T03:04	1.1	30	18.97 ± 0.04	16.62 ± 0.02	15.32 ± 0.01	13.23 ± 0.02	13.781 ± 0.003
IGR J16358-4726	2004-07-10T04:40	1.2	30	$> 23.42 \pm 0.28$	$> 23.67 \pm 0.33$	23.75 ± 0.34	20.49 ± 0.10	18.59 ± 0.08
IGR J16393-4643	2004-07-10T06:56	1.8	30	$> 24.97 \pm 0.80$	21.53 ± 0.13	19.62 ± 0.05	17.92 ± 0.05	16.99 ± 0.02
IGR J17391-3021	2004-07-10T06:22	1.3	1	$> 21.16 \pm 0.71$	14.97 ± 0.02	12.94 ± 0.02	11.28 ± 0.02	10.458 ± 0.001

Table 3. Log of optical and NIR spectra. We indicate the name of the source, the telescope used, the date and UT time of the observations, the airmass (AM), the exposure time in seconds in optical and NIR (blue and red grisms respectively). All spectra were obtained at ESO/NTT with EMMI and SofI instruments, except the optical spectra of IGR J17252-3616 and IGR J18027-2016 obtained at ESO/3.6m with EFOSC2.

Source	Tel	Date	AM	optical	NIR blue grism	NIR red grism
IGR J16320-4751 C1	NTT	2004-07-08T23:18	1.255	-	2160	2160
IGR J16320-4751 C2	NTT	2004-07-10T03:36	1.112	1440	-	-
"	NTT	2004-07-08T23:18	1.255	-	2160	2160
IGR J16358-4726	NTT	2004-07-09T02:06	1.052	-	2160	2160
IGR J16479-4514	NTT	2004-07-10T23:35	1.222	-	720	720
IGR J17252-3616	3.6m	2005-10-01T01:49	1.683	4800	-	-
"	NTT	2004-07-11T01:08	1.083	-	720	720
IGR J17391-3021	NTT	2004-07-10T05:36	1.177	720	-	-
IGR J17391-3021	NTT	2004-07-09T04:24	1.038	-	1080	1080
IGR J18027-2016	3.6m	2005-09-30T02:38	2.006	1800	-	-
"	NTT	2004-07-11T02:34	1.036	-	720	720
IGR J19140+0951	NTT	2004-07-11T04:38	1.289	-	720	720

be somewhat underestimated since the source was $9\overset{'}{.}7$ from the *Chandra* aimpoint so that the point-spread function is significantly broadened. This source is a transient source, its hard X-ray spectrum being well fitted with a heavily absorbed power-law: $\Gamma \sim 0.5$ and $N_H \sim 3.3\,10^{23}\mathrm{cm}^{-2}$, with the presence of Fe Kα emission line (Patel et al., 2007). By performing detailed spectral and timing analysis of this source using multi-satellite archival observations, Patel et al. (2007) have detected 5880 ± 50 s periodic variations, which could be due either to the spin of a neutron star, or to an orbital period, and they identified a 94 s spin-up in 8 days, corresponding to a mean spin period derivative of 1.9×10^{-4} s/s, pointing to a neutron star origin. Assuming that this spin up is due to accretion, they estimate the source magnetic field to be between 10^{13} and 10^{15} G, suggesting that the compact object might be a magnetar. These

Table 4. Results in NIR. We indicate the name of the source (C1, C2, etc. indicate the different candidates as labeled in the finding charts of Figure 2), the date and UT time of the observations, the airmass, the exposure time (Exptime) in seconds, and the J, H and Ks magnitudes.

Source	Date	Airmass	Exptime	J	H	Ks
			(s)	1.25 μm	1.65 μm	2.2 μm
IGR J16320-4751 C1	2004-07-08T23:05	1.3	108	17.24±0.11	13.28±0.04	11.21±0.05
IGR J16320-4751 C2	2004-07-08T23:05	1.3	108	12.30±0.03	11.41±0.03	11.05±0.05
IGR J16320-4751 C3	2004-07-08T23:05	1.3	108	18.86±0.20	17.70±0.17	16.85±0.15
IGR J16320-4751 C4	2004-07-08T23:05	1.3	108	-	-	18.21±0.33
IGR J16358-4726	2004-07-09T01:43	1.1	450	15.46±0.04	13.57±0.03	12.60±0.05
IGR J16393-4643 C1	2004-07-09T06:25	1.5	108	14.62±0.03	13.26±0.03	12.67±0.05
IGR J16393-4643 C2	2004-07-09T06:25	1.5	108	16.25±0.08	15.46±0.09	14.88±0.10
IGR J16393-4643 C3	2004-07-09T06:25	1.5	108	-	17.87±0.97	15.47±0.24
IGR J16393-4643 C4	2004-07-09T06:25	1.5	108	16.24±0.10	14.79±0.07	14.68±0.13
IGR J16418-4532 C1	2004-07-11T05:55	1.4	108	14.03±0.03	16.62±0.03	11.61±0.05
IGR J16418-4532 C2	2004-07-11T05:55	1.4	108	16.48±0.09	19.44±0.26	14.76±0.09
IGR J16418-4532 C3	2004-07-11T05:55	1.4	108	17.48±0.17	20.60±0.51	16.12±0.27
IGR J16418-4532 C4	2004-07-11T05:55	1.4	108	18.06±0.17	21.05±0.51	16.96±0.30
IGR J16479-4514 C1	2004-07-10T23:21	1.3	108	13.06±0.02	10.92±0.02	9.79±0.05
IGR J16479-4514 C2	2004-07-10T23:21	1.3	108	16.22±0.07	15.53±0.08	15.02±0.10
IGR J16558-5203	2004-07-11T06:18	1.5	108	12.82±0.03	11.66±0.03	10.52±0.05
IGR J17091-3624 C1	2004-07-11T06:35	1.5	108	16.73±0.05	15.83±0.05	15.36±0.07
IGR J17091-3624 C2	2004-07-11T06:35	1.5	108	18.19±0.11	17.12±0.12	16.65±0.14
IGR J17252-3616 C1	2004-07-11T00:39	1.2	108	14.19±0.02	11.90±0.03	10.67±0.05
IGR J17252-3616 C2	2004-07-11T00:39	1.2	108	17.40±0.10	15.13±0.05	13.92±0.07
IGR J17252-3616 C3	2004-07-11T00:39	1.2	108	-	15.00±0.06	13.82±0.09
IGR J17252-3616 C4	2004-07-11T00:39	1.2	108	-	18.61 1.17	15.17±0.13
IGR J17391-3021	2004-07-09T04:08	1.0	108	9.09±0.02	8.70±0.02	8.16±0.05
IGR J17597-2201 C1	2004-07-11T01:36	1.1	108	16.78±0.10	14.84±0.07	14.13±0.08
IGR J17597-2201 C2	2004-07-11T01:36	1.1	108	16.13±0.08	14.24±0.06	13.49±0.07
IGR J17597-2201 C3	2004-07-11T01:36	1.1	108	18.50±0.23	17.36±0.28	17.28±0.44
IGR J17597-2201 C4	2004-07-11T01:36	1.1	108	17.80±0.13	16.62±0.12	16.30±0.22
IGR J17597-2201 C5	2004-07-11T01:36	1.1	108	19.19±0.25	17.89±0.20	17.22±0.36
IGR J17597-2201 C6	2004-07-11T01:36	1.1	108	17.62±0.25	15.59±0.12	14.68±0.11
IGR J18027-2016 C1	2004-07-11T02:08	1.1	180	12.81±0.02	11.95±0.03	11.50±0.05
IGR J18027-2016 C2	2004-07-11T02:08	1.1	180	13.97±0.03	13.3±0.04	13.14±0.06
IGR J18027-2016 C3	2004-07-11T02:08	1.1	180	17.61±0.22	16.75±0.23	16.08±0.29
IGR J18027-2016 C4	2004-07-11T02:08	1.1	180	16.88±0.14	15.65±0.15	15.20±0.24
IGR J18483-0311	2004-07-11T07:44	1.7	180	10.77±0.03	9.21±0.03	8.39±0.04
IGR J19140+0951	2004-07-11T04:26	1.3	108	11.32±0.02	9.73±0.02	8.84±0.04

Table 5. GLIMPSE fluxes (in mJy) for the sources IGR J16393-4643, IGR J16418-4532, IGR J18027-2016 and IGR J18483-0535. The fluxes for the other sources are given in Rahoui et al. (2008).

Sources	3.6 μm	4.5 μm	5.8 μm	8 μm
IGR J16393-4643	3.53 ± 0.52	2.89 ± 0.47	–	–
IGR J16418-4532	12.46 ± 0.90	9.45 ± 0.58	5.57 ± 0.58	3.58 ± 0.41
IGR J18027-2016	10.70 ± 0.28	7.40 ± 0.18	5.30 ± 0.26	2.50 ± 0.05
IGR J18483-0535	217.00 ± 8.90	164.00 ± 7.20	124.00 ± 5.50	67.00 ± 2.10

observations suggest that this source is an X-ray pulsar at a distance of $\sim 6-8$ kpc. No radio emission has been detected.

A 2MASS counterpart has been suggested by Kouveliotou et al. (2003) based on the accurate *Chandra* position (2MASS J16355369-4725398, with J = 15.41, H = 13.44, K = 12.59). We performed accurate astrometry of the field (rms of fit = 0.″45), and overplot the 0.″6 *Chandra* error circle, as shown in Figure 2. The 2MASS counterpart is at 1.2″ from the centre, therefore outside the error circle. On the other hand, this 2MASS counterpart might be a blended object, since it shows an extension towards the East, right at the position of the error circle. A better spatial resolution would allow to confirm or not whether the 2MASS candidate is the real counterpart of this source. However, its brightness favors this candidate, and in the following we consider it as the candidate counterpart. Optical and NIR magnitudes of this 2MASS candidate are given in Tables 2 and 4 respectively.

Table 6. Summary of parameters we used to fit the SEDs of the sources. We give in the table their name, the interstellar extinction in magnitudes A_i, the X-ray extinction of the source in magnitudes A_X and then the parameters of the fit: the extinction in the optical A_V, the temperature T_* and the $\frac{R_*}{D_*}$ ratio of the companion (more details on these parameters are given in the text). The 90%-confidence ranges of these parameters are given in parenthesis. We also give the reduced χ^2. The parameters for the other sources are given in Rahoui et al. (2008).

Sources	A_i	A_X	A_V	$T_*(K)$	$\frac{R_*}{D_*}$	χ^2/dof
IGR J16393-4643	11.71	133.61	11.5(10.9 – 11.8)	24400(12800 – 34200)	$2.21(1.81 - 3.13) \times 10^{-11}$	3.25/2
IGR J16418-4532	10.05	53.45	14.5(13.1 – 14.9)	32800(10600 – 36000)	$3.77(2.64 - 6.85) \times 10^{-11}$	1.5/4
IGR J17091-3624	4.13	5.34	6.8(2.0 – 9.6)	6900(3000, 34300)	$1.15(0.50 - 2.00) \times 10^{-11}$	1.005/1
IGR J17597-2201	6.251	24.05	16.1(13.1 – 17.1)	31700(6500 – 36000)	$1.28(1.30 - 3.00) \times 10^{-11}$	2.9/1
IGR J18027-2016	5.56	48.42	8.8(8 – 9.1)	20800(12800 – 32200)	$3.7(2.8 - 4.76) \times 10^{-11}$	6.00/4
IGR J18483-0535	8.66	148.1	17.4(16.9 – 18.3)	22500(16400 – 36000)	$2.15(1.75 - 2.75) \times 10^{-10}$	10/5

The NIR spectra of IGR J16358-4726 are shown in Figure 4. We report the detected lines in Table 8. The NIR spectrum is very faint and extremely absorbed, however we detect some lines even in the blue part of its spectrum, mainly HeII emission lines. The red part of the NIR spectrum exhibits a red continuum, and the presence of absorption and emission lines, with tentative P-Cygni profiles: the H Brackett series with P-Cygni profiles between 1.5 and 2.2 μm, and HeI and He II absorption lines. The presence of these lines, associated with P-Cygni profiles, are typical of an O/B supergiant star, which is therefore probably the spectral type of the companion star. In this case it would be a supergiant HMXB. In addtion, we clearly detect the forbidden [FeII] line at 2.22 μm (and tentatively the allowed FeII line at 1.98 μm), suggesting that the companion star is a sgB[e] star. Furthermore, it is interesting to note that Rahoui et al. (2008) propose, using an independent method of SED fitting, that the companion might be a sgB[e] star. Our result would therefore be in agreement with the fit of its SED, shown in Figure 1.

3.3. IGR J16393-4643

IGR J16393-4643 was discovered by Malizia et al. (2004) at the position (RA, DEC, J2000.0) = ($16^h39\overset{m}{.}3, -46°43'$) (2′ uncertainty). The improved position from *XMM-Newton*/EPIC is (RA DEC, J2000.0) = ($16^h39^m05\overset{s}{.}4, -46°42'12''$) (4″ uncertainty) which is compatible with that of 2MASS J16390535-4642137 (Bodaghee et al., 2006). It is a persistent, heavily-absorbed ($N_H = 2.5 \times 10^{23}$ cm^{-2}), and hard ($\Gamma = 1.3 \pm 1.0$) wind-accreting pulsar, and a pulse period of 912.0 ± 0.1 s was discovered in the ISGRI and EPIC light curves, characteristic of a spin period of an X-ray pulsar (Bodaghee et al., 2006). High column density and hard spectral index suggest that IGR J16393-4643 is an HMXB. This source exhibits large variations in intensity, and shows X-ray lines. An orbital period of 3.6875±0.0006 days has been detected from *Rossi-XTE* data, implying a mass function of $6.5 \pm 1.1\ M_\odot$ (or up to 14 $M_\odot$ if the orbit is eccentric; Thompson et al. 2006), this lower limit on the mass confirming that the system is an HMXB.

We performed accurate astrometry of the field (rms of fit = 0.″54). Inside the error circle, there is the 2MASS candidate counterpart proposed by Bodaghee et al. (2006) (2MASS J16390535-4642137), and in addition there are 3 more candidates, all labeled 1 to 4 respectively in Figure 2. They are located at 1.7, 3.1, 3.4 and 3.″3 respectively from the centre of the error circle. Optical and NIR magnitudes of these candidates are given in Tables 2 and 4 respectively. A more precise localization of the hard X-ray source is therefore necessary to know which is the real counterpart of the source, however Candidate 1 seems to be the likely counterpart based on the astrometry and on its NIR brightness.

We fitted its SED with the model described in Section 2.4, taking optical and NIR magnitudes of Candidate 1. We obtain a stellar temperature $T_* = 24400$K, typical of a B spectral type companion star. The other parameters are given in Table 6, and the SED is shown in Figure 1. By taking the R_*/D_* (2.21×10^{-11}) minimizing χ^2, and assuming a radius $R_* = 10\ R_\odot$ typical of a BIV-V spectral type companion star, we derive a distance of $D_* = 10.6$ kpc. On the other hand, by taking the minimum radius of a B supergiant star, i.e. at least 20 $R_\odot$, we derive a distance of nearly 20.4 kpc, probably too big to be plausible. The fit therefore is entirely consistent with its HMXB nature and favours a BIV-V companion star.

3.4. IGR J16418-4532

IGR J16418-4532 was discovered on 2003 February 1-5 at the position (RA DEC J2000.0) = ($16^h41\overset{m}{.}8, -45°32'$, 2′ uncertainty), towards the Norma region (Tomsick et al., 2004b). *XMM-Newton* localized the source at ($16^h41^m51\overset{s}{.}0, -45°32'25''$) with 4″ accuracy (Walter et al., 2006). *XMM-Newton* observations have shown that it is a heavily absorbed X-ray pulsar exhibiting a column density of $N_H \sim 1.0 \times 10^{23}$ cm^{-2}, a peak-flux of ∼80 mCrab (20-30 keV), and a pulse period of 1246 ± 100 s (Walter et al., 2006). This source is an SFXT candidate, as proposed by Sguera et al. (2006) using *INTEGRAL* observations. A 3.75 day modulation has been found in *Rossi-XTE*/ASM and *Swift*/BAT lightcurves, with a possible total eclipse, which would suggest either a high binary inclination, or the presence of a supergiant companion star (Corbet et al., 2006). We point out that the latter case would be consistent with the position of this object in the Corbet diagram.

We performed the astrometry of this source with 1139 2MASS stars (rms of fit = 0.″38). The field is shown in Figure 2. The centre of the *XMM-Newton* error circle is 2.2″ away

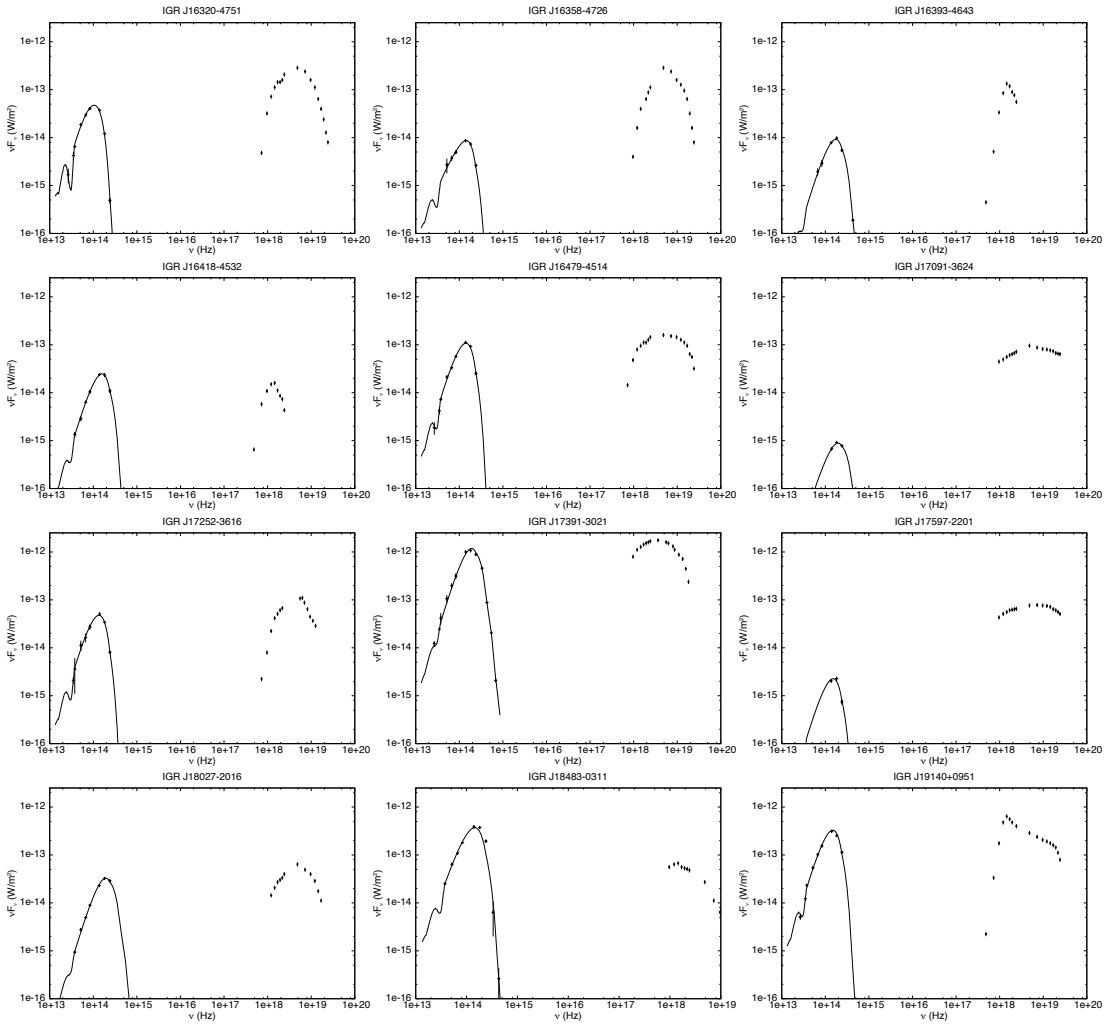

Fig. 1. SEDs of all these *INTEGRAL* sources, showing the observations from hard X-rays to MIR wavelengths. In each case, we overplot the black-body emission representing the stellar spectral type of the companion star, which is given in Table 7 for the sources IGR J16393-4643, IGR J16418-4532, IGR J17091-3624, IGR J17597-2201, IGR J18027-2016 and IGR J18483-0535, and in Rahoui et al. (2008) for the remaining sources. See Section 2.4 for more details on the X-ray data. From top to bottom, and left to right: IGR J16320-4751, IGR J16358-4726, IGR J16393-4643, IGR J16418-4532, IGR J16479-4514, IGR J17091-3624, IGR J17252-3616, IGR J17391-3021, IGR J17597-2201, IGR J18027-2016, IGR J18483-0311 and IGR J19140+0951.

from a bright 2MASS source (2MASS J16415078-4532253, labelled Candidate 1), as pointed out by Walter et al. (2006), however there are at least three more possible counterparts in the 4″ *XMM-Newton* error circle, not present in the 2MASS catalogue, at 1.9, 1.3 and 2.1″ respectively from the centre of the error circle. These additional candidate counterparts are labeled 2 to 4 respectively. We give their optical and NIR magnitudes in Tables 2 and 4 respectively. From the brightness in NIR we favor Candidate 1 as the candidate counterpart.

The fit of its SED, shown in Figure 1, and taking optical and NIR magnitudes as described in Section 2.4, gives a stellar temperature $T_* = 32800$K, suggesting an O/B spectral type companion star. The other parameters of the fit are given in Table 6. The R_*/D_* ratio which minimizes χ^2 (3.77×10^{-11}) allows to derive a minimal distance of 13 kpc for a supergiant, which is plausible. This source is therefore an HMXB, and could be a supergiant HMXB, consistent with its position in the Corbet diagram. We point out however its appartenance to the SFXT class is uncertain, based on its X-ray behaviour (Zurita Heras et al. in prep.).

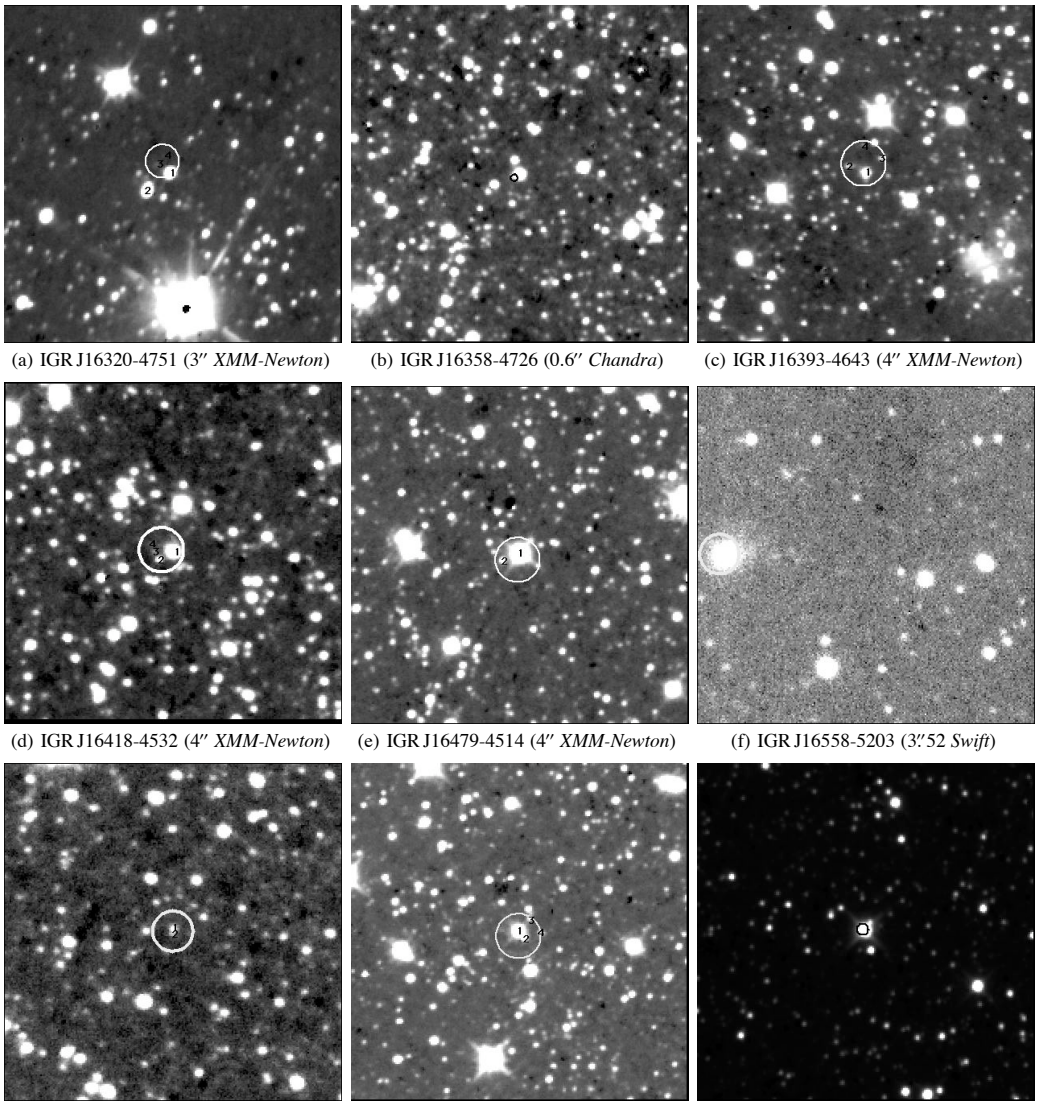

(a) IGR J16320-4751 (3″ *XMM-Newton*) (b) IGR J16358-4726 (0.6″ *Chandra*) (c) IGR J16393-4643 (4″ *XMM-Newton*)

(d) IGR J16418-4532 (4″ *XMM-Newton*) (e) IGR J16479-4514 (4″ *XMM-Newton*) (f) IGR J16558-5203 (3.″52 *Swift*)

(g) IGR J17091-3624 (3.6″ *Swift*) (h) IGR J17252-3616 (4″ *XMM-Newton*) (i) IGR J17391-3021 (1″ *Chandra*)

Fig. 2. Finding charts of the studied *INTEGRAL* sources, observed at ESO NTT telescope in the infrared Ks band (2.2 μm). Size: 1′x1′; North is to the top and East to the left. They are all centered apart from IGR J16558-5203, because the source was caught at the edge of the CCD. We overplot the most accurate localisation available to date.

3.5. IGR J16479-4514

IGR J16479-4514 has been discovered on 2003 August 8-9 at the position (RA DEC J2000.0) = ($16^h47.^m9$, −45°14′), uncertainty ∼ 3′, by Molkov et al. (2003). *XMM-Newton* observations localized the source at ($16^h48^m06.^s6$, −45°12′08″) with a 4″ accuracy (Walter et al., 2006). These *XMM-Newton* observations have shown that it exhibits a column density of $N_{\rm H} = 0.77 - 1.2 \times 10^{23}$ cm^{-2}. This source exhibits recurrent outbursts, making this source a fast transient with a peak-flux of ∼ 120 mCrab (20-60 keV) (Sguera et al. 2005; Sguera et al. 2006). There is an IR source IRAS 16441-4506 in the error circle.

We performed accurate astrometry of the field (rms of fit = 0.″41), shown in Figure 2. There is a bright J= 12.9, H=10.8 and K= 9.8 2MASS source (2MASS J16415078-4532253 = USNO-B1.0 0447-053133) 1.1″ away from the centre of the *XMM-Newton* error circle, which is the closest 2MASS source,

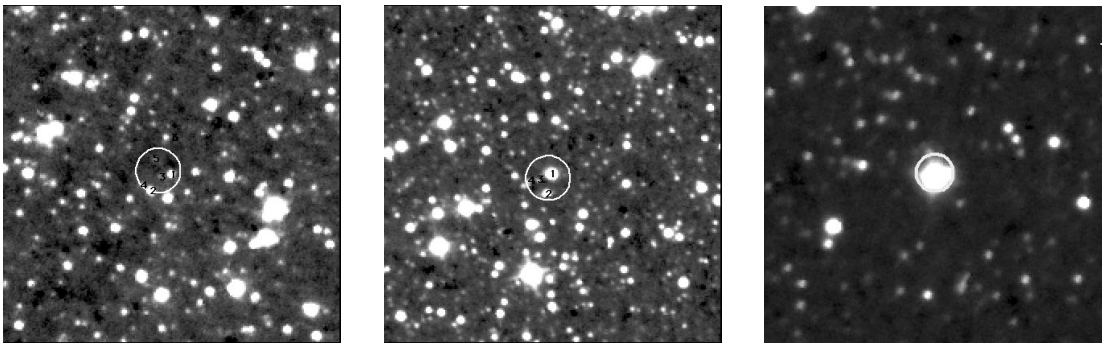

(a) IGR J17597-2201 (4″ *XMM-Newton*) (b) IGR J18027-2016 (4″ *XMM-Newton*) (c) IGR J18483-0311 (3.3″ *Swift*)

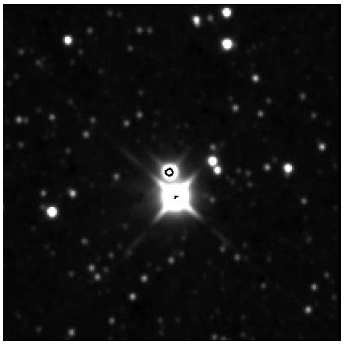

(d) IGR J19140+0951 (0.6″ *Chandra*)

Fig. 3. Figure 2 cont'd: finding chart of the studied *INTEGRAL* sources.

suggested by Walter et al. (2006) as being a candidate counterpart. In addition, we find another candidate counterpart inside the error circle, at 2.6″ from the centre of the error circle, labeled 2 in Figure 2. The optical and NIR magnitudes of both candidate counterparts are given in Tables 2 and 4 respectively. However, on the basis of the astrometry (close to the error circle centre) and the photometry (NIR brightness) we favour Candidate 1 as the candidate counterpart.

NIR spectra of Candidate 1 are shown in Figure 4. We report the detected lines in Table 8. We find emission of H (Brackett series) between 1.5 – 2.17 μm, and also HeI, HeII and FeII emission lines. These NIR spectra are typical of a supergiant O/B star, therefore strengthening Candidate 1 as the likely counterpart of this source, the companion star of IGR J16479-4514 having an OB spectral type. This source would therefore be a supergiant HMXB system, probably belonging to the SFXT class. Its SED, consistent with the HMXB nature of the system, is shown in Figure 1.

3.6. IGR J16558-5203

IGR J16558-5203 was discovered at the position (RA DEC J2000.0) = ($16^h55\overset{m}{.}8, -52°03$) with a 2′ uncertainty (Walter et al., 2004a). This source has a *ROSAT* counterpart (1RXS J165605.6-520345) at the position ($16^h56^m05\overset{s}{.}60, -52°03'45\overset{''}{.}5$), which allowed to reduce the uncertainty to 8″ (Stephen et al., 2005). Recently, the position has been refined by *Swift* observations at ($16^h56^m05\overset{s}{.}73, -52°03'41\overset{''}{.}18$) with a 3.″52 error circle radius (Malizia et al., 2007).

We performed accurate astrometry of the field, shown in Figure 2, and find that there is a bright 2MASS object inside the 3.″52 *Swift* error circle. The optical and NIR magnitudes of this object are given in Tables 2 and 4 respectively. This object is clearly extended on the NIR images, suggesting an extragalactic source. This is in agreement with the result from Masetti et al. (2006), who showed that this object was a Seyfert 1.2 AGN at a redshift of 0.054, exhibiting Hβ and OIII emission lines.

3.7. IGR J17091-3624

IGR J17091-3624 was discovered at the position (RA DEC J2000.0) = ($17^h09\overset{m}{.}1, -36°24'38''$), uncertainty ~ 3′ (Kuulkers et al., 2003). Follow-up analysis of archival data of TTM telescope aboard KVANT module of MIR orbital station revealed that this source had been detected in several observations performed on Oct.1-10, 1994, at the position (RA DEC J2000.0) = ($17^h09^m06^s, -36°24'07''$), error radius about 0.8′. This TTM position is within 0.6′ from the *INTEGRAL* posi-

tion (Revnivtsev et al., 2003a). It is also coincident with the SAX source 1SAX J1709-36. A variable radio counterpart has been detected in follow-up radio observations at the position ($17^h09^m02\overset{s}{.}3 \pm 0.4, -36°23'33''$), giving an error circle of 5″ radius (Rupen et al., 2003). Since this source was exhibiting some radio emission it has been classified as a galactic X-ray binary, and a candidate microquasar, probably hosting a black hole. It exhibits a large variability in X-rays, and it is uncertain if this source is a Be/X-ray binary or a LMXB. Capitanio et al. (2006) confirm the low absorption ($N_{\rm H} < 1 \times 10^{22}$ cm^{-2}) and comptonised spectrum of this source. Negueruela & Schurch (2007) proposed the 2MASS J17090199-3623260 source as a candidate counterpart, based on photometric catalogues. They report that this object is a late F8 V companion star. However, a more accurate position has been obtained by Kennea & et al. (2007): (RA DEC J2000.0) = ($17^h09^m07\overset{s}{.}6, -36°24'24\overset{''}{.}9$), error radius about $3\overset{''}{.}6$, which excludes the association of the high energy source with the radio source.

We have performed accurate astrometry of the field, shown in Figure 2, and we overplot the $3\overset{''}{.}6$ Swift error circle. We find that the claimed counterpart 2MASS J17090199-3623260 of Negueruela & Schurch (2007) is well outside this error circle, we can therefore reject it. We report the discovery of 2 blended candidate counterparts inside the error circle, labeled 1 and 2 in Figure 2 respectively, located at $0\overset{''}{.}5$ and $0\overset{''}{.}4$ from the centre of the error circle. We give the NIR magnitudes of these 2 candidate counterparts in Table 4. We need a more precise position for this source in order to pinpoint the real counterpart of this source, but we favour Candidate 1 as the likely counterpart, on the basis of its NIR brightness.

With only three infrared magnitudes for the two candidate counterparts labeled C1 and C2, the fit of their SEDs is not very accurate, with the model described in Section 2.4. In addition, there is no counterpart of this source in the Spitzer GLIMPSE survey (3.6 and 4.5 μm). We can therefore not firmly conclude on the nature of this binary system. However, it is interesting to note that the R_*/D_* 90% best fit values are very low ($= 1.15 \times 10^{-11}$). From these values we can compute the range of maximal radius that the massive star would have if it was at the maximal distance inside our Galaxy, at $D_* = 30$ kpc: we find $R_*max = [6.7 - 12.8\ R_\odot]$. Since the maximal radius of the companion star would be $\sim 13\ R_\odot$, this star can not be neither a supergiant, nor a giant. Alternatively, it could be a main sequence early-type star, but then located very far in our Galaxy. We therefore conclude that this object is more probably an LMXB system in the Galactic bulge.

3.8. IGR J17252-3616

IGR J17252-3616 was discovered on 2004 February 9 in the Galactic bulge region, at the position ($17^h25\overset{m}{.}2, -36°16'$) by Walter et al. (2004a). Observations performed by *XMM-Newton* on 2004 March 21 by Zurita Heras et al. (2006) localized the source at ($17^h25^m11\overset{s}{.}4, -36°16'58\overset{''}{.}6$) with 4″ accuracy. This source is a rediscovery of the *EXOSAT* source EXO 1722-363, based on similar timing and spectral properties. It has been shown to be a heavily absorbed ($N_{\rm H} \sim 1.5 \times 10^{23}$ cm^{-2}) and persistent source, exhibiting apparent total eclipses, and a hard X-ray spectrum with either an absorbed compton (kT~5.5 keV and $\tau \sim 7.8$) or a flat power law ($\Gamma \sim 0.02$), a very large column density, and Fe Kα line at 6.4 keV. The detection of a spin period of ~ 413.7 s and an orbital period of ~ 9.72 days securely classified this source as a binary X-ray Pulsar (Zurita Heras et al., 2006). Thompson et al. (2007) refined the orbital period to P=9.7403 days with data collected over more than 7 years. They also derived a mass function of the system of 11.7 solar masses, suggesting an HMXB nature. In addition, we point out that putting the spin and orbital periods of this source on a Corbet diagram (Corbet, 1986) allows us to suggest a supergiant HMXB nature.

We performed accurate astrometry of the source, and overplot the *XMM-Newton* error circle, as shown in Figure 2. There is a bright 2MASS counterpart, 2MASS J17251139-3616575 (Ks=10.7, labelled Candidate 1), inside the error circle, as suggested by Walter et al. (2006). However, we point out that in addition to the 2MASS source, there are three fainter candidate counterparts inside the 4″ *XMM-Newton* error circle, labelled 2 to 4 respectively. All these candidates are located at 0.7, 1.4, 3.7 and 3.9″ respectively from the centre of the error circle. One of these is blended with the 2MASS counterpart. IGR J17252-3616 would therefore benefit of a more accurate localization, however based on astrometry and NIR brightness, we favour Candidate 1 as the most likely candidate counterpart. Optical and NIR magnitudes of these candidate counterparts are given in Tables 2 and 4 respectively.

Optical and NIR spectra of the 2MASS counterpart (Candidate 1) are shown in Figure 5. We report the detected lines in Table 8. We find emission lines of H (Paschen and Brackett), HeI and HeII lines with likely P-Cygni profiles at 2.06 μm, and perhaps FeII. From these NIR spectra, typical of an OB star we conclude that the companion star of this source has an OB spectral type. This result is in agreement with the suggestion by Zurita Heras et al. (2006), based on the presence of this bright 2MASS source in the error circle. This source is therefore an HMXB system, probably hosting a supergiant companion star, in agreement with the results by Thompson et al. (2007), and in agreement with its position in the Corbet diagram. The SED, consistent with the HMXB nature of the system, is shown in Figure 1.

3.9. IGR J17391-3021

IGR J17391-3021 was discovered on 2003 August 26 at the position (RA DEC J2000.0) = ($17^h39\overset{m}{.}1, -30°21\overset{'}{.}5$) with a 3′ uncertainty by Sunyaev et al. (2003). *Chandra* observations performed on 2003 October 15 localized the source at ($17^h39^m11\overset{s}{.}58, -30°20'37\overset{''}{.}6$) with a $\sim$ 1″ accuracy (Smith et al., 2006). It is a rediscovery of a previously known *ASCA* and *Rossi-XTE* source AX J1739.1-3020 = XTE J1739-302 (Smith, 2004). Negueruela et al. (2006a) have suggested that the optical counterpart of IGR J17391-3021 is a USNO A2.0 source (USNO B1.0 0596-058586) with B=17 and R=12.9, and that the NIR counterpart is a bright 2MASS source (2MASS J17391155-3020380 with J=8.600 ± 0.021,

H=7.823 ± 0.027 and Ks=7.428 ± 0.023; Smith et al. 2006). They also showed that the source is highly reddened, with a variable absorption column density between outbursts. During both low and high level states it exhibits hard X-ray spectra. The fast X-ray transient behaviour (typical of an SFXT) and neutron star spectrum have been confirmed by analyzing archival *INTEGRAL* data, with flares lasting between 30 min and 3 hours (Sguera et al., 2005), the bright ones reaching 330 mCrab (Türler et al., 2007). Negueruela et al. (2006a) state that this source is most likely an HMXB, however the outbursts are shorter than expected for HMXBs or Be/NS binaries, consistent with the SFXTs.

We performed accurate astrometry of the field (rms of fit = 0.″47), and overplot the *Chandra* error circle, as shown in Figure 2. Optical and NIR magnitudes of the candidate counterpart are given in Tables 2 and 4 respectively. However we point out that the NIR magnitudes are out of the domain of linearity of SofI, which explains the discrepancy with the 2MASS magnitudes. We find that this 2MASS source is a blended source, however from the astrometry, it is clear that the 1″ *Chandra* error circle confirms that the 2MASS source is the counterpart of this source.

We examine the optical and NIR spectra shown in Figure 5. We report the detected lines in Table 8. In the optical spectrum, we first detect interstellar lines at 5800, 5890-6 (NaI Doublet), Hα, H lines (Paschen), HeI and HeII emission lines, NI lines. The NIR spectrum is very rich in H lines from the Paschen and Brackett series, and also in HeI and HeII emission lines, some exhibiting P-Cygni profiles, and OI lines. All these lines are characteristic of early-type stars, more precisely of a supergiant O star, in agreement with the O8Iab(f) spectral type derived by Negueruela et al. (2006a). IGR J17391-3021 is therefore a supergiant HMXB, located at a distance of ∼ 2.3 kpc (Negueruela et al., 2006a), and not a Be as stated in Bird et al. (2006). The SED, consistent with the HMXB nature of the system, is shown in Figure 1.

We can determine the column density along the line of sight, using the equivalent width of the NaI Doublet = 9Å; E(B-V) = $0.25 \times W$(Å) = 2.25 magnitudes (using Munari & Zwitter (1997)); $N(HI + H2) = 5.8 \times 10^{21} \times E(B-V) = 1.3 \times 10^{22}$ atoms/cm^2 (using Bohlin et al. 1978), the column density is consistent with the one indicated in Table 7.

3.10. IGR J17597-2201

IGR J17597-2201 was discovered at the position (RA DEC J2000.0) = ($17^h59^m.7, -22°01'$) with ∼ 2′ uncertainty (Lutovinov et al., 2003). *XMM-Newton* observations localized the source at ($17^h59^m45^s.7, -22°01'39''$) with a 4″ accuracy (Walter et al., 2006). It exhibits an absorption of $N_{\rm H} = 4.5 \pm 0.7 \times 10^{22}$ cm^{-2}, or $2.70 \pm 0.15 \times 10^{22}$ cm^{-2} when a partial-covering absorber is included. This source, associated with the *Rossi-XTE* source XTE J1759-220, is a Low Mass X-ray Binary system, a late-type transient type I X-ray burster, therefore hosting a neutron star, with a dipping behavior of ∼ 30% with ∼ 5 min dip duration (Markwardt & Swank, 2003).

We performed accurate astrometry of the field, shown in Figure 2. Walter et al. (2006) proposed a 2MASS counterpart for this source (2MASS J17594556-2201435), however it is well outside the error circle, towards the South-West, at 5.1″ from the centre of the error circle. There are one bright and two faint candidate counterparts which are well inside the *XMM-Newton* error circle (labeled 1, 3 and 5 and located respectively at 2.25, 0.95 and 2.05″ from the centre of the *XMM-Newton* error circle). In addition, there are one faint and one bright candidate counterparts, sitting on the error circle (labeled 2 and 4, and located respectively at 3.8 and 3.9″ from the centre of *XMM-Newton* error circle). We give the NIR magnitudes of these candidate counterparts in Table 4. Since the previously proposed counterpart is outside the error circle, and since we propose new candidate counterparts, this source deserves further observations to find which one is the right counterpart.

By fitting the SED of the brightest candidate labeled 1, which is also the closest to the error circle centre, with the model described in Section 2.4, we obtain a stellar temperature $T* = 31700$ K, consistent with an O type star. The other parameters are given in Table 6, and the SED is shown in Figure 1. However we point out that our spectral fit is not accurate enough to unambiguously constrain the spectral type of the companion star, because we have only the three NIR magnitudes (we did not detect any MIR counterpart in the Spitzer GLIMPSE survey). Therefore, taking into account the errors, this SED fitting is consistent at 90% both with an LMXB and HMXB system. Assuming the source is a supergiant, with a minimum radius of 20 $R_\odot$, and taking a mean R_*/D_* of 2×10^{-11}, we obtain a distance of 35.2 kpc, which is not plausible. Alternatively, taking a radius $R_* = 10\ R_\odot$ typical of a B V companion star, we derive a distance of $D_* = 15.2$ kpc, a more reasonable estimate although still high. We therefore conclude that the source is most likely an LMXB, consistent with the X-ray properties, given the detection of type I X-ray bursts.

3.11. IGR J18027-2016

IGR J18027-2016 was discovered at the position (RA DEC J2000.0) = ($18^h02^m46^s, -20°16'.3$) (Revnivtsev et al., 2004). *XMM-Newton* observations allowed to localize the source at ($18^h02^m42^s.0, -20°17'18''$) with a 4″ accuracy (Walter et al., 2006). We point out that the source was originally called IGR J18029-2016, and that it is associated with the SAX source SAX J18027-2017. The absorption is $N_{\rm H} = 9.1 \pm 0.5 \times 10^{22}$ cm^{-2} (Walter et al., 2006). It is an X-ray pulsar, and a transient source, an eclipsing HMXB, likely at a distance of 10 kpc. An orbital period of 4.57 days and a pulse period of 139.47 s have been discovered by Hill et al. (2005). These authors have derived the system parameters, with an excentricity of e< 0.2, a mass function of f(M)∼ 17 ± 5 $M_\odot$, implying a mass of the companion of 18.8 − 29.3 $M_\odot$.

We performed accurate astrometry of this source (rms of fit = 0.″51), showed in Figure 2. There is a 2MASS counterpart (2MASS J18024194-2017172) at ∼ 1″ from the centre of the *XMM-Newton* error circle, which is the candidate counterpart proposed by Walter et al. (2006). However there is another

bright source well inside the error circle, labeled Candidate 2. There is also at least one faint counterpart inside the error circle. We give the NIR magnitudes of Candidate 1 and Candidate 2 in Table 4 respectively. Based on the proximity to the error circle centre, and its NIR brightness, we favour Candidate 1 as the likely candidate.

The optical and NIR spectra of Candidate 1 are shown in Figure 5. We report the detected lines in Table 8. In the optical spectrum we detect Hydrogen (α to ζ) and HeII emission lines, and in the NIR spectrum we detect H (Paschen and Brackett series), HeI and HeII emission lines, some tentatively exhibiting P-Cygni profiles. These NIR spectra are typical from a supergiant OB star, which is therefore likely the spectral type of the companion star: IGR J18027-2016 is therefore a supergiant HMXB system. Fitting the data with the model described in Section 2.4, we obtain a stellar temperature $T_* = 20800$K, which is typical of a B supergiant star. The other parameters are given in Table 6, and the SED is shown in Figure 1. By taking the R_*/D_* minimizing χ^2 (3.7×10^{-11}), and assuming a typical radius of a B supergiant star, i.e. $R_* = 20\ R_\odot$, we derive a distance of $D_* = 11.9$ kpc. We therefore favour the supergiant nature of the companion star, with a B spectral type, in agreement with the results derived from the spectra.

3.12. IGR J18483-0311

IGR J18483-0311 was discovered at the position (RA DEC J2000.0) = ($18^h48^m3, -03°11'$), with uncertainty $\sim 2'$ (Chernyakova et al., 2003). The *Swift* observations allowed Sguera et al. (2007) to refine the position of the source to ($18^h48^m17^s.17, -03°10'15''.54$), uncertainty 3.3″. The *Swift* refined position allowed them to identify an optical counterpart from the USNO-B1.0 and 2MASS catalogue located at ($18^h48^m17^s.2, -03°10'16''.5$) with magnitudes R=19.26, I=15.32, J=10.74, H=9.29 and K=8.46. The source exhibits a column density of $N_{\rm H} = 9 \times 10^{22}$ cm^{-2}, a $\Gamma = 1.4$ and an energy cutoff at $E_{cut} = 22$ keV (Sguera et al., 2007). Timing analysis of *Rossi-XTE*/ASM light curve have allowed to derive an orbital period of 18.55 ± 0.05 days (Levine & Corbet, 2006). Sguera et al. (2007) also report that the source contains a pulsar with a spin period of 21.0526 ± 0.0005 s with a pulse fraction of $65 \pm 10\%$, while the highly reddened optical counterpart suggests by analogy with other such systems that the source is an HMXB. They further argue that it is a likely Be system due to its localization in a Corbet diagram (Corbet, 1986), but they can not rule out an SFXT, although the typical ratio between maximum and minimum luminosity they observed is at least 10 times lower than that of typical SFXT.

We performed accurate astrometry of this source (rms of fit = 0.″67), showed in Figure 2. There is a bright 2MASS counterpart inside the *Swift* error circle, which is the candidate counterpart proposed by Sguera et al. (2007). However this source seems to be blended with another fainter source, at 2.5″ from the centre of the error circle. We give the NIR magnitudes of the bright candidate counterpart in Table 4.

Fitting the SED of this counterpart with the model described in Section 2.4, allows us to derive a stellar temperature of $T_* = 22500$K in the limit of 90% of χ^2, which is typical of a B star. The other parameters are given in Table 6, and the SED is shown in Figure 1. The stellar temperature is consistent with a B spectral type companion star. Since the R_*/D_* ratio minimizing χ^2 is 2.15×10^{-10}, the distance of this source would then be 0.9 kpc if the companion star is a main sequence star (with a typical stellar radius of $R_* = 3\ R_\odot$), 1.5 kpc for a sub-giant and 2.7 kpc for a supergiant star (with a typical stellar radius of $R_* = 20\ R_\odot$). This source exhibits a strong NIR excess, which might indicate the presence of a disk/wind such as in massive stars. Furthermore, its position in the Corbet diagram is inbetween Be and wind accretor-supergiant X-ray binary systems. Although we can not firmly conclude on the spectral type and class, this SED fitting definitely shows that this source is an HMXB system.

3.13. IGR J19140+0951

IGR J19140+0951 has been discovered on 2003 March 6-7 at the position (RA DEC J2000.0) = ($19^h13^m55^s, +9°51'.6$), uncertainty 1′) by Hannikainen et al. (2003). *Chandra* observations performed on 2004 May 11 localized the source at ($19^h14^m4^s.232, +09°52'58''.29$) with a 0.6″ accuracy (in't Zand et al., 2006). Fitting the hard X-ray spectrum from *Rossi-XTE* observations allowed to derive a $\Gamma \sim 1.6$ and $N_{\rm H} \sim 6 \times 10^{22}$cm^{-2} (Swank & Markwardt, 2003) with variations of $N_{\rm H}$ up to $\sim 10^{23}$ cm^{-2} (Rodriguez et al., 2005). An orbital period of 13.55 days has been found from timing analysis of *Rossi-XTE* data, with an X-ray activity detected with *Rossi-XTE*/ASM as early as 1996 (Corbet et al., 2004), confirming the binary nature of the source. Rodriguez et al. (2005), after a comprehensive analysis of *INTEGRAL* and *Rossi-XTE* data, showed the source was spending most of its time in a faint state but reported high variations of luminosity and absorption column density. It is a persistent HMXB with evidence for the compact object being a neutron star rather than a black hole, exhibiting a variable absorption column density, and a bright iron line (Rodriguez et al., 2005). We point out that this source has other names: IGR J19140+098 (Hannikainen et al., 2003), and EXO 1912+097. in't Zand et al. (2006) proposed the 2MASS source 2MASS J19140422+0952577 as the NIR counterpart of this source.

We performed accurate astrometry of the field (rms of fit = 0.″35), showed in Figure 2. The accurate error circle allows us to localize a candidate counterpart (J=11.8, H=11.5 and K= 11.4 magnitude) in the glare of the bright source 2MASS 19140422+0952577 located at 1.5″ (J=8.55, H=7.67 and Ks= 7.06 magnitude). We give the NIR magnitudes of the deblended source in Table 4 respectively.

We show the NIR spectra of this source in Figure 4. We report the detected lines in Table 8. The spectrum is dominated by H (Paschen and Brackett series), and HeI and HeII in emission. The NIR spectra are typical from an OB spectral type companion star, and the narrowness of the lines points towards a supergiant type, which is consistent with the results by Nespoli et al. (2007) of a B1I stellar type companion, derived from spectra obtained at ESO/NTT/SofI. This classification has been refined

to B0.5I based on spectra obtained at UKIRT (Hannikainen et al., 2007), making IGR J19140+0951 a supergiant X-ray binary. Both classifications confirm the supergiant HMXB nature of IGR J19140+0951, hosting a neutron star. The SED, consistent with the HMXB nature of the system, is shown in Figure 1.

We point out that in't Zand et al. (2006) also suggest a MIR counterpart at 8.3 μm found in the Midcourse Space Experiment (*MSX*, Mill 1994), however Rahoui et al. (2008) show that in't Zand et al. (2006) are in fact reporting the summed flux of a blended source, composed of the MIR counterparts of both IGR J19140+0951 and the bright 2MASS source at the South, which is unrelated with IGR J19140+0951. Rahoui et al. (2008) give the MIR fluxes of the counterpart of IGR J19140+0951.

4. Discussion

We begin this Section by giving a summary of the results on all individual sources constituting our studied sample. We continue by showing the large scale environment of these sources, and reporting the presence of absorption in their environment. We then recall the general characteristics of HMXBs, before finishing by putting together and discussing all the results obtained in this paper, in the context of the *INTEGRAL* era.

4.1. Summary of results on the sample of studied sources

In this paper, we found by spectroscopy of the most likely candidate counterparts the spectral types of IGR J16320-4751, IGR J16358-4726, IGR J16479-4514, IGR J17252-3616 and IGR J18027-2016: they are all of supergiant OB types, IGR J16358-4726 likely hosting a sgB[e] companion star. We also confirm the supergiant O nature of IGR J17391-3021, and the supergiant B nature of IGR J19140+0951. By fitting the SED of the most likely candidates we found that IGR J16418-4532 is an HMXB, probably hosting a supergiant O/B spectral type companion star, that IGR J16393-4643 is an HMXB system probably hosting a BIV-V companion star, and that IGR J18483-0311 is very likely an HMXB system. By an accurate astrometry we rejected the counterpart proposed for IGR J17091-3624 and IGR J17597-2201, we propose two new candidate counterparts for each of them, which by SED fitting we found consistent with an LMXB nature. Finally, we confirm the AGN nature of IGR J16558-5203.

We summarize in Table 7 the results we obtained both by spectroscopy and SED fitting on the sample of studied *INTEGRAL* sources. We put together in this Table the results on the column density in optical/IR, spectral type of the companion stars, and type of sources for all individual sources of our studied sample. Furthermore, we add in this Table all the parameters known about these sources, such as the spin and orbital period, when known, and column density derived from X-ray observations, in order to facilitate the following discussion. The interstellar column density and absorption in the optical and NIR domain have been derived from our observations, given in Table 6 for the sources IGR J16393-4643, IGR J16418-4532, IGR J17091-3624, IGR J17597-2201, IGR J18027-2016 and IGR J18483-0535, and in Rahoui et al. (2008) for the remaining sources. We then converted the column density into absorption in magnitudes, using the relation given in Cardelli et al. (1989): $N_{\rm H}/A_{\rm v} = 1.87 \times 10^{21}$ cm^{-2}/ magnitudes.

The results, concerning the spectral type of the companion star, given by these SED fittings are in complete agreement with those directly derived from the spectroscopy, when available. On the other hand, they allow us to derive the likely spectral type of the companion star, when there is no spectroscopic information. We can therefore conclude that most of these obscured sources host luminous, massive, hot and early-type companion stars, i.e. of O/B spectral type, most of them being evolved stars of the supergiant spectral class.

From these SEDs, all reported in Figure 1, we can directly compare the optical to MIR with the hard X-ray domain integrated flux (corresponding to the energy output). All sources for which both fluxes are comparable are supergiant HMXBs: IGR J16418-4532, IGR J16479-4514, IGR J17252-3616, IGR J17391-3021, IGR J18027-2016, IGR J19140+0951. These comparable optical–MIR and hard X-ray fluxes are expected from the HMXB nature of the systems. Most of the sources for which the hard X-ray flux is much higher than the optical–MIR flux are HMXBs, hosting either a supergiant or B type companion star: IGR J16320-4751, IGR J16358-4726, IGR J16393-4643. IGR J17091-3624 and IGR J17597-2201 are the only cases with a hard X-ray flux higher than the optical–MIR flux, consistent with their LMXB nature. Finally, there is only one case where the hard X-ray flux is much less than the optical–MIR flux: the HMXB IGR J18483-0311. We point out however that the multi-wavelength observations put together in these SEDs were not taken simultaneously, and that the hard X-ray fluxes are variable.

4.2. Environment

Four sources among the studied sample exhibit large-scale regions of absorption in the NIR images, very close to the line of sight of the hard X-ray source: IGR J16358-4726, IGR J16418-4532, IGR J16479-4514 and IGR J17391-3021. We show in Figure 6 the large field J band image of these sources (except for IGR J16479-4514 for which we show the large field Ks band image). This absorption region might be due to the presence of extended molecular clouds and/or H II regions. The presence of such highly absorbed regions is not so surprising close to these peculiar hard X-ray sources, since they must be strongly linked to their formation. For instance, the Norma arm region is one of the richest star-forming region of our Galaxy, where many high-mass stars form and evolve (Bronfman et al., 1996). There exists therefore a high probability for binary systems constituted of high-mass stars to form, and evolve into HMXBs (see for instance Tauris & van den Heuvel 2006). This might eventually explain why so many binary systems with high-mass companion stars and progenitors of compact objects

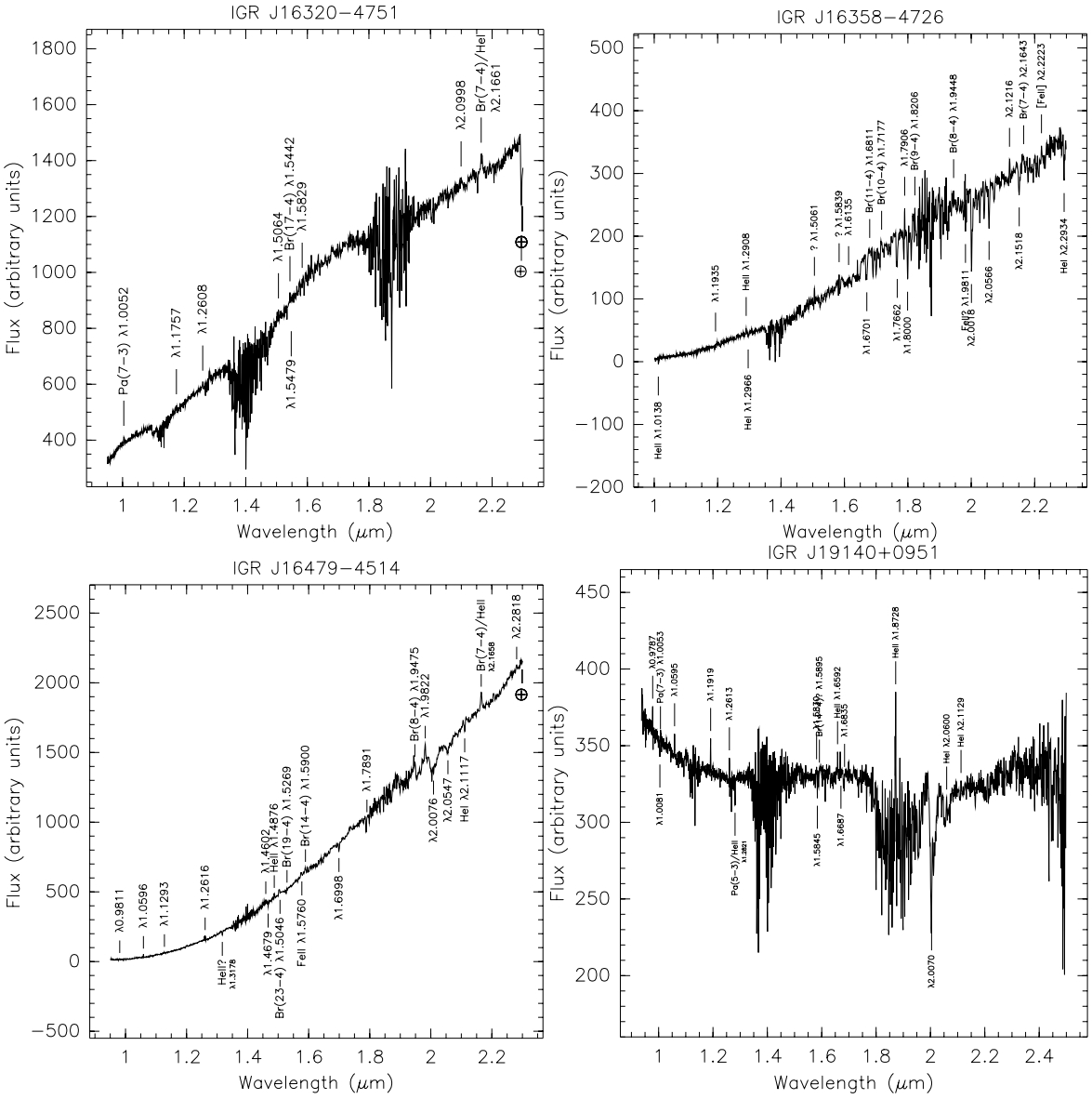

Fig. 4. From top to bottom, and left to right: combined blue and red grism NIR spectra of IGR J16320-4751 (Candidate 1), IGR J16358-4726, IGR J16479-4514 (Candidate 1) and IGR J19140+0951 (the y axis is in arbitrary units).

such as black hole or neutron stars can have formed in this region of our Galaxy.

Bodaghee et al. (2007) have compared the spatial distribution of HMXBs discovered by *INTEGRAL* –for which the distance is known– and of star-forming complexes –mainly OB regions reported by Russeil (2003)–. They have shown that their spatial distribution is similar, suggesting that HMXBs are associated with these complexes. The discovery of large-scale absorption regions in the direction of these sources is therefore not surprising, since the formation sites of HMXBs are closely linked to rich star forming regions. Indeed, the short life of HMXBs prevents these systems to go far away from their birthplace. One thing which would need to be done in the future is to characterize these large-scale absorption regions, and to measure the metallicity of stars hosted by these regions.

Table 7. Summary of results and characteristics of our studied sample of *INTEGRAL* sources. We give in this Table the name of the sources, the region of the Galaxy in the direction of which they are located, their spin and orbital period, the interstellar column density (N_HI), the absorption derived from optical to infrared observations (N_HIR), the absorption derived from X-ray observations (N_HX), the spectral type (SpT) of their most likely candidate obtained or confirmed by spectroscopy (spec) or by fitting the SED (sed), the nature and type of the binary system, and the reference (Ref) about the spectral type. More details on each source are given in Section 3. Details on how were obtained N_HI, N_HIR and N_HX are given in Section 2.4. Type abbreviations: AGN = Active Galactic Nucleus, B = Burster (neutron star), BHC = Black Hole Candidate, D = Dipping source, LMXB = Low Mass X-ray Binary, HMXB = High-Mass X-ray Binary System, OBS = obscured source, SFXT = Supergiant Fast X-ray Transient, T: Transient source, XP: X-ray Pulsar. The classification as SFXT is still subjective, since we miss some accurate observations on a long-term scale for most of the sources. The spectral types come from optical/NIR spectroscopy, reported in the references given in the column Ref. c: this paper, h: Hannikainen et al. (2007), m: Masetti et al. (2006), neg: Negueruela et al. (2006a), nes: Nespoli et al. (2007).

Source	Region	Pspin	Porb	$N_{\rm H}$I	$N_{\rm H}$IR	$N_{\rm H}$X	SpT	Nature	Ref
		(s)	(d)	10^{22} cm^{-2}	10^{22} cm^{-2}	10^{22} cm^{-2}			
IGR J16320-4751	Norma	1250	8.96(1)	2.14	6.6	21	spec: sgOB	HMXB/XP/T/OBS	c
IGR J16358-4726	Norma	5880		2.20	3.3	33	spec: sgB[e]?	HMXB/XP/T/OBS	c
IGR J16393-4643	Norma	912	3.6875(6)	2.19	2.19	24.98	sed: BIV-V?	HMXB/XP/T	c
IGR J16418-4532	Norma	1246	3.753(4)	1.88	2.7	10	sed: sgOB?	HMXB/XP/SFXT	c
IGR J16479-4514	Norma			2.14	3.4	7.7	spec: sgOB	HMXB/SFXT?	c
IGR J16558-5203	-	-	-	-	-	-	AGN	Seyfert 1.2	m
IGR J17091-3624	GC			0.77	1.03	1.0	sed: LMXB	BHC	c
IGR J17252-3616	GC	413	9.74(4)	1.56	3.8	15	spec: sgOB	HMXB/XP/OBS	c
IGR J17391-3021	GC			1.37	1.7	29.98	spec: O8Iab(f)	HMXB/SFXT/OBS	neg
IGR J17597-2201	GC			1.17	2.84	4.50	sed: LMXB	LMXB/B/D/P	c
IGR J18027-2016	GC	139	4.5696(9)	1.04	1.53	9.05	spec: sgOB	HMXB/XP/T	c
IGR J18483-0311	GC	21.05	18.55	1.62	2.45	27.69	sed: HMXB?	HMXB/XP	c
IGR J19140+0951			13.558(4)	1.68	2.9	6	spec: B0.5I	HMXB/OBS	h, nes

4.3. HMXBs in the INTEGRAL era

HMXBs are separated in 2 distinct groups. The first group contains the majority of the HMXB systems, constituted of known or suspected Be/X-ray Binary systems (BeXBs), called Be/X-ray transients. In Be systems, the donor is a Be star and the compact object is a neutron star typically in a wide, moderately eccentric orbit, spending little time in close proximity to the dense circumstellar disk surrounding the Be companion (Coe 2000; Negueruela 2004). X-ray outbursts occur when the compact object passes through the Be-star disk, accreting from the low-velocity and high-density wind around Be stars, and exhibiting hard X-ray spectra.

The second group of HMXB systems contains the Supergiant/X-ray Binaries (SXBs), where the compact object orbits deep inside the highly supersonic wind of a supergiant early-type star, which plays the role of the donor star (Kaper et al., 2004). The X-ray luminosity is powered either by accretion from the strong stellar wind of the optical companion, or by Roche-lobe overflow. In a wind-fed system accretion from the stellar wind results in a persistent X-ray luminosity of 10^{35-36} erg/s, while in a Roche-lobe overflow system, matter flows via the inner Lagrangian point to form an accretion disc. In this case, a much higher X-ray luminosity ($\sim 10^{38}$ erg/s) is then produced during the outbursts.

In the pre-*INTEGRAL* era, known HMXBs were mostly BeXBs systems. For instance, in the catalogue of HMXBs of Liu et al. (2000), there were 54 BeXBs and 7 SXBs identified, out of 130 HMXBs, representing a proportion of 42% and 5% respectively. Then, between the two last editions of HMXB catalogues (Liu et al. 2000 and Liu et al. 2006), the proportion of SXBs compared to BeXBs has increased, with the first HMXBs identified in the *INTEGRAL* data. The third IBIS/ISGRI soft γ-ray survey catalogue (Bird et al., 2007), spanning nearly 3.5 years of operations, contains 421 sources detected with the *INTEGRAL* observatory, of which 214 ($\sim$ 50 %) have been discovered by this satellite. This catalogue, extending up to 100 keV, includes 118 AGNs, 147 X-ray binaries (79 LMXBs and 68 HMXBs), 23 Cataclysmic Variables, 23 other objects, and still 115 unidentified objects. Among the 68 HMXBs, 24 have been identified as BeXBs and 19 as SXBs, representing a proportion of 35% and 28% respectively. The proportion of BeXBs, relative to the total of HMXBs, has decreased by a factor 1.2 while the proportion of SXBs has increased by a factor 5.6 between the catalogue of Liu et al. (2000) and the one of Bird et al. (2007). Related to this increasing proportion of SXBs, the other highlight of the *INTEGRAL* catalogue is the emergence of the SFXT class, with 12 *INTEGRAL* sources being firm or possible candidates.

Our studied sample of *INTEGRAL* sources allows us to add four newly identified SXBs which were not classified as such

in Bird et al. (2007): IGR J16320-4751, IGR J16358-4726, IGR J17252-3616 and IGR J18027-2016. The other sources which we have identified in this paper as supergiants were already put as SXBs, based either on spectral classification – IGR J17391-3021 and IGR J19140+0951– or on X-ray properties –the SFXT candidates IGR J16418-4532 and IGR J16479-4514–). With these new SXBs, the proportion of SXBs has reached the one of BeXBs: 35% of all HMXBs for each population. This clearly shows that the launch of *INTEGRAL* has drastically changed the statistical situation concerning the nature of HMXBs, by revealing a new dominant population of supergiant X-ray binaries, which are purely wind accretor systems.

Although this came as a surprise, it is *a posteriori* consistent with the fact that these hard X-ray emitters constitute the sources which are ideally detected by *INTEGRAL*, as discussed in Lutovinov et al. (2005a), Dean et al. (2005) and Bodaghee et al. (2007). Indeed, *INTEGRAL* observing at energies higher than the threshold above which photoelectric absorption becomes negligible in most matter, it can easily detect bright sources above a few tens of keV, while they are not detectable below, and therefore had remained hidden up to now. HMXBs accreting by stellar wind create a naturally dense and highly absorbing circumstellar wind compared to Roche lobe overflow in LMXBs, hiding the X-ray emission in a similar way to Seyfert 2 AGNs (Dean et al. 2005; Malizia et al. 2003).

4.4. The nature of *INTEGRAL* HMXBs

Let us now consider our results, summarized and put together with other characteristics of these sources in Table 7. In this sample of 13 *INTEGRAL* sources, concentrated both towards the direction of the Norma arm and the Galactic Centre, we classified 10 HMXBs (8 sources hosting sgOB and 2 sources hosting BIV-V companion stars), 2 LMXBs and 1 AGN. We clearly confirm the predominance of HMXBs hosting supergiants, as opposed to those hosting Be companion stars: in our sample, 80% of HMXBs host compact objects (probably neutron stars) orbiting around O/B supergiant secondaries. As already discussed, this result is in agreement with the increase of SXBs in the HMXBs population. However, quantitatively, the proportion of SXBs in our studied sample is higher than in the Bird et al. (2007) catalogue. There are two reasons: first, our sample is much more limited; second, most of the sources of our sample are in the direction of the Norma arm, which is associated with rich star-forming regions, natural birthplace of massive stars, as discussed in Section 4.2. Most of these new *INTEGRAL* sources are wind accretors, consistent with their location in the Corbet diagram (Corbet, 1986): nearly all of the HMXBs discovered by *INTEGRAL*, for which both spin and orbital periods have been measured, are located in the upper part of this diagram, among other wind accretors, typical of supergiant HMXBs. These systems exhibit extra absorption by a factor of ~ 4 compared to the average of all HMXBs, and they are X-ray pulsars, with longer pulsation periods than previously known HMXBs (Bodaghee et al., 2007).

In the companion paper by Rahoui et al. (2008) it is shown that only 3 sources –IGR J16318-4848, IGR J16358-4726 and IGR J16195-4945– on a sample of 12 *INTEGRAL* sources exhibit a MIR excess, due to an absorbing component enshrouding the whole binary system. The MIR emission of the remaining sources comes from the supergiant companion star, showing that an absorbing material is enshrouding the compact object itself for most of the sources (preliminary results of this paper were described in Chaty & Rahoui 2006). We are therefore facing two classes of *INTEGRAL* sources, i.e. highly absorbed sources such as IGR J16358-4726, for which the extreme representant is IGR J16318-4848, and SFXTs such as IGR J17391-3021, for which the archetype is IGR J17544-2619.

As shown in Table 7, these classes share similar properties –for instance they both host supergiant companion stars– however they do not seem to have exactly the same configuration, and one way to explain their different characteristics can be found in their excess in absorption, which does not seem to have the same origin. It is caused by two different phenomena in the case of the highly absorbed sources: the observations from hard X-ray to MIR domains suggest the presence of absorbing material concentrated around the compact object, and also some dust and/or cold gas, perhaps forming a cocoon, enshrouding the whole binary system (Filliatre & Chaty 2004; Rahoui et al. 2008). Their characteristics might be explained by the presence of a compact object (neutron star or black hole) orbiting within the dense wind surrounding the companion star. On the other hand, in the case of SFXTs, characterised by fast X-ray outbursts, the presence of the absorbing material seems concentrated around the compact object only, and MIR observations show that there is no need of any other absorbing material around the whole system (Rahoui et al., 2008). Their characteristics might be explained by the presence of a compact object (neutron star or black hole) located on an eccentric orbit around the companion star, and it would then be when the compact object penetrates the clumpy circumstellar envelope that outbursts are caused. However the situation is more complicated, since some SFXT sources are also highly obscured, and the intrinsic absorption derived from X-ray observations vary for some *INTEGRAL* sources (see e.g. the case of IGR J19140+0951; Prat et al. in prep.).

The X-ray transient or persistent nature of these sources might therefore be related to the geometry of these systems, and it is possible to distinguish the nature of both classes by speculating on the geometry of these systems (see also Chaty & Rahoui 2006). However only the knowledge of their orbital periods, which is currently unknown for most of these sources, will allow to confirm or not this view. Many questions are still open, most of them being related to the interaction between the compact object and the supergiant star, and to the nature of the absorbing material, which seems to be present in the environment either of the compact object, or of the whole binary system, and even both. To better understand the general properties of these systems, we will need to better characterise the dust, its temperature, composition, geometry, extension around the system, and to investigate where this dust or cold gas comes from. Finally, probably the most important question to solve is: is this unusual circumstellar environment due to stellar evolu-

tion OR to the binary system itself? To answer to this question, this dominant population of supergiant HMXBs now needs to be taken into account in the population synthesis models.

5. Conclusions

To summarize this paper, we have performed an extensive study of a sample of 13 *INTEGRAL* sources, through optical and NIR photometry and spectroscopy, performing for each of them an accurate astrometry, identifying candidate counterparts, deriving their optical and NIR magnitudes, and obtaining spectra for most of them. In addition, we built and fitted the SED of these sources, from MIR to hard X-rays. We thus identified the nature of the companion stars and of the binary systems by spectroscopy for 7 of these sources, and by fitting their SED for 5 of them. We finally reported NIR fields of four of these sources, which exhibit large-scale regions of absorption, probably linked to their formation process. We then discussed the existence of this dominant population of supergiant HMXBs in our Galaxy, born with two very massive components: a population which has been only recently revealed by the *INTEGRAL* observatory.

To conclude, it clearly appears that a study of this new population of supergiant HMXBs that we are now facing, constraining the nature and orbital parameters of these systems, and linked to population synthesis models, will provide a better understanding of the evolution of HMXBs. These systems are probably the primary progenitors of neutron star/neutron star or neutron star/black hole mergers. There is therefore the possibility that they are related with short/hard γ-ray bursts, and also that they might be good candidates of gravitational wave emitters. Our final word will be that, because most of these sources are obscured, the "Norma arm"-like sources can only be studied in the hard X-ray and infrared domains. A joint study of these sources with multi-wavelength hard X-ray, optical, NIR, MIR (and radio) observations is therefore necessary.

Acknowledgements. Based on observations collected at the European Southern Observatory, Chile (observing proposals ESO N° 073.D-0339). We acknowledge Jorge Melnick for special DDT time at 3.6 telescope on EFOSC2. SC thanks the ESO staff and especially Valenti Ivanov and Emanuela Pompei for their precious assistance during the run when we performed these optical and NIR observations. JAT acknowledges partial support from *Chandra* award number GO5-6037X issued by the *Chandra X-Ray Observatory Center*, which is operated by the Smithsonian Astrophysical Observatory for and on behalf of the National Aeronautics and Space Administration (NASA), under contract NAS8-03060. This research has made use of NASA's Astrophysics Data System, of the SIMBAD database, operated at CDS, Strasbourg, France, and of data products from the Two Micron All Sky Survey, which is a joint project of the University of Massachusetts and the Infrared Processing and Analysis Center/California Institute of Technology, funded by the National Aeronautics and Space Administration and the National Science Foundation.

References

Bird, A. J., Barlow, E. J., Bassani, L., et al. 2006, ApJ, 636, 765
Bird, A. J., Malizia, A., Bazzano, A., et al. 2007, ApJS, 170, 175
Bodaghee, A., Courvoisier, T. J.-L., Rodriguez, J., et al. 2007, A&A, 467, 585
Bodaghee, A., Walter, R., Zurita Heras, J. A., et al. 2006, A&A, 447, 1027
Bohlin, R. C., Savage, B. D., & Drake, J. F. 1978, ApJ, 224, 132
Bronfman, L., Nyman, L.-A., & May, J. 1996, A&AS, 115, 81
Capitanio, F., Bazzano, A., Ubertini, P., et al. 2006, ApJ, 643, 376
Cardelli, J. A., Clayton, G. C., & Mathis, J. S. 1989, ApJ, 345, 245
Caron, G., Moffat, A. F. J., St-Louis, N., Wade, G. A., & Lester, J. B. 2003, AJ, 126, 1415
Chaty, S. & Filliatre, P. 2005, Ap&SS, 297, 235
Chaty, S. & Rahoui, F. 2006, in Procs. of 6th INTEGRAL workshop, Moscow, Russia, in press (astro-ph/0609474)
Chernyakova, M., Lutovinov, A., Capitanio, F., Lund, N., & Gehrels, N. 2003, The Astronomer's Telegram, 157, 1
Coe, M. J. 2000, in ASP Conf. Ser. 214: IAU Colloq. 175: The Be Phenomenon in Early-Type Stars, ed. M. A. Smith, H. F. Henrichs, & J. Fabregat, 656–+
Corbet, R., Barbier, L., Barthelmy, S., et al. 2006, The Astronomer's Telegram, 779, 1
Corbet, R., Barbier, L., Barthelmy, S., et al. 2005, The Astronomer's Telegram, 649, 1
Corbet, R. H. D. 1986, MNRAS, 220, 1047
Corbet, R. H. D., Hannikainen, D. C., & Remillard, R. 2004, The Astronomer's Telegram, 269, 1
Dean, A. J., Bazzano, A., Hill, A. B., et al. 2005, A&A, 443, 485
Dickey, J. M. & Lockman, F. J. 1990, ARA&A, 28, 215
Filliatre, P. & Chaty, S. 2004, ApJ, 616, 469
Hannikainen, D. C., Rawlings, M. G., Muhli, P., et al. 2007, MNRAS, 380, 665
Hannikainen, D. C., Rodriguez, J., & Pottschmidt, K. 2003, IAU Circ., 8088, 4
Hill, A. B., Walter, R., Knigge, C., et al. 2005, A&A, 439, 255
in't Zand, J. J. M., Jonker, P. G., Nelemans, G., Steeghs, D., & O'Brien, K. 2006, A&A, 448, 1101
Kaper, L., van der Meer, A., & Tijani, A. H. 2004, in Revista Mexicana de Astronomia y Astrofisica Conference Series, ed. C. Allen & C. Scarfe, 128–131
Kennea, J. A. & et al. 2007, The Astronomer's Telegram, 1
Kouveliotou, C., Patel, S., Tennant, A., et al. 2003, IAU Circ., 8109, 2
Kuulkers, E., Lutovinov, A., Parmar, A., et al. 2003, The Astronomer's Telegram, 149, 1
Landolt, A. U. 1992, AJ, 104, 340
Lebrun, F., Leray, J. P., Lavocat, P., et al. 2003, A&A, 411, L141
Levine, A. M. & Corbet, R. 2006, The Astronomer's Telegram, 940, 1
Liu, Q. Z., van Paradijs, J., & van den Heuvel, E. P. J. 2000, Astron. Astrophys. Suppl. Ser., 147, 25
Liu, Q. Z., van Paradijs, J., & van den Heuvel, E. P. J. 2006, A&A, 455, 1165

Lutovinov, A., Revnivtsev, M., Gilfanov, M., et al. 2005a, A&A, 444, 821
Lutovinov, A., Rodriguez, J., Revnivtsev, M., & Shtykovskiy, P. 2005b, A&A, 433, L41
Lutovinov, A., Walter, R., Belanger, G., et al. 2003, The Astronomer's Telegram, 155, 1
Malizia, A., Bassani, L., di Cocco, G., et al. 2004, The Astronomer's Telegram, 227, 1
Malizia, A., Bassani, L., Stephen, J. B., et al. 2003, ApJ, 589, L17
Malizia, A., Landi, R., Bassani, L., et al. 2007, ArXiv e-prints, 706
Markwardt, C. B. & Swank, J. H. 2003, The Astronomer's Telegram, 156, 1
Masetti, N., Morelli, L., Palazzi, E., et al. 2006, A&A, 459, 21
Mill, J. D. 1994, in Proc. SPIE Vol. 2232, p. 200-216, Signal Processing, Sensor Fusion, and Target Recognition III, Ivan Kadar; Vibeke Libby; Eds., ed. I. Kadar & V. Libby, 200–216
Molkov, S., Mowlavi, N., Goldwurm, A., et al. 2003, The Astronomer's Telegram, 176, 1
Munari, U. & Tomasella, L. 1999, A&AS, 137, 521
Munari, U. & Zwitter, T. 1997, A&A, 318, 269
Negueruela, I. 2004, in Revista Mexicana de Astronomia y Astrofisica Conference Series, ed. G. Tovmassian & E. Sion, 55–56
Negueruela, I. & Schurch, M. P. E. 2007, A&A, 461, 631
Negueruela, I., Smith, D. M., Harrison, T. E., & Torrejón, J. M. 2006a, ApJ, 638, 982
Negueruela, I., Smith, D. M., Reig, P., Chaty, S., & Torrejón, J. M. 2006b, in ESA Special Publication, Vol. 604, ESA Special Publication, ed. A. Wilson, 165–170
Nespoli, E., Fabregat, J., & Mennickent, R. 2007, The Astronomer's Telegram, 982, 1
Patel, S. K., Zurita, J., Del Santo, M., et al. 2007, ApJ, 657, 994
Pellizza, L. J., Chaty, S., & Negueruela, I. 2006, A&A, 455, 653
Persson, S. E., Murphy, D. C., Krzeminski, W., Roth, M., & Rieke, M. J. 1998, AJ, 116, 2475
Predehl, P. & Schmitt, J. 1995, A&A, 293, 889
Rahoui, F., Chaty, S., Lagage, P.-O., & Pantin, E. 2008, A&A, in press
Revnivtsev, M., Gilfanov, M., Churazov, E., & Sunyaev, R. 2003a, The Astronomer's Telegram, 150, 1
Revnivtsev, M., Tuerler, M., Del Santo, M., et al. 2003b, IAU Circ., 8097, 2
Revnivtsev, M. G., Sunyaev, R. A., Varshalovich, D. A., et al. 2004, Astronomy Letters, 30, 382
Rodriguez, J., Bodaghee, A., Kaaret, P., et al. 2006, MNRAS, 366, 274
Rodriguez, J., Cabanac, C., Hannikainen, D. C., et al. 2005, A&A, 432, 235
Rodriguez, J., Tomsick, J. A., Foschini, L., et al. 2003, A&A, 407, L41
Rupen, M. P., Mioduszewski, A. J., & Dhawan, V. 2003, The Astronomer's Telegram, 152, 1
Russeil, D. 2003, A&A, 397, 133
Sguera, V., Barlow, E. J., Bird, A. J., et al. 2005, A&A, 444, 221
Sguera, V., Bazzano, A., Bird, A. J., et al. 2006, ApJ, 646, 452
Sguera, V., Hill, A. B., Bird, A. J., et al. 2007, A&A, 467, 249
Smith, D. M. 2004, The Astronomer's Telegram, 338, 1
Smith, D. M., Heindl, W. A., Markwardt, C. B., et al. 2006, ApJ, 638, 974
Stephen, J. B., Bassani, L., Molina, M., et al. 2005, A&A, 432, L49
Sunyaev, R., Lutovinov, A., Molkov, S., & Deluit, S. 2003, The Astronomer's Telegram, 181, 1
Swank, J. H. & Markwardt, C. B. 2003, The Astronomer's Telegram, 128, 1
Tauris, T. M. & van den Heuvel, E. P. J. 2006, Formation and evolution of compact stellar X-ray sources (Compact stellar X-ray sources), 623–665
Thompson, T. W. J., Tomsick, J. A., Rothschild, R. E., in't Zand, J. J. M., & Walter, R. 2006, ApJ, 649, 373
Thompson, T. W. J., Tomsick, J. A., Zand, J. J. M. i., Rothschild, R. E., & Walter, R. 2007, ApJ, 661, 447
Tomsick, J. A., Chaty, S., Rodriguez, J., et al. 2006, ApJ, 647, 1309
Tomsick, J. A., Lingenfelter, R., Corbel, S., Goldwurm, A., & Kaaret, P. 2004a, in ESA SP-552: 5th INTEGRAL Workshop on the INTEGRAL Universe, ed. V. Schoenfelder, G. Lichti, & C. Winkler, 413–416
Tomsick, J. A., Lingenfelter, R., Corbel, S., Goldwurm, A., & Kaaret, P. 2004b, The Astronomer's Telegram, 224, 1
Tomsick, J. A., Lingenfelter, R., Walter, R., et al. 2003, IAU Circ., 8076, 1
Türler, M., Balman, S., Bazzano, A., et al. 2007, The Astronomer's Telegram, 1019, 1
Walter, R., Bodaghee, A., Barlow, E. J., et al. 2004a, The Astronomer's Telegram, 229, 1
Walter, R., Courvoisier, T. J.-L., Foschini, L., et al. 2004b, in ESA Special Publication, Vol. 552, 5th INTEGRAL Workshop on the INTEGRAL Universe, ed. V. Schoenfelder, G. Lichti, & C. Winkler, 417–422
Walter, R., Zurita Heras, J., Bassani, L., et al. 2006, A&A, 453, 133
Zurita Heras, J. A., de Cesare, G., Walter, R., et al. 2006, A&A, 448, 261

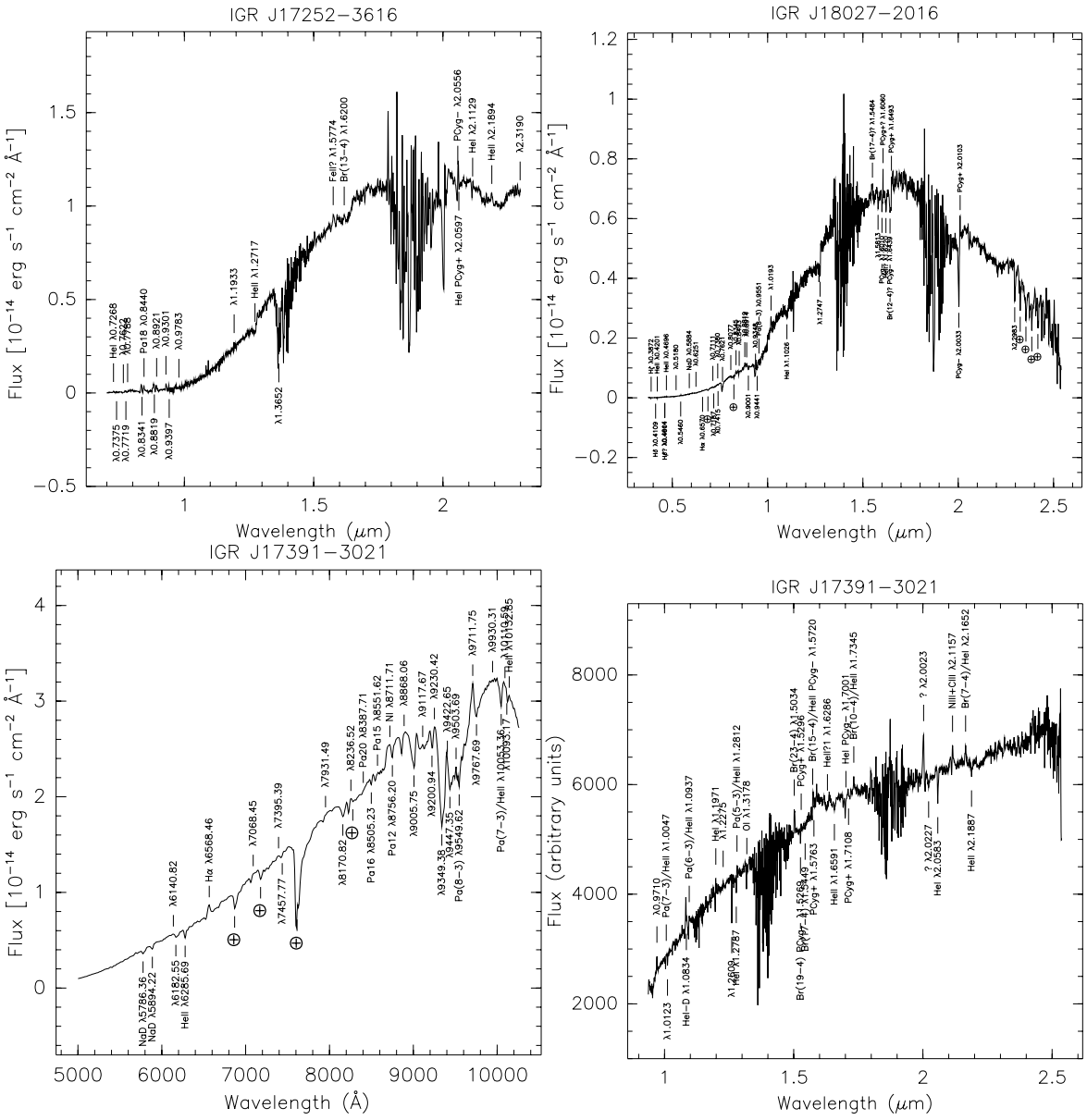
IGR J17252−3616
IGR J18027−2016
IGR J17391−3021
IGR J17391−3021
Flux [10^−14 erg s^−1 cm^−2 Å^−1]
Wavelength (μm)
Wavelength (Å)
Flux (arbitrary units)
HeI λ0.7268
Pa18 λ0.8440
λ0.8921
λ0.9301
λ0.9783
λ0.7375
λ0.7719
λ0.8341
λ0.8819
λ0.9397
λ1.1933
HeII λ1.2717
λ1.3652
FeII? λ1.5774
Br(13−4) λ1.6200
PCyg− λ2.0556
HeI λ2.1129
HeII λ2.1894
λ2.3190
HeI PCyg+ λ2.0597
λ1.0183
λ1.1026
λ1.2747
λ0.9551
λ0.9441
λ0.9001
λ0.5460
HeI λ0.4686
λ0.3180
λ0.4109
λ0.4221
λ0.4340
λ0.4861
λ0.6563
λ0.6678
λ0.7065
λ0.7281
λ0.7711
λ0.7965
λ0.8178
λ0.8274
λ0.8392
λ0.8413
λ0.8467
λ0.8502
λ0.8545
λ0.8598
λ0.8750
λ0.8862
λ0.8914
λ0.9015
λ0.9063
λ0.9229
λ0.9340
λ0.9405
λ0.9464
λ0.9546
λ0.9605
λ0.9708
λ0.9815
λ0.9903
λ1.0049
λ1.0126
λ1.0183
λ1.0281
λ1.0358
λ1.0411
λ1.0477
λ1.0532
λ1.0581
λ1.0617
λ1.0644
λ1.0680
λ1.0713
λ1.0747
λ1.0784
λ1.0813
λ1.0833
λ1.0858
λ1.0880
λ1.0913
λ1.0938
λ1.0962
λ1.0983
λ1.1013
λ1.1033
λ1.1054
λ1.1080
λ1.1103
λ1.1128
λ1.1153
λ1.1183
λ1.1208
λ1.1233
λ1.1258
λ1.1283
λ1.1308
λ1.1333
λ1.1358
λ1.1383
λ1.1408
λ1.1433
λ1.1458
λ1.1483
λ1.1508
λ1.1533
λ1.1558
λ1.1583
λ1.1608
λ1.1633
λ1.1658
λ1.1683
λ1.1708
λ1.1733
λ1.1758
λ1.1783
λ1.1808
λ1.1833
λ1.1858
λ1.1883
λ1.1908
λ1.1933
λ1.1958
λ1.1983
λ1.2008
λ1.2033
λ1.2058
λ1.2083
λ1.2108
λ1.2133
λ1.2158

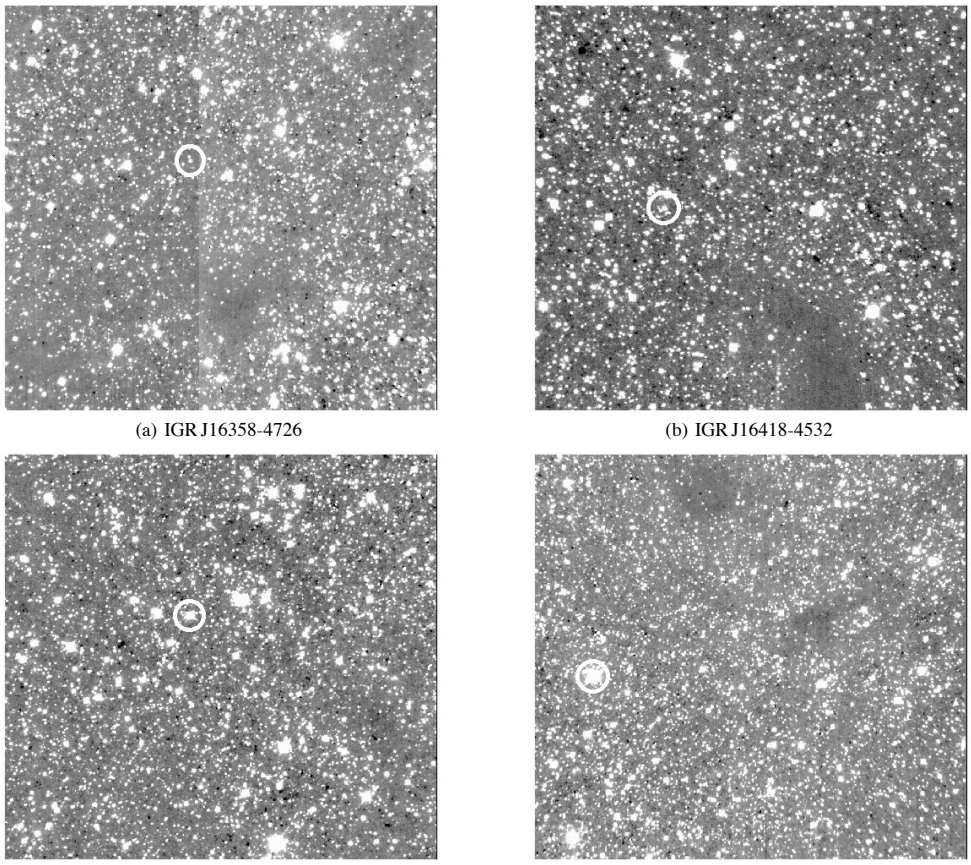

(a) IGR J16358-4726 (b) IGR J16418-4532

(c) IGR J16479-4514 (d) IGR J17391-3021

Fig. 6. Large fields of 4 studied sources exhibiting high absorption along their line of sight. Size: $5.5' \times 5.5'$; North is to the top and East to the left. We overplot a white circle to indicate the position of the *INTEGRAL* sources.

Table 8: Spectroscopy results. We indicate the name of the sources, the identification of the lines, the rest wavelength (μm), the fitted central wavelength (μm), the flux (in erg $s^{-1}cm^{-2}$ for optical spectra and in arbitrary units for NIR spectra), the equivalent width (EQW in Å), and Full Width Half Maximum (FWHM in Å). T stands for telluric.

Source	Identification	λ	λ_{fit}	Flux	EQW	FWHM
IGR J16320-4751						
	Pa(7-3)	1.005	1.0052	1296.88	-3.773±1.3	55.6
			1.1757	855.62	-1.889	51.35
			1.2609	673.3	-1.275	29.4
			1.5064	689.659	-0.9421	8.044
	Br(17-4)	1.544	1.5442	1214.05	-1.529±0.4	12.76
			1.5479	2708.57	-3.044	112.4
			1.5829	0.0120243	-0.175554	14.6
			2.0998	2160.39	-1.656	88.75
	Br(7-4)/HeI	2.166/2.166	2.1661	7327.22	-5.454±1.0	114.6
	T		2.2962	-10695.5	7.402	51.66
	T		2.3248	-8645.31	6.087	38.76
IGR J16358-4726						
	HeII	1.0133	1.0138	-331.65	24.01	7.408
			1.1935	803.177	-9.219	2.876
	HeII	1.2914	1.2908	878.037	-5.591	25.71
	HeI	1.2971	1.2966	-285.973	1.77	12.26
	?		1.5061	5060.16	-14.96	25.61
	?		1.5839	3229.4	-7.776	25.37
			1.6135	2407.31	-5.477	21.55
			1.6701	-1731.86	10.56	46.58
	Br(11-4)	1.681	1.6811	5716.71	-40.69	133.3
	Br(10-4)	1.737	1.7177	1292.73	-7.716	46.55
			1.7662	-2008.36	10.33	40.9
			1.7906	902.755	-4.666	13.32
			1.8000	-1825.61	9.3	23.42
	Br(9-4)	1.818	1.8206	3066.46	-15.68	92.93
	Br(8-4)	1.945	1.9448	561.476	-2.306	14.81
	FeII?	1.9746	1.9811	1281.53	-5.106	2.16
			2.0018	-4330.84	16.86	38.31
			2.0566	-2011.82	7.386	30.4
			2.1216	944.583	-3.257	23.41
			2.1518	-2205.66	7.095	47.87
	Br(7-4)	2.166	2.1643	1585.54	-5.174	70.49
	[FeII]	2.224	2.2223	3877.44	-12.85	126.6
	HeI	2.3069	2.2934	-1053.51	3.128	17.71
IGR J16479-4514						
			0.9811	417.44	-39.77	28.98
			1.0597	282.616	-8.639	5.383
			1.1293	661.497	-10.13	69.46
			1.2616	376.308	-2.184	5.55
	HeII?	1.3150	1.3178	-489.818	2.034	17.33
			1.4602	336.183	-0.7073	7.066
			1.4679	-280.531	0.5932	7.727
	HeII	1.4882	1.4876	595.672	-1.141	15.05
	Br(23-4)	1.504	1.5046	2512.46	-4.622	39.73
	Br(19-4)	1.526	1.5269	-1037.44	1.767	18.67
	FeII	1.576	1.5760	1858.42	-2.719	35.1
	Br(14-4)	1.588	1.5900	3130.59	-4.995	70.96
			1.6998	-1075.65	1.29	22.05

Table 8: continued.

Source	Identification	λ	λ_{fit}	Flux	EQW	FWHM
			1.7891	-2371.63	2.32	20.62
	Br(8-4)	1.945	1.9475	8758.25	-6.548	92.96
			1.9822	4953.06	-3.442	38.83
			2.0076	-22693.7	15.46	192.7
			2.0547	-4648.77	2.992	90.7
	HeI	2.1126	2.1117	-2376.81	1.379	30.27
	Br(7-4)/HeII	2.166/2.166	2.1658	6605.93	-3.652	51.56
			2.2818	2197.39	-1.054	47.44
	T		2.3294	-2606.04	1.184	22.37
IGR J17252-3616						
	HeI		0.7268	9.590E-17	-61.37	32.97
			0.7375	6.308E-17	-34.66	21.14
			0.7622	-1.29E-16	48.04	66.65
			0.7719	1.136E-16	-39.71	37.44
			0.7788	-1.06E-16	22.64	31.12
	T		0.8277	-1.30E-16	31.32	26.38
			0.8341	9.047E-16	-195.9	39.92
	Pa18	0.8437	0.8440	6.046E-16	-106.5	44.48
			0.8819	1.176E-15	-169.9	58.22
			0.8921	6.742E-16	-91.68	46.02
			0.9301	5.538E-16	-50.68	33.24
			0.9397	1.435E-16	-15.17	21.22
			0.9783	5.476E-16	-48.98	57.03
			1.1933	17258.4	-1.55	6.047
	HeII	1.2719	1.2717	-205225.	12.25	116.1
			1.3652	-1927788.	80.62	151.6
	FeII?	1.576	1.5774	170625.	-4.023	63.2
	Br(13-4)	1.611	1.6200	167968.	-3.916	95.54
	PCyg-		2.0555	-277866.	5.281	63.73
	HeI PCyg+	2.0587	2.0597	163020.	-3.08	23.96
	HeI	2.1126	2.1129	-105139.	2.004	29.24
	HeII	2.1891	2.1894	158546.	-3.309	63.66
			2.3190	-203026.	3.913	25.96
IGR J17391-3021						
	NaD	0.5780	0.5786	-9.84E-15	2.512	29.57
	NaD	0.5890	0.5894	-5.74E-15	1.316	16.76
			0.6141	7.903E-15	-1.462	28.81
			0.6183	-9.74E-15	1.736	31.93
	HeII		0.6286	-1.18E-14	2.01	15.24
	Hα	0.6562	0.6568	2.207E-14	-2.804	23.84
	T		0.6888	-7.97E-14	7.934	52.38
			0.7068	-7.77E-15	0.6783	16.38
	T		0.7189	-2.15E-14	1.767	24.4
			0.7395	9.707E-15	-0.7171	32.32
			0.7458	3.928E-15	-0.2813	11.34
	T		0.7629	-6.50E-13	41.87	78.06
			0.7931	-1.15E-14	0.6468	22.8
			0.8171	-5.01E-14	2.624	41.
			0.8237	-2.64E-14	1.349	18.94
	T		0.8290	-4.75E-15	0.241	22.14
	Pa20	0.8392	0.8388	-1.62E-15	0.07962	8.758
	Pa16	0.8502	0.8505	-1.11E-14	0.5035	13.02
	Pa15	0.8545	0.8552	-1.23E-14	0.5532	18.17
	NI	0.8703	0.8712	1.028E-13	-4.347	50.04
	Pa12	0.8750	0.8756	-3.44E-14	1.348	22.97

Table 8: continued.

Source	Identification	λ	λ_{fit}	Flux	EQW	FWHM
			0.8868	-4.96E-14	1.887	25.83
			0.9006	-1.66E-13	6.293	49.69
			0.9118	7.353E-15	-0.2933	17.46
			0.9201	4.781E-14	-1.887	28.79
			0.9230	-4.13E-14	1.545	22.38
			0.9349	-5.66E-13	22.48	64.58
			0.9423	-1.49E-12	57.2	309.8
			0.9447	-2.00E-12	72.96	274.8
			0.9504	-8.41E-13	32.56	178.7
	Pa(8-3)	0.954	0.9550	-1.19E-13	4.949	44.28
			0.9712	1.268E-13	-4.463	36.45
			0.9768	-2.08E-13	6.634	73.77
			0.9930	7.416E-13	-25.57	218.4
			1.0111	1.372E-14	-0.4479	13.33
			1.0093	5.657E-14	-1.853	34.91
	Pa(7-3)/HeII	1.005/1.0049	1.0053	-6.23E-14	1.959	25.14
	HeII	1.0133	1.0133	-1.24E-14	0.4036	12.24
			0.9710	13487.8	-2.658	24.21
	Pa(7-3)/HeII	1.005/1.0049	1.0047	-3997.88	0.7305	9.054
			1.0123	-4141.89	0.7398	9.734
	HeI-D	1.0832-3	1.0834	45732.6	-7.06	42.2
	Pa(6-3)/HeII	1.094/1.0938	1.0937	-9981.06	1.472	15.88
	HeI	1.1972	1.1971	-11849.5	1.522	15.93
			1.2275	8130.68	-1.014	27.2
			1.2609	-7058.26	0.851	1.225
	HeI	1.2789	1.2787	-7781.74	0.9251	9.955
	Pa(5-3)/HeII	1.282/1.2817	1.2812	24041.7	-2.847	69.16
	OI	1.3165	1.3178	-9810.79	1.124	10.69
	Br(23-4)	1.504	1.5034	33968.9	-3.427	39.53
	Br(19-4) PCyg-	1.526	1.5269	-10867.7	1.074	11.76
	PCyg+		1.5296	2753.08	-0.2737	7.687
	Br(17-4)	1.544	1.5449	-5302.73	0.5161	12.05
	Br(15-4)/HeII PCyg-	1.571/1.5719	1.5720	-8690.81	0.816	11.44
	PCyg+		1.5763	28064.4	-2.625	34.17
	HeII?	1.6241	1.6286	-14464.6	2.554	83.49
	HeII	1.6584	1.6591	-8012.45	1.407	59.07
	HeI PCyg-	1.7007	1.7001	-9883.17	1.721	25.47
	PCyg+		1.7108	7183.83	-1.248	46.05
	Br(10-4)/HeII	1.737/1.7355	1.7345	18147.7	-3.105	82.78
	?		2.0023	48773.3	-8.054	53.72
	?		2.0227	-8537.24	1.394	54.94
	HeI	2.0587	2.0583	-19765.2	3.163	32.95
	NIII+CIII	2.116	2.1157	11898.8	-1.87	28.88
	Br(7-4)/HeI	2.166/2.166	2.1652	14485.3	-2.267	48.56
	HeII	2.1891	2.1887	-5196.59	0.8194	24.93
IGR J18027-2016						
	Hζ	0.3889	0.3872	-1.64E-16	85.36	13.75
	Hδ	0.4101	0.4109	1.403E-15	INDEF	13.79
	HeII	0.4200	0.4201	-7.06E-16	2460.	8.549
			0.4614	-5.94E-16	79.65	7.906
	HeII	0.4686	0.4696	2.762E-16	-28.62	20.08
	Hβ?	0.4861	0.4901	9.769E-16	-75.71	10.23
			0.5180	-7.98E-16	51.37	9.967
			0.5460	2.099E-16	-7.693	12.53
	NaD	0.5890	0.5884	-1.99E-16	3.885	20.76

Table 8: continued.

Source	Identification	λ	λ_{fit}	Flux	EQW	FWHM
			0.6251	3.172E-16	-5.072	42.17
	Hα	0.6562	0.6570	6.033E-16	-6.788	44.4
	T		0.6885	-1.21E-15	10.03	59.22
			0.7111	-6.80E-17	0.4671	7.604
			0.7187	-1.65E-16	1.096	21.06
			0.7380	3.866E-16	-2.221	43.12
			0.7415	-3.43E-16	1.845	31.
			0.7621	-8.49E-15	40.47	66.51
			0.8077	3.062E-16	-1.061	20.52
	T		0.8240	-4.18E-16	1.409	10.03
			0.8345	1.376E-15	-4.163	33.41
			0.8493	-1.38E-15	3.771	22.71
			0.8819	2.979E-15	-7.014	50.99
			0.8914	2.231E-15	-5.194	42.9
			0.9001	-1.79E-15	4.164	40.1
			0.9348	-5.29E-15	13.54	50.03
			0.9441	-1.93E-15	5.08	34.31
	Pa(8-3)	0.9549	0.9551	-4.02E-15	9.739	83.46
			1.0193	169299.	-16.81	67.81
	HeI	1.1016	1.1026	-188368.	13.04	111.4
			1.2747	-267133.	11.87	89.39
	Br(17-4)?	1.544	1.5484	257952.	-8.298	116.5
			1.5813	-137910.	4.266	59.41
	PCyg-		1.6010	-87404.2	2.733	35.72
	PCyg+?		1.6060	46540.9	-1.455	7.072
	HeII?	1.6241	1.6220	-105641.	3.331	41.99
	Br(12-4)? PCyg-	1.641	1.6439	-340789.	10.27	82.88
	PCyg+		1.6493	-14621.9	0.4325	1.403
	PCyg-		2.0033	-644298.	25.66	59.55
	PCyg+		2.0103	123941.	-4.991	29.17
			2.2983	-299051.	14.65	55.77
	T		2.3262	-103670.	5.96	25.2
	T		2.3563	-226137.	14.08	59.82
	T		2.3867	-113159.	7.989	29.05
	T		2.4189	-141757.	9.892	37.36
IGR J19140+0951						
			0.9787	254.752	-0.5518	8.255
	Pa(7-3)	1.005	1.0053	-179.359	0.397	10.52
	-		1.0081	113.557	-0.2515	8.25
	-		1.0595	193.383	-0.4397	6.494
	-		1.1919	554.	-1.31	15.17
	-		1.2613	247.094	-0.5914	7.01
	Pa(5-3)/HeII	1.282/1.2817	1.2821	-359.765	0.86	13.84
	-		1.5830	1002.7	-3.077	83.78
	-		1.5845	-414.155	0.9797	7.817
	Br(14-4)?	1.588	1.5895	-517.017	1.205	29.69
	HeII	1.6584	1.6592	324.516	-0.9892	12.57
			1.6687	1036.81	-3.168	95.57
			1.6834	-149.388	0.4517	7.682
	HeII	1.8725	1.8728	1335.31	-4.457	11.47
			2.0070	-12037.2	37.72	187.7
	HeI	2.0587	2.0600	563.242	-1.878	30.69
	HeI	2.1126	2.1129	169.253	-0.5294	18.93

3.5.5 Sources Galactiques de rayons X durs découvertes par *INTEGRAL* révélées par des observations multi-longueurs d'onde : II. Environnement de l'étoile compagnon

"Galactic hard X-ray sources discovered by *INTEGRAL* brought to light by multiwavelength observations : II. The environment of the companion star" par F. Rahoui, S. Chaty, P.-O. Lagage, E. Pantin, 2008, A&A in press

Dans cet article sont compilées des observations dans le domaine infrarouge moyen de vingt nouvelles sources *INTEGRAL*. Les observations dans ce domaine, ainsi qu'une modélisation précise de l'émission, en tenant compte de l'étoile compagnon ainsi que dans certains cas d'une composante de poussière et/ou de gaz froid, montrent que dans 3 cas, incluant IGR J16318-4848, l'ajustement des observations nécessite l'ajout d'une composante additionnelle. Ainsi, dans ces 3 cas, il semble qu'une composante de poussière se soit formée dans l'environnement de ces étoiles compagnon, des sgB[e] pour la plupart, à partir de fortes composantes de vent stellaire. Cette composante de poussière est donc à l'origine de l'absorption élevée vue en direction de ces sources (voir le paragraphe 3.3.4 pour plus de détails).

Astronomy & Astrophysics manuscript no. igr˙mir˙frahoui2
December 28, 2007
© ESO 2007

Galactic hard X-ray sources discovered by *INTEGRAL* brought to light by multi-wavelength observations⋆

II. The environment of the companion star

F. Rahoui[1,2], S. Chaty[2], P-O. Lagage[2], and E. Pantin[2]

[1] European Southern Observatory, Alonso de Córdova 3107, Vitacura, Santiago de Chile
e-mail: frahoui@eso.org
[2] Laboratoire AIM, CEA/DSM - CNRS - Université Paris Diderot, DAPNIA/Service d'Astrophysique, Bât. 709, CEA-Saclay, F-91191 Gif-sur- Yvette Cédex, France

Received ; accepted

ABSTRACT

Context. The *INTEGRAL* mission has led to the discovery of a new type of Supergiant X-ray Binaries (SGXBs) whose physical properties differ from those of previously known SGXBs. Those sources are in the course of being unveiled by means of multi-wavelength X-rays, optical, near- and mid-infrared observations and two classes are appearing. The first class is constituted of obscured persistent SGXBs and the second class is populated by the so-called Supergiant Fast X-ray Transients (SFXTs).
Aims. We report here on mid-infrared (MIR) observations of the companion stars of twelve SGXBs from these two classes which aimed at assessing the contribution of the star and the material enshrouding the system to the total emission.
Methods. We used data from observations we carried out at ESO/VLT using VISIR as well as archival and published data to perform broad-band Spectral Energy Distributions of the companion stars and fitted them with a combination of two black-bodies representing the star and a MIR excess due to the absorbing material enshrouding the star, if any.
Results. We detect a MIR excess in the emission of IGR J16318-4848, IGR J16358-4726 and perhaps IGR J16195-4945. The other sources do not exhibit any MIR excess even when the intrinsic absorption is very high. Indeed, the stellar winds of supergiant stars are not suitable for dust production and we show that this behaviour is not changed by the presence of the compact object. Concerning IGR J16318-4848 and probably IGR J16358-4726, the MIR excess can be explained by their sgB[e] nature and the presence of an equatorial disk around the supergiant companion in which dust can be produced. Moreover, our results suggest that some of the supergiant stars in those systems could exhibit an absorption excess compared to isolated supergiant stars, this excess being possibly partly due to the photoionization of their stellar wind in the vicinity of their atmosphere. We also show that the differences of behaviour between the obscured SGXBs and the SFXTs in the high-energy domain do not exist from optical to MIR wavelengths, but supergiant stars in SFXTs could nevertheless be most of the time less absorbed than supergiant stars in obscured SGXBs, due to the geometry of the systems. At last, our results confirm the presence of a very dense cocoon of material around the compact object as the extinction in the X-ray domain is generally several order of magnitudes higher than the extinction in the visible.

Key words. Infrared: stars – X-rays: binaries, individuals: IGR J16195-4945, IGR J16207-5129, IGR J16318-4848, IGR J16320-4751, IGR J16358-4726, IGR J16418-4532, IGR J16465-4507, IGR J16479-4514, IGR J17252-3616, IGR J17391-3021, IGR J17544-2619, IGR J19140+0951 – binaries: general – supergiants – Stars: fundamental parameters

1. Introduction

High-Mass X-ray Binaries (HMXBs) are X-ray sources for which high-energy emission is due to accretion onto a compact object (black hole or neutron star) of material coming from a massive companion star. Until recently, the huge majority of known HMXBs were Be/X-ray binaries, i.e a neutron star accreting from a disc around a Be star. Most of these sources are transient, even if a few are persistent weak X-ray emitters ($L_X \sim 10^{34}$ erg s^{-1}). The other known HMXBs were Supergiant X-ray Binaries (SGXBs), composed of a compact object orbiting around an early-type supergiant and fed by accretion from the strong radiative wind of the companion. These objects are persistent sources ($L_X \sim 10^{36}$ erg s^{-1}) and their relative low number compared to the population of Be/X-ray

Send offprint requests to: F. Rahoui
⋆ Based on observations carried out at the European Southern Observatory under programmes ID 075.D-0773 and 077.D-0721.

binaries was explained as a consequence of the short lifetime of supergiant stars.

The launch of the *INTErnational Gammay-Ray Astrophysics Laboratory* (*INTEGRAL*, Winkler et al. 2003) in October 2002 completely changed the situation as many more HMXBs whose companion stars are supergiants were discovered during the monitoring of the Galactic Center and the Galactic Plane using the onboard IBIS/ISGRI instruments (Ubertini et al. 2003; Lebrun et al. 2003). Most of these sources are reported in Bird et al. (2007) and Bodaghee et al. (2007), and their studies revealed two main features which where not present on previously known SGXBs:

- first, many of them exhibit a considerable intrinsic absorption, with a column density up to $N_H \sim 2 \times 10^{24}\,cm^{-2}$ in the case of IGR J16318-4848 (Matt & Guainazzi 2003), which explains why previous high-energy missions had not detected them.
- second, some of these new sources revealed a transitory nature. They are undetectable most of the time and occasionally present a fast X-Ray transient activity lasting a few hours. Moreover, they exhibit a quiescent luminosity of $L_X \sim 10^{33}$ erg s^{-1}, well below the persistent state of other SGXBs.

It then appears that supergiant HMXBs discovered by *INTEGRAL* can be classified in two classes: one class of considerably obscured persistent sources that we will simply call obscured SGXBs in this paper and one class of Supergiant Fast X-ray Transients (SFXTs, Negueruela et al. 2006b).

High-energy observations can give some information about the compact object or about the processes that lead to the emission but do not allow to study the companion star. It is therefore very important to perform multi-wavelength observations of these sources - from optical to MIR wavelengths - as this represents the only way to characterize the companion or to detect dust around these highly obscured systems. However, positions given by *INTEGRAL* are not accurate enough (∼2′) to identify their optical counterparts, due to the large number of objects in the error circle. Observations with X-ray telescopes like *XMM-Newton* or *Chandra* are therefore crucial because they allow a localisation with a position accuracy of 4″or better, which lowers the number of possible optical counterparts.

We performed optical to MIR wavelengths observations of several candidate SGXBs recently discovered with *INTEGRAL*.

Optical and NIR observations were carried out at ESO/NTT using EMMI and SOFI instruments and aimed at constraining the spectral type of the companions through accurate astrometry as well as spectroscopy and photometry of the candidate counterparts. They are reported in the companion paper (Chaty et al., 2007, CHA07 hereafter), and it is shown that most of these sources are actually supergiant stars.

In this paper, we report on MIR observations of the companions of twelve *INTEGRAL* candidate SFXTs and obscured SGXBs (listed in Table 1) which aimed at studying the circumstellar environment of these highly absorbed sources and particularly to detect any MIR excess in their emission which could be due to the absorbing material. This sources were chosen because they had very accurate positions and confirmed 2MASS counterparts.

Using these observations, the results reported in the companion paper (CHA07) as well as archival data from the USNO, 2MASS and GLIMPSE catalogues when needed, we performed broad-band Spectral Energy Distributions (SEDs) of these sources and fitted them with a two-components blackbody model in order to assess the contribution of the star and the enshrouding material in the emission.

ESO observations as well as our model are described in Section 2. In Section 3, results of the fits for each source are given and these results are discussed in Section 4. We conclude in Section 5.

2. Observations

2.1. MIR observations and data reduction

MIR observations were carried out on 2005 June 20-22 and 2006 June 29-30 using VISIR (Lagage et al. 2004), the ESO/VLT mid-infrared imager and spectrograph, composed of an imager and a long slit-spectrometer covering several filters in N and Q bands and mounted on Unit 3 of the VLT (Melipal). Standard "chopping and nodding" MIR observational technique was used to suppress the background dominating at these wavelengths. Secondary mirror chopping was performed in the North-South direction with an amplitude of 16″at a frequency of 0.25 Hz. Nodding technique, necessary to compensate for chopping residuals, was chosen as parallel to the chopping and applied using telescope offsets of 16″.

Due to the high thermal MIR background for ground-based observations, the detector integration time was set to 16 ms.

We performed broad-band photometry in 3 filters, PAH1 (λ=8.59±0.42 μm), PAH2 (λ=11.25±0.59 μm) and Q2 (λ=18.72±0.88 μm) using the small field in all bands (19.″2x19.″2 and 0.″075 plate scale). All the observations were bracketed with standard stars observations for flux calibration and PSF determination. The weather conditions were good and stable during the observations.

Raw data were reduced using the IDL reduction package written by Eric Pantin. The elementary images are co-added in real-time to obtain chopping-corrected data then the different nodding positions are combined to form the final image. VISIR detector is affected by stripes randomly triggered by some abnormal high-gain pixels. A dedicated destriping method has been developed (Pantin, 2007, in prep.) to suppress them.

MIR fluxes of all observed sources including 1σ errors are listed in Table 2.

2.2. Archival data

When we did not have optical to MIR data of our sources, we searched for the counterparts in 3 catalogues:

- in the United States Naval Observatory (USNO) catalogues in B, R and I for USNO-B1.0, B and R for USNO-A.2. Positions and fluxes accuracies are 0.″25 and 0.3 magni-

tudes in the case of USNO-B.1, 0.″2 and 0.5 magnitudes in the case of USNO-A.2.
- in the 2 Microns All Sky Survey (2MASS), in J (1.25±0.16 μm), H (1.65±0.25 μm) and Ks (2.17±0.26 μm) bands. Position accuracy is about 0.″2.
- in the *Spitzer*'s Galactic Legacy Infrared Mid-Plane Survey Extraordinaire (GLIMPSE, Benjamin et al. 2003), survey of the Galactic Plane ($|b| \leq 1^\circ$ and between l=10° and l=65° on both sides of the Galactic Center) performed with the *Spitzer Space Telescope*, using the IRAC camera in four bands, 3.6±0.745 μm, 4.5±1.023 μm, 5.8±1.450 μm and 8±2.857 μm.

All sources had a confirmed 2MASS counterpart and three of them (IGR J16195-4945, IGR J16207-5129 and IGR J16318-4848) had a GLIMPSE counterpart given in the literature. We found all the other GLIMPSE counterparts using the 2MASS positions and they are listed in Table 3. We used all the fluxes given in the GLIMPSE catalogue except in the case of IGR J17252-3616, IGR J17391-3021 and IGR J17544-2619 because fluxes were not present in the catalogue tables. Nevertheless, we used the archival images and directly measured their fluxes, using aperture photometry. Uncertainties on the measurements were computed in the same way using the error maps given with the data.

2.3. Absorption

Absorption at wavelength λ, A_λ, is a crucial parameter to fit the SEDs, especially in the MIR. Indeed, inappropriate values can lead to a bad assessment of the MIR excess.

Visible absorption A_V was a free parameter of the fits. An accurate interstellar absorption law - i.e. the wavelength dependence of the $\frac{A_\lambda}{A_V}$ ratio in the line of sight - was then needed to properly fit the SEDs.

In the optical bands, we used the analytical expression given in Cardelli et al. (1989, CAR89 hereafter) who derived the average interstellar extinction law in the direction of the Galactic Center.

From 1.25 μm to 8 μm, we used the analytical expression given in Indebetouw et al. (2005, IND05 hereafter). They derived it from the measurements of the mean values of the color excess ratios $\frac{(A_\lambda - A_K)}{(A_J - A_K)}$ from the color distributions of observed stars in the direction of the Galactic Center. They used archival data from 2MASS and GLIMPSE catalogues, which is relevant in our case as we use GLIMPSE fluxes.

Above 8 μm, where absorption is dominated by the silicate features at 9.7 μm and 18 μm, we found several extinction laws in the literature (Rieke et al. 1989; Lutz et al. 1996; Moneti et al. 2001) which exhibit some differences. Considering the high importance of a good assessment to correctly fit the MIR excess, we decided to assess the ratio $\frac{A_\lambda}{A_V}$ in 2 VISIR bands - PAH1 and PAH2 - from our data in order to build the relevant law for our observations.

Rieke & Lebofsky (1985) gave the interstellar extinction law up to 13 μm and from their results, we derived $0.043 \leq \frac{A_{pah1}}{A_V} \leq 0.074$ and $0.047 \leq \frac{A_{pah2}}{A_V} \leq 0.06$. To get the best values corresponding to our data in PAH1 and PAH2, we proceeded in 3 steps:

- we first selected the sources for which we had VISIR fluxes in PAH1 and/or PAH2 and fitted their SEDs with extinction laws given in CAR89 and IND05 from 0.36 to 8 μm and half-interval values taken in PAH1 and PAH2.
- then, when we did not need any MIR excess to fit the IRAC fluxes, we adjusted the $\frac{A_{pah1}}{A_V}$ and $\frac{A_{pah2}}{A_V}$ ratios to improve the χ^2 of our fits.
- we finally averaged all the extinction values obtained for all sources to get what we consider as the right ratios in PAH1 and PAH2 in the direction of the Galactic Plane.

The resulting values are in good agreement with those given by the extinction law from Lutz et al. (1996), therefore we chose the Lutz' extinction law to fit our SEDs above 8 μm, Q2 filter included.

$\frac{A_\lambda}{A_V}$ values we used in each band are listed in Table 4, and the overall extinction law is displayed on Fig 1.

2.4. SEDs

Using all the archival and observational data from optical to MIR wavelengths, we performed the SEDs of these sources. We fitted them (using a χ^2 minimization) with a model combining two absorbed black-bodies, one representing the companion star emission and a spherical one representing a possible MIR excess due to the absorbing material enshrouding the companion star:

$$\lambda F(\lambda) = \frac{2\pi hc^2}{{D_*}^2 \lambda^4} 10^{-0.4 A_\lambda} \left[\frac{{R_*}^2}{e^{\frac{hc}{\lambda k T_*}} - 1} + \frac{{R_d}^2}{e^{\frac{hc}{\lambda k T_d}} - 1} \right] \quad \text{in W m}^{-2}$$

We added to the flux uncertainties systematic errors as following:

- 2% systematic error in each IRAC band as given in the IRAC manual[1]
- comparing the variations of the flux calibration values obtained from standards with VISIR during our observation nights, we figured out that systematic errors with VISIR were about 5% at 10 μm and 10% at 20 μm

The free parameters of the fits were the absorption in the V-band A_V, the companion star black-body temperature T_* and radius to distance ratio $\frac{R_*}{D_*}$ as well as the additional spherical component black-body temperature and radius T_d and R_d.

Best-fitting parameters for individual sources as well as corresponding χ^2 are listed in Table 5 and fitted SEDs are displayed on Fig 3. Moreover, 90%-confidence ranges of parameters are listed in Table 6.

[1] http://ssc.spitzer.caltech.edu/documents/som/som8.0.irac.pdf

Table 1. Summary of sources studied in this paper. We give in the table their name, their coordinates (J2000 and galactic), the total galactic column density of neutral hydrogen (N_H(HI)) and the total galactic column density of molecular hydrogen ($N_H(H_2)$)in the line of sight, the X-ray column density of the source (N_{Hx}), their type (SFXT or OBS - obscured sources), their spectral type (SpT) and the reference (Ref) about the spectral type. Their spectral types come from optical/NIR spectroscopy, reported in the following references: c: Chaty et al (2007, submitted) f: Filliatre & Chaty (2004), i: in't Zand et al. (2006), n1: Negueruela et al. (2005), n2: Negueruela et al. (2006a), n3: Nespoli et al. (2007), p: Pellizza et al. (2006), t: Tomsick et al. (2006).
N_H(HI) is computed using the web version of the N_H FTOOL from HEASARC. This tool uses the data from Dickey & Lockman (1990), who performed HI observations from Lyman-α and 21cm line. N_H(HI) is the total galactic column density, which means it is integrated along the line of sight over all our Galaxy. Therefore, it is likely overestimated compared to the real value at the distance of the sources.
$N_H(H_2)$ is computed using the velocity-integrated map (W_{CO}) and the X-ratio given in Dame, Hartmann, & Thaddeus (2001). It is also likely overestimated compared to the real value at the distance of the sources as it is integrated along the line of sight over all our Galaxy.
On the contrary, N_{Hx} is computed from the fitting of the high-energy SED so it takes into account all the absorption at the right distance of the source.

Sources	α(J2000)	δ(J2000)	l	b	N_H(HI)(10^{22})	$N_H(H_2)$(10^{22})	N_{Hx}(10^{22})	Type	SpT	Ref
IGR J16195-4945	16 19 32.20	−49 44 30.7	333.56	0.339	2.2	5.4	7.0	SFXT ?	O/B	t
IGR J16207-5129	16 20 46.26	−51 30 06.0	332.46	−1.050	1.7	2.2	3.7	OBS	O/B	t
IGR J16318-4848	16 31 48.60	−48 49 00.0	335.62	−0.448	2.1	3.6	200.0	OBS	sgB[e]	f
IGR J16320-4751	16 32 01.90	−47 52 27.0	336.30	0.169	2.1	4.4	21.0	OBS	O/BI	c
IGR J16358-4726	16 35 53.80	−47 25 41.1	337.01	−0.007	2.2	7.3	33.0	OBS	sgB[e]	c
IGR J16418-4532	16 41 51.00	−45 32 25.0	339.19	0.489	1.9	3.6	10.0	SFXT ?	O/B	c
IGR J16465-4507	16 46 35.50	−45 07 04.0	340.05	0.135	2.1	5.9	60.0	SFXT	B0.5I	n1
IGR J16479-4514	16 48 06.60	−45 12 08.0	340.16	−0.124	2.1	8.2	7.7	SFXT ?	O/BI	c
IGR J17252-3616	17 25 11.40	−36 16 58.6	351.50	−0.354	1.6	3.9	15.0	OBS	O/BI	c
IGR J17391-3021	17 39 11.58	−30 20 37.6	358.07	0.445	1.4	4.5	30.0	SFXT	08Iab(f)	n2
IGR J17544-2619	17 54 25.28	−26 19 52.6	3.26	−0.336	1.4	7.8	1.4	SFXT	O9Ib	p
IGR J19140+0951	19 14 04.23	+09 52 58.3	44.30	−0.469	1.7	3.7	6.0	OBS	B1I	n3

Table 2. Summary of VISIR observations of newly discovered *INTEGRAL* sources. We give in the table their name and their MIR fluxes (mJy) in the PAH1 (8.59 μm), PAH2 (11.25 μm) and Q2 (18.72 μm) filters. When we did not detect a source, we give the upper limit. When no flux nor upper limit is given, the source was not observed in the considered filter.

Sources	PAH1	PAH2	Q2
IGR J16195-4945	< 6.1	< 7.8	< 50.3
IGR J16207-5129	21.7 ± 1.4	9.4 ± 1.3	< 53.4
IGR J16318-4848	426.2 ± 3.0	317.4 ± 3.4	180.7 ± 15.3
IGR J16320-4751	12.1 ± 1.7	6.3 ± 1.8	
IGR J16358-4726	< 6.9		
IGR J16418-4532	< 5.8		
IGR J16465-4507	6.9 ± 1.1	< 5.0	
IGR J16479-4514	10.9 ± 1.2	7.0 ± 1.6	
IGR J17252-3616	6.1 ± 0.6	< 5.0	
IGR J17391-3021	70.2 ± 1.6	46.5 ± 2.6	
IGR J17544-2619	46.1 ± 2.8	20.2 ± 2.1	
IGR J19140+0951	35.2 ± 1.4	19.1 ± 1.4	

3. Results

3.1. IGR J16195-4945

IGR J16195-4945 was detected by *INTEGRAL* during observations carried out between 2003 February 27 and October 19 (Walter et al. 2004) and corresponds to the ASCA source AX J161929-4945 (Sugizaki et al. 2001; Sidoli et al. 2005). Analyzing *INTEGRAL* public data, Sidoli et al. (2005) derived an average flux level of ∼17 mCrab (20-40 keV). Performing a follow-up with *INTEGRAL*, Sguera et al. (2006) showed it behaved like a SFXT and reported a peak-flux of ∼35 mCrab (20-40 keV).

Tomsick et al. (2006) observed the source with *Chandra* between 2005 April and July and gave its position with a 0.″6 accuracy. They fitted its high-energy emission with an absorbed power-law and derived $\Gamma \sim 0.5$ and $N_H \sim 7\times10^{22}$cm^{-2}. Moreover, using their accurate localization, they found its NIR and MIR counterparts in the 2MASS (2MASS J16193220-4944305) and in the GLIMPSE (G333.5571+00.3390) catalogues and performed its NIR photometry using ESO/NTT observations. They showed its spectral type was compatible

Table 3. List of GLIMPSE counterparts we found for 9 sources. We give in the table their name, the name of their GLIMPSE counterparts, their separation from the 2MASS counterparts and their fluxes in mJy at 3.6 μm, 4.5 μm, 5.8 μm and 8 μm. When the counterparts' fluxes were not available in the database, we reduced the corresponding images and directly computed the fluxes.

Sources	GLIMPSE counterpart	Separation	3.6 μm	4.5 μm	5.8 μm	8 μm
IGR J16320-4751	G336.3293+00.1689	0.″17	48.2 ± 1.9	44.3 ± 2.1	36.0 ± 2.0	17.3 ± 1.0
IGR J16358-4726	G337.0994-00.0062	0.″46	5.9 ± 0.5	5.6 ± 0.6	5.3 ± 1.7	
IGR J16418-4532	G339.1889+00.4889	0.″28	12.5 ± 0.9	9.5 ± 0.6	5.6 ± 0.6	3.6 ± 0.4
IGR J16465-4507	G340.0536+00.1350	0.″16	45.0 ± 2.0	32.6 ± 1.5	22.0 ± 0.9	13.7 ± 0.6
IGR J16479-4514	G340.1630-00.1239	0.″13	68.6 ± 3.1	49.6 ± 2.0	41.2 ± 2.3	19.4 ± 0.9
IGR J17252-3616			32.6 ± 3.7	24.7 ± 4.7	21.8 ± 5.0	9.6 ± 6.5
IGR J17391-3021			375.9 ± 44.0	297.0 ± 31.0	205.0 ± 33.0	111.0 ± 28.0
IGR J17544-2619			213.9 ± 25.4	137.0 ± 18.9	99.6 ± 7.6	66.5 ± 12.1
IGR J19140+0951	G044.2963-00.4688	0.″48	185.0 ± 9.3	152.0 ± 11.1	103.9 ± 5.4	62.0 ± 2.1

Table 4. Adopted $\frac{A_\lambda}{A_v}$ values.

Filters	U	B	V	R	I	J	H	Ks	3.6 μm	4.5 μm	5.8 μm	8 μm	8.59 μm	11.25 μm	18.72 μm
$\frac{A_\lambda}{A_v}$	1.575	1.332	1	0.757	0.486	0.289	0.174	0.115	0.0638	0.0539	0.0474	0.0444	0.0595	0.0605	0.040

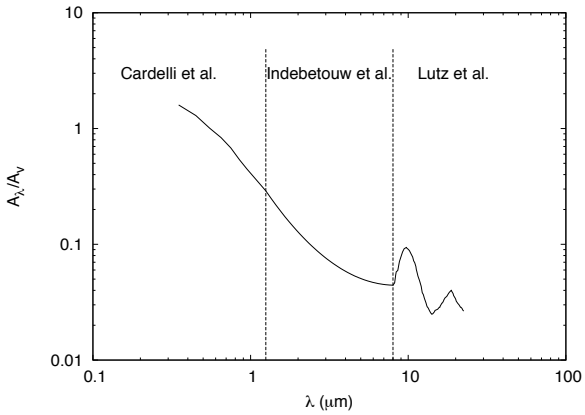

Fig. 1. Adopted extinction law. We used the law given in Cardelli et al. (1989) in the optical, the one given in Indebetouw et al. (2005) from 1.25 μm to 8 μm, and the law from Lutz et al. (1996) above 8 μm.

with an O, B or A supergiant star. They also found possible USNO-A.2 and USNO-B.1 counterparts. Nevertheless, as it was already suggested in their paper, the USNO source is a blended foreground object (Tovmassian et al. 2006).

We observed IGR J16195-4945 on 2006 June 30 in PAH1 during 1200s but we did not detect it. Typical seeing and airmass were 0.″88 and 1.07.
We nevertheless fitted its SED using NIR and GLIMPSE flux values given in Tomsick et al. (2006) and best-fitting parameters are A_V=15.5, T_*=23800K, $\frac{R_*}{D_*}=5.96\times10^{-11}$, T_d=1160K, $R_d=5.1R_*$ and the reduced χ^2 is 3.9/2.
The best-fitting parameters without the additional component are A_V=16.1, T_*=13800K, $\frac{R_*}{D_*}=8.94\times10^{-11}$ and the corresponding reduced χ^2 is 15.8/4. We then found a MIR excess.

The additional component is then necessary to correctly fit the SED as this source exhibits a MIR excess. Nevertheless, as it is shown in Fig 4, this excess is small and the lack of data above 8 μm does not allow to reach definitive conclusions.

Moreover, in both cases (with and without dust), the stellar component is consistent with an O/B supergiant, as it was already suggested in Tomsick et al. (2006).

3.2. IGR J16207-5129

IGR J16207-5129 is an obscured SGXB that was discovered by *INTEGRAL* during observations carried out between 2003 February 27 and October 19 (Walter et al. 2004).

Table 5. Summary of parameters we used to fit the SEDs of the sources. We give in the table their name, the total galactic extinctions in magnitudes A_{HI} and A_{H2}, the X-ray extinction of the source in magnitudes A_X and then the parameters themselves: the extinction in the optical A_V, the temperature T_* and the $\frac{R_*}{D_*}$ ratio of the companion and the temperature and radius T_d and R_d (in R_* unit) of the dust component when needed. We also add the reduced χ^2 we reach for each fit.
A_{HI} and A_{H2} are computed from N_H(HI) and $N_H(H_2)$ given in Table 1 using the relation $A_H = \frac{3.1}{5.8\times10^{21}\,cm^{-2}} N_H$ (Bohlin, Savage, & Drake 1978; Rieke & Lebofsky 1985).

Sources	A_{HI}	A_{H2}	A_X	A_V	T_*(K)	$\frac{R_*}{D_*}$	T_d(K)	$\frac{R_d}{D_*}\left(\frac{R_*}{D_*}\right)$	χ^2/dof
IGR J16195-4945	11.7	28.6	37.4	15.5	23800	5.96×10^{-11}	1160	5.1	3.9/2
IGR J16207-5129	9.3	11.8	19.8	10.5	33800	9.42×10^{-11}			28.5/9
IGR J16318-4848	11.0	19.2	1069.5	17.0	22200	3.74×10^{-10}	1100	10.0	6.6/6
IGR J16320-4751	11.4	23.6	112.2	35.4	33000	1.38×10^{-10}			7.7/6
IGR J16358-4726	11.8	39.4	176.4	17.6	24500	3.16×10^{-11}	810	10.1	3.6/2
IGR J16418-4532	10.1	19.3	53.5	14.5	32800	3.77×10^{-11}			1.4/4
IGR J16465-4507	11.3	31.4	320.7	5.9	25000	6.40×10^{-11}			13.9/7
IGR J16479-4514	11.4	43.8	41.2	18.5	32800	1.00×10^{-10}			7.4/6
IGR J17252-3616	8.3	20.1	80.2	20.8	32600	7.57×10^{-11}			3.8/5
IGR J17391-3021	7.3	23.9	160.4	9.2	31400	1.80×10^{-10}			11.7/10
IGR J17544-2619	7.7	41.5	7.70	6.1	31000	1.27×10^{-10}			6.1/8
IGR J19140+0951	9.0	14.0	32.1	16.5	22500	1.92×10^{-10}			14.4/6

Table 6. Ranges of parameters that give acceptable fits (90% confidence) for each source. We give in the table their name and then the ranges themselves: ΔA_V, ΔT_*, $\Delta\frac{R_*}{D_*}$, ΔT_d and ΔR_d.

Sources	ΔA_V	ΔT_*	$\Delta\frac{R_*}{D_*}$	ΔT_d	ΔR_d
IGR J16195-4945	14.8 – 15.8	13100 – 25900	$5.68\times10^{-11} - 6.68\times10^{-11}$	950 – 1460	3.9 – 6.6
IGR J16207-5129	10.4 – 10.6	25200 – 36000	$9.36\times10^{-11} - 1.05\times10^{-10}$		
IGR J16318-4848	16.6 – 17.4	19300 – 24500	$3.65\times10^{-10} - 3.84\times10^{-10}$	960 – 1260	8.8 – 11.8
IGR J16320-4751	34.8 – 35.5	22000 – 35600	$1.33\times10^{-10} - 1.69\times10^{-10}$		
IGR J16358-4726	17.1 – 18.1	19500 – 36000	$2.64\times10^{-11} - 3.52\times10^{-11}$	630 – 1020	8.0 – 13.8
IGR J16418-4532	13.6 – 14.7	10600 – 36000	$3.58\times10^{-11} - 5.44\times10^{-11}$		
IGR J16465-4507	5.0 – 6.1	15400 – 33600	$5.50\times10^{-11} - 7.95\times10^{-11}$		
IGR J16479-4514	18.4 – 18.8	26200 – 36000	$9.48\times10^{-11} - 1.13\times10^{-10}$		
IGR J17252-3616	20.3 – 21.0	20500 – 36000	$7.17\times10^{-11} - 9.48\times10^{-11}$		
IGR J17391-3021	8.8 – 9.4	16100 – 32200	$1.78\times10^{-10} - 2.63\times10^{-10}$		
IGR J17544-2619	6.0 – 6.2	26700 – 35500	$1.18\times10^{-10} - 1.38\times10^{-10}$		
IGR J19140+0951	15.7 – 16.7	13200 – 28100	$1.71\times10^{-10} - 2.53\times10^{-10}$		

Tomsick et al. (2006) observed it with *Chandra* during the same run as IGR J16195-4945 and gave its position with a 0.″6 accuracy. They also fitted its high-energy emission with an absorbed power-law and derived $\Gamma \sim 0.5$ and $N_H \sim 3.7\times10^{22}cm^{-2}$. Using their accurate localization, they found its NIR and MIR counterparts in the 2MASS (2MASS J16204627-5130060) and in the GLIMPSE (G333.4590+01.0501) catalogues and performed its NIR photometry using ESO/NTT observations. They showed its temperature was to be ⩾18000K, which indicates the system is a HMXB. They also found its USNO-B1.0 (USNO-B1.0 0384-0560875) counterpart.

We observed IGR J16207-5129 on 2006 June 29 in PAH1 and PAH2 during 1200s in each filter and in Q2 during 2400s. Typical seeing and airmass were 0.″72 and 1.09. We did not detect it in Q2 but in PAH1 and PAH2. Fluxes we derived are 21.7±1.4 mJy and 9.4±1.3 mJy respectively.

Using those values as well as fluxes from ESO/NTT observations and GLIMPSE archives found in Tomsick et al. (2006), we fitted its SED and best-fitting parameters are A_V=10.5, T_*=33800K, $\frac{R_*}{D_*}$=9.42×10^{-11} and the reduced χ^2 is 28.5/9. Negueruela & Schurch (2007) found the spectral type was to be earlier than B1I; our parameters are therefore in good agreement with their results.
The best fit with the additional component gives a larger reduced χ^2 of 30/7 and $T_d < 200$K, which is not significant as the presence of such cold material marginally enhances the MIR flux. We therefore think IGR J16207-5129 is an O/B massive star whose enshrouding material marginally contributes to its MIR emission.

3.3. IGR J16318-4848

Main high-energy characteristics of this source can be found in Matt & Guainazzi (2003) and Walter et al. (2003). IGR J16318-4848 was discovered by *INTEGRAL* on 2003 January 29 (Courvoisier et al. 2003) and was then observed with *XMM-Newton* which allowed a 4″localization. Those observations showed that the source was exhibiting a strong absorption of $N_H \sim 2 \times 10^{24} cm^{-2}$, a temperature kT = 9 keV and a photon index $\sim$ 2.

Using this accurate position, Filliatre & Chaty (2004) discovered its optical counterpart and confirmed the NIR counterpart proposed by Walter et al. (2003) (2MASS J16314831-4849005). They also performed photometry and spectroscopy in optical and NIR on 2003 February 23-25 at ESO/NTT and showed that the source presented a significant NIR excess and that it was strongly absorbed ($A_V \sim 17.4$). The spectroscopy revealed an unusual spectrum with a continuum very rich in strong emission lines, which, together with the presence of forbidden lines, pointed towards a sgB[e] companion star (see e.g. Lamers et al. 1998; Zickgraf 1999, for definition and characteristics of these stars).

Using 2MASS magnitudes, GLIMPSE (G335.6260-00.4477) and MSX fluxes, Kaplan et al. (2006) fitted its SED with a combination of a stellar black-body and a dust component black-body and showed that presence of warm dust around the system was necessary to explain the NIR and MIR excess. From their fit, they derived $A_V \sim 18.5$, T_d=1030K and R_d=10R_*.

We observed IGR J16318-4848 with VISIR twice:

- the first one on 2005 June 21 during 300s in PAH1 and PAH2 and 600s in Q2. Typical seeing and airmass were 0.″81 and 1.14. We detected the source in all bands and derived fluxes are 409.2±2.4 mJy, 322.4±3.3 mJy and 172.1±14.9 mJy in PAH1, PAH2 and Q2 respectively.
- the second one on 2006 June 30 during 600s in all bands. Typical seeing and airmass were 0.″68 and 1.09. We detected the source in all bands and derived fluxes are 426.2±3.0 mJy, 317.4±3.4 mJy and 180.7±15.3 mJy in PAH1, PAH2 and Q2 respectively.

Those observations show that IGR J16318-4848 is very bright in the MIR (it is actually the brightest source is our sample) and that its flux was constant within a year, considering VISIR systematic errors.

Using data from our last run as well as magnitudes given in Filliatre & Chaty (2004) in the optical and the NIR and fluxes from the GLIMPSE archives, we fitted its SED and best-fitting parameters are A_V=17, T_*=22200K, $\frac{R_*}{D_*}=3.74 \times 10^{-10}$, T_d=1100K, R_d=10R_* and the reduced χ^2 is 6.6/6.
The best-fitting parameters without the additional component are A_V=17.9, T_*=18200K, $\frac{R_*}{D_*}=5.1 \times 10^{-10}$ and the corresponding reduced χ^2 is 425/8.
We then confirm that the MIR excess is likely due to the presence of warm dust around the system, as already suggested by Filliatre & Chaty (2004) and reported in Kaplan et al. (2006).

3.4. IGR J16320-4751

IGR J16320-4751 was detected by *INTEGRAL* on 2003 February (Tomsick et al. 2003) and corresponds to the ASCA source AX J1631.9-4752. Rodriguez et al. (2003) reported observations with *XMM-Newton*. They gave an accurate localization (3″) and fitted its high-energy spectrum with an absorbed power-law. They derived $\Gamma \sim 1.6$ and $N_H \sim 2.1 \times 10^{23} cm^{-2}$.

Lutovinov et al. (2005) reported on the discovery of X-Ray pulsations (P$\sim$ 1309s) which proved the compact object was a neutron star. Moreover, Corbet et al. (2004) obtained the light curve of IGR J16320-4751 between 2004 December 21 and 2005 September 17 with Swift and reported on the discovery of a 8.96 days orbital period. IGR J16320-4751 is then a X-ray binary whose compact object is a neutron star.

Negueruela & Schurch (2007) searched for its NIR counterpart in the 2MASS catalogue and found its position was consistent with 2MASS J16320215-4752289. They also concluded that if it was an O/B supergiant, it had to be extremely absorbed.

Optical and NIR photometry and spectroscopy of this source were carried out at ESO/NTT and results are reported in CHA07. It is shown that its NIR spectrum is consistent with an O/B supergiant and that its intrinsic absorption is very high, as it was not detected in any of the visible bands.

We searched for its MIR counterpart in the GLIMPSE archives and found it was consistent with G336.3293+00.1689.

We observed IGR J16320-4751 with VISIR on 2005 June 20 in PAH1 and PAH2 and respective exposure times were 1800s and 2400s. Typical seeing and airmass were 0.″63 and 1.13. We detected it in both filters and respective fluxes are 12.1±1.7 mJy and 6.3±1.8 mJy.

Using the ESO/NTT NIR magnitudes given in CHA07 as well as the GLIMPSE and VISIR fluxes, we fitted its SED and best-fitting parameters are A_V=35.4, T_*=33000K, $\frac{R_*}{D_*}=1.38 \times 10^{-10}$ and the reduced χ^2 is 7.7/6. This result is in good agreement with an extremely absorbed O/B supergiant as reported in CHA07.
The best fit with the additional component gives a larger reduced χ^2 of 8/4 and $T_d < 200$K.

We therefore think that IGR J16320-4751 is an O/B supergiant whose enshrouding material marginally contributes to its MIR emission, even if its intrinsic absorption is extremely high.

3.5. IGR J16358-4726

IGR J16358-4726 was detected with *INTEGRAL* on 2003 March 19 (Revnivtsev et al. 2003) and first observed with *Chandra* on 2003 March 24 (Patel et al. 2004). They gave its position with a 0.″6 accuracy and fitted its high-energy spectrum with an absorbed power-law. They derived $\Gamma \sim 0.5$ and $N_H \sim 3.3 \times 10^{23} cm^{-2}$. They also found a 5880±50s modulation, which could be either a neutron star pulsation or an orbital modulation. Nevertheless, Patel et al. (2006) performed detailed spectral and timing analysis of this source using multi-satellite archival observations and identified a 94s spin up, which points to a neutron star origin. Assuming this spin up

was due to accretion, they estimated the source magnetic field was between 10^{13} and 10^{15} G which could support a magnetar nature of IGR J16358-4726.

Kouveliotou et al. (2003) proposed 2MASS J16355369-4725398 as the possible NIR counterpart and NIR spectroscopy and photometry of this counterpart were performed at ESO/NTT and are reported in CHA07. They show that its spectrum is consistent with a B supergiant belonging to the same family as IGR J16318-4848, the so-called B[e] supergiants.

We also found its MIR counterpart in the GLIMPSE archives (G337.0994-00.0062).

We observed IGR J16358-4726 with VISIR on 2006 June 29 but did not detect it in any filter. Using NIR magnitudes given in CHA07 and GLIMPSE fluxes, we fitted its SED and best-fitting parameters are A_V=17.6, T_*=24500K, $\frac{R_*}{D_*}$=3.16 × 10^{-11}, T_d=810K, R_d=10.1R_* and the reduced χ^2 is 3.6/2.
The best-fitting parameters without the additional component are A_V=16.7, T_*=9800K, $\frac{R_*}{D_*}$=6.05×10^{-11} and the corresponding reduced χ^2 is 8.8/4.

The additional component is then necessary to correctly fit the SED as this source exhibits a MIR excess (see Fig 4). Even if we lack MIR data above 5.8 μm, we think this excess is real and is due to warm dust as it is consistent with the source to be a sgB[e] as reported in CHA07.

3.6. IGR J16418-4532

IGR J16418-4532 was discovered with *INTEGRAL* on 2003 February 1-5 (Tomsick et al. 2004). Using *INTEGRAL* observations, Sguera et al. (2006) reported a SFXT behaviour of this source and a peak-flux of ∼ 80 mCrab (20-30 keV). Moreover, using *XMM-Newton* and *INTEGRAL* observations, Walter et al. (2006) reported a pulse period of 1246±100s and derived $N_H \sim 10^{23}$cm^{-2}. They also proposed 2MASS J16415078-4532253 as its likely NIR counterpart. NIR photometry of this counterpart was performed at ESO/NTT and is reported in CHA07. We also found the MIR counterpart in the GLIMPSE archives (G339.1889+004889).

We observed IGR J16418-4532 with VISIR on 2006 June 29 but did not detect it in any filter. Using NIR magnitudes given in CHA07 as well as GLIMPSE fluxes, we fitted its SED and best-fitting parameters are A_V=14.5, T_*=32800K, $\frac{R_*}{D_*}$=3.77 × 10^{-11} and the reduced χ^2 is 1.4/4.
The best fit with the additional component gives a larger reduced χ^2 of 3.9/2 and T_d < 200K.

Uncertainties on the data are high and this is the reason why reduced χ^2 are low. Nevertheless, parameters of the fit as well as the 90%-confidence ranges of parameters listed in Table 6 are consistent with an O/B massive star nature. The temperature of the additional component being insignificant, we conclude this source is an O/B massive star whose enshrouding material marginally contributes to its MIR emission.

3.7. IGR J16465-4507

IGR J16465-4507 is a transient source discovered with *INTEGRAL* on 2004 September 6-7 (Lutovinov et al. 2004). Observations were carried out on 2004 September 14 with *XMM-Newton* and Zurita Heras & Walter (2004) reported a position with a 4″accuracy, allowing to identify a NIR counterpart in the 2MASS catalogue (2MASS J16463526-4507045=USNO-B1.0 0448-00520455). Using the ESO/NTT, Negueruela et al. (2005) performed intermediate resolution spectroscopy of the source, estimated the spectral type was a B0.5I and proposed it to be a SFXT. Using *XMM-Newton* and *INTEGRAL*, Walter et al. (2006) found a pulse period of 227±5s and derived $N_H \sim 6 \times 10^{23}$cm^{-2}. We found its MIR counterpart in the GLIMPSE archives (G340.0536+00.1350) using the 2MASS position.

We observed IGR J16465-4507 with VISIR twice:

- the first one on 2005 June 20 during 600s in PAH1. Typical seeing and airmass were 0.″81 and 1.14. We detected the source and derived flux is 8.7±1.8 mJy.
- the second one on 2006 June 30 during 1200s in PAH1 and PAH2. Typical seeing and airmass were 0.″68 and 1.09. We detected the source in PAH1 but not in PAH2. Derived flux is 6.9±1.1 mJy.

These observations show that IGR J16465-4507 MIR flux was constant within a year.

Using USNO-B1.0, 2MASS and GLIMPSE flux values as well as our VISIR data, we fitted its SED and best-fitting parameters are A_V=5.9, T_*=25000K, $\frac{R_*}{D_*}$=6.4 × 10^{-11} and the reduced χ^2 is 13.9/7.
The best fit with the additional components gives a larger reduced χ^2 of 20/5 and T_d < 200K.

We then conclude that no additional component is necessary to explain the MIR emission of this source, and the parameters derived from our fit are in good agreement with IGR J16465-4507 to be a B0.5I as reported in Negueruela et al. (2005).

3.8. IGR J16479-4514

IGR J16479-4514 was discovered with *INTEGRAL* on 2003 August 8-9 (Molkov et al. 2003). Sguera et al. (2005) suggested it was a fast transient after they detected recurrent outbursts and Sguera et al. (2006) reported a peak-flux of ∼ 120 mCrab (20-60 keV). Walter et al. (2006) observed it with *XMM-Newton* and gave its position with a 4″accuracy. Moreover, they derived $N_H \sim 7.7 \times 10^{22}$cm^{-2} from their observations. They also proposed 2MASS J16415078-4532253=USNO-B1.0 0447-0531332 as its likely NIR counterpart. NIR spectroscopy and photometry of this counterpart were performed at ESO/NTT and are reported in CHA07 and it is shown that its spectrum is consistent with an O/B supergiant. We also found the MIR counterpart in the GLIMPSE archive (G339.1889+004889).

We observed IGR J16479-4514 with VISIR on 2006 June 29 in PAH1 and PAH2 and exposure time was 1200s in each

filter. Typical seeing and airmass were 0.″9 and 1.14. We detected it in both filters and respective fluxes are 10.9±1.2 mJy and 7.0±1.6 mJy. Using the NIR magnitude given in CHA07 as well as GLIMPSE and VISIR fluxes, we fitted its SED and best-fitting parameters are A_V=18.5, T_*=32800K, $\frac{R_*}{D_*}$=1.00 × 10^{-10} and reduced χ^2 is 7.4/6.
The best fit with the additional component gives a larger reduced χ^2 of 9/4 and T_d < 200K.

We then do not need any additional component to fit the SED and our result is then consistent with IGR J16479-4514 to be an obscured O/B supergiant in good agreement with CHA07.

3.9. IGR J17252-3616

IGR J17252-3616 is a heavily-absorbed persistent source discovered with *INTEGRAL* on 2004 February 9 and reported in Walter et al. (2004). It was observed with *XMM-Newton* on 2004 March 21 and Zurita Heras et al. (2006) gave its position with a 4″accuracy. Using the *XMM-Newton* observations as well as those carried out with *INTEGRAL*, they showed the source was a binary X-ray pulsar with a spin period of ∼413.7s and an orbital period of ∼ 9.72 days and derived $N_H \sim 1.5 \times 10^{23}$cm^{-2}. Moreover, they fitted its high-energy spectrum with either an absorbed compton (kT∼5.5 keV and $\tau \sim 7.8$) or a flat power law ($\Gamma \sim 0.02$).

In their paper, they proposed 2MASS J17251139-3616575 to be its likely NIR counterpart as did Negueruela & Schurch (2007). NIR spectroscopy and photometry of this counterpart were performed at ESO/NTT and are reported in CHA07 and it is shown that its spectrum is consistent with an O/B supergiant. Using the 2MASS position, we searched for its MIR counterpart in the GLIMPSE catalogue. Unfortunately, we did not find its IRAC fluxes in the database. Nevertheless, we found post-Basic Calibrated Data (post-BCD) images of the source in all filters. We then reduced those data and derived fluxes directly from the images. They are listed in Table 3.

We observed IGR J17252-3616 with VISIR on 2006 June 30 in PAH1 and PAH2 and exposure time was 1200s in each filter. Typical seeing and airmass were 0.″97 and 1.09. We detected it in PAH1 and derived flux is 6.1±0.6 mJy. Using the NIR magnitudes given in CHA07 as well as the GLIMPSE and VISIR fluxes, we fitted its SED and best-fitting parameters are A_V=20.8, T_*=32600K, $\frac{R_*}{D_*}$=7.57 × 10^{-11} and reduced χ^2 is 3.8/5.
The best fit with the additional component gives a larger reduced χ^2 of 6.9/3 and T_d < 200K.

We then do not need any additional component to fit the SED and our result is consistent with IGR J17252-3616 to be an obscured O/B supergiant in good agreement with CHA07.

3.10. IGR J17391-3021

IGR J17391-3021 is a transient source discovered with *INTEGRAL* on 2003 August 26 (Sunyaev et al. 2003) and corresponds to the *Rossi X-ray Timing Explorer* (*RXTE*) source XTE J1739-302. Sguera et al. (2005) analyzed archival *INTEGRAL* data and classified the source as a Fast X-ray transient presenting a typical neutron star spectrum. Smith et al. (2006) observed it with *Chandra* on 2003 October 15 and gave its precise position with a 1″accuracy. They also gave its optical/NIR counterpart 2MASS J17391155-3020380=USNO B1.0 0596-0585865 and classified IGR J17391-3021 as a SFXT. Negueruela et al. (2006a) performed optical/NIR photometry and spectroscopy of the companion using ESO/NTT and found it was a O8Iab(f) star whose distance was ∼2.3kpc. CHA07 also report on optical and NIR spectroscopy and photometry of the companion carried out at ESO/NTT and confirm the nature of the companion. Using the 2MASS position, we searched for its MIR counterpart in the GLIMPSE catalogue and as for IGR J17252-3616, we had to reduce post-BCD data and derive fluxes directly from the images. Fluxes are listed in Table 3.

We observed IGR J17391-3021 with VISIR on 2005 June 20 in PAH1 and PAH2 and exposure time was 600s in each filter. Typical seeing and airmass were 0.″63 and 1.13. We detected it in both filters and derived fluxes are 70.2±1.6 mJy and 46.5±2.6 mJy. Using optical and NIR magnitudes given in CHA07 as well as GLIMPSE and VISIR fluxes, we fitted its SED and best-fitting parameters are A_V=9.2, T_*=31400K, $\frac{R_*}{D_*}$=1.8 × 10^{-10} and reduced χ^2 is 11.7/10.
The best fit with the additional component gives a larger reduced χ^2 of 15.3/8 and T_d < 200K.

We then do not need any additional component to fit the SED and the parameters derived from our fit are in good agreement with IGR J17391-3021 to be an O8Iab(f) supergiant star, as initially reported in Negueruela et al. (2006a).

3.11. IGR J17544-2619

IGR J17544-2619 is a transient source discovered with *INTEGRAL* on 2003 September 17 (Sunyaev et al. 2003). González-Riestra et al. (2004) observed it with *XMM-Newton* and derived $N_H \sim 2 \times 10^{22}$cm^{-2}. They also confirmed the association of the companion with 2MASS J17542527-2619526=USNO-B1.0 0636-0620933, as proposed in Rodriguez (2003). in't Zand (2005) reported about observations performed with *Chandra*, gave its position with a 0.″6 accuracy, $N_H \sim 1.36 \times 10^{22}$cm^{-2} and showed that its high-energy spectrum was typical of an accreting neutron star. Moreover, they identified the counterpart as a blue supergiant. Sguera et al. (2006) reported a peak-flux of ∼240 mCrab. Using ESO/NTT, Pellizza et al. (2006) performed optical/NIR spectroscopy and photometry of the companion and gave its spectral type to be O9Ib at 2.1-4.2 kpc. Using the 2MASS position, we searched for its MIR counterpart in the GLIMPSE catalogue and as for IGR J17252-3616 and IGR J17391-3021, we had to reduce post-BCD data and derived fluxes directly from the images. Fluxes are listed in Table 3.

We observed IGR J17544-2619 with VISIR on 2005 June 20 in PAH1 and PAH2 and exposure time was 600s in PAH1

and 1200s in PAH2. Typical seeing and airmass were 0.″64 and 1.13. We detected it in both filters and derived fluxes are 46.1±2.8 mJy and 20.2±2.1 mJy. Using magnitudes from Pellizza et al. (2006), GLIMPSE and VISIR fluxes, we fitted its SED and best-fitting parameters are A_V=6.1, T_*=31000K, $\frac{R_*}{D_*}$=1.27×10^{-10} and reduced χ^2 is 6.1/8.
The best fit with the additional component gives a larger reduced χ^2 of 9/6 and T_d < 200K.

We then do not need any additional component to fit the SED and the parameters derived from our fit are in good agreement with IGR J17544-2619 to be an O9Ib supergiant star, as initially reported in Pellizza et al. (2006).

3.12. IGR J19140+0951

IGR J19140+0951 is a persistent source that was discovered with *INTEGRAL* on 2003 March 6-7 (Hannikainen et al. 2003). Observations carried out with *RXTE* allowed to derived $\Gamma \sim 1.6$ and $N_H \sim 6 \times 10^{22}$cm^{-2} (Swank & Markwardt 2003). Timing analysis of the *RXTE* data showed a period of 13.55 days (Corbet et al. 2004) which shows the binary nature of the source. Rodriguez et al. (2005), after a comprehensive analysis of *INTEGRAL* and *RXTE* data, showed the source was spending most of its time in a faint state but reported high variations of luminosity and absorption column density (up to $\sim 10^{23}$cm^{-2}). They also found evidence that the compact object was a neutron star rather than a black hole. Using *Chandra* observations carried out 2004 May 11, in't Zand et al. (2006) gave its position with a 0.″6 accuracy. This allowed them to find its NIR counterpart in the 2MASS catalogue (2MASS J19140422+0952577). Moreover, they searched for its MIR counterpart in the Mid-course Space Experiment (MSX Mill 1994) and found an object at 8.3 μm. NIR photometry and spectroscopy of this source were performed at ESO/NTT and results are reported in CHA07. It is shown that its spectrum is consistent with an O/B massive star, in good agreement with Nespoli et al. (2007) who showed it was a B1I supergiant. Using the 2MASS position, we also found its MIR counterpart in the GLIMPSE archive (G044.2963-00.4688).

We observed IGR J19140+0951 with VISIR on 2006 June 30 in PAH1 and PAH2 and exposure time was 1200s in each filter. Typical seeing and airmass were 1.″12 and 1.17. We detected it in both filters and derived fluxes are 35.2±1.4 mJy and 19.1±1.4 mJy. We point out that the object given as the MSX counterpart of IGR J19140+0951 in in't Zand et al. (2006) is a blended source. Indeed, VISIR images, whose resolution is far better, clearly show there are two sources in the field, IGR J19140+0951 and a very bright southern source (see Fig 2).

Using magnitudes given in CHA07 as well as fluxes from GLIMPSE and our observations with VISIR, we fitted its SED and best-fitting parameters are A_V=16.5, T_*=22500K, $\frac{R_*}{D_*}$=1.92×10^{-10} and reduced χ^2 is 14.4/6.
The best fit with the additional component gives a larger reduced χ^2 of 20.2/4 and T_d < 200K.

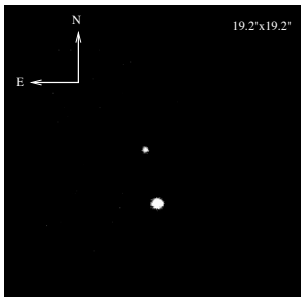

Fig. 2. VISIR image of IGR J19140+0951 in PAH1 (8.59 μm). 19.″2x19.″2 field of view and 0.″075 plate scale. We clearly see the two sources which were blended with MSX. The MIR counterpart of IGR J19140+0951 is the northern source.

We do not need any additional component to fit the SED and the parameters derived from our fit are in good agreement with IGR J19140+0951 to be an B1I supergiant star, as initially reported in Nespoli et al. (2007).

4. Discussion

4.1. B vs B[e] supergiants stellar winds

All SEDs were best-fitted without any dust component (even the very absorbed one like IGR J16320-4751) except three of them (IGR J16195-4945, IGR J16318-4848 and IGR J16358-4726, see Fig. 3) which exhibit a MIR excess likely due to the presence of dust in their stellar wind.

Blue supergiants are known to exhibit a very strong but sparse stellar wind of high velocity (~1000-2000 km.s^{-1}). This was explained through the so-called radiation line-driven CAK model (Castor, Abbott, & Klein 1975) in which the wind is driven by absorption in spectral lines. Hot stars emit most of their radiation in the ultraviolet (UV) where their atmosphere have many absorption lines. Photons coming from the photosphere of the star with the same wavelength are absorbed and re-emitted to the expanding medium in a random direction with almost the same momentum, which results in acceleration of the wind. This process is very effective because the line spectrum of the scattering ions in the wind is Doppler-shifted compared to the stellar rest-frame. So, the scattering atoms are shifted with respect to their neighbours at lower velocities and can interact with an unaffected part of the stellar spectrum.

IGR J16318-4848 was proved to belong to a particular class of B1 supergiants, the B[e] supergiants or sgB[e] (Filliatre & Chaty 2004). A physical definition of B[e] stars can be found in Lamers et al. (1998). We will just remind here two of the characteristics: the presence of forbidden emission lines of [Fe II] and [O I] in the NIR spectrum and the presence of a strong MIR excess due to hot circumstellar dust which re-emits the absorbed stellar radiation through free-free emission. A sgB[e] is defined by the B[e] phenomenon plus the indication of mass loss in the optical spectrum (P-cygni

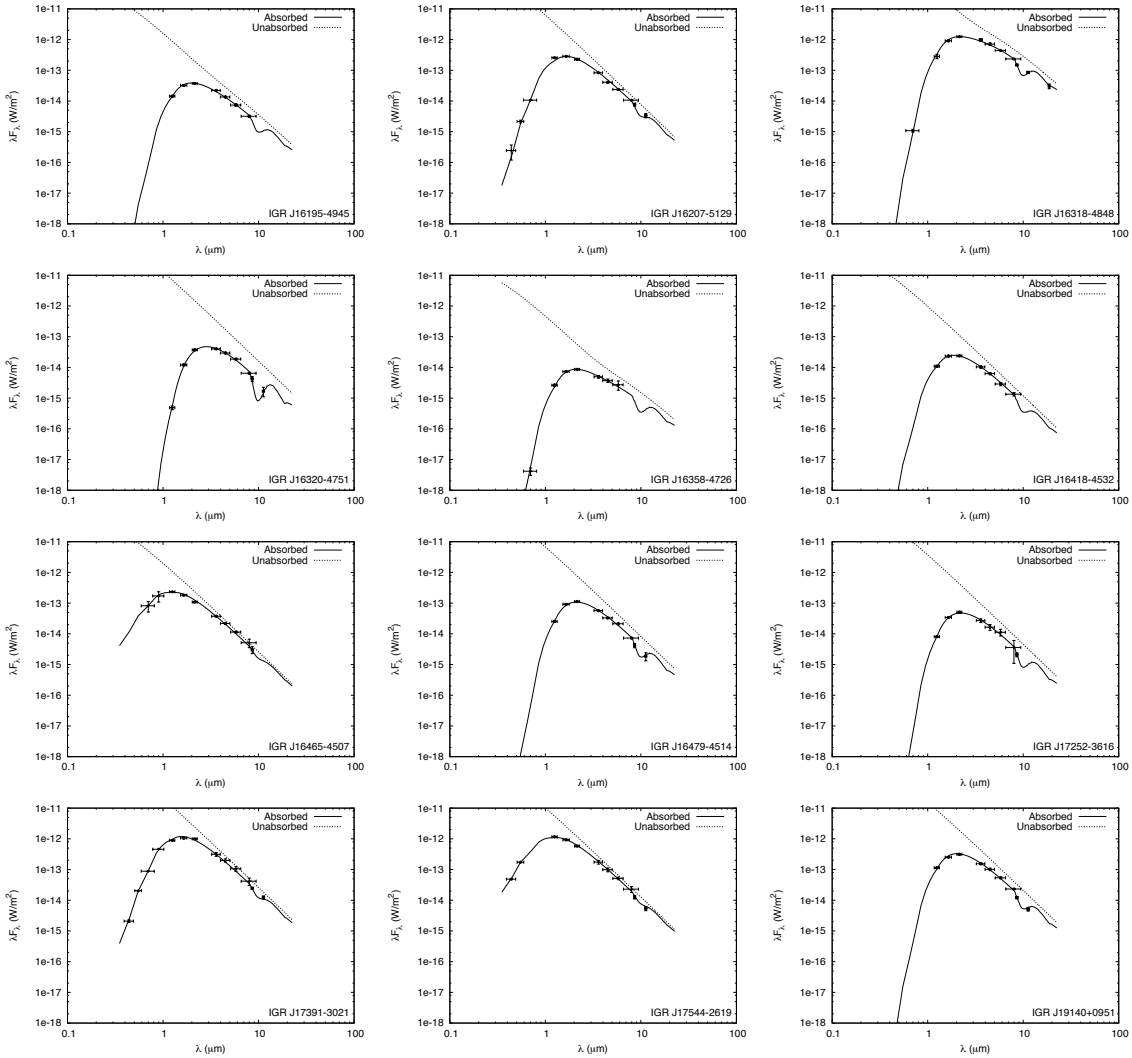

Fig. 3. Optical to MIR absorbed (line) and unabsorbed (dotted-line) SEDs of 12 *INTEGRAL* sources, including data from ESO/NTT, 2MASS, GLIMPSE and VISIR.

profiles) as well as an hybrid spectrum characterized by the simultaneous presence of narrow low-excitation lines and broad absorption features of high-excitation lines. This hybrid nature was empirically explained by the simultaneous presence of a normal supergiant hot polar wind (fast and sparse) and responsible for the broad lines and a cool equatorial outflowing disk-like wind (slow and dense) responsible for the narrow lines (Shore & Sanduleak 1983; Zickgraf et al. 1985; Shore et al. 1987). This empirical model received some confirmation from polarimetry (Oudmaijer & Drew 1999).

There are a few models to explain the creation of this outflowing disk and all of them consider the star rotation to be an important parameter in the process. In this paper, we will only present the most consistent of them, the Rotation Induced Bi-stability mechanism (RIB), but a review can be found in Kraus & Miroshnichenko (2006).

The lines responsible for the creation of the wind are dependent on the ionization structure, and a change in this structure leads to a change of the radiative flux. This is the bi-stability jump, found by Lamers & Pauldrach (1991), which appears for

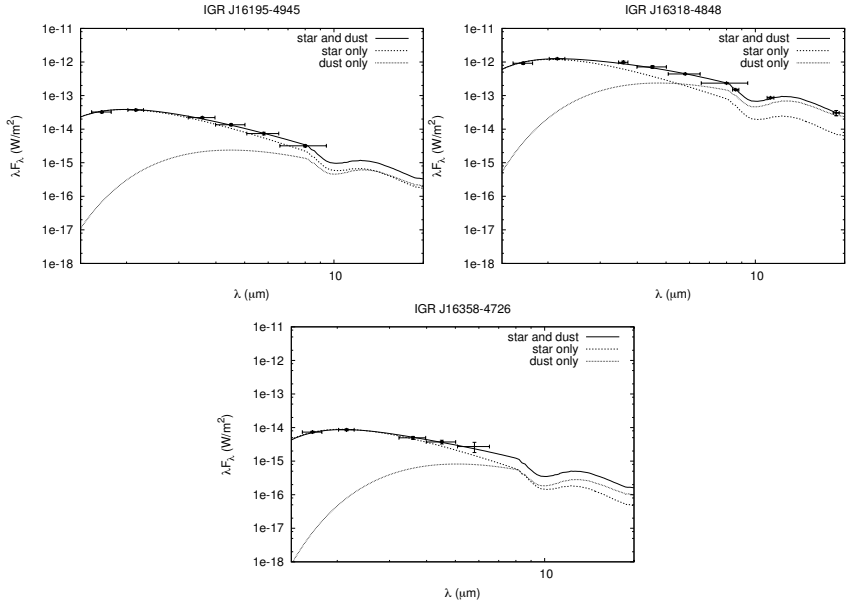

Fig. 4. Optical to MIR SEDs of IGR J16195-4945, IGR J16318-4848 and IGR J16358-4726 in the NIR and the MIR. We show their SEDs including the contribution of the star and the dust (line), the star only (dashed-line) and the dust only (dotted-line).

B stars with effective temperatures of about 23000k. Above this temperature, the wind tends to be fast and sparse. Below, the mass loss rate if five times larger and the terminal velocity two times slower which leads to a wind ten times denser.

Cassinelli & Ignace (1997) proposed that the same effect was important from polar to equatorial regions for rapidly rotating B stars. Indeed, the rapid rotation leads to polar brightening which increases the poles temperature to the hot side of the jump. At the same time, the rotation leading to gravity darkening, the equatorial region may be on the cool side of the jump. Consequently, the wind in the equatorial region is denser than the wind in the polar region. Nevertheless, Pelupessy et al. (2000) showed that the rotational velocity of the star should be very close to its critical value to allow the equatorial wind to reach the density necessary to create the disk. However, supergiant stars cannot be close to critical rotational velocity because of likely disruption. Additional mechanisms are therefore necessary to allow the supergiant star to reach its critical velocity (see e.g. Owocki 2006). In the particular case of a sgB[e] star in an X-ray binary system, the spin-up should occur during the supergiant phase of the companion, which indicates a different evolutionary stage from other HMXBs.

This disk itself cannot explain the strong MIR excess the sgB[e] stars exhibit. Nevertheless, Bjorkman & Cassinelli (1993) showed the existence of a zone in the disk (about 50-60 stellar radii from the star) in which the temperature is below the temperature of sublimation of the dust (about 1500K) and density high enough to allow for its creation.

IGR J16318-4848 is the source in our sample that exhibits the strongest MIR excess and we believe it is due to the sgB[e] nature of its companion star. Indeed, many other strongly absorbed sources in our sample do not present any MIR excess.

Moreover, IGR J16358-4726, the second source in our sample that exhibits a MIR excess and whose SED needs an additional component to be properly fitted, was suggested to be a sgB[e] as its spectrum has all the characteristic features of supergiant stars plus the [Fe II] feature (CHA07). Our fit is therefore in good agreement with their result and the only other source of our sample that surely exhibits a MIR excess is indeed a sgB[e] star.

In the case of IGR J16195-4945, we are more cautious concerning the presence of warm dust which could be responsible for a MIR excess as we lack data above 8 μm. Indeed, Fig 4. shows that these source could exhibit a MIR excess but much lower than the two others. Nevertheless, if this excess was to be confirmed, we believe it would be also due to the sgB[e] nature of the companion.

Finally, we would like to stress out the fact that in a sgB[e] star, the dust being mostly located in an equatorial disk, the simple model we used to fit the SEDs cannot reproduce the complex distribution of the dust around these stars. Nevertheless, it allows the detection of a warm MIR excess due to the presence of dust in the stellar winds.

At last, concerning all the stars in our sample, we cannot exclude the presence of a cold component - responsible for their intrinsic absorption - which we cannot detect due to the lack of data above 20 μm.

Table 7. Summary of spectral types (SpT) and distances (D_*) we derived from our fits for confirmed supergiant stars in our sample. (*) are sources with an accurate spectral type found in the literature, (†) are confirmed supergiant stars whose temperature derived from our fits was used to assess their accurate spectral type using the O/B supergiant classifications given in Martins et al. (2005) and Crowther et al. (2006). References on the determination of the spectral type and/or spectral class of these sources are found in Table 1.

Sources	SpT	D_*(kpc)
IGR J16318-4848*	sgB[e]	~ 1.6
IGR J16320-4751†	O8I	~ 3.5
IGR J16358-4726*	sgB[e]	~ 18.5
IGR J16465-4507*	B0.5I	~ 9.4
IGR J16479-4514†	O8.5I	~ 4.9
IGR J17252-3616†	O8.5I	~ 6.1
IGR J17391-3021*	O8I	~ 2.7
IGR J17544-2619*	O9I	~ 3.6
IGR J19140+0951*	B1I	~ 3.1

Table 8. Summary of distances (D_*) we derived from our fits for sources with unconfirmed spectral classes. We give in the table their spectral types as derived from our fits and their expected distances depending on their possible spectral classes.

Sources	SpT	D_*(kpc)		
		V	III	I
IGR J16195-4945	B1	~ 3.1	~ 5.7	~ 9.8
IGR J16207-5129	O7.5	~ 1.8	~ 2.8	~ 4.1
IGR J16418-4532	O8.5	~ 4.9	~ 8.3	~ 13

4.2. Spectral type and distance

Among our sample, six sources are supergiant stars with a known spectral type - IGR J16318-4848 and IGR J16358-4726 are sgB[e], IGR J16465-4507 is a B0.5I, IGR J17391-3021 is an 08Iab(f), IGR J17544-2619 is an O9Ib and IGR J19140+0951 is a B1I - and three are found to be O/B supergiants whose temperatures derived from our fits allow an assessment of the spectral types using the classification given in Martins et al. (2005) and Crowther et al. (2006) for O and B galactic supergiants respectively, given the uncertainties of observational results (~ 2000K) and uncertainties on the fits temperatures as given in Table 6. We therefore derived that IGR J16320-4751 could be an 08I and IGR J16479-4514 and IGR J17252-3616 could be 08.5I stars.

Concerning the last three sources whose spectral class is unknown, results of the fits listed in tables 5 and 6 show that they likely are all O/B massive stars and we also used their derived temperatures to assess their spectral type using the classification given in both papers quoted above. IGR J16195-4945 could be a B1 star, and as already stressed above, it could be sgB[e] due to its MIR excess, and IGR J16207-5129 and IGR J16418-4532 could be O7.5-O8.5 stars. Nevertheless, even if the high intrinsic X-ray absorption of their associated compact objects points out towards a supergiant nature as it means the accretion is likely wind-fed, the fits themselves do not allow an assessment of their spectral classes. We will then consider they could be either main sequence, giant or supergiant stars.

Martins & Plez (2006) give a UBVJHK synthetic photometry of galactic OI, OIII and OV stars, with which one can get the expected unabsorbed absolute magnitude in J band M_j for stars having a given spectral classification. Using the absorbed apparent magnitudes m_j of our sources and the J band absorption we derived from our fits, $A_j = 0.289 \times A_V$, it is then possible to assess the distance of O stars in our sample using the standard relation:

$$D_* = 10^{0.2(m_j - A_j - M_j + 5)} \quad \text{in pc}$$

We did not find any synthetic photometry for B supergiants. Nevertheless, expected radii of galactic BI, BIII and BV stars are given in Vacca et al. (1996) and we divided these values by the $\frac{R_*}{D_*}$ ratio derived from our fits to get the star distance.

Derived distances for the sources whose spectral class is known are listed in Table 7, in Table 8 for the others.

4.3. X-ray properties

Except in the case of IGR J17544-2619, X-ray absorptions are systematically significantly larger than the visible absorptions. This indicates the presence in the system of a two components absorbing material: one around the companion star, responsible for the visible absorption, and a very dense one around the compact object coming from the stellar winds that accrete onto the compact object and responsible for the huge X-ray absorption those sources exhibit.

The obscuration of the compact object by the stellar wind is due to the photoelectric absorption of the X-ray emission by the wind, and this absorption varies along the orbit of the compact object. This orbital dependence was for instance observed and modelled on 4U 1700-37 (Haberl, White, & Kallman 1989).

Moreover, an effect on the X-ray absorption due to the photoionization of the stellar wind in the vicinity of the compact object by its X-ray emission was predicted (Hatchett & McCray 1977). Indeed, in SGXBs, the compact object moves through the stellar wind of the companion star, and the X-rays are responsible for the enhancement or the depletion of the ionized atoms responsible for the acceleration of the wind (e.g. C_{IV} and N_V). This has a direct consequence on the velocity profile of the wind; when the wind enters into an ionized zone, it follows a standard CAK law until it reaches a location in which it is sufficiently ionized that no further radiative driving takes place and the wind velocity is "frozen" to a constant value from this point. This results into a lower wind velocity close to the compact object and consequently a higher wind density which leads to a higher obscuration of the compact object.

Most of the sources studied in this work are very absorbed in the high-energy domain. Nevertheless, this absorption may

Table 9. Summary of parameters we used to fit the SEDs of the isolated supergiants. We give in the table their name, their galactic coordinates, their spectral types, the interstellar extinction in magnitudes A_i and then the parameters themselves: the extinction in the optical A_V, the temperature T_* and the $\frac{R_*}{D_*}$ ratio of the star.
Distances of these stars are known, and A_i is obtained from N_{Hi} computed with the N(HI) calculator available on the MAST website, which gives the column density of neutral hydrogen in the line of sight out to their distance.

Sources	l	b	SpT	A_i	A_V	$T_*(K)$	$\frac{R_*}{D_*}$
HD 144969	333.18	2.0	B0.5Ia	3.34	3.9	26000	4.01×10^{-10}
HD 148422	329.92	−5.6	B0.5Ib	0.75	0.9	24700	8.76×10^{-11}
HD 149038	339.38	2.51	B1Ia	0.81	1	24000	5.30×10^{-10}
HD 151804	343.62	1.94	O8Iaf	0.83	1.3	32000	4.20×10^{-10}
HD 152234	343.46	1.22	B0.5Ia	1.17	1.5	25100	4.94×10^{-10}
HD 152235	343.31	1.1	B1Ia	3.37	3.9	24500	1.13×10^{-9}
HD 152249	343.35	1.16	O9Ib	1.34	1.7	30100	2.89×10^{-10}
HD 156201	351.51	1.49	B0.5Ia	2.68	2.9	26500	2.90×10^{-10}

not be always that high. Indeed, in the case of very wide eccentric orbits, their column density could normally vary along their orbit and suddenly increase when very close to the companion star because of the wind ionization. On the contrary, if these objects were to be always very absorbed, it could mean that their orbit is very close to the companion star and weakly eccentric. If this effect were to be observed, we think it could explain the difference of behaviour between obscured SGXBs (close quasi-circular orbits) and SFXTs (wide eccentric orbits).

4.4. Optical properties

We were able to fit all the sources but three with a simple stellar black-body model. Concerning these three sources, we explained that the MIR excess was likely due to the presence of warm dust created within the stellar wind due to the sgB[e] nature of the companions. Therefore, it seems that the optical to MIR wavelengths emission of these SGXBs corresponds to the emission of absorbed blue supergiants or sgB[e].

Moreover, the results of the fits listed in the Table 5 show that it is *a priori* not possible to differentiate an obscured SGXB and a SFXT from their optical to MIR wavelengths SEDs and it then seems that the difference of behaviour between both kinds of SGXBs depends only on the geometry of the system, i.e. its orbital distance or its orbit eccentricity (Chaty & Rahoui 2007).

Nevertheless, in order to assess a possible effect of the compact object on the companion star, we took a sample of eight isolated O/B supergiants in the direction of the Galactic Center and fitted their optical to NIR wavelengths SEDs with an absorbed stellar black-body. Best-fitting parameters are listed in Table 9. Distances of these supergiants are known, and this allowed to calculate the accurate HI column density out to their position using the tool available on the MAST website (Fruscione et al. 1994).

We see that their visible absorption is of the same order of magnitude as the interstellar HI absorption and well below the level of absorption of our sources. This could mean that some supergiant stars in SGXBs exhibit an excess of absorption due to a local absorbing component. Unfortunately, the total interstellar absorption out to the distance of our sources is unknown and we cannot compare their visible absorptions derived from our fits to the total interstellar absorption out to their position.

Nevertheless, if this was the case, we think that this excess of absorption could also be partly due to the photoionization of the wind in the vicinity of the companion star by the high-energy emission of the compact object, as this would make their winds slower than in isolated supergiant stars. Since the wind velocity is smaller, the medium is denser and suitable to create a more absorbing material.

Indeed, in the case of persistent sources with very close and quasi-circular orbits, we think that this possible effect could be particularly strong as the wind around the companion star would be permanently photoionized and would have lower velocities than in isolated supergiants. This could be the general scheme of obscured SGXBs.

On the other hand, in the case of very wide and eccentric orbits, the compact object would be most of the time far from the secondary and its X-ray emission would not photoionize the wind close to the companion star, which would not exhibit any visible absorption excess until the compact object get closer. This could be the general scheme of SFXTs.

At last, in both cases, it would be possible to observe a variation of the P-Cygni profiles of the companion star (i.e. a variation of the wind velocity) with the phase angle of the compact object along its orbit.

As a possible confirmation of this general behaviour, we point out that the visible absorptions derived from our fits for the companion stars of the only sources in our sample that surely exhibit the SFXT behaviour (IGR J16465-4945, IGR J17391-3021 and IGR J17544-2619) are far smaller than the visible absorptions of the others. Moreover, concerning obscured SGXBs, the wind velocity of IGR J16318-4848 was found to be ∼410 km/s (Filliatre & Chaty 2004), far smaller than the expected wind velocity for O/B supergiants (∼1000-2000 km/s).

5. Conclusions

In this paper, we presented results of observations performed at ESO/VLT with VISIR which aimed at studying the MIR emission of twelve *INTEGRAL* obscured HMXBs, whose companions are confirmed or candidate supergiants. Moreover, using the observations performed at ESO/NTT and reported in the companion paper (CHA07), previous optical/NIR observations found in the literature and archival data from USNO, 2MASS and GLIMPSE, we fitted the broad-band SEDs of these sources using a simple two-components black-body model in order to obtain their visible absorptions and temperatures and to assess the contribution of their enshrouding material in their emission.

We confirmed that all these sources were likely O/B supergiant stars and that for most of them the enshrouding material marginally contributed to the emission. Moreover, in the case of IGR J16318-4848, IGR J16358-4726 and perhaps IGR J16195-4945, the MIR excess could be explained by the sgB[e] nature of the companion stars.

By comparing optical and high-energy characteristics of these sources, we showed that the distinction SFXTs/obscured SGXBs does not seem to exist from optical to MIR wavelengths. Nevertheless, most of the sources in our sample are significantly absorbed in the optical and we think that the wind can be denser around some supergiants in SGXBs, which could be due to the photoionization by the high-energy emission of the compact object.

Several improvements in our study are necessary to allow definitive conclusions. Indeed, the data used to perform the SEDs were not taken simultaneously, which can for instance lead to a incorrect assessment of the MIR excess in the emission.

Moreover, the lack of optical magnitudes for several sources could have led to an incorrect fitting of their intrinsic visible absorption A_V.

At last, the absence of an accurate measurement of the total interstellar absorption out to the distance of these sources does not allow us to say whether the presence of the compact object can lead to a stellar wind denser in some supergiants belonging to SGXBs than in isolated supergiants.

We then recommend further optical investigation on these sources to study any possible variation of their P-cygni profile with the phase of the compact object.

Moreover, we think that the measurement of the distance of these sources is crucial to allow a good assessment of the real interstellar absorption up to their distance, in order to detect any local absorbing component around companion stars.

We also recommend X-ray monitoring in order to study the dependence of their column density with orbital phase angle, which could help to understand the difference between obscured SGXBs and SFXTs.

Acknowledgements. We are pleased to thank Jérôme Rodriguez for his very useful website in which all the *INTEGRAL* sources are referenced (http://isdc.unige.ch/~rodrigue/html/igrsources.html).
Based on observations carried out at the European Southern Observatory, Chile (through programmes ID. 075.D-0773 and 077.D-0721). This research has made use of NASA's Astrophysics Data System, of the SIMBAD and VizieR databases operated at CDS, Strasbourg, France, of products from the US Naval Observatory catalogues, of products from the Two Micron All Sky Survey, which is a joint project of the University of Massachusetts and the Infrared Processing and Analysis Center/California Institute of Technology, funded by the National Aeronautics and Space Administration and the National Science Foundation as well as products from the Galactic Legacy Infrared Mid-Plane Survey Extraordinaire, which is a *Spitzer Space Telescope* Legacy Science Program.

References

Benjamin, R. A., Churchwell, E., Babler, B. L., et al. 2003, PASP, 115, 953
Bird, A. J., Malizia, A., Bazzano, A., et al. 2007, ApJS, 170, 175
Bjorkman, J. E. & Cassinelli, J. P. 1993, ApJ, 409, 429
Bodaghee, A., Courvoisier, T. J.-L., Rodriguez, J., et al. 2007, A&A, 467, 585
Bohlin, R. C., Savage, B. D., & Drake, J. F. 1978, ApJ, 224, 132
Cardelli, J. A., Clayton, G. C., & Mathis, J. S. 1989, ApJ, 345, 245
Cassinelli, J. P. & Ignace, R. 1997, in Astronomical Society of the Pacific Conference Series, Vol. 120, Luminous Blue Variables: Massive Stars in Transition, ed. A. Nota & H. Lamers, 166–+
Castor, J. I., Abbott, D. C., & Klein, R. I. 1975, ApJ, 195, 157
Chaty, S. & Rahoui, F. 2007, Proceeding of the VIth INTEGRAL Workshop, "The Obscured Universe", Space Research Institute, Moscow, Russia, 2006, ESA's Publications Division: Special Publication SP-622
Corbet, R. H. D., Hannikainen, D. C., & Remillard, R. 2004, The Astronomer's Telegram, 269, 1
Courvoisier, T. J.-L., Walter, R., Rodriguez, J., Bouchet, L., & Lutovinov, A. A. 2003, IAU Circ., 8063, 3
Crowther, P. A., Lennon, D. J., & Walborn, N. R. 2006, A&A, 446, 279
Dame, T. M., Hartmann, D., & Thaddeus, P. 2001, ApJ, 547, 792
Dickey, J. M. & Lockman, F. J. 1990, ARA&A, 28, 215
Filliatre, P. & Chaty, S. 2004, ApJ, 616, 469
Fruscione, A., Hawkins, I., Jelinsky, P., & Wiercigroch, A. 1994, ApJS, 94, 127
González-Riestra, R., Oosterbroek, T., Kuulkers, E., Orr, A., & Parmar, A. N. 2004, A&A, 420, 589
Haberl, F., White, N. E., & Kallman, T. R. 1989, ApJ, 343, 409
Hannikainen, D. C., Rodriguez, J., & Pottschmidt, K. 2003, IAU Circ., 8088, 4
Hatchett, S. & McCray, R. 1977, ApJ, 211, 552
Indebetouw, R., Mathis, J. S., Babler, B. L., et al. 2005, ApJ, 619, 931
in't Zand, J. J. M. 2005, A&A, 441, L1
in't Zand, J. J. M., Jonker, P. G., Nelemans, G., Steeghs, D., & O'Brien, K. 2006, A&A, 448, 1101
Kaplan, D. L., Moon, D.-S., & Reach, W. T. 2006, ApJ, 649, L107
Kouveliotou, C., Patel, S., Tennant, A., et al. 2003, IAU Circ., 8109, 2
Kraus, M. & Miroshnichenko, A. S., eds. 2006, Astronomical Society of the Pacific Conference Series, Vol. 355, Stars with the B[e] Phenomenon
Lagage, P. O., Pel, J. W., Authier, M., et al. 2004, The Messenger, 117, 12
Lamers, H. J. G. & Pauldrach, A. W. A. 1991, A&A, 244, L5
Lamers, H. J. G. L. M., Zickgraf, F.-J., de Winter, D., Houziaux, L., & Zorec, J. 1998, A&A, 340, 117
Lebrun, F., Leray, J. P., Lavocat, P., et al. 2003, A&A, 411,

Chapitre 4

Conclusions et perspectives scientifiques

Ou comment je vois les grands axes d'étude des systèmes binaires de haute énergie, dans les années à venir

Sommaire

4.1 Étude de population de sources Galactiques 225
4.1.1 Poursuite de l'étude des microquasars 225
4.1.2 Détermination de la nature des sources *INTEGRAL* 225
4.1.3 Contraintes sur les modèles de synthèse de population 226
4.1.4 L'apport de GLAST 227
4.2 Formation et évolution des systèmes binaires serrés 228
4.2.1 Formation des systèmes binaires : lien avec leur environnement 229
4.2.2 Evolution des systèmes binaires : importance du donneur 230
4.3 À la recherche des progéniteurs de trous noirs et d'étoiles à neutron 235
4.3.1 Formation, évolution et fin de vie des étoiles massives 236
4.3.2 Étude des phénomènes physiques à chaque étape de l'évolution 238
4.4 Le mot de la fin 239
4.4.1 Le rêve d'un observateur 239

Mots clés : Variable cataclysmique, naine blanche, étoile à neutron, trou noir

Abstract :

What has been accomplished in the understanding of high energy binary systems, what remains to be done in this field, and the important questions which need to be resolved, and which will occupy my time during the next years... This chapter is divided in three parts. In the first one, I describe questions related to the population of Galactic sources, taken as a whole, and how they can allow to better understand high energy binary systems. In the second one, I focus on the study of the formation and evolution of high energy binary systems as an object, and on

phenomena occuring in these systems. In the third one, I give details on a project that I am very interested in, and which takes roots in the two previous ones : the distinction between progenitors of neutron stars and black holes.

Résumé :

Ce qui a été accompli dans la compréhension des systèmes binaires de haute énergie, ce qu'il reste à faire dans ce domaine, et les questions importantes qui nécessitent d'être résolues, et qui vont occuper mon temps dans les années à venir... Ce chapitre est divisé en trois parties. Dans la première, j'aborde les questions liées aux population de sources Galactiques prises en tant que tout, et comment elles peuvent permettre de mieux comprendre les systèmes binaires de haute énergie. Dans la deuxième, je me concentre sur l'étude de la formation et de l'évolution des systèmes binaires de haute énergie en tant que tels, et sur les phénomènes présents dans ces systèmes. Dans la troisième, je détaille un projet qui me tient à coeur, et qui regroupe les deux précédents : la distinction entre progéniteurs d'étoiles à neutron et de trous noirs.

4.1 Étude de population de sources Galactiques

4.1.1 Poursuite de l'étude des microquasars

Des avancées considérables ont été effectuées sur les microquasars, depuis leur découverte en 1992. D'objets extraordinaires, ils sont devenus presque communs, extrêmement étudiés, grâce à d'intensives campagnes d'observations, et des simulations numériques. Des jets ont été résolus sur beaucoup de microquasars, les rendant presque banals, les interactions avec le milieu environnant semblent maintenant évidentes... Que de chemin parcouru entre le premier congrès des microquasars, où je présentais mes premiers résultats de thèse portant sur des observations en infrarouge et millimétrique de GRS 1915+105, en 1995 à Washington, jusqu'au sixième congrès en septembre 2006 en Italie, où des statistiques peuvent maintenant être établies sur un nombre toujours croissant de microquasars. Pourtant, malgré les assauts des observateurs, des modélisateurs et des théoriciens, la nature de l'émission à haute énergie reste encore hautement mystérieuse, une couronne de plasma entourant, avec une géométrie inconnue, un disque d'accrétion. Les jets eux-mêmes émettent-ils aussi dans le domaine des rayons X ? Pléthore d'observations montrant le lien entre l'accrétion et l'éjection ont été effectuées, depuis la découverte en 1997 de ce lien sur le microquasar superluminique GRS 1915+105 (Chaty 1998 ; Mirabel et al. 1998). Pourtant, et encore une fois ce n'est pas faute d'avoir essayé, les mécanismes d'accrétion–éjection ne sont toujours pas au rendez-vous, et ce sont toujours les modèles de Blandford-Payne et Blandford-Znajek qui dominent. Beaucoup d'autres questions restent encore en suspens, et en particulier concernant la nature des jets, l'interaction matière éjectée–environnement, et les processus d'émission à haute énergie. Seules des campagnes d'observations multi-longueurs d'onde, couplées à des simulations et des modèles théoriques, devraient permettre dans un avenir plus ou moins proche des avancées dans la résolution de ces questions fondamentales.

Concernant l'émission de rayonnement à haute énergie, les modèles et les observations actuelles semblent montrer que les systèmes binaires X de grande masse contenant une étoile à neutron magnétisée sont de meilleurs émetteurs potentiels de rayonnement γ que les autres systèmes, et en particulier les microquasars. Ceci sera cependant testé avec en particulier les observations qu'effectuera le satellite GLAST, et permettra peut-être de clore le débat concernant les émetteurs de haute énergie : sont-ils des microquasars ou des sources binaires de grande masse constituées d'une étoile géante et d'une étoile à neutron magnétisée ?

4.1.2 Détermination de la nature des sources *INTEGRAL*

Bien que des progrès aient été accomplis dans la détermination de la nature de plusieurs des 214 sources *INTEGRAL* (Bodaghee et al., 2007), il reste encore 111 sources pour lesquelles la nature est inconnue, représentant donc encore 52 %. À la fois leur distribution spatiale et leur émission de rayons X suggèrent une population galactique composée principalement de LMXBs, plutôt que AGN derrière le plan galactique. Si beaucoup de ces sources non classifiées sont des LMXBs, alors elles ont probablement échappé à une identification et donc à une classification à cause de contreparties optiques plutôt faibles, à cause de leur localisation dans le bulbe et le plan galactique où de la poussière absorbe les rayonnements, et à cause de la confusion de

source. Toutes ces raisons rendent en effet la tâche d'identification de la contrepartie optique difficile. De plus, leur émission en rayons X est souvent transitoire, et donc incompatible avec des observations de suivi. Ainsi, seulement 6 sources (3%) ont été classifiées comme LMXB, la moitié au cours de l'année 2006, grâce à de multiples campagnes ToO ciblant les sources *INTEGRAL*.

Probablement la plus grande surprise réside dans le grand nombre de HMXBs ainsi que dans les propriétés de ces systèmes. Plusieurs HMXBs présentent un niveau élevé d'absorption intrinsèque, avec $N_{\rm H} = 10^{23-24}$ cm^{-2} (cf Matt & Guainazzi 2003 ; Rodriguez et al. 2003 ; Combi et al. 2004 ; Beckmann et al. 2005 ; Walter et al. 2006), et, au moins dans un cas, il est clair qu'un vent stellaire fort est responsable de l'absorption (Filliatre & Chaty, 2004). En plus de fortes densités de colonne, quelques membres du groupe des HMXBs d'*INTEGRAL* présentent d'autres caractéristiques extrêmes, incluant les sursauts X de grande amplitude des supergéantes transitoires rapides de rayons X (SFXTs, Negueruela et al. 2006b ; Sguera et al. 2006) et des étoiles à neutron avec de très longues périodes de spin, de 1000 à 6000 s (Patel et al. 2004 ; Lutovinov et al. 2005b). Cependant, il n'est pas forcément si étonnant qu'*INTEGRAL* ait détecté autant de systèmes binaires de grande masse : comme discuté par Lutovinov et al. (2005a), Dean et al. (2005) et Bodaghee et al. (2007), les systèmes binaires de grande masse constituent les astres idéalement vus par *INTEGRAL*. En effet, *INTEGRAL* observant au-delà du seuil d'énergie à partir duquel l'absorption photoélectrique devient négligeable dans la plupart des constituants de la matière, il peut détecter des astres brillants au-dessus de quelques dizaines de keV, alors qu'ils sont indétectables en dessous. Dans le cas des HMXBs, l'accrétion par vent stellaire dominant dans ces systèmes, par opposition au dépassement du lobe de Roche chez les LMXBs, procure un vent circumstellaire dense et très absorbant, cachant l'émission X, de la même manière que dans le cas des AGN Seyfert 2 (Malizia et al., 2003).

En se basant sur le taux actuel de découverte de HMXBs d'*INTEGRAL*, il est probable que les 111 sources de nature inconnue incluent 30 HMXBs (28%), et, l'une des tâches dans un futur proche, est d'identifier ces systèmes ou d'autres sources Galactiques inhabituelles. La couverture relativement uniforme obtenue par le satellite *INTEGRAL* dans le plan Galactique le rend utile afin de recenser les populations de sources Galactiques. Un tel échantillon (incluant les HMXBs déjà connues et celles découvertes par *INTEGRAL*) permet en effet de mieux contraindre la population des HMXBs dans le contexte de l'évolution des systèmes binaires, ainsi que du nombre et de la distribution des objets compacts dans la Galaxie (comme par exemple la localisation des HMXBs relativement aux bras spiraux, cf Lutovinov et al. 2005a ; Dean et al. 2005 ; Bodaghee et al. 2007) en plus de nous permettre d'étudier la physique des objets compacts accrétants.

4.1.3 Contraintes sur les modèles de synthèse de population

Une étude liée à l'évolution des systèmes binaires serrés consiste à connaître, au sein des HMXBs, quelle est la proportion de binaires X Be, par rapport aux systèmes contenant des supergéantes. Les études de population théoriques donnent comme estimation qu'il y aurait 10^4 systèmes binaires dans la Galaxie contenant une étoile B et une étoile à neutron ou un trou noir (Meurs & van den Heuvel, 1989). Pour ces systèmes, les scénarios d'évolution, où la masse et le moment angulaire sont conservés pendant la majeure partie de l'évolution, conduisent à des

binaires Be, alors que des scénarios non-conservatifs conduisent à des systèmes de supergéantes (cf Verbunt & van den Heuvel dans Lewin et al. 1995). Bien que la vision conventionnelle soit que la population est dominée par le premier type, plus de la moitié des HMXBs d'*INTEGRAL* identifiées à ce jour tombent dans la catégorie des supergéantes (Filliatre & Chaty 2004 ; Negueruela et al. 2006a ; Masetti et al. 2006 ; Bodaghee et al. 2007). Continuer à identifier les sources *INTEGRAL* améliorera les contraintes sur le nombre de supergéantes par rapport aux systèmes Be dans la Galaxie, et aura un impact sur notre compréhension de l'évolution des HMXBs. Ceci, de plus, a des implications sur les estimations du nombre de binaires NS/NS et NS/BH dans la Galaxie (Tauris & van den Heuvel, 2006), de telles estimations étant critiques pour estimer la probabilité de détecter des ondes gravitationnelles (voir discussion dans le paragraphe 4.3).

En se fondant sur les résultats de synthèse de population des HMXBs, Lommen et al. (2005) suggère la possibilité qu'un sous-ensemble des sources *INTEGRAL* représente une population manquante d'HMXBs avec des compagnons fusionnant l'He dans leur coeur (supergéantes, géantes, ou étoiles Wolf-Rayet). Alors qu'une infime fraction de cette population posséderait un disque d'accrétion (comme Cygnus X-3, la binaire X à Wolf-Rayet bien connue), la plupart de cette population serait constituée d'accréteurs par vent avec des luminosités X d'environ 10^{36} erg s^{-1} et des absorptions intrinsèques significatives. Lommen et al. (2005) prédit que des douzaines de tels objets avec étoiles à neutron et trous noirs accrétant par vent devraient exister dans la Galaxie (cf figures 4 et 5 de Lommen et al. 2005). Les observations futures de ces sources permettront donc de faire des comparaisons directes avec les résultats des modèles de synthèse de population. Pour ce faire, il va falloir identifier le groupe complet d'HMXBs vus par *INTEGRAL*, afin de déterminer la nature des composantes de la binaire (type spectral du compagnon et nature de l'objet compact) à partir d'observations multi-longueurs d'onde, ainsi que le type de l'accrétion se produisant (vent ou disque), et de déterminer si la population est similaire à ce qui est prédit par les modèles de synthèse de population (Lommen et al. 2005 ; Portegies Zwart & Verbunt 1996).

Une question spécialement intéressante est de savoir si beaucoup de ces HMXBs contiennent des trous noirs, car nous ne connaissons actuellement qu'un petit nombre de trous noirs dans des HMXBs. De plus, les observations de ces sources *INTEGRAL* permettront probablement de découvrir d'autres types de sources intéressantes. Par exemple, en dépit du nombre relativement faible de répéteurs de sursauts de rayons γ mous ("Soft Gamma-ray Repeaters", SGRs) et de pulsars de rayons X anormaux ("Anomalous X-ray Pulsars", AXPs) connus dans la Galaxie, 7 de ces sources sont assez brillantes pour avoir été détectées par *INTEGRAL* (den Hartog et al. 2007 ; Bassani et al. 2004 ; Bodaghee et al. 2007), et plus encore de ces étoiles à neutron au champ magnétique extrêment élevé pourraient se trouver dans le groupe de sources non identifiées. Enfin, quelques-unes des sources (comme par exemple IGR J20188+3647) coincident avec les cercles d'erreur des sources EGRET non-identifiées, et il pourrait y avoir un recouvrement entre ces groupes.

4.1.4 L'apport de GLAST

Le nombre d'accélérateurs de haute énergie de notre Galaxie a augmenté dans la dernière décennie, avec les observations du télescope EGRET à bord du satellite Compton Gamma-Ray

Observatory, et avec les découvertes récentes des télescopes au sol observant dans le TeV, tels que HESS, MAGIC, et MILAGRO. 40 sources de rayons γ ont été détectées le long de la Voie Lactée dans le domaine du GeV, et 30 dans celui du TeV. Cependant, la nature à la fois des processus d'émission à haute énergie, que des particules accélérées, reste encore très énigmatique. La plupart de ces objets n'ont pas encore été identifiés, après plusieurs années d'étude, et ceux qui ont été identifiés posent beaucoup de questions importantes auxquelles l'échantillon actuel, restreint et biaisé, ne permet pas de répondre.

Dans le domaine d'étude des sources de haute énergie, et les contraintes sur les modèles de synthèse de population, le lancement par la NASA fin 2007 du nouveau satellite Gamma-ray Large Area Space Telescope (GLAST), la prochaine mission fondamentale en astrophysique des rayons γ, constituera un évènement de première ampleur, car il améliorera drastiquement la situation, en détectant des centaines de nouvelles sources γ dans la Voie Lactée, et en les localisant avec une précision de la minute d'arc. Cette précision de localisation permettra des analyses multi-longueurs d'onde approfondies, afin d'identifier ces nouvelles sources, et d'explorer leurs propriétés. GLAST détectera des pulsars, des nébuleuses de vent de pulsar, des rémanents de supernova, et des systèmes binaires de grande masse contenant des étoiles à neutron plus ou moins magnétisées, ou même de nouvelles classes d'objets présentant des phénomènes de haute énergie. Evidemment, ces nouvelles sources risquent de poser encore plus de questions, et il sera nécessaire d'entreprendre une approche commune dans les hautes énergies (satellites *XMM, Chandra, Swift, INTEGRAL*, et télescopes au sol comme HESS-2), liée à une étude multi-longueurs d'onde dans les autres domaines du spectre électromagnétique, et aux travaux de modélisation, pour comprendre la physique des émetteurs à haute énergie, et apporter quelques éléments de réponse...

Dans le cadre du groupe multi-longueur d'onde, et en tant que membre affilié de la collaboration GLAST, je prévois d'identifier les contreparties détectées par le LAT (Large Area Telescope), en particulier en recherchant les contreparties dans les grandes bases de données d'archive des observatoires radio, IR, optique, UV et X, à partir de critères de sélection permettant de sélectionner les contreparties candidates dans les divers catalogues. À partir de ces contreparties dans plusieurs longueurs d'onde, il sera possible de construire des distributions spectrales d'énergie des sources LAT, et d'identifier/classifier ces sources. Un suivi de ces sources pourra être effectué grâce à des propositions de temps sur des télescopes au sol ou dans l'espace.

Ce n'est que lorsque plusieurs centaines de sources auront été détectées dans le domaine des hautes énergies dans les MeV/GeV, et qu'une bonne partie de ces sources aura été identifiée/classifiée, qu'il sera possible d'entreprendre une étude statistique de ces objets, et avancer dans la compréhension des objets sièges de phénomènes des hautes énergies.

4.2 Formation et évolution des systèmes binaires serrés

En Astrophysique, les phénomènes se produisant dans les galaxies sont gouvernés par l'évolution stellaire. Depuis la contraction de nuages moléculaires donnant naissance aux étoiles, la nucléosynthèse forgeant les atomes ensuite fournis au milieu interstellaire, au phénomène de supernova, l'effondrement d'étoiles en fin de vie en objet compact –naines blanches, étoiles à neu-

tron ou trous noirs–, une description correcte de ces phénomènes nécessite une compréhension précise de chaque étape de l'évolution stellaire. En plus de sa masse, beaucoup de paramètres additionnels influencent la vie d'une étoile : la région où elle est née, reliée à sa composition chimique et métallicité, son moment angulaire, si elle est gravitationnellement liée dans un système binaire, etc. Nous allons dans la suite détailler les divers mécanismes physiques qui influencent la formation et l'évolution des systèmes binaires serrés.

4.2.1 Formation des systèmes binaires : lien avec leur environnement

L'environnement dans lequel se forme une étoile est fondamental dans la constitution de ses propriétés intrinsèques et de ses caractéristiques. En effet, selon la densité et la métallicité de l'environnement par exemple, l'étoile sera plus ou moins massive, avec un vent plus ou moins fort, qui permettra éventuellement de former une enveloppe de poussière plus ou moins dense autour d'elle. Or, ce qui est vrai pour une étoile isolée l'est encore plus pour une étoile qui est l'une des composantes d'un système binaire. En effet, l'évolution d'une étoile située dans un système binaire serré peut être influencée par l'interaction avec son étoile compagnon, telle que par la perte et/ou le transfert de masse et de moment angulaire, et aussi par l'évolution de l'étoile compagnon elle-même (Tauris & van den Heuvel, 2006). Les systèmes binaires de haute énergie en constituent le meilleur exemple.

Une preuve que l'environnement où naissent les étoiles est très important est donnée par l'analyse statistique du dernier catalogue de sources *INTEGRAL* effectuée par Dean et al. (2005) et Bodaghee et al. (2007). Cette analyse montre que les systèmes binaires X de faible masse sont concentrés dans les régions du centre de la Galaxie, et plus précisément du bulbe galactique, alors que ceux de grande masse sont répartis dans l'ensemble du plan galactique, mais confinés dans le disque, et préférentiellement à proximité des points tangentiels de la structure des bras spiraux (voir figure 4.1). On s'attendait en effet à cette distribution spatiale (cf figure 1.1), car les systèmes binaires de faible masse étant constitués de compagnons optiques appartenant à une vieille population stellaire, on les trouve surtout dans le bulbe Galactique, où ils ont eu le temps de migrer en dehors du plan de la Galaxie ($|b| > 3 - 5°$). Par contre, les systèmes de grande masse contenant des étoiles compagnons jeunes, ils restent proches des sites de formation stellaire récente. Ceci est d'ailleurs corroboré par la distribution galactique des sources binaires de grande masse dont la distance est connue, superposée à un modèle de la Galaxie incluant la localisation des complexes de formation d'étoiles, comme le montre la figure 4.2.

Ainsi, théoriquement, l'époque d'apparition des systèmes binaires de grande masse devrait suivre le passage de l'onde de densité liée au bras spiral, passage induisant une flambée de formation d'étoiles. Dans ce contexte, les modèles prédisent une fenêtre temporelle plutôt importante, puisque l'intervalle de temps entre la formation des étoiles et l'apparition des systèmes binaires de grande masse dépend des masses initiales des astres composant le système binaire. L'intervalle de temps d'apparition de ces systèmes de grande masse devrait donc naturellement refléter la gamme de masses des deux composantes des systèmes binaires, ainsi que le suggère Dean et al. (2005). Or la formation d'un système binaire de grande masse prenant seulement quelques dizaines de millions d'années (Tauris & van den Heuvel, 2006), elle devrait constituer un bon traceur du passage de l'onde de densité dans la Galaxie. Pour qu'une telle étude statistique soit

précise, il faudrait disposer non seulement de plus de systèmes binaires de grande masse pour lesquels on connaît précisément la distance, mais aussi d'un modèle dynamique de la structure spirale des bras de la Galaxie précis et fiable.

Les points d'étude importants dans ce domaine, qui permettront dans le futur de mieux comprendre l'influence et l'impact de l'environnement sur les étoiles des systèmes binaires de haute énergie, sont :

- • une étude des systèmes binaires X de grande masse situés dans différentes régions de la Galaxie, afin de mesurer précisément l'impact de l'environnement à grande échelle sur ces systèmes,
- • une étude du lien entre la métallicité des étoiles compagnons et leur présence dans des régions plus ou moins riches en formation d'étoiles,
- • une étude du lien entre les sources X ultralumineuses (ULXs) d'autres galaxies, et leur présence dans des régions plus ou moins riches en formation d'étoiles,
- • une comparaison de la perte de masse par vent stellaire, liée ou non à l'évolution des binaires serrées, avec la pente de la fonction de masse initiale (IMF, "Initial Mass Function").

Les domaines de l'infrarouge moyen et du sub-millimétrique vont peu à peu prendre une place fondamentale dans l'étude de ces objets et de leur environnement, puisque c'est uniquement dans ces domaines que l'environnement proche des étoiles géantes et supergéantes peut être caractérisé, à savoir la présence de poussière ou de gaz froid, sa composition, sa température et son extension.

4.2.2 Evolution des systèmes binaires : importance du donneur

L'évolution des systèmes binaires est dominée par celle de chacune de ses composantes, cependant celles-ci n'évoluent pas de la même manière que les étoiles isolées, car chaque composante d'un système binaire est affectée par la présence de son compagnon (objet compact ou non) dans son environnement proche. Ainsi, l'évolution d'un système binaire serré est extrêmement complexe, car elle dépend de beaucoup de mécanismes physiques, dont on peut avoir un aperçu dans Meurs & van den Heuvel (1989).

Pour donner un exemple simple où l'objet compact modifie de façon tangible l'environnement proche de leur étoile compagnon, prenons celui des étoiles Be : le disque de décrétion des étoiles Be est tronqué sous l'effet de la présence de l'étoile neutron, placée sur une orbite excentrique autour de l'étoile Be (Reig, 2007). Plus généralement, la nature même d'une étoile détermine les propriétés d'un système binaire. Par exemple, nous avons vu dans le chapitre 3 que les propriétés d'un système binaire, dans les domaines des hautes énergies et de l'infrarouge, dépendaient de la nature de l'étoile compagnon, et plus particulièrement de son type spectral. Or il est important de se rappeler que l'environnement circumstellaire des étoiles sgB[e] diffère fondamentalement de celui des supergéantes de type B : les premières étoiles éjectent un vent dense et lent au niveau de l'équateur, qui est propice à la formation d'un cocon de poussière entourant l'étoile, ce qui n'est pas le cas des secondes étoiles. Les propriétés aux hautes énergies différeront alors, vu que l'objet compact n'accrétera pas autant et de la même façon en fonction de la présence ou non de ce cocon de poussière. Dans ce contexte, la découverte par le satellite

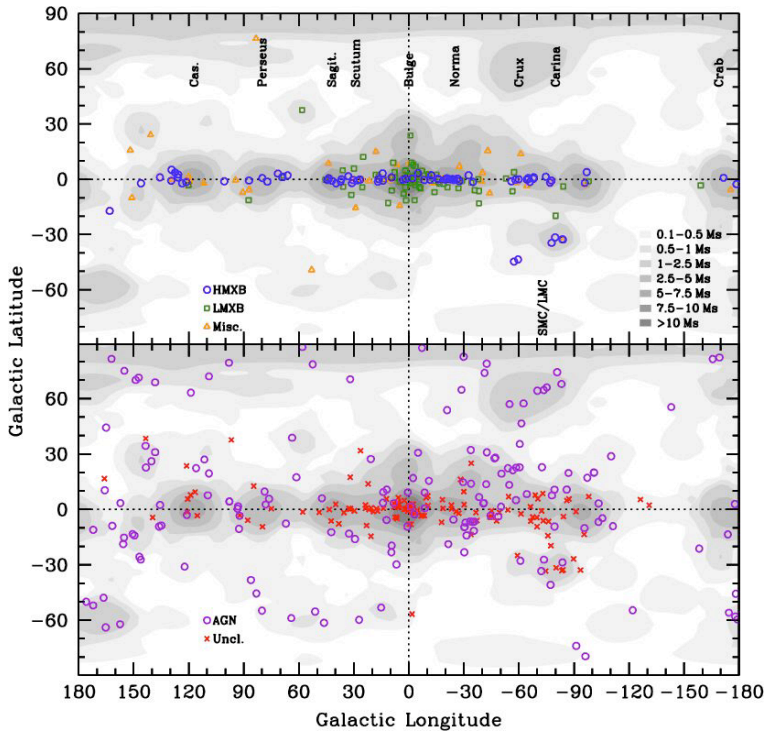

FIG. 4.1 – Distribution spatiale en coordonnées galactiques des sources détectées par *INTEGRAL*/ISGRI (Bodaghee et al., 2007). La figure du haut présente la distribution des systèmes binaires de grande masse (cercles), de faible masse (carrés) et des sources diverses (triangles). La figure du bas montre les sources extragalactiques (cercles) et non classifiés (croix). Les directions tangentielles des bras spiraux sont indiquées, ainsi que les temps d'exposition cumulatifs dans chaque direction (à partir de données publiques dans les révolutions 30-484).

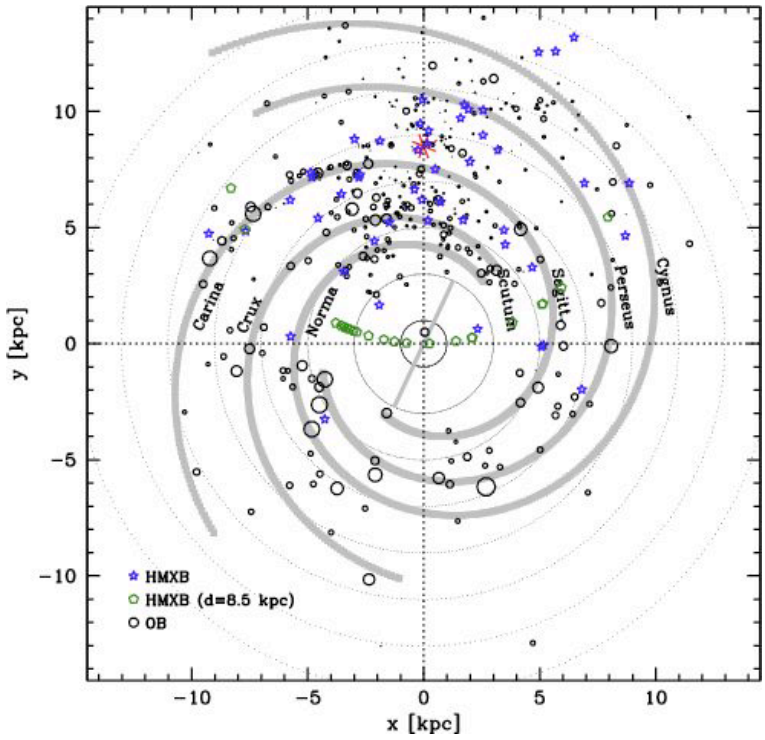

FIG. 4.2 – Distribution Galactique des systèmes binaires de grande masse (Bodaghee et al., 2007) dont la distance est connue (49, symbole d'étoile) et les localisations de complexes de formation d'étoiles de Russeil (2003) (464, cercles). La taille du symbole des derniers est proportionnelle à l'activité du complexe. Les HMXBs dont les distance sont inconnues ont été placées à 8.5 kpc (23, symbole pentagone).

INTEGRAL d'une importante population dans la Galaxie de systèmes binaires de grande masse abritant une supergéante et accrétant par vent permettra certainement de mieux appréhender l'influence de l'objet compact sur l'évolution des étoiles supergéantes. En effet, les propriétés d'un objet compact accrétant à l'intérieur du vent stellaire de l'étoile compagnon, et en particulier l'efficacité de l'accrétion de ce vent, dépendent beaucoup de la géométrie du système, ainsi que de la taille et de la forme de la région optiquement mince et totalement ionisée du gaz, l'analogue de la sphère de Strömgren (Pringle 1973, cf discussion dans Hatchett & McCray (1977)[1]).

Des systèmes binaires de faible masse au systèmes de masse intermédiaire...

Comme indiqué dans le chapitre 1, les étoiles compagnon présentes dans un système binaire ont souvent aussi eu le temps d'évoluer depuis leur naissance ou la formation du système binaire, et la masse de l'étoile déduite des observations de vitesse radiale ne fournit pas forcément une indication de la masse qu'avait l'étoile lors de sa formation ou de la plus grande partie de sa vie. J'avais déjà signalé dans le chapitre 1 le cas des étoiles compagnon de faible masse que constituent les sous-géantes de type F-G, comme par exemple pour Cygnus X-2 : cette catégorie d'étoiles compagnon est probablement le rémanent d'étoiles qui ont perdu de la masse par transfert de masse, et qui originellement étaient des étoiles de masse intermédiaire ($M \sim 1.5-4\ M_{\odot}$; Podsiadlowski & Rappaport 2000 ; Tauris et al. 2000). Ceci a été très clairement vu dans le cas du microquasar et candidat trou noir XTE J1118+480 (cf chapitre 2), grâce à des observations spectroscopiques en ultraviolet (Haswell et al., 2002) : l'étoile compagnon présente des signatures claires montrant que le cycle CNO s'est déjà produit dans l'étoile, alors que sa masse ($0.4\ M_{\odot}$), en accord avec son type spectral (Chaty et al., 2003b), n'aurait pas pu initier ce cycle[2]. Ceci signifie donc qu'il ne reste plus que le coeur d'une étoile massive... Cette étoile a donc certainement éjecté son enveloppe externe avant d'initier le transfert de masse vers l'objet compact. Une autre possibilité est que l'enveloppe de cette étoile ait été en partie éjectée, et peut-être en partie accrétée par le trou noir.

Il est apparu ces dernières années que la distinction entre systèmes binaires de faible masse et de grande masse n'est pas aussi claire dans plusieurs cas. En effet, plusieurs systèmes binaires de faible masse se sont vus promus systèmes binaires de masse intermédiaire, et pourraient même être des systèmes binaires de grande masse ! Le cas du microquasar GRO J1655-40 est particulièrement intéressant : Kolb et al. (1997) avaient proposé que l'étoile compagnon de ce système ait une masse de $\sim\ 2.3\ M_{\odot}$, qu'elle ait commencé son évolution sur la séquence principale, mais que depuis elle avait évolué en dehors de cette branche, et serait maintenant à mi-chemin entre la séquence principale et le commencement de la branche des géantes. Des observations infrarouges ont montré que l'étoile compagnon présente un type spectral F3-6 IV, et sa position sur le diagramme Hertzsprung-Russell suggère que l'étoile est en train de traverser l'intervalle d'Hertzsprung, c'est-à-dire de quitter la séquence principale pour se diriger vers la branche des géantes rouges (Chaty et al., 2002). Le cas de V4641 Sgr est tout aussi intéressant, puisque la

[1] Comme ces auteurs l'écrivent, le sujet des vents stellaires est déjà très compliqué *sans* source X à l'intérieur !

[2] C'est encore une fois grâce à la faible absorption de cette source que de telles observations en UV ont pu montrer que le processus CNO s'était déjà déroulé, mais combien d'étoiles pourraient montrer cela si nous avions accès à plus d'observations de ce type, c'est-à-dire à plus d'objets présentant de faibles absorptions ?

position de l'étoile compagnon de ce microquasar sur le diagramme Hertzsprung-Russell montre que son type spectral est B3-A2 IV, et suggère aussi que l'étoile compagnon est en train d'évoluer, en traversant l'intervalle d'Hertzsprung (Chaty et al., 2003a). On peut aussi ajouter le cas plus récent de XTE J1720-318, un système binaire de masse intermédiaire, avec une étoile compagnon de type spectral compris entre B et G (Chaty & Bessolaz, 2006).

Cependant, à la fois la nature de ces systèmes, comme des moyens observationnels, nous empêchent d'aller beaucoup plus loin aujourd'hui dans l'étude de ces systèmes. La nature de ces systèmes d'abord, car les étoiles compagnons des systèmes binaires X de faible masse ne se dévoilent pas facilement : faible en quiescence, la brillance de ces étoiles est dépassée de plusieurs ordres de grandeur par le disque d'accrétion pendant les périodes de sursauts d'activité. Les moyens observationnels ensuite, ne sont souvent pas suffisants pour caractériser de façon précise les étoiles compagnons, observables principalement en optique et en infrarouge. Le VLT, le JWST, MIRI, dicteront donc l'avenir de l'étude des étoiles compagnon. Mais il va sans dire qu'il faudra coupler ces observations aux modèles d'évolution stellaire, pour acquérir une meilleure compréhension des différents stades d'évolution des systèmes binaires de haute énergie.

...jusqu'aux systèmes binaires de grande masse

Il semble donc que les systèmes binaires X de grande masse soient des astres idéaux permettant une étude de l'interaction entre l'objet compact et l'étoile compagnon, et de l'influence de ce premier sur cette dernière. La découverte par le satellite *INTEGRAL* d'une importante population de systèmes binaires X de grande masse dans notre Galaxie sera donc certainement très bénéfique à l'étude de cette interaction et influence. Par contre la question qui subsiste est : où se placent ces sources *INTEGRAL* –ces systèmes binaires constitués d'une étoile à neutron orbitant autour d'une étoile supergéante– dans le schéma de l'évolution des systèmes binaires ? La réponse à cette question n'est certainement pas évidente, car il faut trouver un donneur fournissant un vent stellaire fort avec un taux de perte de masse $\frac{dM}{dt}$ supérieur à $10^{-4}\ M_{\odot}$/an, afin de générer un gaz suffisamment dense autour de l'objet compact pour produire l'émission X. En quoi exactement, et pourquoi est-ce que ces nouveaux systèmes sont différents des systèmes HMXBs plus "classiques" ? Y a-t-il un lien avec les systèmes binaires de masse intermédiaire ? Cette grande absorption, et le fait que l'étoile à neutron orbite dans le vent de l'étoile dans le cas de IGR J16318-4848 évoque le cas de l'enveloppe commune. Mais les modèles prédisent une durée de la phase de l'enveloppe commune de seulement 10^3 ans au maximum, ce qui fait qu'on devrait déjà en voir beaucoup moins que ce qu'*INTEGRAL* a détecté (Meurs & van den Heuvel 1989, cf discussion dans Dean et al. 2005).

Enfin, il reste aussi à déterminer où se placent les sources à jets que sont les microquasars, sur le schéma d'évolution des systèmes binaires. Certains microquasars sont des systèmes binaires de faible masse, d'autres de grande masse. Comme elle dépend du phénomène d'accrétion, la période d'activité de ces objets est certainement reliée au schéma évolutif des systèmes binaires.

4.3 À la recherche des progéniteurs de trous noirs et d'étoiles à neutron

Nous avons vu dans l'ensemble de ce chapitre comment la formation et l'évolution des étoiles, surtout dans des systèmes binaires serrés, étaient fondamentaux pour déterminer leur destin final. Il s'ensuit de ce scénario de l'évolution stellaire, et des mécanismes physiques ayant potentiellement une influence sur cette évolution, qu'il n'est pas aisé de retrouver, en observant une étoile à ses derniers instants, quelle était la nature de cette étoile juste après sa naissance. L'évolution des systèmes binaires est donc liée au problème crucial en astrophysique de la masse des progéniteurs d'objet compact.

Le seuil de masse permettant à une étoile de se transformer en trou noir n'est pas connu : les simulations numériques des fins de vie stellaires prédisent que les progéniteurs d'étoiles à neutron ont une masse comprise entre 8 et $25\ M_{\odot}$, et ceux de trous noirs entre 25 et $40\ M_{\odot}$ (Woosley et al., 1993), cependant les observations montrent qu'il y a un recouvrement dans l'échelle des masses conduisant à une étoile à neutron ou un trou noir, entre 20 et $50\ M_{\odot}$ (Ergma & van den Heuvel, 1998). Ainsi, des étoiles massives donnent naissance à des étoiles à neutron, et d'autres, moins massives, à des trous noirs. Ce fait observationnel implique que ce n'est pas uniquement la masse du coeur du progéniteur qui détermine son destin final en étoile à neutron ou trou noir, mais plusieurs conditions et mécanismes additionnels liés à l'évolution stellaire, comme par exemple la rotation, les champs magnétiques, la perte de masse, l'asymétrie de la supernova, etc...

Pourtant, il est important de pouvoir retracer rétroactivement l'historique d'une étoile, afin d'acquérir une meilleure compréhension de : i) la formation stellaire, ii) l'évolution stellaire à différents stades, et principalement celle des étoiles massives, iii) l'influence réciproque entre les deux composantes d'un système binaire serré, iv) le phénomène de supernova, v) la formation, l'évolution et la distribution spatiale des systèmes binaires de haute énergie dans notre Galaxie, vi) un recensement précis des objets compacts –étoiles à neutron et trou noir– dans notre Galaxie, et vii) des estimations du nombre de coalescences de systèmes binaires formés d'une paire d'objets compacts. Ce sujet d'étude important devrait se développer dans les années qui viennent, au croisement entre formation stellaire, évolution stellaire et Astrophysique des hautes énergies, sur cette question cruciale mais non encore résolue : *"Comment distinguer les progéniteurs d'étoiles à neutron et de trous noirs ?"*. Ainsi que je l'ai décrit ci-dessus, bien que de formulation aisée, cette question n'a pas de réponse simple, car beaucoup de mécanismes physiques, enchevêtrés à toutes les étapes –depuis le début jusqu'à la fin– de l'évolution stellaire, peuvent modifier le destin d'une étoile en fin de vie. Ceci me conduit à formuler plus globalement cette question : *"En connaissant l'environnement d'une étoile à sa naissance, peut-on savoir si elle finira en étoile à neutron ou en trou noir ?"*.

Cette recherche transverse et inter-disciplinaire de la formation, de l'évolution et du destin des étoiles massive, ouvrira certainement de nouveaux horizons et opportunités dans notre vision globale de l'Astrophysique. En effet, la recherche de sa solution nécessite d'invoquer des liens entre divers domaines de l'Astrophysique, tels que le milieu interstellaire, la formation et l'évolution stellaire, l'évolution et de la distribution des systèmes binaires serrés, l'Astrophysique

des hautes énergies, les objets compacts, et les étapes finales de l'évolution stellaire, incluant le phénomène d'explosion de supernova, etc.

4.3.1 Formation, évolution et fin de vie des étoiles massives

Décrivons maintenant quelques mécanismes physiques pris à différents stades de la vie d'une étoile, qui influencent la formation, l'évolution et finalement le destin ultime de l'étoile.

• Au cours des premières étapes de la formation stellaire, les caractéristiques de la jeune étoile dépendent drastiquement du milieu interstellaire, de sa composition, métallicité, mais aussi des régions de la Galaxie où elle est née : des régions riches en formation d'étoiles, à haute densité de gaz, permettront de former beaucoup d'étoiles massives dans des systèmes binaires. La formation stellaire est en effet influencée par la densité, la température, le champ magnétique, la turbulence, la cinématique du milieu ; enfin la masse et la rotation acquises par l'étoile influenceront toute sa vie.

• Pendant leur évolution, les transferts de masse et de moment angulaire jouent un rôle important dans l'évolution stellaire de chaque composante de systèmes binaires serrés. De plus, l'interaction elle-même entre l'objet compact et l'étoile compagnon peut changer l'évolution de cette dernière (Filliatre & Chaty, 2004).

• Une étape importante de l'évolution des systèmes binaires serrés a lieu pendant ce qui est appelé "Phase d'enveloppe commune". Cette phase est initiée par l'objet compact pénétrant à l'intérieur de l'enveloppe de l'étoile compagnon, sur une orbite qui décroît rapidement du fait d'une grande perte de moment angulaire orbital. Cette phase a été invoquée par Paczynski (1976) pour expliquer comment les systèmes binaires de haute énergie à très courte période orbitale peuvent se former, bien que les deux composantes de ces systèmes, qui étaient de grandes étoiles à leur formation, n'auraient pas pu rentrer à l'intérieur d'un système binaire présentant une distance orbitale aussi petite. Cette phase de mouvement de spirale vers l'intérieur, couramment prise en compte dans les modèles de synthèse de population, mais jamais observée, probablement parce qu'elle est est courte (< 1000 ans) comparée à la vie entière d'une étoile massive ($\sim 10^6 - 10^7$ d'années), est donc un ingrédient de première importance pour l'évolution des systèmes binaires de haute énergie.

• Au cours de sa vie, à des étapes particulières de son évolution, une étoile massive peut perdre une quantité importante de sa masse par des vents intenses. Ceci est le cas par exemple des étoiles Wolf-Rayet, qui sont des coeurs nus d'Helium de $3 - 4\ M_\odot$, c'est-à-dire les résidus d'étoiles auparavant massives ($> 25 - 40\ M_\odot$) qui ont perdu la plupart de leur enveloppe par des vents stellaires (Maeder, 1993).

• L'étape finale d'une étoile massive est marquée par un événement extrême qui est crucial pour l'étoile mourante : l'explosion de supernova, qui déterminera le produit final –étoile à neutron ou trou noir– de l'objet compact. Nous avons déjà vu que la masse n'est pas le seul facteur important pour déterminer la fin de l'étoile. Le champ magnétique, la rotation du coeur effondré, et les instabilités de Rayleigh-Taylor, pourraient aussi jouer un rôle majeur (Ergma & van den Heuvel, 1998). L'explosion asymétrique semble influencer à la fois le recul ("kick") et la rotation ("spin") de l'étoile à neutron, son effet étant probablement différent pour un progéniteur de

trou noir qui se forme directement, ou par la matière éjectée retombant sur le coeur. Enfin, il y a beaucoup d'explosions ratées dans les simulations numériques dans le domaine $15 - 25\ M_{\odot}$, qui pourraient potentiellement produire un trou noir.

Ces différentes étapes se produisant pendant l'évolution stellaire montrent que beaucoup de mécanismes physiques influencent le destin ultime d'une étoile qui vient de naître, et qui finira soit en étoile à neutron soit en trou noir.

Étoiles massives

La résolution de cette question requiert une étude innovante et inter-disciplinaire, basée sur les étoiles massives dans les systèmes binaires de haute énergie, à différents stades de leur évolution. Relier les études observationnelles et théoriques sur la formation, l'évolution et la mort des étoiles massives de notre Galaxie, et comparer l'évolution des étoiles massives isolées et celles situées dans un système binaire, avec les résultats des modèles de synthèse de population, devrait permettre de suivre le fil de l'évolution des étoiles, et de trouver quels étaient les progéniteurs des objets compacts.

Les étoiles massives situées dans des systèmes binaires de haute énergie constituent l'échantillon le plus adéquat pour cette recherche, pour les raisons suivantes. La première raison est que plus de la moitié des étoiles sont situées dans des systèmes binaires. Ensuite, les systèmes binaires de haute énergie sont des laboratoires de haute énergie accélérant l'évolution des étoiles, pour lesquels nous avons la possibilité de connaître précisément à quel stade de l'évolution stellaire se trouvent les composantes de ces systèmes. De plus, les paramètres et mécanismes physiques gouvernant l'évolution stellaire, tels que la masse, la rotation, le moment angulaire de chaque composante, et le transfert de masse et de moment angulaire à l'intérieur du système, sont obtenus avec plus de facilité et de précision dans des systèmes binaires serrés que dans les étoiles isolées, à cause de l'influence gravitationnelle d'une composante sur l'autre. Enfin, nous pouvons comparer directement le nombre de systèmes binaires de haute énergie observés dans la Galaxie, au nombre prédit par les modèles de synthèse de population.

Coalescences de deux objets compacts

Cette question est d'une importance primordiale, non seulement car sa solution permettra une meilleure compréhension de ces champs fondamentaux de l'Astrophysique, mais aussi parce qu'elle fournira un recensement précis des objets compacts, étoiles à neutron et trous noirs, dans notre Galaxie, permettant une bonne prédiction des coalescences d'objets compacts. Or, cette prédiction a des implications dans le champ d'étude des sursauts de rayons γ et des ondes gravitationnelles. En effet, les systèmes binaires de haute énergie contenant une étoile compagnon massive, du type des nouvelles sources *INTEGRAL*, pourraient donner lieu à une fin de vie intéressante, à laquelle on pourra peut-être avoir accès dans un avenir proche. Tout commence avec un système binaire serré, et après deux épisodes de transfert de masse, et deux explosions de supernovae, il peut se former un couple d'objets compacts : paires d'étoiles à neutron, de trous noirs, ou d'étoiles à neutron orbitant autour de trous noirs. Cependant une incertitude subsiste,

car l'explosion de supernova peut modifier les paramètres orbitaux du système, pouvant causer la destruction du système binaire, et ceci même si l'explosion est isotrope, car la supernova n'explose pas au centre de masse du système. Dans le cas où les couples restent liés, ces systèmes entreront finalement en collision puis en coalescence après une émission d'ondes gravitationnelles, devenant probablement les progéniteurs de sursauts de rayons γ courts et durs, d'une durée de ~ 0.1 s, tels qu'on les observe à périphérie des galaxies-hôtes. En effet, pendant que ces deux astres se rapprochent, ce qui correspond à un temps très long, le système migre loin de son lieu de formation. On peut alors imaginer dans un avenir proche détecter, avec les futurs détecteurs d'ondes gravitationnelles, au sol ou dans l'espace, comme Advanced-LIGO et LISA, un signal d'ondes gravitationnelles en augmentation, avant une émission de rayons gamma correspondant à la coalescence.

4.3.2 Étude des phénomènes physiques à chaque étape de l'évolution

Décrivons maintenant quels sont les moyens d'observation et d'interprétation des phénomènes physiques qui nous permettront de suivre les étoiles massives à divers stades de leur évolution.

• *Formation stellaire :* Détermination des abondances du milieu interstellaire où les étoiles sont nées, dans différentes régions suivant la distribution Galactique des populations de systèmes binaires de haute énergie, telle qu'elle est donnée par les observatoires de haute énergie *INTEGRAL* aujourd'hui et *GLAST* demain. Comparaison entre cette distribution et la localisation des régions riches en formation d'étoiles, telle qu'elle est donnée par exemple par le satellite *HERSCHEL*, en prenant en compte les mouvements propres des systèmes dans la Galaxie. Cette étude sera facilitée par le fait que le Service d'Astrophysique est impliqué dans ces satellites, *INTEGRAL* observera au moins jusqu'en 2010, *GLAST* sera lancé fin 2007 et *HERSCHEL* en 2008.

• *Évolution stellaire :* Étude statistique des paramètres stellaires au cours de l'évolution stellaire, comparaison entre étoiles massives isolées et situées dans des systèmes binaires serrés, comparaison entre évolution stellaire et modèles de synthèse de population. Détermination des vitesses radiales, permettant une étude précise des masses de chaque composante des systèmes binaires serrés, à différents stades de leur évolution. Contraintes sur les rayons, la métallicité et l'evolution stellaires obtenues avec le satellite *Kepler*, à partir de données d'astérosismologie. Modélisation de l'évolution stellaire dans des systèmes binaires serrés, et plus particulièrement de la Phase d'Enveloppe Commune.

• *Métallicité :* Etude de la composition chimique et des abondances d'étoiles compagnon dans des systèmes binaires de haute énergie, à différents stades de leur évolution (principalement en utilisant les instruments spectroscopique de l'ESO), et comparaison avec les modèles d'évolution stellaire d'étoiles isolées : signature de matériau provenant de l'explosion de supernova de l'étoile primaire, conduisant à la connaissance de la masse du progéniteur, et permettant de remonter au progéniteur de trou noir et d'étoile à neutron, à différents stades de l'évolution des deux composantes de systèmes binaires serrés.

• *Supernova :* Comparaison entre données observationnelles, simulations et théorie des explosions de supernova, en fonction de la masse du progéniteur, et contraintes sur les modèles de synthèse de population.

4.4 Le mot de la fin

Il existe clairement une nécessité de révéler la nature de ces astres de haute énergie, que ce soit ceux découverts par *INTEGRAL* et aujourd'hui encore non identifiés, ou ceux qui seront demain découverts par exemple par le satellite GLAST. Révéler leur nature permet en effet de comprendre où et comment se placent ces astres au sein du schéma général de l'évolution stellaire. Ainsi que nous l'avons vu, deux méthodes complémentaires existent, ayant le même objectif commun : atteindre une meilleure compréhension des systèmes binaires, de leur formation et de leur évolution. La première méthode consiste à effectuer des observations de suivi multi-longueurs d'onde sur des sources X et γ choisies en fonction de leurs caractéristiques, afin d'identifier leur contrepartie et d'étudier la source avec moult détails, sur une gamme d'énergie la plus grande possible. Cette méthode, exhaustive, ne permet malheureusement que d'étudier un petit nombre de sources. La deuxième méthode, plus globale, consiste à étudier un échantillon sur des bases statistiques, et de comparer les caractéristiques globales des objets constituant cet échantillon, avec d'autres jeux de données génériques connus d'objets astronomiques. Evidemment il existe un grand degré de complémentarité entre ces deux méthodes. Les études des systèmes binaires de haute énergie ont jusqu'à aujourd'hui été principalement tournées vers des études exhaustives d'astres uniques. Cependant, la sensibilité accrue à haute énergie des nouveaux instruments va permettre des études statistiques poussées d'échantillons représentatifs. C'est déjà le cas pour *INTEGRAL*, avec plus de 200 sources au bout de 5 ans d'observations, ce sera encore plus vrai pour GLAST, dont le premier catalogue, au bout d'un an, contiendra dejà plus d'un millier de sources.

Enfin, j'ai présenté un projet d'étude sur la formation, l'évolution et la fin de vie des systèmes binaires de haute énergie, et principalement ceux abritant des étoiles de grande masse. Cette étude est intimement liée et conduit naturellement à la recherche des progéniteurs d'étoiles à neutron et de trous noirs. Je suis convaincu que ces astres constituent la clé de beaucoup de questions fondamentales en Astrophysique, depuis la formation stellaire, jusqu'à leur destin final.

4.4.1 Le rêve d'un observateur

Il est possible de rêver dès à présent à des campagnes simultanées d'observations multi-longueurs d'onde, permettant de mettre en évidence des phénomènes se produisant à l'échelle de la nano-seconde au sein des microquasars, ainsi qu'une couverture complète du spectre électromagnétique, incluant les ondes gravitationnelles et les neutrinos, pour l'étude de l'ensemble des sources de haute énergie.

• ALMA permettra de mieux connaître la structure de la Galaxie, les concentrations en gaz moléculaire et hydrogène, et donc aidera à chercher les liens entre concentration de systèmes

binaires de haute énergie et formation d'étoiles...

• VLT, JWST, MIRI : permettront d'étudier de l'UV à l'infrarouge moyen les étoiles compagnons, et les parties externes des disques d'accrétion, de déterminer les masses des deux composantes des systèmes binaires par vitesse radiale, de déterminer la géométrie, la température et la composition de cocons potentiels de gaz froid et de poussière situés autour des systèmes binaires...

• SIMBOL-X, (et XEUS ?), pourraient étudier des systèmes tous à la même distance, permettant une comparaison plus facile entre les différents systèmes, en s'affranchissant des effets de distance.

• GLAST permettra d'étudier non seulement l'émission γ des systèmes binaires de grande masse contenant des étoiles à neutron très magnétisées ($\sim$ pulsars), émission créé par l'interaction entre le vent du pulsar et celui de l'étoile supergéante, mais aussi certainement de découvrir de nouvelles classes d'objets émettant dans le domaine des hautes énergies...

• LIGO, LISA... permettront de rechercher les signatures de coalescence d'objets compacts, étoile à neutron ou trou noir...

• ANTARES, ICECUBE, KM3... : les futurs détecteurs de neutrinos permettront d'étudier les disques d'accrétions autour de trous noirs galactiques ou extra-galactiques, les modèles prédisant des émissions de neutrinos, ainsi que de sonder les coeurs des étoiles compagnons...

On le voit, le futur est riche de promesses d'observations, de modélisations, de simulations... Il faudra agir, lier ces travaux observationnels à des travaux théoriques, de modélisations ou de simulations, pour que ces promesses se réalisent et se convertissent en une compréhension plus profonde de la physique sous-jacente à ces formidables machines relativistes et gravitationnelles que sont les systèmes binaires de haute énergie...

Bibliographie

Aharonian, F., Akhperjanian, A. G., Aye, K.-M., et al. 2005, Science, 309, 746

Albert, J., Aliu, E., Anderhub, H., et al. 2006, Science, 312, 1771

Bassani, L., Malizia, A., Stephen, J. B., et al. 2004, The Astronomer's Telegram, 232, 1

Beckmann, V., Kennea, J. A., Markwardt, C., et al. 2005, ApJ, 631, 506

Bird, A. J., Barlow, E. J., Bassani, L., et al. 2006, ApJ, 636, 765

Bodaghee, A., Courvoisier, T. J.-L., Rodriguez, J., et al. 2007, A&A, 467, 585

Bolton, C. T. 1972, Nature, 235, 271

Bosch-Ramon, V., Romero, G. E., & Paredes, J. M. 2006, A&A, 447, 263

Bouchet, L., Mandrou, P., Roques, J.-P., et al. 1991, ApJ, 383, L45

Bradt, H. V. D. & McClintock, J. E. 1983, ARA&A, 21, 13

Bronfman, L., Nyman, L.-A., & May, J. 1996, A&AS, 115, 81

Cadolle Bel, M., Ribó, M., Rodriguez, J., et al. 2007, ApJ, 659, 549

Castro-Tirado, A. J., Brandt, S., Lund, N., et al. 1994, ApJ, 92, 469

Chaty, S. 1998, PhD thesis, AA(Service d'Astrophysique, CE Saclay, France)

Chaty, S. & Bessolaz, N. 2006, A&A, 455, 639

Chaty, S., Charles, P. A., Martí, J., et al. 2003a, MNRAS, 343, 169

Chaty, S. & Filliatre, P. 2005, Ap&SS, 297, 235

Chaty, S., Haswell, C. A., Malzac, J., et al. 2003b, MNRAS, 346, 689

Chaty, S., Mirabel, I. F., Goldoni, P., et al. 2002, MNRAS, 331, 1065

Chaty, S. & Rahoui, F. 2006, in Procs. of 6th INTEGRAL workshop, Moscow, Russia, in press (astro-ph/0609474)

Chaty, S., Rahoui, F., Foellmi, C., et al. 2008, A&A, in press

Chaty, S., Rodríguez, L. F., Mirabel, I. F., Geballe, T., & Fuchs, Y. 2001, A&A, 366, 1041

Coe, M. J. 2000, in ASP Conf. Ser. 214 : IAU Colloq. 175 : The Be Phenomenon in Early-Type Stars, ed. M. A. Smith, H. F. Henrichs, & J. Fabregat, 656–+

Combi, J. A., Ribó, M., Martí, J., & Chaty, S. 2006, A&A, 458, 761

Combi, J. A., Ribó, M., Mirabel, I. F., & Sugizaki, M. 2004, A&A, 422, 1031

Corbel, S., Fender, R. P., Tzioumis, A. K., et al. 2002, Science, 298, 196

Corbet, R., Barbier, L., Barthelmy, S., et al. 2005, The Astronomer's Telegram, 649, 1

Corbet, R. H. D. 1986, MNRAS, 220, 1047

Courvoisier, T. J.-L., Walter, R., Rodriguez, J., Bouchet, L., & Lutovinov, A. A. 2003, IAU Circ., 8063, 3

Dean, A. J., Bazzano, A., Hill, A. B., et al. 2005, A&A, 443, 485

den Hartog, P. R., Kuiper, L., Hermsen, W., et al. 2007, Ap&SS, 98

Dhawan, V., Mirabel, I., & Rodríguez, L. 2000, ApJ, 543

Distefano, C., Guetta, D., Waxman, E., & Levinson, A. 2002, ApJ, 575, 378

Dubner, G., Holdaway, M., Goss, M., & Mirabel, I. F. 1998, AJ, 116, 1842

Dubus, G. 2006, A&A, 456, 801

Dubus, G. & Chaty, S. 2006, A&A, 458, 591

Ergma, E. & van den Heuvel, E. P. J. 1998, A&A, 331, L29

Ergma, E. V. & Fedorova, A. V. 1991, A&A, 242, 125

Falcke, H., Körding, E., & Markoff, S. 2004, A&A, 414, 895

Fender, R. P. 2001, MNRAS, 322, 31

Filliatre, P. & Chaty, S. 2004, ApJ, 616, 469

Fuchs, Y. ., Mirabel, I. F. ., & Ogley, R. N. 2001, Astrophysics and Space Science Supplement, 276, 99

Fuchs, Y., Rodriguez, J., Mirabel, I. F., et al. 2003, A&A, 409, L35

Gallo, E., Fender, R. P., & Pooley, G. G. 2003, MNRAS, 344, 60

Genzel, R., Schödel, R., Ott, T., et al. 2003, Nature, 425, 934

Giacconi, R., Gursky, H., Paolini, F. R., & Rossi, B. B. 1962, Physical Review Letters, 9, 439

González-Riestra, R., Oosterbroek, T., Kuulkers, E., Orr, A., & Parmar, A. N. 2004, A&A, 420, 589

Grove, J., Johnson, W., Kroeger, R., et al. 1998, ApJ, 500, 899

Haswell, C. A., Hynes, R. I., King, A. R., & Schenker, K. 2002, MNRAS, 332, 928+

Hatchett, S. & McCray, R. 1977, ApJ, 211, 552

Heinz, S. & Sunyaev, R. 2002, A&A, 390, 751

Indebetouw, R., Mathis, J. S., Babler, B. L., et al. 2005, ApJ, 619, 931

in't Zand, J. J. M. 2005, A&A, 441, L1

in't Zand, J. J. M., Jonker, P. G., Nelemans, G., Steeghs, D., & O'Brien, K. 2006, A&A, 448, 1101

Kaper, L., van der Meer, A., & Tijani, A. H. 2004, in Revista Mexicana de Astronomia y Astrofisica Conference Series, ed. C. Allen & C. Scarfe, 128–131

Kolb, U., King, A., Ritter, H., & Frank, J. 1997, ApJ, 485, L33

Körding, E., Falcke, H., & Markoff, S. 2002, A&A, 382, L13

Lebrun, F., Terrier, R., Bazzano, A., et al. 2004, Nature, 428, 293

Lee, J. C., Reynolds, C. S., Remillard, R., et al. 2002, ApJ, 567, 1102

Lewin, W. H. G., van Paradijs, J., & van den Heuvel, E. P. J. 1995, X-ray binaries (Cambridge Astrophysics Series, Cambridge, MA : Cambridge University Press, |c1995, edited by Lewin, Walter H.G. ; Van Paradijs, Jan ; Van den Heuvel, Edward P.J.)

Liu, Q. Z. & Mirabel, I. F. 2005, A&A, 429, 1125

Liu, Q. Z., van Paradijs, J., & van den Heuvel, E. P. J. 2000, Astron. Astrophys. Suppl. Ser., 147, 25

Liu, Q. Z., van Paradijs, J., & van den Heuvel, E. P. J. 2001, A&A, 368, 1021

Liu, Q. Z., van Paradijs, J., & van den Heuvel, E. P. J. 2006, A&A, 455, 1165

Lommen, D., Yungelson, L., van den Heuvel, E., Nelemans, G., & Portegies Zwart, S. 2005, A&A, 443, 231

Lutovinov, A., Revnivtsev, M., Gilfanov, M., et al. 2005a, A&A, 444, 821

Lutovinov, A., Rodriguez, J., Revnivtsev, M., & Shtykovskiy, P. 2005b, A&A, 433, L41

Maeder, A. 1993, Space Sci. Rev., 66, 349

Malizia, A., Bassani, L., Stephen, J. B., et al. 2003, ApJ, 589, L17

Margon, B. 1984, ARA&A, 22, 507

Markoff, S., Falcke, H., & Fender, R. 2001, A&A, 372, L25

Marscher, A. P., Jorstad, S. G., Gómez, J., et al. 2002, Nature, 417, 625

Masetti, N., Morelli, L., Palazzi, E., et al. 2006, A&A, 459, 21

Massi, M., Ribó, M., Paredes, J. M., et al. 2004, A&A, 414, L1

Matt, G. & Guainazzi, M. 2003, MNRAS, 341, L13

Meurs, E. J. A. & van den Heuvel, E. P. J. 1989, A&A, 226, 88

Mirabel, I. F. 2006, Science, 312, 1759

Mirabel, I. F., Dhawan, V., Chaty, S., et al. 1998, A&A, 330, L9

Mirabel, I. F. & Rodríguez, L. F. 1994, Nature, 371, 46

Mirabel, I. F., Rodríguez, L. F., Chaty, S., et al. 1996, ApJ, 472, L111

Mirabel, I. F., Rodríguez, L. F., Cordier, B., Paul, J., & Lebrun, F. 1992, Nature, 358, 215

Negueruela, I. 2004, in Revista Mexicana de Astronomia y Astrofisica Conference Series, ed. G. Tovmassian & E. Sion, 55–56

Negueruela, I., Smith, D. M., & Chaty, S. 2005, The Astronomer's Telegram, 429, 1

Negueruela, I., Smith, D. M., Harrison, T. E., & Torrejón, J. M. 2006a, ApJ, 638, 982

Negueruela, I., Smith, D. M., Reig, P., Chaty, S., & Torrejón, J. M. 2006b, in ESA Special Publication, Vol. 604, ESA Special Publication, ed. A. Wilson, 165–170

Nespoli, E., Fabregat, J., & Mennickent, R. 2007, The Astronomer's Telegram, 982, 1

Novikov, I. D. & Zel'Dovich, Y. B. 1966, Nuova Cimento Sup., 4, 810

Paczynski, B. 1976, in IAU Symposium, Vol. 73, Structure and Evolution of Close Binary Systems, ed. P. Eggleton, S. Mitton, & J. Whelan, 75–+

Pandey, M., Manchanda, R. K., Rao, A. P., Durouchoux, P., & Ishwara-Chandra. 2006, A&A, 446, 471

Paredes, J. M., Martí, J., Ribó, M., & Massi, M. 2000, Science, 288, 2340

Patel, S. K., Kouveliotou, C., Tennant, A., et al. 2004, ApJ, 602, L45

Pellizza, L. J., Chaty, S., & Negueruela, I. 2006, A&A, 455, 653

Podsiadlowski, P. 1991, Nature, 350, 136

Podsiadlowski, P. & Rappaport, S. 2000, ApJ, 529, 946

Portegies Zwart, S. F. & Verbunt, F. 1996, A&A, 309, 179

Pringle, J. E. 1973, Nature, 243, 90

Pylyser, E. & Savonije, G. J. 1988, A&A, 191, 57

Pylyser, E. H. P. & Savonije, G. J. 1989, A&A, 208, 52

Rahoui, F., Chaty, S., Lagage, P.-O., & Pantin, E. 2008, A&A, in press

Reig, P. 2007, MNRAS, 255

Ribó, M., Dhawan, V., & Mirabel, I. F. 2004, in European VLBI Network on New Developments in VLBI Science and Technology, 111–112

Rieke, G. & Lebofsky, M. 1985, ApJ, 288, 618

Rodriguez, J., Tomsick, J. A., Foschini, L., et al. 2003, A&A, 407, L41

Romero, G. E. & Orellana, M. 2005, A&A, 439, 237

Ruderman, M., Shaham, J., & Tavani, M. 1989, ApJ, 336, 507

Russeil, D. 2003, A&A, 397, 133

Salpeter, E. E. 1964, ApJ, 140, 796

Sguera, V., Bazzano, A., Bird, A. J., et al. 2006, ApJ, 646, 452

Shklovsky, I. S. 1967, ApJ, 148, L1+

Sturner, S. J. & Shrader, C. R. 2005, ApJ, 625, 923

Sunyaev, R. A., Grebenev, S. A., Lutovinov, A. A., et al. 2003, The Astronomer's Telegram, 190, 1

Tauris, T. M. 1996, A&A, 315, 453

Tauris, T. M. & van den Heuvel, E. P. J. 2006, Formation and evolution of compact stellar X-ray sources (Compact stellar X-ray sources), 623–665

Tauris, T. M., van den Heuvel, E. P. J., & Savonije, G. J. 2000, ApJ, 530, L93

Thompson, T. W. J., Tomsick, J. A., Rothschild, R. E., in't Zand, J. J. M., & Walter, R. 2006, ApJ, 649, 373

Tomsick, J. A., Chaty, S., Rodriguez, J., et al. 2006a, ApJ, 647, 1309

Tomsick, J. A., Chaty, S., Rodriguez, J., & Walter, R. 2007, The Astronomer's Telegram, 1018, 1

Tomsick, J. A., Chaty, S., Rodriguez, J., Walter, R., & Kaaret, P. 2006b, The Astronomer's Telegram, 959, 1

Tomsick, J. A., Lingenfelter, R., Corbel, S., Goldwurm, A., & Kaaret, P. 2004, in ESA SP-552 : 5th INTEGRAL Workshop on the INTEGRAL Universe, ed. V. Schoenfelder, G. Lichti, & C. Winkler, 413–416

Tovmassian, G., Tomsick, J. A., & Mennickent, R. 2006, The Astronomer's Telegram, 804, 1

Türler, M., Courvoisier, T. J.-L., Chaty, S., & Fuchs, Y. 2004, A&A, 415, L35

Ueda, Y., Yamaoka, K., Sánchez-Fernández, C., et al. 2002, ApJ, 571, 918

van den Heuvel, E. P. J. & van Paradijs, J. 1988, Nature, 334, 227

van Paradijs, J. 1983, in Accretion-Driven Stellar X-ray Sources, ed. W. H. G. Lewin & E. P. J. van den Heuvel, 189–260

van Paradijs, J. 1995, in The Lives of the Neutron Stars. Proceedings of the NATO Advanced Study Institute on the Lives of the Neutron Stars, held in Kemer, Turkey, August 29-September 12, 1993. Editor(s), M.A. Alpar, U. Kiziloglu, J. van Paradijs ; Publisher, Kluwer Academic, Dordrecht, The Netherlands, Boston, Massachusetts, 1995. LC # : QB843.N4 L583 1993. ISBN # : 0-7923-324-6-6., p.281, ed. M. A. Alpar, U. Kiziloglu, & J. van Paradijs, 281–+

Walter, R., Rodriguez, J., Foschini, L., et al. 2003, A&A, 411, L427

Walter, R., Zurita Heras, J., Bassani, L., et al. 2006, A&A, 453, 133

Webster, B. L. & Murdin, P. 1972, Nature, 235, 37

Wolszczan, A. 1994, Science, 264, 538

Woosley, S. E., Langer, N., & Weaver, T. A. 1993, ApJ, 411, 823

Zel'Dovich, Y. B. 1964, Soviet Physics Doklady, 9, 195

Zeldovich, Y. B. & Guseynov, O. H. 1966, ApJ, 144, 840

Zel'Dovich, Y. B. & Novikov, I. D. 1964, Doklady Academii Nauk SSSR, 158, 811